DECIPHERING THE DNA DAMAGE SIGNALING NETWORKS

IN *CAENORHABDITIS ELEGANS*

DISSERTATION

ZUR

ERLANGUNG DER NATURWISSENSCHAFTLICHEN DOKTORWÜRDE
(DR. SC. NAT.)

VORGELEGT DER

MATHEMATISCH-NATURWISSENSCHAFTLICHEN FAKULTÄT

DER

UNIVERSITÄT ZÜRICH

VON

GARIFALIA STERGIOU

AUS

GRIECHENLAND

PROMOTIONSKOMITEE

PROF. MICHAEL O. HENGARTNER (VORSITZ, LEITER DER DISSERTATION)

PROF. KONRAD BASLER

PROF. PATRICK NEF

PROF. PRIMO SCHÄR

ZÜRICH 2005

DECIPHERING THE DNA DAMAGE SIGNALING NETWORKS

IN *CAENORHABDITIS ELEGANS*

SUBMITTED IN ACCORDANCE WITH REQUIREMENTS OF

THE UNIVERSITY OF ZURICH

FOR THE DEGREE OF

DOCTOR OF PHILOSOPHY

GARIFALIA STERGIOU

UNIVERSITY OF ZURICH

To the most beloved people in my life…

Every event is dictated by a "telos", an ultimate goal after a combination of actions. The aim of being is the development of the potential toward reality. Nothing is superfluous in nature, nothing is futile, nothing is there that is not perfect. Just by living in nature, we can witness the existence of a purposeful end in the universal structure, in all of nature's creations, all the big and the small ones…

Aristotle, 384 BC

Acknowledgements

I feel that this page turns out to be the hardest one for numerous reasons.

I owe a big “thank you” to Michael who, apart from trusting me to work in his lab despite my fears about biology back then, has been more than a supervisor to me; it is something rare to find in a boss and hope he knows more than what these lines reveal.

I am thankful to my committee members, Prof. Konrad Basler, Prof. Patrick Nef and Prof. Primo Schär for their exquisite co-operation.

I thank Christophe Grundschober and Beate Hartmann, members of the microarray lab in Hoffmann-La Roche for their enormous help. I am obliged to Randy Hofmann, whose presence in the first two years in our lab was catalytic to me. I owe him my way of thinking in terms of “DNA damage”. I want to thank Jason and Cheng-Wen for endless hours of discussion during our days and nights in the lab, our tough and happy times in Zurich. I feel the need to thank Ati for showing me that a PhD is not only a learning procedure but also a process where I have the chance to offer and the pleasure to get back more. Along with this, the members of the DNA damage group who make our worms proud of us. Many thanks to the people in the lab and to my friend Paola who had and still have the power to make me laugh during my hard days here. I specially thank Jim whom although I met very recently, I appreciated his presence very fast; not only as a scientist but most importantly as a friend.

I am extremely grateful to the invisible heroes of this story, my family, whose support and encouragement were mostly valuable to me. And I am deeply grateful to Kimon, the person who made it possible for the day of my defense to come. The person who believes in me and keeps my lab and non-lab life in balance.

Summary

To monitor genomic integrity in order to ensure the transmission of genetic information with high fidelity, eukaryotic cells mount a robust and complex response to DNA damage. This response translates into arrest of the cell cycle and initiation of repair pathways, and may culminate in cell death in case of non-repairable damage. Cells harboring defects in these pathways respond to DNA damage improperly which, in turn, may enhance the rate of carcinogenesis. Previous and current work in *C. elegans* has developed this organism into a promising working model for DNA damage signaling networks.

DNA damage responsive networks embrace groups of functionally connected genes. I decided to undertake a genome-wide approach to study these biological relationships. I utilized cDNA microarrays to develop the gene expression profile following exposure to Ionizing Radiation (IR) and the mutagenic agent ethyl-nitroso-urea (ENU). Identifying genes that are differentially regulated in response to DNA damage may provide insight into the cellular responses to specific genotoxic agents.

This study revealed *lin-26*, a gene that encodes a member of the Krüppel-type zinc finger proteins, to be transcriptionally induced upon IR, whereas loss of its function abrogates DNA damage-induced apoptosis. I speculate that LIN-26 is repressing the expression of certain pro-survival genes and may be involved in stabilizing the commitment of the dying cells to the death fate.

A forward genetic screen for mutants defective in IR-induced apoptosis identified *rpo-1*, a gene homologous to a splice variant of the second largest subunit of human RNA polymerase I. Compromising its function also affects nuclear and nucleolar size, reflecting an abnormal number of ribosomal RNA transcripts. I postulate the involvement of the nucleolus in the appropriate triggering of DNA damage-induced cell death.

To expand knowledge of DNA damage signaling cascades, I demonstrated that a UV-induced signaling pathway is present in *C. elegans*, which comprises a distinct set of components that partially overlaps with those of the IR responsive pathway. Major regulators are the *atl-1* and *atm-1* genes, that when mutated in humans give rise to severe genetic disorders. In addition, repair factors are important determinants of the initiation of the DNA damage signaling triggered by UV.

As many aspects of the DNA damage response have been highly conserved throughout eukaryotic evolution, studying a simple model organism like *C. elegans* will contribute to the unveiling of the complexities of the DNA damage signaling network in mammals and the underlying biology of human disorders.

Zusammenfassung

Um die Integrität des Genoms zu kontrollieren und um sicherzustellen, dass genetische Information mit hoher Genauigkeit weitergegeben wird, haben eukaryotische Zellen eine robuste und komplexe Antwort auf Schädigung der DNA entwickelt. Diese Antwort besteht aus Zellzyklus-Arretierung wie auch dem Einleiten von Reparatursignalwegen, und kann im programmierten Zelltod gipfeln, falls der Schaden an der DNA irreparabel ist. Zellen mit Defekten in diesen Signaltransduktionswegen können auf Schäden an der DNA nicht angemessen reagieren, was wiederum eine erhöhte Wahrscheinlichkeit einer neoplastischen Veränderung mit sich bringt. Frühere wie auch gegenwärtige Forschung am Nematoden *C. elegans* hat dazu beigetragen, dass dieser Organismus ein vielversprechendes Modell darstellt um Signaltransduktionswege nach DNA-Schädigung zu erforschen.

Aktivierte Netzwerke nach DNA-Schädigung umfassen Gruppen funktionell verbundener Gene. Ich entschloss mich einen genomweiten Ansatz zu wählen, um diese biologischen Netzwerke zu studieren. Ich benutzte cDNA microarrays um Genexpressionsprofile zu erstellen nach ionisierender Strahlung und dem Mutagen Ethyl-nitroso-urea (ENU). Die Identifizierung von Genen, die unterschiedlich nach DNA-Schädigung exprimiert werden, können somit Einblick gewähren, wie eine Zelle auf spezifische genotoxische Einflüsse reagiert.

Diese Arbeit hat zur Identifizierung von *lin-26* geführt, einem Gen, das für ein Mitglied einer neuen Gruppe von Zinkfinger-Proteinen kodiert und auf Ebene der

Transkription hochreguliert wird nach ionisierender Strahlung. Funktionsverlust dieses Genes führt dazu, dass nach DNA-Schädigung der programmierte Zelltod verhindert wird. Ich vermute, dass LIN-26 die Expression gewisser Gene hemmt, die für das Überleben der Zelle zuständig wären und die Zelle in der Entscheidung Richtung Zelltod stabilisiert.

Ein forward genetische Screen mit dem Ziel Mutanten zu finden, die Apoptose nach ionisierender Strahlung nicht einleiten können, führte zur Identifizierung von *rpo-1*, einem Gene, das Homolog zu einer Spleissvariante der zweitgrössten Unterheit der menschlichen RNA Polymerase I ist. Eine Beeinträchtigung der Funktion dieses Gens beeinflusst die Grösse des Zellkerns wie auch des Nukleolus, was eine veränderte Anzahl ribosomaler RNA Transkripte widerspiegelt. Ich postuliere eine Beteiligung des Nukleolus an der korrekten Einleitung des programmierten Zelltodes nach DNA-Schädigung.

Um mehr Einsicht zu gewinnen in Signaltransduktionskaskaden die nach DNA-Schäden aktiviert werden, zeigte ich im weiteren, dass ein Ultraviolettlicht-spezifischer Signalweg in *C. elegans* existiert, der partiell mit dem durch ionisierender Strahlung aktivierten Signalweg überlappt. Hauptregulatoren sind die Gene *atl-1* und *atm-1*, welche im Falle einer Mutation zu schwerwiegenden Krankheiten führen können. Ferner sind gewisse Komponenten der Zellreparatur von entscheidender Wichtigkeit im Einleiten der Signalwege nach DNA-Schädigung durch UV-Licht.

Da viele Aspekte der Zellantwort nach DNA-Schädigung evolutionär konserviert sind, wird die Forschung an einem simplen Modellorganismus wie dem Nematoden *C. elegans* dazu beitragen, die Komplexität der Signalwege nach DNA-Schädigung in Säugetieren zu entschlüsseln und helfen Krankheiten besser zu verstehen, welchen Defekte in diesen zugrundeliegen.

Table of contents

CHAPTER 1

PART I

APOPTOSIS IN *CAENORHABDITIS ELEGANS*

Preface

"We propose to identify every cell in the worm and trace lineages", wrote Sydney in his bid for support for the project in the mid 1960's. "We shall also investigate the constancy of development and study its genetic control by looking for mutants." Sydney later recalled that some people thought the idea was crazy.

Why did Sydney Brenner pick a worm?

There is not a single member in the whole worm community who hasn't recognized by now the importance of that crazy idea and valued the achievements of the first worm geneticist.

Since then, the soil nematode, a simple eukaryotic organism, has proven to be a very good model to study various conserved biological processes due to its extraordinary characteristics: a well-characterized and invariant cell lineage, the small size of a transparent body that allows morphological observations, combined with powerful genetics and a fully sequenced genome, are among the properties that make it so advantageous.

Mostly valuable it was proven for the understanding of programmed cell death (Horvitz *et al.*, 1982, Metzstein *et al.*, 1998, Liu & Hengartner, 1999, Horvitz, 1999). The pioneer studies of the genetics of developmental programmed cell death by Horvitz and his colleagues led to the identification of the principal components of a core apoptotic pathway, which was found to be conserved in several organisms, including mammals.

Already since the mid-nineteenth century, many observations had indicated that cell death plays a considerable role during physiological processes of multicellular organisms, particularly during embryogenesis and metamorphosis (Gluecksmann, 1951 Lockshin *et al.*, 2001). Cell death removes superfluous, damaged or harmful cells to sculpt the structures of the future organism, to form the proper shapes of organs by deleting unneeded structures, and to control the appropriate number of cells that are produced. The term programmed cell death or apoptosis was introduced to propose that cell death during development is not of accidental nature but follows a sequence of genetically controlled steps leading to locally and temporally defined self-destruction (Lockshin & Williams, 1964). Later in life, apoptosis is used to maintain tissue homeostasis, for example, by eliminating immature lymphocytes that have inappropriate receptor specificities during the establishment of the immune tolerance, or virus-infected and injured cells.

Apoptotic processes are, therefore, of widespread biological significance. Dysfunction or dyrsegulation of the apoptotic program is implicated in a variety of pathological conditions. Defects in apoptosis can result in cancer, autoimmune diseases and spreading of viral infections, whereas excessive apoptosis can lead to neurodegenerative disorders, AIDS and ischaemic diseases (Fadeel *et al.*, 1999).

1.1. Cell death occurs during development in *C. elegans*

During development of the *C. elegans* hermaphrodite animal, one hundred and thirty-one cells out of the thousand and ninety that are initially generated die by apoptosis in a highly reproducible manner (Sulston and Horvitz, 1977, Sulston *et al.*, 1983). Namely, always the same cells and at a well-defined and invariant point in embryonic development will be removed, with all of them being extinguished by the time embryos have reached the three-fold stage.

Stereotypical morphological changes, such as cell shrinkage, deformation and loss of contact to the neighboring cells, chromatin condensation, plasma membrane blebbing or budding, and fragmentation into compact membrane-enclosed structures called 'apoptotic bodies', is what one observes under the light microscope, similar to the morphological changes occurring in dying mammalian cells (Sulston & Horvitz, 1977, Robertson & Thomson, 1982).

Extensive genetic screens for mutations that affect the execution of developmental cell death led to the identification of a genetic pathway for programmed cell death. Epistasis studies placed the affected genes in a linear pathway, that requires the hierarchical occurrence of four different phases: induction of programmed cell death, execution of the apoptotic program, engulfment of the dying cell by one of its neighbors and degradation of the corpse within the engulfing cell (Figure 1) (Liu & Hengartner, 1999). Recent studies, however, in both mammals and *C. elegans* suggested that there is interplay among the four steps, with the phagocytes actively promoting the execution of programmed cell death in the doomed cells (Figure 1) (Reddien *et al.*, 2001, Conradt, 2002).

1.1.1. The genetic requirements of programmed cell death

Developmental cell death requires the action of three genes, *ced-3, ced-4* (cell death abnormality) and *egl-1* (egg-laying defective), for its execution. A fourth gene, *ced-9*, has a pro-survival activity and normally protects cells from an inappropriate activation of the apoptotic pathway. *ced-3, ced-4* and *ced-9* form the core apoptotic machinery while the pro-apoptotic activity of EGL-1 relies on the negative regulation of CED-9 (Liu and Hengartner, 1999).

The CED-3 caspase

ced-3 is essential for programmed cell death in *C. elegans,* as strong loss of function mutations in the gene completely block all normally occurring deaths, except those occuring in the male tail (Ellis and Horvitz, 1986). Weaker loss of function alleles of *ced-3,* result in a partial suppression of death, with a fraction of cells dying in a stochastic way. Mosaic analysis and ectopic expression experiments suggest that *ced-3* functions cell autonomously to promote programmed cell death (Ellis and Horvitz, 1986; Yuan and Horvitz 1990; Shaham and Horvitz 1996a).

ced-3 encodes a member of the CED-3/ICE (Interleukin-1b converting enzyme) family of cysteine aspartyl proteases (Yuan *et al.*, 1993, Xue *et al.*, 1996), which act by triggering intracellular proteolytic cascades that ultimately lead to the degradation of vital cell components. Despite the numerous death caspases identified in mammals (Alnemri *et al.*, 1996, Nicholson & Thornberry, 1997), only CED-3 in worms has a

well-defined role in cell death (Shaham, 1998), with little information on its substrates, though.

Overexpression of CED-3 or any of the other ICE family members induces apoptotic cell death in mammalian cells (Miura *et al.*, 1993). Simultaneous overexpression of either Bcl-2, the mammalian *ced-9* homolog, or by viral caspase inhibitors, such as p35 can prevent these deaths (Ray *et al.*, 1992, 1993; Martinou *et al.*, 1995; Xue and Horvitz, 1995).

The CED-4/Apaf1 orthologue

ced-4 was initially regarded as a protein of unknown function (Yuan & Horvitz, 1992) and only when the mammalian apoptotic protease activating factor-1, Apaf-1, was identified and characterized, did its function become known (Zou *et al.*, 1997). *ced-4* is also essential for programmed cell death in *C. elegans*. *ced-4(lf)* mutations completely prevent all developmental cell deaths, except those occurring in the male tail (Ellis and Horvitz, 1986). Interestingly enough, through alternative splicing the *ced-4* locus gives rise to two isoforms, the products of which have antagonistic effects: when overexpressed, CED-4L has anti-apoptotic effects, while CED-4S promotes apoptosis (Yuan & Horvitz, 1992, Shaham & Horvitz, 1996b). However, how exactly these two splice variants are involved in the 'apoptosome' is largely unknown.

CED-4 possesses both an amino-terminal caspase recruitment domain (CARD) (Hofmann *et al.*, 1997), which allows binding of the CARD domain of CED-3, and a nucleotide binding domain (NBD or P-loop). A domain responsible for binding to

CED-9 has been shown to play an important role in sequestrating CED-4 in an inactive complex on the mitochondrial membrane (Chen *et al*., 2000). Upon induction of apoptosis in the *C. elegans* embryo, CED-4 translocates from mitochondria to the perinuclear region independently of CED-3, to cell autonomously promote the death fate. It does so by autoactivating CED-3 when, through its oligomerization brings molecules of the latter into 'close proximity' (Chinnaiyan *et al*., 1997a, b, Yang *et al*., 1998).

The CED-9/Bcl-2 orthologue

The *ced-9* gene was originally defined by a gain-of-function allele that blocks programmed cell death (Hengartner *et al.*, 1992). *cis* dominant suppressors were then isolated that led to an ectopic activation of programmed cell death in cells that normally live, resulting in sterility and maternal effect lethality (Hengartner *et al.*, 1992). The *ced-9* gene product exhibits sequence and functional similarity to Bcl-2 (B cell lymphoma 2) (Hengartner & Horvitz, 1994), a mammalian proto-oncogene originally discovered by a dominant gain-of-function mutation commonly found in follicular lymphomas (Tsujimoto *et al.*, 1984). Overexpression of both prevents or slows down apoptosis in a large variety of cells fated to die (Hengartner & Horvitz, 1994).

CED-9 directly interacts with CED-4 (Chinnaiyan *et al.*, 1997b; James *et al*., 1997; Spector *et al.*, 1997) likely through the conserved BH1, BH2 and BH3 domains (Bcl-2 Homology domain). Both in mammalian cells (Wu *et al.*, 1997) and in *C. elegans*

(Chen *et al.*, 2000) it localizes on the outer mitochondrial membrane where it sequesters CED-4 in an inactive complex, thereby exerting its anti-apoptotic activity.

The EGL-1/BH3-only domain protein

The *egl-1* gene was originally defined by gain-of-function mutations that provoke a dominant egg-laying defect due to the inappropriate death of the two functional Hermaphrodite Specific Neurons (HSNs) (Ellis & Horvitz, 1986). A *cis* dominant suppressor of *egl-1(gf)* egg-laying defect identified a loss-of-function mutation which prevented most if not all developmentally regulated programmed cell deaths in somatic cells (Conradt and Horvitz, 1998).

The *C. elegans egl-1* gene encodes a small protein with molecular and functional similarity to the 'BH3-only' subfamily of the Bcl-2-like proteins. A short region of 9 amino-acids is responsible for the physical interaction with CED-9 which, upon binding, results in the displacement of CED-4 from the mitochondrial associated complex, thereby allowing CED-4 to trigger cell death. Many cells control the induction of programmed cell death by transcriptionally regulating *egl-1* expression. Depending on the cell type and the developmental stage, transcription factors including CES-1, CES-2 (Ellis & Horvitz, 1991b) or TRA-1A (Conradt & Horvitz, 1999) can have a positive or negative effect.

1.2. Programmed cell death in the *C. elegans* germline

1.2.1. The *C. elegans* adult hermaphrodite germline

The gonad of the *C. elegans* adult hermaphrodite is a bilaterally symmetrical tube with a distal-to-proximal polarity and with proximal ends that are joined to a common uterus. It is composed of germ cell nuclei that are surrounded by incomplete membranes and share a common syncytial cytoplasm via cytoplasmic bridges (Figure 2) (Schedl, 1997).

Cells in the distal arm undergo rounds of mitotic division, serving as a germline stem cell population. The proliferative state is maintained by a distal tip cell (DTC) that caps the distal portion of the gonad. As germ line nuclei progress proximally out of the DTC influence, they enter meiosis in the transition zone and progress into the pachytene stage of meiotic prophase I (Crittenden *et al.*, 1994). Progression beyond the pachytene stage of meiosis I requires activation of the MAP kinase signaling pathway (Church *et al.*, 1995) and occurs near the bend of the gonad arm. Upon exit from this stage, they complete meiotic prophase, enlarge in size to form oocytes, undergo the final stages of maturation and finish meiosis after fertilization through the spermatheca.

1.2.2. Regulation of physiological programmed cell death

The reproductive system presents some of the best examples of programmed cell death. An excess or non-viable germ and granulosa cells are eliminated early in ontogeny during human ovarian function and development, and thereafter

continuously throughout reproductive life (Morita & Tilly, 1999, Johnson & Bridgham, 2002, Vaskivuo & Tapanainen, 2003).

Similarly, apoptosis is a hallmark of the *C. elegans* germline development, where almost half of all potential oocytes die during meiotic maturation (Gumienny *et al.*, 1999). These deaths are stochastic in nature, in contrast to the reproducible pattern seen in somatic tissues. In addition, cell death increases with the age of the animal. This could either be due to accumulation of replicative errors in the mitotic nuclei resulting in terminally damaged cells, or the steady state levels of death could reflect a larger amount of existing cells.

Genetic requirements of physiological cell death

Germ cell death and developmental cell death share the same execution machinery: strong loss-of-function mutations in either *ced-3* or *ced-4* dramatically decrease germ cell death, and the *ced-9* loss-of-function mutation similarly results in increased levels of apoptosis (Gumienny *et al.*, 1999). The main difference, however, lies in the necessity for EGL-1 activity in the induction of apoptosis, namely *egl-1(lf)* mutants show wild-type levels of physiological cell death. In addition, a *ced-9(gf)* mutation that affects the CED-9/EGL-1 interaction has little effect on germ cell death. These facts strongly imply the existence of additional molecular mechanisms, mainly BH3-independent ones, to regulate the initiation and control the progression of programmed cell death in the hermaphrodite germline (Figure 1).

Interestingly, triggering of germ line apoptosis relies on the Ras/MAPK kinase pathway. Its role for the exit of germ cells form the pachytene stage is coupled to the

induction of cell death. It appears to play a permissive role in the proper progression of apoptosis, as activation of the pathway is necessary, but not sufficient, for the cells to die. The ras/MAPK pathway might also directly regulate the cell death machinery (Gumienny *et al.*, 1999, Gibert *et al.*, 1984).

One of the genes that was found to specifically influence programmed cell death in the germline codes for a predicted RNA helicase. Knocking down expression of *cgh-1* results in increased levels of death, making lack of *cgh-1* function the first stimulus identified that can trigger killing of all developing oocytes by the apoptotic mechanism. If the protein controls the metabolism or translation of certain mRNA molecules, this could be implicative of the mode of regulation of physiological cell death. In the same line of evidence, several *gla* genes (germ line apoptosis) have been isolated by a former member of the Hengartner lab, that lead to increased apoptosis when mutated (Milstein, PhD thesis, 2001). Some of them encode potential RNA binding proteins and their study could possibly shed some light on the molecular mechanisms controlling physiological germ apoptosis. It is possible, however, that the activation of apoptosis is due to a non-specific mechanism.

1.3. Engulfment of apoptotic cells in *C. elegans*

Engulfment is the biological process activated for the efficient elimination of cells undergoing programmed cell death. Removal of apoptotic cells is crucial for the shaping and remodeling of organs during development and for normal tissue homeostasis. It is also important to prevent unwanted immune responses to self-antigens derived from the dying cells.

With a diverse physiological importance, engulfment of apoptotic cells is a very complex process. Genetic studies in *C. elegans* have led to a framework for this process. Although the organism lacks professional phagocytic cells, it uses cells that are immediately adjacent to the apoptotic cell to remove it, usually within less than an hour of the onset of apoptosis.

1.3.1. The function of engulfing genes to mediate clearance of apoptotic corpses

The work with *C. elegans* revealed at least seven major genes, *ced-1, -2, -5, -6, -7, -10* and *ced-12*, that define two signal transduction pathways acting redundantly to control engulfment (Ellis *et al.*, 1991a, Gumienny & Hengartner, 2001, Wu *et al.*, 2001). In the respective mutants cells deaths occur normally, but many of the dying cells fail to be engulfed and persist in the animal for several hours. Animals that combine mutations in genes belonging to the two different pathways display an even more severe engulfment defect.

The first pathway comprises CED-1/SREC/LRP, a candidate receptor that probably recognizes an unknown ligand on the apoptotic cell and signals via its cytoplasmic tail to the adaptor protein CED-6/GULP to mediate cytoskeleton

remodeling. CED-7/ABCA1 is thought to play a role in membrane dynamics and is required for proper CED-1 localization. In the second pathway, CED-2/CrkII recruits the CED-5/DOCK180::CED-12/ELMO complex to the membrane to achieve actin rearrangement through CED-10/Rac (Kinchen & Hengartner, 2005). Recent genetic studies carried out with a recently isolated *ced-10* null allele have placed CED-10/Rac to act genetically downstream of both pathways, to mediate corpse removal (Kinchen *et al*., 2005). This evidence provides a functional link between the two engulfment pathways and reveals that actin remodeling during activation of the CED-1 - CED-6 - CED-7 pathway proceeds through signaling of CED-10.

Despite the considerable progress made in the field, there are still important questions regarding the molecular mechanisms that control apoptotic cell corpse engulfment and other factors involved in. For example, the major receptor that activates the CED-2 - CED-5 - CED-12 pathway as well as the ligands on the surface of the dying cell that activate each one of the engulfment pathways remain to be discovered. Moreover, the molecules acting downstream of CED-6 are still obscure. And, how activation of CED-6 provokes activation of CED-10, and the latter subsequently leading to actin remodeling, are unclear issues.

Interestingly, all the *C. elegans* engulfment genes have orthologs in higher vertebrates, suggesting that the mechanisms mediating cell corpse removal are evolutionary conserved. Thus, continuation of studies in the worm might help us gain significant insight into this fundamental aspect of metazoan biology.

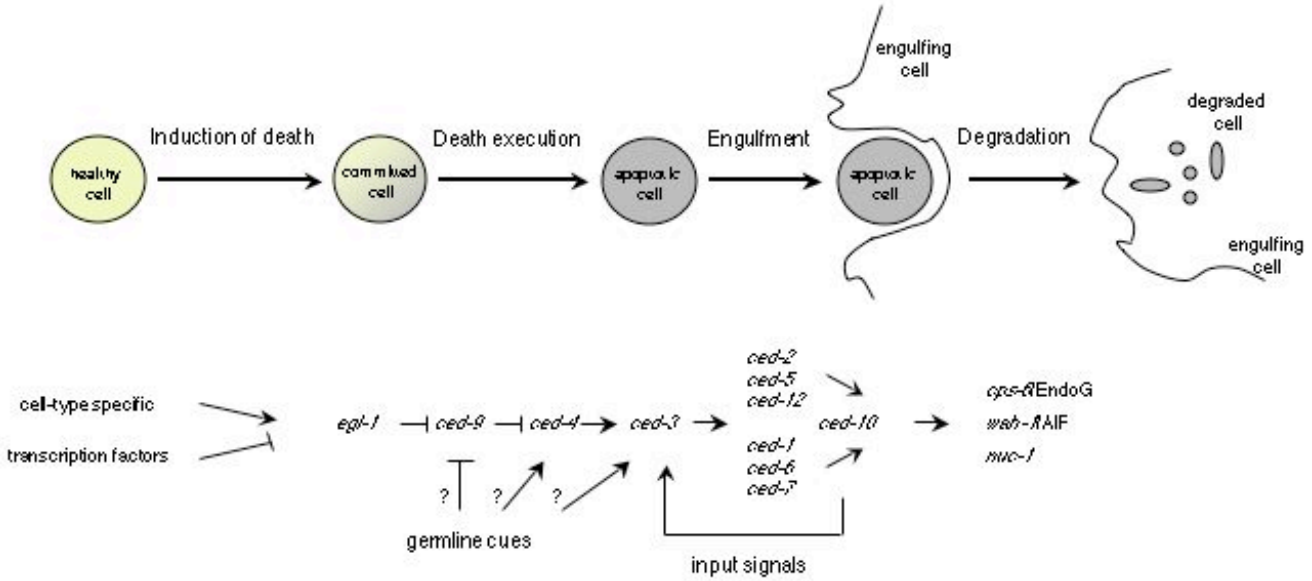

Figure 1. A conserved genetic pathway mediates programmed cell death in *C. elegans*

Four different phases constitute the genetic pathway for programmed cell death in *C. elegans*. Induction of death is cell-specific, whereas the apoptotic machinery (*egl-1, ced-9, ced-4, ced-3*) and the engulfing machinery (*ced-1, -2, -5, -6, -7, -10, -12*) that eliminate the germ cells are cell-type independent. Input from the engulfing components contributes to the proper induction of cell death (Reddien et al., 2001, Hoeppner et al., 2001). Scheme is adapted from Liu & Hengartner, 1999.

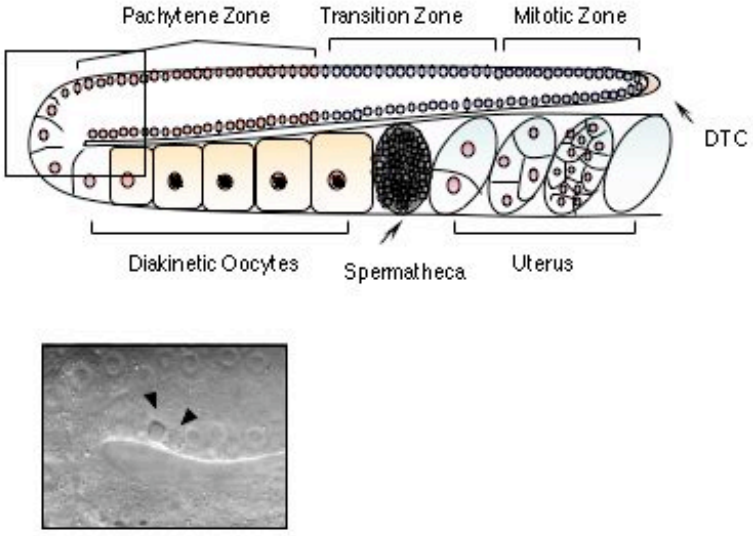

Figure 2. The adult hermaphrodite germline tissue of *C. elegans*

The germline tissue displays a distal-to-proximal polarity in its pattern of proliferation, meiotic prophase progression and gametogenesis (See more details in the text). In the window below, DIC microscopy of the bend of the gonad with two apoptotic corpses marked by the arrowheads.

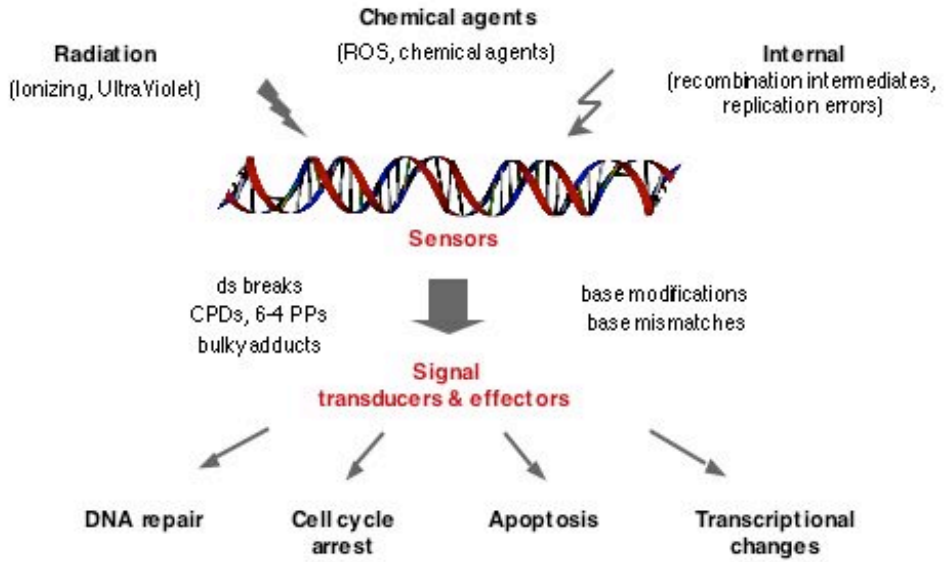

Figure 3. Activation of cellular responses upon DNA damage

A number of exogenous and endogenous factors inflict various types of damage in the genome. Different sensors detect different lesions and activate a protein kinase-based signaling cascade. The biological output comprises repair processes, cell cycle arrest, apoptosis and changes in the transcriptional profile of the cells.

PART II

DEATH AND MORE: DNA DAMAGE RESPONSE PATHWAYS IN THE NEMATODE *C. ELEGANS*

Cell Death and Differentiation

Volume 11, p. 21-28

Preface

To monitor genomic integrity in order to ensure the transmission of genetic information with high fidelity, cells have evolved elaborate mechanisms, named checkpoints. These are signal transduction pathways that enforce the orderly execution of the cell cycle and arrest its progression upon the occurrence of undesirable events. DNA damage in the form of irradiation, replication stress, recombination unresolved structures, reactive oxygen species and helix distortion events constitute such primary threats for the cells (Figure 3).

A number of additional responses are subsequently mounted by the cells that direct DNA repair or apoptosis. These actions prevent the conversion of aberrant DNA structures into inheritable mutations and compromise the survival of cells with unrepairable damage. Cells harboring defects in checkpoint pathways respond to DNA damage improperly, which in turn may enhance the rate of cancer development.

Genetic components of these pathways have been identified in yeast and humans. Work from the past few years in *C. elegans* has also identified such key components with largely conserved function and has contributed to our understanding of the organism (Gartner *et al.*, 2000, Ahmed *et al.*, 2001, Derry *et al.*, 2001, Schumacher *et al.*, 2001, Hofmann *et al.*, 2002). As reviewed in the following paper and as discussed in the subsequent chapters of this dissertation, a nice working model on the DNA damage signaling networks is beginning to emerge.

Cell Death and Differentiation (2004) 11, 21–28

www.nature.com/cdd

Review

Death and more: DNA damage response pathways in the nematode *C. elegans*

L Stergiou[1] and MO Hengartner*,[1]

[1] Institute of Molecular Biology, University of Zurich, Winterthurerstrasse 190, CH-8057 Zurich, Switzerland
* Corresponding author: MO Hengartner, Tel: +41 1 635 3140; Fax: +41 1 635 6861; E-mail: michael.hengartner@molbio.unizh.ch

Received 30.6.03; accepted 05.8.03
Edited by G Melino

Abstract

Genotoxic stress is a threat to our cells' genome integrity. Failure to repair DNA lesions properly after the induction of cell proliferation arrest can lead to mutations or large-scale genomic instability. Because such changes may have tumorigenic potential, damaged cells are often eliminated via apoptosis. Loss of this apoptotic response is actually one of the hallmarks of cancer. Towards the effort to elucidate the DNA damage-induced signaling steps leading to these biological events, an easily accessible model system is required, where the acquired knowledge can reveal the mechanisms underlying more complex organisms. Accumulating evidence coming from studies in *Caenorhabditis elegans* point to its usefulness as such. In the worm's germline, DNA damage can induce both cell cycle arrest and apoptosis, two responses that are spatially separated. The latter is a tightly controlled process that is genetically indistinguishable from developmental programmed cell death. Upstream of the central death machinery, components of the DNA damage signaling cascade lie and act either as sensors of the lesion or as transducers of the initial signal detected. This review summarizes the findings of several studies that specify the elements of the DNA damage-induced responses, as components of the cell cycle control machinery, the repairing process or the apoptotic outcome. The validity of *C. elegans* as a tool to further dissect the complex signaling network of these responses and the high potential for it to reveal important links to cancer and other genetic abnormalities are addressed.
Cell Death and Differentiation (2004) **11**, 21–28. doi:10.1038/sj.cdd.4401340

Keywords: apoptosis; programmed cell death; checkpoint; cell cycle; DNA repair

Abbreviations: Rad, radiation sensitive; PCNA, proliferating Cell Nuclear Antigen; Hus1, hydroxyurea-sensitive 1; Mre11, meiotic recombination 11; Nbs1, nibrin (mutated in Nijmegen breakage syndrome) ; BRCA1, breast cancer 1; ATM, ataxia telangiectasia mutated kinase; ATR, ataxia telangiectasia-related kinase; Tel1, telomere length regulation 1; Chk1, checkpoint kinase 1; Cdk, cyclin-dependent kinase; Cdc, cell division control; Apaf-1, apoptotic protease-activating factor-1; Bcl-2, B-cell lymphoma 2; BH3, BCL-2 homology domain 3; PUMA, p53 upregulated modulator of apoptosis; ced, cell death abnormal; *egl-1*, egg-laying abnormal-1; *mrt-2*, mortal germ line-2; *clk-2*, clock gene; Spo 11, sporulation, meiosis-specific protein; *msh*, mismatch repair gene; *cep-1*, *C. elegans* p53

Introduction

Living organisms expend considerable energy to preserve integrity of their genomes. Multiple mechanisms have evolved to ensure the fidelity of genome duplication and to guarantee faithful partitioning of chromosomes at each cell division. Furthermore, cells are under the constant threat of DNA damaging agents, such as ionizing radiation, oxygen radicals and monofunctional alkylating agents. Maintenance of genome stability thus also depends on an appropriate response when DNA damage is inflicted by these agents. Indeed, eukaryotes have developed complex biochemical signaling networks that activate numerous processes following DNA damage: activation of the repair machinery, transient cell cycle arrest, transcriptional upregulation of a number of other response proteins and in metazoans, induction of apoptosis. Together, these response pathways insure efficient repair of the lesion or, if necessary, elimination of the damaged cell. Much of our understanding of DNA damage response pathways originate from elegant genetic studies in the yeasts *Saccharomyces cerevisiae* and *S. pombe*. These studies, together with work performed in Aspergillus, *Caenorhabditis elegans*, Drosophila, various mammalian species including humans, have revealed much conservation, but also some surprising changes in DNA damage response pathways through evolution.

In this review, we very briefly discuss the general features of DNA damage response pathways and their main players, and then concentrate on what has been learned about DNA damage response from studies in the nematode *C. elegans*.

DNA Damage Response Proteins: Sensors, Transducers and Effectors

Depending on their distinct positions and functions within the signaling cascades, proteins involved in DNA damage response have been classified as sensors that detect the damage, transducers that transmit the signal that damage is present, or effectors that elicit the various specific biological responses (Table 1).

Table 1 Orthologous checkpoint proteins in *C. elegans*, yeasts and mammalian cells

Protein function	*C. elegans*	*S. pombe*	*S. cerevisiae*	Mammals
Sensors				
RFC1-like	HPR-17	Rad17	Rad24	RAD17
PCNA-like	HPR-9	Rad9	Ddc1	RAD9
	HUS-1	Hus1	Mec3	HUS1
	MRT-2	Rad1	Rad17	RAD1
BRCT-containing	HSR-9	Rhp9/Crb2	Rad9	BRCA1
DSB recognition/repair				
	MRE-11	Rad32	Mre11	MRE11
	RAD-50		Rad50	RAD50
		1	1	NBS1
Transducers				
PI3-kinases	ATM-1	Tel1	Tel1	ATM
	ATL-3	Rad3	Mec1	ATR
Rad3 regulatory subunit	1	Rad26	Ddc2	1
Effector kinases	CHK-1	Chk1	Chk1	CHK1
	CHK-2	Cds1	Rad53	CHK2
Downstream effectors	CEP-1	—	—	p53

Sensor proteins are thought to associate with damaged DNA directly or indirectly and they serve as recognition complexes to recruit and modulate the function of specific transducer proteins. Different types of DNA damage can activate different molecular pathways, suggesting that the nature of the DNA structure that is recognized by the sensors defines each time the steps to follow. However, despite the large number of possible DNA lesion types, only a limited number of response pathways have been identified. It is likely that the DNA damage response pathways sense common intermediates, rather than the original damage. Indeed, the current view for eukaryotic cells is that all types of DNA damage are eventually converted to either single-strand (ssDNA) and double-strand DNA breaks (DSBs).

Two complexes – the Rad17-RFC and the 9-1-1 complexes – cooperate to detect DSBs. Rad17 interacts with four replication factor C subunits (Rfc2, Rfc3, Rfc4, Rfc5) to form a pentameric structure,[1,2] whereas the proliferating cell nuclear antigen (PCNA) homologs Rad9, hydroxyurea-sensitive 1 (Hus1) and Rad1 form a heterotrimeric ring around DNA. These two complexes are thus reminiscent of the 'clamp loader' and the 'sliding clamp' involved in DNA replication,[3] and recent evidence suggests that a similar mechanism might be used to load the 9-1-1 complex onto sites of DNA damage.[4] A third protein complex, known as the Mre11–Rad50–Nbs1 complex (MRN), Mre11=meiotic recombination 11; Nbs1 nibrin (mutated in Nijmegen breakage syndrome), also localizes to sites of double-strand breaks; this complex furthermore has a role in repair, meiotic recombination and telomere maintenance. Mutants for the Mre11 or Nbs1 proteins exhibit a radioresistant DNA synthesis (RDS) phenotype, indicating that these proteins are also involved in checkpoints during S-phase of the cell cycle.[5–7] Finally, breast cancer 1 (BRCA1), which likely acts as an adaptor molecule and colocalizes with proteins such as Rad51, the PCNA and MRN complexes, plays an important role in several distinct DNA damage response pathways.[8–10] Mutations in the BRCA1 gene are associated with more than half of all cases of familial breast cancer, underscoring the importance of genome integrity in protecting against cancer development.

Downstream of the sensor molecules, transducers of the initial signal initiate phosphorylation cascades that amplify and diversify the signal by targeting multiple downstream effectors. This class of proteins includes two prominent members of the PI3K superfamily (phosphatidyl-inositol-3-kinase), ATM and ATR (the homologs of *S. pombe* Tel1 and Rad3, respectively) (ATM=active telangiectasia mutated kinase; ATR=ataxia telangiectasia-related kinase; Tel1=telomere length regulation 1). Upon their activation by DNA damage, ATM and/or ATR phosphorylate a number of substrates, whose identity can vary according to the nature of the lesion. DNA damage responses are highly abnormal in cells lacking ATM or ATR, leading to accumulation of mutations and chromosomal aberrations, which increase the probability of developmental abnormalities and genetic diseases.[11–14] The serine–threonine kinases checkpoint kinase 1 (Chk1) and Chk2 are among the phosphorylated substrates and the molecules that will carry on the signal, and are required for cell cycle arrest following DNA damage.[12,14,15]

Cell Cycle Arrest

DNA damage temporarily arrests cell cycle progression, in order to permit repair prior to DNA replication or cell division. The presence of eukaryotic cell cycle checkpoints that respond to DNA damage were first inferred from the identification of radiation-sensitive (rad) yeast mutants that fail to delay entry into mitosis after DNA damage. Subsequently, checkpoint pathways have also been identified that control entry into or progression through S phase.

The G1/S checkpoint

When damage occurs in the G1 phase, most eukaryotic cells exhibit a delay prior to S-phase onset. This prevents replication of a damaged template that might result in the

fixation of mutations or in a chromosome bearing a DSB. Whereas this checkpoint is weak and most of the damage remains unrepaired in budding yeast,[16] the G1/S checkpoint is prominent in mammals, where it acts by preventing activation of Cdk2-cyclin E (Cdk=cyclin-dependent kinase). This is accomplished by stabilizing p53 through phosphorylation to cause transcriptional activation of p21 and by degrading Cdc25A (Cds=cell division control) to maintain the inhibitory phosphorylation on Cdk2.[17,18]

The intra-S-phase checkpoint

Most of what is known about this checkpoint control comes from studies in budding and fission yeasts, with mammalian cells showing features similar to the latter. Upon encountering a DNA lesion, the replication forks stall transiently to block early- and late-firing onsets. Forks are then converted to structures that are prevented from undergoing nuclease attack and collapse. Those that are processed by nucleases activate the ATR homolog, Rad3, and Cds1/Chk2 activity. Inhibition of CDK2 activity through Cdc25A degradation in mammalian cells leads to a several-hour delay in S-phase progression, whereas prolonged blockade in yeast may cause regaining of replication.[19]

The G2/M checkpoint

In both yeast and higher eukaryotes, the G2/M transition is blocked by the maintenance of the inhibitory phosphorylation on Cdc2, and thus blockade of Cdc2-cyclin B activity. Activation of ATR or ATM by DNA damage leads to Chk1 or Chk2 activation, respectively which, in turn, act on Cdc25C phosphatase to promote its association with 14-3-3 proteins.[20–22] Additionally, regulation of cyclin B both at the transcriptional level and by its cytoplasmic localization, may also contribute to the G2/M arrest.[23,24]

Apoptotic Cell Death

In multicellular organisms, in addition to cell cycle arrest and repair, genotoxic stress can lead to the apoptotic demise of the damaged cell. DNA damage-induced cell deaths share the morphological characteristics of developmental programmed cell deaths, with features like cell rounding, cellular membrane blebbing, chromosomal condensation and DNA degradation shared between the two types of death.[25]

In mammals, two independent intracellular apoptotic signaling cascades can activate apoptosis: the mitochondrial pathway associated with activation of the apoptotic protease-activating factor-1 (Apaf-1) and caspase-9-containing apoptosome,[26] and the death receptor pathway that acts through caspase-8.[27] p53 contributes mainly to the activation of the former and exerts its function through the transcriptional regulation of its target genes. The mitochondrial pathway is regulated by the B-cell lymphoma 2 (Bcl-2) protein family, which includes both proapoptotic and prosurvival members. The sensors and mediators of apoptosis are the 'BH3-only domain' (BH3=BCL-2 homology domain 3) proapoptotic proteins. In response to DNA damage, at least two BH3 domain proteins, p53 upregulated modulator of apoptosis (PUMA) and Noxa, are transcriptionally induced in a p53-dependent manner.[28,29] Post-translational phosphorylation (Bad, Bik) and proteolytic cleavage (Bid) are additional mechanisms for the regulation of the 'BH3-only domain' proteins in response to an apoptotic stimulus. The signal is then relayed to the 'multidomain' proapoptotic proteins Bax and Bak, which are initially kept at an inactive state. Upon activation, conformational changes result in their stable association into the mitochondrial membrane either to form a pore or interact with channel-forming proteins and increase membrane permeability. Cytochrome *c* and other intermembrane space proteins are then released to efficiently induce caspase-dependent and/or -independent apoptosis.[30] In addition to PUMA and Noxa, a number of other p53 target genes, including but not limited to Bax, have been suggested to promote DNA damage - induced apoptosis.[31]

Programmed Cell Death in *C. elegans*

Significant progress in the field concerning the events in apoptosis was made from studies in the nematode *C. elegans*. In this species, two waves of apoptotic deaths have been found. The first occurs largely during embryogenesis, and helps to sculpt the cell lineages that produce all of the animal's somatic cells. The second wave of death occurs in the adult female germ line, where several hundred cells are eliminated during oogenesis.

Developmental cell death

During the somatic development of the animal, 131 of the 1090 cells generated undergo programmed cell death in a highly reproducible way: always the same cells die, and each cell dies at a characteristic point in development. Extensive genetic analysis of these cell deaths led to the identification of an evolutionarily conserved core apoptotic pathway that regulates all programmed cell deaths in *C. elegans*.[32,33] Two genes, *ced-3* and *ced-4* (ced=cell death abnormal), are required for the killing process. The product of the former is a member of the caspase family of cysteine proteases; the product of the latter is homologous to mammalian Apaf-1 and functions genetically as a positive regulator of CED-3. A third gene, *ced-9*, protects cells that normally survive from undergoing programmed cell death. The CED-9 protein is homologous to the oncoprotein Bcl-2, which likewise promotes cell survival in mammals. Finally, EGL-1 is required for all developmental cell deaths in the animal. It belongs to a subset of Bcl-2 family members that contain only one of four Bcl-2 homology domains, the BH3 domain, and are thus known as BH3 domain only proteins. The BH3 domain allows EGL-1 to associate with and inhibit CED-9.

Biochemical studies have suggested that the key event required for apoptotic cell death in *C. elegans* is the processing of CED-3 from the inactive zymogen state into the active caspase.[34,35] While the activation of CED-3 appears to be autocatalytic in nature, it does require association of the zymogen with oligomerized CED-4, likely forming a worm version of the apoptosome, which in

mammals consists of at least three proteins – caspase-9, Apaf-1, and cytochrome *c*.[36] In cells that should survive, formation of the apoptosome is prevented, at least in part because CED-4 is bound to and sequestered by CED-9 in a stable complex on the surface of mitochondria.[37] Cells fated to die appear to be marked for apoptosis through the expression of EGL-1. Binding of EGL-1 to CED-9 causes the release of CED-4, which is then free to trigger the lethal proteolytic action of CED-3.[38,39]

Germ cell apoptosis

The *C. elegans* hermaphrodite consists of two U-shaped arms, joined proximally together at a common uterus (Figure 1). Unlike the somatic tissues, the germ line proliferates continuously both during larval development and in adult worms. In the adult hermaphrodite, germ cells progress through various stages of differentiation. The distal most germ cells proliferate mitotically and serve as a stem cell population. During their passage through a 'transition zone', they stop dividing and initiate meiosis. The most abundant population of cells resides in the pachytene stage of meiotic prophase that extends until before the bend of the gonad. Upon exit from this stage, they complete meiotic prophase, cellularize, undergo the final stages of maturation and finish meiosis after fertilization, which occurs as the oocyte pass through the spermatheca.[40] Under normal growth conditions, approximately half of the female germ cells are doomed to die by programmed cell death.[41] A steady-state level of zero to four apoptotic cells can be observed at any given time. These so-called 'physiological germ cell deaths' occur presumably to maintain tissue homeostasis.

DNA Damage Responses in *C. elegans*

Studies in *C. elegans* on the effect of genotoxic stress have suggested that there are little or no checkpoint controls exerted during embryonic development, except for a possible transient intra-S checkpoint during early embryonic development.[42] In the germ line, however, DNA damage-induced signaling induce two clear responses – cell cycle arrest and apoptosis – that are spatially separated (Figure 1). Exposure of worms to ionizing radiation causes a transient halt in cell cycle progression in the proliferating zone, resulting in a decreased number of mitotic germ cells. Notably, the volume of the arrested nuclei as well as that of the surrounding cytoplasm become enlarged, since cellular and nuclear growth continue to occur.[43] In the meiotic compartment, after the exit from the pachytene region, increasing doses of ionizing radiation cause a dramatic increase in the number apoptotic cell deaths, which appear as early as 2–3 h after the insult, and persist for 20–60 min as highly refractile disks before being engulfed and degraded by the surrounding somatic sheath cells. Time course analyses have suggested that there are two waves of apoptosis, one early and one late, in response to irradiation (Figure 2a). The second wave of deaths might be caused by the delayed removal of cells that had been damaged in the mitotic region and failed to be repaired properly. Other types of DNA damage, such as treatment with the monofunctional alkylating agent ENU, or the accumulation of aberrant meiotic intermediates, also induce germ cell death, clearly showing that the deaths are a direct consequence of DNA damage.[44]

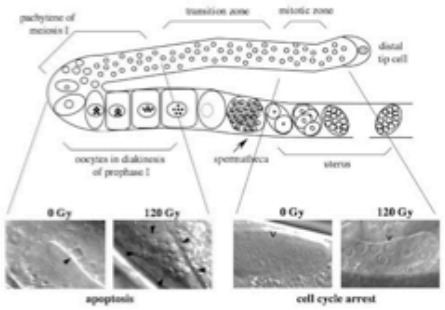

Figure 1 DNA damage responses in the adult hermaphrodite *C. elegans* germ line. Mitotic stem cells proliferate throughout adulthood in the distal end of each gonad arm, then pass through a characteristic set of morphological stages as they undergo meiosis and descend towards the uterus. Following DNA damage germ cells in the mitotic region undergo proliferation arrest (right, open arrowheads), whereas meiotic germ cell nuclei undergo apoptosis (left, filled arrowheads)

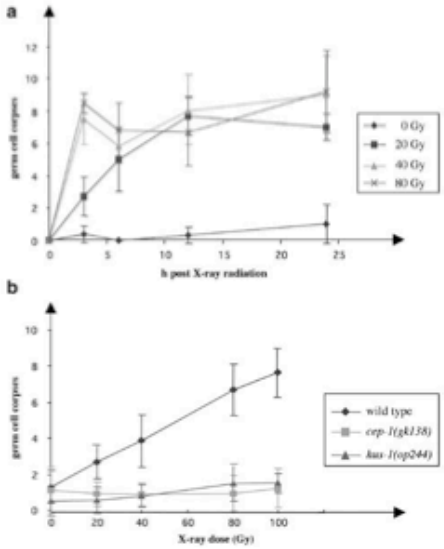

Figure 2 Wild-type worms respond with an early and a late wave of apoptotic deaths following exposure to ionizing radiation, in a dose-dependent manner (**a**). The checkpoint mutants *cep-1* and *hus-1* are defective in DNA damage-induced apoptotic cell death (**b**)

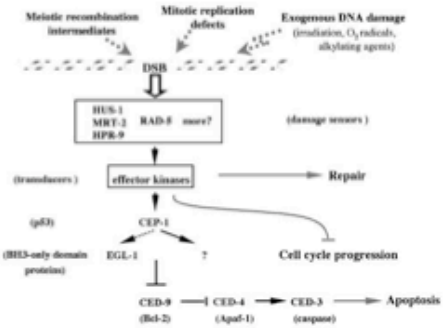

Figure 3 Exogenous DNA damage or damage in the form of meiotic recombination intermediates or mitotic replication defects is sensed by numerous proteins. HUS-1 and MRT-2, as part of a trimeric complex, and RAD-5 are involved in this process to allow for the action of the repair machinery. Cell cycle progression delay facilitates the repair process. The *C. elegans* p53 homolog, CEP-1, is responsible for the transcriptional activation of at least one BH3-only domain protein, EGL-1, that leads ultimately to the activation of the apoptotic machinery

DNA damage-induced apoptosis requires the core apoptotic machinery (Figure 3): there is no cell death induced in the germ line of animals homozygous for the *ced-3(n717)* or *ced-4(n1162)* loss-of-function alleles. However, in contrast to physiological germ cell death, DNA damage-induced cell death is blocked by *ced-9(n1950)* gain-of-function and is severely reduced in the *egl-1(n3082)* (egl-1=egg-laying abnormal-1) loss-of-function mutation, indicating that the DNA damage response machinery is genetically distinct from the pathways that control somatic cell death and physiological germ cell death.

Checkpoint Mutants in *C. elegans*

Various genetic screens for mutants defective in different signaling pathways, such as rad mutants and mutants with a high rate of chromosome nondisjunction, have revealed three strains defective for radiation-induced apoptosis: *hus-1(op244)*, *mrt-2(2663)* (mrt=mortal germline-2) and *rad-5(mn159)* (Figure 3).[43,45,46] All three mutations abrogate cell cycle arrest and apoptosis induced by DNA damage (Figure 2b), without affecting developmental or physiological germ cell death. Consistent with the situation in yeast and mammalian checkpoint gene mutants, they also show increased genomic instability and reduced long-term survival following genotoxic insults, as the high rates of embryonic lethality demonstrate.[44,47]

mrt-2 and *hus-1* identify a conserved sensor pathway

Molecular characterization of *mrt-2* and *hus-1* showed that these genes encode the *C. elegans* homologs of *S. pombe* Rad1 and Hus1 (*S. cerevisiae* Rad17 and Mec3) checkpoint proteins.[46,48] The fact that these two proteins are also required for DNA damage-induced cell cycle arrest in worms suggest that at least part of the DNA damage response pathway characterized in yeasts is conserved through evolution and also functions in nematodes. In fission yeast, Hus1, Rad1 and Rad9 form a heterotrimeric complex that resembles the PCNA complex in structure. Similarly, *C. elegans* HUS-1 is a nuclear protein that requires MRT-2 and the Rad9 homolog HPR-9 for proper localization to the nucleus. HUS-1 interacts physically with MRT-2, and a point mutation that disrupts this interaction compromises HUS-1 function.[48] Furthermore, Hofmann *et al*[48] recently showed that while HUS-1::GFP is uniformly associated with chromatin under normal conditions, upon DNA damage the fusion protein relocates within a few hours to distinct nuclear foci – possibly sites of unrepaired damage – consistent with the proposed function of the 9-1-1 complex as a marker of DNA damage.

Interestingly, while its role in cell cycle arrest appears to have been largely conserved from yeasts to nematodes, work in *C. elegans* has suggested that the 9-1-1 complex has acquired additional functions in nematodes that are either absent or not yet described in yeasts. Most surprise was the report by Ahmed and Hodgkin,[46] that MRT-2 is required for telomere length maintenance: in *mrt-2* mutants, telomeres progressively shorten over many generations, eventually leading to end-to-end chromosome fusion, genomic instability, and late-onset sterility by about the 15th generation. A similar defect has been described in *hus-1* mutants.[48] No such telomere defect is apparent in the yeast 9-1-1 mutants, suggesting either that this complex does not maintain telomere length in yeasts, or that it is redundant with other proteins in this function. Whether the 9-1-1 complex is also required for telomere length maintenance in mammals remains to be determined.

RAD-5/CLK-2 functions in parallel to the HUS-1/MRT-2 complex

A third checkpoint gene, *rad-5*, was originally identified in a screen for mutations that show reduced long-term survival following ionizing radiation. The mutation isolated in this screen, *rad-5(mn159)*, was later found to be allelic to *clk-2(qm37)* (clk-2=clock gene), a mutation characterized by slow growth and a mild increase in animal life span.[47] As with *mrt-2* and *hus-1*, DNA damage-induced cell cycle arrest and apoptosis are abrogated in *rad-5/clk-2* mutants. However, unlike MRT-2 and HPR-9, the *C. elegans* checkpoint protein RAD-5 is dispensable for the subcellular localization of HUS-1.[48] Indeed, several lines of evidence suggest that RAD-5 functions in a pathway distinct from the 9-1-1 complex. First, long-term survival of *hus-1*; *rad-5* and *mrt-2*; *rad-5* double mutants are significantly reduced compared to the single mutants – this should not be the case if these proteins acted in a linear pathway. Second, unlike the 9-1-1 mutants, *rad-5* mutants appear to also be defective in the S-phase replication checkpoint, similar to what is known for the yeast DNA polymerase epsilon.[50] Third, *rad-5* mutants do not show

the mortal germ line phenotype of the 9-1-1 mutants. Finally, unlike the 9-1-1 complex, RAD-5 is an essential gene, as complete elimination of *rad-5* gene function results in developmental arrest and embryonic lethality.

Surprisingly, mutations in *TEL2*, the budding yeast homolog of *rad-5*, do not result in any checkpoint defects or hypersensitivity to DNA damaging agents. Rather, hypomorphic *tel2* mutants have been shown to bear short telomeres, suggesting a role for this gene in telomere maintenance.[49] It is possible that the checkpoint role of RAD-5 is a new function acquired during metazoan evolution, and thus not present in yeasts. Alternatively, a role for Tel2p in DNA damage response might simply have been missed so far due to the essential nature of the gene.

Genes involved in meiotic DNA recombination

Double-strand breaks occur not only following genotoxic stress, but also normally during meiotic prophase to initiate meiotic recombination events.[51] Two coupled processes, the formation and the processing of DSBs are involved in meiotic recombination. The *SPO11* gene product is responsible for enzymatic DNA cleavage to create DSBs and Mre11 subsequently processes these through its intrinsic exonuclease activity. Rad51, a member of the RecA-strand exchange protein family, catalyzes the invasion of the single-strand DNA overhangs generated by Mre11 into a recipient homologous double-strand DNA molecule, thereby initiating the formation of D loops and the later steps of meiotic recombination.[51,52] Mutations in Rad51 confer an enhanced sensitivity to DNA damaging agents in yeast, a reduction in mitotic recombination and impaired meiosis. Silencing of the gene via RNAi in *C. elegans* results in high levels of embryonic lethality and increased frequency of males,[44,53,54] phenotypes encountered commonly in meiotic mutants. Moreover, a dramatic increase in germ cell apoptosis is observed when *rad-51* is inactivated. When meiotic recombination is blocked by the absence of sporulation, meiosis-specific protein (SPO-11), this increase no longer occurs, suggesting that the resulting deaths are indeed triggered by accumulation of recombination intermediates, which are perceived as a form of DNA damage. Mutations in *hus-1*, *mrt-2* and *rad-5* checkpoint genes suppress the *rad-51*-dependent apoptotic death, suggesting that disruption of the DNA damage checkpoint pathway compromises the ability of the cells to sense and respond to the incurred damage.[44] Damage caused by radiation treatment in late embryonic stages, in animals depleted from RAD-51, resulted in several developmental defects in vulva and gonad formation. This effect is likely due to inability of repair of radiation-induced DSBs, and implies that *rad-51* also functions in DNA damage response in the soma.[55]

As is the case with *rad-51*, loss of *mre-11* function results in defective meiotic recombination and increased germ cell apoptosis. Consistent with this, the viability of progeny in these mutants drops dramatically. In mammals, Mre11 has been implicated in DNA damage response.[56] However, the fact that *mre-11* mutants show increased, rather than decreased germ cell apoptosis argues that in *C. elegans*, the DNA damage checkpoint is still functional in *mre-11* mutants.[57]

Another crucial component of the *C. elegans* meiotic recombination machinery is a germline-specific member of the MutS protein family, MSH-5.[58] Crossing over and chiasma formation events depend on *msh-5* gene (*msh*=mismatch repair gene) function: in *msh-5* mutants, both events are severely reduced or eliminated. Nevertheless, *C. elegans msh-5* mutants are able to complete meiosis and gametogenesis with high efficiency and produce embryos without undergoing germ cell apoptosis like their murine counterparts.[59,60] It is likely that *msh-5* mutant cells escape apoptosis because they are still proficient in repairing dsDNA breaks, but in a way that does not lead to crossovers between homologous chromosomes.[58]

Mismatch repair genes

Unlike Msh5 and its heterodimer partner Msh4, which are involved in the control of meiotic crossing over, the other members of the MutS protein family have a substantial role in the correction of DNA polymerase errors, through mechanisms such as postreplication DNA mismatch repair (MMR). In yeast, the Msh2 protein participates in all three different complexes to repair base–base mismatches and DNA loops[61] and mutations in the human and mouse gene result in tumor development.[62] The tumorigenic potential of MMR mutants is likely due to an increased mutation rate in these cells, coupled with a resistance to apoptosis caused by certain mutagens, which would allow the mutated cells to survive.[62]

In *C. elegans*, *msh-2* mutants also show a mutator phenotype, as well as reduced fertility and long-term viability (possibly due to the accumulation of detrimental mutations). *msh-2* mutants also show increased microsatellite instability. Following exposure to ionizing radiation, the apoptotic response of *msh-2* mutants is impaired and/or delayed, but not abrogated. It is possible that binding of the lesions by mismatch repair proteins promotes both the DNA repair process and the elimination of cells by apoptosis, depending on the amount of damage.[63] The role of MSH-2 in apoptosis, though, still remains to be clarified.

No role for CHK-2 in DNA damage response in *C. elegans*?

Unlike the situation in other organisms, where Chk2 proteins participate in several distinct signaling pathways that maintain genome integrity, *C. elegans chk-2* mutants show normal checkpoint responses following DNA damage. While it is possible that in *C. elegans*, CHK-2 is simply redundant with another protein for its well-characterized checkpoint function, an alternative explanation is that in nematodes, CHK-2 has simply lost its role in DNA damage response and has acquired a different function. Indeed, elegant genetic studies have suggested that *C. elegans* CHK-2 is required for establishment of homolog alignment and synapsis.[64] An early role in the initiation of meiotic recombination was also suggested by the observation that *chk-2* mutations, like those in the meiotic endonuclease gene *spo-11*, suppress the increase in apop-

tosis normally observed in worms depleted of RAD-51. Alternatively, *chk-2* mutants might be successful in initiating recombination, but defective in activating the checkpoint in response to a subset of DNA lesions, such as recombination intermediates.

The *C. elegans* p53 homolog CEP-1

The tumor suppressor protein p53 plays a key role in the integration of cellular responses to genotoxic stimuli. In higher organisms, it acts as a guardian of genome integrity, by inducing cell cycle arrest or apoptosis following DNA damage. p53-mediated apoptosis is a consequence of the combined expression of various target-genes, either through its trans-activation function or transcriptional repression.[65,66] Like its mammalian homolog, the *C. elegans* p53 protein, CEP-1, is required for DNA damage-induced germ cell apoptosis (Figure 2b).[67,68] In contrast to mammalian p53, however, CEP-1 is dispensable for cell cycle arrest activation, a property shared also by Drosophila p53.[69] It is likely that this primordial proapoptotic function depends on transcriptional activation of genes that act on the core apoptotic machinery.

Indeed, recent studies have suggested that induction of germ cell apoptosis following DNA damage is transcriptionally regulated: following DNA damage, mRNA levels for the BH3 domain protein EGL-1 are dramatically upregulated, consistent with the previously described role for *egl-1* in DNA damage induced apoptosis in the adult germ line. Interestingly, *egl-1* mRNA levels do not change following DNA damage in *cep-1* mutants, nor in any of the other checkpoint mutants thought to act upstream of *cep-1* (*hus-1*, *rad-5*). An attractive model consistent with these observations would be that CEP-1 acts as a direct transactivator for the *egl-1* gene following DNA damage (Figure 3). A particular appeal of this model is its similarity with the situation in mammals, where DNA damage-induced apoptosis requires the p53-dependent transcriptional activation of the BH3 domain proteins Noxa and PUMA. How CEP-1 becomes activated following DNA damage, and whether it can directly bind to the *egl-1* regulatory region remains to be determined.

Conclusions

Loss of DNA damage checkpoint function can lead to genome instability, one of the driving forces towards carcinogenesis. Understanding how checkpoint pathways maintain genome integrity is thus crucial for a complete understanding of the origin of cancer and of other genetic abnormalities. Such knowledge might ultimately provide insights into novel ways to prevent, diagnose, and treat such diseases. Considering the fact that DNA damage checkpoints in higher eukaryotes are more complicated than those found in the unicellular yeasts, an easily accessible metazoan model organism is required to study these biological processes in depth. *C. elegans* is a promising candidate for this function. Its powerful genetics and molecular tools allow an in-depth study of developmental and various other biological pathways. Indeed, the advances made so far in the area of DNA damage response suggest that this species can provide a useful jumping board, from which acquired knowledge can be used to test specific hypotheses in the human system. As in many other biological problems, the worm's simplicity may be the key to unveiling the complexities of the human organism.

References

1. Griffiths DJ, Barbet NC, McCready S, Lehmann AR and Carr AM (1995) Fission yeast rad17: a homologue of budding yeast RAD24 that shares regions of sequence similarity with DNA polymerase accessory proteins. EMBO J. 14: 5812–5823
2. Green CM, Erdjument-Bromage H, Tempst P and Lowndes NF (2000) A novel Rad24 checkpoint protein complex closely related to replication factor C. Curr. Biol. 10: 39–42
3. Tsurimoto T and Stillman B (1991) Replication factors required for SV40 DNA replication *in vitro*. II. Switching of DNA polymerase alpha and delta during initiation of leading and lagging strand synthesis. J. Biol. Chem. 266: 1961–1968
4. Zou L, Cortez D and Elledge SJ (2002) Regulation of ATR substrate selection by Rad17-dependent loading of Rad9 complexes onto chromatin. Genes Dev. 16: 198–208
5. Chamankhah M and Xiao W (1999) Formation of the yeast Mre11–Rad50–Xrs2 complex is correlated with DNA repair and telomere maintenance. Nucleic Acids Res. 27: 2072–2079
6. Maser RS, Monsen KJ, Nelms BE and Petrini JH (1997) hMre11 and hRad50 nuclear foci are induced during the normal cellular response to DNA double-strand breaks. Mol. Cell Biol. 17: 6087–6096
7. Shiloh Y (1997) Ataxia-telangiectasia and the Nijmegen breakage syndrome: related disorders but genes apart. Annu. Rev. Genet. 31: 635–662
8. Gowen LC, Avrutskaya AV, Latour AM, Koller BH and Leadon SA (1998) BRCA1 required for transcription-coupled repair of oxidative DNA damage. Science 281: 1009–1012
9. Moynahan ME, Chiu JW, Koller BH and Jasin M (1999) Brca1 controls homology-directed DNA repair. Mol. Cell 4: 511–518
10. Snouwaert JN, Gowen LC, Latour AM, Mohn AR, Xiao A, DiBiase L and Koller BH (1999) BRCA1 deficient embryonic stem cells display a decreased homologous recombination frequency and an increased frequency of non-homologous recombination that is corrected by expression of a brca1 transgene. Oncogene 18: 7900–7907
11. Hartwell LH and Kastan MB (1994) Cell cycle control and cancer. Science 266: 1821–1828
12. Zhou BB and Elledge SJ (2000) The DNA damage response: putting checkpoints in perspective. Nature 408: 433–439
13. Khanna KK and Jackson SP (2001) DNA double-strand breaks: signaling, repair and the cancer connection. Nat. Genet. 27: 247–254
14. Shiloh Y (2001) ATM and ATR: networking cellular responses to DNA damage. Curr. Opin. Genet. Dev. 11: 71–77
15. Walworth NC and Bernards R (1996) rad-dependent response of the chk1-encoded protein kinase at the DNA damage checkpoint. Science 271: 353–356
16. Gerald JN, Benjamin JM and Kron SJ (2002) Robust G1 checkpoint arrest in budding yeast: dependence on DNA damage signaling and repair. J. Cell Sci. 115: 1749–1757
17. Ekholm SV and Reed SI (2000) Regulation of G(1) cyclin-dependent kinases in the mammalian cell cycle. Curr. Opin. Cell Biol. 12: 676–684
18. Sherr CJ and Roberts JM (1999) CDK inhibitors: positive and negative regulators of G1-phase progression. Genes Dev. 13: 1501–1512
19. Bartek J and Lukas J (2001) Mammalian G1- and S-phase checkpoints in response to DNA damage. Curr. Opin. Cell Biol. 13: 738–747
20. Graves PR, Lovly CM, Uy GL and Piwnica-Worms H (2001) Localization of human Cdc25C is regulated both by nuclear export and 14-3-3 protein binding. Oncogene 20: 1839–1851
21. Matsuoka S, Huang M and Elledge SJ (1998) Linkage of ATM to cell cycle regulation by the Chk2 protein kinase. Science 282: 1893–1897
22. Peng CY, Graves PR, Thoma RS, Wu Z, Shaw AS and Piwnica-Worms H (1997) Mitotic and G2 checkpoint control: regulation of 14-3-3 protein binding by phosphorylation of Cdc25C on serine-216. Science 277: 1501–1505

23. Jin P, Hardy S and Morgan DO (1998) Nuclear localization of cyclin B1 controls mitotic entry after DNA damage. J. Cell Biol. 141: 875–885
24. Toyoshima F, Moriguchi T, Wada A, Fukuda M and Nishida E (1998) Nuclear export of cyclin B1 and its possible role in the DNA damage-induced G2 checkpoint. EMBO J. 17: 2728–2735
25. Horvitz HR, Ellis HM and Sternberg PW (1982) Programmed cell death in nematode development. Neurosci. Comment. 1: 56–65
26. Green DR and Reed JC (1998) Mitochondria and apoptosis. Science 281: 1309–1312
27. Ashkenazi A and Dixit VM (1998) Death receptors: signaling and modulation. Science 281: 1305–1308
28. Nakano K and Vousden KH (2001) PUMA, a novel proapoptotic gene, is induced by p53. Mol. Cell 7: 683–694
29. Oda E, Ohki R, Murasawa H, Nemoto J, Shibue T, Yamashita T, Tokino T, Taniguchi T and Tanaka N (2000) Noxa, a BH3-only member of the Bcl-2 family and candidate mediator of p53-induced apoptosis. Science 288: 1053–1058
30. Borner C (2003) The Bcl-2 protein family: sensors and checkpoints for life-or-death decisions. Mol. Immunol. 39: 615–647
31. Miyashita T and Reed J (1995) Tumor suppressor p53 is a direct transcriptional activator of the human bax gene. Cell 80: 293–299
32. Hengartner MO and Horvitz HR (1994a) The ins and outs of programmed cell death during *C. elegans* development. Philos. Trans. R. Soc. Lond. B Biol. Sci. 345: 243–246
33. Hengartner MO and Horvitz HR (1994b) Programmed cell death in *Caenorhabditis elegans*. Curr. Opin. Genet. Dev. 4: 581–586
34. Xue D, Shaham S and Horvitz HR (1996) The *Caenorhabditis elegans* cell-death protein CED-3 is a cysteine protease with substrate specificities similar to those of the human CPP32 protease. Genes Dev. 10: 1073–1083
35. Chinnaiyan AM, O'Rourke K, Lane BR and Dixit VM (1997) Interaction of CED-4 with CED-3 and CED-9: a molecular framework for cell death. Science 275: 1122–1126
36. Yang X, Chang HY and Baltimore D (1998) Essential role of CED-4 oligomerization in CED-3 activation and apoptosis. Science 281: 1355–1357
37. Chen F, Hersh BM, Conradt B, Zhou Z, Riemer D, Gruenbaum Y and Horvitz HR (2000) Translocation of *C. elegans* CED-4 to nuclear membranes during programmed cell death. Science 287: 1485–1489
38. Conradt B and Horvitz HR (1998) The *C. elegans* protein EGL-1 is required for programmed cell death and interacts with the Bcl-2-like protein CED-9. Cell 93: 519–529
39. del Peso L, Gonzalez VM, Inohara N, Ellis RE and Nunez G (2000) Disruption of the CED-9.CED-4 complex by EGL-1 is a critical step for programmed cell death in *Caenorhabditis elegans*. J. Biol. Chem. 275: 27205–27211
40. Schedl T (1997) Developmental genetics of the germ line. In C. elegans II, Riddle DL, Blumenthal T, Meyer BJ and Priess JR (eds) (Plainview, NY: Cold Spring Harbor Laboratory Press), pp. 241–269
41. Gumienny TL, Lambie E, Hartwieg E, Horvitz HR and Hengartner MO (1999) Genetic control of programmed cell death in the *Caenorhabditis elegans* hermaphrodite germline. Development 126: 1011–1022
42. Encalada SE, Martin PR, Phillips JB, Lyczak R, Hamill DR, Swan KA and Bowerman B (2000) DNA replication defects delay cell division and disrupt cell polarity in early *Caenorhabditis elegans* embryos. Dev. Biol. 228: 225–238
43. Hodgkin J, Horvitz HR and Brenner S (1979) Nondisjunction mutants of the nematode *Caenorhabditis elegans*. Genetics 91: 67–94
44. Gartner A, Milstein S, Ahmed S, Hodgkin J and Hengartner MO (2000) A conserved checkpoint pathway mediates DNA damage-induced apoptosis and cell cycle arrest in *C. elegans*. Mol. Cell 5: 435–443
45. Hartman PS and Herman RK (1982) Radiation-sensitive mutants of *Caenorhabditis elegans*. Genetics 102: 159–178
46. Ahmed S and Hodgkin J (2000) MRT-2 checkpoint protein is required for germline immortality and telomere replication in *C. elegans*. Nature 403: 159–164
47. Ahmed S, Alpi A, Hengartner MO and Gartner A (2001) *C. elegans* RAD-5/CLK-2 defines a new DNA damage checkpoint protein. Curr. Biol. 11: 1934–1944
48. Hofmann ER, Milstein S, Boulton SJ, Ye M, Hofmann JJ, Stergiou L, Gartner A, Vidal M and Hengartner MO (2002) *Caenorhabditis elegans* HUS-1 is a DNA damage checkpoint protein required for genome stability and EGL-1-mediated apoptosis. Curr. Biol. 12: 1908–1918
49. Lustig AJ and Petes TD (1986) Identification of yeast mutants with altered telomere structure. Proc. Natl. Acad. Sci. USA 83: 1398–1402
50. Navas TA, Zhou Z and Elledge SJ (1995) DNA polymerase epsilon links the DNA replication machinery to the S phase checkpoint. Cell 80: 29–39
51. Roeder GS (1997) Meiotic chromosomes: it takes two to tango. Genes Dev. 11: 2600–2621
52. Bishop DK, Park D, Xu L and Kleckner N (1992) DMC1: a meiosis-specific yeast homolog *of E. coli* recA required for recombination, synaptonemal complex formation, and cell cycle progression. Cell 69: 439–456
53. Takanami T, Mori A, Takahashi H and Higashitani A (2000) Hyper-resistance of meiotic cells to radiation due to a strong expression of a single recA-like gene in *Caenorhabditis elegans*. Nucleic Acids Res. 28: 4232–4236
54. Dernburg AF, McDonald K, Moulder G, Barstead R, Dresser M and Villeneuve AM (1998) Meiotic recombination in *C. elegans* initiates by a conserved mechanism and is dispensable for homologous chromosome synapsis. Cell 94: 387–398
55. Rinaldo C, Bazzicalupo P, Ederle S, Hilliard M and La Volpe A (2001) Roles for *Caenorhabditis elegans* rad-51 in meiosis and in resistance to ionizing radiation during development. Genetics 160: 471–479
56. D'Amours D and Jackson SP (2002) The Mre11 complex: at the crossroads of DNA repair and checkpoint signalling. Nat. Rev. Mol. Cell Biol. 3: 317–327
57. Chin GM and Villeneuve AM (2001) *C. elegans* mre-11 is required for meiotic recombination and DNA repair but is dispensable for the meiotic G(2) DNA damage checkpoint. Genes Dev. 15: 522–534
58. Kelly KO, Dernburg AF, Stanfield GM and Villeneuve AM (2000) *Caenorhabditis elegans* msh-5 is required for both normal and radiation-induced meiotic crossing over but not for completion of meiosis. Genetics 156: 617–630
59. de Vries SS, Baart EB, Dekker M, Siezen A, de Rooij DG, de Boer P and te Riele H (1999) Mouse MutS-like protein Msh5 is required for proper chromosome synapsis in male and female meiosis. Genes Dev. 13: 523–531
60. Edelmann W, Cohen PE, Kneitz B, Winand N, Lia M, Heyer J, Kolodner R, Pollard JW and Kucherlapati R (1999) Mammalian MutS homologue 5 is required for chromosome pairing in meiosis. Nat. Genet. 21: 123–127
61. Harfe BD and Jinks-Robertson S (2000) DNA mismatch repair and genetic instability. Annu. Rev. Genet. 34: 359–399
62. Buermeyer AB, Deschenes SM, Baker SM and Liskay RM (1999) Mammalian DNA mismatch repair. Annu. Rev. Genet. 33: 359–399
63. Degtyareva NP, Greenwell P, Hofmann ER, Hengartner MO, Zhang L, Culotti JG and Petes TD (2002) *Caenorhabditis elegans* DNA mismatch repair gene msh-2 is required for microsatellite stability and maintenance of genome integrity. Proc. Natl. Acad. Sci. USA 99: 2158–2163
64. MacQueen AJ and Villeneuve AM (2001) Nuclear reorganization and homologous chromosome pairing during meiotic prophase require *C. elegans* chk-2. Genes Dev. 15: 1674–1687
65. Kastan MB, Zhan Q, el-Deiry WS, Carrier F, Jacks T, Walsh WV, Plunkett BS, Vogelstein B and Fornace Jr AJ (1992) A mammalian cell cycle checkpoint pathway utilizing p53 and GADD45 is defective in ataxia-telangiectasia. Cell 71: 587–597
66. Moberg KH, Tyndall WA and Hall DJ (1992) Wild-type murine p53 represses transcription from the murine c-myc promoter in a human glial cell line. J. Cell Biochem. 49: 208–215
67. Derry WB, Putzke AP and Rothman JH (2001) *Caenorhabditis elegans* p53: role in apoptosis, meiosis, and stress resistance. Science 294: 591–595
68. Schumacher B, Hofmann K, Boulton S and Gartner A (2001) The *C. elegans* homolog of the p53 tumor suppressor is required for DNA damage-induced apoptosis. Curr. Biol. 11: 1722–1727
69. Ollmann M, Young LM, Di Como CJ, Karim F, Belvin M, Robertson S, Whittaker K, Demsky M, Fisher WW, Buchman A, Duyk G, Friedman L, Prives C and Kopczynski C (2000) Drosophila p53 is a structural and functional homolog of the tumor suppressor p53. Cell 101: 91–101

References

Alnemri, E.S., Livingston, D.J., Nicholson, D.W., Salvesen, G., Thornberry, N.A, Wong, W.W. & Yuan, J. Human ICE/CED-3 protease nomenclature. *Cell* **87**, 171 (1996).

Chen, F., Hersh, B.M., Conradt, B., Zhou, Z., Riemer, D., Gruenbaum, Y. & Horvitz, H.R. Translocation of *C. elegans* CED-4 to nuclear membranes during programmed cell death. *Science* **287**, 1485-1489 (2000).

Chinnaiyan, A.M., Chaudhary, D., O'Rourke, K., Koonin, E.V. & Dixit, V.M. Role of CED-4 in the activation of CED-3. *Nature* **388**, 728- 729 (1997a).

Chinnaiyan, A.M., O'Rourke, K., Lane, B.R. & Dixit, V.M. Interaction of CED-4 with CED-3 and CED-9: A molecular framework for cell death. *Science* **275**, 1122-1126 (1997b).

Church, D.L., Guan, K.L., Lambie, E.J. Three genes of the MAP kinase cascade, *mek-2, mpk–1/sur-1 and let-60 ras,* are required for meiotic cell cycle progression in *Caenorhabditis elegans*. *Development* **121**, 2525-2535 (1995).

Conradt, B. & Horvitz, H.R. The *C. elegans* protein EGL-1 is required for programmed cell death and interacts with the Bcl-2-like protein CED-9. *Cell*. **93**, 519-529 (1998).

Conradt, B. & Horvitz, H.R. The TRA-1A sex determination protein of *C. elegans* regulates sexually dimorphic cell deaths by repressing the *egl-1* cell death activator gene. *Cell* **98**, 317-327 (1999).

Conradt, B. With a little help from your friends: cells don't die alone. *Nat. Cell. Biol.* **4**, 139-143 (2002).

Crittenden, S.L., Troeml, E.R., Evans, T.C., Kimble, J. GLP-1 is localized to the mitotic region of the *C. elegans* germ line. *Development* **120**, 2901-2911 (1994).

Ellis, H,M. & Horvitz, H.R. Genetic control of programmed cell death in the nematode *C. elegans*. *Cell* **44**, 817-829 (1986).

Ellis, R.E. & Horvitz, H.R. Two *C. elegans* genes control the programmed deaths of specific cells in the pharynx. *Development* **112**, 591-603 (1991b).

Ellis, R.E., Jacobson, D.M. & Horvitz, H.R. Genes required for the engulfment of cell corpses during programmed cell death in *Caenorhabditis elegans*. *Genetics* **129**, 79-94 (1991a).

Fadeel, B., Orrenius, S. & Zhivotovsky, B. Apoptosis in human disease: a new skin for the old ceremony? *Biochem Biophys Res Commun* **266(3)**, 699-717 (1999).

Gibert, M.A., Starck, J. & Beguet, B. Role of the gonad cytoplasmic core during oogenesis of the nematode *Caenorhabditis elegans*. *Biol Cell*. **50(1)**, 77-85 (1984).

Gluecksmann, A. Cell death in normal vertebrate ontogeny. Biological Reviews **26**, 59-86 (1951).

Gumienny, T., Lamble, E., Hartwieg, E., Horvitz, H.R. & Hengartner, M.O. Genetic control of programmed cell death in the Caenorhabditis elegant hermaphrodite germline. *Development* **126**, 1011-1022 (1999).

Gumienny, T.L. & Hengartner, M.O. How the worm removes corpses: the nematode *C. elegans* as a model to study engulfment. *Cell Death Differ*. **8**, 564-568 (2001).

Hedgecock, E.M., Sulston, J.E. & Thomson, J.N. Mutations affecting programmed cell deaths in the nematode *Caenorhabditis elegans*. *Science* **220**, 1277-1279 (1983).

Hengartner, M.O. & Horvitz, H.R. *C. elegans* cell survival gene *ced-9* encodes a functional homolog of the mammalian proto-oncogene *bcl-2*. *Cell* **76**, 665-676 (1994).

Hengartner, M.O., Ellis, R.E. & Horvitz, H.R. *C. elegans* gene *ced-9* protects cells from programmed cell death. *Nature* **356**, 494-499 (1992).

Hoeppner, D.J., Hengartner, M.O. & Schnabel, R. Engulfment genes cooperate with *ced-3* to promote cell death in *Caenorhabditis elegans*. *Nature* **412(6843)**, 202-6 (2001).

Hofmann, K., Bucher, P. & Tschopp, J. The CARD domain: a new apoptotic signaling motif. *Trends Biochem. Sci.* **22**, 155-156 (1997).

Horvitz, H.R. Genetic control of programmed cell death in the nematode *Caenorhabditis elegans*. *Cancer Res.* **59**, 1701s-1706s (1999).

Horvitz, H.R., Ellis, H.M. & Sternberg, P.W. Programmed cell death in nematode development. *Neurosci. Comment.* **1**, 56-65 (1982).

James, C., Gschmeissner, S., Fraser, A. & Evan, G.I. CED-4 induces chromatin condensation in *Schizosaccharomyces pombe* and is inhibited by direct physical association with CED-9. *Curr. Biol.* **7**, 246-252 (1997).

Johnson, A.L. & Bridgham, J.T. Caspase-mediated apoptosis in the vertebrate ovary. *Reproduction* **124(1)**, 19-27 (2002).

Kinchen, J.M. & Hengartner, M.O. Tales of cannibalism, suicide, and murder: Programmed cell death in *C. elegans*. *Curr Top Dev Biol.* **65**, 1-45 (2005).

Kinchen, J.M., Cabello, J., Klingele, D., Wong, K., Feichtinger, R., Schnabel, H., Schnabel, R. & Hengartner, M.O. Two pathways converge at CED-10 to mediate actin rearrangement and corpse removal in *C. elegans*. *Nature*. **434(7029)**, 93-9 (2005).

Liu, Q.A. & Hengartner, M.O. The molecular mechanism of programmed cell death in *C. elegans*. *Ann N Y Acad Sci*. **887**, 92-104 (1999).

Lockshin, R.A. & Williams, C.M. Programmed cell death. II. Endocrine potentiation of the breakdown of the intersegmental muscles of silkmoths. *J Insect Physiol* **10**, 643-649 (1964).

Lockshin, R.A. & Zakeri, Z. Programmed cell death and apoptosis: origins of the theory. *Nat Rev Mol Cell Biol* **2(7)**, 545-50 (2001).

Martinou, I., Fernandez, P.A., Missotten, M., White, E., Allet, B., Sadoul, R. & Martinou, J.C. Viral proteins E1B19K and p35 protect sympathetic neurons from cell death induced by NGF deprivation. *J. Cell Biol.* 128, 201-208 (1995).

Metzstein, M.M., Stanfield, G.M. & Horvitz, H.R. Genetics of programmed cell death in *C. elegans:* past, present and future. *Trends Genet.* **14**, 410-416 (1998).

Milstein, S. Genetic analysis of programmed cell death in the *Caenorhabditis elegans* germline. PhD thesis. State University of New York, New York (2001).

Miura, M., Zhu, H., Rotello, R., Hartwieg, E.A. & Yuan, J. Induction of apoptosis in fibroblasts by IL-1b converting enzyme, a mammalian homolog of the *C. elegans* cell death gene *ced-3*. *Cell* **75**, 653-660 (1993).

Morita, Y. & Tilly, J.L. Oocyte apoptosis: like sand through an hourglass. *Dev Biol.*

213(1), 1-17 (1999).

Navarro, R.E., Shim, E.Y., Kohara, Y., Singson, A. & Blackwell, T.K. *cgh-1*, a conserved predicted RNA helicase required for gametogenesis and protection from physiological germline apoptosis in *C. elegans*. *Development*. **128(17)**, 3221-32 (2001).

Nicholson, D.W. & Thornberry, N.A. Caspases: killer proteases. *Trends Biochem. Sci.* **22**, 299-306 (1997).

Ray, C.A., Black, R.A., Kronheim, S.R., Greenstreet, T.A., Sleath, P.R., Salvesen, G.S. & Pickup, D.J. Viral inhibition of inflammation: Cowpox virus encodes an inhibitor of the interleukin-1b converting enzyme. *Cell* 69, 597-604 (1992).

Reddien, P.W., Cameron, S. & Horvitz, H.R. Phagocytosis promotes programmed cell death in *C. elegans*. *Nature* **412**, 198-202 (2001).

Robertson, A.M. & Thomson, J.N. Morphology of programmed cell death in the ventral nerve cord of *Caenorhabditis elegans* larvae. *J. Embryol. exp. Morph.* **67**, 89-100 (1982).

Schedl, T. Developmental genetics of the germ line. In C. elegans II, Riddle DL, Blumenthal T, Meyer BJ and Priess JR (eds) (Plainview, NY: Cold Spring Harbor Laboratory Press), pp. 241–269 (1997).

Shaham S and Horvitz HR. Developing *Caenorhabditis elegans* neurons may contain both cell-death protective and killer activities. *Genes Dev*. **10**, 578-591 (1996a).

Shaham, S. & Horvitz, H.R. An alternatively spliced *C. elegans ced-4* RNA encodes a novel cell death inhibitor. *Cell* **86**, 201-208 (1996b).

Shaham, S. Identification of multiple *Caenorhabditis elegans* caspases and their potential roles in proteolytic cascades. *J. Biol. Chem*. **273**, 35109-35117 (1998).

Spector, M.S., Desnoyers, S., Hoeppner, D.J. & Hengartner, M.O. Interaction between the *C. elegans* cell death regulators CED-9 and CED-4. *Nature* **385**, 653-656 (1997).

Sulston, J.E. & Horvitz, H.R. Post-embryonic cell lineages of the nematode *Caenorhabditis elegans*. *Dev. Biol*. **82**, 110-156 (1977).

Sulston, J.E., Shierenberg, E., White, J.G. & Thomson N. The embryonic cell lineage of the nematode *Caenorhabditis elegans*. *Dev. Biol*. **100**, 64-119 (1983).

Tsujimoto, Y., Finger, L.R., Yunis, J., Nowell, P.C., Croce, C.M. Cloning of the chromosome breakpoint of neoplastic B cells with the t(14;18) chromosome translocation. *Science* **226**, 1097-1099 (1984).

Vaskivuo, T.E., Tapanainen, J.S. Apoptosis in the human ovary. *Reprod Biomed Online* **6(1)**, 24-35 (2003).

Wu, D., Wallen, H.D. & Nunez, G. Interaction and regulation of subcellular localization of CED-4 by CED-9. *Science* **275**, 1126-1129 (1997).

Wu, Y.C., Tsai, M.C., Cheng, L.C., Chou, C.J. & Weng, N.Y. *C. elegans* CED-12 acts in the conserved crkII/DOCK180/Rac pathway to control cell migration and cell corpse engulfment. *Dev Cell*. **1(4)**, 491-502 (2001).

Xue, D. & Horvitz, H.R. Inhibition of the *Caenorhabditis elegans* cell-death protease CED-3 by a CED-3 cleavage site in baculovirus p35 protein. *Nature* **377**, 248-251 (1995).

Xue, D., Shaham, S. & Horvitz H.R. The *Caenorhabditis elegans* cell death protein CED-3 is a cysteine protease with substrate specificities similar to those of the human CPP32 protease. *Genes & Dev*. **10**, 1073-1083 (1996).

Yang, X., Chang, H.Y. & Baltimore, D. Essential role of CED-4 oligomerization in CED-3 activation and apoptosis. *Science* **281**, 1355-1357 (1998).

Yuan, J. & Horvitz, H.R. The *Caenorhabditis elegans* cell death gene *ced-4* encodes a novel protein and is expressed during the period of programmed cell death. *Development* **116**, 309-320 (1992).

Yuan, J., Shaham, S., Ledoux, S., Ellis, H.M. & Horvitz H.R. The *C. elegans* cell death gene *ced-3* encodes a protein similar to mammalian interleukin-1 beta converting enzyme. *Cell* **75**, 641-652 (1993).

Zhou, Z., Caron, E., Hartwieg, E., Hall, A. & Horvitz, H.R. The *C. elegans* PH domain protein CED-12 regulates cytoskeletal reorganization via a Rho/Rac GTPase signaling pathway. *Dev Cell.* **1(4)**, 477-89 (2001).

Zou, H., Henzel, W.J., Liu, X., Lutschg, A. & Wang, X. Apaf-1, a human protein homologous to *C. elegans* CED-4, participates in cytochrome *c*-dependent activation of caspase-3. *Cell* **90**, 405-13 (1997).

CHAPTER 2

CAENORHABDITIS ELEGANS HUS-1 IS A DNA DAMAGE CHECKPOINT PROTEIN REQUIRED FOR GENOME STABILITY AND EGL-1-MEDIATED APOPTOSIS

Current Biology

Volume 12, p. 1908-1918

Preface

Mammalian cells exhibit complex, but intricate cellular responses to genotoxic stress, including cell cycle checkpoints, DNA repair and apoptosis. These processes act in a concerted fashion and remain functionally linked through mechanisms not completely understood. Inactivation of these important biological events may result in genomic instability and cell transformation, as well as alterations of therapeutic sensitivity.

Although having been proven very useful for the identification of checkpoint mutants (Murakami and Nurse, 2000), the two yeasts, *S. cerevisiae* and *S. pombe*, lack an apoptotic program. The availability of *C. elegans* as a model organism, on the other hand, has greatly increased our understanding of the genetic control of cell death. The existence of DNA damage responses and the preliminary genetic characterization of the ionizing radiation-induced responses first became known in the year 2000 (Gartner *et al.*, 2000). These, together with the limitation of the mouse model for easy genetic manipulations and conditional or viable knock-outs render the worm a very promising system to delineate the multiple interconnected cellular pathways.

Randy Hofmann, a former post doc in the Hengartner lab, initiated studies on *hus-1*, by mapping and cloning the *op241* allele and identifying the gene as the homolog of the *S. pombe* gene *hus1*$^{+}$. In an independent reverse genetic screen for deletions in *C. elegans* of known checkpoint genes, the *op244* allele of the same gene

was recovered. In the paper presented in this chapter, we demonstrate that the *C. elegans hus-1* is required for DNA damage-induced apoptosis, in an EGL-1-mediated fashion. At the beginning of my career as a graduate student in the Hengartner lab, I was engaged into this project, where my task was to show the transcriptional requirements for the initiation of cell death upon ionizing radiation. Following the paper presented below is my contribution, as well as additional experiments I had performed to reach the theory we support.

Current Biology, Vol. 12, 1908–1918, November 19, 2002, ©2002 Elsevier Science Ltd. All rights reserved. PII S0960-9822(02)01262-9

Caenorhabditis elegans HUS-1 Is a DNA Damage Checkpoint Protein Required for Genome Stability and EGL-1-Mediated Apoptosis

E. Randal Hofmann,[1,6,8] Stuart Milstein,[1,2,3,8] Simon J. Boulton,[3,4] Mianjia Ye,[1] Jen J. Hofmann,[1,6] Lilli Stergiou,[5] Anton Gartner,[5] Marc Vidal,[3] and Michael O. Hengartner[1,6,7]

[1]Cold Spring Harbor Laboratory
1 Bungtown Road
Cold Spring Harbor, New York 11724
[2]Graduate Program in Genetics and Department of Molecular Genetics and Microbiology
The State University of New York at Stony Brook
Stony Brook, New York 11794
[3]Dana-Farber Cancer Institute
Department of Genetics
Harvard Medical School
Boston, Massachusetts 02115
[4]Cancer Research UK
Clare Hall
Clare Hall Laboratories
South Mimms
Hertfordshire EN6 3LD
United Kingdom
[5]Max-Planck-Institute for Biochemistry
Department of Cell Biology
Am Klopferspitz 18a
Martinsried 82152
Germany
[6]University of Zürich
Institute for Molecular Biology
Winterthurerstrasse 190
8057 Zürich
Switzerland

Summary

Background: The inability to efficiently repair DNA damage or remove cells with severely damaged genomes has been linked to several human cancers. Studies in yeasts and mammals have identified several genes that are required for proper activation of cell cycle checkpoints following various types of DNA damage. However, in metazoans, DNA damage can induce apoptosis as well. How DNA damage activates the apoptotic machinery is not fully understood.

Results: We demonstrate here that the *Caenorhabditis elegans* gene *hus-1* is required for DNA damage-induced cell cycle arrest and apoptosis. Following DNA damage, HUS-1 relocalizes and forms distinct foci that overlap with chromatin. Relocalization does not require the novel checkpoint protein RAD-5; rather, relocalization appears more frequently in *rad-5* mutants, suggesting that RAD-5 plays a role in repair. HUS-1 is required for genome stability, as demonstrated by increased frequency of spontaneous mutations, chromosome nondisjunction, and telomere shortening. Finally, we show that DNA damage increases expression of the proapoptotic gene *egl-1*, a response that requires *hus-1* and the *p53* homolog *cep-1*.

Conclusions: Our findings suggest that the RAD-5 checkpoint protein is not required for HUS-1 to relocalize following DNA damage. Furthermore, our studies reveal a new function of HUS-1 in the prevention of telomere shortening and mortalization of germ cells. DNA damage-induced germ cell death is abrogated in *hus-1* mutants, in part, due to the inability of these mutants to activate *egl-1* transcription in a *cep-1/p53*-dependent manner. Thus, HUS-1 is required for p53-dependent activation of a BH3 domain protein in *C. elegans*.

[7]Correspondence: michael.hengartner@molbio.unizh.ch
[8]These authors contributed equally to this work.

Introduction

Tumorigenesis is characterized by the accumulation of genetic mutations, rearrangements, amplifications, and deletions — any of which can drive the progressive transformation of normal cells into highly malignant derivatives [1]. Cancer avoidance therefore requires precise and efficient means to maintain the integrity of the genome. Damage to DNA triggers checkpoint controls that result in cell cycle arrest and repair of the lesion. In metazoans, DNA damage often results in the programmed demise of the cell, possibly due to extensive damage that is not rectifiable [2]. Alternatively, it may be prudent for the organism to eliminate dangerous cells in tissues that have an extensive proliferative capacity, even when damage has been minimal [3, 4]. Loss of communication between the DNA lesion and the apoptotic program, which allows the persistence of cells with damaged and/or unstable genomes, can lead to tumorigenesis.

Our understanding of the genetics of the DNA damage checkpoint pathway has been heavily dependent on studies done in the yeasts *Saccharomyces cerevisiae* and *Schizosaccharomyces pombe* [5]. The DNA damage checkpoint in *S. pombe* includes six "rad" genes: *rad1*$^+$, *rad3*$^+$, *rad9*$^+$, *rad17*$^+$, *rad26*$^+$, and *hus1*$^+$. DNA damage activates Rad3, a phosphatidylinositol kinase family member that is structurally and functionally related to human ATM and ATR [6]. Rad3 is required for phosphorylation of Hus1, Rad26, Chk1, and Cds1. Phosphorylation of the kinases Chk1 and Cds1 transduces DNA damage and replication checkpoint signals to the cell cycle machinery [5]. Despite our exceptional understanding of checkpoint arrest and repair, yeast lack an apoptotic program; thus, our understanding of how a cell decides to repair or die is lagging.

The genetics of apoptosis has been extensively studied in the nematode *Caenorhabditis elegans* [7]. Although the majority of this work has focused on developmental aspects of somatic apoptosis, recent research has also focused on the germline [8]. Unlike the invariable pattern of somatic cell deaths during development, germline apoptosis is not determined by lineage and can

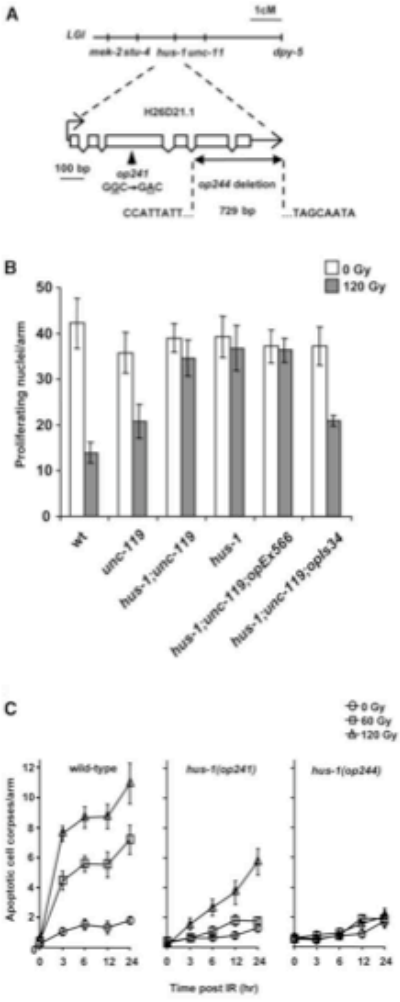

Figure 1. Identification of *hus-1* Mutants

(A) Genetic map and genomic structure of the *hus-1* gene. Boxes represent coding sequence. The position and nature of the *hus-1* mutations are indicated.

(B) Quantification of cell proliferation arrest in wild-type, *hus-1(op241)*, and *hus-1(op241);unc-119(ed3)* strains with integrated *(opIs34)* and nonintegrated *(opEx566)* transgenic constructs. The number of cells in the proliferating region of the germline was viewed by DIC and scored 50 μm from the distal end of the gonad 12 hr following irradiation, as described in Supplementary Experimental Procedures. Each bar represents five worms ± SD.

(C) Comparison of the germline apoptotic response to irradiation between wild-type and *hus-1* mutants. Corpses were scored in the distal arm of the gonad of adult animals following indicated doses of irradiation. *hus-1* deletion mutants are completely defective for DNA damage-induced apoptosis; however, physiological germ cell death is present.

be regulated by multiple pathways. We have previously demonstrated that *C. elegans* is an excellent genetic tool that can be used to understand DNA damage-induced cell cycle arrest and apoptosis [9, 10]. DNA damage-mediated apoptosis is dependent on *ced-3* and *ced-4* and is negatively regulated by *ced-9*. The positive death regulator, *egl-1*, is partially required, but it is not essential for radiation-induced apoptosis. Recently, three *C. elegans* checkpoint mutants, *op241*, *rad-5(mn159)*, and *mrt-2(e2663)*, have been identified that block DNA damage-induced apoptosis and cell cycle arrest [9, 11]. It is unclear how these checkpoint genes regulate the apoptotic machinery. One possibility is by means of a p53 homolog, *cep-1*, which is required for DNA damage-induced germ cell death but not cell cycle arrest [12, 13].

Here we show that *op241* is a hypomorphic allele in the *C. elegans* homolog of the *S. pombe hus1*$^+$ checkpoint gene. *hus-1* mutants fail to induce apoptosis and proliferation arrest following DNA damage and show increased sensitivity to DNA damage-induced lethality. Using a newly identified candidate null allele, we show that *hus-1* function is also required for telomere length maintenance. HUS-1 is a nuclear protein that is expressed in early embryos and the adult germlines and relocalizes to putative sites of DNA damage. Finally, we demonstrate that DNA damage induces the proapoptotic gene *egl-1*. This is dependent on *hus-1* and the p53 homolog, *cep-1*.

Results

Identification of Mutations in *C. elegans hus-1*

We have previously described mutants defective in cell cycle arrest and apoptosis induced by DNA damage [9, 10]. Included in this group was the mutation *op241*, originally identified in a strain containing the *him-7(e1480)* mutation and later named *dam-1(op241)* (DNA damage response) [9, 10]. We mapped *op241* to a 2.1-cM interval, between *stu-4* and *unc-11*, on the left side of chromosome I (Figure 1A). An in silico search for candidate genes in this interval identified *H26D21.1*, a homolog of the *S. pombe* gene *hus1*$^+$. Sequence analysis of *H26D21.1* from *op241* revealed a G to A transition at base pair +296, resulting in a G to D substitution at amino acid 99. Because of the high sequence conservation between *H26D21.1* and *hus-1* homologs from other species, we renamed this gene *hus-1*.

In an independent reverse genetic screen for deletions in *C. elegans* homologs of known checkpoint genes, we recovered a single *hus-1* allele, *op244*. The *op244* allele is a 729-bp deletion that removes the last two exons and most of the 3′ untranslated region of *hus-1* (bp 4725–5453 on cosmid H26D21) (Figure 1A). *hus-1(op244)* mutants from homozygous parents show an

Table 1. *hus-1* Deletion Mutants Display Chromosome Nondisjunction and Embryonic Lethality

	F3	F3		F6	
Genotype	Males (%)	Brood Size	Survival (%)	Brood Size	Survival (%)
Wild-type; n = 15	0.0 ± 0.0	257.4 ± 13.5	99.5 ± 2.6	239.1 ± 21.3	99.2 ± 4.3
hus-1(op241); n = 10	0.2 ± 0.2	303.6 ± 25.9	96.9 ± 2.3	334.7 ± 24.4	96.2 ± 3.6
hus-1(op244); n = 15	5.7 ± 10.3	222.5 ± 90.0	78.5 ± 15.7	60.1 ± 41.6	50.0 ± 17.6

incompletely penetrant maternal effect embryonic lethality (Table 1). Complementation tests confirmed that *op241* and *op244* are allelic (see the Experimental Procedures). An extrachromosomal array (*opEx566*) of a full-length translational fusion of HUS-1::GFP under the control of the *hus-1* promoter, which does not express in the germline, fails to rescue both cell cycle arrest and DNA damage-induced apoptosis in *op241* (Figure 1B). However, a germline-expressing transgene, *opIs34*, of the same construct fully rescues the DNA damage cell cycle arrest and partially rescues the apoptotic defect of *op241* (4.2-fold induction of apoptotic cells in *op241;unc-119;opIs34* animals compared to 1.3-fold induction in *op241;unc-119;opEx566* and 8.6-fold induction in wild-type) (Figure 1B).

DNA Damage Responses Are Defective in *hus-1* Mutants

Ionizing radiation induces several responses in *C. elegans*, including germ cell apoptosis, cell cycle arrest, and embryonic lethality [9]. We have previously shown that *op241* is defective for DNA damage-induced germ cell death and cell cycle arrest [9]. We found that the *op244* allele had more severe defects in both of these responses (Figures 1C, S1A, and S1B; Figure S1 is contained in the Supplementary Material available with this article online). In addition, *op244* is more sensitive to the embryonic lethal effects of ionizing radiation (Figure S1C).

hus-1(op241) Disrupts a Checkpoint Protein Interaction

The G99D mutation in *op241* affects a residue that, while poorly conserved at the primary sequence level, borders a helix that has been proposed to interact with *S. pombe* and human Rad9 proteins (Figure 2A) [14]. Although *C. elegans* HUS-1 does not interact with HPR-9, the *C. elegans* homolog of Rad9, on its own in the two-hybrid system [15], in vivo interaction in worms is likely (see below). To analyze the molecular nature of the *hus-1(op241)* defect, we tested the mutant form of the protein for its ability to interact with four proteins (MRT-2, PDI-2, K21H4.1, and F56D12.5) that interact with HUS-1 in the yeast two-hybrid system [15]. HUS-1(+) interacted with these four proteins with varying degrees (Figure 2B). In contrast, HUS-1(G99D) is defective for its ability to interact with the conserved checkpoint protein MRT-2, the *C. elegans* homolog of *S. pombe* Rad1, and with PDI-2, a protein disulfide isomerase homolog, in the yeast-two hybrid system (Figure 2B).

Furthermore, HUS-1(G99D) failed to interact with MRT-2 in GST pull-down experiments from transfected cells (Figure 2C). However, HUS-1(+) and HUS-1(G99D) interacted comparably with F56D12.5 and K12H4.1 (Figure 2A). These findings suggest that the *op241* mutation does not completely abolish the structural integrity of the mutant protein but specifically compromises a protein interaction domain that is important for association with MRT-2 and PDI-2. Our findings suggest that an inability to form a HUS-1/MRT-2 complex in vivo compromises the integrity of the DNA damage checkpoint in *op241*, thus providing a molecular explanation for this mutation.

HUS-1 Is a Nuclear Protein that Requires the Checkpoint Proteins MRT-2 and HPR-9, but Not RAD-5, for Proper Localization

S. pombe Hus1p has been shown to be a nuclear protein [16]. Microscopic analysis of *opIs34[hus-1::gfp]* animals revealed HUS-1::GFP localization in the nuclei of proliferating germ cells, meiotic germ cells, mature oocytes, and embryos (Figure 3A). We also observed nuclear GFP expression in a subset of somatic cells, particularly proliferating cells, in larvae (data not shown). Rad1, Rad9, and Hus1 form a heterotrimer complex that structurally resembles the proliferating cell nuclear antigen (PCNA) trimer [14, 17]. Rad17 is believed to load this complex onto DNA at or near sites of DNA damage [18]. To determine the role of these interactions in *C. elegans*, we analyzed HUS-1::GFP expression in a *mrt-2(e2663)* background. Surprisingly, the expression of HUS-1::GFP in the germline was greatly reduced and was excluded from the nucleus (Figure 3A). Crossing these worms back to wild-type worms restored proper localization of HUS-1::GFP to the nucleus (data not shown). This reduction of expression is likely due to degradation, possibly as a result of improper localization, rather than transcriptional regulation, as GFP under the control of the *hus-1* promoter (*opIs29(pRH04)*) was not affected by loss of MRT-2 (data not shown).

We also analyzed the expression of HUS-1::GFP in a *rad-5(mn159)* background. RAD-5 is homologous to *S. cerevisiae* Tel2p and is required for germ cell replication and DNA damage checkpoints [9, 11]. HUS-1::GFP localization was not different in *rad-5(mn159)* than in the parental strain (Figure 3A), and this finding is consistent with evidence that *rad-5* acts independently of *hus-1* and *mrt-2* [11]. Interestingly, HUS-1::GFP levels were significantly lower in *rad-5(mn159)* mutants compared to the parental strain.

MRT-2 interacts with HPR-9 in a two-hybrid assay, suggesting that the Rad1/Rad9/Hus1 complex is conserved in *C. elegans* [15]. Inhibition of *hpr-9* expression via RNAi was sufficient to disrupt HUS-1::GFP localization and expression similarly to a *mrt-2* RNAi-positive control, indicating that HPR-9 is also required for HUS-1

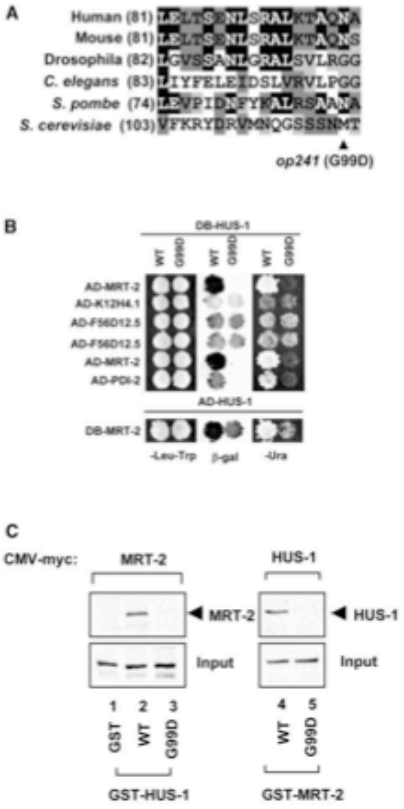

Figure 2. HUS-1(G99D) Is Defective for MRT-2 and PDI-2 Binding

(A) Using the Blosum62mt2 matrix (Align-X), the alignment of the putative helical Rad9 interacting region of Hus1 from human, mouse, fly, worm, and fission yeast and Mec3 from budding yeast was determined. The affected residue in *op241* is indicated by an arrowhead. See text for details.

(B) The yeast two-hybrid system was used to test for protein interactions with wild-type (WT) and mutant (G99D) HUS-1–GAL4 DNA binding domain (DB) fusions by scoring for LacZ expression and growth on −Ura plates (no selection: −Leu −Trp). HUS-1(WT) interacts with GAL4 activation (AD) fusions of MRT-2, K12H4.1, F56D12.5, and PDI-2. HUS-1(G99D) does not interact with MRT-2 and PDI-2, but it still interacts with K12H4.1 and F56D12.5.

(C) In vitro interaction of HUS-1 and MRT-2. GST-HUS-1(WT), but not GST-HUS-1(G99D) or GST alone, interacts with Myc-epitope-tagged MRT-2 (lanes 1–3). GST-MRT-2 is able to interact with wild-type (WT) but not mutant Myc-epitope-tagged HUS-1(G99D) (lanes 4 and 5).

localization and stabilization (Figure 3B). In contrast, *hpr-17(RNAi)*- and *ced-3(RNAi)*-treated worms showed normal HUS-1::GFP localization (Figure 3B). HUS-1::GFP nuclear localization is independent of the other HUS-1-interacting proteins that we tested (PDI-2, K21H4.1, and F56D12.5; data not shown).

HUS-1::GFP Relocalizes to Distinct Foci that Colocalize with Chromatin following DNA Damage

In order to determine the subcellular localization of HUS-1 following DNA damage, we analyzed HUS-1::GFP localization in germ cells before and after exposure to ionizing radiation. HUS-1::GFP was diffuse in proliferating germ nuclei and weakly chromatin localized in pachytene cells under normal conditions. However, following exposure to ionizing radiation, HUS-1::GFP concentrates at distinct nuclear foci in all stages of germ cell development (Figures 4A, 4C, and 4D). The presence of these foci could be observed as early as 3 hr following exposure to ionizing radiation. These foci overlap with chromatin, as demonstrated by counterstaining with DAPI (Figures 4C and 4D).

Genetic evidence of increased DNA damage sensitivity in *hus-1(op241);rad-5(mn159)* and *rad-5(mn159) mrt-2(e2663)* double mutants suggest that *rad-5* functions in a parallel pathway to *hus-1* and *mrt-2* [11]. In order to determine if relocalization of HUS-1::GFP was dependent on *rad-5*, we irradiated worms containing the *hus-1::gfp* transgene in a *rad-5(mn159)* background. We found that rather than being blocked, HUS-1::GFP relocalization was enhanced in the absence of *rad-5* function. The number of foci were present in greater numbers in the absence of RAD-5 prior to and after exposure to ionizing radiation (Figure 4B). Further, we found that, while HUS-1::GFP foci numbers decreased in *rad-5(+)* controls after 20 hr, the number of foci did not change in *rad-5* mutants (Figure 4B).

Double-strand breaks also occur under normal conditions during meiotic prophase from initiation events during recombination. These double-strand breaks fail to "heal" in several yeast mutants, resulting in pachytene cell cycle arrest. RNAi of the RecA-strand exchange family member, *rad-51*, similarly blocks recombination in *C. elegans* germ cells and results in increased germ cell apoptosis [9, 19]. Under normal conditions, a limited number of HUS-1::GFP foci can occasionally be observed in the pachytene region of the germline (Figure 4D). In contrast, *rad-51*(RNAi) worms showed a dramatic increase in HUS-1::GFP foci (Figure 4D).

The *hus-1* Deletion Mutant Exhibits Genome Instability

Several lines of evidence suggest that loss of *hus-1* function leads to genomic instability. First, *hus-1* mutants show high levels of chromosomal nondisjunction, as evidenced by the high proportion of males (the result of X chromosome nondisjunction) in the self-progeny of *op244* mutants. Whereas nondisjunction of the X chromosomes produces less than 0.2% male progeny in the wild-type [20], early *op244* generations produce about 6% males (Table 1). Second, as has been observed for other mutants defective in genome stability, *hus-1* mutants show abnormal levels of embryonic lethality [21]: early generations of *op244* mutants produce about

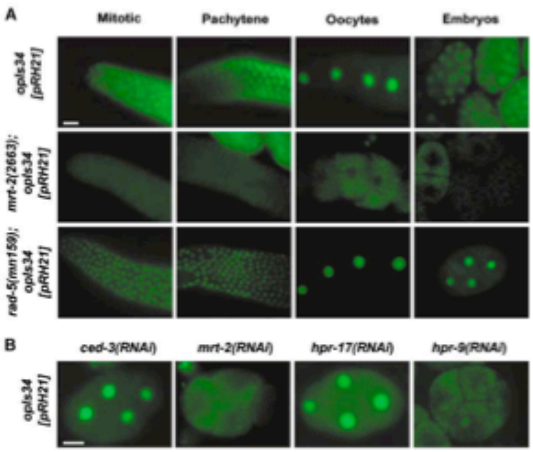

Figure 3. HUS-1 Nuclear Localization Requires MRT-2 and HPR-9

(A) Fluorescent microscopy of integrated transgenic strains expressing fusion constructs in gonads and embryos of wild-type, *mrt-2(e2663)*, and *rad-5(mn159)* mutant backgrounds. The genotype and construct used are indicated, and expression is shown in the indicated stage of oogenesis and early embryos. pRH21 is a full-length translational fusion containing 2252 bp of genomic sequence 5′ to the stop codon.

(B) Fluorescent microscopy of 4-cell-stage embryos from F2-integrated transgenic worms fed dsRNA produced from indicated genes as described in the Experimental Procedures. For confirmation of *ced-3(RNAi)* and *hpr-17(RNAi)*, germ cell death and hypersensitivity to radiation-induced embryonic lethality, respectively, were scored. The scale bars represent 10 μm.

78% healthy progeny that survive to adulthood (the level of larval lethality was minimal) (Table 1). Embryonic survival is even lower in later generations. Embryonic survival of *op241* mutants was not significantly different from wild-type worms. Nondisjunction of autosomes could well explain most or all of the embryonic lethality seen in *op244* mutants, although other defects, such as failure to repair endogenous damage, cannot be excluded. Indeed, spontaneous mutations are more frequent, as measured by an *unc-93* reversion assay (see below).

Mutations in the checkpoint gene *mrt-2* result not only in a failure to induce apoptosis in response to DNA damage [9], but also in progressive telomere loss, eventually leading to end-to-end chromosome fusion and aneuploidy [22]. As a consequence of these defects, the brood sizes of *mrt-2* mutants decrease over generations until the animals become sterile – the Mrt (mortal germline) phenotype from which the gene derived its name. While early generations of freshly outcrossed *op244* mutants have brood sizes similar to wild-type worms, later generations showed dramatically lower fertility (Table 1) and became sterile after about 15 generations (producing very few embryos, none of which hatch). We did not see a Mrt phenotype in *op241* mutants kept at 20°C (Table 1). However, when grown at 25°C, *op241* mutants also became sterile after approximately 15 generations, suggesting that *op241* might be a temperature-sensitive allele.

To test whether the Mrt phenotype of *hus-1* mutants was due to telomere loss, we probed Southern blots of genomic DNA from multiple generations of *op244* and *op241* strains. In *op244* mutants grown at 20°C, we saw a progressive loss of telomere sequence in late generations of worms (Figure 5A). As reported before, the ends of telomeres do not decrease in *op241* mutants grown at 20°C [11]; however, worms grown at 25°C did display telomere shortening (data not shown). In wild-type worms, six chromosomal bivalents can be observed by DAPI staining of oocytes in diakinesis. In contrast, late generations of *op244* mutants often contained fewer than six bivalents. In *op244* generations no longer producing viable progeny, only 3–4 bivalents could be seen (Figure 5B); consistent with the idea that loss of telomeres led to chromosome fusions. Correspondingly, the incidence of males increases dramatically after several generations and gives rise eventually to dominant Him (high incidence of males) strains (data not shown).

One function of checkpoint genes is to prevent cells with a damaged genome from progressing through the cell cycle without correcting the DNA lesion. Mutations in genes that repair these lesions or regulate the checkpoints that prevent cell cycle progression have been shown to display higher spontaneous mutation frequencies [23, 24]. Since *hus-1* has a checkpoint function, we used the well-characterized *unc-93* reversion assay to look at spontaneous mutation frequencies in *hus-1* worms [25]. We found the spontaneous suppression frequency of *unc-93(e1500)* worms in our assay to be 1×10^{-5} (Figure 5C). In two independent *hus-1(op244);unc-93(e1500)* strains, we found the mutation frequency to be 10- to 20-fold higher than in the control strain (Figure 5C). Consistent with this, the appearance of spontaneous mutations has also been observed during strain maintenance (data not shown).

Ionizing Radiation Induces *egl-1* Transcript Upregulation in a *hus-1*- and *cep-1*-Dependent Manner

In order to determine whether *hus-1* is transcriptionally regulated following DNA damage, we isolated mRNA from adult wild-type and *hus-1(op244)*-irradiated worms and probed Northern blots with *hus-1* cDNA. A single transcript of the expected size was seen in wild-type; however, the transcript was truncated and levels were dramatically reduced in the *hus-1(op244)* deletion mu-

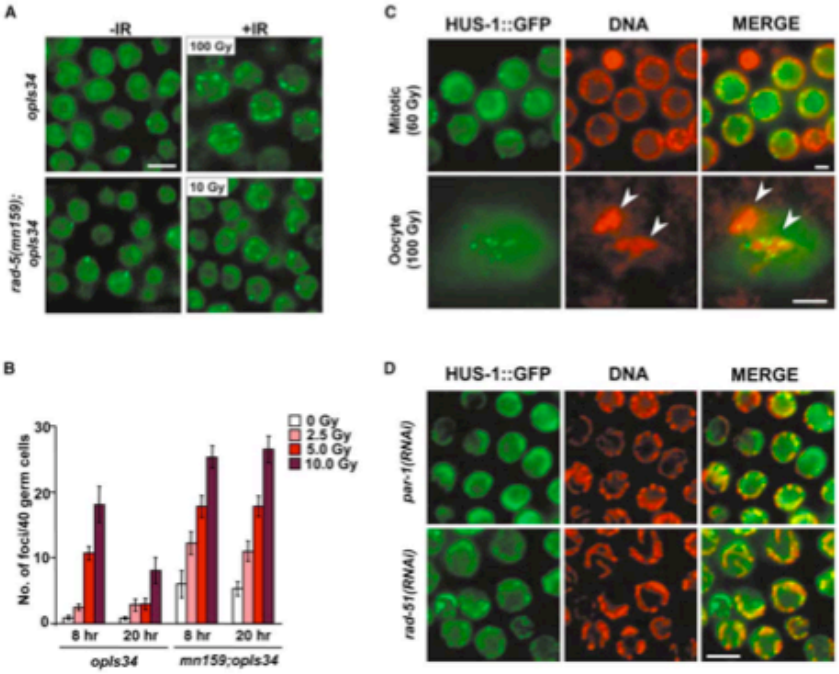

Figure 4. Subcellular Relocalization of HUS-1::GFP following DNA Damage

(A) Fluorescent microscopy of proliferating germ cells expressing HUS-1::GFP (*opIs34*). Irradiated worms (*opIs34* = 100 Gy; *rad-5(mn159);opIs34* = 10 Gy) were viewed 8 hr following irradiation. HUS-1::GFP is diffuse in controls. Relocalized HUS-1::GFP is seen as bright foci. The scale bar represents 5 μm.

(B) Quantification of HUS-1::GFP foci in wild-type and *rad-5(mn159)* backgrounds. Foci were scored in 40 proliferating germ cells in a single Z stack following mild doses of X-rays at indicated times. Each bar represents ten worms ± SEM.

(C) Colocalization of HUS-1::GFP with chromatin following exposure to ionizing radiation. The top panel shows proliferating germ cells. The bottom panel shows a single oocyte nucleus in diakinesis. Arrowheads point to two DAPI-stained bivalents from an oocyte in diakinesis. The scale bar represents 2 μm.

(D) Fluorescent microscopy of meiotic germ cells from worms fed dsRNA from *rad-51* and a *par-1* control. As in (C), HUS-1::GFP foci overlap with chromatin stained with Hoechst 33342 dye. The scale bar represents 5 μm.

tant. Levels of *hus-1* mRNA did not change significantly 60 and 180 min after exposure to IR (Figure 6A).

In *C. elegans*, the BH3 domain protein, EGL-1, activates the apoptotic machinery. Furthermore, *egl-1* is transcriptionally regulated in order to activate apoptosis during somatic development [26]. We subsequently hybridized the same blot to an *egl-1* probe. We found that, in wild-type young adults, *egl-1* is induced by 60 min and increases by 180 min after irradiation (Figures 6A and 6B). Induction is significantly lower in *glp-4(bn2)* (a temperature-sensitive mutant that lacks a germline at the restrictive temperature) animals, suggesting that *egl-1* induction is largely restricted to the germline (Figure 6B). Consistent with this hypothesis, we found germline induction of an *egl-1::gfp* transcriptional reporter construct following exposure to ionizing radiation (Figure 6C). Importantly, *egl-1* levels did not increase in the *hus-1(op244)* deletion worms after irradiation (Figures 6A and 6B). These results are consistent with the hypothesis that *hus-1*-dependent induction of *egl-1* transcription is an important element of the apoptotic DNA damage response in *C. elegans* and that it promotes the increased germ cell apoptosis observed following genotoxic stress.

Recent work showed that the *cep-1* gene, which encodes a *C. elegans* homolog of p53, is required for DNA damage-induced germ cell apoptosis [12, 13]. In order to determine if *cep-1* is also required for *egl-1* induction, we analyzed *egl-1* expression by using real-time quantitative RT-PCR (Q-RT-PCR) before and after exposure to

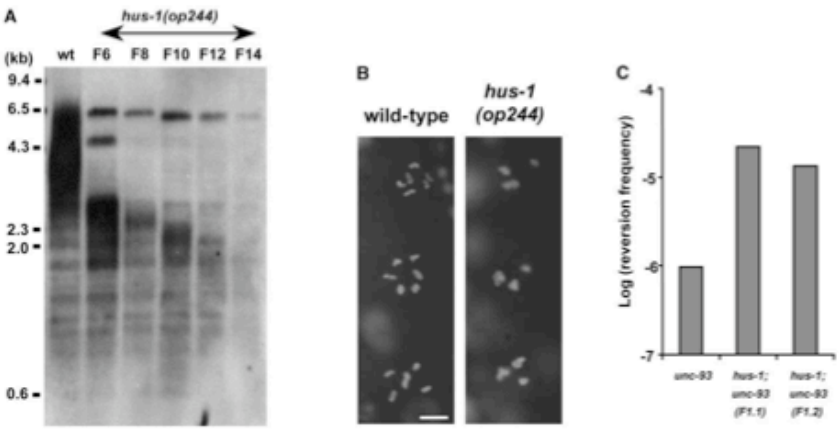

Figure 5. *hus-1* Deletion Mutants Show a Telomere Maintenance Defect and a High Rate of Spontaneous Mutations

(A) Southern blots were performed with a *C. elegans* telomere-specific probe on genomic DNA from wild-type (WT) and indicated inbred generations of *op244* after outcrossing.

(B) Oocytes in diakinesis were stained with DAPI from wild-type and late-generation *hus-1(op244)* mutants that no longer produced viable progeny. Wild-type oocytes contain six easily visible bivalents, while late-generation *hus-1(op244)* mutants often have only 3–5 visible bivalents. The scale bar represents 2 μm.

(C) Spontaneous *unc-93(e1500)* reversion frequencies (log) in *hus-1(+)* and two independently generated *hus(op244)* strains (F1.1 and F1.2). The *unc-93(e1500)* gain-of-function mutation results in severe paralysis that can be suppressed by loss of function of any one of five different genes; this loss of function includes inactivating second site mutations within the *unc-93* gene itself [47].

ionizing radiation in two different *cep-1* mutant strains. Using this technique, we confirmed that *egl-1* transcripts are strongly induced in wild-type worms (Figure 6B). Induction of *egl-1* transcripts was reduced but not abolished in *cep-1(w40)* (Figure 6B), consistent with the observation that *cep-1(w40)* worms have some increased germ cell apoptosis following DNA damage, albeit to a much lesser extent than wild-type ([12] and unpublished data). In contrast, animals homozygous for the deletion allele *cep-1(gk138)*, which completely blocks DNA damage-induced apoptosis (W.B. Derry and J.H. Rothman, personal communication), showed a total absence of *egl-1* induction (Figure 6B). This suggests that *hus-1* and *cep-1* likely act in the same pathway to mediate DNA damage-induced apoptosis.

In order to learn more about the role of *hus-1* in cell cycle regulation, we determined the expression levels of two cyclin kinase inhibitor homologs, *cki-1* and *cki-2* [27, 28]. In mammalian cells, the cyclin kinase inhibitor p21 is induced by p53 expression following DNA damage [29]. However, neither *cki-1* nor *cki-2* was significantly induced transcriptionally by irradiation at 60 or 180 min (Figure 6A).

Discussion

We have shown that HUS-1 is required for a DNA damage checkpoint in *C. elegans*. As in yeast, loss of *hus-1* function abrogates DNA damage-induced cell cycle arrest and sensitizes animals to the lethal effects of ionizing radiation. In *C. elegans*, HUS-1 also mediates an apoptotic response to DNA damage, a pathway that is absent in yeast. Consistent with the observed mutant phenotype, *hus-1* expression is predominantly in the germline. However, we do observe expression in a subset of proliferating somatic cells. HUS-1 may have a role in repair and checkpoints in these cells as well. While we have not performed a detailed mosaic analysis, the fact that transgenes with no germline expression (but with high somatic cell expression) failed to rescue *hus-1(op241)* suggests that HUS-1 acts cell-autonomously to control mitotic checkpoints.

Following DNA damage, HUS-1 is relocalized in the nucleus to distinct foci. These foci are likely sites of double-strand breaks (DSBs), as RNAi suppression of *rad-51*, a gene required for DSB repair during meiotic recombination, or elimination of the checkpoint gene *rad-5* also resulted in increased HUS-1 relocalization. The *C. elegans* checkpoint gene *rad-5* was not required for HUS-1 relocalization. Rather, *rad-5(mn159)* mutants showed an increased number of HUS-1::GFP foci in proliferating germ cells under normal conditions. Following mild insults, HUS-1::GFP foci also failed to decrease in *rad-5* mutants compared to controls. These data suggest that RAD-5 is required for efficient repair of endogenous and exogenous DNA damage either downstream or independent of HUS-1.

Interestingly, the two *hus-1* alleles, *op241* and *op244*, have similar checkpoint defects, yet the deletion of *hus-1* reveals additional functions of HUS-1 in the main-

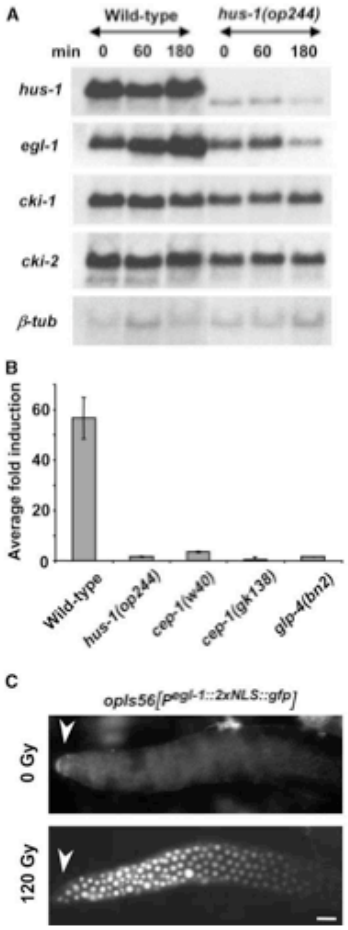

Figure 6. *egl-1* Is Transcriptionally Induced by Irradiation in a *hus-1*- and *cep-1*-Dependent Manner

(A) Northern blots were performed with 2 μg polyA-enriched RNA isolated from wild-type and *hus-1(op244)* mutant young adult worms at indicated times after exposure to 120 Gy γ-irradiation. The same blot was reprobed with a PCR-generated probe from the indicated gene on the left.

(B) Average fold induction of *egl-1* gene expression in wild-type, *hus-1(op244)*, *cep-1(w40)*, *cep-1(gk138)*, and *glp-4(bn2)* mutants after 100 Gy X-ray irradiation as determined by real-time quantitative RT-PCR. *glp-4(bn2)* worms were grown at the nonpermissive temperature, and 90–100 worms were selected that lacked a germline. Each bar represents the average ± SD.

(C) Induction of *egl-1::gfp* expression in the germline. A construct containing 2.7 kb of genomic sequence 5′ to the translation start site of *egl-1* fused to GFP equipped with two nuclear localization signals. Worms were synchronized and irradiated as L4 animals. GFP expression was analyzed in dissected gonads 30 hr following irradiation. Expression was seen in both proliferating and late-pachytene germ cells in most (12/16) irradiated animals. Background expression could be seen in the late-pachytene germ cells in few (2/23) nonirradiated controls, but not (0/23) in the proliferating germ cells. The arrowhead indicates the distal end of the gonad. The scale bar represents 10 μm.

tenance of genome stability. Deletion mutants show a high frequency of meiotic nondisjunction and/or chromosome loss, resulting in increased male progeny, due to loss of the X chromosome, and high levels of embryonic lethality. Chromosome abnormalities have also been reported in mouse *Hus1*−/− cells [30]. One possible cause for the increase in genome instability is the inability to recognize or repair various forms of DNA damage. Indeed, we found that *hus-1* mutants have a mutator phenotype.

Our results also demonstrate that, unlike in yeast, HUS-1 is required for the prevention of telomere shortening during replication of the genome [31]. *hus-1* deletion worms show a progressive shortening of telomeres, which is associated with a progressive reduction in brood size, reaching complete sterility by the 15th generation. In late-generation worms, outcrossing reveals a dominant Him phenotype that is consistent with end-to-end fusions of the X chromosome with autosomes, due to loss of telomeric ends [22]. Fusions are also apparent in oocytes of late-generation worms in which only three or four bivalents, rather than the typical six, can be detected in diakinesis. A similar mortal germline phenotype and chromosome fusions associated with telomere loss have previously been reported for a mutant in the HUS-1-interacting protein MRT-2, and this finding suggests that the same MRT-2/HUS-1 complex that acts in checkpoint control might also control telomere length. It is not known what role HUS-1 has in telomere maintenance in vertebrates.

Studies of DNA damage responses in *C. elegans* have revealed intriguing differences from responses in mammals. DNA damage induces both a G1/S and G2/M arrest in mammalian cells. These cell cycle arrest checkpoints are mediated, in part, by the cyclin kinase inhibitor p21 in a p53-dependent manner [29]. However, we did not see an increase of mRNA levels of two candidate cyclin kinase inhibitors, *cki-1* and *cki-2*, at the times examined. It remains possible that one or both of these CIP homologs is induced at later time points or is posttranscriptionally regulated. Unlike in mammals, but similarly to *Drosophila* [32], loss of CEP-1 (p53) function in *C. elegans* does not result in a cell cycle arrest defect in response to DNA damage [12, 13], suggesting that induction of apoptosis might have been the original function of p53 family members during evolution. Mutants of the homologs of yeast Cdc2 and Cdc25 have been shown to disrupt normal cell cycle in the germline of *C. elegans*; thus, as in yeast, these are possible candidates for downstream effectors of HUS-1-mediated checkpoints [33, 34].

In mammalian cells, DNA damage induces the tran-

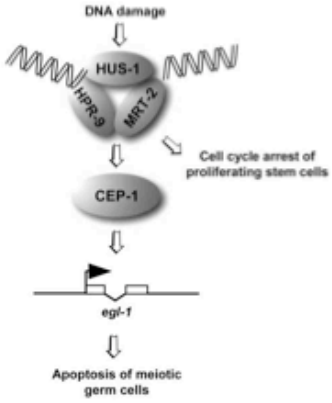

Figure 7. Model: A Pathway for DNA Damage-Induced Apoptosis and Cell Cycle Arrest in *C. elegans*

DNA damage recruitment of the HUS-1/MRT-2/HPR-9 complex to the site of the lesion, where it activates cell cycle arrest of proliferating stem cells. This complex also signals to the apoptotic machinery via CEP-1-dependent upregulation of *egl-1*.

scription of many genes, including the proapoptotic BH3 domain-containing proteins Bax, Puma, and Noxa [35–38]. Transcriptional activation of Bax is dependent on p53 in a tissue-dependent manner but is independent of Atm [39]. However, it is not known whether the genes that sense damaged DNA, such as the Rad family proteins, are required for the induction of Bax, Puma, or Noxa. We demonstrate in *C. elegans* a dramatic increase in mRNA levels for the proapoptotic protein EGL-1 following irradiation. We conclude that this induction is mostly in the germline, as *gip-4* mutants lack strong *egl-1* induction and a GFP reporter displayed high germline expression following irradiation. Induction of *egl-1* by γ-irradiation is dependent on *hus-1*. This provides a molecular explanation for how DNA damage induces apoptosis in germ cells of *C. elegans* and suggests a key link between a DNA damage checkpoint gene and the apoptotic machinery (Figure 7). However, as in mammals, DNA damage likely activates other proapoptotic genes since *egl-1(lf)* mutants are only partially defective in this response.

In mice, all *Hus1*−/− embryos die by 11.5 days postcoitum (dpc) [30], and this death is at least in part due to a high level of chromosome abnormalities, which result in increased apoptosis during embryogenesis. Similarly, we showed that, while worm HUS-1 is not absolutely required for embryonic survival, a significant fraction of *hus-1* embryos die during embryogenesis, likely due to genomic instability. However, we failed to detect any increase in somatic developmental cell death in *hus-1* mutants (data not shown), and these findings are consistent with our previous report that DNA damage does not induce somatic cell apoptosis [9].

In *C. elegans*, p53 function is essential for *hus-1*-mediated apoptosis. In contrast, p53 status does not influence apoptosis and embryonic lethality in *Hus1*−/− mice, as the *Hus1*−/−*p53*−/− embryonic lethality is morphologically indistinguishable from that of *Hus1*−/− embryos [40]. Furthermore, induction of p53 target genes, such as Bax, is normal in *Hus1*−/− mice. However, in *C. elegans*, induction of *egl-1* requires *hus-1* and the *p53* homolog, *cep-1*. Thus, unlike in mouse embryos [40], *hus-1* and *cep-1* likely act in a common pathway to activate the apoptotic machinery (Figure 7).

In contrast to *hus-1(op244)* mutants, which are highly sensitive to IR-induced double-strand breaks (DSBs), mouse *Hus1*−/− cells are highly sensitive to hydroxyurea (HU) and ultraviolet (UV) radiation, but not to ionizing radiation (IR) [30]. One explanation may be that Hus1 in mice is required primarily for the replication checkpoint (UV and HU), but not the DSB checkpoint (IR) during embryogenesis. Indeed, lack of Hus1 or low levels of IR fail to induce cell cycle arrest in mouse embryos; however, apoptosis is induced [4, 30]. However, HUS1, along with Atm and p53, may also play a primary role in responding to DSBs after cells become more differentiated [41]. In several knockouts (*Hus1*−/−, *Atm*−/−, *Brca*−/−), apoptotic cells have been shown to have constitutively higher levels of Bax. Here we demonstrate that, in *C. elegans*, loss of DNA damage sensors upstream of p53 results in loss of activation of the apoptotic machinery and results in radioresistant cells. As with the loss of p53, this may be a crucial step toward transformation into malignant tumors [42].

While the deletion mutant *hus-1(op244)* shows evidence of embryonic defects due to genomic instability and telomere loss, *hus-1(op241)* only appears to be defective in the DNA damage checkpoint response under normal laboratory growth conditions. The fact that mutations can disrupt checkpoint function without impairing essential genome maintenance functions during embryogenesis (chromosome segregation) and oogenesis (telomere maintenance) in *C. elegans* might explain how checkpoint genes essential for viability in mammals can also act as tumor suppressors. For example, even though *Chk1*+/− (in a *Wnt-1* oncogenic background) and *Atr*+/− can promote tumorigenesis, loss of heterozygosity is not seen in these tumors, because loss of either Atr or Chk1 is cell lethal [43, 44]. Thus, while complete loss of DNA damage checkpoint genes can induce mitotic catastrophe, more subtle mutations may contribute to oncogenic transformation by preventing cell cycle arrest and apoptosis.

Conclusions

C. elegans HUS-1 is a conserved checkpoint protein that is required for DNA damage-induced cell cycle arrest and apoptosis. Following DNA damage, HUS-1 relocalizes to putative sites of DSBs independently of the novel checkpoint protein RAD-5. HUS-1 is also required for genome stability and telomere maintenance. We also demonstrate that HUS-1 checkpoint, but not essential genome maintenance, functions are dispensable for embryogenesis, suggesting a possible requirement for HUS-1 in tumor suppression. DNA damage upregulates EGL-1 in a HUS-1- and CEP-1-dependent manner, pro-

viding a molecular link between DNA damage sensors and p53-mediated activation of BH3 proteins in *C. elegans*.

Experimental Procedures

Isolation of *op244*

A deletion library was constructed by using trimethylpsoralen and UV mutagenesis as previously described [45]. This library was screened for deletion mutants of *H26D21.1* via nested PCR by using the following primer sequences: first round 5′-ATGGTCCTGCAGG GAAATAG-3′ and 5′-ATCCGTTAACAGTGAGATACTC-3′ and nested 5′-AGGCACATACAATAATACGGTG-3′ and 5′-ATCACGATCATGT GAAGCCG-3′. Pooled genomic DNA from 96-well plates was screened, and positive plates were screened again by rows and columns to get a single well address. Thawed worms from a positive address were screened by single worm PCR to confirm the presence of the mutation. Homozygous worms were used to prepare genomic DNA for sequence analysis of the mutated *H26D21.1* gene. *op244* mutants were backcrossed to the wild-type eight times before phenotypical analysis.

Spontaneous Mutation Frequencies of *op244*

Mutants of each genotype were singled (*unc-93*, n = 100; *hus-1;unc-93* F1.1, n = 88; *hus-1;unc-93* F1.2, n = 83) and monitored for three generations until plates were starved. Starved animals were then transferred to new plates, and the number of plates with revertants were scored as independent reversion events (*unc-93*, 6/100; *hus-1;unc-93* F1.1, 47/88; *hus-1;unc-93* F1.2, 27/83). These events were then divided by the total number of haploid genomes screened, based on the average brood size of each genotype, to determine the reversion frequency.

Transgenic Worms

HUS-1::GFP lines were constructed with pRH04 and pRH21. pRH04 is a transcriptional fusion containing 1144 bp of genomic sequence upstream of the start codon. pRH21 is a translational fusion construct containing 2252 bp including upstream regulatory sequence and all coding sequence of *H26D21.1* fused in-frame to the C-terminal GFP tag. pRH21 contains GFP and *let-858* sequences from pPD117.01 (gift of A. Fire) and rescuing *unc-119* genomic sequence from pDPMM016 [46]. pRH25 was made by subcloning a 2.7-kb PCR fragment of the sequence 5′ to the *egl-1* start codon into pRH20, which contains a Kpn-1 and ApaI (2xNLS::GFP::let-858 3′UTR) fragment from pPD135.83 (gift of A. Fire) and the *unc-119(+)* rescuing sequence. Constructs were bombarded into *unc-119(ed3)* worms as previously described [46]. Integration of each construct was determined by loss of visible Unc-119 offspring. At least three integrated lines were generated for each construct. Gonads were dissected and were stained with Hoechst 33342 (0.5 μg/ml) or were fixed with 4% paraformaldehyde followed by cold methanol and stained with DAPI (0.2 μg/ml). Images were captured with an ORCA-ER digital CCD camera and were processed with OpenLab software.

Quantitative RT-PCR

Synchronized wild-type, *ced-1(w40)*, *ced-1(gk138)*, *glp-4(bn2)*, and *hus-1(op244)* adult hermaphrodites were irradiated with 100 Gy of X-rays and were left for 3 hr to recover. *glp-4(bn2)* worms were grown at the nonpermissive temperature, and 90–100 worms were selected that lacked a germline. Total RNA was isolated with RNAzol B (*ams* Biotechnology) according to the manufacturer's protocol, treated with DnaseI, and further purified with the RNeasy kit (Qiagen). For cDNA synthesis, purified total RNA was reverse transcribed with 250 U MultiScribe Reverse Transcriptase (Applied Biosystems) by using random primers. Relative amounts of *egl-1* cDNA were subsequently estimated by real-time quantitative PCR in an ABI Prism 7700 Sequence detector system, by using the primers 5′-CAGGACTTCTCCTCGTGTGAAGATTC-3′ and 5′-GAAGTCATCG CACATTGCTGCTA-3′, which span the single *egl-1* intron. 18S rRNA was used for the internal standard. Average fold induction represents the relative expression of *egl-1* following irradiation (sample) compared to the untreated control (calibrator), normalized based on 18S rRNA levels.

Supplementary Material

Supplementary Material including comparative data of cell cycle arrest and radiation sensitivities of both *hus-1* alleles (Figure S1) as well as additional methodological detail is available at http://images.cellpress.com/supmat/supmatin.htm.

Acknowledgments

We thank B. Derry and J. Rothman for the *ced-1(w40)* mutant and the *C. elegans* Knockout Consortium for *ced-1(gk138)*; V. Pratis and J. Austin for the *unc-119* genomic rescuing plasmid and the bombardment protocol; A. Fire for pPD117.01, pPD135.83, and pPD129.36; Y. Kohara for cDNA clone yk238e9; A. Coulson for the cTel55x plasmid; and A. Brincat for help with bombardment. We thank A. Hajnal and members of the Hengartner Lab for comments. Some *C. elegans* strains were obtained from the *Caenorhabditis* Genetics Center, which is funded by the National Institutes of Health (NIH) National Center for Research Resources (NCRR). This work was supported by grants from the NIH (GM52540 to M.O.H., F32 GM20801 to E.R.H., and 7 R33 CA81658-02 to S.J.B. and M.V.) and the Ernst Hadorn Foundation (to M.O.H.).

Received: May 12, 2002
Revised: September 18, 2002
Accepted: September 23, 2002
Published: November 19, 2002

References

1. Hoeijmakers, J.H. (2001). Genome maintenance mechanisms for preventing cancer. Nature *411*, 366–374.
2. Rich, T., Allen, R.L., and Wyllie, A.H. (2000). Defying death after DNA damage. Nature *407*, 777–783.
3. Bach, S.P., Renehan, A.G., and Potten, C.S. (2000). Stem cells: the intestinal stem cell as a paradigm. Carcinogenesis *21*, 469–476.
4. Heyer, B.S., MacAuley, A., Behrendtsen, O., and Werb, Z. (2000). Hypersensitivity to DNA damage leads to increased apoptosis during early mouse development. Genes Dev. *14*, 2072–2084.
5. Murakami, H., and Nurse, P. (2000). DNA replication and damage checkpoints and meiotic cell cycle controls in the fission and budding yeasts. Biochem. J. *349*, 1–12.
6. Bentley, N.J., Holtzman, D.A., Flaggs, G., Keegan, K.S., DeMaggio, A., Ford, J.C., Hoekstra, M., and Carr, A.M. (1996). The *Schizosaccharomyces pombe rad3* checkpoint gene. EMBO J. *15*, 6641–6651.
7. Horvitz, H.R. (1999). Genetic control of programmed cell death in the nematode *Caenorhabditis elegans*. Cancer Res. *59*, 1701s–1706s.
8. Gumienny, T.L., Lambie, E., Hartwieg, E., Horvitz, H.R., and Hengartner, M.O. (1999). Genetic control of programmed cell death in the *Caenorhabditis elegans* hermaphrodite germline. Development *126*, 1011–1022.
9. Gartner, A., Milstein, S., Ahmed, S., Hodgkin, J., and Hengartner, M.O. (2000). A conserved checkpoint pathway mediates DNA damage-induced apoptosis and cell cycle arrest in *C. elegans*. Mol. Cell *5*, 435–443.
10. Hofmann, E.R., Milstein, S., and Hengartner, M.O. (2000). DNA damage-induced checkpoint pathways in the nematode *Caenorhabditis elegans*. Cold Spring Harb. Symp. Quant. Biol. *65*, 467–473.
11. Ahmed, S., Alpi, A., Hengartner, M.O., and Gartner, A. (2001). *C. elegans* RAD-5/CLK-2 defines a new DNA damage checkpoint protein. Curr. Biol. *11*, 1934–1944.
12. Derry, W.B., Putzke, A.P., and Rothman, J.H. (2001). *Caenorhabditis elegans* p53: role in apoptosis, meiosis, and stress resistance. Science *294*, 591–595.
13. Schumacher, B., Hofmann, K., Boulton, S., and Gartner, A. (2001). The *C. elegans* homolog of the p53 tumor suppressor

is required for DNA damage-induced apoptosis. Curr. Biol. *11*, 1722–1727.
14. Venclovas, C., and Thelen, M.P. (2000). Structure-based predictions of Rad1, Rad9, Hus1 and Rad17 participation in sliding clamp and clamp-loading complexes. Nucleic Acids Res. *28*, 2481–2493.
15. Boulton, S.J., Gartner, A., Reboul, J., Vaglio, P., Dyson, N., Hill, D.E., and Vidal, M. (2002). Combined functional genomic maps of the *C. elegans* DNA damage response. Science *295*, 127–131.
16. Caspari, T., Dahlen, M., Kanter-Smoler, G., Lindsay, H.D., Hofmann, K., Papadimitriou, K., Sunnerhagen, P., and Carr, A.M. (2000). Characterization of *Schizosaccharomyces pombe* Hus1: a PCNA-related protein that associates with Rad1 and Rad9. Mol. Cell. Biol. *20*, 1254–1262.
17. Kaur, R., Kostrub, C.F., and Enoch, T. (2001). Structure-function analysis of fission yeast Hus1-Rad1-Rad9 checkpoint complex. Mol. Biol. Cell *12*, 3744–3758.
18. Zou, L., Cortez, D., and Elledge, S.J. (2002). Regulation of ATR substrate selection by Rad17-dependent loading of Rad9 complexes onto chromatin. Genes Dev. *16*, 198–208.
19. Takanami, T., Mori, A., Takahashi, H., and Higashitani, A. (2000). Hyper-resistance of meiotic cells to radiation due to a strong expression of a single recA-like gene in *Caenorhabditis elegans*. Nucleic Acids Res. *28*, 4232–4236.
20. Hodgkin, J., Horvitz, H.R., and Brenner, S. (1979). Nondisjunction mutants of the nematode *Caenorhabditis elegans*. Genetics *91*, 67–94.
21. Chin, G.M., and Villeneuve, A.M. (2001). *C. elegans mre-11* is required for meiotic recombination and DNA repair but is dispensable for the meiotic G(2) DNA damage checkpoint. Genes Dev. *15*, 522–534.
22. Ahmed, S., and Hodgkin, J. (2000). MRT-2 checkpoint protein is required for germline immortality and telomere replication in *C. elegans*. Nature *403*, 159–164.
23. Myung, K., Datta, A., and Kolodner, R.D. (2001). Suppression of spontaneous chromosomal rearrangements by S phase checkpoint functions in *Saccharomyces cerevisiae*. Cell *104*, 397–408.
24. Myung, K., Chen, C., and Kolodner, R.D. (2001). Multiple pathways cooperate in the suppression of genome instability in *Saccharomyces cerevisiae*. Nature *411*, 1073–1076.
25. De Stasio, E., Lephoto, C., Azuma, L., Holst, C., Stanislaus, D., and Uttam, J. (1997). Characterization of revertants of *unc-93(e1500)* in *Caenorhabditis elegans* induced by N-ethyl-N-nitrosourea. Genetics *147*, 597–608.
26. Conradt, B., and Horvitz, H.R. (1999). The TRA-1A sex determination protein of *C. elegans* regulates sexually dimorphic cell deaths by repressing the *egl-1* cell death activator gene. Cell *98*, 317–327.
27. Feng, H., Zhong, W., Punkosdy, G., Gu, S., Zhou, L., Seabolt, E.K., and Kipreos, E.T. (1999). CUL-2 is required for the G1-to-S-phase transition and mitotic chromosome condensation in *Caenorhabditis elegans*. Nat. Cell Biol. *1*, 486–492.
28. Hong, Y., Roy, R., and Ambros, V. (1998). Developmental regulation of a cyclin-dependent kinase inhibitor controls postembryonic cell cycle progression in *Caenorhabditis elegans*. Development *125*, 3585–3597.
29. Bunz, F., Dutriaux, A., Lengauer, C., Waldman, T., Zhou, S., Brown, J.P., Sedivy, J.M., Kinzler, K.W., and Vogelstein, B. (1998). Requirement for p53 and p21 to sustain G2 arrest after DNA damage. Science *282*, 1497–1501.
30. Weiss, R.S., Enoch, T., and Leder, P. (2000). Inactivation of mouse Hus1 results in genomic instability and impaired responses to genotoxic stress. Genes Dev. *14*, 1886–1898.
31. Dahlen, M., Olsson, T., Kanter-Smoler, G., Ramne, A., and Sunnerhagen, P. (1998). Regulation of telomere length by checkpoint genes in *Schizosaccharomyces pombe*. Mol. Biol. Cell *9*, 511–521.
32. Ollmann, M., Young, L.M., Di Como, C.J., Karim, F., Belvin, M., Robertson, S., Whittaker, K., Demsky, M., Fisher, W.W., Buchman, A., et al. (2000). *Drosophila* p53 is a structural and functional homolog of the tumor suppressor p53. Cell *101*, 91–101.
33. Boxem, M., Srinivasan, D.G., and van den Heuvel, S. (1999). The *Caenorhabditis elegans* gene *ncc-1* encodes a *cdc2*-related kinase required for M phase in meiotic and mitotic cell divisions, but not for S phase. Development *126*, 2227–2239.
34. Ashcroft, N., and Golden, A. (2002). CDC-25.1 regulates germline proliferation in *Caenorhabditis elegans*. Genesis *33*, 1–7.
35. Miyashita, T., and Reed, J.C. (1995). Tumor suppressor p53 is a direct transcriptional activator of the human Bax gene. Cell *80*, 293–299.
36. Oda, E., Ohki, R., Murasawa, H., Nemoto, J., Shibue, T., Yamashita, T., Tokino, T., Taniguchi, T., and Tanaka, N. (2000). Noxa, a BH3-only member of the Bcl-2 family and candidate mediator of p53-induced apoptosis. Science *288*, 1053–1058.
37. Nakano, K., and Vousden, K.H. (2001). PUMA, a novel proapoptotic gene, is induced by p53. Mol. Cell *7*, 683–694.
38. Yu, J., Zhang, L., Hwang, P.M., Kinzler, K.W., and Vogelstein, B. (2001). PUMA induces the rapid apoptosis of colorectal cancer cells. Mol. Cell *7*, 673–682.
39. Barlow, C., Brown, K.D., Deng, C.X., Tagle, D.A., and Wynshaw-Boris, A. (1997). Atm selectively regulates distinct p53-dependent cell-cycle checkpoint and apoptotic pathways. Nat. Genet. *17*, 453–456.
40. Weiss, R.S., Matsuoka, S., Elledge, S.J., and Leder, P. (2002). Hus1 acts upstream of Chk1 in a mammalian DNA damage response pathway. Curr. Biol. *12*, 73–77.
41. Herzog, K.H., Chong, M.J., Kapsetaki, M., Morgan, J.I., and McKinnon, P.J. (1998). Requirement for Atm in ionizing radiation-induced cell death in the developing central nervous system. Science *280*, 1089–1091.
42. Symonds, H., Krall, L., Remington, L., Saenz-Robles, M., Lowe, S., Jacks, T., and Van Dyke, T. (1994). p53-dependent apoptosis suppresses tumor growth and progression *in vivo*. Cell *78*, 703–711.
43. Liu, Q., Guntuku, S., Cui, X.S., Matsuoka, S., Cortez, D., Tamai, K., Luo, G., Carattini-Rivera, S., DeMayo, F., Bradley, A., et al. (2000). Chk1 is an essential kinase that is regulated by Atr and required for the G(2)/M DNA damage checkpoint. Genes Dev. *14*, 1448–1459.
44. Brown, E.J., and Baltimore, D. (2000). ATR disruption leads to chromosomal fragmentation and early embryonic lethality. Genes Dev. *14*, 397–402.
45. Jansen, G., Hazendonk, E., Thijssen, K.L., and Plasterk, R.H. (1997). Reverse genetics by chemical mutagenesis in *Caenorhabditis elegans*. Nat. Genet. *17*, 119–121.
46. Praitis, V., Casey, E., Collar, D., and Austin, J. (2001). Creation of low-copy integrated transgenic lines in *Caenorhabditis elegans*. Genetics *157*, 1217–1226.
47. Greenwald, I.S., and Horvitz, H.R. (1980). *unc-93(e1500)*: a behavioral mutant of *Caenorhabditis elegans* that defines a gene with a wild-type null phenotype. Genetics *96*, 147–164.

2.1. Transcriptional regulation of BH3-only domain proteins

2.1.1. Ionizing radiation induces *egl-1* transcript upregulation in a *hus-1*- and *cep-1*-dependent manner (Figure 6B)

The BH3-only domain protein, EGL-1, is required for apoptosis during somatic development and is transcriptionally regulated in order to activate the apoptotic machinery (Conradt and Horvitz, 1999). Already in Figure 6A, the observation that *egl-1* transcripts are increased upon ionizing radiation and during time, prompted us to look for the genetic requirements for this induction. For this reason I established the real-time quantitative RT-PCR method to measure precisely this alteration in *egl-1* mRNA levels in certain genetic backgrounds. Confirming the Northern result, in the *hus-1(op244)* mutants *egl-1* induction is compromised. In the *cep-1(w40)* mutants, there are still some transcripts detectable upon DNA damage, compared to the *cep-1(gk138)* where this response is completely abrogated. This is consistent with the presence of a wild-type copy of *cep-1* in the former background, whereas the latter is a null. To validate the Q-RT-PCR data, I repeated the Northern analysis (Figure 1). To our surprise, in the *cep-1(w40)* mutant, the signal was much stronger, but this is probably due to a saturation effect and a limitation of the technique.

To make sure that the transcriptional up-regulation is restricted to the germline tissue where apoptosis is also observed, I used the *glp-4(bn2)* mutants. The animals lack a germline, and the comparison between the soma and the germline was feasible. Indeed, the induction we observed in the wild-type was totally abolished. This finding

is also in agreement with the lack of radiation-induced apoptosis in young adult animals, in any other tissue but the germline (Gartner *et al.*, 2000).

2.1.2. *egl-1* is regulated at the transcriptional and not the post-transcriptional level upon ionizing radiation

The question then arose of whether the increase in the mRNA levels is actually due to a transcriptional induction or occurs at the post-transcriptional level. To test this possibility I used the *ama-1(m118)* mutants, which carry a mutation in the large subunit of RNA polymerase II, required for mRNA transcription. The *m118* mutation confers resistance to the toxin α-amanitin, whereas in wild-type worms the activity of the protein is inhibited by half at a toxin concentration of 0.007 μg/mL (Table 1) (Rogalski *et al.*, 1988, Sanford *et al.*, 1983, Bullerjahn and Riddle, 1988). The change in the mRNA levels of *egl-1* upon ionizing radiation was measured then in wild-type worms in the presence or absence of α-amanitin. The gene failed to be induced when the worms were fed with the toxin prior to treatment with X-rays, showing to us that transcription could be blocked efficiently upon stress. Moreover, the *ama-1(m118)* mutants, which can grow and reproduce in concentrations of α-amanitin that arrest development of wild type animals, did not show a significant decrease in the presence of the toxin (6.1-fold compared to 1.6-fold, Table 2), although the response seemed to be much weaker in the first place (6.1-fold compared to 61-fold, Table 2).

2.1.3. Transcriptional regulation of *egl-1* and *ced-13* occurs also during development

Already at the beginning of my thesis I was really astonished by the fine regulation of the phenomenon of apoptosis in the nematode, and its spatial restriction in the germline tissue in response to an external stimulus like ionizing radiation. I wanted, therefore, to test if there is an effect at the molecular level in the soma. I quantified the initial and the final (upon application of X-rays) transcript levels of both *egl-1* and *ced-13*, the two so far known BH3-only proteins, at all developmental stages. As Figure 2 shows, both genes are already expressed in the embryos, with *ced-13* being quite abundant. This is consistent, first, with the established role of *egl-1* in mediating all the somatic cell deaths (Conradt and Horvitz, 1998), and second with the recent finding that overexpression of *ced-13* in the embryos induces cell death in a *ced-3*, *ced-4* and *ced-9*-dependent manner (Schumacher *et al*., 2005). Both the genes are then silenced during the L1 and L2L3 larval stages and transcripts begin to appear again at the L4 and young adult stages, supporting their role in the subsequent death decision upon DNA damage. The unexpected finding, though, that ionizing radiation results in an increase at their transcripts in animals that do not have a fully developed germline, yet, raises the question as to where this is attributed to. Could there be an effect in the soma that never reaches, though, the final output of the execution fate, meaning the apoptotic event itself?

Indeed, we are very much interested in clarifying this and additional observations that we made the following years, as to the involvement of the soma in the DNA damage responses (see future directions, Chapter 8) . For this we are in an ongoing collaboration with Prof. Koo HS from the Yonsei University in Seoul.

References

Bullerjahn, A.M. & Riddle, D.L. Fine-structure genetics of *ama-1*, an essential gene encoding the amanitin-binding subunit of RNA polymerase II in *Caenorhabditis elegans*. *Genetics* **120(2)**, 423-34 (1988).

Conradt, B. & Horvitz, H.R. The *C. elegans* protein EGL-1 is required for programmed cell death and interacts with the Bcl-2-like protein CED-9. *Cell* **93(4)**, 519–29 (1998).

Conradt, B. & Horvitz, H.R. The TRA-1A sex determination protein of *C. elegans* regulates sexually dimorphic cell deaths by repressing the *egl-1* cell death activator gene. *Cell* **98**, 317-327 (1999).

Gartner, A., Milstein, S., Ahmed, S., Hodgkin, J. & Hengartner, M.O. A conserved checkpoint pathway mediates DNA damage-induced apoptosis and cell cycle arrest in *C. elegans*. *Mol. Cell* **5**, 435-443 (2000).

Murakami, H. & Nurse, P. DNA replication and damage checkpoints and meiotic cell cycle controls in the fission and budding yeasts. *Biochem. J.* **349**, 1-12 (2000).

Rogalski, T.M., Bullerjahn, A.M. & Riddle, D.L. Lethal and amanitin-resistance mutations in the Caenorhabditis elegans *ama-1* and *ama-2* genes. *Genetics* **120(2)**, 409-22 (1988).

Sanford, T., Golomb, M. & Riddle, D.L. SanRNA polymerase II from wild type and alpha-amanitin-resistant strains of *Caenorhabditis elegans*. *J Biol Chem* **258(21)**, 12804-9 (1983).

Schumacher, B., Schertel, C., Wittenburg, N., Tuck, S., Mitani, S., Gartner, A., Conradt, B. & Shaham, S. *C. elegans ced-13* can promote apoptosis and is induced in response to DNA damage. *Cell Death Differ*. **12(2)**, 153-61 (2005).

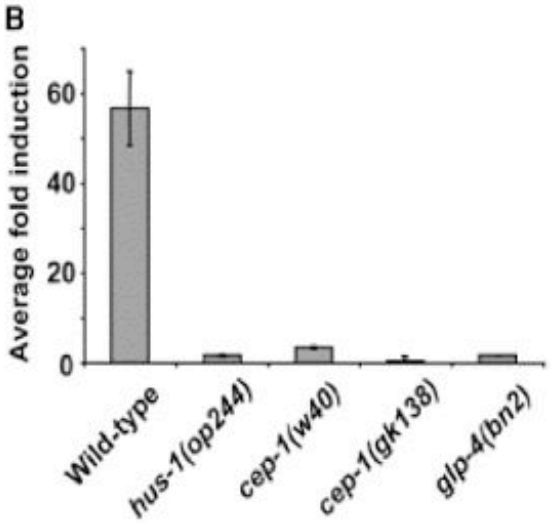

Figure 6B. *egl-1* is transcriptionally induced by irradiation in a *hus-1*- and *cep-1*-dependent manner

Average fold induction of *egl-1* gene expression in wild-type, *hus-1(op244)*, *cep-1(w40)*, *cep-1(gk138)*, and *glp-4(bn2)* mutants after 100 Gy X-ray irradiation as determined by real-time quantitative RT-PCR. *glp-4(bn2)* worms were grown at the non permissive temperature, and 90–100 worms were selected that lacked a germline. Each bar represents the average ± SD.

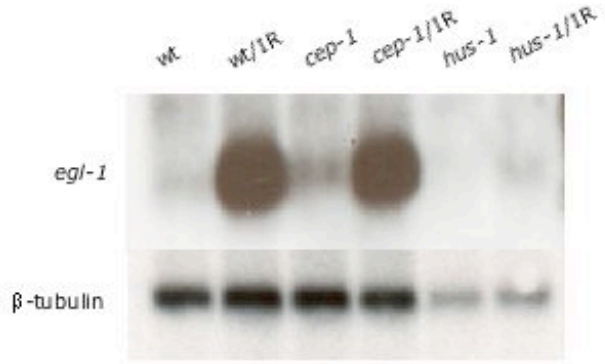

Figure 1. Transcriptional induction of *egl-1* upon ionizing radiation is compromised in *hus-1(op244)* mutants

Northern blot analysis of *egl-1* mRNA in wild-type worms and in *cep-1(w40)* and *hus-1(op244)* mutants, before and 3 h after treatment with 120 Gy of X-rays. A 500 nt genomic fragment from the *egl-1* locus was radiolabeled (Strip-EZ DNA kit, Ambion) and used as a probe on a blot where total RNA had been transfered. Northern analysis was performed using the NorthernMax kit (Ambion). β-tubulin was used as an internal control.

Table 1. Inhibition of the RNA PolII activity by the toxin α-amanitin

Two mutations in the large subunit of RNA PolII that confer resistance to the toxin α-amanitin are described below. The concentrations with which inhibition of the activity of each one of the RNA polymerases is succeeded, are mentioned.

	RNA Pol II	RNA Pol III	RNA Pol I
	50% inhibition by		0% inhibition by
WT	0.007 μg/mL	25±10 μg/mL	500 μg/mL
ama-1(m118)	1 μg/mL		
**** ama-1(m118m526)***	150 μg/mL		

* 150x more resistant than *m118*

* 20000x more resistant than wt

Table 2. Transcriptional induction of *egl-1* upon ionizing radiation is compromised in the presence of α-amanitin

The change in the mRNA levels of *egl-1* was determined by real-time Q-RT-PCR, 3 h following treatment with 120 Gy of X-rays. Wild-type worms and *ama-1(m118)* mutants were used, either after treatment with 15 ng/mL of α-amanitin or in the absence of the toxin. Data shown is the average fold-change of two independent experiments.

	***egl-1* induction** α**-amanitin**		
	-	**+**	**fold-decrease**
wt	61	0.2	300
ama-1(m118)	6.1	1.6	4

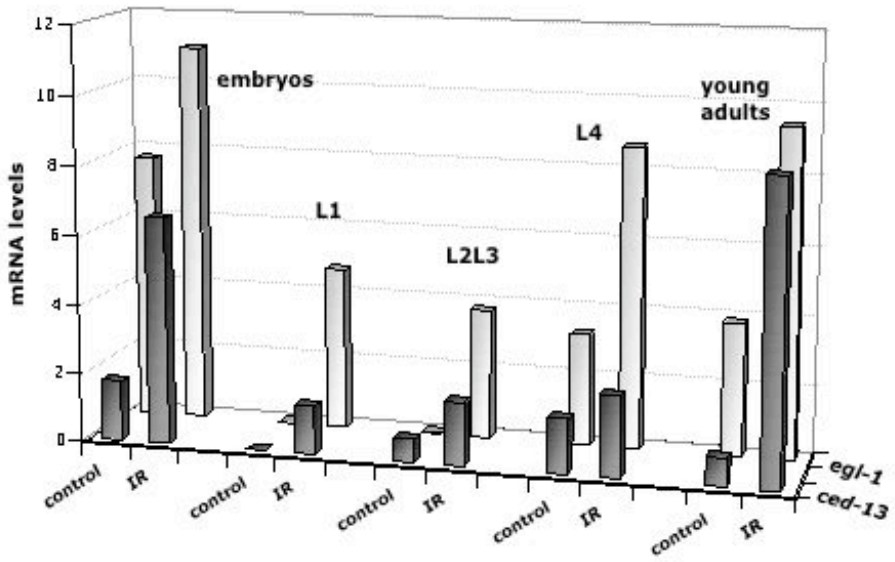

Figure 2. Transcriptional regulation of *egl-1* and *ced-13* during development and upon ionizing radiation

The mRNA levels of *egl-1* and *ced-13* at all the developmental stages of wild-type animals were determined by real-time Q-RT-PCR. Moreover, animals were exposed to 120 Gy of X-rays and transcriptional levels were again quantified 3 h following treatment. Data shown are expressed in a.u.

CHAPTER 3

FUNCTIONAL GENOMICS ANALYSIS TO STUDY DNA DAMAGE TRANSCRIPTIONAL RESPONSES UPON IONIZING RADIATION IN *CAENORHABDITIS ELEGANS*

Preface

Eukaryotic cells mount a robust and complex response to DNA damage, that translates into arrest of the cell cycle, initiation of repair pathways and culminates in cell death in case of non-repairable damage. Nowadays, we are witnessing an accumulative amount of data regarding these events and an explosive scientific interest.

Because DNA damage responsive networks embrace groups of highly connected genes and proteins and because multiple interconnected cellular pathways respond to damage, we decided to undertake a genome-wide approach and study these phenomena.

The DNA microarray technology has a great deal of potential, due to the fact that there are a number of features advantageous to its use. The biggest advantage concerns the ability to study the behavior of many genes simultaneously, enabling the comprehensive molecular "profiling" of different organisms.

I utilized cDNA microarrays to develop the gene expression profile for ionizing radiation-exposed wild-type animals and animals treated with the mutagenic agent ENU. In order to relate the changes in the expression profiles to the underlying biological processes, I also used two different genetic backgrounds. Namely, the *hus-1(op244)* and the *cep-1(gk138)* mutants were also exposed to ionizing radiation and subsequently monitored for a change in the transcriptional profile. I was hoping to find genes that are related to the recognition of DNA damage, to a halt in cell cycle progression and to the activation of the apoptotic process. By differential analysis, I

could be able to identify genes that depend on the two players of the ionizing radiation pathway mentioned above, for their induction.

3.1. Experimental set-up of the microarray analysis

3.1.1. The strategy of the microarray experiment and the Affymetrix GeneChip technology

As every researcher embarking on a microarray project, I had to concisely document all the stages of the experiment. A simple technical definition for a microarray experiment refers to "a set of one or more hybridizations, each of which relates one or more samples to one or more arrays". Figure 1 shows the pipeline of the experiment, starting from the experimental design that was made to elucidate the questions I wanted to answer (discussed later, Table 1). To succeed my goal, Prof. Michael Hengartner initiated a collaboration with the pharmaceutical company Hoffmann-La Roche in Basel, and the laboratory of Prof. Patrick Nef.

The technology that was already established in this lab was the Affymetrix GeneChip technology. A brief description of the basic principles, accompanied by a schematic representation of the chip design is shown in Figure 2. The Affymetrix GeneChip technology is a high-density probe array where DNA targets in the form of oligonucleotide probes are chemically synthesized on a solid phase with the use of photolithographic techniques. The whole *C. elegans* genome (18683 predicted genes) is mounted on two chips (Figure 2A). The oligonucleotide probe is designed such that the sequence information comes from the 3' end of the mRNA (Figure 2B). Each gene on the array is represented by 14 cells or features, which are clusters of 10000 identical sequences (Figure 2C). On the upper row, the probes match perfectly the mRNA from which they were designed (called matched probes). On the lower row,

the probes have the same sequence except that there is a single mismatch in the middle to ascertain the degree of cross hybridization. After hybridization takes place, both signals are detected by a laser scanner (Figure 1). When the upper signal is stronger than the lower, the software, which further does the analysis, calculates the difference for each pair and then takes the average signal intensity. To reach meaningful biological conclusions, one needs to perform multiple experiments, including replicates and compare these with each other (Figure 1). Therefore, the previous calculation is done three times for the three independent samples per experimental condition to obtain the mean hybridization intensity (Figure 2C).

3.1.2. Sample preparation for the hybridization onto the chips

The chemistry that was applied to prepare the probe to be hybridized onto the chips is summarized in the schematic graph of Figure 3. The labeling procedure begins with the synthesis of cDNA from the mRNA molecules by means of an oligo (dT) primer linked to an RNA polymerase promoter region. Antisense RNA is then transcribed from the cDNA by T7 RNA polymerase, which also incorporates a DIG modified nucleotide (dUTP-DIG). Extraneous mRNA is then removed from the mixture. After purification, the DIG-labeled cDNA is ready for hybridization to the microarray, where a signal, based on the degree of the gene expression in the initial sample, will be generated.

3.1.3. Normalization of the results of the Affymetrix GeneChip technology

In microarray experiments there are many sources of systematic variation, which affect the measured gene expression levels. Normalization is the term used to describe the process of removing such variation.

Most methods of normalization make the assumption that the average (geometric mean) ratio is 1, or the average (arithmetic mean) log ratio is zero. Namely, that the average gene does not change its expression under the condition being studied. Typically, a normalization method has two components. First, a set of elements on the microarray is selected, and second, that set of elements is used to calculate either a normalization value, or normalization function, which is then be applied to all of, or a subset of, the raw data.

From the few possible methods for element selection, we (in the laboratories of Roche) chose the so-called 'control elements'. Certain elements on the array exist specifically for normalization purposes, and transcripts that will hybridize to them are spiked into the labeling mix at known concentration. The method of choice to calculate a normalization factor or function was the 'intensity-dependent normalization'. A function is generated using the selected elements that is intensity-dependent. This function is then applied to the data.

3.1.4. Independence and reproducibility of the microarray experiment

The issue of reproducibility across microarray platforms is an important one for the robust analysis of the results obtained. To assess data quality and reliability, therefore,

one needs information arising from repetitions of the experiment. In these experiments we proceeded with biological repeats, which is actually the source of the greatest noise in most of the cases.

Comparing two of the "wild-type" arrays generated the scatter plot shown in Figure 4. The correlation coefficient (r) of the log2 values of the normalized hybridization signal intensity was calculated in a pair-wise fashion, using all the genes. Each data point corresponds to the compiled normalized weighted average of the spot on a single microarray that corresponds to one gene. The red lines demarcate threshold values (change factors 1 and 4) that were set up by me to control the differences in gene expression relative to the inner black line. Generally, the microarrays should give highly reproducible results with typically very few genes showing greater than 2-fold differences between different measurements (change factor 1). In this comparison, the number of genes with a change factor of more than 1 and less than –1 was 1642, a 8.8% of the total number. The number of genes with a change factor of more than 4 and less than –4 was only 56, that is, 0.3% of the total genes regulated. I kept the genes that showed values bigger than a "cut off" value of 10 (to eliminate undesirable signals), and at the same time the genes that lied between the two inner red lines. After all these checkpoints, I ended up with 93% of the genes from the two wild-type replicates, having a very similar signal intensity. The same analysis was performed for every biological replicate in a pair-wise fashion. I obtained a strong positive correlation for all the cases, indicating a high degree of reproducibility for my results.

3.2. Data processing of the microarray analysis

3.2.1. Visualization of the differential gene expression

A high degree of data reproducibility allowed me to make further comparisons between the datasets. It might also facilitate in the future comparisons between specific data sets within any database, obtained by a totally independent scientific experiment.

In the scatter plot shown in Figure 5, I tried to correlate the results from a "wild-type" and a "wild-type/IR" array. Similar to the already described process, the correlation coefficient (r) of the log2 values of the signal intensity was calculated in a pair-wise fashion. Each data point corresponds to the compiled normalized weighted average of the spot on a single microarray that corresponds to one gene. The red lines demarcate threshold values (change factors 1 and 4) that were set up by me to monitor the differences in gene expression relative to the inner black line, which represents no change at all. Spots that are spread beyond the two inner red lines, representing a 2-fold induction or repression in the gene expression levels, were kept as significant changes. Again the "cut off" value was set at 10, to eliminate undesirable signals. The total number of genes found to be regulated under these conditions was 565. Representing data this way makes it easy to view results and immediately detect genes that display an interesting change in their expression upon any treatment.

3.2.2. Gene expression profiling in *C. elegans* upon treatment with ionizing radiation and ENU

In the microarray study that I performed, I anticipated to detect large-scale changes in gene expression after ionizing radiation and application of damage with the alkylating agent ENU. As briefly mentioned in paragraph 3.1.1, the experimental design was done in a way such that I am able to identify downstream targets and effectors of defined genes that have been clearly implicated in DNA damage responses. These are the checkpoint gene, *hus-1*, and the p53 homolog, *cep-1*. Additionally, I expected to discover new ways of regulation of the DNA damage signal, via potentially new pathways. Table 1 shows the overall output of the microarray experiments. The conditions I analyzed with regard to the genotypes used and the conditions I compared, are all described. The number of genes found to be regulated (up- or down-) under each condition tested is also included.

Of attention is the list with the 49 genes that showed no change between *hus-1* mutants and wild-type animals, and no change even after irradiation was applied on the mutants. These genes I conferred are dependent on *hus-1* for induction, and are therefore referred to as the "HUS-1-dependent set". A similar list with 178 genes was generated, with the ones that showed no change between the *cep-1* mutants and the wild-type animals, or after irradiation of the mutants. These genes I concluded to be dependent on *cep-1* for induction, and are therefore referred to as the "CEP-1-dependent set". A long list of genes regulated up- and down- was generated upon ENU treatment of the wild-type, some of them being in common with the "IR responsive set".

The whole experimental output in the form of lists, where the precise change factor [$\log_2$(fold-change in mRNA)] for each condition tested is written, can be viewed in the Tables 2-7. The lists contain also a short description of the gene to be affected, as it is annotated in WormBase.

3.2.3. Validation of the microarray results using real-time Q-RT-PCR

One of the most important steps before proceeding with the analysis of the microarray experiments is to find a way to validate the results. Verification methods insure that one has received the correct molecular information from the microarrays, since both the technical and biological treatments can affect the measured expression.

I applied quantitative real-time RT-PCR as the method of validation. A number of genes from the "IR" and the "ENU" experimental set were picked randomly to test for a change in their mRNA levels. In Table 8, the results are expressed as fold-change and the microarray values are shown for comparison. Values that would fall into a reasonable range defined arbitrarily were kept as a positive result. Moreover, the same tendency in one genetic background (wild-type) and lack of such a trend in a mutant background (*hus-1* or *cep*-1) was regarded as a reliable result. Among the 26 genes tested, 19 were confirmed in this way. Although this is only a small fraction represented by this method, it is considered indicative of the power of the microarray technique.

Overall, the real-time RT-PCR confirmed the majority of the microarray results (87%), giving a physiological relevance of the transcriptional responses measured to the biological phenomenon we are studying.

3.2.4. Hierarchical clustering analysis

It is particularly advantageous to visualize overall similarities and differences in the expression patterns observed in a microarray experiment. By this means, one could find interesting internal structures or relationships in a given data set. Hierarchical clustering is a commonly used technique in genomic data analysis that enables this.

A general definition of clustering is the segmentation in a collection of objects into subsets or 'clusters', such that those within each cluster are more closely related to one another than objects assigned to different clusters. Hierarchical clustering may be represented by a two-dimensional diagram known as dendrogram, which illustrates the fusions or divisions made at each successive stage of the analysis.

After having obtained the expression of individual genes in a numerical form, I used the hierarchical clustering method to group genes in relatively homogenous clusters, representing a similar expression profile. For this reason, I applied the Cluster and Treeview software.

Figure 6 displays the results for the "HUS-1-dependent set", containing 49 genes, as a dendrogram and in color mosaic pattern. The color scale shows the trend and levels of expression, whereas the column headings refer to the conditions analyzed (see table under the figure). The genes are arranged in a continuum profile, which is subdivided into two major expression clusters. As an example, genes in the lower cluster do not only remain unchanged (as in the upper cluster, black color) but are actually repressed upon ionizing radiation in the absence of the HUS-1 protein.

In Figure 7 the results for the "CEP-1-dependent set", containing 178 genes, are depicted. Similarly, with the green color the down-regulated genes are shown, with red the induced ones, whereas black means no change. This profile is subdivided into four major expression clusters. Highlighted is part of the third cluster. The last two clusters are the 'signature' of the response to irradiation, which are actually the genes that remain unchanged in the absence of CEP-1. Another example is the upper most cluster, which is characterized by a consistent and strong repression upon irradiation in the wild-type and at the same time no change in expression in the *cep-1* background.

3.3. Functional classification of the identified genes

3.3.1. Distribution of the "IR" and the "ENU" experimental set into functional classes

The microarray experiment I performed was designed in such a way that it could profile gene expression patterns in *C. elegans* upon DNA damage and identify genes that are particularly affected by genotoxic stress. To identify cellular functions that might be critical for proper DNA damage responses, I tried to determine whether certain classes of genes would be represented in the total output.

In Figure 8, I used the total number of genes that were found to be regulated (up- or down-) upon ionizing radiation in all the different genetic backgrounds tested (wild-type, *hus-1* and *cep-1* mutants) to generate a pie chart. The gene annotations

were derived from WormBase and were used to manually place the genes into functional classes. The numbers of genes in each class are shown.

Among the genes that belong to an obvious class, genes encoding protein kinases were the most abundant ones, representing a 27.5%. Both serine/threonine and tyrosine kinases are included and the vast majority is predicted to be cytoplasmic kinases rather than receptor kinases. Likewise, both serine/threonine and tyrosine protein phosphatases were present, constituting 16.2% of the non-metabolic genes. Because the DNA damage responsive pathways are known to be activated phosphorylation cascades, these results confirm the involvement of such protein equivalents in the response and strongly imply the identification of potentially novel genes. Neither ATM nor ATR, the initiators of the mammalian DNA damage signaling network (discussed in detail in chapter 5), nor the immediate downstream targets of theirs, checkpoint kinases Chk1 and Chk2, were members of the kinase group. This is not surprising, though, since there is no real evidence for transcriptional regulation, as a mode for their activation. It has been clear that activation is restricted to the post-translational level, either via interaction with DNA or with repair complexes (Shiloh, 2003, Lee & Paull, 2005, Cortez *et al.*, 2001, Ng *et al.*, 2004, Falck *et al.*, 2001, Liu et l., 2000, Tanaka *et al.*, 2001). The same holds true for the mitogen-activated kinases (MAPKs), which, upon activation by various sources of genotoxic stress, transduce the signals to the nucleus (Yang *et al.*, 2003).

The “IR” cluster was particularly enriched in ribosomal proteins (18%), either subunits of the 40S or the 60S complex, or proteins that have to do with ribosomal biogenesis. Being the final step in the flow of the genetic information, translation and

the regulation at this level allows an immediate, rapid and reversible response to changes in physiological conditions. Especially during conditions of cellular stress, this type of regulation is quite advantageous. Under such circumstances, global translation is reduced, both to preserve energy and to prevent the synthesis of unnecessary proteins. Confirming this notion, the majority of the gene products of the ribosomal genes identified are part of the ribosomal assembly complex and found to be down-regulated. Notably, though, the stress-induced attenuation of global translation is often accompanied by translation of a selective set of proteins that are required either for cell survival or for cell demise under stress (Harding *et al.*, 2000, Holcik *et al.*, 2000, Holcik and Sonenberg, 2005). Indeed, in the "IR-responsive" set, a small number of ribosomal-related genes were found to be up-regulated, but the protein function is not linked to any known or characterized proteins. At the moment, though, it is not possible to explain how specific the transcriptional regulation of these proteins after treatment with ionizing radiation is to the stress response.

A small fraction from the non-metabolic class of genes included proteins linked to the cell cycle progression control. The transition from one cell cycle phase to another occurs in an orderly fashion and is regulated by different cellular proteins. Key regulatory proteins are the cyclin-dependent kinases (CDK), a family of serine/threonine protein kinases that are activated at specific points of the cell cycle and whose protein levels remain stable during the cell cycle. In contrast, cyclins, their activating proteins, contain sequences required for efficient ubiquitin-mediated proteolysis at the end of a cell cycle phase (Cyclins A and B contain a destruction box, cyclins D and E contain a PEST motif). In this study, two G2 specific cyclins, one not previously characterized in *C. elegans* and the other *cyb-3*, were identified.

Components of the multiple protein complex that includes the SCF ubiquitin ligase were represented more than once. The worm homolog genes, which are called *skr-4* and *skr-5*, are, though, uncharacterized. In yeast such complexes have been found to ubiquitinate proteins during the G1/S transition, leading them to degradation (Connelly and Hieter, 1996, Zachariae and Nasmyth, 1999).

Moreover, the gene coding for a DNA-binding cell cycle division control protein, *mat-1*, belongs to this group. The yeast homolog is a subunit of the Anaphase-Promoting Complex/Cyclosome (APC/C), a ubiquitin-protein ligase required for degradation of anaphase inhibitors, including mitotic cyclins, during the metaphase/anaphase transition (Tugendreich, 1995, Zachariae and Nasmyth, 1999). The equivalent gene in humans is p27Kip1, known for its implication in various human cancers (Nho and Sheaff, 2003, Coqueret, 2003). Indeed, a group of cell cycle inhibitory proteins, called CDK inhibitors, can counteract CDK activity. In mammals, the Cip/Kip family (p21 (Waf1, Cip1), p27, p57) inactivates G1/CDK complexes and to a lesser extent CDK1-cyclin B complexes. Interestingly, the expression of p21 is under transcriptional control of the p53 tumor suppressor gene (el Deiry *et al*., 1993). The INK4 family (including p15, p16, p18, p19) specifically inactivates G1/CDK(4,6) complexes.

The nature of the cell cycle proteins that were found to be regulated upon ionizing radiation, in all the genetic backgrounds examined, implies a possible mode of regulation of the cell cycle arrest response in *C. elegans*. Since there is no information available as to how the cell cycle is ceased in worms, a more careful approach of this study might shed light into these events.

A similar analysis was performed, where I used all the genes that were found to be regulated (up- or down-) upon ENU treatment in the wild-type. The gene annotations were derived from WormBase and were used to manually place the genes into functional classes. Figure 9 shows the pie chart that was generated that way, with the numbers of genes in each class shown.

Genes coding for protein kinases, both serine/threonine and tyrosine, were again the most abundant ones, representing a 30.6% of the non-metabolic genes. Likewise, serine/threonine and tyrosine protein phosphatases were present at a 16%.

The "ENU" cluster was similarly overrepresented by ribosomal proteins (25.1%), both subunits of the 40S or the 60S complex, and proteins that are related to ribosomal biogenesis.

Genes that are related to the cell cycle progression control were also identified. The biggest portion was G2 mitotic specific cyclins, with *cyb-3* and *cyb-1* among them. The phosphatase *cdc-25.3*, a member of the cell division cycle 25 (CDC25) family of cell cycle regulators that includes *S. pombe* CDC25 and Drosophila string, and one of four *cdc-25* genes in *C. elegans*, appeared in this subgroup. Cell cycle arrest in the G2 phase, for example, is known to be initiated both in the presence and absence of p53, via inhibition of Cdc25 and activation of p21, as already presented in Chapter 1.

Moreover, a fair number of repair genes were recognized, in both the "IR" and "ENU" clusters (10.8% and 5.9% of the non-metabolic clustered genes, respectively). These either belong to the double strand break repair or the nucleotide excision repair machinery. Representatives of the former ones in the "IR" group, are the recombinational repair gene *rad-54* (see Chapter 5 for a detailed analysis) and the yeast Rad18 homolog, a protein involved in structural maintenance of chromosomes and required for interchromosomal and sister chromatid recombination (Lehmann *et al.*, 1995). The *mre-11* gene, the human homolog of which is part of a complex subunit with Rad50 and Nbs1 (MRN complex) which functions in repair of DNA double-strand breaks and in telomere stability, was part of the "ENU" group (Chin and Villeneuve, 2001). The homolog of the human XPF gene, a single-stranded DNA endonuclease that cleaves single-stranded DNA during nucleotide excision repair and double-strand break repair, as well as the yeast gene Rad16, the product of which recognizes and binds damaged DNA in an ATP-dependent manner (with Rad7) during nucleotide excision repair (Reed *et al.*, 1998) were identified to be regulated upon ionizing radiation. On the other hand, the homolog of the XPG human gene, a single-stranded DNA endonuclease that cleaves single-stranded DNA during nucleotide excision repair appeared to be regulated upon ENU treatment (de Laat, 1999). Rad23, a subunit of the nucleotide excision repair factor 2 in yeast belonged into the same group (Prakash and Prakash, 2000, Jansen *et al.*, 1998).

The fact that members of both major repair pathways appeared in this analysis is quite expected and consistent with the types of lesions that need to be repaired upon application of either X-rays or ENU. As a general statement, though, repair genes were rather down-regulated, at least under the conditions I chose to perform the

experiment (time-points and doses selected). The important issue is the nature of the genes whose transcriptional levels were altered upon DNA damage.

Several helicases were recognized as being members of both clusters. The action of DNA helicases is required in fundamental cellular processes such as DNA replication, repair, recombination, and transcription. From the known crystal structures it appears that the enzymatic machinery of DNA helicases has been highly conserved, although their functions can be distinguished by co-factor utilization, substrate preference, directionality of unwinding, processivity, and interaction with other proteins (Villani and Le Gac, 2000). In *C. elegans* only three of those have been characterized to a certain extent. The Bloom's syndrome RecQ helicase homolog, *him-6*, gives rise to an enhanced irradiation sensitivity phenotype, a partially defective S-phase checkpoint and reduced levels of DNA-damage induced apoptosis, when mutated (Wicky *et al*., 2004). The Werner syndrome protein homolog, *wrn-1*, was shown to act as a checkpoint protein for DNA damage and replication blockage (Lee *et al*., 2004). Mutant animals for the RecQ5 homolog, *rcq-5*, are significantly more sensitive to ionizing radiation, implying a possible involvement for the protein in DNA repair (Jeong *et al*., 2003). Because DNA helicases are among the first proteins that would encounter DNA damage during these processes, a complete understanding of their interaction with lesions is crucial.

Minority in this subgroup were RNA helicases, members of the DExD/H-box family, shown in other organisms to be involved in many processes and complexes within the cell. While individual members have been studied extensively, the mechanisms through which they affect multiprotein complexes are just beginning to

be investigated (Silverman *et al.*, 2003). Our knowledge in *C. elegans* about their modulation and action is very poor.

Interestingly, under treatment with both sources of genotoxic stress, the worm homolog of the BRCA1 tumor suppressor gene was identified. It was shown recently that mutant *brc-1* animals display abnormalities, such as elevated levels of p53-dependent germ cell death before and after irradiation, and impaired progeny survival and chromosome fragmentation after irradiation (Boulton *et al.*, 2004).

Last but not least, an important class of genes that is the main interest of both my project and the area of focus of other members of the lab, is the pro-apoptotic or pro-survival genes. The two already characterized and known to be transcriptionally regulated upon DNA damage pro-apoptotic factors, *egl-1* and *ced-13*, failed to be recognized since there was no sequence tethered for them on the chip. *ced-9*, the only *C. elegans* homolog of Bcl-2, major inhibitor of developmental and radiation-induced cell deaths (Hengartner *et al.*, 1992, Gartner *et al.*, 2000) was found to be down-regulated upon ENU treatment.

The recently identified (Schumacher *et al.*, 2005), sole suppressor of the *C. elegans* p53, *gld-1*, is similarly repressed. The same way that study had shown that the regulation of *cep-1* translation influences DNA damage-induced apoptosis, this study reveals the potent need for repression of negative regulation on *cep-1*, for the proper induction of cell death.

A gene with inhibitor of apoptosis domains, member of the baculoviral inhibitor-of-apoptosis (IAP) repeat (BIR) proteins (BIRPs) family, *bir-1*, appeared to be also down-regulated. The protein has only been shown to be part of the Aurora B kinase complex in *C. elegans*, a critical regulator of chromosome segregation and

cytokinesis, required for AIR-2 (Aurora B) localization (Romano *et al.*, 2003). No direct function in apoptosis, though, has been established for the protein yet (Fraser *et al.*, 1999).

Among the repressed genes, this study also identified *mac-1* whose product has been found to be a CED-4 interactor, member of the AAA ATPases (Wu *et al.*, 1999). The protein was shown to form a multi-protein complex that also includes CED-3 or CED-9 and in mammalian cells, it could prevent initiation of death by CED-4 and CED-3. The way the last two described genes might regulate cell death upon DNA damage is unclear at the moment, but it might be worth of investigation.

Finally, the only known death related gene that I could recognize down-regulated in the list of "IR" genes was *nuc-1*. This is the DNase II homolog in worms which functions in an intermediate step of apoptotic DNA degradation, after the killing step and prior to engulfment (Wu *et al.*, 2000). At the same time it is required for the degradation of dietary DNA. In an independent forward genetic screen performed by Dr A. Gartner, with subsequent mapping by Kimon Doukoumetzidis in our lab, *nuc-1* was identified as a gene that results in increased apoptosis, when mutated. Ongoing studies by the latter have revealed a possible role in DNA damage responses (Doukoumetzidis K., unpublished data). Interestingly, several *crn* genes (cell death-related nucleases) have human homologs that are important for RNA processing, protein folding, DNA replication, and DNA damage repair (Parrish and Xue, 2003).

3.3.2. Differential distribution of the "IR" gene set into the different genetic backgrounds – functional groups

The rationale of using the two mutant backgrounds in this microarray analysis was, as already mentioned, to recover genes that depend on HUS-1 and CEP-1 for their transcriptional induction. For the first case, these sets of genes are listed in Table 4 where, genes that are up-regulated in the wild-type in response to ionizing radiation, but do not show any change in the *hus-1(op244)* background, were selected to be presented.

The linearity of the IR-pathway, though, with *cep-1* acting downstream of *hus-1*, made it reasonable to search for genes that require only HUS-1 or both proteins to become transcriptionally activated. In Table 9, the 21 genes that I manually recovered and found to belong to the former category are indicated. The predicted gene function was obtained from WormBase and the NCBI Blast tool. To receive information about germline expression, the tissue I study and mostly see the DNA damage responses, I looked into reported microarray experiments (Kim S. lab, Stanford Microarray Database) and RNA in situ hybridization data (Kohara group). For 12 out of the 14 genes for which information exists in either database, there was expression of the transcript in the germline. Considering, at the period when I did the analysis, that some of these genes could be important to further study I started looking for mutants. Some were already available in the *C. elegans* Gene Knockout Consortium (CGC), some others I requested to be generated. The alleles that are up to this moment available are shown in the third column of the table. For two of these mutants I am presenting additional information in the paragraphs to follow.

Following this analysis, I chose to select for the genes from each experimental set (wild-type, *hus-1(op244)*, *cep-1(gk138)*) that were up-regulated in wild-type or remain unchanged in the mutants after IR. With those I designed a Venn Diagram, as a way to compare the gene sets and identify common members, illustrated in Figure 10. The number of genes that fall into each category are indicated in the circles. The overlap between any two circles shows the common individuals between these two sets. The intersection among the three sections of the diagram (the dark red area) represents the 28 genes whose transcriptional induction is dependent on both HUS-1 and CEP-1.

Table 10 summarizes the above genes with the predicted gene function obtained from WormBase and the NCBI Blast tool. Information about germline expression was again retrieved from reported microarray experiments (Kim S. lab, Stanford Microarray Database) and RNA in situ hybridization data (Kohara group). For 16 out of the 18 genes for which information exists in either database, there was expression of the transcript in the germline. As mentioned earlier, I looked for available mutants or requested their generation from the CGC.

To visualize which functional classes are represented by the "HUS-1/CEP-1 common set", I generated I pie chart (Figure 11). Gene annotations were derived from WormBase and were used to manually place these genes into functional groups. The number of genes in each group is shown. The distribution of these 28 potential downstream effectors of HUS-1 and CEP-1 is quite divergent. It ranges from proteins involved in the translational / transcriptional process (activators or repressors or ribosome-related proteins) and signaling molecules, to enzymatic molecules (methyl- and acetyl-transferases) and proteins involved in the degradation process by the

proteasome. Various other classes concern mitochondrial and structural proteins, as well as transporters or ion channels.

3.3.3. Descriptive analysis and preliminary characterization of some "IR"-responsive genes

Below follows a short description of some of the genes I was able to find information about in the literature, either after having been characterized in *C. elegans* or another model organism, such as the yeasts or mouse, or after having been described in humans. I present this information for each gene separately and I also show a basic analysis I performed for some of these genes :

C36B7.6

The gene codes for cleft lip and palate transmembrane protein 1 (CLPTM1). Several eukaryotic sequences comprise a family. Cleft lip, with or without cleft palate, is a common birth defect that is genetically complex. The nonsyndromic forms have been studied genetically using linkage and candidate-gene association studies with only partial success in defining the loci responsible for orofacial clefting. CLPTM1 encodes a transmembrane protein and has strong homology to two *C. elegans* genes, suggesting that CLPTM1 may belong to a new gene family. This family also contains the human cisplatin resistance related protein CRR9p, which is associated with cisplatin-induced apoptosis. The connection of this protein with the response to ionizing radiation is at the moment elusive.

F29B9.1

The gene encodes a methyltransferase with a SAM binding motif. Transfer of the methyl group from the ubiquitous S-adenosyl-L-methionine (AdoMet) to either nitrogen, oxygen or carbon atoms is frequently employed in diverse organisms ranging from bacteria to plants and mammals. The reaction is catalyzed by methyltransferases and modifies DNA, RNA, proteins and small molecules, such as catechol for regulatory purposes. The various aspects of the role of DNA methylation in a number of cellular processes in eukaryotes, including gene regulation and differentiation, is well documented (Jeltsch, 2002).

F54D10.7

This is the *C. elegans* homolog of the SMC4 yeast gene. The evolutionarily-conserved eukaryotic SMC (structural maintenance of chromosomes) proteins are ubiquitous chromosomal components in prokaryotes and eukaryotes. The eukaryotic SMC proteins form two kind of heterodimers: the SMC1/SMC3 and the SMC2/SMC4 types, that constitute an essential part of higher order complexes involved in chromatin and DNA dynamics. The two most prominent and best-characterized complexes are cohesin and condensin. The Smc4 protein is a subunit of the condensin complex which, together with its Smc2p partner that has ATP-hydrolyzing and DNA-binding activity, reorganizes chromosomes during cell division (Strunnikov and Jessberger, 1999, Stray and Lindsley, 2003). In a recent study the Smc4 protein was identified as a substrate for Cdk1 activity, the only Cdk that controls cell cycle in *S.*

cerevisiae (Ubersax, 2003). Careful analysis of this *in vivo* phosphorylation event is likely to yield insights into cell-cycle regulation.

K03D10.3

The gene codes for a MYST histone acetyltransferase. In *S. cerevisiae* the protein is the catalytic subunit of the native multisubunit complex (NuA4) that acetylates nucleosomal histone H4 at the N-terminal tail. The protein is the product of the ESA1 gene, an essential gene required for cell cycle progression (Allard *et al.*, 1999). Temperature-sensitive mutant alleles abolish the enzymatic activity *in vitro* and result in partial loss of an acetylated isoform of histone H4 *in vivo*. Yeast strains carrying these mutations, although succeed in replicating their DNA, they fail to proceed normally through mitosis and cytokinesis (Clarke *et al.*, 1999).

Interestingly, another subunit of the NuA4 complex is the product of TRA1, an ATM-related essential gene homologous to human TRRAP, essential cofactor for c-Myc- and E2F-mediated oncogenic transformation (Allard *et al.*, 1999). The function of the essential Esa1 protein as the HAT subunit of NuA4 and the presence of Tra1p supports an essential link between histone dynamic modification, transcriptional regulation and cell cycle control.

K08E3.8 (*mdt-29*)

"MDT" is a unified nomenclature for protein subunits of mediator complexes linking transcriptional regulators to RNA polymerase II (Bourbon *et al.*, 2004). Promoter-specific initiation of transcription by RNA polymerase II (Pol II) requires

both gene-specific regulators and general transcription factors (GTFs). Biochemical and genetic studies in yeast led to the discovery of a Mediator (MED) complex of 20 protein subunits, linking transcriptional regulators to Pol II and GTFs. *In vitro*, Mediator stimulates basal transcription, enables activated transcription, and relieves the interfering effect of a strong transcriptional activator (Kim *et al*., 1994). Further genetic studies demonstrated the role of Mediator in repression as well as activation, and established the relevance of Mediator to transcription control *in vivo*.

T06D8.8 (*rpn-9*)

In worms *rpn-9* is predicted to encode a non-ATPase subunit of the 19S regulatory complex of the proteasome. It contains a PINT motif (Proteasome, Int-6, Nip-1 and TRIP-15), a homology domain that occurs in the C-terminal region of several regulatory components of the 26S proteasome. Apparently, all of the characterized proteins containing such domains are parts of larger multi-protein complexes. Proteins with PINT domains include budding yeast proteasome regulatory components Rpn3(Sun2), Rpn5, Rpn6, Rpn7 and Rpn9 ; mammalian proteasome regulatory components p55, p58 and p44.5, and translation initiation factor 3 complex subunits p110 and INT6 ; and several uncharacterized ORFs from plants, nematodes and mammals.

In yeast, the *rpn-9* homolog is a non-ATPase regulatory subunit of the 26S proteasome, with the null mutant being temperature sensitive and exhibiting proteasome assembly defects. Moreover, the cells arrest in G2/M of the cell cycle and show slow degradation of the anaphase and M phase inhibitors, Pds1p and Clb2p, respectively (Takeuchi and Toh-e, 2001). Knocking down the gene in worms affects

body morphology, embryonic viability, locomotion, larval viability, fertility, and growth. These are the only phenotypes that have been identified in a screen for genes involved in control of cell division in the ectoderm (Mengarelli *et al.*, West Coast Meeting, 2004).

rpn-9 was one of the genes for which I had requested a CGC mutant strain. The homozygote *rpn-9* animals are sterile because of severe meiotic defects. As Figure 12 shows there is practically no pachytene zone, despite the presence of a normal looking mitotic region and transition zone. For this reason, there are also defects in oogenesis, without any normally developed oocyte. Additionally, there are "gaps" in the germline, "ring structures" that look like empty space or necrotic areas. For DNA damage phenotypes in *rpn-9(gk401)* animals in terms of apoptosis and cell cycle arrest I had, therefore, to look in the heterozygote animals. Figures 13 shows the apoptotic phenotype in the course of time upon 120 Gy of X-rays.

Overall, the animals display reduced apoptosis, with a two to three-fold decrease in the number of corpses compared to the wild-type. However, the initial levels of cell death are slightly increased and there is a further increase upon IR at later time-points. A defect in cell cycle arrest was hard to score for in the heterozygote *gk401*, but interestingly enough the homozygote mutants show mitotic cells that are enlarged, even in the absence or IR (see Figure 12). This might suggest a permanent arrest in one of the cell cycle phases, concomitant with the yeast phenotype. At the moment it is unclear where the lack of death observed is attributed. On a hypothetical basis, the protein could have a pro-survival factor as a substrate to lead to degradation under conditions of genotoxic stress that would normally require the initiation of cell death.

T09B4.10 (*chn-1*)

The gene name stands for C-term of Hsp70-iNteracting protein. The protein belongs to the CHIP family of proteins and acts as a chaperone-dependent E3 ubiquitin ligase. The protein contains a modified RING finger domain, without the full complement of Zn^{2+}-binding ligands, guiding to its involvement in E2-dependent ubiquitination. To succeed quality control of intracellular proteins, an essential step for cellular homeostasis, molecular chaperones recognize and contribute to the refolding of misfolded or unfolded proteins. In addition, the ubiquitin-proteasome system mediates the degradation of such abnormal proteins. Ubiquitin-protein ligases (E3s) determine the substrate specificity for ubiquitylation and have been classified into HECT and RING-finger families. More recently proteins that contain a U box of about 70 amino acids that is conserved from yeast to humans, have been identified as a new type of E3. All mammalian U-box proteins have been reported to interact with molecular chaperones or co-chaperones, (including Hsp90, Hsp70, DnaJc7, EKN1, CRN, and VCP), acting as assistants that modulate the folding machinery in a positive or negative manner. CHIP is such a cofactor that interacts with Hsp70 and, in general, attenuates its most well characterized functions. In addition, CHIP accelerates ubiquitin-dependent degradation of chaperone substrates. Surprisingly, a major target of the ubiquitin ligase activity of CHIP is Hsc70 itself (Jiang *et al*., 2001).

The amino acid sequence also contains tetratrico peptide repeats (TPR), a structural motif present in a wide range of proteins, known to mediate protein-protein interactions and the assembly of multiprotein complexes. The TPR motif consists of 316 tandem-repeats of 34 amino acids residues, although individual TPR motifs can be dispersed in the protein sequence. Such motifs have been identified in various

different organisms, ranging from bacteria to humans. Proteins containing TPRs are involved in a variety of biological processes, such as cell cycle regulation, transcriptional control, mitochondrial and peroxisomal protein transport, neurogenesis and protein folding.

There are recent reports that the mammalian CHIP activates HSF1 and confers protection against apoptosis and cellular stress (Dai *et al.*, 2003). Induction of molecular chaperones is regulated by a transcriptional program that depends on heat shock factor 1 (HSF1), which is normally under negative regulatory control by molecular chaperones Hsp70 and Hsp90. That study demonstrated that CHIP regulates activation of the stress-chaperone response through induced trimerization and transcriptional activation of HSF1, and is required for protection against stress-induced apoptosis in murine fibroblasts. Mice lacking CHIP, develop normally but are temperature-sensitive and develop apoptosis in multiple organs after environmental challenge.

Another report showed that CHIP is associated with Parkin, a gene responsible for familial Parkinson's disease, and enhances its ubiquitin ligase activity (Imai *et al.*, 2002). The unfolded Pael receptor (Pael-R) is a substrate of the E3 ubiquitin ligase Parkin. Accumulation of Pael-R in the endoplasmic reticulum (ER) of dopaminergic neurons induces ER stress leading to neurodegeneration. CHIP, Hsp70, Parkin, and Pael-R were shown to form a complex with the amount of CHIP being increased during ER stress. CHIP promoted the dissociation of Hsp70 from Parkin and Pael-R, thus facilitating Parkin-mediated Pael-R ubiquitination. Furthermore, CHIP enhanced the ability of Parkin to inhibit cell death induced by Pael-R.

In *C. elegans* loss of CHIP function arrests the development of the animal at the larval stage (Khan and Nukina, 2004). The gene is expressed ubiquitously in all tissues with some tissue specific variations, though. A dose dependent phenotype was observed *in vivo*. Although overexpression of CHIP causes embryonic lethality, a comparatively lower level of over expression causes locomotion and egg laying defects.

I tested the role of *chn-1* in DNA damage responses, since it was another gene for which I had requested a CGC mutant strain. The homozygote *chn-1(ok459)* animals arrest at early larval stages, and the heterozygotes display a partially penetrant germline phenotype, with morphological defects at the pachytene zone. Therefore, I decided to look for an apoptotic phenotype in animals that were exposed to RNAi after the L1 stage. Figure 14 shows the number of corpses in two different time-points after the L4 stage, after gene inactivation in a wild-type, *ced-3(n717)*, *cep-1(gk138)* and *hus-1(op244)* background. The initial levels of cell death in *chn-1(RNAi)* are clearly elevated and this is also in agreement with the mutant phenotype (6.8 ±2.2 corpses at the 12h-post L4 stage). This death is caspase-mediated since it is abrogated in a *ced-3(lf)* background. Moreover, it is likely induced by endogenous DNA damage, since *cep-1(lf)* completely blocks it. In contrast to that, *hus-1(lf)* fails to suppress this death, suggesting that the checkpoint protein is not required for sensing this damage. Subsequently, the apoptotic response was followed up in the course of time, before and after the application of X-rays. As is illustrated in Figure 15, there is successful induction of apoptosis upon IR, although the fold-induction is nearly half of that of the wild-type (see Figure 13 for comparison). The same result is also presented in Figure 16 and in addition to that, the UV apoptotic response was measured. For reasons that will only become clear in Chapter 5, I will not comment

extensively on the obtained result at this point, although there seems to be a defect upon this type of stress.

Whether the *C. elegans* CHN-1 exerts a role in tuning the response to stress by regulation of protein quality control, remains to be elucidated. An appealing hypothesis would be the regulation, in terms of protein degradation, of a pro-apoptotic factor whose improper accumulation leads to the increased levels of death in a *chn-1* loss of function situation.

T24H7.1 (*phb-2*)

The gene product is a subunit of the mitochondrial ProHiBitin complex. Prohibitins comprise a remarkably conserved protein family in eukaryotic cells with proposed functions in cell cycle progression, senescence, apoptosis, and the regulation of mitochondrial activities. Two prohibitin homologues in yeast, Phb1 and Phb2, were shown to assemble into a high molecular weight complex in the mitochondrial inner membrane, forming membrane-bound rings (Tatsuta *et al.*, 2005). Deletion of the two *S. cerevisiae* genes results in a defect in mitochondrial membrane potential and a decreased replicative lifespan, connecting the metabolic efficiency of the cells with the ageing process (Coates *et al.*, 1997).

In mammalian cells, prohibitin was identified as a potential regulator of growth arrest and a tumor suppressor (McClung *et al.*, 1995, Nuell *et al.*, 1991). In yeast there is evidence of a role for prohibitin in mitochondrial inheritance and in the regulation of mitochondrial morphology (Berger and Yaffe, 1998).

Prohibitins in *C. elegans*, similarly to yeast and humans, form a high molecular weight complex in the mitochondrial inner membrane. RNA-mediated gene

inactivation, has shown that they are essential during embryonic development and are required for somatic and germline differentiation in the larval gonad (Artal-Sanz *et al.*, 2003).

What the implication of the worm protein in the cellular responses to DNA damage is remains largely unknown. The previous knowledge that abundance in the prohibitin transcripts blocks entry into S phase of cultured cells, therefore proliferation, in combination with the amenability of the worm to genetic analysis might shed more light into the functions of the protein in diverse cellular processes, including development and tumor suppression.

W08E3.1 (*snr-2*)

The gene codes for a small nuclear ribonucleoprotein, a U1 snRNP component very well conserved in humans. The U1, U2, U4/U6, and U5 small nuclear ribonucleoprotein particles (snRNPs) are involved in pre-mRNA splicing. They have seven Sm proteins (B/B', D1, D2, D3, E, F and G) in common, which assemble around the Sm site present in four of the major spliceosomal small nuclear RNAs. The Sm proteins are essential for pre-mRNA splicing and facilitate RNA-protein interactions and structural changes required for the formation of stable, biologically active snRNP structures (Kufel *et al.*, 2003). Sm proteins are also found in archaebacteria, which do not have any splicing apparatus, suggesting a more general role for these proteins.

In *C. elegans* there is a mutant available, which in a homozygote state confers embryonic lethality, consistent with the role of the gene in RNA biogenesis and

function. This phenotype hinders further analysis to elucidate the role, if any, of *snr-2* in DNA damage responses.

W04B5.5

This gene encodes a phospholipid-independent AKT/PKB kinase, homologous to the human 3-phosphoinositide dependent protein kinase-1 (hPDK1). In *S. pombe* the protein is a serine/threonine protein kinase, known as ksg1, involved in the control of cell cycle arrest via a phosphoinositide signaling pathway. The gene is essential for growth, mating and sporulation, since mutant cells undergo growth arrest in the G2 phase of the cell cycle at the restrictive temperature (Niederberger and Schweingruber, 1999). Additional studies showed that ksg1 is a novel regulator of cell wall integrity in the fission yeast (Graub *et al*., 2003). In *S. cerevisiae* the protein is named PKH1 (Pkb-activating Kinase Homolog) and is involved in the sphingolipid-mediated signaling pathway that controls the internalization step of endocytosis (Friant *et al*., 2001). Interestingly enough, a downstream kinase of PDK1 in mammals, SGK (serum- and glucocorticoid-inducible kinase 1), has been reported to be significantly induced in a p53-dependent manner after DNA damage. This induction occurred through ERK (extracellular signal-regulated kinase 1/2)-mediated post-translational regulation (You *et al*., 2004), and resulted in the inhibition of the FOXO3a activity.

The *C. elegans* homolog belongs to the serine or threonine-specific kinase subfamily. Structurally, it contains a conserved catalytic core but lacks a phospholipid binding pleckstrin homology domain, suggestive of its phospholipids-independent

kinase activity. The so-called PIAK worm protein was found to phosphorylate mammalian AKT/PKB and activate the survival pathway that may be utilized during periods of cellular quiescence (Li, *et al.*, 2001).

W04B5.5 was one of the genes for which the CGC generated a mutant strain for me. I looked at the *ok1309* allele for DNA damage phenotypes in terms of apoptosis and cell cycle arrest. Figure 17 shows the apoptotic response in the course of time, after the animals where irradiated with 120 Gy of X-rays. The overall behavior suggests a defect in the activation of apoptosis, with a three-fold decrease in the number of corpses compared to the wild-type. However, there is a gradual increase in the death levels at later time-points, suggesting that the worm homolog of the 3-phosphoinositide dependent protein kinase-1 shares redundancy with another protein. I observed no defect in cell cycle arrest upon ionizing radiation (data not shown) but a role for the protein in DNA repair cannot be excluded, since embryonic lethality upon IR was elevated compared to the wild-type levels (approximately 30% vs 3%) (Figure 18).

Although further analysis is required, I speculate that this 3-phosphoinositide dependent protein kinase-1-like could act in an antagonistic to the *C. elegans* SGK-1 pathway to mediate general stress or DNA damage responses. Indeed, the latter has been shown to be a crucial factor for the control of development, stress response, and longevity (Hertweck *et al.*, 2004). It acts in parallel to the AKT-1/2 kinases to mediate DAF-2 signaling, and together with PDK-1 (homolog of the isoform 1 of human 3-phosphoinositide dependent protein kinase-1) is able to directly phosphorylate and inactivate DAF-16/FKHRL1.

In the last decade we have experienced a rapid expansion in the field of functional genomics, mainly due to the global gene expression profiling capabilities provided by techniques, such as microarray analysis. Application of this technology in very diverse fields shows the versatility of this tool and the potential to revolutionize biological research.

Identifying genes that are differentially expressed in response to DNA damage may help elucidate markers for genetic damage and provide insight into the cellular responses to specific genotoxic agents.

The current study provided us with a plethora of data, but the benefits that this study might hold have not yet been exploited to their full power. I anticipate, though, that it could expand our understanding of the DNA damage signaling networks regulating the responses of the nematode *C. elegans* to ionizing radiation and other sources of genotoxic stress.

References

Adams, R.R., Carmena, M. & Earnshaw, W.C. Chromosomal passengers and the (aurora) ABCs of mitosis. *Trends Cell Biol*. **11(2)**, 49-54 (2001).

Allard, S., Utley, R.T., Savard, J., Clarke, A., Grant, P., Brandl, C.J., Pillus, L., Workman, J.L. & Cote, J. NuA4, an essential transcription adaptor/histone H4 acetyltransferase complex containing Esa1p and the ATM-related cofactor Tra1p. *EMBO J*. **18(18)**, 5108-19 (1999).

Artal-Sanz, M., Tsang, W.Y., Willems, E.M., Grivell, L.A., Lemire, B.D., van der Spek, H. & Nijtmans, L.G. The mitochondrial prohibitin complex is essential for embryonic viability and germline function in Caenorhabditis elegans. *J Biol Chem*. **278(34)**, 32091-9 (2003).

Berger, K.H. & Yaffe, M.P. Prohibitin family members interact genetically with mitochondrial inheritance components in Saccharomyces cerevisiae. *Mol Cell Biol*. **18(7)**, 4043-52 (1998).

Boulton, S.J., Martin, J.S., Polanowska, J., Hill, D.E., Gartner, A. & Vidal, M. BRCA1/BARD1 orthologs required for DNA repair in *Caenorhabditis elegans*. *Curr Biol*. **14(1)**, 33-9 (2004).

Bourbon, H.M., *et al*. A unified nomenclature for protein subunits of mediator

complexes linking transcriptional regulators to RNA polymerase II. *Mol Cell*. **14(5)**, 553-7 (2004).

Brenner, S. The genetics of Caenorhabditis elegans. *Genetics* **77(1)**, 71-94 (1974).

Chin, G.M. & Villeneuve, A.M. *C. elegans mre-11* is required for meiotic recombination and DNA repair but is dispensable for the meiotic G(2) DNA damage checkpoint. *Genes Dev*. **15(5)**, 522-34 (2001).

Clarke, A.S., Lowell, J.E., Jacobson, S.J. & Pillus, L. Esa1p is an essential histone acetyltransferase required for cell cycle progression. *Mol Cell Biol.* **19(4)**, 2515-26 (1999).

Coates, P.J., Jamieson, D.J., Smart, K., Prescott, A.R. & Hall PA. The prohibitin family of mitochondrial proteins regulate replicative lifespan. *Curr Biol*. **7(8)**, 607-10 (1997).

Connelly, C. & Hieter, P. Budding yeast SKP1 encodes an evolutionarily conserved kinetochore protein required for cell cycle progression. *Cell* **86(2)**, 275-85 (1996).

Coqueret, O. New roles for p21 and p27 cell-cycle inhibitors: a function for each cell compartment? *Trends Cell Biol*. **13(2)**, 65-70 (2003).

Cortez, D., Guntuku, S., Qin, J. & Elledge, S.J. ATR and ATRIP: partners in checkpoint signaling. *Science* **294(5547)**, 1713-6 (2001).

Dai, Q., Zhang, C., Wu, Y., McDonough, H., Whaley, R.A., Godfrey, V., Li, H.H., Madamanchi, N., Xu, W., Neckers, L., Cyr, D. & Patterson, C. CHIP activates HSF1 and confers protection against apoptosis and cellular stress. *EMBO J.* **22(20)**, 5446-58 (2003).

el-Deiry, W.S., Tokino, T., Velculescu, V.E., Levy, D.B., Parsons, R., Trent, J.M., Lin, D., Mercer, W.E., Kinzler, K.W. & Vogelstein, B. WAF1, a potential mediator of p53 tumor suppression.

Ellis, N.A. DNA helicases in inherited human disorders. *Curr Opin Genet Dev*. **7(3)**, 354-63 (1997).

Falck, J., Mailand, N., Syljuasen, R.G., Bartek, J. & Lukas, J. The ATM-Chk2-Cdc25A checkpoint pathway guards against radioresistant DNA synthesis. *Nature* **410(6830)**, 842-7 (2001).

Fraser, A.G., James, C., Evan, G.I. & Hengartner, M.O. *Caenorhabditis elegans* inhibitor of apoptosis protein (IAP) homologue BIR-1 plays a conserved role in cytokinesis. *Curr Biol*. **9(6)**:292-301 (1999).

Friant, S., Lombardi, R., Schmelzle, T., Hall, M.N., Riezman, H. Sphingoid base signaling via Pkh kinases is required for endocytosis in yeast. *EMBO J.* **20(23)**, 6783-92 (2001).

Gartner, A., Milstein, S., Ahmed, S., Hodgkin, J. & Hengartner, M.O. A conserved

checkpoint pathway mediates DNA damage--induced apoptosis and cell cycle arrest in *C. elegans*. *Mol. Cell* **5**, 435-443 (2000).

Graub, R., Hilti, N., Niederberger, C. & Schweingruber, M.E. Ksg1, a homologue of the phosphoinositide-dependent protein kinase 1, controls cell wall integrity in Schizosaccharomyces pombe. *J Basic Microbiol*. **43(6)**, 473-82 (2003).

Harding, H.P., Novoa, I., Zhang, Y., Zeng, H., Wek, R., Schapira, M. & Ron, D. Regulated translation initiation controls stress-induced gene expression in mammalian cells. *Mol Cell* **6(5)**, 1099-108 (2000).

Hengartner, M.O., Ellis, R.E. & Horvitz, H.R. *Caenorhabditis elegans* gene *ced-9* protects cells from programmed cell death. *Nature*. **356(6369)**, 494-9 (1992).

Hertweck, M., Gobel, C., & Baumeister, R. C. elegans SGK-1 is the critical component in the Akt/PKB kinase complex to control stress response and life span. *Dev Cell* **6(4)**, 577-88 (2004).

Holcik, M. & Sonenberg, N. Translational control in stress and apoptosis. *Nat Rev Mol Cell Biol*. **6(4)**, 318-27 (2005).

Holcik, M., Sonenberg, N. & Korneluk, R.G. Internal ribosome initiation of translation and the control of cell death. *Trends Genet*. **16(10)**, 469-73 (2000).

Imai, Y., Soda, M., Hatakeyama, S., Akagi, T., Hashikawa, T., Nakayama, K.I. & Takahashi, R. CHIP is associated with Parkin, a gene responsible for familial Parkinson's disease, and enhances its ubiquitin ligase activity. *Mol Cell* **10(1)**, 55-67 (2002).

Jansen, L.E., Verhage, R.A. & Brouwer, J. Preferential binding of yeast Rad4.Rad23 complex to damaged DNA. *J Biol Chem.* **273(50)**, 33111-4 (1998).

Jeltsch, A. Beyond Watson and Crick: DNA methylation and molecular enzymology of DNA methyltransferases. *Chembiochem.* **3(4)**, 274-93 (2002).

Jeong, Y.S., Kang, Y., Lim, K.H., Lee, M.H., Lee, J. & Koo, H.S. Deficiency of *Caenorhabditis elegans* RecQ5 homologue reduces life span and increases sensitivity to ionizing radiation. *DNA Repair (Amst).* **2(12)**, 1309-19 (2003).

Jiang, J., Ballinger, C.A., Wu, Y., Dai, Q., Cyr, D.M., Hohfeld, J. & Patterson, C. CHIP is a U-box-dependent E3 ubiquitin ligase: identification of Hsc70 as a target for ubiquitylation. *J Biol Chem.* **276(46)**, 42938-44 (2001).

Juang, Y.L., Huang, J., Peters, J.M., McLaughlin, M.E., Tai, C.Y. & Pellman D. APC-mediated proteolysis of Ase1 and the morphogenesis of the mitotic spindle. *Science* **275(5304)**, 1311-4 (1997).

Kamath, R.S., Fraser, A.G., Dong, Y., Poulin, G., Durbin, R., Gotta, M., Kanapin, A., Le Bot, N., Moreno, S., Sohrmann, M., Welchman, D.P., Zipperlen, P., & Ahringer, J.

Systematic functional analysis of the Caenorhabditis elegans genome using RNAi. *Nature* **421(6920)**, 231-7 (2003).

Khan, L.A. & Nukina, N. Molecular and functional analysis of Caenorhabditis elegans CHIP, a homologue of Mammalian CHIP. *FEBS Lett*. **565(1-3)**, 11-8 (2004).

Kim, Y.J., Bjorklund, S., Li, Y., Sayre, M.H. & Kornberg, R.D. A multiprotein mediator of transcriptional activation and its interaction with the C-terminal repeat domain of RNA polymerase II. *Cell* **77(4)**, 599-608 (1994).

Kostrouchova, M., Kostrouch, Z., Saudek, V., Piatigorsky, J. & Rall, J.E. BIR-1, a *Caenorhabditis elegans* homologue of Survivin, regulates transcription and development. *Proc Natl Acad Sci U S A*. **100(9)**, 5240-5 (2003).

Kufel, J., Allmang, C., Petfalski, E., Beggs, J. & Tollervey, D. Lsm Proteins are required for normal processing and stability of ribosomal RNAs. *J Biol Chem*. **278(4)**, 2147-56 (2003).

de Laat, W.L., Jaspers, N.G. & Hoeijmakers, J.H. Molecular mechanism of nucleotide excision repair. *Genes Dev*. **13(7)**, 768-85 (1999).

Lee, S.J., Yook, J.S., Han, S.M. & Koo, H,S. Werner syndrome protein homolog affects *C. elegans* development, growth rate, life span and sensitivity to DNA damage by acting at a DNA damage checkpoint. *Development* **131(11)**, 2565-75 (2004).

Lee, J.H. & Paull, T.T. ATM activation by DNA double-strand breaks through the Mre11-Rad50-Nbs1 complex. *Science* **308(5721)**, 551-4 (2005).

Lehmann, A.R., Walicka, M., Griffiths, D.J., Murray, J.M., Watts, F.Z., McCready, S. & Carr, A.M. The rad18 gene of *Schizosaccharomyces pombe* defines a new subgroup of the SMC superfamily involved in DNA repair. *Mol Cell Biol* **15(12)**, 7067-80 (1995).

Li, Y., Dowbenko, D. & Lasky, L.A. *Caenorhabditis elegans* PIAK, a phospholipid-independent kinase that activates the AKT/PKB survival kinase. *J Biol Chem*. **276(23)**, 20323-9 (2001).

Liu, Q., Guntuku, S., Cui, X.S., Matsuoka, S., Cortez, D., Tamai, K., Luo, G., Carattini-Rivera, S., DeMayo, F., Bradley, A., Donehower, L.A. & Elledge, S.J. Chk1 is an essential kinase that is regulated by Atr and required for the G(2)/M DNA damage checkpoint. *Genes Dev*. **14(12)**, 1448-59 (2000).

McClung, J.K., Jupe, E.R., Liu, X.T. & Dell'Orco, R.T. Prohibitin: potential role in senescence, development, and tumor suppression. *Exp Gerontol*. **30(2)**, 99-124 (1995).

Mengarelli, I., Wood, C.G., Cheam, L., Kamath, R.S., Fraser, A.G., Ahringer, J. & Rothman, J.H. Identification and phenotypic analysis of 5 genes involved in the control of cell division in the endoderm. West Coast Worm Meeting 2004.

Ng, C.P., Lee, H.C., Ho, C.W., Arooz, T., Siu, W.Y., Lau, A. & Poon, R.Y. Differential mode of regulation of the checkpoint kinases CHK1 and CHK2 by their regulatory domains. *J Biol Chem.* **279(10)**, 8808-19 (2004).

Nho, R.S. & Sheaff, R.J. p27kip1 contributions to cancer. *Prog Cell Cycle Res.* **5**, 249-59 (2003).

Niederberger, C. & Schweingruber, M.E. A *Schizosaccharomyces pombe* gene, ksg1, that shows structural homology to the human phosphoinositide-dependent protein kinase PDK1, is essential for growth, mating and sporulation. *Mol Gen Genet.* **261(1)**, 177-83 (1999).

Nuell, M.J., Stewart, D.A., Walker, L., Friedman, V., Wood, C.M., Owens, G.A., Smith, J.R., Schneider, E.L., Dell' Orco, R., Lumpkin, C.K., *et al.* Prohibitin, an evolutionarily conserved intracellular protein that blocks DNA synthesis in normal fibroblasts and HeLa cells. *Mol Cell Biol.* **11(3)**, 1372-81 (1991).

Parrish, J.Z. & Xue, D. Functional genomic analysis of apoptotic DNA degradation in *C. elegans*. *Mol Cell.* **11(4)**, 987-96 (2003).

Prakash, S. & Prakash, L. Nucleotide excision repair in yeast. *Mutat Res* **451(1-2)**, 13-24 (2000).

Reed, S.H., You, Z. & Friedberg, E.C. The yeast RAD7 and RAD16 genes are required for postincision events during nucleotide excision repair. In vitro and in vivo

studies with rad7 and rad16 mutants and purification of a Rad7/Rad16-containing protein complex. *J Biol Chem* **273(45)**, 29481-8 (1998).

Romano, A., Guse, A., Krascenicova, I., Schnabel, H., Schnabel, R. & Glotzer, M. CSC-1: a subunit of the Aurora B kinase complex that binds to the survivin-like protein BIR-1 and the incenp-like protein ICP-1. *J Cell Biol*. 161(2), 229-36 (2003).

Schumacher, B., Hanazawa, M., Lee, M.H., Nayak, S., Volkmann, K., Hofmann, R., Hengartner, M., Schedl, T. & Gartner A. Translational repression of *C. elegans* p53 by GLD-1 regulates DNA damage-induced apoptosis. *Cell* 120(3), 357-68 (2005).

Shiloh, Y. ATM and related protein kinases: safeguarding genome integrity. *Nat Rev Cancer* 3(3), 155-68 (2003).

Silverman, E., Edwalds-Gilbert, G. & Lin, R.J. DExD/H-box proteins and their partners: helping RNA helicases unwind. *Gene* **312**, 1-16 (2003).

Stray, J.E. & Lindsley, J.E. Biochemical analysis of the yeast condensin Smc2/4 complex: an ATPase that promotes knotting of circular DNA. *J Biol Chem*. **278(28)**, 26238-48 (2003).

Strunnikov, A.V. & Jessberger, R. Structural maintenance of chromosomes (SMC) proteins: conserved molecular properties for multiple biological functions. *Eur J Biochem*. **263(1)**, 6-13 (1999).

Takeuchi, J. & Toh-e, A. Genetic dissection of the yeast 26S proteasome: cell cycle

defects caused by the Deltarpn9 mutation. *Biochimie* **83(3-4)**, 333-40 (2001).

Tanaka, K., Boddy, M.N., Chen, X.B., McGowan, C.H. & Russell, P. Threonine-11, phosphorylated by Rad3 and atm in vitro, is required for activation of fission yeast checkpoint kinase Cds1. *Mol Cell Biol.* **21(10)**, 3398-404 (2001).

Tatsuta, T., Modelm K. & Langer, T. Formation of membrane-bound ring complexes by prohibitins in mitochondria. *Mol Biol Cell.* **16(1)**, 248-59 (2005).

Tugendreich, S., Tomkiel, J., Earnshaw, W. & Hieter P. CDC27Hs colocalizes with CDC16Hs to the centrosome and mitotic spindle and is essential for the metaphase to anaphase transition. *Cell* **81(2)**, 261-8 (1995).

Ubersax, J.A., Woodbury, E.L., Quang, P.N., Paraz, M., Blethrow, J.D., Shah, K., Shokat, K.M. & Morgan, D.O. Targets of the cyclin-dependent kinase Cdk1. *Nature* **425(6960)**, 859-64 (2003).

Villani, G. & Tanguy, Le Gac N. Interactions of DNA helicases with damaged DNA: possible biological consequences. *J Biol Chem.* **275(43)**, 33185-8 (2000).

Wicky, C., Alpi, A., Passannante, M., Rose, A., Gartner, A. & Muller, F. Multiple genetic pathways involving the Caenorhabditis elegans Bloom's syndrome genes *him-6*, *rad-51*, and *top-3* are needed to maintain genome stability in the germ line. *Mol Cell Biol.* **24(11)**, 5016-27 (2004).

Wu, D., Chen, P.J., Chen, S., Hu, Y., Nunez, G. & Ellis RE. *C. elegans* MAC-1, an essential member of the AAA family of ATPases, can bind CED-4 and prevent cell death. *Development.* **126(9)**, 2021-31 (1999).

Wu, Y.C., Stanfield, G.M. & Horvitz, H.R. NUC-1, a *Caenorhabditis elegans* DNase II homolog, functions in an intermediate step of DNA degradation during apoptosis. *Genes Dev.* (2000) **14(5)**, 536-48 (2003).

Yang, J., Yu, Y. & Duerksen-Hughes, P.J. Protein kinases and their involvement in the cellular responses to genotoxic stress. *Mutat Res.* **543(1)**, 31-58 (2003).

You, H., Jang, Y., You-Ten, A.I., Okada, H., Liepa, J., Wakeham, A., Zaugg, K. & Mak, T.W. p53-dependent inhibition of FKHRL1 in response to DNA damage through protein kinase SGK1. *Proc Natl Acad Sci U S A.* **101(39)**, 14057-62 (2004).

Zachariae, W. & Nasmyth, K. Whose end is destruction: cell division and the anaphase-promoting complex. *Genes Dev.* **13(16)**, 2039-58 (1999).

Methods

Microarrays. (a) Total RNA isolation. Fresh tissue from the different genetic backgrounds tested, before or 3 h following treatment with either IR or ENU, was used as a starting material. Total RNA was isolated using the RNAzol B (ams Biotechnology) according to the manufacturer's protocol, dissolved in RNase-free water (Sigma) and tested on a 1% formamide-agarose gel.

(b) First strand synthesis of direct cDNA. A total of 20 μg RNA in 8 μL of H_2O was used to synthesize cDNA with a microarray custom cDNA synthesis kit (Gibco BRL, #18090-019) and using an oligo dT24-T7 promoter, HPLC purified primer.

(c) Second strand synthesis of direct cDNA. The 20 μL of the previous reaction were used to synthesize the second cDNA strand (Gibco BRL, #18090-019). No RNase A or proteinase K treatment followed the T4 DNA polymerase incubation and 150 μL of DEPC-H_2O was added instead.

(d) cDNA purification. The product was purified using PhaseLock gel light tubes (Eppendorf, #0032007.961) and precipitated with 7.5 M NH_4Oac and glycogen (Gibco BRL, #10814-010), according to the instructions.

(e) *In vitro* transcription labeling (IVT). Of the purified cDNA, 3.5 μL were mixed with 75 mM each of NTPs (Ambion), supplemented with 10 mM Bio-11-CTP and 10 mM Bio-16-UTP (Enzo, #42818 and #42814, respectively). A T7 enzyme mix was used for a 4 h incubation of the *in vitro* transcription reaction (MEGAscript T7 kit, Ambion, #1334).

(f) IVT product purification. The product was immediately purified using RNeasy spin columns (Qiagen, #74104), eluted in a total of 60 μL of DEPC-H_2O and was

stored at –80°C. The transcripts (1-10%) were checked on a formaldehyde agarose gel and the OD_{260} was measured.

(g) Fragmentation of the IVT product. A total of 30 μg of the IVT product was fragmented in fragmentation buffer (Roche laboratories, Basel). The mixture was denatured in a thermocycler and subsequently placed on ice.

(h) Genechip hybridization. A pre-treatment solution was prepared to be applied to the Affymetrix *C. elegans* GeneChip. The fragmented cRNA was mixed with a control stock mix, a biotinylated oligo, herring sperm DNA, acetylated BSA and hybridization buffer. The mixture was heated up, kept in a 45°C waterbath, loaded onto the chip and incubated on rotisserie overnight.

(i) Washing, amplification and staining. The washing steps were done with buffers on Roche Fluidics according to the lab's protocol. A streptavidin stain solution was applied to the chip and incubated on rotisserie, followed by washing steps. For the amplification, the chip was incubated with a biotinylated-anti-streptavidin solution. After the washes, a stain solution supplemented with phycoerythrin was applied on the chip, followed by incubation on rotisserie.

(j) Scanning. After the washing steps, the chip was filled completely with washing buffer, was scanned in a laser scanner to detect the signals, and analyzed using the Affymetrix GeneChip System Expression Analysis package.

*** The exact protocols and reagents (g-j) are confidential for the Roche laboratories**

Genetics. All strains were grown at 20ºC on NGM agar seeded with *E. coli* OP50 (Brenner, 1974). The Bristol N2 strain was used as the wild-type strain. The following alleles and transgenic strains were used: LGI: *hus-1(op244)*, *chn-1(ok459)*, *cep-1(gk138)*; LGII: *rpn-9(gk401)*; LGIII: W04B5.5*(ok1309)*; LGIV: *ced-3(n717)*. The *chn-1(ok459)* and *rpn-9(gk401)* strains were maintained as *chn-1(ok459)*/ok59 I and *rpn-9(gk401)*/mIn1[mIs14 *dpy-10(e128)*] II, respectively.

Germline apoptosis. Young adult staged worms from different genetic backgrounds were exposed to 120 Gy of X-rays and/or 100 J/m^2 of UV-C radiation and corpses were scored in the meiotic region of one gonad arm during the course of time or at the indicated time points, using Nomarski optics. For the RNAi experiments, L1 staged worms were put on plates seeded with the respective RNAi clone (Kamath *et al.*, 2003) and young adults were scored for germline apoptosis in the course of time.

Embryonic lethality assay. Wild-type and *ok1309* mutant animals, 48 h post the L1 stage, were subjected to 120 Gy of X-rays and one day later were left lay eggs for 4-6 h. Non-hatched eggs were scored the next day as a positive embryonic lethal phenotype and expressed as a fraction of the total eggs laid. Data shown is the average percent lethality of 50 animals. Error bars indicate SEM.

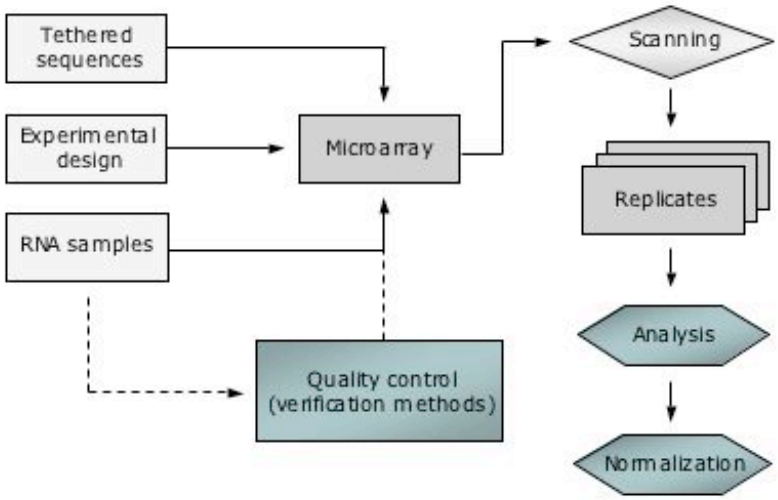

Figure 1. Basic stages of a microarray experiment

The experimental design is made to elucidate the questions that the experiment is supposed to answer. Sample information regarding the origin of the RNA samples, as well as gene information regarding the tethered sequences on the array need to be defined. To reach meaningful biological conclusions, one needs to perform multiple experiments, including replicates and compare these with each other. Normalization removes technical variation and improves the comparisons between experiments. Verification methods insure that one has received the correct molecular information from the microarrays.

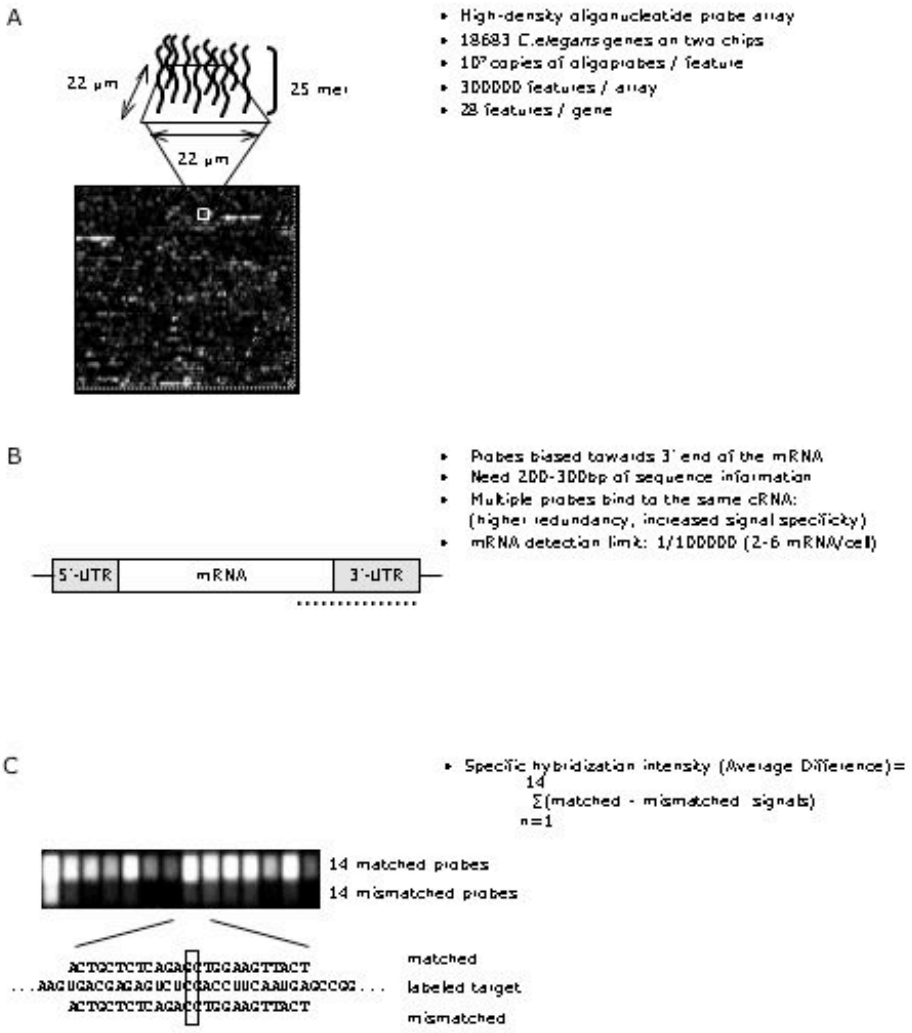

Figure 2. The Affymetrix GeneChip technology

(A) Part of the high-density oligonucleotide probe array is depicted. (B) Schematic show and properties of the probe on the chip. (C) Probe design is based on a match vs mismatch signal, which specifies the final mean hybridization intensity.

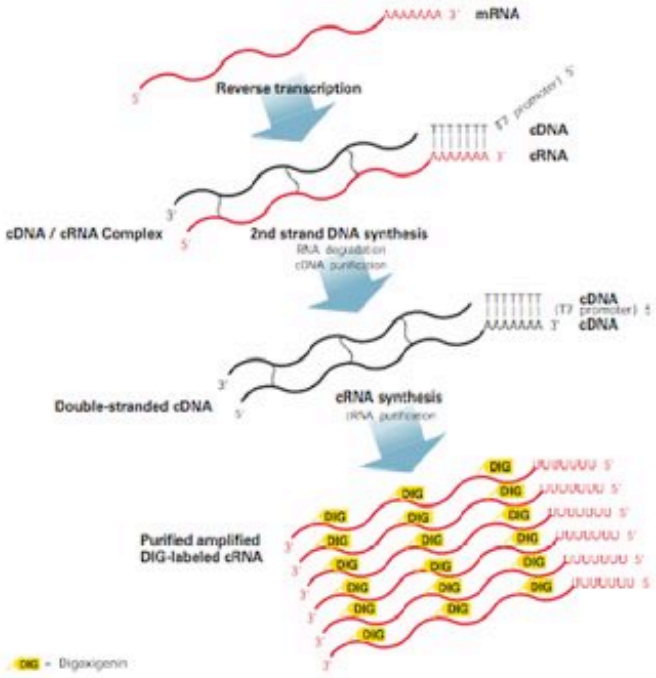

Figure 3. Schematic graph of the sample labeling for the hybridization onto chips

The labeling procedure begins with the synthesis of cDNA from the RNA sequence by means of an oligo (dT) primer linked to an RNA polymerase promoter region. Antisense RNA is then transcribed from the cDNA by T7 RNA polymerase, which also incorporates a DIG modified nucleotide (dUTP-DIG). Extraneous mRNA is then removed from the mixture. After purification, the DIG-labeled cDNA is ready for hybridization to the microarray.

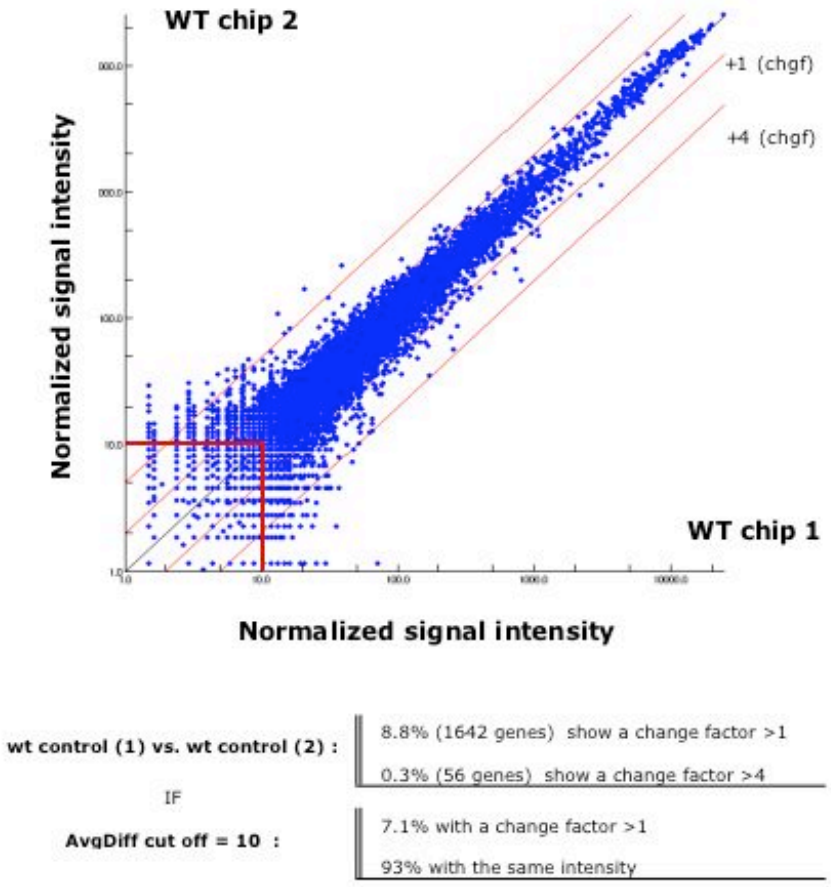

Figure 4. The reproducibility of the replicates in the microarray experiments is high

Scatter plot showing pair-wise correlation of two "wild-type" arrays. The correlation coefficient (r) of the log2 values of the signal intensity was calculated in a pair-wise fashion using all the genes. Each data point corresponds to the compiled normalized weighted average of the spot on a single microarray that corresponds to one gene. The red lines demarcate threshold values (change factors 1 and 4) for significant difference in gene expression relative to the inner black line. After a "cut off" value of 10, genes that lied between the two inner red lines were kept.

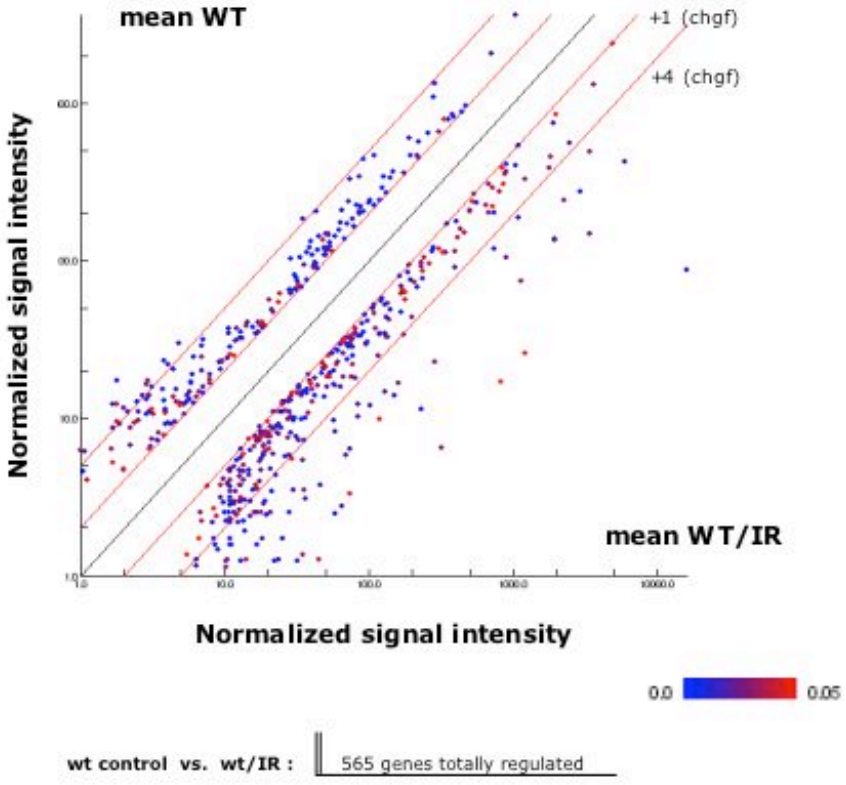

Figure 5. Plotting the normalized signal intensities reveals the difference in gene expression between two samples

Scatter plot showing pair-wise correlation between a "wild-type" and a "wild-type/IR" array. The correlation coefficient (r) of the log2 values of the signal intensity was calculated in a pair-wise fashion. Each data point corresponds to the compiled normalized weighted average of the spot on a single microarray that corresponds to one gene. The red lines demarcate threshold values (change factors 1 and 4) for significant difference in gene expression relative to the inner black line. After a "cut off" value of 10, genes that lied outside the two inner red lines were kept.

Table 1. Gene expression profiling in *C. elegans* upon treatment with ionizing radiation and ENU

The overall output of the microarray experiments is shown. The criteria for the analysis with regard to the genotypes used and the conditions compared, are described. The number of genes regulated under each condition, as well as the type of regulation are shown.

	Conditions compared	No of genes regulated	Tendency
1	wt vs. wt/IR	565	up- and down-regulation
2	*hus-1* vs. *hus-1* /IR	944	up- and down-regulation
3	wt vs. *hus-1*		no change
	hus-1 vs. *hus-1* /IR	49	no change
	wt vs. wt/IR		up-regulation
4	wt vs. *hus-1*		no change
	wt vs. wt/IR	27	up- and down-regulation
	wt/IR vs. *hus-1* /IR		down- and up-regualtion
5	*cep-1* vs. cep-1 /IR	238	up- and down-regulation
6	wt vs. cep-1		no change
	cep-1 vs. cep-1 /IR	178	no change
	wt vs. wt/IR		up- and down-regulation
7	wt vs. wt/ENU	1706	up- and down-regulation

Table 8. Validation of the microarray results using real-time Q-RT-PCR

A number of genes from the "IR" and the "ENU" experimental set were picked randomly to test for a change in their mRNA levels, using real time Q-RT-PCR. The microarray results are shown for comparison. Among the genes tested, 87% were confirmed.

	Gene model	Change-fold				Validation (yes/no)
		Microarrays	QRT-PCR			
		wt	wt	*hus-1*	*cep-1*	
IR						
	T19B4.5	19.8	14	1.8		y
	R119.7	4.7	5.9	1.2		y
	Y43E12A.3	4.5	4.7	1.4		y
	K01G12.3	12.1	282	1.7		y
	C04B4.2	9.3	635	0.2		y
	M03F4.7	7.7	3.9	3.1		n
	C25F9.4	7.5	0.5	0.4		n
	ZC239.12	5.6	1.3	1.1		n
	T20F7.6	9.3	3.1	2.4		n
	R12G8.2	8.6	6.6	1.1	_	y
	C36B7.6	2.0	25.6	1.1	0.5	y
	K03D10.3	8.6	25.6	1.6	0.04	y
	T09B4.10	2.2	5.3	1.7	0.07	y
	K08E3.8	2.4	59.3	1.8	6.2	n
	C42C1.10	2.6	2.3	1.2	_	y
	F47H4.1	2.0	30.3	1.2	_	y
	K05B2.2	4.1	3.9	2.4	_	n
	ZK180.2	4.2	0.5	1.0	_	n
ENU						
	F55G11.5	14.8	9.6			y
	C17H12.8	2.4	35			y
	C02F4.4	58	2.2			y
	Y47G6A.26	51	1.8			y
	E03A3.4	42	8.9			y
	R08F11.4	111	10.4			y
	AC3.3	0.3	0			y
	C24H11.1	0.3	0.7			y

Table 9. The list of genes that dependent on HUS-1 but not on CEP-1 for transcriptional induction

The predicted gene function was obtained from WormBase and the NCBI Blast tool. Germline expression data were obtained from reported microarray experiments (Stanford Database) and RNA in situ data (Kohara group).

Gene	Function	Germline Expression		Mutant Allele present
		Microarray Data	RNA in situ data	
C04B4.2	Unnamed protein. Calcium-binding EF-hand	germline +	-	*ok1212*
C10G8.5	NCX-2 protein *(Na/Ca eXchanger)*		germline / pharynx	
C16A11.4	PHD Zn-finger protein	germline ++	germline	*ok1236*
C17D12.1a	DHHC-type Zn-finger protein		germline	
C27D6.7	SRB-4 protein *(Serpentine Receptor, class B)*		-	
C38C10.4	GPR-2 protein *(G Protein Regulator)*		-	*tm964*
C50B6.1	Unknown protein		-	*ok1343*
F10D2.2	UDP-glucuronosyl and UDP-glucosyl transferase		-	
F18A1.2	LIN-26 protein. C2H2 zinc finger-containing protein	germline	germline	*n156, ga91, ok939*
F34D6.1	F-box containing protein	germline	embryos	
F42A8.3	Uncharacterized conserved protein	germline	germline / embryos	*gk165*
F47B7.5	Extracellular protein with cysteine rich structures		-	
F52D10.2	Uncharacterized conserved protein		?	*ok1205*
F52H3.4	Unknown protein	germline ++	germline / embryos	
F54C9.10	ARL-1 protein (ARF-like)		-	
T07C4.6	TBX-9 protein (T BoX family)		germline / embryos	*ms31*
W04B5.5	phospholipid-independent AKT/PKB kinase		germline	*ok1309*
Y106G6H.14	SH3 domain and Ankyrin repeat containing protein	germline	?	
Y43E12A.3	Unnamed protein. BTB/POZ domain	germline +	-	
Y52B11C.1	N-acetylglucosaminyl phosphatidylinositol de-N-acetylase		-	
Y57A10A.25	Poly(A)-specific exoribonuclease PARN		-	

(+) germline enriched, (-) no information available, (?) hard to estimate

Table 10. The list of genes that dependent on both HUS-1 and CEP-1 for transcriptional induction

The predicted gene function was obtained from WormBase and the NCBI Blast tool. Germline expression data were obtained from reported microarray experiments (Stanford Database) and RNA in situ data (Kohara group).

Gene	Function	Germline Expression		Mutant Allele present
		Microarray Data	RNA in situ data	
C36B7.6	Cleft lip and palate transmembrane protein		germline (bend)	
C42C1.10	Mitochondrial solute carrier protein	germline	-	
F29B9.1	Methytransferase (SAM binding motif)	germline	-	
F32D8.5b	Uncharacterized membrane protein		embryos	
F44E2.8	Unnamed protein (protein kinase-like)	germline +	-	
F47H4.1	Zinc finger, C2H2 type		germline (bend)	*tm593, tm605*
F54D10.7	Ubiquitin family protein	germline ++	germline	
K02B2.3	Uncharacterized conserved protein		?	
K02E10.2	HID-1 protein (High temperature-Induced Dauer formation)		germline / embryos	*sa722, sa1058*
K03D10.3	MYST histone acetyltransferase		germline (bend)	
K05B2.2	Predicted cell growth/differentiation regulator with RA domain		germline	
K08E3.8	MDT-29 protein (MeDiaTor), transcriptional co-repressor		germline (meiotic zone)	*ok965*
K10H10.1	Permease of the major facilitator superfamily		germline (bend)	
R07D5.1	UNC-7 protein. Innexin-type channel		-	*e5, e139, hs9*
R12G8.2	TWK-36 protein (TWIK family of potassium channels).		-	
T06D8.8	RPN-9 protein (Proteasome Regulatory Particle, Non-ATPase)	germline +	germline / oocytes / embryos	*gk401*
T09B4.10	CHN-1 protein (C-term of Hsp-70-iNteracting protein, CHIP)		-	*ok459*
T23G11.9	Unknown protein		-	
T24H7.1	PHB-2 protein (mitochondrial ProHiBitin complex)	germline +	germline / embryos	
W08E3.1	SNR-2 protein (Small Nuclear Ribonucleoprotein)		germline / embryos	*gk209*
Y34B4A.8	GTPase acivator protein, Rho-GAP		-	
Y38C1BA.1	Unknown protein		-	
Y48G10A.4	Unknown protein		germline	
Y49F6C.8	Unknown protein		-	
Y57A10A.3	Uncharacterized protein		-	
Y71F9AR.1	BAM-2 protein (Branching Abnormal)		germline / embryos	
ZC239.12	Polymerase delta-interacting protein PDIP1		-	*tm1617*
ZK180.2	GABA-B ion channel receptor subunit GABABR1		-	

(+) germline enriched, (-) no information available, (?) hard to estimate

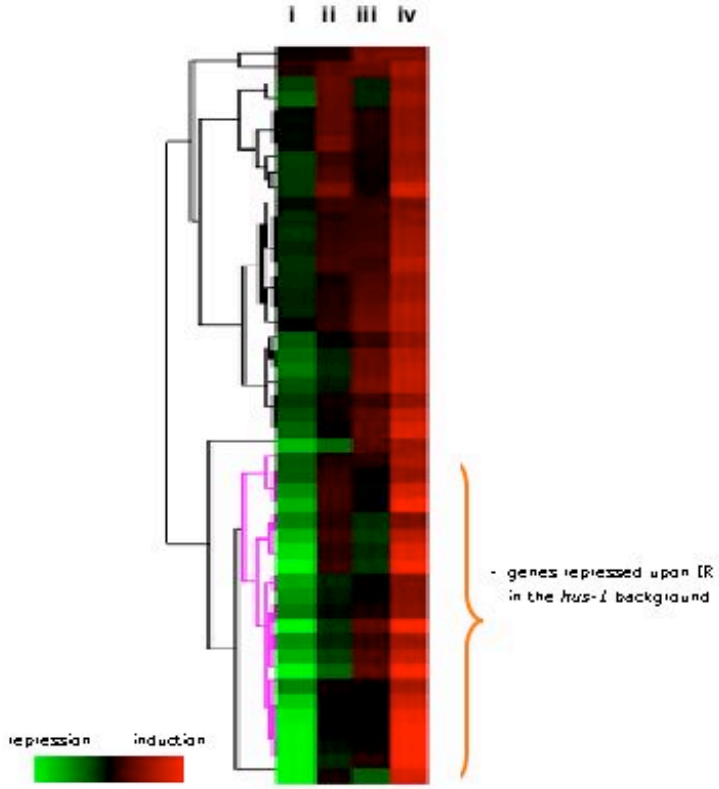

	genotypes compared			tendency
i	wt/IR	vs.	*hus-1* /IR	down-regulation
ii	wt	vs.	*hus-1*	no change
iii	*hus-1*	vs.	*hus-1* /IR	no change
iv	wt	vs.	wt/IR	up-regulation

Figure 6. Hierarchical clustering analysis of the "HUS-1-dependent set" categorizes genes with similar expression profiles

The average expression levels of the 49 genes with significant changes in expression between the wild-type and the *hus-1* mutants are shown. The color scale shows levels of expression. Column headings refer to the conditions analyzed (see table above). The Cluster and Treeview software were applied for this analysis.

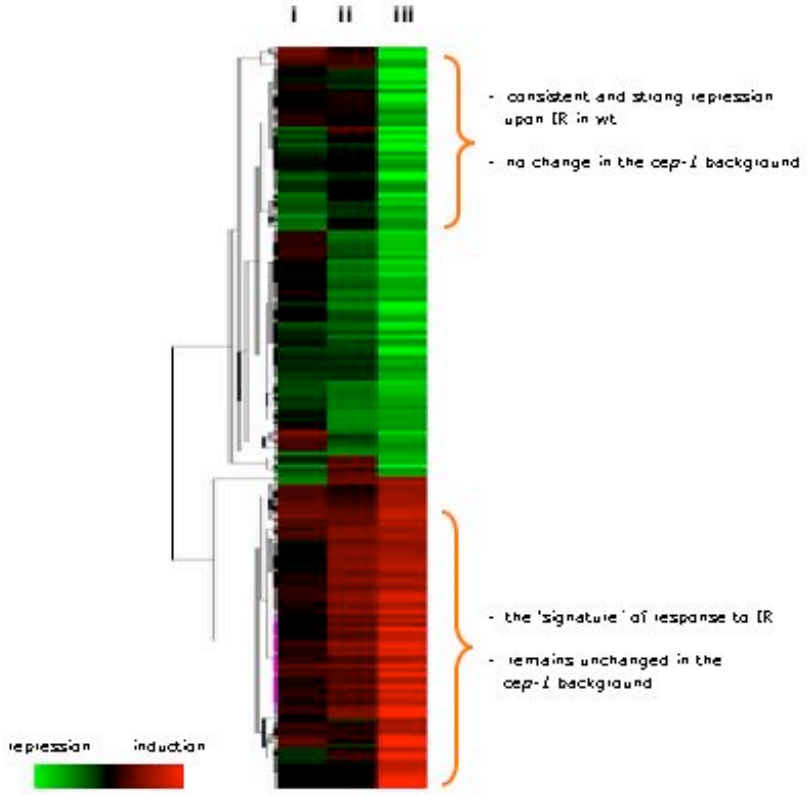

	genotypes compared			tendency
i	*cep-1*	vs.	*cep-1* /IR	no change
ii	wt	vs.	*cep-1*	no change
iii	wt	vs.	wt/IR	up- and down-regulation

Figure 7. Hierarchical clustering analysis of the "CEP-1-dependent set" categorizes genes with similar expression profiles

The average expression levels of the 178 genes with significant changes in expression between the wild-type and the *cep-1* mutants are shown. The color scale shows levels of expression. Column headings refer to the conditions analyzed (see table above). The Cluster and Treeview software were applied for this analysis.

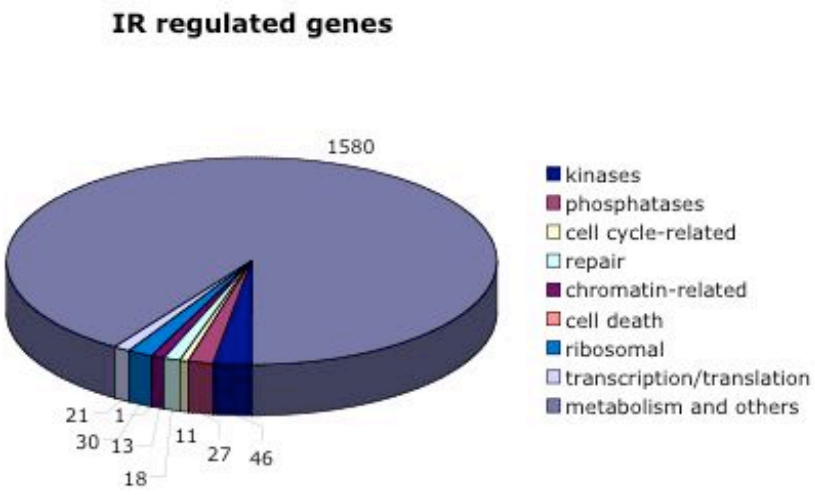

Figure 8. Pie chart showing the distribution of the genes regulated upon ionizing radiation into functional classes

The total number of genes that were found to be regulated (up- or down-) upon ionizing radiation in all the different genetic backgrounds tested (wild-type, *hus-1* and *cep-1* mutants), were used to generate a pie chart. Gene annotations were derived from WormBase and were used to manually place the genes into functional classes. The numbers of genes in each class are shown.

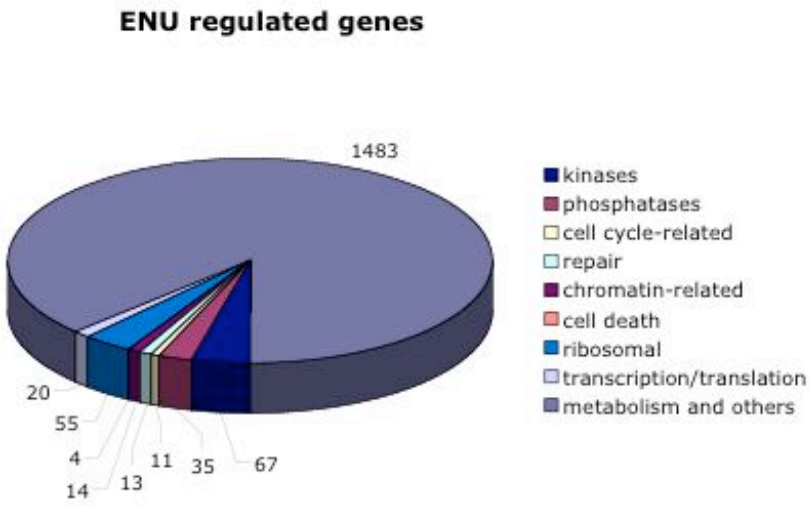

Figure 9. Pie chart showing the distribution of the genes regulated upon ENU treatment into functional classes

The total number of genes that were found to be regulated (up- or down-) upon ENU treatment in the wild-type animals, were used to generate a pie chart. Gene annotations were derived from WormBase and were used to manually place the genes into functional classes. The numbers of genes in each class are shown.

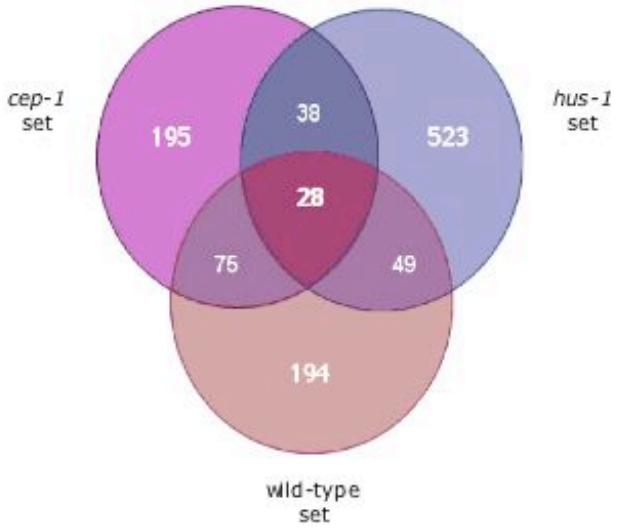

Figure 10. Venn diagram showing the differential distribution of genes regulated upon ionizing radiation in all genetic backgrounds

The number of genes from each experimental set that are up-regulated or remain unchanged after IR is indicated in the circles. The intersection among the three sections of the Venn diagram (the dark red portion) represents the 28 genes whose transcriptional induction is dependent on CEP-1 and HUS-1.

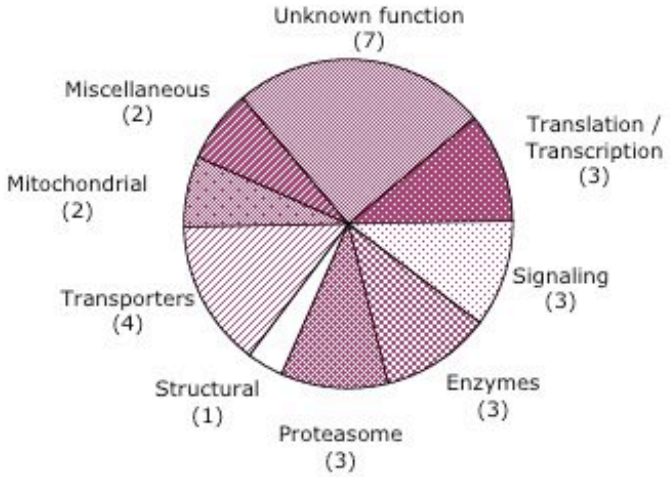

Figure 11. Pie chart showing the distribution of the 28 genes, potential downstream effectors of CEP-1 and HUS-1, into functional classes

The 28 genes that were found to depend on CEP-1 and HUS-1 for transcriptional up-regulation upon ionizing radiation, were used to generate a pie chart. Gene annotations were derived from WormBase and were used to manually place these genes into functional classes. The number of genes in each class is shown.

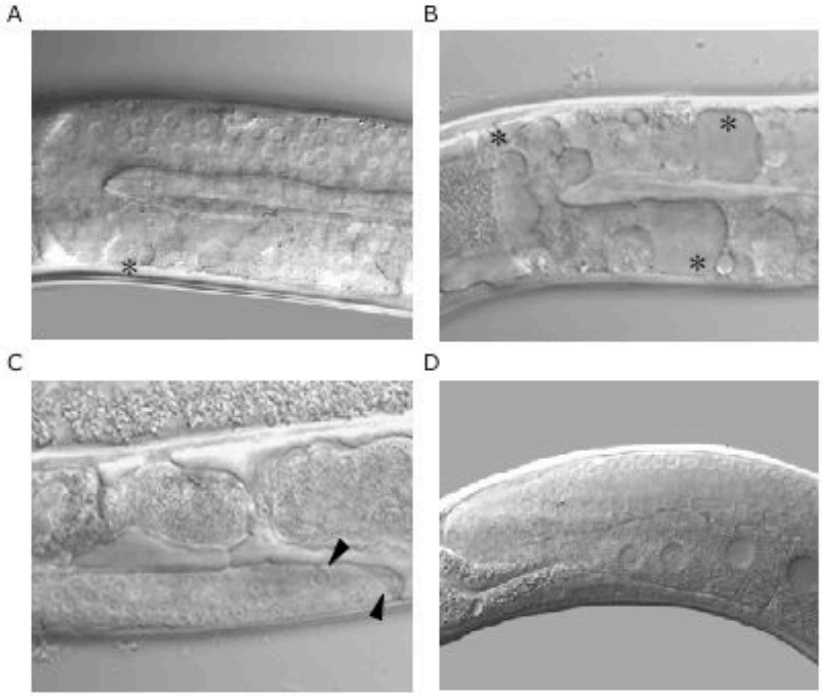

Figure 12. Phenotypic germline characteristics of the *rpn-9(gk401)* mutants

DIC pictures of the germline of the *gk401* allele are depicted. (A+B) Homozygotes for the *gk401* mutation animals display defects in oogenesis with the pachytene zone practically absent. Additionally, empty circular areas appear all around the bend of the gonad (marked with an asterisk). (C) Certain mitotic cells appear to be arrested and interspersed with normal looking nuclei in homozygote *gk401* animals (arrowheads). (D) The heterozygote over the mIn1 balancer animals appear wild-type.

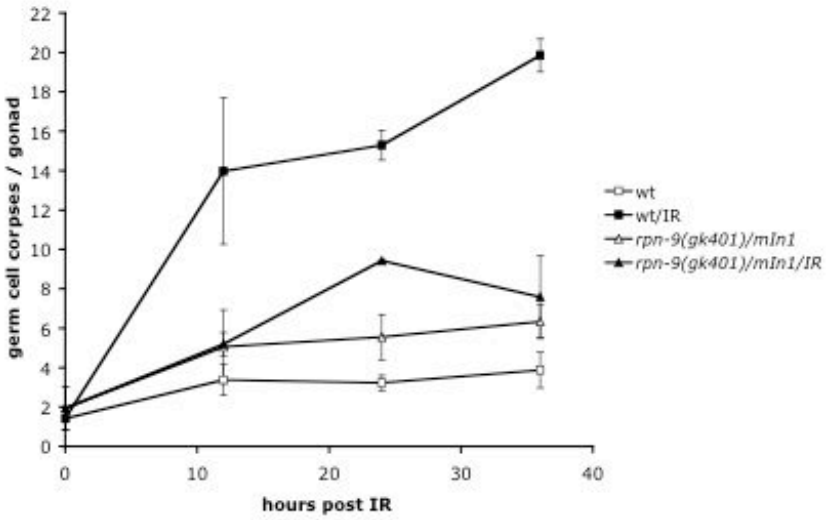

Figure 13. *rpn-9* mutants are defective for ionizing radiation-induced apoptosis

Time course analysis was performed with wild-type animals and *rpn-9(gk401)/mIn1* mutants. Apoptotic corpses were scored in the meiotic region of one gonad arm of young adult animals, during the course of time and following 120 Gy of X-rays. Data shown represent the average number of two independent experiments ± SD.

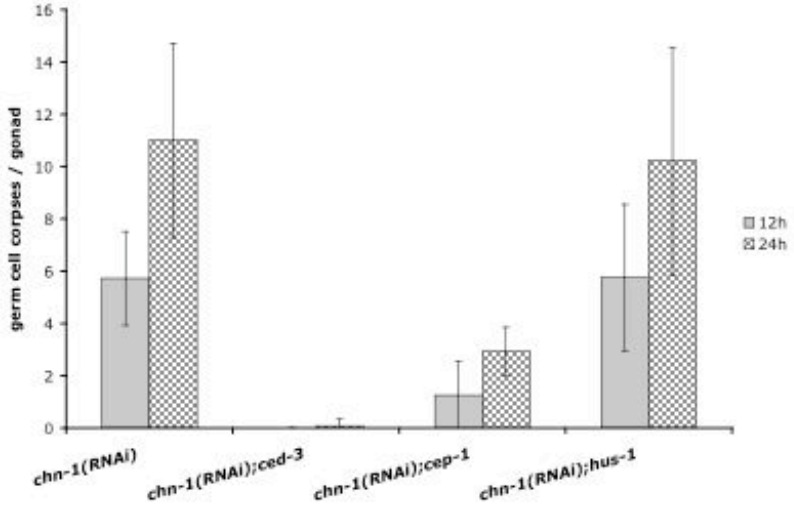

Figure 14. Loss of *chn-1* function results in increased germ cell death, that is apoptotic in nature and likely due to endogenous DNA damage

RNAi was applied against *chn-1* in wild-type animals, *ced-3(n717)*, *cep-1(gk138)* and *hus-1(op244)* mutants. Apoptotic corpses were scored in the meiotic region of one gonad arm of animals 12 and 24 h after the L4 stage. Data shown represent the average number of two independent experiments ± SD.

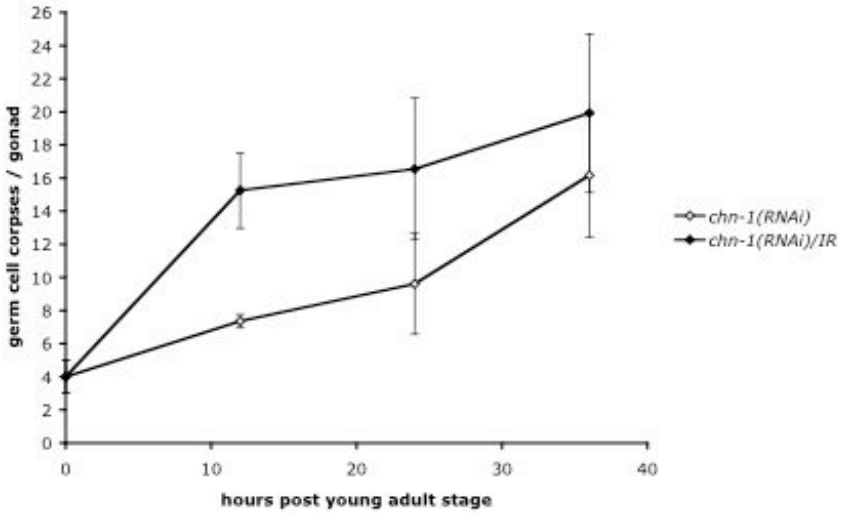

Figure 15. Loss of *chn-1* function results in increased germline apoptosis and rather limited IR-induced apoptosis

Time course analysis was performed with wild-type animals subjected to *chn-1(RNAi)* at the L1 stage (2 mM IPTG). Apoptotic corpses were scored in the meiotic region of one gonad arm of young adult animals, during the course of time and following 120 Gy of X-rays. Data shown represent the average number of two independent experiments ± SD.

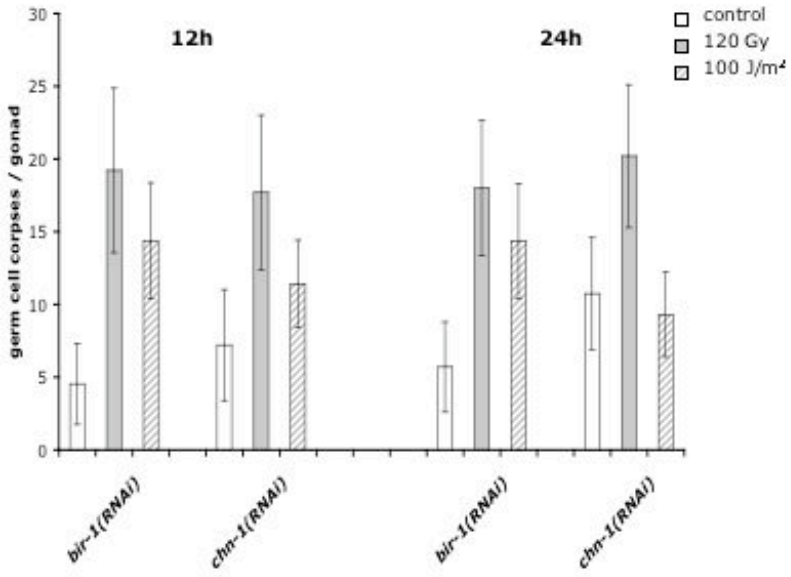

Figure 16. Induction of cell death upon IR is slightly compromised in a *chn-1* loss of function situation. Cell death upon UV-C radiation is profoundly affected

Apoptotic corpses were scored in the meiotic region of one gonad arm of wild-type animals that were subjected to *chn-1*(RNAi), before and after the application of 120 Gy of X-rays or 100 J/m^2 of UV radiation. *bir-1*(RNAi) was used as a control. Data shown represent the average number of two independent experiments ± SD.

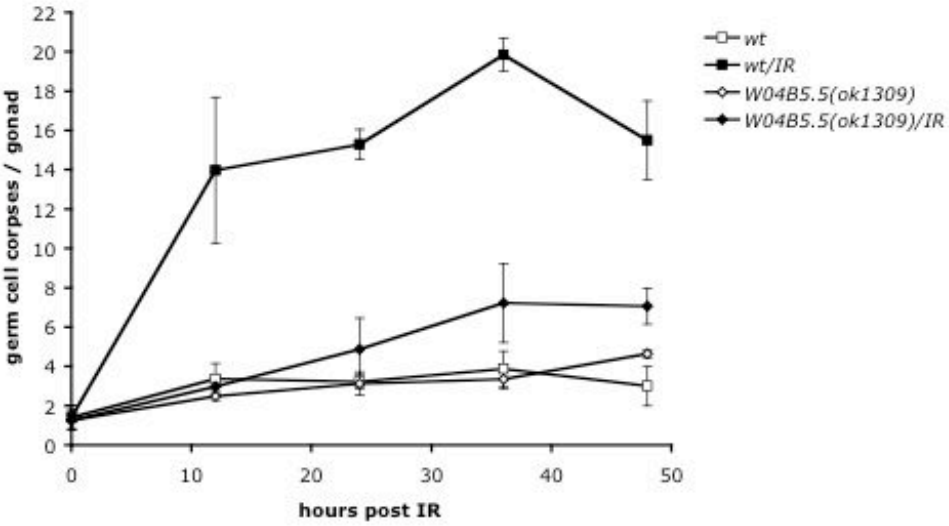

Figure 17. W04B5.5*(ok1309)* mutants are defective for ionizing radiation-induced apoptosis

Time course analysis was performed with wild-type animals and W04B5.5*(ok1309)* mutants. Apoptotic corpses were scored in the meiotic region of one gonad arm of young adult animals, during the course of time and following 120 Gy of X-rays. Data shown represent the average number of three independent experiments ± SD.

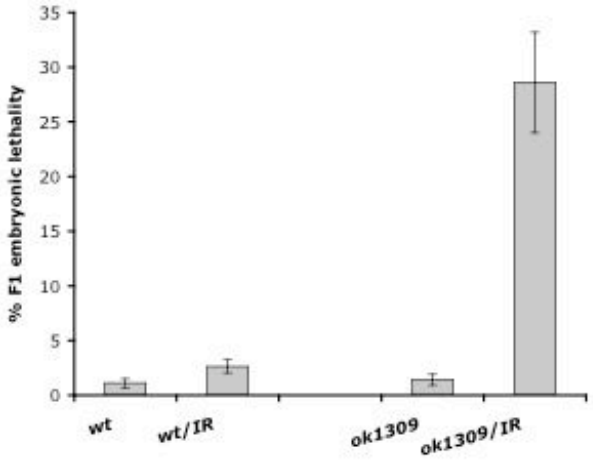

Figure 18. W04B5.5*(ok1309)* mutants display moderate levels of embryonic lethality upon ionizing radiation

Animals at the L4 stage of the indicated genotype were irradiated with 120 Gy or left untreated. After 12 h they were let lay eggs and finally unhatched embryos were counted and expressed as a fraction of the total number laid. Data shown is the average percent lethality of 50 animals for each genotype. Error bars indicate SEM.

Table 2. The expression of the 565 genes in the "IR" experimental set in wild-type

Listed below are the *C. elegans* genes that are up- or down-regulated in wild-type in response to ionizing radiation. For comparison, the tendency in the *hus-1(op244)* background is shown.

Gene model	Description	Change Factor			
		wt vs. wt/IR	wt vs. *hus-1*	*hus-1* vs. *hus-1* /IR	wt/IR vs. *hus-1* /IR
ZK228.7	similarity in C. elegans olfactory receptor odr-10	5.24	5.79	-1.73	-1.51
C06E1.5		4.78	15.92	-1.76	0.65
T19B4.5		4.31	2.33	-0.61	-1.56
F32D8.5b	uncharacterized membrane protein	4.3	0	0	-4.3
C17D12.1a	zinc finger protein	4.22	-0.8	0.67	-4.62
T27F6.4		3.83	-1.54	0.52	-7.1
B0403.4	probable protein disulfide isomerase p5 precursor	3.68	-3.98	28.75	-0.07
Y52B11C.1	N-acetylglucosaminyl phosphatidylinositol de-N-acetylase	3.68	-0.35	8.7	-2.71
K01G12.3		3.6	1.05	-0.26	-1.84
T27E4.3	heat shock protein hsp16-48	3.47	1.62	12.4	6.84
F56A4.3f	similar to glutathione s-transferase	3.39	-0.93	6.33	-0.16
F43D9.3	sec1 family	3.34	0	1.13	-1.04
C27C7.3	elo-74	3.32	16.88	-1.46	0.68
T28F7.6	AMP-activated protein kinase	3.22	1.72	0.64	0.06
C04B4.2	similarity to Ca binding EF-hand domain	3.21	-0.27	0.22	-3.56
K03D10.3	histone acetyltransferase	3.11	-0.1	0.07	-3.22
R12G8.2	putative potassium channel subunit n2p26	3.11	0.38	-0.38	-3.11
F52D10.2	uncharacterized conserved protein, contains phosphotyrosine interaction domain	2.98	0.4	0.04	-1.72
M03F4.7	calcium binding protein	2.95	1.75	0.48	0.03
C08B11.5	poly(A) RNA binding protein	2.93	-0.69	2	-1.22
C25F9.4		2.91	1.84	8.2	-0.15
Y71D11A.6	hypothetical glycine receptor like protein f59c12.1	2.91	4.93	-2.6	-1.37
F56D5.4		2.77	0.6	1.26	-0.04
C48B6.2	putative 40S ribosomal protein s4-like	2.57	7.39	-1.82	-0.2
ZC239.12	similar to human tumor necrosis factor-alpha-induced protein bl2	2.49	0	0	-2.49
C40H1.2	hypothetical 23.8 kda protein	2.46	0.96	1.43	0.37
C12D8.6		2.45	4.52	-2.92	-1.45
Y57G11C.15	protein transport protein sec61 alpha subunit	2.45	-11.11	24.42	-0.64
T04A8.9		2.43	0.11	1.61	-0.19
F23F1.1	coset-binding factor subunit ghp5p	2.34	-3.02	9.22	-0.32
ZC404.10	similarity to mammalian mu- and kappa-type opioid receptors	2.29	1.25	-1.25	-2.29
F57B10.9		2.27	-0.13	1.39	-0.54
R07D5.1	unc-7 protein	2.24	0.28	-0.28	-2.24
C36D4.1		2.23	-1.91	2.07	-1.12
C16H11.4	similar to udp-glucuronosyltransferases	2.22	1.96	-0.03	-0.12
R119.7		2.22	-4.33	0.32	-12.02
F07H5.2	gamma-sarcoglycan	2.18	2.79	0.88	1.25
Y43E12A.3	BTB/POZ (also known as br-c/ttk) domain-containing protein	2.16	0.02	8.7	-0.83
F29B9.1	methyltransferase, SAM binding motif	2.15	0.15	-0.74	-3.76
Y71H2B.2	phosphorylated adaptor for RNA export	2.14	-0.42	1.41	-0.86
F29F11.6	serine/threonine protein phosphatase	2.13	-46.8	48.38	-2.16
Y62F5A.1a		2.13	13.08	-2.17	0.42
F47B7.5	extracellular protein with cysteine rich structures	2.07	0.44	-0.05	-1.25
ZK180.2	GABA-B ion channel receptor subunit GABABR1 and related subunits	2.06	0	0	-2.06
C02A12.1	glutathione s-transferase	2.04	1.23	0.08	-0.26
K05B2.2	predicted cell growth/differentiation regulator, contains RA domain	2.04	0.96	0.12	-0.38
T12C9.4	similar to cyclins	2.04	-0.24	1.32	-0.62
Y47H9C.5	thioredoxin protein	2.02	1.8	0.43	0.33
C14B1.7	similar to C. elegans protein c14b1.7	1.96	-11.55	5.28	-4.91
T23G11.9	dopamine responsive protein drg-1	1.9	-0.46	0.56	-1.72
ZC513.6	zinc finger protein	1.89	-19.86	0.04	-57.2
R02C2.2	protein kinase	1.86	4.27	-2.35	-0.82
Y102A5C.22	transmembrane receptor (rhodopsin family)	1.86	2.58	-1.14	-0.71
C38C10.4	gpr-2 (G protein regulator)	1.83	0.09	0.63	-0.6
K01D12.13	glutathione s-transferases	1.83	3.35	-0.22	0.26
W10C8.3		1.83	5.1	-1.86	-0.33
F49D9.1	ankyrin homologue	1.82	3.66	-0.85	-0.12
K10H10.1	permease of the major facilitator superfamily	1.81	-0.28	0.77	-1.03
Y48G10A.4	unknown protein	1.79	-0.17	0.97	-0.65
C01G10.11	unc-76	1.77	-4.22	4.78	-1.51
ZK858.7	novel protein similar to predicted worm, yeast and plant proteins	1.77	1.68	-0.03	-0.06
D2013.6	similar to C. elegans predicted protein d2013.6	1.76	-1.58	1.86	-1.49
ZK402.3		1.76	1.53	-2.37	-2.67
C07D10.4	hypothetical zinc metalloproteinase	1.75	1.17	0.08	-0.18
F14D2.10	similarity to RNA recognition motifs	1.75	0	1.17	-0.27
F34D6.1	F-box containing protein	1.75	0.41	-0.41	-1.75
F25H8.1		1.75	0.34	1.44	0.19
F55C5.3	twk-11 potassium channel protein	1.75	0	3.45	0.62
F08B6.1		1.73	5.41	-2.23	-0.26
F17E9.2		1.73	2	-2.48	-2.18
C50B6.1	unknown protein	1.7	0.47	0.36	-0.26
Y56A3A.20	ccr4-associated factor 1	1.69	-6.95	8.08	-1.66
F12B6.3	ligand-gated ionic channel	1.68	3.32	-1.46	-0.53
W04B5.5	protein kinase	1.67	0.23	0.75	-0.24
C08B6.4	chitinase	1.64	0	2.72	0.41
T07C4.6	tbx-9 (TBX2 and related T-box transcription factors)	1.64	-0.22	0.74	-0.86
ZK1098.1	ww/rsp5/wwp domain containing proteins (2 domains)	1.64	0	6.63	1.89
K08D10.3	a1 small nuclear ribonucleoprotein a	1.63	-0.08	1.1	-0.35
Y105E8B.4	speckle-type POZ and related proteins with TRAF, MATH and BTB/POZ domains	1.61	-6.75	5.66	-2.04
F53H8.1	clathrin coat assembly protein	1.59	1.4	0.02	-0.05
T09A5.11	probable dolichyl-diphosphooligosaccharide glycosyltransferase precursor	1.58	-0.89	1.89	-0.5
T14B4.5		1.58	1.21	1.18	0.87
Y57A10A.25	poly(A)-specific exoribonuclease PARN	1.58	0.3	8.9	-0.04
C10G8.5	ncx-2 sodium/calcium exchanger protein 1	1.54	0.17	0.25	-0.74
ZC204.4	srg-10 protein	1.54	5.6	-0.89	0.38
F41D3.9		1.53	7.98	-9.58	-1.98
C53A5.3	probable histone deacetylase 1	1.52	-6.34	4.88	-2.14
ZC395.10	S. cerevisiae 24.1 kda protein in vma12-apn1 intergenic region	1.51	0.11	1.07	-0.09
W03C9.2		1.49	-1.03	1.83	-0.79
Y45F6C.8	unknown protein	1.49	0.09	0.04	-1.19

Y43F8C.14	PH (pleckstrin homologe) domain	1.48	-0.82	1.02	-1
F43G6.3	leucine rich repeat (2 copies)	1.48	-1.41	2.29	-0.8
F53G2.6	nuclear transport receptor	1.48	-1.34	3.43	-0.3
Y57A10A.3	uncharacterized protein	1.45	0.36	0.48	-0.24
B0001.7	hypothetical 83.8 kda protein	1.44	-1.83	3.02	-0.72
F41G4.3	stc-5 stomatin-like protein	1.44	2.82	-0.02	0.54
C25A1.1		1.42	-1.38	0.88	-2.04
D2096.5		1.42	8.21	-2.75	0.02
F59B1.8	similarity to bovine cAMP-dependent protein kinase ii-b-binding protein	1.42	1.86	1.23	1.62
Y75B8A.30	ser/thr protein phosphatase	1.41	-1.28	1.59	-1.1
C42C1.10	mitochondrial carrier protein	1.39	0.3	0.38	-0.35
F10D2.2	glucuronosyltransferase	1.39	0.62	0.82	0.24
F18A1.2	transcription factor lin-26	1.39	-0.26	0.32	-1.28
R04E5.8	hydroxyproline-rich glycoprotein dz-hrgp precursor	1.39	-1.4	0.62	-2.54
Y25C1A.5	beta adaptin-like protein	1.39	-3.74	6.8	-0.46
F52B11.2	phosphomannomutase 2	1.37	0.83	1.23	0.73
Y111B2D.F	sr family splicing factor	1.37	-1.98	2.43	-1.06
C27D6.7	srb-4	1.36	0.69	-0.24	-0.73
C34G6.4	pgp-2 ABC transporter	1.36	-0.04	2.73	0.52
C41A3.1	polyketide synthase	1.36	3.09	-1.16	-0.24
F44E7.5		1.36	-1.51	2.21	-0.85
F52H3.4	in *S. cerevisiae* .. nucleolar protein for pre-rRNA processing and ribosome biogenesis	1.36	0.54	8.1	-0.4
T06D8.8	26S proteasome subunit p40.5	1.36	0.2	0.61	-0.22
ZK228.3	similar the gPain rhodopsin family of 7-transmembrane receptors	1.36	3.74	0.11	1.24
F25D7.2		1.35	-5.51	4.59	-1.74
F44E2.8	unnamed protein	1.34	-0.85	0.58	-1.75
F54D10.7	in *S. cerevisiae* , subunit of the condensin complex	1.33	0.34	0	-0.74
C06G3.2	kinesin-like protein	1.32	-7.68	6.55	-1.66
B0410.2		1.31	1.8	-0.52	-0.25
F08F1.2		1.31	4.62	-1.17	0.12
F54C9.10	putative ADP-ribosylation factor 2	1.31	0.86	0.16	-0.08
F08G12.1	ras-related like protein	1.3	0	1.88	0.25
T22A3.3		1.3	-5.15	4.85	-1.43
T28A8.6		1.3	2.62	-0.64	-0.04
Y45F10A.4	probable selenide, water dikinase, selenophosphate synthetase	1.3	-0.32	1.03	-0.49
B0284.3		1.29	5.9	-4.2	-0.72
F42G2.4		1.29	4.86	-1.6	-0.02
H05C05.1	profilaggrin fragment	1.28	-1.63	4.49	-0.09
K08E3.8	MDT-28 protein (MeDiaTor), transcriptional co-repressor	1.28	0.14	0.55	-0.3
C18A11.4		1.28	5.11	-1.44	0.1
F17C11.1	bzip DNA binding domain	1.28	-0.33	1.97	-0.02
F46G11.2		1.28	5.26	-0.33	1.07
F49F1.2		1.28	10.56	-2.85	0.31
Y45F10D.8	putative WD-repeat membrane protein	1.28	1.16	-0.37	-0.45
Y47G6A.18		1.28	-0.45	1.78	-0.19
R107.6		1.27	-5.21	5.95	-1.03
F56H1.4	ATPase	1.26	-3.63	4.64	-0.85
Y106G6H.14	Src homology domain 3 ; ank repeat	1.26	-0.03	0.37	-0.7
B0304.4	hypothetical 14.4 kda protein	1.24	1.71	-0.35	-0.12
F28H1.6		1.23	-3.36	4.12	-0.9
Y38C1BA.1	unknown protein	1.23	-0.08	0.17	-1.06
Y62E10A.11b		1.22	1.29	0.24	0.28
H162.1		1.21	1.9	-3.74	-2.61
T28D9.7	diogenerin	1.21	0.46	1.01	0.32
C16A11.4	PHD Zn-finger protein	1.2	0.14	0.38	-0.41
H17B01.2	collagen	1.2	2.34	-0.09	0.4
K02E10.2	hid-1 (protein containing regions of low-complexity)	1.2	0.7	8.2	-0.08
Y41E3.7	peripheriel benzodiazepine receptor associated protein	1.2	-1.78	3.2	-1.77
W08E3.1	small nuclear ribonucleoprotein (snrnp)	1.18	0.34	0.13	-0.44
C26F1.3		1.17	2.12	-0.47	-0.02
C06A1.6	serine 2 ultra high sulfur protein	1.16	2.09	-0.56	-0.09
OC2.5	dehydrogenase	1.16	5.31	-0.34	1.19
F18F10.9		1.16	5.14	0.68	3.82
F23H11.1	sequence 1 from patent wo9700323	1.16	-4.19	2.01	-2.74
F42A8.3	hypothetical 37.3 kda protein	1.16	0.67	0.21	-0.07
Y71F9AR.1	unknown protein	1.15	0.24	0.35	-0.28
T09B4.10	similarity to a single tpr domain	1.14	0.77	-0.21	-0.46
T26C12.2		1.14	3.62	-3.18	-0.94
R05F9.10	tpr domain repeats	1.13	-3.61	7.9	-0.12
F15C11.2	ubiquitin family	1.12	-11.45	16.31	-0.52
T23D8.7	putative RNA-binding protein g89	1.12	-1.73	2.08	-0.88
Y113G7B.7		1.12	1.66	-0.78	-0.42
F54C4.4		1.11	4.44	-2.7	-0.44
F10C1.1		1.1	1.32	-0.03	0.08
Y17G7B.5	mcm2/3/5 family	1.1	-7.61	4.64	-2.2
C10H11.3	similar to UDP-glucuronosyltransferases	1.08	1.49	-0.1	0.09
F25H9.4	hypothetical 42.8 kda protein	1.08	1.7	-0.3	0
ZK353.1		1.08	1.61	-0.29	-0.03
B0281.5	similar to human tumor necrosis factor-alpha-induced protein b12	1.07	3.66	-1.14	0.05
C06A1.4	similar to *C. elegans* protein zk757.3	1.07	-4.22	8.8	-0.39
F54C9.8	pumilio-family RNA binding domains (aka pum-hd, pumilio homologe domain)	1.07	-5.19	2.23	-2.97
K02B2.3	uncharacterized conserved protein	1.07	-0.17	0.03	-1.35
Y37D8A.9		1.06	-1.98	0.35	-3.36
C07E3.6	pha-1 mRNA	1.05	3.22	-3.22	-1.05
C10G11.7		1.05	-8.78	6.67	-1.55
C16C8.14	similarity to ubiquitin	1.05	-2.04	2.64	-0.71
Y34B4A.8	SH3-binding protein 3bp-1	1.05	-0.28	0	-1.58
T15B5.3		1.04	-28.65	28.26	-1.65
T12F5.1		1.04	-1.1	1.57	-0.66
C26E6.5		1.03	-16.39	4.71	-5.19
F47H4.1	zinc finger, c2h2 type (2 domains)	1.03	0.25	-0.3	-1.12
K05C4.7		1.03	-0.95	1.11	-0.87
F30F8.1		1.02	-5.06	4.11	-1.4
W04H10.1		1.02	1.9	-0.48	-0.04
B0207.10		1.01	2.39	-1.04	-0.21
K08F4.7	gst-4 glutathione-s-tranferase	1.01	7.67	-0.73	1.49
ZK1320.7	single ankyrin motif	1.01	4.7	-0.14	1.48
C36B7.6	cleft lip and palate transmembrane protein 1	1	0.14	0.94	0.11
D2085.2		1	2.82	-1.58	-0.35
EEED8.12	probable RNA binding protein	1	8.9	-8.9	-1
F16H9.1a	regulator of g protein signalling domain	1	1.58	-0.5	-0.16
T24H7.1	prohibitin	1	0.37	0.33	-0.1

T24H7.4		1	6.09	-11.31	-2.46
W01A11.2		1	-0.78	1.04	-0.75
C25B8.6	nuclear hormone receptor family member nhr-10	-1	-0.98	-0.86	-0.82
F28H6.1	Akt-2 ph (pleckstrin homology) domain, protein kinase c terminal domain	-1.02	-3.85	0.73	-0.39
VM106R.1	tumor necrosis factor, alpha-induced protein 1, endothelial (b12 protein)	-1.02	-5.36	1.59	-0.21
C25H12.6		-1.03	-0.32	-1.33	-0.51
K02A6.2		-1.03	-0.06	-1.72	-0.41
T01B6.3	similar to inosine-5' -monophosphate dehydrogenases	-1.03	-3.67	0.95	-0.19
T02H6.3	sarcoplasmic reticulum histidine-rich calcium-binding protein precursor	-1.03	-5.19	5.28	1.05
T10H10.1	hum-6 myosin	-1.03	0.18	1.31	4.55
C18B2.5		-1.04	-1.39	0.92	0.64
C34F11.4	major sperm protein	-1.04	-0.87	8.2	0.31
F47E1.2	DNA binding protein	-1.04	-0.32	-1.71	-0.75
M03A8.1	fat-3 alcohol dehydrogenase; non-specific lipid transfer protein	-1.04	1.15	0.01	3.43
Y39A3CR.6	helix-loop-helix DNA-binding domain	-1.04	-6.35	0.95	-0.85
C02E7.5	chemoreceptor	-1.05	-1.13	0.26	0.21
K09D9.6		-1.05	-0.11	-1.1	-0.13
M28.4	similar to glycoproteins	-1.05	0.01	-0.96	0.06
F25E12.6		-1.06	0.09	0.26	1.81
F10G2.1	similarity to pneumocystis carinii msg102 major surface glycoprotein	-1.07	-0.29	0.05	0.69
F21C10.6		-1.07	1.33	-1.62	0.84
F52H3.5		-1.07	-0.17	0.64	1.9
F28E10.6		-1.08	-5.36	1.56	-0.2
Y56D4B.f	unknown protein	-1.08	1.48	-4.16	0
C34D10.1	novel protein similar to predicted human and worm genes	-1.1	-9.77	7.27	0.62
F53A9.2	histidine-rich	-1.1	0	-0.1	0.92
Y53F4B.30	glutathione s-transferase	-1.1	0.05	0.27	1.81
F49H6.5	molybdenum cofactor synthesis-step 1 protein a splice type 1	-1.11	-8.8	1.61	-0.78
ZK673.1	excretory/secretory mucin muc-5	-1.11	-4.84	-0.15	-2.08
C14C11.1		-1.12	-2.18	0.72	0.15
F38E9.2		-1.12	-1.22	0.49	0.42
K07D4.4		-1.12	0.73	-1.94	0.25
C01B7.3		-1.13	-0.03	-0.13	0.84
F29B9.5	similar to thioredoxin	-1.13	0.29	-0.51	0.82
Y73F8A.f	unknown protein	-1.13	0.16	0.11	1.75
F44C8.2	nuclear hormone receptor	-1.14	-0.87	-0.63	-0.43
F22E12.4	egl-9	-1.15	-9.39	5.11	0.27
T13F2.1	fat-4 cytochrome b5 containing fusion protein	-1.15	-0.83	0.35	0.6
F21D4.4	lectin c-type domain short and long forms	-1.16	-3.1	2.38	0.78
F59F4.1	acyl-coa oxidase	-1.16	-0.41	1.05	2.14
R09F10.1	peptidase	-1.16	-1.28	1.28	1.17
ZK757.3a	translation initiation factor eIF2c	-1.16	-1.38	0.36	0.24
F46F5.6		-1.17	-0.29	-0.64	0.03
K10B3.1b	spc-1 spectrin alpha chain	-1.17	-12.99	6.5	0.16
C16D9.2	tyrosine-protein kinase	-1.18	-0.88	1.19	1.54
F29B9.2		-1.18	-0.29	0.68	1.84
H02I12.3	transmembrane receptor (rhodopsin family)	-1.18	-6.01	1.48	-0.3
T28C12.4a	esterase	-1.19	-0.92	-0.58	-0.26
Y23H5A.5	alpha2-catulin	-1.19	-0.63	-0.16	0.16
B0218.7	in 5. cerevisiae , zinc finger transcription factor, stress-responsive	-1.2	-0.37	0.68	1.7
K02D7.1	phosphorylase	-1.2	-3.93	1.41	0.08
Y106G6E.4	5-formyltetrahydrofolate cyclo-ligase	-1.2	0.3	-0.3	1.2
C07A12.1	ham-2 zinc finger protein	-1.21	-1.19	0.05	0.06
C35A5.7	transmembranous domains	-1.22	1.17	-1.92	0.65
F49E11.11	testis-specific protein tpn-1 like	-1.22	-3.53	2.53	0.73
M60.5	klp-2 channel protein	-1.22	0.27	0.08	2.04
T25G12.3		-1.22	0.01	-1.63	-0.17
Y106G6D.6		-1.22	1.05	-2.59	0.27
B0240.1	rhr-2 erythrocyte plasma membrane glycoprotein like	-1.23	0.15	-0.87	0.37
F44D12.4		-1.23	-3.42	1.19	0.1
C37C3.8		-1.24	-1.43	0.02	-0.07
T25B2.2		-1.24	-0.58	-0.58	-0.12
Y11D2A9.a	unknown protein	-1.24	0.04	-0.21	0.92
F26D11.4		-1.25	0.61	-2.61	0
Y76A2A.1		-1.25	-0.5	0.17	0.75
C05D10.1	hypothetical 53.2 kda protein	-1.26	-0.84	8.2	0.48
F26B1.4	similar to collagen	-1.27	0.17	-0.43	0.66
F42D1.2	tyrosine aminotransferase	-1.27	-2.13	-0.37	-0.89
K07E3.3	methylenetetrahydrofolate dehydrogenase	-1.27	-1.65	0.83	0.57
Y46G5A.26	ionotropic gaba receptor subunit unc-49a	-1.27	-1.12	1.33	1.49
C16D2.1		-1.28	-0.05	8.1	1.39
F42G9.4		-1.28	-0.12	-1.75	-0.34
K06A9.1a	glucoamylase s1/s2 precursor (glucan 1,4-alpha- glucosidase)	-1.29	-3.45	3.33	1.23
Y46G5A.30	glycine transporter type-2	-1.29	-0.91	0.53	0.84
C14B1.3		-1.3	-0.88	-0.01	0.21
DC2.4		-1.32	0.41	-1.03	0.61
F29B9.9	collagen	-1.32	-2.19	0.33	-0.04
T04B2.5	85 kda calcium-independent phospholipase a2	-1.32	-11.03	9.29	0.98
C06E8.2		-1.33	-6.04	3.03	0.34
C26E1.2		-1.33	-0.55	-0.22	0.23
F07H5.5		-1.33	-82.06	21.36	-0.21
F32H5.4	transport protein	-1.33	1.95	-6.98	-0.16
E02H9.4		-1.34	0.81	-1.48	0.71
ZK218.3	similarity to toxocara canis tes-26 protein	-1.34	-0.14	-1.41	-0.17
C45H3.12		-1.35	0.37	-2.2	0.01
C03A7.2		-1.36	-1.17	0.18	0.26
C36C9.3		-1.36	-1.13	-0.16	-0.05
F18E9.2		-1.36	0.02	-0.27	0.89
M04D8.6		-1.36	-1.48	-0.01	-0.06
Y105E8B.e	unknown protein	-1.36	0.31	0.07	2.32
C01G10.2	similarity to xenopus dopamine d2 receptor	-1.37	0.33	-0.31	1.41
C31B8.6	chemoreceptor	-1.37	0.41	-2.33	0
C34E11.2		-1.37	0.69	-1.94	0.36
F15E6.3	RNA binding protein	-1.37	-2.96	-0.05	-0.76
F21D9.4	similar the gfam rhodopsin family of 7-transmembrane receptors	-1.37	-0.73	1.11	1.89
Y17D7A.2	domain of unknown function	-1.37	0.43	-0.59	1.13
B04F6.9	similarity to bombesinlike peptide - african clawed frog	-1.38	-0.33	0.68	2.02
F20D6.5		-1.38	1.24	-2.93	0.36
K07A1.4		-1.38	0.25	0.07	2.18
T24A11.3	toh-1 zinc metalloprotease	-1.38	-2.71	8.3	-0.2
W05H9.1		-1.38	-3.94	7.69	3.18
ZK54.2	trehalose phosphate synthase	-1.38	-9.87	3.24	-3.06

F35H10.2		-1.39	0.53	-1.52	0.45
Y65B4BL.1	unnamed protein	-1.39	0.39	-0.76	0.89
B0252.6	hypothetical 23.6 kda protein	-1.4	-0.2	-0.41	0.42
C17G1.3	udp-glucosyltransferase	-1.4	-1.37	1.23	1.26
D2045.5	serine/threonine kinase	-1.4	-1.06	0.61	0.87
R10E9.2		-1.4	-1.32	0.58	0.65
T23B12.8		-1.41	0.24	-1.37	0.26
T05A10.5	testis-specific protein like	-1.42	-0.37	-2.22	-0.82
Y47D7A.15	egg shell protein	-1.42	-0.7	-2.89	-1.74
ZK849.4	putative membrane protein	-1.42	-3.44	-0.11	-1.03
C46F4.2	long-chain-fatty-acid coa ligase	-1.43	-2.37	0.48	0.07
F32H5.3		-1.43	0.34	-5.8	-1.09
F59B10.4	hypothetical 29.4 kda protein	-1.44	-0.87	-0.76	-0.26
M01F1.5	glucose transport protein	-1.44	-0.46	-0.15	0.45
T28B4.4	claudin homolog that may be required for normal cohesion of apical junctions	-1.44	0.01	-0.15	1.14
W04H10.3	zinc finger protein	-1.44	-4.6	0.28	-0.84
ZK75.1	probable insulin-like peptide beta-type 1 precursor	-1.44	-3.41	0.25	-0.45
C48B4.2	rhomboid	-1.45	-0.81	-0.1	0.23
F52E1.5		-1.45	0.65	-1.3	0.75
R06A10.4	protein kinase	-1.45	0.22	-1.1	0.43
T23C6.2		-1.45	1.4	-4.88	0
C07B5.5	nuc-1	-1.46	-0.71	-0.06	0.36
F42G4.6		-1.47	-0.54	0.34	1.15
T01D3.6a	EGF-like domains	-1.48	-0.35	-0.61	0.15
F47B3.1	protein-tyrosine phosphatase	-1.5	-8.77	4.82	0.49
D2096.3	similar to glucan 1	-1.51	-0.93	0.82	1.36
C04H5.1	hspc152	-1.52	-1.44	0.77	0.82
Y71F9B.a	unknown protein	-1.52	-0.42	-0.08	0.65
B0272.4	enoyl-coa hydratase/isomerase	-1.53	0.7	-0.31	2.29
C05H5.7	phophatase	-1.53	-0.31	-0.13	0.71
R04F11.1		-1.53	0.35	-0.51	1.25
ZK1320.4	putative cytochrome p450	-1.53	-0.32	0.08	1.07
F18A12.8	peptidase	-1.54	-3.93	1	0.03
D1046.5	seven transmembrane domain orphan receptor	-1.55	-1.52	-0.21	-0.2
K02E2.3	chemoreceptor	-1.56	-0.68	-0.53	0
ZK337.1a	alpha-2-macroglobulin family (3 domains)	-1.56	-2.78	3.65	2.15
F57F4.3	putative serine/threonine-protein kinase	-1.57	-2.22	0.28	0.01
K10G9.2		-1.57	-2.03	1.87	1.43
Y57G11C.31		-1.57	0.03	0.88	4.02
C24H11.1	protein phosphatase-1 (pp1)	-1.58	-0.45	0.08	0.92
F16H6.1	lectin c-type domain short and long forms, cub domain	-1.58	-1.58	0	0
K10D6.4		-1.58	-4.51	0.98	-0.07
Y44A6D.5	aminotransferase class iv	-1.58	-0.65	0.18	0.84
C54E10.5	zinc finger, c4 type (two domains)	-1.59	-0.15	-0.92	0.17
F46C5.7	hypothetical 23.2 kda protein	-1.59	0.4	-0.49	1.43
C14E2.4	similarity to prolyl 4-hydroxylase alpha subunit	-1.6	0.3	-1.02	0.68
F53F4.12		-1.6	0.51	-0.13	2.5
F58F6.1	cuticular collagen	-1.6	-0.83	-0.04	0.37
T03F1.5	serine/threonine protein phosphatase pp1	-1.6	-1.49	0.66	0.73
Y116A8B.4		-1.6	1.65	-1.82	1.44
Y73F8A.12	unnamed protein	-1.6	-0.03	0.15	1.9
ZC373.1	cystathionine beta-synthase	-1.6	-0.27	-0.08	0.9
C41D7.2	similar to *C. elegans* protein H4F4.4	-1.61	-4.84	1.07	-0.08
AC3.3	similarity to erbb-3 receptor protein-tyrosine kinase	-1.62	-0.98	0.16	0.53
F35B3.4		-1.63	-0.98	-3.13	-0.7
F35D11.3	novel protein similar to predicted yeast and worm proteins	-1.64	-6.97	0.54	-0.96
R09E12.2		-1.64	-1.64	1.34	1.34
F11A5.1	similarity to *C. elegans* olfactory receptor odr-10	-1.65	0.21	-1.11	0.52
Y25C1A.1		-1.65	-0.57	0.42	1.4
AC8.3		-1.68	0.9	-2.55	0.44
F10G2.3	similarity to cub domains	-1.7	-0.47	-1.76	-0.5
F42F12.1		-1.7	-0.98	-3.22	-0.66
Y52B11A.10		-1.7	1.63	-0.27	4.6
F15A8.4		-1.71	0.27	-2.43	0.01
R05D2.3	hypothetical zinc finger protein	-1.71	-2.15	1.56	1.21
T26H5.5	similarity to rana pipiens rhodopsin	-1.71	-1.75	0.25	0.23
F13H6.5		-1.72	-9.24	0.68	-1.24
F58H1.7	low-density lipoprotein receptor	-1.72	-2.5	0.36	0.05
W02D7.8		-1.73	-1.69	-0.01	0
C12D5.5		-1.74	-0.64	-0.92	-0.15
F28E10.1	d-dt3	-1.74	-0.23	-0.43	0.56
B0213.12	cytochrome p450	-1.75	-0.82	0.62	1.44
B0240.3	daf-11 guanylate cyclase	-1.75	-1.2	-0.25	0
C01A2.6		-1.75	-1.5	-0.1	0
C08G6.2	putative porin precursor	-1.75	-0.17	-0.08	1.17
C13C4.4	probable n-acetylglucosamine-6-phosphate deacetylase	-1.75	-0.22	0.04	1.33
C38C8.3		-1.75	-0.58	0.77	2.08
C54C8.5	glycoprotein specific udp-glucuronyltransferase	-1.75	0.06	-0.52	0.91
F42C5.2	protein-coupled receptor	-1.75	0.27	-1.75	0.27
F49E12.10	erg-3 like protein	-1.75	-1.75	0	0
R11H6.3		-1.75	0.46	-1.2	0.82
T06C12.13	zinc finger, c4 type (two domains)	-1.75	-0.41	-0.34	0.46
Y43F8B.9		-1.75	-2.03	-5.81	-6.5
B0034.1	hypothetical 22.9 kda protein	-1.76	-1.35	-0.51	-0.29
F45D3.3		-1.77	-3.8	1.17	0.25
ZC410.5	microfilarial antigen like	-1.77	-0.24	-0.01	1.21
F08G5.6		-1.78	7.87	0.09	25.93
F53E2.2	cd9 antigen like	-1.78	-1.33	-0.19	0
ZK180.5	similarity to ccaat/enhancer binding protein beta	-1.78	-19.03	4.31	-0.26
K11D2.1	human pk19 protein like	-1.81	-1.09	-0.19	0.13
ZK377.2	sax-3	-1.81	-6.17	2.94	0.54
B0344.2		-1.82	-1.77	1.38	1.42
F38A5.10	beta-galactoside-binding lectin	-1.82	-0.03	-15.63	-5.06
F22B7.9	hypothetical 32.9 kda protein	-1.84	-13.31	2.92	-0.28
W08E12.4		-1.85	0.05	-1.74	0.09
F36H12.4	in *S. cerevisiae* , putative RNA helicase involved in mRNA degradation	-1.86	-0.15	0.55	2.87
F58G1.6		-1.86	-1.36	-0.63	-0.34
C33G3.4	probable beta-mannosidase precursor	-1.87	-1	1.07	1.97
F09C6.6		-1.87	-0.24	-0.44	0.61
M28.9		-1.87	-0.48	0.27	1.46
Y40C5A.5	membrane interacting protein of rgs16	-1.87	-4.09	1.58	0.44
Y60A3A.18	skr-4 (ubiquitinates proteins during the G1/S transition)	-1.87	-1.87	2.78	2.76

ZK1010.7	collagen	-1.87	-28.53	33.85	2.39
C45B11.3	alcohol dehydrogenase	-1.89	0.18	-0.48	1.3
R12E2.7	similarity to coast/enhancer binding protein beta	-1.89	0.73	-2.08	0.62
F56B6.4	svt-5 glycagonin	-1.9	-1.85	-0.27	-0.25
K06H6.2		-1.9	-1.9	0	0
W01B11.2	sulfate transporter	-1.9	-1.9	1.82	1.82
Y69F12A.2		-1.9	-0.19	0.03	1.52
ZK622.3	phosphoethanolamine n-methyltransferase	-1.9	-17.91	6.44	0.14
W01B11.5		-1.92	-1.92	0	0
F49E2.5F		-1.93	-3.23	2.58	1.49
H23L24.2	85 kda calcium-independent phospholipase a2	-1.93	-0.41	-0.31	0.58
Y11B2A.9a		-1.93	-4.08	0.73	0
F21E9.5	reverse transcriptase	-1.96	-1.96	0	0
C54F6.13	probable na(+)/h(+) antiporter	-1.97	0.41	-1.97	0.41
F39H12.2		-1.97	-0.29	-0.95	0.18
R12H4.7		-1.97	0.19	-0.73	1.05
ZK682.5	human platelet glycoprotein v precursor	-1.98	-2.15	1.98	1.83
K07C11.4	esterase	-1.99	-1.39	1.26	1.82
B0414.3	hydratase-dehydrogenase-epimerase	-2	-0.6	1.2	1.25
K02E7.9	similarity to mouse zinc finger 5 protein	-2	-2.76	-0.57	-0.96
ZC395.5		-2	0	-2.77	-0.26
AH10.1	4-coumarate:coenzyme a ligase	-2.01	-3.46	2.11	1.1
F55C12.3		-2.01	0.77	-0.73	2.1
C52E2.6		-2.03	-0.57	-0.93	0
F36F2.2	unknown protein	-2.03	-0.88	1.54	3.09
C52B9.3	cofactor e	-2.05	-4.55	-0.38	-1.5
W07E11.1	glutamate synthase	-2.05	-6.44	1.26	-0.08
C05D2.3	aromatic-l-amino-acid decarboxylase	-2.07	-7.37	2.63	0.33
H28G03.4	transposase	-2.08	0.29	-2.97	0
F37B4.2	ifc-1 intermediate filament protein	-2.09	-4.04	-0.34	-1.19
C13G3.2		-2.11	0.21	-4.63	-0.5
F34H10.2	hypothetical 11.9 kda protein	-2.11	-0.65	-1.23	-0.18
H02G9.3	similarity to erbb-3 receptor protein-tyrosine kinase	-2.14	-1.84	-0.06	0.04
C05E7.2		-2.15	-0.09	-3.37	-0.52
C14C6.12	similarity to pneumocystis carinii msg102 major surface glycoprotein	-2.17	-2.17	0.12	0.12
C54G10.4	mitochrondrial carrier protein	-2.2	-2.72	0	-0.16
F47B8.2		-2.2	-1.93	0.33	0.45
F53B3.4		-2.21	-2.21	9.35	9.35
F53C3.4	uncharacterized protein, contains CX module	-2.21	-0.27	-0.22	1.07
F16C3.2		-2.22	-1.68	-2.49	-1.91
F11E6.6		-2.23	-0.48	-1.29	-0.05
F56B3.7	adp-glucuronosyltransferase	-2.23	-0.97	-0.64	0
R06B9.1	dihydroxyvitamin d3-induced protein	-2.23	-4.14	0	-0.59
R11G11.2	ztn-58 zinc finger protein	-2.23	-9.23	2.9	0.23
Y43F8A.2		-2.23	-2.28	0.71	0.69
ZK637.13	putative globin-like protein	-2.23	-2.68	1.04	0.79
F13C5.1	unknown protein	-2.24	-0.86	0.26	1.2
F42G9.7	synaptotagmin	-2.25	-1.09	-0.56	0
K11D12.4	acetyltransferase	-2.25	-3.37	34.33	26.3
T21B6.6	7tm receptor	-2.25	0.16	-2.79	0
F43C11.3		-2.26	0.24	-42.21	-9.64
K06D10.10		-2.26	-0.75	0.12	1.08
F09B12.1a		-2.27	-3.49	19.54	13.94
C43E11.5	similarity to human leukocyte common antigen 1 precursor	-2.29	-1.51	0.78	1.34
F27E5.1	acid ceramidase precursor	-2.32	-3.1	-0.11	-0.37
F08A10.1		-2.33	-3.39	0	-0.32
D1086.2		-2.34	-0.81	-1.11	-0.01
F46F5.9		-2.39	-1.31	-1.16	-0.48
Y57G11A.2	cell surface glycoprotein 1 precursor (outer layer protein b)	-2.4	-2.35	0.48	0.5
R05D8.10	alcohol dehydrogenase	-2.42	-2.42	0	0
K12H6.9		-2.43	0.87	-0.25	4.15
K10G4.2	similarity to rana pipiens rhodopsin	-2.46	0.26	-1.47	0.77
B0238.1	carboxylesterase	-2.47	-0.37	0.96	0.96
F54B3.2	hypothetical 43.7 kda protein	-2.48	-2.48	1.75	1.75
K12H6.5		-2.48	-1.42	1.18	2.14
F58G1.9		-2.49	0.03	-1.09	0.73
C54F6.14	ferritin heavy chain	-2.51	-3.67	0.91	0.44
F49C5.7		-2.52	-2.52	0	0
C18D1.3	flp-4	-2.53	-1.07	1.02	2.43
T03F6.4		-2.53	-2.53	0	0
F11A6.1a	furin like serine protease	-2.54	-4.6	1.87	0.81
F52B11.5		-2.56	1.11	-0.67	3.48
F23F1.6	amino acid permease	-2.59	0.03	-4.15	-0.4
R02F11.2	similarity to a c-type lectin domain	-2.59	-1.98	0.14	0.37
F44E2.8	zinc finger protein	-2.6	-0.67	0.17	1.53
C27D8.3		-2.64	-5.88	3.58	1.49
Y42G9A.1		-2.65	-3.98	1.78	1.02
C24B9.9		-2.66	-4.19	2.95	1.78
C44B7.8	similar to *C. elegans* protein f59b2.2	-2.66	-1.02	-0.77	0.02
Y69E1A.8		-2.66	-0.67	0.19	1.62
T01B10.5		-2.69	-2.69	0	0
T07C4.4		-2.69	-0.97	0.07	1
T28D3.1	carnitate acyltransferase	-2.69	-3.09	-0.31	-0.45
C30G7.1	histone H1 like	-2.73	-4.5	0	-0.47
Y60A3A.5	similarity in *C. elegans* olfactory receptor odr-10	-2.76	0.67	-0.49	3.21
Y65H2.8	zinc finger, c4 type (two domains)	-2.76	0.56	-1.14	1.75
F49G10.2		-2.87	-3.47	0.73	0.5
F56F3.3		-2.93	2.3	-2.49	2.71
Y39B6A.1		-2.93	-4.23	3.89	2.76
C07A4.3	extracellular protein	-3.05	0.43	-2.71	0.56
T10B10.1	col-41 collagen	-3.07	-1.18	-1.58	-0.38
C06G3.1	zinc finger protein	-3.08	-0.86	-0.81	0.21
F11F1.6		-3.13	-0.92	0.51	2.25
T28A11.16	similarity to pneumocystis carinii msg102 major surface glycoprotein	-3.13	-3.13	4.12	4.12
F13D11.3	tyrosine-phosphatase family	-3.15	-2.02	-0.05	0.31
Y44A6C.1		-3.18	-16.42	4.71	0.37
C28F5.1	hypothetical 7.5 kda protein	-3.19	0.31	-4.5	0
T05A10.1	plant seed storage proteins, zinc finger, c2h2 type (3 domains)	-3.19	-3.19	0	0
K06A6.2		-3.21	-3.21	0	0
Y47D3A.9	sex-determining transformer protein 1	-3.23	-0.04	-0.13	2.59
B0213.3		-3.36	-0.09	-2.86	0.04
T22F3.5	chemoreceptor	-3.37	0.01	-0.98	1.24

Y43C5A.3	glycine-rich	-3.42	-3.39	1.4	1.41
H05H21.9		-3.45	-4.24	2.42	1.91
Y57A10B.7		-3.45	-2.43	1.13	1.76
K05F6.5	serum paraoxonase/arylesterase 2, serum aryldialkylphosphatase 2	-3.49	-0.89	-1.08	0.14
T28H10.3	vacuolar processing enzyme like	-3.54	-1.38	8.6	2.07
F42A6.2		-3.55	9	-2.51	0.3
F49E11.10	testis-specific protein tpn-1 like	-3.57	-5.81	0.27	-0.14
W03D2.6		-3.61	-1.98	2.87	5.04
R12E2.7	similarity to coat/enhancer binding protein beta	-3.65	0.31	-1.39	1.54
ZK1251.5	protein-tyrosine phosphatase	-3.66	-0.98	0.08	1.57
T08A4.2		-3.68	0.4	-0.45	3.5
T08H4.3	ets protein	-3.68	-0.17	-1.29	0.75
B0563.5	hypothetical 10.2 kda protein	-3.82	0.53	-6.36	0
K01A2.4		-3.87	-4.03	-0.41	-0.46
T07H3.1		-3.93	-3.25	-0.16	0
Y75B12B.3		-3.93	0.31	-1.04	2.16
F11D11.9	hypothetical 29.3 kd protein	-4.01	-0.57	-0.41	1.27
K08D10.8	phospholipid scramblase 1	-4.16	-3.91	0.87	0.66
F47H4.10	skr-5 (ubiquitinates proteins during the G1/S transition)	-4.23	-1.49	-1.1	0
Y38H6C.17	similar to C. elegans protein f59b2.2	-4.26	-2.51	-0.6	-0.07
C52A11.4	inpp-1	-4.32	-0.16	-1.61	0.75
F21D12.3		-4.35	-4.35	0.55	0.55
Y51H4A.0	putative 32.6 kda lipase	-4.36	-0.46	-2.67	0
C18D11.2	acyl coa binding protein	-4.54	-0.43	-0.03	2.77
F21C10.10		-4.88	-7.9	0.93	0.27
T07G12.5	permease	-4.88	-2.5	-0.68	0
M01H9.1	similarity to thioredoxin redox-active center	-4.94	-0.79	0.17	2.89
F40F4.3	fatty acid-binding protein homolog 2 precursor	-5.17	-1.14	-3.61	-0.8
C05E7.1a		-5.3	-0.21	-0.21	3.33
F59E11.7		-5.48	-1.88	-0.43	0.58
ZC204.12		-5.84	-4.09	1.57	2.45
F32A5.5	similarity to mip family of transmembrane proteins	-5.94	-5.23	-0.11	0.01
F22E10.3	p-glycoprotein (mdr)	-6.08	-6.08	0.52	0.52
F21A3.2	acid phosphatase	-6.2	-1.19	0.15	2.77
F48E10.6		-6.48	0.31	-0.05	8.26
Y48A6A.1	zig-5 ig (immunoglobulin) superfamily	-6.47	-2.21	-1.33	0
B0393.4	mRNA similar to megakaryocyte stimulating factor precursor	-7.88	-7.98	2.03	2.03
F46B6.8	lipase	-7.3	-1.42	-0.72	1
F41E6.5	glycolate oxidase	-7.48	-6.55	0.92	1.15
B0564.3	putative membrane protein	-7.55	-15.64	1.06	0.06
F09B9.4		-7.69	-7.69	12.18	12.18
T01C3.4	lipase	-7.83	-4.93	-0.44	0.04
T12D8.5		-7.85	-0.89	-0.31	2.62
F27A8.1		-8.05	-8.05	6.57	6.57
F08F7.6		-8.35	-13.11	0.41	-0.07
F09B9.1		-8.63	-12.29	1.14	0.55
F28F8.2	long-chain-fatty-acid-coa ligase	-9.44	-20.41	0.24	-0.65
F08G2.6	ins-37	-10.01	-3.78	0.68	2.89
F56G4.1	similarity to acyltransferases	-10.23	0.08	0.08	12.22
R04B5.5	sorbital dehydrogenase	-10.54	-1.21	-1.06	1.55
K01A2.3		-10.66	-1.5	-3.22	0.11
C35C5.7		-11.07	-13.57	-0.16	-0.44
K01A2.3		-11.26	-0.94	-3.59	0.38
B0213.15	cytochrome p450	-11.74	-11.05	0.06	0.12
K12G11.3	alcohol dehydrogenase	-12.72	-44.44	2.77	0.14
ZK973.7	nonmuscle myosin ii heavy chain a	-13.13	-168.81	37.76	2.23
B0564.3	putative membrane protein	-13.17	-34.19	2.53	0.42
F56A11.6		-13.48	-13.48	2.72	2.72
F49C5.1	hypothetical 13.4 kda protein	-14.48	-13.46	-0.11	-0.04
C15H9.1	NAD(P) transhydrogenase, mitochondria	-15.27	-15.14	-0.01	0
F09E8.5	testis-specific protein tpn-1 like	-17.48	-4.4	-2.42	0
F43C11.7	similar to glp-binding protein ard-1 and s. pyogenes m protein	-19.22	-9.41	-0.77	0.1
F53A9.8	histidine-rich	-21.72	-1.8	-0.45	4.6
K01A2.2		-46.53	-18.36	-0.81	1.31
K11G9.6	metallothionein-i (mt-i)	-47.66	-4.97	-0.45	4.62
F49F1.5	similarity to toxocara canis tex-26 protein	-48	-7.76	-8.05	-0.62
T22F3.11	similar to Na+ dependent-phosphate cotransporters	-179.71	-586.02	2.58	0.1

Table 3. The expression of the 944 genes in the "IR" experimental set in *hus-1(op244)*

Listed below are the *C. elegans* genes that are up- or down-regulated in *hus-1(op244)* in response to ionizing radiation. For comparison, the tendency in the wild-type is shown.

Gene model	Description	Change Factor			
		hus-1 vs. *hus-1* /IR	wt vs. wt/IR	wt vs. *hus-1*	wt/IR vs. *hus-1* /IR
C30C11.4		122.93	0.92	-93	0.2
Z66Z7.2a	putative clathrin-coated vesicle/synaptic vesicle proton pump subunit	111.26	0.47	-52.02	0.44
Y9C9A.d	micronemle antigen	106.26	-0.05	-76.6	0.46
C24F3.1a	tram protein (translocating chain-associating membrane protein)	83.9	1.35	-23.08	0.5
D2045.1		69.34	1.37	-31.56	-0.1
Y43F8B.2b	hspc210	38.59	-0.31	-48.35	0.09
F48E8.5	probable protein phosphatase pp2a regulatory subunit	38.19	0.89	-38.76	-0.11
Y53F4B.4d	alpha-contractin (contractin) (centrosome-associated actin homolog)	37.24	1.47	-13.96	0.03
W06H8.f	eh-domain containing protein 2	37.2	0.57	-21.64	0.07
C47D12.6	probable threonyl-tRNA synthetase, cytoplasmic	36.83	0.83	-11.18	0.69
T28D9.1	hypothetical 14.2 kda protein	33.56	0.47	-38.12	-0.67
T01D3.5		33.26	0.45	-47.37	-1.05
Y54E2A.11	eukaryotic translation initiation factor 3 subunit 9 (eIF-3 eta)	31.73	0.88	-35.73	-0.21
T23D8.4	probable eukaryotic translation initiation factor 3 subunit 8	30.79	0.85	-11.21	0.41
T10H9.4	snb-1 synaptobrevin	28.82	0.15	-40.64	-0.6
Y40B1B.5		28.33	0.82	-18.5	-0.22
Y71H2B.10	beta-adaptin 1 (plasma membrane adaptor ha2/ap2 adaptin beta subunit)	24.51	0.58	-11.07	0.34
VF13D12L.3	pyrococcus horikoshii malate dehydrogenase	24.36	-0.34	-110.43	-2.27
B0261.10	synaptobrevin	23.29	-0.1	-28.61	0.24
B0403.4	probable protein disulfide isomerase p5 precursor	20.75	2.68	-2.98	-0.07
Y116A8C.25	splicing factor u2af 38 kda subunit (u2 auxiliary factor 38 kda subunit)	20.67	1.74	-6.71	0.16
C38C3.5a	actin depolymerizing factor 1	19.87	0.65	-23.46	-0.69
F40F8.7	histone H2A-like protein	19.02	0.38	-17.7	-0.29
T22B11.5	2-oxoglutarate dehydrogenase	18.84	-0.13	-28.95	-0.34
Y32H12A.4	protein phosphatase inhibitor 2 (ipp-2)	18.58	0.78	-15.26	-0.48
F29B2.10		18.37	0.43	-6.38	0.83
C34E10.6	probable atp synthase beta chain, mitochondrial precursor	17.82	-0.1	-33.03	-0.64
T05H4.6	eukaryotic peptide chain release factor subunit 1	15.86	2.42	-2.24	0.52
Y46G5A.1	aricagene	15.55	0.5	-15.49	-0.49
F32A11.1		15.17	0.81	-29.51	-0.33
M03A1.6	similarity over a short region to drosophila retinal degeneration b protein	14.41	-0.5	-9.04	1.31
F10G8.7	DNA excision repair protein	14.32	1.35	-8.98	-0.39
C34E10.1		14.09	0.48	-10.74	-0.15
F46F11.6		13.7	0.94	-6.73	-0.02
K10D3.2	snc-14	13.32	-0.02	-11.51	0.17
Y110A7A.17	mat-1 (metaphase/anaphase transition defect)	13.32	0.69	-12.93	-0.65
K12H4.8	hypothetical helicase	13.24	0.27	-0.98	4.73
Z6484.1	ornithine decarboxylase antizyme	12.73	-0.37	-18.95	0.05
K01G5.4	gtp-binding protein	12.57	0.24	-13.5	-0.33
B0416.5		12.43	0.53	-6.01	0.25
Y75B12B.5	peptidyl-prolyl cis-trans isomerase 3	12.23	-0.43	-16.5	0.06
T12F5.3	glh-4 helicase	10.91	1.11	-12.22	-1.34
B0280.3	probable ribose 5-phosphate isomerase	10.69	0.46	-7.72	-0.09
Y53H1B.2		10.67	-0.19	-16.49	-0.25
T07A9.10	acetylcholine regulator	10.54	1.28	-2.69	0.08
K11D9.2A	e1-e2 atpases	10.36	8.7	-10.69	-0.75
W09D6.6	multidrug resistance protein (p-glycoprotein)	10.01	0.62	-3.36	0.56
R12B2.5	similar to notch protein in and just upstream of the poly-gln region	9.91	-0.07	-9.87	0.16
Y47D3A.15	5' -amp-activated protein kinase, beta-2 subunit	9.89	-0.79	-10.56	0.69
F25B4.5	similarity to tpr domains	9.71	1.28	-3.89	0.15
F27B1.1	glutathione s-transferase	9.64	0.61	-3.47	0.48
Y41E3.10	elongation factor 1	9.6	0.22	-10.14	-0.29
B0205.7	casein kinase ii, alpha chain	9.46	0.16	-7.38	0.08
F23F1.1	coat-binding factor subunit php5p	9.22	2.34	-2.82	-0.32
C25A11.4A	200 kda antigen p200	9.02	0.82	-13.64	-0.49
C28H8.3	hypothetical helicase	9.01	-0.5	-4.13	1.93
F43D9.4	stp-1 heat shock hsp20 proteins	8.91	-0.1	-21.32	-1.04
K07C5.1	actin-like protein 2	8.87	0.25	-6.54	0.05
B0205.5	farnesyltransferase alpha subunit	8.85	0.25	-7.18	-0.04
F25H2.10	60S acidic ribosomal protein	8.64	-0.07	-17.14	-0.75
K07E12.1		8.54	-0.41	-4.49	1.46
C44C1.1		8.23	0.55	-3.84	0.23
C33F10.12	mitochondrial phosphate carrier protein	8.21	-0.71	-11.95	0.22
C45H3.10	similarity to S. cerevisiae lst1 protein	7.98	0.93	-2.51	0.33
F26A3.2	cap binding protein	7.95	-0.12	-7.77	0.15
Y51H4A.8	ras-like gtp-binding protein rhea	7.86	-0.28	-3.48	1.51
W02C12.3	transcriptice factor	7.79	-0.54	-14.36	-0.13
F09F7.2	myosin, essential light chain	7.74	-0.16	-25.91	-1.67
M01B12.5	extragenic suppressor of the bimd6 mutation	7.47	8.7	-3.98	0.22
F44E7.4	peptidase	7.42	8.5	-3.22	0.33
D2024.6	f-actin capping protein alpha subunit	7.4	0.76	-6.98	-0.25
M01B12.2	ino4p homolog	7.26	8	8	7.26
T03F1.1	similar to molybdoterin biosynthesis moeb proteins	7.18	0.76	-2.35	0.07
Y45G12B.2		7.11	1.16	-2.52	-0.21
F42A6.7	rbp-1 RNA-binding protein	7.1	2.65	-1.39	-0.08
Y39A1C.3	'cold-shock' DNA-binding domain	7.03	0.43	-5.82	-0.22
K09G1.1		7.02	-0.13	-6.4	0.23
C46G7.1		6.96	-0.5	-25.7	-1.23
R07G3.5		6.93	0.42	-2.66	0.19
T10C6.11	histone H2B.1 and H2B.2	6.9	-0.33	-13.7	-0.39
F58A6.2	leucine rich repeat (2 copies) (2 domains)	6.78	1.97	-1.32	0.13
F23B2.6	vimentin like	6.72	0.75	-6.78	-0.76
D2013.5	gtp-binding protein	6.69	3	-0.78	0.08
Y71F9AL.16	drosophila melanogaster actin-like protein 3	6.59	0.95	-2.74	0.04
C34B2.8	mitochondrial lon protease homolog precursor	6.47	-0.27	-0.24	6.62
F52C9.1		6.45	0.89	-5.81	0.03
T01C3.7	fibrillarin	6.39	0.55	-3.23	0.13
T21B10.3		6.35	0.89	-1.45	1.75
F22F7.1	conserved hypothetical protein	6.31	1.45	-1.68	0.11
D1007.15	human hypothetical protein klaa0195	6.23	0.55	-3.47	0.04

K09H9.6	second-step splicing factor 1, ssf1 protein	6.2	1.36	-0.89	0.61
ZC506.3	phosphatidylserine synthase i	6.14	0.74	-3.51	-0.1
C15F1.7	superoxide dismutase (cu-zn)	6.1	0.11	-9.59	-0.66
T05B11.1		6.07	-3.82	-9.88	2.14
F15E11.9	c-type lectin	5.98	0.29	-6.12	-0.32
Y75H2A.6	human sop2-like protein	5.88	0.5	-4.38	0.02
T05E11.5		5.81	0.74	-1.4	0.62
Y57A10A.P	dictyostelium discoideum myosin ii heavy chain, non muscle	5.76	0.35	-4.38	-0.03
F33H1.1	daf-19 DNA binding transcription factor	5.72	0.55	-4	-0.15
F53F1.4	cuticlin protein	5.7	0.21	-5.16	-0.11
C23F12.1	human endothelial actin-binding protein (abp-280)	5.69	-0.43	-12.24	-0.38
M03C11.6		5.69	-0.03	-18.69	-1.56
C16H3.3		5.68	0.69	-1.75	0.44
C29E6.3	protein tyrosine phosphatase	5.68	-0.01	-6.81	0.16
C18A3.3	hypothetical 52.1 kda protein	5.66	1.98	-0.62	0.39
W04D2.3	ins-11 ogre family	5.58	0.6	-5.88	-0.67
Y47G6A.8	endonuclease	5.57	0.36	-6.26	-0.51
Y57A10A.13	predicted 3'-5' exonuclease	5.57	-0.44	-6.37	0.76
ZK546.14	putative surf6 protein	5.52	0	0	5.52
Y38C1BA.3	collagen	5.49	-0.38	-19.69	-1.31
C44E4.1a	alkoxyd2 pushover	5.43	-3.63	-2.54	7.4
Y113G7A.4	sodium-calcium exchanger	5.41	-0.61	-22.77	-1.31
F22D6.6		5.36	0.75	-2.77	-3.04
C02F4.2	serine/threonine protein phosphatase	5.35	-0.07	-4.74	0.19
C06G3.7	probable thioredoxin reductase	5.35	-1.3	-6.19	0.15
K04F10.4c	endoprotease bli-4 precursor	5.33	0.97	-1.82	0.14
F42G4.3A	lim domain containing proteins	5.31	-1.4	-15.24	-0.83
F09E5.3	putative dienoxribose-phosphate aldolase	5.3	0.47	-3.44	-0.03
C14B1.7	similar to *C. elegans* protein c14b1.7	5.29	1.96	-11.55	-4.91
C25H3.8	*S. cerevisiae* vacuolar protein sorting-associated protein vps13	5.28	0.38	-3.63	-0.02
Y39A1C.2	exi-1 hect-domain (ubiquitin-transferase)	5.27	1.22	-1.68	0.06
F52B11.7	human bumetanide-sensitive sodium-(potassium)-chloride cotransporter 1	5.17	0.5	-8	-1.19
Y17G9B.9		5.17	1.2	-30.46	-10.22
C16C8.13	similarity to ubiquitin	5.09	3.72	-0.44	-0.12
F42G9.1	probable protein phosphatase	5.09	1.33	-1.35	0.11
F54C9.9		5.09	-0.18	-0.38	5.09
C56C10.3	similar to *S cerevisiae* nuclear protein esf7	4.99	0.87	-2.83	-0.01
Y57A10A.3		4.99	1.6	-2.02	0.24
D2024.3	putative multipass transmembrane	4.96	-2.58	-1.5	7.57
B0207.4	air-2 protein kinase	4.91	1.4	-2.97	-0.18
C05E4.3	serine protease inhibitor	4.86	-0.58	-18.59	-1.11
T04A8.7	1,4-alpha-glucan branching enzyme	4.85	0.57	-7.47	-1.28
Y54H5A.2		4.85	-0.07	-6.03	-0.12
R07H5.2	cel8937 carnitine palmitoyltransferase ii	4.83	0.76	-1.85	0.61
ZC404.3		4.83	0.59	-1.33	0.57
F56G4.5	thioredoxins	4.75	-0.01	-2.21	0.81
C30A5.4	probable serine/threonine protein phosphatase	4.72	1.9	0	2.01
C26E6.5		4.71	1.03	-16.26	-1.19
T03E6.7	cathepsin-like protease	4.7	0.25	-5.34	-0.4
F28D2.2	chicken myosin heavy chain, fast skeletal muscle, embryonic	4.62	-0.12	-1.99	1.11
Y18D10A.20	pfn-1 profilins	4.57	0.83	-6.97	-1.61
T05C3.5		4.54	1.05	-1.78	-0.03
T08G11.4		4.54	0.81	-0.78	0.74
F09A5.4a		4.49	-0.03	-4.78	-0.02
Y71F9AL.D	human coatomer alpha subunit (alpha-coat protein)	4.47	0.74	-0.95	0.61
T07D4.3	probableATP-dependent RNA helicase a (nuclear DNA helicase ii)	4.42	1.89	-0.83	0.1
ZK1127.10	putative cystathionine gamma-lyase	4.39	-0.24	-3.37	0.53
C47A10.2	similarity to *C. elegans* olfactory receptor odr-10	4.35	4.21	-0.01	0.02
K02G10.6	similar to *S. cerevisiae* tag1	4.31	1.86	-0.81	0.16
T27C4.4a	metastasis associated 1-like protein	4.3	0.25	-4.3	-0.25
F27C1.6	myeloblast klee0266	4.29	1.43	0	1.18
D2021.2		4.28	0.3	-0.3	2.12
K02D7.3	cuticular collagen	4.25	1.88	-10.78	-3.7
M01D1.5		4.23	-0.06	-1.37	1.33
EEED8.5	putative pre-mrna splicing factor ATP-dependent RNA helicase	4.22	3.49	-0.24	-0.07
F59E10.2	peptidyl-prolyl cis-trans isomerase 4	4.16	0.15	-1.61	0.73
F32D8.5a	uncharacterized membrane protein	4.12	0.87	-2.67	-0.12
C07H6.1	DNA ligase iv	4.07	0.83	-0.75	0.59
F28B3.7	chromosome segregation protein smc5	4.01	0.66	-0.86	1.83
F38E1.3	serine /threonine-protein kinase	3.98	0.1	-2.16	0.43
B0205.3	26S proteasome regulatory subunit rpn	3.97	0.64	-2.99	-0.65
ZC262.3	n-cam ig domain	3.97	-0.23	-9.9	2.21
C25A11.2		3.96	1.29	-2.01	-0.26
F27D4.2	guanine nucleotide exchange factor unc-73a	3.95	1.11	-2.67	-0.31
F55C7.7d	acyl-coa dehydrogenase	3.95	-0.8	-12.82	-0.55
Y53H1A.5	histone deacetylase family	3.92	0.2	-4.72	-0.39
F42A8.2	putative succinate dehydrogenase iron-sulfur protein, mitochondrial precursor	3.88	-0.08	-10.2	-1.12
B0213.1	transposable element tc1 transposase	3.82	-0.35	-7.2	-0.26
T27E9.7	ABC transporters (2 domains)	3.81	-0.65	-5.84	0.31
Y73B6A.1	protein kinase	3.8	0.29	-0.99	0.87
C13F10.4		3.79	0.48	-2.08	0.05
T28D3.2	tropomin	3.77	-0.29	-13.34	-1.34
F23F1.8	probable 26S protease regulatory subunit s10b	3.73	0.45	-2.92	-0.2
K03H1.2	putative pre-mRNA splicing factor ATP-dependent RNA helicase	3.73	-0.08	-0.52	2.4
K11H3.1	probable glycerol-3-phosphate dehydrogenase [NAD+], cytoplasmic	3.73	0.31	-4.38	-0.49
C05E7.A	*S. cerevisiae* intracellular protein transport protein uso1	3.71	-0.68	-0.68	3.71
C33A12.7	glyoxalase ii	3.66	-0.13	-1.73	0.62
R06C7.4	katnin a	3.66	0.45	-4.7	-0.76
Y51B9A.3		3.63	-3.24	-13.53	0.35
C26C6.1	hmg (high mobility group) box, bromodomain (5 domains), zinc finger, c2h2 type	3.61	1.42	-2.37	-0.77
T23B12.6	ny-ren-45 antigen	3.57	0.1	-5.74	-0.62
T01G6.1	histidyl-tRNA synthetase	3.49	0.38	-2.03	0.07
F31D4.2		3.47	0.25	-1.33	0.54
F55C5.3	twk-11 potassium channel protein	3.45	1.75	0	0.62
F25D7.1	putative NADH oxidoreductase complex i subunit	3.44	0.54	-2.62	-0.6
F45E1.1	hypothetical 10.8 kda protein	3.44	-0.84	-4.8	0.41
F53G2.6	nuclear transport receptor	3.43	1.46	-1.34	-0.3
Y71F9B.1		3.42	0.7	-2.53	-0.74
Y105C5B.P	similar to small histidine-alanine-rich protein precursor	3.38	-0.1	-0.88	1.57
Y54E5B.4	ubiquitin-conjugating enzymes	3.38	0.67	-2.02	-0.15
F55A3.1	*S. cerevisiae* rsm4 protein	3.36	0.37	-2.34	-0.05

R06A4.8	alpha amylase	3.36	-0.13	-2.89	0.27
Y45G12B.3	transcriptional regulator, putative	3.33	0.88	-7.82	-1.01
R02D5.1	dehydrogenase	3.32	-0.2	-5.12	-0.18
T27D12.2	chloride channel protein	3.32	-0.24	-14.64	-1.93
Y17G7B.3	metallo-beta-lactamase superfamily	3.32	0.54	-0.92	0.46
B0285.5	c5-glucuronyl epimerase	3.31	7.26	0.39	-0.38
W09B6.4		3.28	0.24	-4.2	-0.5
F54E12.4	histone H2B	3.27	-0.33	-6.01	-0.23
H17B01.4		3.27	0.45	-1.83	0.12
K09B3.2		3.26	-0.57	-4.77	0.16
ZK973.2		3.21	0.25	-3.01	-0.19
R02F2.1	Cyclin B and related kinase-activating protein	3.2	0.14	-10.61	-2.15
Y75B12B.2	peptidyl-prolyl cis-trans isomerase 7	3.18	0.51	-2.54	-0.28
C35C5.4	inig-2 ras-related protein	3.17	0.25	-2.49	-0.05
F33D4.5		3.17	0.69	0.03	1.53
H27M09.6		3.13	0.61	0.12	3.59
Y39B6B.FF	rat serine/threonine protein phosphatase 5	3.13	1.76	-1.22	-0.5
B0491.1	hypothetical transmembrane protein	3.11	1.33	-0.46	0.2
C24H12.5		3.09	0.53	-2.74	-0.4
C47B2.2a	probable uracil phosphoribosyltransferase	3.09	0.45	-2.14	-0.11
T24H7.2	similar to heat shock protein	3.08	-0.04	-0.82	3.16
C06E8.2		3.03	-1.33	-6.84	0.34
F41H10.3	transcriptional activator ercap	3.03	0.74	-1.73	-0.18
K08H10.1	lea-1	3.03	-0.88	-9.85	-2.32
C47B2.6	NAD dependant epimerase/dehydratase family	3.02	2.33	0.3	0.58
ZK470.2a		3	0.22	-4.13	-0.56
B0365.3	eat-6 na(+)/k(+) atpase alpha subunit	2.99	0.83	-1.42	0.01
F55C5.7	serine/threonine kinase	2.98	0.83	-1.84	0.19
F17C8.5	twk-5	2.94	1.84	0.84	1.01
C13A10.3	similarity to human guanine nucleotide regulatory protein	2.93	-0.57	-2.68	0.67
F14D12.6	g-protein coupled receptor	2.92	-0.65	-1.79	1.32
F19B2.5		2.91	1.23	0.57	1.75
T08A9.4		2.9	0.87	-2.88	-0.06
C47E12.5	ubiquitin-activating enzyme	2.88	0.92	-1.52	-0.25
Y48A6B.3	ribosomal protein l7ae	2.88	0.34	-2.27	-0.13
F18C5.3	similar to s. cerevisiae hypothetical 287.5 kda protein in pdr region	2.87	0.26	-0.45	1.11
E01A3.2	DNA helicase	2.85	0.23	0.28	2.93
Y60A3A.6	similarity in c. elegans olfactory receptor odr-10	2.85	-0.11	-4.84	-0.18
K09H9.6	second-step splicing factor 1, slf1 protein	2.84	1.18	-0.37	0.28
R10E11.1	cbp-1 protein	2.82	0.59	-2.14	-0.31
T03F1.4	hypothetical 23.7 kda protein	2.81	0.76	-1.63	-0.22
B0261.3	organic cation transporter oct2r	2.78	-0.71	-0.31	3.64
K08F4.1	yeast chd2p like	2.78	-0.08	-0.71	1.39
C01G6.5	forkhead-associated (fha) domain	2.74	0.61	-0.52	0.53
F56A11.6		2.72	-13.48	-13.48	2.72
Y54B9A.8	similar to small histidine-alanine-rich protein precursor	2.71	0.87	-0.57	1.22
M02E1.1		2.7	-0.28	-2.19	0.13
T03E7.3	ras-related protein	2.69	0.69	-6.68	-1.26
F47F6.7	gtpase activating protein	2.66	0.1	-6.78	-1.34
F58A3.1a	lin-domain binding factor 1	2.66	0	1.02	6.41
F58B3.5	probable methionyl-tRNA synthetase (methionine--trna ligase)	2.66	1.38	-0.01	0.53
F33G12.5	similar to the human 95k golgi antigen	2.65	0.94	-0.3	0.44
C06A5.8		2.63	1.85	-1.25	-0.27
C28H8.4	putative er lumen protein retaining receptor	2.63	0.99	-1.1	-0.15
F20D6.4	serine protease inhibitor	2.62	0.41	-0.91	0.35
F10C2.5	mannosyl-oligosaccharide alpha-1,2-mannosidase	2.61	1.18	0.25	1.07
W02D9.2	yeast yip1 protein like	2.61	0.22	-3.59	-0.55
Y54G11A.9		2.61	0.57	-1.18	0.06
T10C6.6a	camp inducible 2 protein	2.6	0.15	-2.98	-0.27
T12G3.7		2.6	0.48	-1.13	0.14
F26H11.5		2.58	0.87	-3.99	-0.49
Y71H9A.3	stc-4 protein	2.57	0.39	-1.54	0.01
F46A9.6	mec-8 mechanosensory gene mec-8	2.56	0.52	-2.86	-0.66
F59G11.3		2.55	0.86	-0.9	-0.05
T18H9.2	protein kinase	2.55	-0.4	-5.25	-0.26
B0564.3	putative membrane protein	2.53	-13.17	-34.19	0.42
C05G5.2	nucleolar phosphoprotein	2.52	0.65	-1.11	0.01
C37C3.6B	lacunin precursor	2.51	-0.5	-6.78	-0.47
F42A10.4	elongation factor 2 kinase (eef-2 kinase)	2.51	-0.65	-6.23	-0.25
Y52B11A.3	heme-binding domain in cytochrome b5 and oxidoreductases	2.51	2.75	0	-0.07
W02B12.2	pre-mrkna splicing factor like protein	2.5	0.92	-1.74	-0.5
K06A1.5	hypothetical 52.8 kda trp-asp repeats containing protein	2.49	-0.19	-2.42	0.21
B0334.8	phosphatidylinositol 3-kinase age-1	2.48	0.87	-0.72	0.08
W05H7.4		2.48	0.88	-6.25	-1.26
C06A5.2		2.47	0.28	-0.34	1.02
T08E4.1	chicken myosin heavy chain, nonmuscle	2.47	0.45	-1.99	-0.25
B0334.5	phytoene synthase precursor	2.46	0.49	-1.33	0
K04H4.1	emb-9 collagen	2.46	-0.68	-5.88	-0.15
Y47D9A.1a	mannose-1-phosphate guanyl transferase	2.45	0.4	-0.71	0.44
B0511.12		2.44	0.88	-1.85	-0.12
K05B2.1		2.44	-0.11	-2.69	0.04
Y18D10A.14		2.43	-0.13	-2.73	0.04
F56C3.9		2.42	0.24	-0.11	1.49
K03D10.1	wap-type (whey acidic protein) ' four-disulfide core ', fibronectin type iii domain	2.4	-0.13	-3.42	-0.15
T22H9.3		2.4	-1.56	-2.83	1.88
F31D4.4	cub domain, lectin c-type domain short and long forms	2.39	-1.16	-3.1	0.76
M03C11.4	human histone acetyltransferase type b catalytic subunit	2.39	-0.11	-3.78	-0.27
F08B4.6	s-heparan sulfate sulfotransferase	2.38	0.9	-0.37	0.3
T13B5.3	acid phosphatase	2.37	-0.18	-1.78	0.43
F43G9.1	probable isocitrate dehydrogenase [NAD] subunit alpha, mitochondrial precursor	2.36	-0.02	-3.74	-0.26
Y45F10D.9		2.36	0.19	-1.26	0.25
C44H4.4		2.33	0.81	-1.15	-0.18
T04A8.5	amidophosphoribosyltransferase	2.32	2.9	1.61	1.22
B0511.1		2.31	0.59	0	1.06
D1037.2	semaphorin 1a precursor	2.29	0.77	-1.99	-0.61
Y71A12D.B	transcription initiation factor TFIID 250 kda subunit	2.28	0.11	-0.18	1.51
ZC504.2	serine/threonine kinase (stk2)/stka subfamily)	2.28	0.74	-1.88	-0.1
F25D2.2	similar to EGF-like repeats	2.27	0.53	-0.79	0.2
Y105E8C.D	RNA polymerase precursor	2.27	-0.52	0.31	5.5
F26H11.3a	bromodomain	2.26	0.16	-0.72	0.64
Y57A10A.15	mitochondrial DNA polymerase gamma, catalytic subunit	2.26	0.24	-1.99	-0.14
C15C8.4	human alpha-2-macroglobulin receptor-associated protein like	2.24	1.88	-0.87	0.45

C42C1.11	peptidase	2.23	0.5	-1.52	-0.17
Y11B2C.D	golgi-associated microtubule-binding protein	2.23	0.7	-0.84	0.03
C01C10.2	hypothetical 24.1 kda protein	2.22	-0.77	-4.43	0.05
ZK849.1	pdz domain (also known as dlh or glgf)	2.22	-0.5	-1.41	1
F44E7.5		2.21	1.36	-1.51	-0.85
F37B12.3		2.2	0.42	-3.81	-1.14
Y38A8.3	similarity to a small region of smt4_yeast	2.2	0.35	-1.08	0.14
C10G11.9	human splicing factor, arginine/serine-rich 4 (pre-mRNA splicing factor srp75)	2.19	-0.38	-19.58	-3.75
Y116ABC.13	S. cerevisiae DNA repair and recombination protein rad54	2.19	1.81	-1.45	-0.54
T01G5.6	nuclear hormone receptor	2.16	-0.06	-1.47	0.36
Y43F11A.6		2.16	-0.96	-0.96	2.16
F53B1.2		2.13	0.72	-1.61	-0.44
RD6B10.1	protein-tyrosine phosphatase	2.13	0.38	0	1.26
Y48C3A.17	human transcription factor e2f3	2.13	0	-0.35	1.31
F58B4.3		2.12	-0.38	-2.22	0.02
AH10.1	4-coumarate:coenzyme a ligase	2.11	-2.01	-2.46	1.1
C41G7.2	drosophila claret segregational protein like	2.11	0.37	-1.69	-0.18
T09A5.9	sdz22 protein	2.11	0.19	-1.56	0.02
R12E2.12		2.1	0.56	-1.56	-0.29
C04G6.1	ser/thr protein kinase	2.09	-0.14	-2.87	-0.1
F23H2.5	DNA polymerase family b	2.09	1.1	-0.71	-0.16
H27C11.1	zinc finger, c4 type ; ligand-binding domain of nuclear hormone receptors	2.09	-0.38	-2.81	0.13
T24D1.2	zinc finger, c2h2-4 type (ring finger) (2 domains)	2.08	0.7	-1.19	-0.21
B0035.8	histone H2B	2.07	-0.27	-4.15	-0.32
F22B5.6		2.07	-1.2	-2.48	-0.21
Y67A6A.1	similar to the s1 family of peptidases	2.06	0	0	2.06
T20G5.11	double-stranded RNA binding motif	2.03	1.36	-0.08	0.19
C16C10.6	ccr-1	2.02	0.91	-0.19	0.32
F56F11.4	26s protease regulatory subunit	2.01	0.9	-0.29	0.23
F29D11.1	low-density lipoprotein receptor-related protein precursor	1.99	0.89	-2.88	-0.12
T28F2.7	similar to an amiloride-sensitive sodium channel beta-subunit	1.99	-0.12	-3.19	-0.25
ZK682.5	human platelet glycoprotein v precursor	1.99	-1.98	-2.15	1.83
B0787.8	phospholipase	1.98	0	0	1.98
K04C2.2		1.97	0.41	-0.95	0.08
F29F11.1	probable udp-glucose 6-dehydrogenase	1.96	0.85	-2.4	-0.2
F48G11.3	serine/threonine-protein kinase	1.96	0.82	-1.37	0.34
K10C3.5	elongation factor ef-2 like	1.96	1	2.19	3.72
C04G2.6	dis3 protein homolog	1.91	0.86	-0.28	0.23
Y48B6A.1		1.91	0.21	-1.76	-0.15
C06G1.5	protein phosphatase pp2a	1.9	0	-1.54	0.14
F46B3.15		1.9	-4.81	-6.23	1.71
F43E2.8	heat shock 70 kda protein d	1.88	0.82	-0.31	0.14
F49E2.4	glutin	1.87	-0.56	-2.2	0.4
LLC1.1	tra-3 calpain	1.87	0.31	-1.49	-0.14
Y38C9A.2	gtp-binding protein	1.87	0.59	-2.51	-0.95
ZC123.1	mouse sperm mitochondrial capsule selenoprotein	1.87	-0.32	-0.32	1.87
Y54E10A.6	yeast phenylalanyl-tRNA synthetase alpha chain cytoplasmic	1.86	0.71	-1.74	-0.64
Y49F6B.A		1.85	1.84	-1.15	-0.55
T13H5.2	retinal-binding like protein	1.84	0.83	-0.22	0.27
Y47D3A.8	sex-determining transformer protein 1	1.84	0.41	-0.4	0.43
C54G4.8	cytochrome c1, heme protein	1.83	0.82	-2.81	-0.38
Y45F10D.3	glycosyl transferases	1.83	1.28	0.11	0.39
C34E7.1	triticum aestivum high mw glutenin subunit	1.82	0	0	1.82
Y119C1A.1		1.8	0.48	-0.64	0.16
B0361.4	hypothetical 42.9 kda protein	1.79	-0.38	-1.41	0.6
R151.7	hsp c82.5	1.79	-0.31	0.16	3.27
Y57G11C.4	29 kda golgi snare	1.79	0.3	-1.19	-0.02
F25G6.9		1.78	3.84	0.67	-0.05
B0506.8	phospholipase	1.76	0.86	-0.58	0.05
C16H3.4		1.75	-0.59	-2.2	0.37
C29F9.1		1.75	0.38	-0.64	0.42
T25D10.4	hypothetical 27.8 kda protein	1.75	0.84	-1.85	-0.08
Y46H3A.1	similar to reverse transcriptase	1.75	0.66	-0.82	-0.1
C04H5.6	putative pre-mRNA splicing factor ATP-dependent RNA helicase	1.74	2.12	0.27	0.12
ZK1127.4	tak-1beta	1.74	0.88	0.25	2.16
K01G5.2a	`chromo` (chromatin organization modifier) domain	1.73	0.6	-1.66	-0.56
T03F6.1	alcohol/ether dehydrogenases, short chain type	1.73	-0.33	-2.29	0.11
C52E4.6A	cyl-1 (cyclin L)	1.72	0.75	-0.54	0.01
F57C7.3	probable syndecan precursor	1.72	0.56	-0.86	-0.07
F25H8.6	putative udp-glucuronosyltransferase ugt5 precursor	1.7	-0.55	-2.14	0.01
K07B1.4		1.7	-0.01	-2.18	-0.17
C07E3.4	protein-tyrosine phosphatase	1.69	-0.26	-0.72	0.67
F11A6.2	phospholipid scramblase 1	1.69	0	0	1.69
K11E4.5	ets-71 zinc finger, c4 type (two domains)	1.68	-0.37	-2.53	-0.23
F15E6.1	200 kda antigen p200	1.67	0.58	-4.17	-2.08
F54F2.8	chinese hamster peroxisomal farnesylated protein	1.67	1.34	0.2	0.37
T09E8.2	cyb-3 (G2/mitotic-specific cyclin B3)	1.66	0.84	-1.33	-0.61
T10B11.6		1.66	0.18	-1.28	0
W02D7.6		1.66	0.88	-0.25	0.97
Y105E8B.D	novel protein (ortholog of rat exo84)	1.66	0.1	-0.9	0.27
C07E3.2	arabidopsis thaliana hypothetical protein t30d6.27	1.65	0.59	-0.3	0.28
F07E5.5	zinc-finger protein	1.65	-0.34	-2.11	0.14
T05G5.9	coiled-coil protein	1.65	1.89	-0.84	-0.14
C35A5.9	histone deacetylase/ecuc/apha family protein	1.61	0.89	0	1.39
R11A8.5	glutathione s-transferases	1.61	0.45	-0.38	0.55
T06D8.5		1.61	0.85	-0.44	0.72
F26E4.8	tubulin alpha-2 chain	1.6	0.2	-2.22	-0.49
C56D2.7	putative novel acyl transferase	1.59	2.48	0.8	0.34
RD1K2.2	kil receptor	1.59	0.13	-1.35	-0.01
F52G3.1	similar to C. elegans unc-89	1.58	0.3	-0.45	0.36
C33H5.8	similar to mitochondrial precursor proteins import receptors	1.57	0.76	0.01	0.48
F25B5.4	caenorhabditis elegans ubiquitin	1.55	-0.08	-2.78	-0.71
F46C8.3		1.55	-0.23	-1.02	0.55
K07F5.4	kin-24 tyrosine-protein kinase	1.55	-1.37	-2.68	0.64
Y65B8A.5	g-protein	1.55	0.22	-0.5	0.39
ZK354.2	protein kinase	1.55	-0.93	-2.27	0.15
ZK792.3	ins-9 ogre family	1.55	0.34	-1.35	-0.24
F36F2.2		1.54	-2.03	-0.88	3.09
F28A5.2	similar to enterococcus faecalis trab	1.53	0.93	-0.41	-0.07
R74.1	probable leucyl-tRNA synthetase	1.53	0.36	-0.11	0.68
T04F8.2		1.52	0.87	0	0.35
T14B4.6	cuticle collagen dpy-2 precursor	1.52	0	0	1.52

C06B8.1	sdp-glucuronosyl transferase	1.51	0.78	0.34	0.92
C18E3.3		1.51	-0.3	-2.58	-0.1
F16H9.1A	regulator of g protein signalling domain	1.51	-0.69	-0.69	1.51
Y17G9B.5		1.51	0.19	-0.85	1.02
Y34B4A.8		1.51	0.12	-0.07	1.06
F17E9.12	caenorhabditis elegans h4	1.5	-0.52	-5.82	-0.79
C53D5.5	gamma-glutamyltranspeptidase	1.49	-0.35	0.23	3.16
T05B9.1		1.49	0.89	-9.38	-3.55
Y113G7A.9		1.49	0.42	-0.12	0.56
R11A5.1a	human beta-nap protein like	1.47	1.47	0.75	0.74
C04E6.5	similarity to the peptidase family c19	1.46	-0.11	-1.57	0.06
T28F5.7		1.45	1.22	-1.51	-1.28
T23B12.3	ribosomal protein	1.45	0.13	-2.22	-0.96
Y62E10A.11a		1.45	0.81	-0.51	-0.18
Y46G5A.5	rat cdp-diacylglycerol--inositol 3-phosphatidyltransferase	1.43	0.63	-1.15	-0.44
Y110A7A.9		1.42	0.19	-0.56	0.3
F13H6.1	zinc-finger protein	1.41	-2.6	-2.6	1.41
Y71H2B.5	aminotransferase, putative	1.4	0.23	-0.59	0.22
F15B9.8	thrombospondin type 1 domain	1.39	0	-0.25	0.92
R102.4a	yeast gly1 like	1.39	0.86	0.86	3.19
B0244.2	c-herdain	1.38	-1.82	-1.77	1.42
M01E5.4		1.38	0.24	-4.37	-1.8
B0238.4		1.37	1.34	0.13	0.15
F27C8.1	integral membrane protein ets6 like	1.37	-4.2	-0.85	0.46
M163.3	histone H1.1	1.37	-0.25	-1.79	0.06
C14C6.1		1.36	1.51	0	-0.06
Y95B8A.6	similarity to procollagen alpha chain 1(v) chain	1.35	-0.68	-9.49	-1.63
Y47G6A.22		1.34	-0.04	-1.83	0.19
F46F11.9		1.3	-0.33	0.14	2.49
F53E10.6		1.29	1.18	-1.82	-0.93
F23F12.6	probable 26s protease regulatory subunit 6b	1.27	0.32	-0.75	-0.02
W07E11.1	glutamate synthase	1.26	-2.05	-6.44	-0.08
C35A5.8	ran binding protein 16 form 1	1.24	0.92	0.14	0.32
C41H7.7	similar to c-type lectin domain	1.22	-0.31	-2.87	-0.05
R10E11.4	sqv-3 galactosyltransferase	1.22	0.44	-0.98	-0.28
C30G4.3	gcy-11 guanylate cyclase receptor	1.21	-0.89	-6.39	-1.77
F25H2.6	ph domain	1.2	0.85	-0.3	0.03
M01G5.4		1.2	0	-1.81	-0.27
F22B3.1	C. elegans histone H4	1.19	-0.67	-4.87	-0.6
T25G12.7	dehydrogenase	1.19	-0.28	-13.01	-4.01
W02F12.3	gastric mucin (fragment)	1.19	0.64	-1.46	-0.85
W08C5.7	putative transmembrane protein g5p	1.19	1.83	-0.81	0.67
F14D2.10	similarity to RNA recognition motifs	1.17	1.75	0	-0.27
F41C3.3	long-chain-fatty-acid coa ligase	1.17	-0.53	-5.55	-0.98
VF36H2L.1		1.15	0.81	-1.3	-0.08
C55C3.3	S. cerevisiae glucoamylase s1/s2 precursor	1.14	-1.21	-2.47	0.36
F26D2.12	lectin c-type domain	1.14	0.28	-1.15	-0.29
H06O01.2	chromodomain-helicase-DNA-binding protein	1.13	1.43	0.34	0.17
Y113G7A.8	NADPH-dependent FMN and FAD containing oxidoreductase	1.13	0.81	-0.21	0.73
B0495.9	hypothetical 30.6 kda protein	1.12	0.48	-0.41	0.02
C14A11.6		1.12	0.42	-1.12	-0.42
C44B9.5	similar to protein tyrosine phosphatase	1.12	0.57	-0.08	0.25
W06H12.1		1.12	0.86	-2.2	-0.59
Y48C3A.16	parvulin	1.12	0.53	0.05	0.45
ZK524.1	integral membrane protein spe-4	1.11	-0.57	-1.19	0.51
B0025.1	sps-34 phosphatidylinositol 3-kinase	1.1	0.44	-0.08	0.35
F02A9.1a	hypothetical 22.4 kda protein	1.1	-0.12	-1.75	-0.18
F33A8.1	let-858	1.1	0.45	0.03	0.58
H16D14.e	cotransporter 3	1.1	-8.1	-2.84	-0.31
T27E9.3	serine/threonine kinase (cdc2/cdkx subfamily)	1.1	0.45	-0.81	-0.25
Y43F8C.7		1.1	8.1	-1.35	-0.23
C35E9.8		1.07	-0.17	-2.28	-0.36
C23G10.3		1.06	0.86	-9.7	0.14
K07D4.3	26S proteasome-associated pad1 homolog	1.06	1.22	-0.88	-0.16
C12C8.1	heat shock protein 70	1.05	1.36	-2.74	-3.21
Y67H2B.C	serine/threonine protein phosphatase	1.05	-0.88	-0.66	1.32
ZK829.10	sodium-dependent neurotransmitter symporter like	1.05	0.24	0.38	1.27
F18A12.3	peptidase	1.04	-1.5	-1.45	1.06
F25H2.4		1.04	0.23	-2.33	-1.02
F35E2.5		1.04	-0.67	-0.86	2.22
W07E6.4	prp-21 splicing factor	1.04	0.32	-0.82	-0.24
B0041.2		1.02	0.63	-0.76	-0.42
F44A2.5		1.02	0.82	-1.82	-0.43
B0412.3	similar in serine repeat region to rat thyroxine-binding globulin	1	0	-0.06	0.9
C04F5.1		1	1.66	-1.34	-1.41
F37D6.1	brca1 c terminus (brct) domain (4 domains)	1	1.73	0.15	-0.19
T05A7.4	hmg-11 nuclear phosphoprotein (weak)	1	0.82	-2.27	-0.67
Y106G6H.7		1	0.85	0.88	0.16
C31H1.2		-1.01	0.39	2.6	0.29
H05L14.1	casein kinase	-1.01	-1.02	0.88	0.87
M162.3	similarity to cytochrome c oxidase subunit 1 from manduca sexta	-1.01	-0.44	0.9	0.36
T06F4.2	chloride channel protein	-1.01	0.39	0.73	-0.62
T28D4.17	similarity to aneumocystis carinii msg102 major surface glycoprotein	-1.01	0.26	1.05	-0.23
W10D9.3		-1.01	0.32	1.42	-0.09
F54E4.3		-1.02	0.19	0.2	-1.01
Y37D8A.15		-1.02	-1.08	-1.01	-0.95
C40D2.3	similarity to toxocara canis surface coat glycoprotein tex-120	-1.04	-0.02	2.9	0.95
C46H11.8	similarity to the superfamily dbl transforming proteins. 6/2000	-1.04	0.62	1.27	-0.46
C16C10.2		-1.05	-0.02	1.85	0.42
F55F1.1	similarity to the superfamily dbl transforming proteins. 6/2000	-1.05	-0.44	1.03	0.42
W04C9.2		-1.05	0.21	1.54	0.02
D2092.8		-1.06	-0.37	0.21	-0.24
ZK970.7	sv-17 antigen precursor	-1.06	0.23	0.44	-0.74
C34D4.11	petunia glycine-rich cell wall structural protein 1 precursor	-1.07	-0.13	0.85	0.01
F28B3.4		-1.07	0.81	0.98	-0.06
T06C12.7	str-84 zinc finger, o4 type (two domains)	-1.07	0.72	1.93	-0.21
C06B8.8	60s ribosomal protein l38	-1.09	0.14	0.64	-0.45
F07B10.1	human clk3 protein like	-1.09	0.38	4.86	1.03
F29B9.11		-1.09	-0.03	0.45	-0.28
T04A8.13	neurofilament triplet m protein	-1.1	-0.52	0.81	0.31
C55A1.9		-1.11	0.81	0.77	-0.2
F07F6.4	zinc finger protein	-1.11	-0.47	0.02	-0.41

R13.4		-1.11	0.28	3.03	0.49
W02A2.6	titin, skeletal muscle isoform	-1.11	0.74	0.31	-1.8
Y37H9A.6	bacterial mutt protein	-1.11	0.26	2.1	0.17
F44A2.6	similarity to yeast hypothetical protein in atp3 region	-1.12	0.33	0.72	-0.64
T13C5.1	cytochrome p450	-1.12	-0.2	0.84	0.04
C16E9.1	similarity to collagen chain alpha	-1.13	-1.04	-0.2	-0.25
Y62E10A.1	cryptochiton stelleri 60S acidic ribosomal protein p2	-1.13	-0.21	0.7	-0.04
C38C3.1		-1.14	-0.07	0.1	-0.82
Y61B8B.1		-1.14	-0.83	1.1	0.79
T28H11.7		-1.15	-0.13	1	0.05
Z63S3.5	hypothetical 13.8 kda protein	-1.15	-0.85	0.19	0.03
DH11.2		-1.17	-0.21	-0.41	-1.53
F29B9.10	similarity to bacillus stearothermophilus 30S ribosomal protein s21	-1.17	0.48	1.64	-0.22
K12H4.2	hypothetical 23.2 kda protein	-1.17	0.13	3.02	0.64
C06G3.11	small zinc finger-like protein	-1.18	0.13	1.42	-0.02
F36A2.6	40S ribosomal protein s15	-1.18	0.18	0.72	-0.5
T01B8.6	putative mitochondrial 28S ribosomal protein s14	-1.19	0.61	4.12	0.45
C05D11.10	hypothetical 11.8 kda protein	-1.2	0.76	3.19	0.08
F29B9.5		-1.21	-0.64	0.04	-0.3
F21H7.4	similarity to a c-type lectin domain	-1.21	-0.38	0.64	0.03
F32H2.2	sdt1 protein like	-1.21	0.35	2.77	0.27
F45E7.3	neurokinin receptor like	-1.21	-0.7	0.25	-0.04
Y59A8B.U		-1.21	0.62	1.48	0.1
C34F6.6		-1.22	-0.8	0.51	0.22
F31D5.2	putative translation product	-1.22	-0.61	0.33	-0.03
F36D4.4	similarity to alpha 1c-adrenergic receptors	-1.22	0.21	0.83	-0.65
F40A3.5	protein kinase	-1.22	-0.42	0.12	-0.4
R11.1	mitochondrial transporter protein	-1.22	0.2	2.21	0.21
T05F1.3	40S ribosomal protein s19	-1.22	-0.1	0.88	-0.09
E04F6.1	chemoreceptor	-1.23	0.97	4.02	0.14
H02F4.2		-1.23	0.26	1.89	0.03
R102.1		-1.23	-0.1	0.27	-0.59
AC8.2	similar to serine/threonine-protein kinase	-1.25	-0.71	-0.57	-1.06
F21D5.9	zinc finger, c2h2 type	-1.25	-1.03	-0.15	-0.27
F58H6.11	similarity to acyltransferases	-1.25	-0.21	0.19	-0.57
K08E7.2	hsb-1	-1.26	0.41	0.88	-0.91
Y75B8A.23		-1.26	0.28	4.08	0.75
C53C11.2		-1.27	-0.28	1.7	0.52
Y48B6A.2	60S ribosomal protein l37a.	-1.28	-0.07	0.42	-0.5
B0218.2	hypothetical zinc finger protein	-1.29	0.23	0.57	-0.8
F11E6.6		-1.29	-2.23	-0.48	-0.05
M151.4	human synaptonemal complex protein 1 (scp-1 protein)	-1.29	-0.11	0.38	-0.49
R12E2.15	similarity to ccaat/enhancer binding protein beta	-1.29	-0.83	-0.03	-0.3
F56H11.2		-1.3	-0.03	0.21	-0.84
Y50E8A.2	major sperm protein 56	-1.3	-0.68	-0.15	-0.33
2C581.3		-1.31	0.1	0.27	-1
C18E9.6		-1.32	0.2	3.41	0.59
F17C8.2	cuticular collagen	-1.32	-0.21	0.19	-0.61
F48D6.1	similar to drosophila melanogaster transcriptice factor tfid	-1.32	0.23	1.65	-0.06
K09F5.1		-1.32	-0.02	0.81	-0.25
C32D5.12	3 beta-hydroxysteroid dehydrogenase/delta 5--->4-isomerase (3beta-had)	-1.33	-0.2	1.07	0.06
T09A5.5	hypothetical 19.4 kda protein	-1.33	0.42	2.33	0.01
T14G12.4	fork head domain transcription factor	-1.33	-1.03	2.01	1.63
Y23H5A.6	alpha-catenin related protein	-1.33	-0.42	0.2	-0.36
C50D2.5		-1.34	0.76	4.29	0.29
C26F1.10		-1.35	-0.77	0.19	-0.12
F17E9.8	similar to acetycholine receptor and to *C. elegans* protein r13a5.4	-1.35	0	1.75	0.17
C47E12.10		-1.36	0.92	6.23	0.59
Y54E5A.5	hspc245	-1.36	0.84	0.88	-1.26
C25G4.8		-1.37	-0.85	0.88	0.3
F47D2.6	similar to reverse transcriptase	-1.37	-0.2	1.83	0.34
F59G1.7	mouse frataxin precursor	-1.37	0.84	3.32	-0.01
AH6.1	guanylate cyclase receptor-type gcy-1 precursor	-1.38	0.16	2.76	0.26
C39D10.2		-1.38	-0.47	-0.36	-1.21
H21G24.1	pherombarin-s precursor	-1.38	0.81	1.25	-0.06
T04A6.1		-1.38	-0.68	-0.36	-0.92
B0250.4		-1.4	0.17	-0.22	-2.44
F31D4.9		-1.4	-0.18	0.78	-0.15
R12D7.4	similarity to family 1 of g-protein coupled receptors	-1.4	0.69	2.31	-0.23
T15H9.4	hypothetical 47.7 kda protein	-1.4	1.47	5.65	0.12
B0280.2	hypothetical 115.2 kda protein	-1.41	-0.27	-0.89	-1.07
F22H10.3		-1.41	0	1.56	0.06
C06E4.5	similarity to *S. cerevisiae* DNA damage-response protien elk1	-1.44	0.34	1.02	-0.62
C37A2.7	ribosomal protein	-1.44	-0.06	0.77	-0.3
Y43F8C.1		-1.44	0.81	2.66	0.49
F28F4.8	pr-domain containing protein 10	-1.45	0.12	3.45	0.63
T10G3.6	gut-2 yeast hypothetical 11.2 kd protein like	-1.45	0.24	0.94	-0.57
T27A1.3		-1.45	0.2	0.71	-0.72
ZK121.8	glutaredoxin 2	-1.45	0.32	2.53	0.09
F37C12.12	bacillus subtilis hypothetical oxidoreductase in arar-lmms intergenic region	-1.46	-1.08	0.97	0.67
F40F4.2	fatty acid-binding protein homolog 3 precursor	-1.46	0.1	2.25	0.2
F53G12.10	probable 60S ribosomal protein l7	-1.46	-0.09	0.84	-1.17
R02F11.1		-1.46	0.34	3.15	0.26
Y116F11C.D		-1.46	-0.08	-0.25	-1.85
F23D12.2		-1.47	0.23	1.48	-0.22
E04A4.8	ribosomal protein	-1.48	-0.17	0.51	-0.4
C16A3.9	probable 40S ribosomal protein s13	-1.49	-0.28	0.38	-0.45
C30A5.5	hypothetical 11.7 kda protein	-1.49	0.14	1.9	0.62
F28E4.2	EGF-like repeat	-1.49	0	1.86	0.15
ZK1248.7	similar to *C. elegans* protein dk757.3	-1.49	0.71	1.33	-0.83
D1065.4	similarity in *C. elegans* olfactory receptor odr-10	-1.5	0.33	1.39	-0.26
F58E2.1	chemoreceptor	-1.5	0.63	1.72	-0.5
C33C12.4		-1.51	-0.34	0.56	-0.2
F25G6.7	sugar transporter	-1.51	-1.09	3.13	2.43
Y54E10A.12	plasmodium falciparum glutamic acid-rich protein precursor	-1.52	1.85	3.13	-0.74
F23A7.1		-1.53	-0.25	0.37	-0.46
R09H2.3		-1.53	-0.26	0.56	-0.28
T21C9.7	srp-13 protein	-1.53	0.6	1.75	-0.28
C05A9.1	p-glycoprotein	-1.54	-0.04	8.84	3.03
T25B6.5		-1.56	-0.15	0.68	-0.32
C44E4.6	acyl-CoA-binding protein homolog (acbp)	-1.58	0.28	2.63	0.1
T08E4.11	q3w646 chemagenin feminor	-1.59	-1.14	0.58	0.29

F40F11.1	ribosomal protein s11	-1.6	0.14	0.98	-0.49
ZC412.9		-1.6	0.27	0.29	-1.56
ZK1251.6	major sperm protein 10	-1.6	-0.28	0.22	-0.69
K09D9.2	cytochrome p450	-1.61	0.22	17.22	4.72
C26F1.9	ribosomal protein l39	-1.62	-0.07	1.24	-0.09
R04B3.3		-1.62	-0.18	1.97	0.31
Y55B1AR.E		-1.62	-0.2	5.59	2.03
F09C6.2		-1.63	0.25	1.25	-0.46
F22H10.6		-1.63	-0.22	1.15	0
F37D6.4		-1.63	0.22	0.6	-1.01
K04C1.4	myosin light chain	-1.63	-0.41	3.02	1.15
Z6686.1	ATP-dependent RNA helicase	-1.63	-0.11	0.59	-0.49
F45G2.10		-1.64	0.83	2.1	0.14
K06H6.4	similarity to a putative single-stranded nucleic acid binding protein	-1.64	0	1.64	0
C23H3.9	xenopus laevis integumentary mucin c.1	-1.65	-0.22	0.72	-0.26
C38D4.9	methylase	-1.65	-0.16	1.19	-0.04
Y49E10.15	human small nuclear ribonucleoprotein e (snrnp-e)	-1.65	0.25	1.57	-0.29
F25D2.5	transcriptional activator hap4 and regulatory domain of lcr and pilfia	-1.66	-0.38	0.5	-0.28
T07C4.9	nex-2 annexin	-1.66	-1.38	-0.58	-0.76
C26C9.2	ribosomal protein	-1.67	0.35	2.78	0.05
T07E3.3		-1.67	0.37	0.67	-1.2
EEED8.4	probable RNA binding protein	-1.68	0.3	2.29	-0.06
F19F10.4		-1.68	-1.03	0.87	0.42
B0240.8	similarity to bovine cAMP-dependent protein kinase ii-b-binding protein	-1.69	0.18	1.93	-0.08
K08E7.8	leucine rich repeat (2 copies) (2 domains)	-1.69	1.81	7.31	0.53
T01G5.8	similarity to C. elegans olfactory receptor odr-10	-1.7	0.28	2.33	-0.04
C05H5.2	elpase	-1.71	0.97	0.42	-2.76
K07D4.2		-1.71	0	1.71	0
R160.6		-1.71	0.31	0.5	-1.37
T21C9.4	enhancer of rudimentary homolog	-1.71	0.94	4.58	0.06
Y53F4B.EE		-1.71	-1.03	0.27	-0.05
F28C6.7A	probable 60S ribosomal protein l28	-1.73	-0.15	0.68	-0.44
F18A12.6	peptidase	-1.74	0.27	2.41	-0.02
F26G1.6	neprilysin	-1.74	0	2.71	0.35
W08E12.4		-1.74	-1.85	0.05	0.09
C03E10.1		-1.75	0.16	1.75	-0.16
C05G6.3	chicken collagen alpha 1(xii) chain precursor (fibrochimerin)	-1.75	-0.4	0.59	-0.24
C06G3.6	zinc finger protein	-1.75	-1.38	-0.62	-0.18
C18C4.8		-1.75	0.29	1	-0.77
C26B2.8		-1.75	0.35	1.75	-0.26
C46H3.2	gcy-8	-1.75	-0.52	0.81	0
C50C10.3		-1.75	0.65	1.03	-0.42
F13E9.4	bovine RNA-binding protein fus/tls (nuclear antigen)	-1.75	0	1.75	0
F18E9.6	similar to small histidine-alanine-rich protein precursor	-1.75	-0.37	0.28	-0.57
F27E5.2	'gained box' domain, homeobox protein	-1.75	0	1.75	0
F28D9.2		-1.75	0.2	1.75	-0.2
F35H10.6		-1.75	1.54	8.22	0.32
F37A4.6	hypothetical 43.5 kda protein	-1.75	0.62	1.75	-0.62
F40D4.11	similarity to C. elegans olfactory receptor odr-10	-1.75	0	1.75	0
F42C5.2	g protein-coupled receptor	-1.75	-1.75	0.27	0.27
F42G9.4		-1.75	-1.28	-0.12	-0.34
F47G3.1		-1.75	0.88	1.13	-1.16
F47G9.2	similarity to C. elegans olfactory receptor odr-10	-1.75	-0.88	0.48	0
F56A4.3	similar to glutathione s-transferase	-1.75	0	1.75	0
F56H8.1	similarity to drosophila fringe protein precursor	-1.75	1.6	2.39	-1.11
F59C6.4	exosome component rrp40	-1.75	0.5	3.11	0
F59H5.3		-1.75	0.39	1.75	-0.39
R03H4.3		-1.75	-0.28	1.15	0
R04E5.9		-1.75	-0.04	0.57	-0.69
T02G6.4		-1.75	-0.14	1.42	0
T23B4.2	collagen	-1.75	0.89	0	-1.99
T23F11.4	zinc finger protein (c2h2 type) (cambridge)	-1.75	0.58	1.75	-0.58
W03H5.5		-1.75	-0.65	0.69	-0.56
W08H1.3		-1.75	-0.66	0.08	-0.54
Y17D7B.5		-1.75	0	1.75	0
Y27F2A.1		-1.75	0.84	1.3	-0.24
Y68A4A.10		-1.75	0	1.75	0
Y6E2A.8	erythrocyte binding protein	-1.75	0	1.75	0
ZC317.4		-1.75	0	1.75	0
ZC411.1		-1.75	0.83	1.75	-0.03
F28F8.1	acr-18 acetylcholine receptor	-1.76	-0.16	0.74	-0.37
Y46H3D.8	similarity to toxocara canis tex-26 protein	-1.76	0.1	0.25	-1.42
F09E5.12		-1.78	0	1.78	0
F16H6.7		-1.78	0.05	2.08	0.05
F19E10.3		-1.78	0.87	1.26	-1.42
F56H8.3		-1.78	-0.4	0.4	-0.42
F58A4.9	probable DNA-directed RNA polymerases I/III	-1.78	0.59	8.03	1.05
K12B6.3	lipase, putative	-1.78	-0.72	-0.03	-0.67
R102.6	proline-rich	-1.79	-0.56	0.71	-0.05
Y51B11A.1	reverse transcriptase	-1.79	0.31	0.58	-1.33
F21D5.8	ganglioside-induced differentiation associated protein 3	-1.8	0.6	5.2	0.38
C24B9.4	similar to reverse transcriptase	-1.81	0.51	2.9	-0.09
Y50E8A.11		-1.81	0.84	0.56	-0.87
C48B6.2	putative 40S ribosomal protein s4-like	-1.82	2.57	7.39	-0.2
T13F2.11	major sperm protein 31/40/142	-1.82	-0.33	0.31	-0.61
C01G10.12		-1.83	0.75	4.23	0.06
H23N18.4	transferase	-1.83	0	1.83	0
Y51A2A.6		-1.83	0.43	0.85	-1.17
Y37A1B0.2		-1.84	-0.21	0.82	-0.29
W07E11.3	tg-2	-1.85	-0.08	-0.28	-2.36
K06A4.4		-1.86	-0.1	0.9	-0.37
W10C8.3		-1.86	1.83	5.1	-0.33
C04G2.1	transthyretin-like family	-1.87	-0.8	0.78	0.12
F09B12.4		-1.88	-2.55	2.38	3.17
F23B2.13	RNA polymerases I, II and III shared polypeptide (approx 7kd)	-1.89	0.16	1.58	-0.31
6RS5.2		-1.9	-0.18	0.59	-0.54
K09C4.1	glucose transporter	-1.9	-0.31	-0.22	-1.69
ZK512.4	signal recognition particle 9 kda protein homolog (srp9)	-1.9	0.35	2.98	0.02
W05E10.3	60S ribosomal protein l29	-1.91	-0.11	1.27	-0.16
C23H5.7	cyclic nucleotide-binding protein	-1.92	0.67	1.05	-1.37
T19B10.9		-1.92	0	1.92	0
T28B12.5	hypothetical 15.9 kda protein	-1.92	-0.07	0.49	-0.83

Y5H2A.A	similarity to erbb-3 receptor protein-tyrosine kinase	-1.92	0.31	0.54	-1.48
Y9C12A.B	similar to phospholipase adrab-b precursor	-1.92	0.82	1.92	-0.02
C05D9.6	major sperm protein 31/40/142	-1.94	-0.14	0.82	-0.41
C34E11.2		-1.94	-1.37	0.69	0.36
Y23B4A.1		-1.94	-0.52	0.94	0
Y52B11A.5	similarity to a c-type lectin domain	-1.94	1.42	1.94	-1.42
F18A11.4		-1.95	0.5	1.6	-0.48
F23A7.5		-1.95	-0.62	-0.5	-1.38
T13F2.10	major sperm protein 31/40/142	-1.96	-0.25	0.42	-0.67
VC5.1		-1.96	0.13	1.77	-0.2
C17D12.4		-1.97	0.44	2.03	-0.4
F45H7.2	guanine nucleotide releasing factor	-1.98	-0.24	0.68	-0.46
T05C12.8		-1.98	-0.02	0.44	-1.03
T09F5.7	reverse transcriptase	-1.98	0	1.98	0
K12C11.4	ankyrin and protein kinase	-1.99	-0.05	2.33	0.18
ZK354.1	major sperm protein 31/40/142	-1.99	-0.06	0.47	-0.92
F16D3.1	tubulin	-2.01	-0.11	0.03	-1.63
Y75B8A.33		-2.01	0.62	2.95	-0.24
F28F8.5		-2.03	0.7	1.44	-1.11
F47D2.1	similarity to cytochrome c oxidase subunit 1 from manduca sexta	-2.03	-0.41	1.14	0
B04F6.4	x. virus protein k4	-2.05	-0.25	1.07	-0.18
F29C5.3		-2.06	-0.06	0.93	-0.49
Y62H9A.7		-2.06	0.65	1.54	-0.27
B0035.16	probable tRNA (5-methylaminomethyl-2-thiouridylate)-methyltransferase	-2.07	0.47	2.73	-0.21
F07C6.11	similarity to C. elegans let-23 receptor protein-tyrosine kinase precursor	-2.07	-2.51	1.85	3.19
K01D12.5		-2.07	-0.35	1.39	0.05
C06G3.5	adenosine deaminase	-2.08	-1.08	-0.01	-0.48
C16E9.5		-2.08	0.22	1.83	-0.43
R12E2.7	similarity to coast/enhancer binding protein beta	-2.08	-1.89	0.73	0.62
W07B8.1	thiol protease	-2.1	-0.7	1.53	0.39
B0348.2		-2.12	-0.73	2.11	0.73
ZK637.2	hypothetical 12.5 kda protein	-2.14	0.26	1.51	-0.57
F44F1.7		-2.15	0.36	2.15	-0.36
F55C10.3	putative cuticle collagen	-2.15	-0.48	-0.29	-1.79
R05D6.7	similar to the insect-type alcohol dehydrogenase/inbitol dehydrogenase family	-2.15	-0.15	0.27	-1.16
Y46G5A.7		-2.15	-0.12	1.82	0
R04A9.1		-2.16	-0.27	0.6	-0.54
F28A5.8		-2.18	-0.38	0.55	-0.48
R07A4.1	egl-36 potassium channel protein	-2.18	-0.13	0.97	-0.42
C46H3.12		-2.2	-1.35	0.37	0.01
F40F8.9		-2.2	0.22	1.56	-0.52
K02B12.6		-2.2	0.67	2.02	-0.13
B0166.3	serine esterase	-2.21	-0.02	-0.44	-3.55
F48G7.11	nuclear hormone receptor	-2.21	-0.55	0.01	-1.05
Y54E10A.13		-2.21	-0.63	2.08	0.56
T05A10.5	tetton-specific protein like	-2.22	-1.42	-0.37	-0.92
Y43F4B.7	similar to C. elegans protein f59b2.2	-2.22	1.2	5.13	-0.16
F08B6.1		-2.23	1.73	5.41	-0.38
B0513.3	60S ribosomal protein l29	-2.24	-0.06	2.09	0.01
C40H5.4	b.subtilis penicillin-binding protein like	-2.25	-0.67	0.65	0
F35D11.8		-2.25	0	2.25	0
F46A8.2		-2.25	-0.18	0.57	-0.77
R13H9.4	major sperm protein 31/40/142	-2.26	-0.13	0.65	-0.76
T22F3.4	probable 60S ribosomal protein l31	-2.26	-0.17	0.39	-1.01
R05F9.8	major sperm protein 33	-2.27	-0.38	0.82	-0.31
Y87G2A.9	human ubiquitin conjugating enzyme g2	-2.27	0.1	0.94	-0.86
F07C4.6	similarity to toxocara canis tes-26 protein	-2.28	0.28	1.79	-0.5
C54E10.4	RNA dependent RNA polymerase	-2.29	0.13	1.48	-0.5
D2024.9		-2.29	-0.54	2.13	0.47
ZC168.5	proline-rich	-2.29	-1.71	-4.39	-5.55
F32B6.6	major sperm protein 31/40/142	-2.3	-0.42	0.72	-0.36
F42G2.1		-2.3	-0.3	2.68	0.45
T25B9.1	5-aminolevulinic acid synthase	-2.3	-0.17	2.57	0.26
Y62E10A.12	u6 snRNA-associated sm-like protein	-2.3	0.41	1.41	-0.93
T06G6.11	thioredoxin ; fyve zinc finger	-2.34	0.6	1.89	-0.85
R02C2.2	protein kinase	-2.35	1.86	4.27	-0.92
R13D7.3	chemoreceptor	-2.35	0.85	2.81	0.06
K09C6.6		-2.36	0.25	1.85	-0.48
Y105E8D.4	serine/threonine kinase	-2.36	0.37	3.92	0.07
ZK402.3		-2.37	1.76	1.53	-2.67
C06G3.8		-2.38	1.87	5.53	-0.07
B03A3.3	histone H3	-2.38	-0.22	1.01	-0.38
F49E12.9	arg-3 like protein	-2.38	0.52	2.09	-0.66
R11G11.15	chemoreceptor	-2.39	0	2.39	0
Y51A2D.16	human myosin heavy chain, perinatal skeletal muscle	-2.39	0.8	2.39	-0.8
W05B2.6	similar to cuticular collagen	-2.4	-0.48	-0.83	-1.37
Y73C8C.6	similarity to C. elegans olfactory receptor odr-10	-2.4	-1.59	0.22	-0.08
C06B8.4	7tm receptor	-2.42	-0.1	1.57	-0.21
F09C12.7	major sperm protein 56	-2.42	-0.09	0.76	-0.76
ZK546.6	major sperm protein 31/40/142	-2.42	-0.34	0.6	-0.59
Y56A3A.11		-2.43	0.56	1.15	-1.49
F49F12.1	transthyretin-like family	-2.44	-0.2	1.38	-0.2
T11F8.1		-2.44	0.5	4.79	0.29
T19E7.1	similarity to c-type lectin family domain	-2.44	-0.24	2.91	0.41
R10E.2		-2.46	-0.06	1.78	-0.17
F37B4.10		-2.49	0	1.19	-0.59
B0238.13	carboxylesterase	-2.51	-0.15	2.05	0
K11D2.2	human pbp32 protein like	-2.51	-1.64	-1.85	-2.78
C28G2.5	zinc finger protein	-2.52	-0.18	0.7	-0.76
AC8.3		-2.55	-1.68	0.9	0.44
F53F1.11	srd-1 protein	-2.55	-0.18	1.67	-0.12
F08F1.3		-2.57	0.24	3.03	-0.1
R09F10.2	similarity to erbb-3 receptor protein-tyrosine kinase	-2.57	-0.72	0.1	-0.89
F14H3.7		-2.58	-0.08	0.02	-2.24
B0222.7	similarity to a part of the triple-helical region of collagen alpha chain	-2.59	-0.47	-0.85	-1.56
C06F9.3	ank repeat	-2.59	-0.34	0.42	-0.88
B0213.2		-2.6	-0.56	0.72	-0.34
F58B3.3	lysozyme endolysin	-2.6	-0.31	-0.87	-4.13
F01F1.3		-2.62	-0.01	0.92	-0.86
T22B2.6	vitellogenin 2 precursor	-2.62	0.86	0.32	-1.9
C42D8.2	transthyretin-like family	-2.63	-0.08	0.55	-1.17
T14G10.4	transthyretin-like family	-2.65	-0.17	1.82	-0.11

W04G5.6	kin-23 tyrosine-protein kinase (kin15/kin16 subfamily)	-2.86	-0.59	1.44	0.06
F58E6.10	unc-42 homeobox domain	-2.87	0	2.87	0
Y39C12A.3		-2.87	-0.09	0.33	-1.52
Y51H4A.D	putative 32.6 kda lipase	-2.87	-4.38	-0.48	0
F54C4.4		-2.7	1.11	4.44	-0.44
C07A4.3	extracellular protein	-2.71	-3.05	0.43	0.56
C04F12.6	dual specificity phosphatase, catalytic domain	-2.72	-0.04	2.15	-0.14
F41E7.1	Na+/H+-exchanging protein Na+/H+ antiporter	-2.72	-0.11	1.01	-0.67
K08H2.4		-2.72	-0.02	1.28	-0.61
T04C9.2		-2.74	0.12	2.87	-0.36
F36A4.5		-2.75	-0.77	0.6	-0.32
K03H1.3	transthyretin-like family	-2.76	-0.13	1.83	-0.27
R144.1	klp-6	-2.76	0.21	2.05	-0.5
W01A8.6	carboxypeptidase b like	-2.77	0.22	0.85	-1.49
F53F4.1	chorion protein like	-2.82	-1.35	0.63	0
M03B6.4		-2.82	0.35	2.64	-0.42
F42H10.2	hypothetical 12.8 kda protein	-2.84	1.26	4.14	-0.69
Y50E8A.1		-2.84	-0.7	0.02	-1.21
ZK682.1	similar to mariner transposon	-2.88	-0.04	2.24	-0.15
Y47D7A.8	phaseolus vulgaris glycine-rich cell wall structural protein 1.8 precursor	-2.89	-1.42	-0.7	-1.74
C12D8.6		-2.92	2.46	4.52	-1.46
R10F2.1	calherin-containing cell adhesion protein	-2.96	0.67	3.34	0.02
F56B6.6	cysteine-rich	-2.98	-0.87	-0.49	-2.18
T01B7.2	srg-11 protein	-2.98	-0.02	2.2	0.67
F19F10.7		-2.99	0	2.99	0
F26B1.6	srg-11 protein	-2.99	0	2.99	0
F35C11.6		-2.99	0.37	2.55	-0.54
C49A9.8	sdp-glucuronosyltransferase	-3.02	0.57	7.93	0.41
Y64G10A.1	similarity to m musculus properdin	-3.05	0.28	1.39	-1.16
ZC462.2		-3.05	0	3.05	0
F56F11.1		-3.08	-1.56	0.42	-0.12
F39B2.5	src homology domain 2	-3.11	0.27	1.24	-1.33
T10B5.8	NADH oxidase	-3.11	-0.17	1.84	-0.33
C08F11.11		-3.12	-0.4	1.03	-0.46
F26D2.4	similarity to C. elegans olfactory receptor odr-10	-3.13	0	3.13	0
F35B3.4		-3.13	-1.63	-0.98	-0.7
T24H10.6	bithoracoid-like protein	-3.16	0.71	2.59	-0.98
B0025.13	lipase	-3.17	-0.53	0.54	-0.76
F48B9.6	reverse transcriptase	-3.19	-0.54	1.13	-0.27
F44F1.5		-3.2	-0.05	2.46	-0.16
T04C12.1		-3.21	-0.2	1.42	-0.45
F40F11.3		-3.22	0.74	8.46	0.29
B04F6.2		-3.28	-0.53	1.8	0
C30G12.5		-3.29	0.14	0.96	-1.49
F30A10.2		-3.29	-0.6	0.75	-0.54
F21A3.2		-3.29	-1.9	1.84	0.62
C05E4.6	chemoreceptor	-3.31	-1.4	0.8	0
C10A4.1	transposases hf1 (d. melanogaster)	-3.31	-0.5	0.13	-1.54
F07G11.7		-3.31	-0.62	2.23	0.44
C17H12.11		-3.37	-0.34	1.32	-0.41
F32H2.6	fatty acid synthase (n-terminus)	-3.37	0.85	3.14	-0.74
F23A7.4	glutamate receptor epsilon subunit like	-3.38	0.21	1.49	-1.14
Y73B6A.3		-3.39	0	3.39	0
C18H9.5	sodium/phosphate transport protein	-3.43	0.18	3.43	-0.18
D1054.10		-3.43	-0.03	1.78	-0.56
D1054.6	similarity to a c-type lectin domain	-3.43	-0.53	-0.28	-2.7
F16H6.7		-3.49	0.93	3.49	-0.93
R03G8.6	zinc metallopeptidase	-3.5	0.36	3.92	-0.24
W05B10.3		-3.5	-0.13	1.18	-0.83
T11F9.8	zinc metalloprotease	-3.51	-0.27	2.18	-0.12
F52A8.3		-3.55	0	3.55	0
R11D1.11	probable carbonyl reductase [NADPH]	-3.56	-0.54	1.31	-0.28
F41E6.6	nucleic-acid binding protein	-3.57	-0.03	1.09	-1.12
F58E1.14	similarity to retrovirus-related polyproteins	-3.58	0.36	3.58	-0.36
ZK822.3	probable na(+)/h(+) antiporter	-3.59	-1.22	0.89	-0.09
K05B2.4	similar to the rat kan-1 protein	-3.59	0.1	5.42	0.27
T13F2.8	cawolin-1	-3.6	0.81	0.16	-3.02
F40F4.3	fatty acid-binding protein homolog 3 precursor	-3.61	-5.17	-1.14	-0.6
ZK507.4	hypothetical 27.7 kda protein	-3.62	-1.28	0.58	-0.26
K08H10.9		-3.67	1.84	7.8	-0.08
C29G2.2		-3.77	0.59	0.31	-4.81
B0035.4	paramyosin like	-3.94	0.66	6.03	-0.16
Y39B6B.BB		-3.95	-0.01	1.84	-0.73
C46H11.1		-3.96	0.39	1.7	-1.55
K11B4.2		-4.03	0.58	2.34	-1.38
T04C9.5	lim binding domain	-4.04	-0.09	2.03	-0.53
F23F1.6	amino acid permease	-4.15	-2.59	0.03	-0.4
C31H5.4		-4.17	-0.75	0.31	-1.27
B0284.3		-4.2	1.29	5.9	-0.72
C25H12.3		-4.27	0.83	1.92	-0.66
F26D2.15	alcohol/ether dehydrogenases, short-chain type	-4.27	-0.35	1.35	-0.66
H12I19.1		-4.33	0.12	1.76	-1.15
F13D12.1	proton-relay domains	-4.4	-0.47	0.81	-1.03
Y39A3CR.D		-4.45	-0.68	0.28	-1.52
F28D1.11		-4.49	0.87	2.16	-0.86
C28F5.1		-4.5	-3.19	0.31	0
D1086.6	xenopus laevis integumentary mucin c.1	-4.5	-0.39	0.75	-1.26
W06D12.1	cuticlin 1 precursor	-4.5	-0.91	1.89	0
Y49F6B.D		-4.5	0	4.5	0
C17H11.5		-4.56	0.55	2.6	-1.4
F59D12.5		-4.57	0.84	3.45	-1.3
Y50E8A.3		-4.6	-0.63	-0.31	-3.5
F35H10.5		-4.68	-0.05	1.02	-1.67
T08G5.7	zinc finger, c2h2 type (3 domains)	-4.75	0.98	8.71	-0.17
T23F2.3	protein-barley	-4.84	-0.52	0.43	-1.7
Y47D7A.L		-4.92	0	4.92	0
F16D3.6		-4.99	-0.17	1.2	-1.32
R10D12.12	novel protein similar to predicted yeast and plant proteins	-4.99	0.28	4.49	-0.4
Y95B8A.1	peptidase	-5.19	0	5.19	0
ZK669.3	gamma-interferon inducible lysosomal thiol reductase	-5.27	-0.74	1.96	-0.22
C15A11.1	col-35 collagen	-5.29	1.83	0.88	-5.77
F15B9.1	s.vellelus antigen peptide like	-5.4	0.51	1.38	-3.08

R07G3.2	lipase	-5.41	-0.25	0.19	-3.3
Y53F4B.7		-5.42	1.49	2.38	-3.76
F14B8.4		-5.51	-0.46	5.08	0.36
B0284.1	putative vicilin storage protein (globulin-like)	-5.86	0.72	3.21	-1.73
C30E1.5	similar to transposase	-5.74	0.28	5.53	-0.32
F26E4.2		-5.77	-0.13	1.77	-1.17
D1037.4		-6.1	0.94	5.01	-1.29
JC8.8	transthyretin-like family	-6.12	-0.29	1.58	-1.15
F59A2.5		-6.16	1.66	12.65	-0.39
F28D2.13	similarity to toxocara canis tex-26 protein	-6.24	0.88	4.83	-0.34
Y47D7A.F		-6.33	-0.68	3.42	0
Z6B16.5	short-chain alcohol dehydrogenase	-6.91	0	6.91	0
Z6662.2		-6.93	0.13	8.32	0.04
F32H5.4	transport protein	-6.98	-1.33	1.95	-0.16
K08B4.6		-7.09	0	3.89	-0.65
T05C1.2		-7.25	0	7.25	0
F42A10.7		-7.3	0.58	15.13	0.23
T04B2.6	cd03613 dehydrogenase	-7.44	-0.77	0.31	-2.62
Y47D7A.H		-7.95	-1.62	1.01	-1.21
F14D2.11		-8.23	8.6	5.3	-1.34
W03C9.5		-8.25	0.35	1.72	-3.59
F14D7.7		-8.68	-0.17	0.95	-3.27
E6ED8.12	probable RNA binding protein	-9.9	1	9.9	-1
C49C3.12	lectin c-type domain	-9.36	0.61	6.93	-1.11
F49C12.14		-9.85	-0.45	1.72	-1.74
F42A9.6		-11	0.44	5.89	-1.5
T24H7.4		-11.31	1	6.09	-2.46
C01G12.6	similarity to zinc finger motif	-12.06	-0.62	0.08	-8.45
C48B4.12a		-14.46	0.96	14.46	-0.96
F35F10.10		-14.68	0.86	8.2	-2.18
C54D10.10	serine protease inhibitor	-16.68	-1.37	0.79	-3.17
Y17G9B.2		-18.38	-0.47	1.7	-3.87
F45E4.5	similarity to echinometra matheai bindin	-19.31	-1.28	1.61	-2.41
C45B2.3		-19.44	0.18	4.26	-3.58
Z6512.7	hypothetical 16.8 kda protein	-24.76	0.29	10.05	-2
T09F5.9	c-type lectin	-28.9	-0.35	1.58	-7.59
F15E6.4	RNA binding protein	-30.59	0.82	28.09	-1.13
C49F5.7		-58.5	-1.06	1.02	-13.6

Table 4. The expression of the 49 genes in the "IR" experimental set in *hus-1(op244)*

Listed below are the *C. elegans* genes that are up-regulated in the wild-type in response to ionizing radiation, but do not show any change in the *hus-1(op244)* background.

Gene model	Description	Change Factor			
		wt vs. wt/IR	wt vs. *hus-1*	*hus-1* vs. *hus-1* /IR	wt/IR vs. *hus-1* /IR
F32D8.5b	uncharacterized membrane protein	4.2	0	0	-4.3
C17D12.1a	zink finger protein	4.22	-0.6	0.67	-4.62
Y52B11C.1	N-acetylglucosaminyl phosphatidylinositol de-N-acetylase	3.68	-0.35	0.7	-2.71
C04B4.2	similarity to Ca binding EF-hand domain	3.21	-0.27	0.22	-3.26
K03D10.3	histone acetyltransferase	3.11	-0.1	0.07	-3.22
R12G8.2	putative potassium channel subunit n2p26	3.11	0.38	-0.38	-3.11
F52D10.2	uncharacterized conserved protein, contains phosphotyrosine interaction domain	2.98	0.4	0.04	-1.72
ZC239.12	similar to human tumor necrosis factor-alpha-induced protein b12	2.49	0	0	-2.49
R07D5.1	unc-7 protein	2.24	0.28	-0.28	-2.24
Y43E12A.3	BTB/POZ (also known as br-c/ttk) domain-containing protein	2.38	0.02	0.7	-0.83
F29B9.1	methyltransferase, SAM binding motif	2.15	0.15	-0.74	-3.76
F47B7.5	extracellular protein with cysteine rich structures	2.07	0.44	-0.05	-1.25
ZK180.2	GABA-B ion channel receptor subunit GABABR1 and related subunits	2.06	0	0	-2.06
K05B2.2	predicted cell growth/differentiation regulator, contains RA domain	2.04	0.96	0.12	-0.38
T23G11.5	dopamine responsive protein drg-1	1.9	-0.48	0.58	-1.72
C38C10.4	gpr-2 (G protein regulator)	1.83	0.09	0.63	-0.6
K10H10.1	permease of the major facilitator superfamily	1.81	-0.28	0.77	-1.03
Y48G10A.4	unknown protein	1.79	-0.17	0.97	-0.65
F34D6.1	F-box containing protein	1.75	0.41	-0.41	-1.75
C50B6.1	unknown protein	1.7	0.47	0.16	-0.26
W04B5.5	protein kinase	1.67	0.23	0.75	-0.24
T07C4.6	tbx-9 (TBR2 and related T-box transcription factors)	1.64	-0.22	0.74	-0.86
Y57A10A.25	poly(A)-specific exoribonuclease PARN	1.56	0.3	0.9	-0.04
C10G8.5	ncx-2 sodium/calcium exchanger protein 1	1.54	0.17	0.25	-0.74
Y48F6C.8	unknown protein	1.49	0.09	0.04	-1.19
Y57A10A.3	uncharacterized protein	1.45	0.36	0.46	-0.24
C42C1.10	mitochondrial carrier protein	1.39	0.3	0.36	-0.26
F10D2.2	glucuronosyltransferase	1.39	0.62	0.82	0.24
F18A1.2	transcriptice factor lin-26	1.39	-0.26	0.32	-1.26
C27D6.7	srb-4	1.38	0.69	-0.24	-0.73
F52H3.4	in S. cerevisiae , nucleolar protein for pre-rRNA processing and ribosome biogenesis	1.38	0.54	8.1	-0.4
T06D8.8	26S proteasome subunit p40.5	1.38	0.2	0.61	-0.22
F44E2.8	unnamed protein	1.34	-0.85	0.58	-1.75
F54D10.7	in S. cerevisiae , subunit of the condensin complex	1.33	0.34	0	-0.74
F54C9.10	putative ADP-ribosylation factor 2	1.31	0.86	0.18	-0.08
K08E3.8	MDT-29 protein (MeDiaTor), transcriptional co-repressor	1.29	0.14	0.55	-0.3
Y106G6H.14	Src homology domain 3 ; ank repeat	1.25	-0.03	0.37	-0.7
Y38C1BA.1	unknown protein	1.23	-0.08	0.17	-1.06
C16A11.4	PHD Zn-finger protein	1.2	0.14	0.38	-0.41
K02E10.2	lid-1 (protein containing regions of low-complexity)	1.2	0.7	8.2	-0.08
W08E3.1	snoRI nuclear ribonucleoprotein (snrnp)	1.18	0.34	0.13	-0.44
F42A8.3	hypothetical 37.3 kda protein	1.16	0.67	0.21	-0.07
Y71F9AR.1	unknown protein	1.15	0.24	0.35	-0.26
T09B4.10	similarity to a single tpr domain	1.14	0.77	-0.21	-0.46
K02B2.3	uncharacterized conserved protein	1.07	-0.17	0.03	-1.35
Y34B4A.8	mouse sh3-binding protein 3bp-1	1.05	-0.26	0	-1.58
F47H4.1	zinc finger, c2h2 type (2 domains)	1.03	0.25	-0.3	-1.12
C36B7.6	cleft lip and palate transmembrane protein 1	1	0.14	0.94	0.11
T24H7.1	prohibitin	1	0.37	0.33	-0.1

Table 5. The expression of the 27 genes in the "IR" experimental set in *hus-1(op244)*

Listed below are the *C. elegans* genes that are differentially regulated between the wild-type and the *hus-1(op244)* mutants in response to ionizing radiation, but do not change under normal conditions.

Gene model	Description	Change Factor		
		wt vs. wt/IR	wt vs. *hus-1*	wt/IR vs. *hus-1* /IR
C17D12.1a	zinc finger protein	4.22	-0.6	-4.62
Y52B11C.1	N-acetylglucosaminyl phosphatidylinositol de-N-acetylase	3.68	-0.35	-2.71
C04B4.2	similarity to Ca binding EF-hand domain	3.21	-0.27	-3.16
K02D10.3	histone acetyltransferase	3.11	-0.1	-3.22
R12G8.2	putative potassium channel subunit n2p26	3.11	0.38	-3.11
ZC239.12	similar to human tumor necrosis factor-alpha-induced protein b12	2.49	0	-2.49
R07D5.1	unc-7 protein	2.24	0.28	-2.24
F29B9.1	methyltransferase, SAM binding motif	2.15	0.15	-3.76
ZK180.2	GABA-B ion channel receptor subunit GABABR1 and related subunits	2.08	0	-2.06
K10H10.1	permease of the major facilitator superfamily	1.81	-0.98	-1.03
F34D6.1	F-box containing protein	1.75	0.41	-1.75
F44E2.8	unnamed protein	1.34	-0.85	-1.75
K02B2.3	uncharacterized conserved protein	1.87	-0.17	-1.35
Y34B4A.e	mouse sh3-binding protein 3bp-1	1.85	-0.26	-1.58
B0218.7	in S. cerevisiae , zinc finger transcription factor, stress-responsive	-1.2	-0.37	1.7
Y106G6E.4	mitochondrial 5-formyltetrahydrofolate cyclo-ligase	-1.2	0.3	1.2
M60.5	klp-2 channel protein	-1.22	0.27	2.04
T28B4.4	claudin homolog that may be required for normal cohesion of apical junctions	-1.44	0.01	1.14
Y73F8A.12	unnamed protein	-1.6	-0.03	1.9
F26H11.4	in S. cerevisiae , putative RNA helicase involved in mRNA degradation	-1.86	-0.15	2.67
C33G3.4	probable beta-mannosidase precursor	-1.87	-1	1.97
F26F2.2	unknown protein	-2.03	-0.88	3.08
F53C3.4	uncharacterized protein, contains CX module	-2.21	-0.27	1.07
F13C5.1	unknown protein	-2.24	-0.86	1.2
B0238.1	carboxylesterase	-2.47	-0.37	3.96
Y60A3A.5	similarity in C. elegans olfactory receptor odr-10	-2.76	0.67	3.21
ZK1251.5	protein-tyrosine phosphatase	-2.66	-0.96	1.57

Table 6. The expression of the 238 genes in the "IR" experimental set in *cep-1(gk138)*

Listed below are the *C. elegans* genes that are up- or down-regulated in *cep-1(gk138)* in response to ionizing radiation.

Gene model	Description	Change Factor *cep-1* vs. *cep-1* /IR
W03G1.7	sphingomyelin phosphodiesterase	5.62
F19F10.9	ralt-1	5.36
C30G4.4		5.3
C03G6.15	cytochrome p450	5.17
F56A8.8		3.7
C08F11.8	udp-glucuronosyl and udp-glucosyl transferases	3.2
Y39C12A.2	ankyrin homolog precursor	3.01
F53C3.8		2.99
T23F6.3		2.93
F08A8.2	acyl-coenzyme a oxidase, peroxisomal	2.8
B0213.4	S. cerevisiae nucleolar protein 3 (mitochondrial targeting suppressor 1 protein)	2.7
F20B4.2		2.67
K07E3.7	probable cation-transporting ATPase	2.64
C54H2.3	ring1 interactor rybp	2.64
T28F4.5		2.53
C03G6.15	cytochrome p450	2.42
M199.4		2.39
Y45G12C.2	glutathione s-transferase p	2.38
AC3.5	glutamyl aminopeptidase	2.34
F45E4.10		2.34
F32B6.3	human hprp18 protein like	2.33
F36A4.14	nuclear hormone receptor family member nhr-22	2.31
F20E11.12	similarity in C. elegans olfactory receptor odr-10	2.29
T04B8.3	similar to human dihydroxyvitamin d3-induced protein and beta arrestin 1	2.28
C02F12.8	breast cancer type 1 susceptibility protein (brca1)	2.28
C16C4.6		2.27
M106.1	mix-1 protein	2.21
F56A4.3	similar to glutathione s-transferase	2.13
K08G2.2	similarity to C. elegans olfactory receptor odr-10	2.11
F10A3.13	olfactory receptor odr-10	2.09
C02F5.1	hypothetical 113.2 kda protein	2.08
F45E1.4	hypothetical 7.1 kda protein	2.03
F47B7.5		2.03
F11C1.2		2.02
Y17D7A.3	nhr-65 zinc finger, c4 type (two domains)	2.02
C55B7.2	alpha-1,3(6)-mannosylglycoprotein beta-1,6-n-acetyl-glucosaminyltransferase	1.98
C33H5.8	similar to mitochondrial precursor proteins import receptors	1.96
B0495.8		1.94
F38A1.13	receptor like	1.93
C25B8.4	asialoglycoprotein receptor	1.88
R09E10.2	protein-tyrosine phosphatase	1.84
D2024.2	conserved hypothetical protein	1.82
F01D5.11		1.79
F13E6.6	tiam-1 like protein	1.76
F17C8.5	twk-5	1.76
F27D4.2		1.72
ZK973.8		1.69
B0432.9	zinc finger protein	1.66
Y50D4B.D	pngase (fragment)	1.65
C33A12.7	best hit: q96332 glyoxalase ii	1.64
F14F4.1	transmembrane receptor (rhodopsin family)	1.64
Y17G9B.6		1.64
F28C6.5		1.62
F56B6.5	uvt-6 g-protein coupled receptor	1.61
F17A9.1		1.6
F53F1.11	srd-1 protein	1.6
K06H7.8	similar to casein kinase	1.59
C34D4.14	human thyroid receptor interacting protein 12	1.59
R05D3.11		1.56
F25H9.5		1.55
Y75B12A.2		1.55
F36H12.3		1.55
C03G6.15	cytochrome p450	1.52
AC3.7	udp-glucuronosyltransferase	1.51
F53H2.2		1.51
D1086.3		1.51
C05D2.8		1.5
C32H11.5	similar to keratins in a glycine-rich region	1.46
T22F3.5	chemoreceptor	1.45
W09G12.1		1.43
F26E4.12	probable glutathione peroxidase	1.42
K07C6.14	transposase	1.39
F21A3.3	EGF-domain protein	1.38
F40F12.2	reverse transcriptase	1.37
ZK287.4	serine protease inhibitor	1.36
F58G4.1	myosin	1.36
B0464.5a	putative serine/threonine-protein kinase	1.36
B0238.12	similarity to EGF-like domain cysteine signature repeat	1.3
K11H12.4		1.3
B0432.8	40S ribosomal protein s3a	1.28
F20C5.1	poly(ADP-ribose) glycohydrolase	1.28
B0238.1	carboxylesterase	1.27

C01A2.5	*S. pombe* hypothetical protein c1d4.05c like	1.27
H06I04.3a	*S. cerevisiae* putative rRNA methyltransferase spb1	1.26
R08D7.1	conserved hypothetical protein	1.25
C16B8.2		1.24
CD6B3.3	cytochrome p450	1.24
F16A11.2	methanococcus hypothetical protein 0682 like	1.22
R07E5.4	glutaredoxin	1.19
B0304.2	hypothetical 24.2 kda protein	1.19
F09E5.9		1.19
B0285.9	hypothetical choline kinase like	1.19
F29C4.6	dictyostelium discoideum veg136 protein	1.15
R11A5.3		1.14
B0B25.2	signalosome subunit 2	1.13
C05E4.1	serine protease inhibitor	1.13
Y11D7A.13		1.12
C50F4.6	his-36	1.11
C01C10.2	hypothetical 24.1 kda protein	1.1
F45C12.6	similarity to mouse zinc finger 5 protien	1.1
C49C8.4	cytochrome p450	1.1
R05A10.4		1.09
B0361.3	organic cation transporter oct2r	1.09
R05D3.9	hypothetical 37.5 kda protein	1.09
F26A3.6		1.09
C50F4.12		1.08
F17C11.10	sop domain	1.07
K07D4.4		1.07
C14A4.4	autoantigen pm-scl	1.06
R03G8.6	zinc metallopeptidase (m1 family)	1.05
D1081.9		1.04
F36A4.3		1.04
K12H4.8	hypothetical helicase	1.02
F39H11.1	yeast yb81 protein like	1.02
C37A5.8		1.02
F36A4.6	col-33 cuticular collagen	1.01
F36D4.2		1.01
F54D5.14	*S. pombe* DNA repair protein rad18	1.01
F54C8.3	hypothetical 115.1 kda protein	1
F28B12.3	protein kinase	1
C29F9.8	similarity to rana pipiens rhodopsin	-1.01
F13G11.2		-1.02
T05E12.5		-1.03
K03H1.12		-1.03
Y57A10C.9		-1.03
R06B10.3		-1.03
F44C4.3	cathepsin b-like cysteine proteinase 4 precursor	-1.04
C23G10.7		-1.04
ZK673.7	hypothetical calcium-binding protein	-1.06
C49H3.2	pcy-8	-1.06
B0294.1		-1.07
F56H9.2		-1.07
F08G12.8		-1.07
K02A4.1	branched-chain amino acid aminotransferase, cytosolic	-1.07
F48F5.4		-1.08
T27A1.3		-1.08
T25B9.6	similarity to *S. cerevisiae* transcription factor mbp1	-1.09
C39F7.1		-1.12
F48G7.11	nuclear hormone receptor	-1.12
F50B3.1	lysozyme (n-acetylmuraminidase)	-1.13
W07E11.3	flp-2	-1.14
C11E4.6	ankyrin repeats	-1.14
CD8D4.1	similarity to bacillus and pseudomonasprobable glucarate transporters	-1.16
CD4.9		-1.16
ZK377.3	sax-3	-1.17
T02C12.1	hum-5 myosin ia	-1.17
T05E12.6		-1.18
T23B3.4	g-protein coupled receptor	-1.18
T08A9.7		-1.2
Y51H4A.I	similar to mariner transposase	-1.2
Y37D8A.13	adm-1 disintegrin	-1.22
F46A8.7		-1.22
ACB.4		-1.22
R12E2.14	similarity to ccaat/enhancer binding protein beta	-1.22
C27F2.6		-1.23
F54B8.1		-1.24
ZK546.4		-1.33
F49H12.6a	putative lysophosphatidic acid acyltransferase	-1.33
F52H3.6	serine/threonine specific protein phosphatase	-1.39
F53A9.1	histidine-rich	-1.4
C35A11.1	similar to thyrotropin-releasing hormone receptors	-1.41
F41H8.2		-1.41
W08E12.4		-1.44
F37H8.3	haloacid dehalogenase-like hydrolase	-1.45
F46F5.9		-1.47
C07A4.3	extracellular protein	-1.5
C55A6.3	dehydrogenase	-1.5
C54C8.11	beta-1,6-n-acetylglucosaminyltransferase like	-1.51
C02B8.6	DNA repair protein rad16 (yeast, weak)	-1.53
F17C11.1	bzip DNA binding domain	-1.54
C33A12.6	udp-glucuronyltransferase	-1.54
H32K16.1	similar to *C. elegans* protein f59b2.2	-1.54
T01C4.2		-1.55
ZK682.5	human platelet glycoprotein v precursor	-1.56
F26E4.2		-1.57

C23G10.11		-1.63
C10C6.2	g-protein coupled receptor	-1.63
Y69P12A.1	protein kinase	-1.63
F28E10.2	hypothetical 31.5 kda protein	-1.63
C50E3.7		-1.63
F07C4.12	carboxylesterase	-1.63
F14D12.6	g-protein coupled receptor	-1.63
F22B3.8	tyrosine-protein kinase	-1.63
F53A9.5	g-protein coupled receptor	-1.63
R04B3.3		-1.64
W03F8.6		-1.64
C44B7.6		-1.65
F07C4.3	srd-1 protein	-1.69
T22E5.2	putative sodium-dependent excitatory amino acid transporter	-1.69
T27F2.2	mouse gtpase-activating protein spa-1 like	-1.74
C45H4.2	cytochrome p450	-1.75
M03F4.3	g-protein coupled receptor	-1.77
F21H12.3	hypothetical 23.6 kda protein	-1.78
F47B7.7		-1.79
F08F8.1		-1.82
Y51H4A.D	putative 32.6 kda lipase	-1.88
R03D7.2	helicase domain	-1.88
F56F3.3		-1.9
F52D1.3	adenylyl cyclase	-1.93
Y60A3A.18	ser-4 (ubiquitinates proteins during the G1/S transition)	-1.94
F32A5.5	similarity to mip family of transmembrane proteins	-1.96
F57A8.1	ets domain	-1.98
F09C12.6	hypothetical 18.6 kda protein	-2
R05H5.1	srd-2 protein	-2
E04F6.1	chemoreceptor	-2.01
K05H9.5		-2.07
F07A5.5	c2 domain	-2.09
F40G9.8	tyrosine kinase receptor	-2.15
C47E8.1		-2.18
F23H12.6	gcy-13 guanylate cyclase (2 domains)	-2.22
ZC168.5	proline-rich	-2.22
K08F9.1	glucose transporter	-2.23
K01A2.10		-2.25
T10C6.3	similarity to family 1 of g-protein coupled receptors	-2.25
F14B6.2		-2.33
W01C8.5		-2.38
C52B9.1	choline kinase	-2.38
W09B6.1	acetyl-coa carboxylase	-2.48
F23B12.1	serine/threonine protein phosphatase	-2.5
C06C6.7	similar to protein-tyrosine phosphatase	-2.75
F53A9.8	histidine-rich	-2.89
F53A9.6	histidine-rich	-2.94
ZK228.7	similarity in *C. elegans* olfactory receptor odr-10	-2.95
C13G3.2		-3.05
C29E4.7	human glutathione-s-transferase homolog	-3.06
T05A1.7	similar to zk637.1 and tetracycline resistance protein	-3.13
ZK970.6	gcy-5 guanylate cyclase	-3.13
F47H4.10	ser-5 (ubiquitinates proteins during the G1/S transition)	-3.4
B0294.2		-3.43
R09B5.6	3-hydroxyacyl-coa dehydrogenase	-3.46
F49H6.13		-3.7
CD9H10.7		-3.8
F45E4.1	ADP-ribosylation factor 3	-4.46
C10B5.3		-4.83
B0244.A		-5.05
AC7.2	soc-2	-5.13
Y38E10A.13		-7.47
F46F5.9		-8.52

Table 7. The expression of the 1706 genes in the "ENU" experimental set in wild-type

Listed below are the *C. elegans* genes that are up- or down-regulated in wild-type in response to Ethyl-Nitroso-Urea.

Gene model	Description	Change Factor wt vs. wt/ENU
AC3.3	similarity to erbb-3 receptor protein-tyrosine kinase	518.11
C09E8.2	similarity to cell wall-plasma membrane linker protein	343.78
F23A8.7		197.03
F19C7.7	cuticular collagen	151.92
R09B5.5	similarity to erbb-3 receptor protein-tyrosine kinase	126.92
F59E12.12	bli-2	126.61
R08F11.4	similarity to methyltransferases	111.13
C50E10.1		99.04
H42K12.3		84.87
C24H11.1	protein phosphatase-1 (pp1)	78.55
T02E9.2	similarity to bovine cartilage-derived morphogenetic protein 2	75.75
F09B9.4		67.42
F26F4.2		65.22
ZK1025.3		60.16
C02F6.4		58.47
C46H11.6	similarity to toxocara canis surface coat glycoprotein tcs-120	51.53
Y47G6A.26		50.97
W09D6.4		48.31
T10E9.3		47.14
T08H10.2	chemoreceptor	45.25
F18A12.2		43.22
B03A3.4	histone H3	41.7
F29C6.5		40.84
H10E21.4	calcium-binding protein	38.24
C14F11.6	ddp-4-dehydrorhamnose 3,5-epimerase (rfbc gene)	37.19
C36F7.3		35.78
F13E6.5	phosphatidic acid phosphatase 2a2	35.09
C34D4.2	probable serine/threonine protein phosphatase	33.9
F28G4.1	cytochrome p450	33.78
ZK836.1	collagen	33.07
F13E9.8	similar to keratins in a glycine-rich region	31.91
C06G3.3		31.18
C54F6.14	ferritin heavy chain	30.43
F28B6.5	cuticular collagen	29.55
Y57A10A.1	putative cuticle collagen	29.39
C23H3.8		28.27
D1086.3		27.37
R03C1.1		27.22
C34G6.6		25.7
T03D8.6	gamma-glutamyltranspeptidase	25.39
K01A2.11B		25.33
ZK377.1	wrt-6	25.26
F36A4.6		25.13
B03D2.1	neuropeptide	24.84
ZK617.3	spermatogenesis-defective protein spe-17	23.57
C09E9.2		23.55
Y116F11A.6		23.38
F46A9.1		23.23
F11C7.2		23.2
T28F2.5	calcium channel subunit	23.07
M03F8.1		22.86
F58E6.2		22.04
F19F10.4		21.95
Y53H1C.2		21.62
F20B6.1	protein tyrosine phosphatase	21.61
F52D1.3	adenylyl cyclase	21.35
ZK1025.2		20.87
ZK637.12	hypothetical 23.9 kda protein	20.73
C28C12.3	similar to keratins in a glycine-rich region	20.67
C56C10.4		20.61
F39E2.9		20.07
C05C12.5		19.69
W04G3.3		19.35
Y116A8C.24	putative tyrosine-protein kinase	18.7
C06G1.1		18.6
ZK1025.7	similar to serine/threonine-protein kinase	18.46
F56D3.1	wheat gamma-gliadin precursor	18.45
T14B4.7	cuticle collagen dpy-18 precursor	18.13
C54A12.1	similar to drosophila membrane protein patched	17.93
C54G7.3	lgn-1	17.93
C03A7.14	similarity to erbb-3 receptor protein-tyrosine kinase	17.65
ZK682.5	human platelet glycoprotein v precursor	16.97
ZK652.2		16.72
F18C5.5		16.4
F36D1.4		15.93
C17C3.4	probable insulin-like peptide gamma-type 1 precursor	15.79
F22F4.1	hypothetical 61.7 kda protein	15.67
ZK666.7	lectin c-type domain short and long forms, von willebrand factor type a domain	15.45
Y53F4B.OD	glutathione s-transferase 1	15.44
F10D11.6	similarity to human lipopolysaccharide-binding protein precursor	15.44
T06E4.11	chemogenin hinmor	15.41
W08E12.8	hypothetical protein	15.26
D2096.6	hypothetical 18.6 kda protein	15.22
F35C11.2	protein-tyrosine phosphatase	14.3
T01D3.4	somatostatin receptor	14.14
C06H5.2		14.12
AH10.1	4-coumarate:coenzyme a ligase	14.07
B0491.2	cuticle collagen sqt-1	13.99
C26B9.3		13.97
F09F9.2		13.81
F35H10.2		13.37
C03A7.11	similar to UDP-glucuronosyltransferases	13.08

F45H7.4	prk-2 serine/threonine kinase	13.03
C06G1.3		13.03
F15B9.6	thrombospondin type 1 domain	13.02
F58G1.5		12.76
ZK512.8	hypothetical 19.1 kda protein	12.53
Y6E2A.9	tricarboxylate carrier-like protein	12.49
M162.5	similar to Na+ dependent-phosphate cotransporters	12.42
C23H5.2	gletin	12.41
Y56A3A.27	top-3 (DNA topoisomerase III)	12.37
T03F1.11	similar to EF-hand calcium binding proteins	12.27
R09B5.8		12.19
M04G7.2	protein-tyrosine phosphatase	11.91
F58H1.2		11.7
F36A4.2		11.66
B0511.4	protein kinase	11.33
ZC328.1		11.3
T21E12.5		11.26
C45B2.7	similar to drosophila membrane protein patched	11.22
Y11D7A.9		11.1
K09H9.2	cuticular collagen	11.02
F52E4.6	wrt-2	11
F26E1.1		10.91
C24B5.3	similar to drosophila membrane protein patched	10.89
F29D10.2		10.86
Y65B4BL.A		10.59
ZK596.2	serine/threonine kinase	10.54
T22B7.2		10.48
E04F6.7	ribitol dehydrogenase	10.47
C35A5.2	UDP-glucuronosyltransferase	10.35
C09E7.F	hypothetical protein	10.29
W05G11.3	cuticular collagen	10.23
Y57A10A.AF		10.09
F35G12.3A	serine/threonine kinase	10.01
F01G10.10	lipopolysaccharide-binding protein like	9.98
H88.3		9.91
C40H1.4	yeast hypothetical ycr34w	9.9
H23N18.5		9.86
F01D5.10		9.8
K10D2.4	serine proteinase inhibitor (kunitz type)	9.78
F25B4.7	ADP/ATP carrier protein	9.73
F52F10.2	similarity to two short region of multi-drug resistance proteins	9.65
K08B4.6		9.63
H08J11.8		9.62
T25E12.4B		9.62
C29E6.2	protein tyrosine phosphatase	9.6
T03G11.8	zig-6 human leukocyte surface protein	9.59
Y43C5B.2	src homology domain 2, tyrosine-protein kinase	9.55
ZK550.5	probable peroxisomal phytanoyl-coa alpha-hydroxylase	9.53
Y50E8A.12		9.51
ZK1067.7	similarity to erbb-3 receptor protein-tyrosine kinase	9.46
Y65H2.7		9.45
ZK1290.3	cuticle collagen 6	9.35
F15E11.12		9.18
C36A4.2	cytochrome p450	9.13
Y38F1A.1		9.11
C09E8.2		8.87
F27E5.3	homeobox domain	8.81
ZK507.3	protein kinase domain	8.79
C09E7.E	hypothetical protein	8.72
Y47G6A.15		8.69
F13D11.3	protein tyrosine phosphatase family	8.68
F23B2.5	frrfamide-like neuropeptides precursor	8.63
F31A3.3		8.63
C18E9.8		8.42
F07H5.8	keratin like	8.35
F23B12.1	serine/threonine protein phosphatase	8.3
C49F8.1		8.3
F55H12.2	protein-tyrosine phosphatase	8.25
T01B7.7	cuticle collagen rol-6	8.24
C27C7.8		8.22
F54C1.8		8.21
F02E9.7	acid phosphatase	8.21
ZK380.4		8.19
K07C11.8		8.13
Y65B4BR.A	similarity to ccaat/enhancer binding protein beta	7.97
T22H6.2	probable delta 1-pyrroline-5-carboxylate synthetase	7.93
C06G1.2		7.8
C15C7.5		7.79
F58D2.2		7.79
C24B5.1		7.77
Y11D7A.15		7.68
F47D12.7	cell951 mipp repeats	7.62
R07B1.2	probable galaptin lec-7	7.6
C09G5.3	putative cuticle collagen	7.59
R11G11.2	ehn-58 zinc finger protein	7.59
M03E7.2	similarity to bovine elastin-cbe1	7.56
Y105C5A.4	similarity to erbb-3 receptor protein-tyrosine kinase	7.55
F54B3.2	hypothetical 43.7 kda protein	7.46
C02D5.1	probable isovaleryl-coa dehydrogenase	7.36
K07F5.6	kin-24 tyrosine-protein kinase	7.31
F29C12.1	adenylyl cyclase	7.29
Y65B4BR.8		7.26
Y43F8C.1		7.21
F36H12.14		7.19
F41C6.5	cuticular collagen	7.11
Y105E8B.H		7.06
K08E7.5	S. cerevisiae glucoamylase s1/s2 precursor	7
F57H12.3		6.99
F28B6.4		6.93
C32H11.10		6.92
K11H3.2	hypothetical 25.9 kda protein	6.83
F37C4.2	similarity to acyltransferases	6.78

F08B4.2	cadherin repeat-containing protein	6.76
C01B12.1	cuticular collagen	6.64
T10H10.2	gcc-3	6.63
ZC455.6	UDP-glucuronyltransferase	6.59
F35C11.3	serine/threonine kinase	6.53
R107.1	sodium-dependent high-affinity dicarboxylate transporter	6.53
C30B5.3		6.49
T04H1.6	lrn-1 low-density lipoprotein receptor	6.43
C49C3.2	serine/threonine kinase (2 domains)	6.42
F38D1.7		6.38
F21F3.2	ser/thr-protein kinase	6.37
C34B2.3	protein kinase	6.36
F49C12.7	similarity to bovine camp-dependant protein kinase ii-b-binding protein	6.33
F36D3.8	similar the g'alm rhodopsin family of 7-transmembrane receptors	6.29
F42H10.7	hypothetical 58.3 kda protein	6.29
F30H5.3	serine proteases inhibitor	6.28
F41E6.2	similar to human androgen receptor	6.25
ZC449.1		6.2
F54D5.1	quaking isoform 2	6.19
F13D12.1	proton-relay domains	6.13
ZK1290.8	hypothetical 26.3 kda protein	6.12
C55C2.4		6.12
JC8.12		6.08
W04G3.1		6.06
F41H10.5		6.05
ZC250.3		6.03
F38A5.6	similarity to emericella nidulans kinesin-like protein bimc	5.98
K09B11.10		5.97
T06A1.5	extracellular protein with conserved cysteines	5.97
C08F11.1		5.94
F09C6.6		5.94
Y40H7A.11		5.92
C25F5.2		5.9
T03G6.1		5.88
T19B10.2		5.83
ZK1053.6		5.83
C25F3.5		5.8
W06F12.2	serine/threonine kinase	5.74
C04G2.5		5.69
C08E8.4		5.66
T02D1.5	ABC transporters	5.64
F10F2.3	lipase	5.63
W04G3.8		5.61
T01D1.6	similarity to erbb-3 receptor protein-tyrosine kinase	5.5
W09D10.5		5.49
F21A3.4	dystrophin like protein	5.48
R05D3.2	hypothetical zinc finger protein	5.46
F12E12.6	similar to c2h2-type zinc finger	5.44
F27E3.3		5.41
F28E10.3	similar to reverse transcriptase	5.38
ZK637.13	putative globin-like protein	5.37
C38C6.6		5.37
B0252.5	hypothetical 33.9 kda protein	5.37
Y59A8B.1		5.34
C26B2.2		5.32
F08G5.4	collagen	5.31
ZK154.1		5.29
C08E3.1		5.26
F21A10.3		5.25
ZK809.5	myosin containing PDZ domain	5.25
F18A12.4	peptidase	5.19
C05D10.3	putative ABC transporter	5.19
T19D7.3		5.18
F45D11.14	hypothetical protein	5.16
F25B3.4		5.16
F56D2.3	hypothetical 47.2 kda protein	5.15
F09B12.1A		5.12
F26A1.10		5.11
ZK180.6	similarity to ccaat/enhancer binding protein beta	5.1
Y44E3B.2	tyrosinase	5.1
Y105C5A.5	similarity to erbb-3 receptor protein-tyrosine kinase	5.08
C14A4.9		5.07
M02E1.1		5.07
C31H2.2	collagen alpha	5.06
ZC443.3		5.03
C15H9.3	similarity to g-protein coupled receptors	5.01
C27H5.4	similarity to NADH dehydrogenase	5
ZC373.6		4.97
Y39A3A.1	transposase	4.95
F21H11.3	t-box protein 2	4.93
R07E3.5	putative lysophosphatidic acid acyltransferase	4.88
Y75B8A.4	ATPases associated with various cellular activities (aaa)	4.88
Y50E8A.2	major sperm protein 56	4.81
ZK1010.7	collagen	4.8
C06A5.4		4.77
C16A11.7		4.76
F44G4.5		4.76
C05E7.1A		4.71
K06A9.2		4.64
D2062.4		4.62
F58F6.1	cuticular collagen	4.6
ZK455.7	multidrug resistance protein 3	4.53
C24B5.4		4.53
F21A9.2	zinc finger protein	4.52
F53F1.5	cutidin	4.51
T19C3.4	polyposis locus protein 1	4.5
T08B2.2	similar to cuticular collagens	4.48
M03C11.1	cAMP-dependant protein kinase	4.47
W08F4.6		4.43
B0228.2		4.4
C05E7.1B		4.39
F56F4.4		4.37

T07F10.4		4.32
F13D11.4	dihydroflavonol-4-reductase	4.3
F20G2.3	similar to retinal-binding protein	4.27
ZK1251.3	3-oxo-5-alpha-steroid 4-dehydrogenase	4.23
F30B5.1	cuticle collagen dpy-13	4.21
F59C6.6		4.2
R12E2.7	similarity to ccaat/enhancer binding protein beta	4.18
C17G10.8	fat-3 alcohol dehydrogenase	4.17
Y1A5A.1	lim domain containing proteins (2 domains)	4.16
C26C6.8	tyrosine-protein kinase like	4.14
ZK180.5	similarity to ccaat/enhancer binding protein beta	4.09
R05D3.5	hypothetical 15.2 kda protein	4.08
F01D5.6		4.07
Y51B9A.3		4.06
F21H7.4	similarity to a c-type lectin domain	4.05
C49A1.2	putative membrane protein	4.04
ZK792.7	yeast cc1 like	4.03
Y60A3A.18	skr-4 (ubiquitinates proteins during the G1/S transition)	4.02
F21E8.5		4.02
F28A10.1		4.01
Y52B11A.10		4.01
F57F7.3	collagen	4
C06H5.1		3.99
Y73C8B.3	hypothetical protein	3.98
T09F5.10		3.98
C31H1.3		3.97
F35G2.4	phy-2 prolyl 4-hydroxylase alpha subunit	3.97
ZC47.5		3.96
C14C11.1		3.96
C33F10.1	similar to C. elegans protein c03b6.2	3.9
F55G11.5		3.89
C06H5.1		3.88
ZK822.4		3.86
C05C8.3	fkb-3 fkbp-binding protein	3.81
ZK1128.3	hypothetical 42.2 kda protein	3.8
F35A5.3	glutamine-rich	3.75
Y45F10B.3		3.75
C06C6.8		3.73
F32A5.4	immunodominant antigen	3.72
Y34B4A.A	mouse SH3-binding protein 3bp-1	3.7
C09G9.4	aromatic-l-amino-acid decarboxylase	3.69
T01B10.2		3.68
Y47D3B.10	prolyl 4-hydroxylase alpha subunit precursor	3.68
C38C10.3	hypothetical 33.7 kda protein	3.65
C35D10.2		3.64
ZK1037.8	similarity in C. elegans olfactory receptor odr-10	3.63
D1081.5	ankyrin motif	3.63
Y49E10.10		3.62
C35E7.10B	protein kinase	3.56
W03D2.5	wrt-5	3.54
Y105C5A.3	similarity to erbb-3 receptor protein-tyrosine kinase	3.52
ZK1307.3	hypothetical 12.4 kda protein	3.51
F40A3.4		3.51
F44D12.4		3.51
C05D11.5		3.49
F26G1.5		3.48
Y73F8A.H	similarity to erbb-3 receptor protein-tyrosine kinase	3.48
T25B9.5	Src homology domain 2, protein tyrosine kinase (Abl subfamily)	3.44
F37C12.13	autoantigen	3.43
T08B6.5	RNA binding protein	3.41
C55B7.3	protein-tyrosine phosphatase	3.41
F53B1.4	thymidine diphosphoglucose 4,6-dehydratase	3.38
F58A3.8	protein kinase	3.36
K09C6.7		3.36
Y47D7A.F	hypothetical protein	3.35
F14H12.4	protein kinase	3.33
R08H2.13	7tm receptor	3.32
T06E4.8		3.31
Y34B4A.B	hypothetical protein	3.29
R12E2.7	similarity to ccaat/enhancer binding protein beta	3.24
C54D1.6	bar-1 beta-catenin	3.24
K07A1.5		3.23
C12D8.9		3.23
F08F1.6		3.23
Y47D3A.10	t-box protein 9	3.19
T08D8.10	peroxidase	3.19
C52E4.7	similar to ser/thr protein kinase	3.19
C43E11.5	similarity to human leukocyte common antigen 1 precursor	3.16
ZC13.4	similarity to EGF-like domain cysteine pattern signature	3.15
F38E9.2		3.15
C37A2.3	acyl-CoA dehydrogenase	3.12
R07B5.3		3.09
C42D8.5	peptidase	3.08
Y43C5B.3	mitochondrial carrier proteins (2 domains)	3.06
C01C10.3		3.04
Y46G5A.22A		3.03
Y48B6A.5		3.02
Y75B8A.2	nab-1 homeobox domain	2.99
Y47H10A.4		2.98
T07E3.2		2.97
F37A8.4	slp-10	2.96
C49F8.3		2.95
Y73F8A.G	similarity to erbb-3 receptor protein-tyrosine kinase	2.94
F30A10.8A	beta1-syntrophin	2.94
ZK632.8	gtp-binding ADP-ribosylation factor homolog protein	2.94
F07F6.1	hypothetical 46.3 kda protein	2.94
H17B01.2	collagen	2.93
ZK688.8	gly-3 UDP-galnac	2.92
F29D10.1		2.91
C16E9.2B		2.91
F19B10.10		2.89
Y66A7A.6	glycosyl transferases	2.88

B0286.3	probable multifunctional protein ade2	2.87
K09B11.5	eukaryotic protein kinase domain	2.86
F42A10.3	similar to small region of phosphatidylethanolamine n-methyltransferase	2.86
Y106G6G.4		2.85
W01F3.3	kunitz/bovine pancreatic trypsin inhibitor domain (10 domains)	2.85
C35D10.6		2.84
C35E9.5	collagen	2.84
Y65H2.10	ecm 18 (fragment)	2.83
H03A1.3		2.82
C56H5.1		2.82
Y44A8D.5	aminotransferase class iv	2.8
F09B9.3	ER lumen protein retaining receptor	2.8
F11G11.4		2.79
R12E2.7	similarity to ccaat/enhancer binding protein beta	2.78
R07E3.4	ADP/ATP carrier protein	2.75
W01B6.2	serine/threonine kinase	2.75
T23B7.1		2.73
T27A3.5	similarity to protein-tyrosine phosphatase domains	2.73
F25E5.4		2.73
ZK39.4	similarity to a c-type lectin domain	2.72
C09D4.3	ser/thr protein kinase	2.72
F08G2.6	ins-37	2.71
D2045.8	TNF-alpha induced protein ti12	2.69
C33C12.4		2.69
Y39B6B.N		2.68
ZK524.1	integral membrane protein spe-4	2.67
T03F6.4		2.67
T05C12.3	hypothetical oxidoreductase	2.66
F10G8.2	eukaryotic protein kinase domain	2.65
K03H6.2	putative 32.6 kda lipase	2.65
E04D5.3	cutidin like protein	2.64
ZK185.2		2.62
F02E11.1	ABC transpoter	2.62
K10H10.4		2.6
F54D10.3		2.59
T17H7.7		2.59
W03D8.8	similar to the rat kan-1 protein	2.59
Y38H8A.3	serine/threonine kinase	2.55
C15H11.9		2.54
Y57G7A.1		2.5
T27B7.6	zinc finger protein	2.5
T19C3.2	hypothetical 31.4 kda protein	2.49
T13A10.11	probable s-adenosylmethionine synthetase	2.48
C50F4.10	serine/threonine kinase	2.48
F08G2.1	histone H2B.1 and H2B.2	2.48
K05F1.3	acyl-CoA dehydrogenase	2.48
T07C12.9	n-methyltransferase	2.44
K06C4.11	histone H2A	2.42
ZC404.2		2.42
T24B8.3		2.42
F29B6.1	protein tyrosine phosphatase	2.4
Y43C5A.1		2.4
T04B2.2	Src homology domain 2, tyrosine-protein kinase (Fes/Fps subfamily)	2.36
K01A2.5	biphenyl hydrolase-related protein	2.35
F53A9.8	histidine-rich	2.35
F56D6.1		2.33
T14B4.4	similar to leukocyte antigen cd53	2.33
K07E8.3		2.33
ZK353.4	hypothetical 33.2 kda protein	2.32
R53.2	probable thymidylate kinase	2.31
T22H2.6B	human granulins precursor (acrogranin)	2.3
C46H11.9	similarity to toxocara canis surface coat glycoprotein tes-120	2.28
ZK1307.1	beta-hydroxylase, bleomycin/phleomycin binding protein, ankyrin homologue	2.28
T28H10.3	vacuolar processing enzyme like	2.28
C24D10.8		2.26
F53F10.1		2.25
F02H6.5		2.22
B0496.7	mouse cysteine-rich intestinal protein	2.21
F07C3.2		2.21
K06B4.9	g-protein coupled receptor	2.2
C24A11.1		2.19
C27A2.5	serine 1 ultra high sulfur protein	2.19
C54G4.3		2.19
F28A3.2	collagen	2.18
C03C11.1		2.18
K10B3.1		2.17
T24C2.4		2.17
Y67H2B.C	serine/threonine protein phosphatase	2.16
F41E6.11	hydroxyproline-rich glycoprotein	2.16
C16H11.3	similar to UDP-glucuronosyltransferases	2.15
C50E10.2	similar to gamma-glutamyl carboxylase	2.15
C33F10.11	similar to *C. elegans* protein cOSb2.2	2.13
C25D7.1		2.13
AH6.2	tricarboxylate carrier-like protein	2.13
F41E4.3		2.12
R13F6.9	dwarfin sma-3 (mad protein homolog 2)	2.12
F45E4.8		2.11
C24D10.7		2.1
T28C6.8		2.08
C05E7.2		2.08
ZK270.1	similar to *C. elegans* protein R4PA.4	2.08
F36H12.11		2.08
F53G12.6	protein-tyrosine kinase	2.08
F56A11.6		2.06
T24H7.4		2.05
Y37D8A.5		2.04
F57B9.8	putative protein tyrosine kinase	2.04
C34B2.4	oracle 2 protein	2.02
ZK265.4	homeobox protein ceh-6	2.02
F43G6.8	zinc finger, c2hc4 type (ring finger)	2.01
R02F11.1		2
C46H11.7	similarity to toxocara canis surface coat glycoprotein tes-120	1.99

Y47D3A.22	ankyrin 3	1.99
F48A8.10	similarity over a short region to plasmodium falciparum d288	1.98
B0485.9	UDP-glucuronosyltransferase	1.97
M04G12.2	cysteine protease	1.95
C06C3.4		1.94
F44D12.4		1.94
ZK666.6	von willebrand factor type a domain	1.94
F15E6.2	human acetylcholine receptor protein, delta chain precursor	1.94
F42G4.6		1.93
C30H6.2	lea-alanine resistance protein 1	1.93
ZK381.5	similarity with mouse tastin	1.93
C50A2.1		1.92
F47G6.4	hum-3	1.92
Y69E1A.8		1.91
C02C2.3	hypothetical acetylcholine receptor like protein	1.91
K01D12.15		1.9
F56A8.4		1.9
Y5H2A.C	glutamine-rich	1.89
F01D5.9	cytochrome p450	1.87
W07E11.1	glutamate synthase	1.87
K08D10.10		1.86
F54D11.2	human neurofilament triplet h protein (200 kda neurofilament protein)	1.86
ZC8.2		1.86
F10E7.3	similarity to NADH dehydrogenase	1.85
F08A8.2	acyl-coenzyme a oxidase, peroxisomal	1.85
F36H12.9	similar to casein kinases	1.85
C33G3.3		1.84
H43E16.1	similar to a. faecalis poly(3-hydroxybutyrate) depolymerase	1.83
ZK131.1	histone H4	1.83
C34D4.3		1.83
C31H1.1	similarity to S. cerevisiae transcription factor mbp1	1.83
T01G6.4	zinc finger protein	1.81
C35A11.2		1.81
K06A5.3	similarity to EGF-like repeats	1.79
F27E5.4	growth arrest protein extracellular domain	1.78
ZK484.8		1.78
F52B11.3	let-653 mucin like protein	1.74
F09C12.2	ser/thr protein kinase	1.73
T14E8.1	protein-tyrosine kinase	1.72
C44H4.3	syn-1 drosophila chaoptin protein like	1.72
C47E12.8	alp like protein	1.71
Y46H3D.1		1.7
F31D5.2	et putative translation product	1.69
K06A4.3	gelsolin	1.69
T22A3.4		1.68
C26H7.1	casein kinase	1.68
K01D12.9		1.67
Y37D8A.8		1.67
F49E3.5	serine threonine protein phosphatase	1.66
K08C4.13	histone H2B.1 and H2B.2	1.65
C52G5.2		1.65
K07F5.5		1.65
M05B5.2		1.64
C07E3.4	protein-tyrosine phosphatase	1.63
M04G7.2	protein-tyrosine phosphatase	1.62
C45G9.1		1.61
F37H8.3	haloacid dehalogenase-like hydrolase	1.61
C33H5.13		1.61
ZK484.2	transporter protein	1.6
Y47G6A.19	carboxypeptidase	1.59
T19C6.12	histone H2A	1.59
F09C3.1	ras GTPase-activating protein like	1.59
C48D2.2		1.59
B0336.11	hypothetical 59.3 kda protein	1.59
DH11.1	putative glutaminase dh11.1	1.58
F55A12.4	dehydrogenase	1.57
Y105C5A.6	similarity to erbb-3 receptor protein-tyrosine kinase	1.57
E04F6.8		1.57
C04F12.7		1.57
T02C5.1		1.56
F36F2.4	syntaxin	1.55
B0280.6	cell wall protein, putative	1.54
T24D8.2		1.54
T21H3.2	similar to C. elegans protein f44f4.4	1.53
K08C9.2		1.53
C06A1.3	putative serine/threonine protein phosphatase	1.53
F07C6.2		1.53
W06D4.2		1.53
Y37D8A.16		1.52
Y54E5A.6A		1.52
C50B8.4		1.52
ZK484.5		1.51
T05C12.3	hypothetical oxidoreductase	1.51
F09G8.6	putative cuticle collagen	1.5
F45H10.4		1.49
C06F11.13		1.49
T01D1.3		1.49
D1081.4		1.49
C53A3.2	similar to 4-nitrophenylphosphatase	1.48
F08F1.8		1.48
Y66A7A.7		1.47
T12B5.1		1.47
E01G4.6		1.46
K02H1.9		1.45
B0244.4		1.45
M02D8.4	asparagine synthase	1.44
F13G11.2		1.43
Y38C1BA.3	collagen	1.43
T19C6.11	histone H2B.1 and H2B.2	1.42
F52H3.3	lim (also known as tir-c/ttk) domain	1.42
F09G2.3	permease	1.42
ZK1127.2	CoA ligase	1.41

C05D11.10	hypothetical 11.8 kda protein	1.39
ZK1098.9	hypothetical 23.9 kda protein	1.39
Y106G6E.4	5-formyltetrahydrofolate cyclo-ligase	1.38
F47B3.1	protein-tyrosine phosphatase	1.37
C31C9.2	d-3-phosphoglycerate dehydrogenase	1.37
AH6.13	sre-2 protein	1.37
F26F12.4		1.36
F26E4.2		1.35
F55C12.3		1.35
W10G6.2	protein kinase C terminal domain	1.35
F47G4.3	NAD-dependent glycerol-3-phosphate dehydrogenase	1.34
F09F5.4	type 1 thrombospondin (tsp) repeats	1.34
B0414.5	isovaleryl-coa dehydrogenase	1.33
C48B4.2	rhomboid	1.33
C34E7.4		1.32
C05D2.7		1.32
F59F4.1	acyl-CoA oxidase 1	1.31
F07C6.1	lin protein pin-2	1.31
B0414.6		1.31
W02G9.1	nucleoside diphosphate-sugar hydrolase of the mutt (nudix) family	1.31
F17C8.3	conserved hypothetical protein	1.31
B0365.5	c-type lectin domain	1.29
C29F7.2		1.26
C17H12.8		1.27
C33E10.8		1.26
F26A10.1		1.26
T23F6.1	human keratin, ultra high-sulfur matrix protein	1.25
F22D6.9	serine/threonine protein phosphatase	1.25
F17C11.5		1.25
CTEL54X.1		1.24
B0035.13	lipase	1.24
C07E3.3	nicotiana tabacum extensin precursor	1.21
F35E12.7	microfilarial sheath protein shp3	1.21
F26B1.1		1.2
M195.1	cuticle collagen	1.2
F32B6.5	sre-1	1.2
VC5.5	bovine lungworm dve-1 polyprotein precursor	1.18
F53F4.13		1.18
K08D8.5		1.18
Y32F6B.1	similar to inactin f/g	1.17
C44B7.4		1.17
F13E6.1	452 protein	1.16
C01G12.3		1.15
F13B9.8	conserved hypothetical protein	1.15
F01G4.5	n-acetylglucosaminyl transferase component gpi1	1.15
C46A5.3	cuticle collagen 14	1.15
B03H12.7		1.15
C35D10.11		1.14
Y37A1B.7		1.14
D1046.2	calpain	1.13
F58H10.1		1.13
F33H2.8		1.13
ZK1251.5	protein-tyrosine phosphatase	1.13
T05C12.10	hedgehog-like protein	1.13
F10F2.2	phosphoribosylformylglycinamidine synthase	1.12
F44A6.1	nucleolarin	1.11
D2062.7		1.11
T04B2.5	mouse 85 kda calcium-independent phospholipase a2	1.11
C05C10.4	putative acid phosphatase	1.1
F10G7.7		1.1
F56F3.6	asx-5 neuroendocrine convertase 2 precursor like	1.09
F32A7.6	asx-5 neuroendocrine convertase 2 precursor like	1.09
F57B1.6		1.09
T13H5.4	prp4 like protein	1.09
K09B3.1		1.08
F07C3.9		1.08
T08B1.3	aldehyde dehydrogenase	1.07
C33F10.12	mitochondrial phosphate carrier protein	1.07
C01G8.3	oxidoreductase	1.07
F14H3.10	cytochrome p450	1.06
F45F2.4	histone H2A	1.06
ZK84.2		1.06
K09A11.3	cytochrome p450	1.05
R07G3.2	lipase	1.05
ZK643.7	hypothetical 12.8 kda protein	1.05
C06E7.4	similar to human cytomegalovirus protein ul53	1.05
C01H6.1	collagen	1.04
C03G6.15	cytochrome p450	1.03
T22A3.2	alpha crystallin b chain	1.03
F27D9.6	similarity to human follicular variant translocation protein 1 precursor	1.01
K01D12.5		1.01
Y40B1A.1		1
C36H8.1	major sperm protein like	1
ZK596.3		1
F36H9.5		1
C06A1.6	serine 2 ultra high sulfur protein	1
R05F9.13	major sperm protein 31/40/142	-1
R119.4	putative RNA-binding protein prp-1	-1
T03E6.7	cathepsin-like protease	-1
R05F9.8	major sperm protein 33	-1
T05G5.6	probable enoyl-coa hydratase, mitochondrial	-1
ZK856.11	putative translation initiation factor	-1
K11H12.2	60S ribosomal protein l15	-1
K02B4.7		-1
ZK354.3		-1
M142.5		-1
F25H5.3A	pyruvate kinase	-1
F45E12.2	transcription initiation factor IIb	-1
T07F10.3	polyadenylate-binding protein like	-1
Y71A12D.1		-1
C26B2.6		-1
F21F8.7	protease	-1

F45G2.3	xpg n-terminal domain, xpg i-region	-1
T07F12.4	serine/threonine protein kinase	-1.01
F42A9.6		-1.01
C16A3.5	NADH-ubiquinone oxidoreductase b22	-1.01
R09B3.2	RNA recognition motif	-1.01
F53C11.4		-1.01
K10B3.7	glyceraldehyde 3-phosphate dehydrogenase 3	-1.01
H35N09.1		-1.01
C25A1.11	aha-1 aryl hydrocarbon receptor nuclear translocator	-1.01
F58A4.4	pri-1 (DNA polymerase alpha primase subunit D)	-1.01
C49G7.3	similarity to toxocara canis tes-26 protein	-1.01
K11C4.5	unc-68 ryanodine receptor	-1.01
B0336.1	wrm-1	-1.01
B0218.6	similarity to c-type lectin domains	-1.01
B0414.5	RNA binding protein	-1.02
F57B9.6	eukaryotic initiation factor 4a	-1.02
Y38H6C.1		-1.02
F09G2.9		-1.02
K12H6.3		-1.02
F48E8.7	scf complex protein skp2	-1.02
Y65B4BL.8	human long-chain-fatty-acid--coa ligase 2	-1.03
Y39B6B.GG	plasmodium lophurae histidine-rich glycoprotein precursor	-1.03
T13A2.8	5'-3' exonuclease, homolog of the human XPG gene	-1.03
F26H9.4	yeast hypothetical protein yg15 like	-1.03
M18.1	collagen	-1.03
Y62E10A.5		-1.03
ZK858.3	lectin	-1.03
Y51H1A.7		-1.03
C34F6.2	collagen	-1.03
C07D10.2	similar to d. melanogaster bncano-g1-c1 protein and v. virus protein e55	-1.03
F25F2.2	approximately 25 cadherin-repeats, 3 EGF domains and one laminin g domain	-1.03
T25C8.2	act-5 actins	-1.04
K07F5.2	major sperm protein 10	-1.04
W06A7.3C	d-99 e	-1.04
F01G4.6	mitochondrial phosphate carrier protein precursor	-1.04
F56B6.3		-1.04
F49E8.6		-1.04
K09B11.2	hypothetical nuclear protein	-1.04
C09G5.4	putative cuticle collagen	-1.04
C06G8.2	hypothetical oligopeptide transporter	-1.04
T20G5.7		-1.05
R53.6		-1.05
T22F3.4	probable 60s ribosomal protein l11	-1.05
C47A4.2	similarity to tnip26 protein	-1.05
R02D3.1	dehydrogenase	-1.05
C01C7.1	src homology domain 3, tyrosine-protein kinase (ack subfamily)	-1.05
Y41E3.10	elongation factor 1 (beta/delta chain)	-1.05
T25G3.3	yeast nonsense-mediated mRNA decay protein like	-1.05
B0041.4	probable 60s ribosomal protein L4	-1.05
B0222.5	hypothetical 26.3 kda homeobox protein	-1.05
M28.5	vhp2/ns6 family protein yel026w homolog	-1.06
F44E5.1		-1.06
R10E11.2	vacuolar atp synthase 16 kda proteolipid subunit 2	-1.06
H06O01.1	protein disulphide isomerase er-60 precursor like	-1.06
C34F6.7		-1.06
C08F11.11		-1.06
Y17G7B.5	mcm2/3/5 family	-1.06
F54A5.1	chicken hepatocyte nuclear factor 1-alpha (hnf-1a)	-1.06
T05A1.2	collagen	-1.07
ZK488.10	similar to keratins in a glycine-rich region	-1.07
C26E6.5		-1.07
F12F3.2	titin	-1.07
Y57G11C.16	ribosomal protein s13	-1.07
H06O01.3	retinal-binding protein like	-1.07
C14C10.5		-1.07
Y56A3A.20	ccr4-associated factor 1	-1.07
T01G9.5	mei-1, meiatic spindle formation protein	-1.08
R09B3.4	ubiquitin-conjugating enzymes	-1.08
F11C3.3	myosin heavy chain b	-1.08
T22E5.5	tropesin t	-1.08
Y39E4A.2A	rat zinc transporter 2 (znt-2)	-1.08
R12E2.3	mouse 26s proteasome regulatory subunit s12 (proteasome subunit p40)	-1.08
D2005.4		-1.08
W09B6.2	drosophila melanogaster transcription initiation factor TFIIH 62 kda subunit	-1.08
F11E6.7		-1.08
K02F2.1	peptidase	-1.08
K06H7.8	similar to casein kinase	-1.08
C04F12.4	rat 60S ribosomal protein l14	-1.09
W02B12.3	pre-mRNA splicing factor like protein	-1.09
T21D12.1		-1.09
ZK1251.6	major sperm protein 10	-1.09
T06E4.4	collagen	-1.09
T23G5.5		-1.09
M01F1.2	probable 60S ribosomal protein l13a	-1.09
F56A8.6	RNA recognition motif	-1.09
M01F1.8		-1.09
C08C3.4	hypothetical 30.8 kda protein	-1.09
Y49F6B.8		-1.09
R10E7.6	multiple ankyrin	-1.09
F49E8.5	probable protein phosphatase pp2a regulatory subunit	-1.09
F21F8.3	protease	-1.09
F53F10.2	decarboxylase	-1.1
Y48B6A.2		-1.1
K07C5.4	yeast protein ll6167.6-like	-1.1
F54D8.2	probable cytochrome c oxidase polypeptide via precursor	-1.1
C24D10.4		-1.1
F57B10.11	similarity to human navel glucocorticoid receptor-associated protein	-1.1
F49C1.6		-1.1
Y47D7A.H	hypothetical protein	-1.1
ZK1127.10	putative cystathionine gamma-lyase	-1.11
F54C9.1	probable initiation factor 5a	-1.11
C35D10.13		-1.11

C06H9.2	high-density lipoprotein-binding protein	-1.11
F26E4.11	zinc finger, c3hc4 type (ring finger)	-1.11
ZK1236.5	hypothetical 35.7 kda protein	-1.11
B0393.2	probable RabGAP domains	-1.11
H43I07.2	transferase	-1.11
C54G10.2	replication factor C 140 kd subunit like	-1.11
B13H9.2	major sperm protein 31/40/142	-1.12
T05H4.11		-1.12
T11F8.3	rme-2 ldl-like receptor	-1.12
F28D10.10	carbamoyl-phosphate synthase (cpsase) (2 domains)	-1.12
C26F1.4	ribosomal protein/ubiquitin-like protein	-1.12
Y71F9AR.4		-1.12
T07C4.8	apoptosis regulator ced-9	-1.12
T22D1.5	similar to protein phosphatase pp2a	-1.13
F18H3.5A	serine/threonine kinase (cdc2/cdka subfamily)	-1.13
R02F2.1	Cyclin B and related kinase-activating protein	-1.13
F14B8.3	similarity with various transporters	-1.13
C27A7.5A	asparaginase	-1.13
F13D12.4	probable methylmalonate-semialdehyde dehydrogenase [acylating] precursor	-1.13
F48A11.5	mouse fat1 protein (fat-associated factor 1)	-1.13
C49F5.7		-1.13
K02F2.2	adenosylhomocysteinase	-1.13
T25E12.4A	phorbol-esters/diacylglycerol binding domain, serine/threonine kinase	-1.13
F46B3.8		-1.13
F57C9.5	neurofilament-h	-1.14
C06E8.2		-1.14
F57C2.2	BTB (also known as br-c/tbk) domain	-1.14
F53G12.10	probable 60S ribosomal protein l7	-1.14
F35B12.5		-1.14
ZK1320.1		-1.14
Y17G7A.1	hmg-12	-1.15
C11D2.1		-1.15
F56H11.4		-1.15
B0024.2	collagen	-1.15
C32D5.11		-1.15
ZK354.11	major sperm protein 31/40/142	-1.16
K03B4.2		-1.16
R05F9.1	yeast suppressor protein sip40	-1.16
B0205.1	ATP citrate lyase	-1.16
F59F4.2	ribosome-associated membrane protein ramp4	-1.17
D2085.3	translation initiation factor	-1.17
F27C4.1	similarity to acyltransferases	-1.17
F09E5.12		-1.17
ZK593.6	microtubule-associated protein 1 like	-1.18
C35B1.3		-1.18
C25A1.8	lectin	-1.18
H12D21.5	putative thiosulfate sulfurtransferase	-1.18
C08H9.3	putative glucosyltransferase	-1.18
T24A11.2		-1.18
Y47G6A.4		-1.18
F49E12.2		-1.18
F29G6.3A	mucin core polypeptide, tracheal	-1.18
R06C1.4	RNA recognition motif	-1.19
F08D12.1	signal recognition particle 72 kda protein homolog (srp72)	-1.19
Y110A2AR.D	human polyposis locus protein 1	-1.19
R01H2.6		-1.19
W02B12.10		-1.19
F52A8.6	ras-like protein like	-1.19
C48B4.8	hypothetical 22.7 kda protein	-1.2
F59B8.2	isocitrate dehydrogenase	-1.2
K07F5.1	major sperm protein 31/40/142	-1.2
ZC434.2	40S ribosomal protein s7	-1.2
T23G11.3		-1.2
R13J1.3	probable 60S ribosomal protein l6	-1.2
F09D1.1	ubiquitin protease	-1.2
F16B4.4		-1.2
W06B11.2	pumilio repeats	-1.2
ZC21.3		-1.2
T13F2.10	major sperm protein 31/40/142	-1.21
C48B4.9	hypothetical 21.8 kda protein	-1.21
ZK546.3	major sperm protein 31/40/142	-1.21
ZK1010.1		-1.21
C52E4.3	probable small nuclear ribonucleoprotein snr d2 (snrnp core protein d2)	-1.21
ZK809.2		-1.21
Y39A3CL.B	drosophila melanogaster calpain	-1.21
ZK512.6	sodium/phosphate cotransporter	-1.21
C37A2.6	similarity to ribosomal protein l11 methyltransferase	-1.21
W06B11.1		-1.21
C32D5.5		-1.22
T28D9.4	hypothetical 50.4 kda protein	-1.22
C06A1.5	probable DNA-directed RNA polymerase II 14.4 kda polypeptide	-1.22
F39B2.6	40S ribosomal protein s26	-1.22
F35D11.4		-1.22
K03B4.3	similar to human tata-binding protein associated factor 38 kda subunit	-1.22
C05C10.5	hypothetical 24.3 kda protein	-1.22
D1054.10		-1.23
VT2385.1		-1.23
M03D4.1A	zen-4 kinesin-like protein	-1.23
C16H11.9	let-502 Rho-associated kinase	-1.23
K05C4.6	hmp-2 armadillo/beta-catenin-like repeats (4 domains)	-1.24
F56D1.6	hypothetical calcium-binding protein	-1.24
F49C1.5		-1.24
R04F11.3	tiadin	-1.24
C06A8.4	skip3p homolog	-1.24
F57B9.3	eukaryotic initiation factor 4a	-1.24
M60.2	similar to human placental protein 11 precursor	-1.24
T04A8.6	ribonucleoprotein	-1.24
F56E10.4	ribosomal protein	-1.24
C06H5.7		-1.24
K05G3.3	carbonic anhydrase	-1.25
K04D7.1	guanine nucleotide-binding protein beta subunit-like protein	-1.25
F07H5.4		-1.25

Y45F10C.5	hypothetical 29.3 kd protein	-1.25
F32B6.1	nhr-4 ligand-binding domain of nuclear hormone receptors, zinc finger, c4 type	-1.25
T23G7.5	tyrosine specific protein phosphatase	-1.26
K11D12.5		-1.26
F42A8.3	hypothetical 37.3 kda protein	-1.26
Y55B1BR.F		-1.26
T09F3.2	carrier protein c2	-1.26
C24B9.3	chicken collagen alpha 3(vi) chain precursor	-1.26
F59F4.4	putative 1-acyl-sn-glycerol-3-phosphate acyltransferase	-1.26
C42D8.8	agl-1	-1.27
F59A1.7		-1.27
T10G3.6	gut-2 yeast hypothetical 11.2 kd protein like	-1.27
Y43B11AR.B	chicken 40S ribosomal protein s4	-1.27
F20B6.2	probable vacuolar atp synthase subunit b	-1.27
K07B1.10	probable galactin lec-8	-1.28
C05D9.7		-1.28
K07F5.9	sap-10	-1.28
Y40C5A.4	probable g protein-coupled receptor	-1.28
K01E6.3	carbonic anhydrase	-1.28
F26E4.9	cytochrome c oxidase	-1.28
C16H3.2	lec-9 sugar-binding protein	-1.28
B0513.3	60S ribosomal protein l29	-1.28
Y39B6A.H		-1.28
Y116A8C.12	ADP-ribosylation factor 6	-1.28
W08A12.1		-1.28
Y75B12B.4	BTB (also known as br-c/tbk) domain	-1.29
T09B9.4	human h4(d10s170) protein	-1.29
W02D9.1	probable DNA primase large subunit	-1.29
H10E21.5	zinc finger protein	-1.29
K03H1.7		-1.29
W05B2.4	chlamydomonas reinhardtii dynein beta chain, flagellar outer arm	-1.29
F13D12.6	putative serine carboxypeptidase	-1.29
C25A1.10	nucleolar phosphoprotein	-1.3
F07H5.10		-1.3
F45D3.3		-1.3
T02H6.11	ubiquinol-cytochrome c reductase complex subunit	-1.3
F48G7.3	nhr-83 nuclear hormone receptor	-1.3
K01G5.4	GTP-binding protein	-1.3
F23B12.3		-1.31
W03C9.2		-1.31
F56A8.5	similarity with C. elegans pes-2	-1.31
F07A5.1A	asc-7 like	-1.31
T05H10.1	ubiquitin carboxyl-terminal hydrolase	-1.31
F15H10.1	cuticle collagen 12 precursor	-1.31
F14H3.6		-1.32
F27C1.4		-1.32
T08D10.1	DNA binding protein	-1.32
C33A12.16		-1.32
B0234.1	transthyretin-like family	-1.33
C16A4.4		-1.33
F36A2.6	40S ribosomal protein s15	-1.33
Z6546.15	plasminogen	-1.33
R05H10.3		-1.33
F32D8.5A		-1.33
C04E7.1	hypothetical 13.6 kda protein	-1.33
K07H8.6	vitellogenin 6 precursor	-1.34
W01G7.3	RNA polymerase i	-1.34
C25E10.5	similarity to two short region of multi-drug resistance proteins	-1.34
F44A2.1		-1.34
ZK1010.2		-1.34
F23H11.3	succinyl-coa ligase	-1.34
Y73F8A.5	copine i	-1.35
F23C8.6	highly similar to developmental protein dg1118	-1.35
F59A2.3	splicing factor-associated 32k chain	-1.35
F20D1.2		-1.35
F02E8.6	sgc-1	-1.35
C45G9.12	hypothetical 10.1 kda protein	-1.35
F53G12.1	ras-related protein	-1.35
K06H7.3	isopentenyl-diphosphate delta isomerase	-1.35
F52H3.7	lec-2 galactoside-binding lectin	-1.35
Y113G7A.9		-1.35
C30H6.9		-1.36
F52E1.13A		-1.36
M01E11.4	eukaryotic translation initiation factor 6	-1.36
C47B2.5		-1.36
Y59A8B.V		-1.36
Y11D7A.1	clostridium kluyveri 4-hydroxybutyric coenzyme a transferase	-1.36
Y57G11C.33		-1.36
C55A1.8		-1.36
C29F9.12		-1.36
T25B9.1	5-aminolevulinic acid synthase	-1.36
Y39A1A.1	conserved hypothetical protein	-1.37
T01C3.6	probable 40S ribosomal protein s16	-1.37
T24A11.1	mystubularin homologous protein 1	-1.37
F40F11.1	ribosomal protein s11	-1.37
K06F4.2	RNA recognition motif	-1.38
C23H4.2	carboxyesterase	-1.38
Y59A8B.W		-1.38
B0244.D	similar to cysteine-rich repeat regions of ldl receptors and mouse ani2 receptor	-1.38
R11D1.8	ribosomal protein l28 like	-1.38
F55H2.3	hypothetical 20.2 kda protein	-1.38
K08F8.1	ribosomal S6 kinase	-1.38
Y65B4BL.F	hypothetical protein	-1.38
R06C7.1	similar to C. elegans protein	-1.39
F09C12.7	major sperm protein S6	-1.39
R08C7.3	histone H2A variant	-1.39
T07D3.9	similarity to rat cytosolic acyl coenzyme a thioester hydrolase	-1.39
T09A5.11	probable dolichyl-diphosphooligosaccharide, glycosyltransferase precursor	-1.39
R07G3.7	hypothetical 46.7 kda protein	-1.39
T22D1.10	ruvbl2	-1.39
T05A12.2	trehalase precursor	-1.39
C04F6.1	vitellogenin 5 precursor	-1.39

C18F10.7	similar to ank repeat region of fowlpox virus bamhi-orf7 protein	-1.4
K08E7.3	let-99 domain found in dishevelled, egl-10, and pleckstrin	-1.4
Y53F4A.3		-1.4
B0365.3	eat-6 Na[+]/K[+] ATPase alpha subunit	-1.4
F58A4.3	hypothetical histone 3-like protein	-1.4
F58G8.5	nuclear hormone receptor family member nhr-34	-1.4
B0454.9		-1.4
Y54E10A.10		-1.4
H38K22.2A		-1.4
C25H3.10		-1.4
H21P03.3A		-1.41
B0393.8		-1.41
C06F9.2	similarity to EGF-like domain cysteine pattern signature	-1.41
C26F6.2	putative membrane protein	-1.41
F46B6.7	zinc finger, c2h2 type	-1.41
F52C6.2		-1.42
F54E7.2	probable 40S ribosomal protein s12	-1.42
Y57G11C.15	protein transport protein sec61 alpha subunit	-1.42
H06I04.4	40S ribosomal protein s27a	-1.42
T05A10.4	scp-like extracellular proteins	-1.42
T15B7.6		-1.43
B0240.2		-1.43
K09H9.6	second-step splicing factor 1, scf1 protein	-1.43
F19C7.1		-1.43
F42D1.2	tyrosine aminotransferase	-1.43
T04C10.2	possi hypothetical protein f8167.8 like	-1.43
K01G5.5	putative nucleolar protein k01g5.5	-1.44
T19H12.2	similarity to leucine-rich repeats	-1.44
T10E10.E	similar tocollagen	-1.44
C05D2.5		-1.45
R09A1.1		-1.45
C05H10.2	probable 60S ribosomal protein l44	-1.45
C18G1.5	histone H1	-1.45
H02B7.5	similar to *S. cerevisiae* protein transport protein sec7	-1.45
Z6643.2	probable deoxycytidylate deaminase	-1.45
H28O16.1	ATP synthase alpha and beta subunits, ATP synthase alpha chain	-1.45
C04A2.7B	viral nonstructural protein p125	-1.46
F28H11.3	probable malate dehydrogenase, mitochondrial precursor	-1.46
F46C8.7		-1.46
Y48G10A.8		-1.46
F56F3.2	sdg-4	-1.47
C47E8.5	heat shock protein (hsp90)	-1.47
C52E4.1	gut-specific cysteine proteinase precursor	-1.47
F40F8.7	histone H2A-like protein	-1.47
D1081.7		-1.47
F54H12.1	probable aconitate hydratase, mitochondrial precursor	-1.48
C04D8.1	GAP-2 GTPase-activating protein	-1.48
Y43F8B.2B		-1.48
C53B7.4	putative ATP synthase g chain, mitachondrial 1	-1.48
C14B1.1	protein disulfide isomerase	-1.48
K05C4.7		-1.48
CC8.2	smooth muscle protein phosphatase type 1-binding subunit	-1.48
B0280.5	lustrin a	-1.49
C01B4.8	similar to sodium/phosphate transporter protein	-1.49
Z66B2.1	similar to mariner transposon	-1.49
C03C10.1	putative casein kinase I	-1.49
B0273.2	tbf-2 protein	-1.5
H01D7.6	similar to a short region of thymopoietins	-1.5
F28H1.2	colponin	-1.5
F01F1.12	fructose-bisphosphate aldolase 2	-1.5
T05A7.9	small histidine-alanine-rich protein precursor (sharp)	-1.5
R06C1.3	human hypothetical proline-rich protein	-1.5
F39G9.1B		-1.51
Y105C5B.2B	panulirus argus glutamine synthetase	-1.51
T27F2.3	bir-1 inhibitor of apoptosis domain	-1.51
Y37A1C.1A	amino acid permease	-1.51
B0261.1	neurofilament-h	-1.51
T10E10.F	similar tocollagen	-1.51
F21C3.4	putative metal transporter	-1.51
C56C10.8	transcriptice factor btf3 homolog	-1.52
R148.4		-1.52
F54E7.4		-1.52
T09A12.4	nhr-66 zinc finger protein	-1.52
C03H5.1	similarity to cub domains	-1.53
C27F5.1	lin-1	-1.53
C17E7.7		-1.53
T02E1.3A	tb11 protein like	-1.53
Y45F10A.2	puf11p-family RNA binding domains	-1.53
C45H3.9		-1.53
C56G2.6	putative steroid dehydrogenase let-767	-1.53
F17H10.1		-1.54
C45G9.2		-1.54
F33H1.2	glyceraldehyde 3-phosphate dehydrogenase 4	-1.54
F46H5.3	probable arginine kinase	-1.54
B0495.6	hypothetical 9.9 kda protein	-1.54
T03F6.3	probable glucosamine-6-phosphate isomerase	-1.54
F25H2.5	nucleoside diphosphate kinase	-1.54
C47B2.4	proteasome a-type and b-type	-1.54
F18H3.3A	poly-adenylate binding protein	-1.55
Y25C1A.7B		-1.55
F49C12.9		-1.55
C15C8.1		-1.55
Y37D8A.11	nucleolar phosphoprotein	-1.56
T28B12.2	transcriptice initiation factor TFIID (tata-box factor)	-1.56
F07A11.2	glucosamine-fructose-6-phosphate aminotransferase	-1.56
W08C5.7	putative transmembrane protein g5p (atg5)	-1.56
ZC53.7		-1.56
T24D1.3		-1.56
T27A10.2		-1.56
C04A2.1		-1.56
C23H3.1		-1.56
C53D5.6	Ran_GTP binding protein	-1.57

F27C1.7	ATPase	-1.57
T08B6.6	chemoreceptor	-1.57
H03A1.1	vab-1 tyrosine protein kinase receptor	-1.57
H20J04.4	ATP-dependent RNA helicase	-1.57
D2030.6		-1.57
F32D1.7	proteophosphoglycan precursor	-1.58
Y57G11C.20		-1.58
B0393.1	probable 40S ribosomal protein	-1.58
F41F3.4	cuticle collagen	-1.58
H02I12.1	immunosuppressive ovarian message protein	-1.59
C04F5.9	zinc finger protein sdc-1	-1.59
F33G12.4	similar to leucine-rich repeats found in many proteins	-1.59
C31H5.6	similar to the rat kan-1 protein	-1.59
T22A3.3		-1.59
F26G1.7	major sperm protein 31/40/142	-1.59
F33H1.4		-1.59
D1025.4		-1.59
B0273.3	human snRNA activating protein complex 50 kda subunit	-1.59
F56B3.3		-1.6
C03H5.3		-1.6
T01B10.4	nuclear hormone receptor family member nhr-14	-1.6
ZK84.6	probable insulin-like peptide beta-type 5 precursor	-1.6
T10E10.D	similar to collagen	-1.6
T04G9.3	c. familiaris signal sequence receptor beta	-1.6
F11G11.5	pistil-specific extensin-like protein	-1.6
F25D7.4	claustrin like	-1.61
ZK353.5	hypothetical 13.8 kda protein	-1.61
ZC168.4	G2/mitotic-specific cyclin B	-1.62
K11H12.7		-1.62
T24B8.1	60S ribosomal protein l32	-1.62
F26A1.13		-1.62
F56C9.3	similar to r. rickettsii protein p34	-1.63
F12F6.7	DNA polymerase delta, regulatory subunit 55	-1.63
T02G5.9	probable lysyl-tRNA synthetase	-1.63
K11D12.3	similarity to cytochrome b	-1.63
C47E8.6	related to transport protein sec1	-1.64
W09G3.3	similar to fbx21, Substrate-recognition component of the SCF ligase complex	-1.64
Y53C10A.12	hif-type DNA-binding domain	-1.64
T23E7.2C	clostridium thermocellum cell surface glycoprotein 1 precursor	-1.64
C52B11.4	similar to C. elegans protein f22d3.5	-1.65
F25H5.4	elongation factor 2 (ef-2)	-1.66
C46F5.1	probable s-adenosylmethionine synthetase	-1.66
W02B12.8	GTPase-activating (RhoGAP) like protein	-1.67
ZK813.1		-1.67
Y62H9A.5		-1.67
C15F1.7	superoxide dismutase [Cu-Zn]	-1.67
C06B8.8	60S ribosomal protein l38	-1.68
Y37D8A.19		-1.68
F55E10.1		-1.68
F22H10.3		-1.68
Y56A3A.19	drosophila melanogaster acyl carrier protein, mitochondrial precursor	-1.68
C34F6.3	collagen	-1.68
F25H2.10	60S acidic ribosomal protein p0	-1.68
F21F8.8	seven transmembrane receptor 2	-1.68
W06D11.3		-1.69
F01G10.1	transketolase	-1.69
Y45E10.14	zinc finger c-x6-c-x5-c-x3-h type	-1.69
C47E8.4	human xap-5 protein	-1.69
Y17G7B.17	myelodysplasia/myeloid leukemia factor protein	-1.69
C18E3.2		-1.69
W05E7.1		-1.7
C52B11.3	probable g protein-coupled receptor	-1.7
F48A3.7	similarity to rhodopsins	-1.7
T02H6.1	u3 snoRNP associated 55 kda protein	-1.7
B02H5.1	rRNA methyltransferase	-1.71
Y8D1A.2		-1.71
T27E9.1	ADP/ATP carrier protein	-1.72
C27A2.2	probable 60S ribosomal protein l23	-1.72
B02H9.8	nuclear hormone receptor family member nhr-22	-1.72
C28D4.3	glutamine synthase	-1.72
C27A2.3		-1.72
R04D3.2	similar to p. lividus heat shock 70 kda protein iv	-1.73
Y113G7B.5		-1.73
C09D4.5	probable 60S ribosomal protein l19	-1.73
F58A4.6	hypothetical 19.1 kda protein	-1.73
F07D10.1	60S ribosomal protein l11	-1.73
Y46A8B.7	cytidine and deoxycytidylate deaminases zinc-binding region	-1.73
Y18D10A.11	*S. cerevisiae* intracellular protein transport protein uso1	-1.73
C30G11.1	probable serine/threonine protein phosphatase	-1.73
K12D12.1	DNA topoisomerase II	-1.73
F23A7.4	glutamate receptor epsilon subunit like	-1.74
C36A4.5	claustrin like	-1.74
C50A2.2		-1.74
F25H2.11	tct-1 (translationally controlled tumor protein homolog)	-1.74
C02F12.6	breast cancer type 1 susceptibility protein (brca1)	-1.75
C16C10.3	similar to C. elegans protein c14b1.7	-1.76
ZK829.4	glutamate dehydrogenase	-1.76
C04G2.4	major sperm protein 10	-1.76
C04A2.2	egl-27	-1.76
Y62H9A.4		-1.77
F32D8.6	protein transport protein sec61 gamma subunit	-1.77
Y110A7A.18	similar to C. elegans protein ck757.3	-1.77
T07H8.6	similar to drosophila membrane protein patched	-1.77
T25C12.4		-1.78
T22F3.3	glycogen phosphorylase	-1.78
C56E10.4		-1.78
C06H2.1	ATP synthase d chain	-1.78
K11B4.2		-1.78
C44B12.1		-1.79
K02B9.1	isocitrate lyase like	-1.79
B0348.6	eukaryotic translation initiation factor 4e (eIF-4e)	-1.79
F02D10.1	cuticle collagen	-1.79

K09H9.2		-1.8
ZK813.2		-1.8
ZK637.11	cdc-25.3	-1.8
F42C5.8	probable 40S ribosomal protein s8	-1.8
F53B6.1	human platelet tetraspan antigen like	-1.81
F35C5.6	lectin c-type domain short and long forms, von willebrand factor type a domain	-1.81
R03G8.6	zinc metallopeptidase (m1 family)	-1.81
C14B9.7	probable 60S ribosomal protein l21	-1.81
Y54G9A.6	WD domain, g-beta repeat (2 domains)	-1.81
C44B12.2	sperc precursor (secreted protein acidic and rich in cysteine) (osteonectin)	-1.82
B0414.3	histone H1	-1.82
F36A2.7		-1.82
C15A11.5	col-7 collagen	-1.82
R08C7.11		-1.82
Y48B6A.11	S. cerevisiae putative 90.2 kda zinc finger protein in cca1-ade2 intergenic region	-1.83
F58G1.2	zinc finger, c2h2 type (6 domains)	-1.83
F21D9.3		-1.84
F41G4.4		-1.85
C07G2.1	cey-1 endochitinase	-1.85
R05D11.5		-1.85
C43G2.1		-1.85
T24H10.4		-1.86
Y56A3A.22		-1.86
F26F12.1	cuticular collagen	-1.87
F59H6.11		-1.87
W03F9.2B		-1.88
T23G11.3	gld-1 female germline-specific tumor suppressor	-1.88
W03G1.1	amino acid transporter	-1.88
W08E12.6		-1.89
C25F7.3	uridylate kinase	-1.89
B0454.5		-1.9
T05D4.1	fructose-bisphosphate aldolase 1	-1.9
F39B2.11	human metaxin	-1.9
C34E7.2		-1.9
F09E5.2	ahpc/tsa protein	-1.91
C18H7.3	cuticular collagen	-1.91
Y46G5A.10		-1.91
Y110A2AL.A		-1.92
F22E5.9		-1.92
F54D10.5		-1.93
T10B11.8		-1.93
F02E8.4		-1.93
C47C12.4	ATP/GTP-binding protein	-1.93
F46B6.6	initiation factor IF-2	-1.93
C06G3.10	ldlc protein homolog	-1.94
R07E5.11		-1.94
C32E8.6		-1.94
C01F1.4	similar to the family of g-protein coupled receptors	-1.94
F08G12.10	putative gap junction protein pannexin	-1.94
C32E8.7	ric-19 (conserved cytosolic protein involved in neuroendocrine secretion)	-1.94
ZK1053.5	phospholipid scramblase 1	-1.95
D1007.12	60S ribosomal protein l24	-1.95
Y54E5B.3		-1.95
R05D6.7	similar to the insect-type alcohol dehydrogenase/inbitol dehydrogenase family	-1.96
F54D10.7		-1.96
F15H10.2	cuticle collagen 13 precursor	-1.96
CD4.1	cd4.1 protein	-1.97
D1007.6	40S ribosomal protein s10	-1.97
F23C8.4		-1.97
F37C12.9	probable 40S ribosomal protein s14	-1.97
B0513.2B		-1.97
T28C12.5	esterase	-1.98
F52G2.2		-1.98
C33F10.9	major sperm protein 31/40/142	-1.98
C10G11.7		-1.98
F54D5.11	transcriptive initiation factor TFIIE-beta	-1.99
F11E6.3	similar to long tandem repeat region of sialidase	-1.99
F56B3.1	similar to cuticular collagen	-2
K07A1.1		-2
ZK829.9	glucose transporter	-2.01
F52C6.12	ubiquitin-conjugating enzyme e2-17 kda	-2.01
B0416.4	hypothetical 25.8 kda protein	-2.01
F53G12.5	mex-3	-2.01
W06A11.3		-2.01
T28C6.4	cuticle collagen	-2.03
C03C10.3	probable ribonucleoside-diphosphate reductase small chain	-2.03
B0513.3	60S ribosomal protein l29	-2.03
F42H11.2	ankyrin domain	-2.03
T27E9.3	serine/threonine kinase (cdc2/cdkx subfamily)	-2.03
ZK20.3	rad-23 (Nucleotide excision repair factor NEF2)	-2.04
Y62H9A.6		-2.04
T12G3.2		-2.04
T10E10.G	similar tocollagen	-2.04
F54C9.5	probable 60S ribosomal protein l5	-2.06
D1007.11		-2.06
F52C6.2		-2.07
Y73B6A.5	Ral homolog serine/threonine-protein kinase	-2.07
F31E3.5	elongation factor 1-alpha (ef-1-alpha)	-2.08
F52E1.1	pos-1 zinc-finger protein	-2.08
K06A5.7A	protein phosphatase	-2.08
Y4C6A.3	zinc finger protein	-2.09
D2030.9A	hypothetical 65.2 kda trp-asp repeats containing protein	-2.09
M02B1.3		-2.09
T28B12.6	putative hepatic transcription factor	-2.11
K02B12.8		-2.12
F54E7.3	par-3	-2.13
C18B2.5		-2.13
F55A3.7	transcriptive factor	-2.13
M110.3		-2.14
F18A1.2	transcriptive factor lin-26	-2.14
C01B4.6	aldose 1-epimerase	-2.15
T04F8.8	schizont/sporozoite surface protein	-2.15

F25B5.4	ubiquitin	-2.15
C34B7.3	putative cytochrome p450 cyp35a1	-2.15
F14F7.1	collagen	-2.15
C26F1.3		-2.16
ZK686.2	DEAD-box ATP-dependent RNA helicase	-2.16
F56C9.6		-2.17
Y37A1A.2		-2.17
R04E5.7		-2.17
C37H5.8	heat shock 70 kda protein f, mitochondrial precursor	-2.17
K09H9.6	second-step splicing factor 1, saf1 protein	-2.17
W05F2.3		-2.18
C26F1.9	ribosomal protein l39	-2.18
T11F9.8	zinc metalloprotease	-2.18
C11E4.2	glutathione peroxidase precursor	-2.19
F52F12.3	mom-4 tyrosine-protein kinase	-2.19
ZK1128.5	protein homolog	-2.19
T02G5.8	acetoacetyl-coa thiolase	-2.2
T20G5.9		-2.2
F53F8.4		-2.2
Y51H1A.4	RHD-finger	-2.2
Y105E8C.C		-2.21
F43G9.5	mRNA cleavage factor I 25 kda subunit	-2.22
C39D10.7	similar to C. elegans proteins b0288.5, r02f2.4 and c07g2.1	-2.22
F10D7.2	calcium alpha subunit; tetracycline resistance	-2.22
T07H6.3	collagen	-2.23
C18H7.1		-2.24
C36E8.5	tubulin beta chain	-2.24
T28F3.1	c2 domain	-2.25
C07E3.7	homeobox protein	-2.25
C41H7.5	similarity to C. elegans proteins c16h2.1 and t28d9.9	-2.26
Y62E10A.14		-2.26
Y71F9B.M	mouse polyposis locus protein 1 homolog (tb2 protein homolog)	-2.27
C16E9.5		-2.27
F53H10.2	zinc finger, c2h2 type	-2.29
F43H9.4		-2.29
C34F11.6	major sperm protein 31/40/142	-2.29
Y73F8A.NN	slack 7-binding protein	-2.29
ZK228.3	similar the drain rhodopsin family of 7-transmembrane receptors	-2.29
F54C9.8	pumilio-family RNA binding domains	-2.3
F29B9.11		-2.3
F11G11.10	col-17 collagen	-2.3
T21D8.1	procollagen alpha	-2.3
F10D7.4		-2.31
F55A12.8	similar to achlya ambisexualis antheridial steroid receptor	-2.31
C10G8.4	similarity to human von willebrands factor	-2.31
C44B12.5		-2.32
C54F6.13	probable Na(+)/H(+) antiporter	-2.32
M01A10.1	DNA-binding protein	-2.32
F59E2.6	hypothetical 59.2 kda protein	-2.32
ZK652.4	probable 60S ribosomal protein l35	-2.32
F49D11.9	pig glycolipid transfer protein	-2.33
Y37D8A.4		-2.33
Y43F8C.2	abductin	-2.33
Y111B2A9.a	unknown protein	-2.34
C47B2.3	tubulin alpha-2 chain	-2.34
M04F3.5		-2.34
F59B10.4	hypothetical 29.4 kda protein	-2.35
Y42G9A.3	mouse ras suppressor protein 1	-2.35
Y32B12B.5	olfactory receptor odr-10	-2.36
F01G4.4	sea lamprey fibrinogen alpha-1 chain precursor	-2.36
T07C4.5A		-2.36
Y48C3A.18	long hypothetical scd5 protein	-2.36
C04F12.2	transposase	-2.36
F25B5.7		-2.37
Y17G9B.2		-2.37
B0250.1	ribosomal proteins L2	-2.37
F13B10.1A	SAM domain (sterile alpha motif)	-2.37
D1054.11	equine herpesvirus type 1 (strain ab4p) (ehv-1)	-2.38
R12H9.4	major sperm protein 31/40/142	-2.38
H02I12.5		-2.38
W06E11.4	human hypothetical protein cgi-97	-2.38
F26B1.2	RNA-binding protein	-2.39
C16A3.9	probable 40S ribosomal protein s13	-2.39
F13B10.2	60S ribosomal protein l3	-2.39
B0035.6	hypothetical 84.3 kda protein	-2.39
F42A10.5		-2.4
C43E11.9		-2.4
C28C12.9	similarity to very-long-chain acyl CoA dehydrogenases.	-2.4
T19F4.1	similarity to dopamine receptor	-2.4
C30C11.4		-2.41
C05G5.5	putative cuticle collagen	-2.41
F49E2.5A	d-99 n	-2.41
C31G12.1		-2.41
T14G11.1		-2.42
F01F1.2		-2.42
Y39A1A.3	human autoantigen p27	-2.42
R10D12.1	sodium/phosphate transporter	-2.42
Y37D8A.9		-2.43
B0412.2	dauer larva development regulatory growth factor daf-7 precursor	-2.44
C02B10.1	acyl-CoA dehydrogenase	-2.46
C06A8.3		-2.47
C14F5.1	nip3 homolog	-2.48
T13F2.8	cawolin-1	-2.5
F26E1.3	nuclear membrane-associated protein	-2.5
F59E12.1	similarity to human skeletal muscle abundant protein	-2.51
C17G10.4B	cdc14as phosphatase	-2.53
Y37H2A.7		-2.54
F18C5.4		-2.54
F08F3.3	rhr-1 blood group rh(d) polypeptide	-2.55
H09B5.2		-2.55
F13G11.1A		-2.55
C16A3.1	Chromatin remodeling protein HARP/SMARCAL1, DEAD-box superfamily	-2.56

K06B4.11	nuclear hormone receptor family member nhr-53	-2.56
F17C11.9	probable elongation factor 1-gamma	-2.57
Y54E10A.4	similar to C. elegans protein c40h1.1	-2.57
K09A9.3	similarity to hnp36 protein	-2.58
B0222.4	glutamate decarboxylase	-2.58
Y39A1A.14		-2.59
C49A1.6		-2.59
K06D8.6		-2.59
T27D12.2	chloride channel protein	-2.6
F53A3.3	40S ribosomal protein	-2.6
T09E8.2	G2/mitotic-specific cyclin B3	-2.62
Z6507.6	G2/mitotic-specific cyclin A1	-2.62
F59H5.1		-2.64
Y71F9AL.2		-2.65
C36F2.3	silk moth sericin precursor	-2.65
F55A11.3	zinc finger, c2h2 type (ring finger)	-2.66
F59A2.1	nucleoporin	-2.66
F09E10.2	short-chain alcohol dehydrogenase	-2.67
F15E11.9	c-type lectin	-2.68
M151.2		-2.69
C01B7.3		-2.69
K10E11.4	sqv-3 galactosyltransferase	-2.7
Y9C9A.9	olfactory receptor odr-10	-2.7
Y45F10D.2		-2.72
T28B11.1		-2.73
B0412.4	40S ribosomal protein s29	-2.73
T21C9.13		-2.75
F26E4.6	cytochrome c oxidase	-2.78
F42F12.1		-2.79
F44B9.4	cyt-1.1 (cyclin T1, CDK9 kinase-activating protein cyclin T)	-2.79
C54C6.1	probable 60S ribosomal protein l37	-2.81
C05E11.5	ammonium transporter	-2.82
T12C9.4	similar to cyclins	-2.85
C45B2.5	glutamine synthetase	-2.86
F02A9.3	antigen precursor	-2.86
C18F10.5	srg-2 protein	-2.86
F10A3.6	olfactory receptor odr-10	-2.88
R05D11.6		-2.88
F55A4.2		-2.89
C05C8.5		-2.89
T05E11.1	probable 40S ribosomal protein s5	-2.9
C53B4.5	collagen	-2.9
F02A9.1B	hypothetical 37.2 kda protein	-2.92
F21C3.1	twk-7 potassium channel protein like	-2.92
C53A5.1		-2.93
K10D2.2	putative 162.6 kda zinc finger protein	-2.94
C32E8.2	probable 60S ribosomal protein l13	-2.95
F22F7.4		-2.97
H27A05.1	human hypothetical protein	-2.98
Y46H3A.3	heat shock protein hsp16-2	-2.98
C28A5.1		-2.98
F53F10.5	similar to nucleoporins	-2.98
F59F5.6	putative liprin alpha (lar-interacting protein alpha)	-2.99
Y51A2A.4		-3
W02D9.7		-3.01
T21D12.3	poly-glutamine tract-binding protein	-3.03
C34E10.6	probable ATP synthase beta chain, mitochondrial precursor	-3.03
T05G5.7		-3.04
T28C12.4A	esterase	-3.04
C35A11.4	sugar transporter	-3.06
K07A1.2	decoyuridine 5`-triphosphate nucleotidehydrolase	-3.07
C55B6.1	glycerol kinase	-3.08
R02D7.7	sox-1 nanos protein	-3.1
AC3.4	similarity to erbb-3 receptor protein-tyrosine kinase	-3.1
F27E5.2	`paired box` domain, homeobox protein	-3.11
F29C4.2		-3.11
R02F2.2	human cb-1 protein	-3.12
W05B2.5	similar to cuticular collagen	-3.12
Y54G11A.3	ATP-dependent RNA helicase	-3.14
F28G4.2		-3.16
B0524.6		-3.17
C18H7.2	cuticular collagen	-3.18
C08F11.2		-3.22
Y46H3A.3	heat shock protein hsp16-2	-3.26
F42A10.7		-3.29
F23C8.12	similar to 3-isopropylmalate dehydrogenase	-3.29
F54C8.2	hypothetical histone 3-like protein	-3.32
Y6G8.3	zinc finger, c2h2 type (2 domains)	-3.33
C06A1.4	similar to C. elegans protein zk757.3	-3.34
H23N18.1	transferase	-3.35
F59G1.5	ptp-2 protein-tyrosine phosphatase	-3.35
Y62E10A.17	mouse transcription factor ap-2	-3.35
C01G10.4	arabinogalactan-protein	-3.37
F49G10.4	lipase	-3.4
F54D10.1	skp1p homolog	-3.4
T16G12.8		-3.48
T04D1.4	Chromodomain-helicase DNA-binding protein	-3.49
K08H2.2		-3.49
W02F12.3	gastric mucin	-3.5
C02F12.4	guanine-nucleotide releasing factor of the cdc24 family	-3.56
W05B2.6	similar to cuticular collagen	-3.56
Y57G11B.5		-3.58
R02E12.5		-3.58
C54E4.4		-3.58
C33A11.2		-3.59
R02D7.3	cuticular collagen	-3.63
C04F12.1	putative arganaute protein	-3.76
C14F11.5	heat shock protein	-3.76
2C302.1	inne-11 (yeast MRE recombination / repair homolog)	-3.76
T01C3.9		-3.77
F28H11.3A	bromodomain	-3.78
K04C1.5	serine/threonine kinase	-3.89

F28C10.3	protein kinase	-3.89
F20H11.6		-3.92
K04F1.9		-3.92
F49F1.12		-3.99
C02B8.1	G2/mitotic-specific cyclin A1	-3.99
T02G5.11	similarity to drosophila nanos protein	-4.01
F16B12.1	c1n/c1s-like domain	-4.02
C05D2.1	cell-surface receptor daf-4 precursor	-4.05
R11G11.8	similarity to o4-type zinc fingers	-4.07
Y54E10BL.I		-4.08
T27F6.4		-4.09
F15E6.1		-4.12
W03C9.7	mex-1 zinc finger c-x8-c-x5-c-x3-h type	-4.14
ZK370.8	hypothetical 71.8 kda protein	-4.15
F49F1.7	excretory/secretory mucin muc-3	-4.15
M142.1	asc-119 protein	-4.17
F56H11.2		-4.17
T14C1.1	transmembrane receptor (rhodopsin family)	-4.18
F57C9.3	similarity to c2h2-type zinc fingers	-4.18
Y40H7A.5	wdr-1 protein	-4.21
T01C3.1	WD domain, g-beta repeats	-4.21
F25C8.7		-4.24
F46G10.6	helix-loop-helix DNA-binding domain	-4.25
T02G5.10	similar to reverse-transcriptase	-4.26
F20C5.3		-4.26
C07A4.3	extracellular protein	-4.38
E03H12.10	ssp-9	-4.39
F22B7.9	hypothetical 32.9 kda protein	-4.39
C01G6.3		-4.39
H04D03.2A		-4.43
ZC404.8	RNA-binding protein	-4.45
F57G4.9		-4.46
F59D12.5		-4.47
C18H7.2	snc-7 protein	-4.47
F14F4.1	7 transmembrane receptor (rhodopsin family)	-4.48
F38E1.7	mom-2 wnt family protein	-4.51
C31B8.8	matrix metalloproteinase	-4.51
C28A5.5		-4.51
F28C2.1		-4.52
W01A8.3	cuticulin	-4.52
F22E12.4	egl-9	-4.58
F02D10.6		-4.66
C06A5.5	RNA-binding protein	-4.67
F46H5.4	rat trg gene product	-4.73
R05F9.11		-4.77
K02E10.5		-4.77
T27E9.5	phosphatidylserine synthase i	-4.79
Y87G2A.7		-4.79
F13A7.8		-4.8
T28D4.19	similarity to pneumocystis carinii msg102 major surface glycoprotein	-4.93
K11D12.10		-4.97
ZK430.1		-4.99
ZK1058.3	galactose-1-phosphate uridylyltransferase	-5.01
Y38H6C.10		-5.06
C50E10.7	src-1 protein	-5.08
E02H9.7	secreted acid phosphatase 2 (sap2) precursor	-5.08
Y14H12B.2		-5.09
ZC13.1	zinc finger protein	-5.11
F20B4.3		-5.21
Y62H9A.3		-5.24
F38B7.6	g-protein coupled receptor	-5.25
K09F5.2	vitellogenin 1 precursor	-5.3
ZK1127.1	sos-2	-5.3
F08F3.6	similarity with C. elegans pes-2	-5.36
Y48C3A.6	cell survival cad-4-interacting protein mac-1	-5.37
C50F7.8	glycine-rich	-5.42
F53F1.4	cutidin	-5.42
K08B4.1		-5.46
T22H6.6	hmg-box transcription factor	-5.49
Y81B9A.1		-5.51
F42G9.8	putative protein-tyrosine sulfotransferase	-5.52
C53D5.4	zinc finger protein	-5.54
K03B8.8		-5.55
F52D2.2	phosphoprotein 1r20	-5.61
F11H8.3	cuticle collagen 9	-5.63
F52C6.3	polyubiquitin	-5.65
Y54G9A.5		-5.7
ZK84.3	putative insulin-like peptide beta-type 6	-5.71
F54D5.5		-5.74
Y80D3A.3	human homeobox protein dlx-2	-5.77
K02G10.7	transmembrane channel protein	-5.77
F02A9.2		-5.83
F10G2.7		-5.83
F44A6.2	steroid hormone receptor family member cnr14	-5.85
C30E1.5	similar to transposase	-5.87
C35E9.4	testis-specific protein tpx-1 like	-5.88
F39B3.3	similar to retrovirus-related pol polyprotein	-5.91
K01B6.2	hypothetical 16.6 kda protein	-5.94
C27A12.8		-5.96
W09G12.6	serotype b putative major immediate-early genes	-5.96
F15G10.1	similar to glycogen-binding subunit protein phosphatase-1	-5.97
F23D12.2		-6.1
ZK256.1B	calcium-transporting ATPase 1	-6.15
Y53C12A.3		-6.17
C13G3.1		-6.27
B0334.11		-6.29
F28H5.1.6	ttp-like factor	-6.37
F52D10.2		-6.46
Y75D11A.2	hypothetical protein	-6.6
T22E5.6		-6.67
C49F5.3		-6.7
F59D8.2		-6.7

ZK470.2A	hypothetical 19.0 kda protein	-8.74
R17.2	putative transcriptional regulator	-8.79
F43D9.5		-8.99
F28A3.4	protein-tyrosine phosphatase	-7.01
F11G11.12	collagen	-7.02
T25E12.4B		-7.09
C50C3.9	hypothetical 18.6 kda protein	-7.11
Y39A3CR.G		-7.11
C12C8.1	heat shock protein 70	-7.45
C02B4.2	nhr-17 nuclear hormone receptor	-7.56
F54D5.9		-7.58
C25F6.1	collagen	-7.64
Y52B11A.8		-7.68
W09G10.1	collagen	-7.93
Y51H1A.6	zinc finger, c2h2 type	-7.93
C44E12.2		-7.96
Y48B6A.14	high mobility group protein 1.1	-8.74
F25A2.1	putative 32.6 kda lipase	-8.86
C09G4.5	inx-6	-8.86
F43G6.10		-9.01
F58B3.9	transthyretin-like family	-9.24
C31G12.1		-9.69
C07G3.4	chemoreceptor	-9.82
Y39H10A.5		-10.05
C50E3.11	folate-like transporter 2	-10.16
B0546.2	hypothetical 68.5 kd protein	-10.23
T08A9.5	similarity with c. elegans pes-2	-10.43
B0304.2	hypothetical 24.2 kda protein	-10.55
C16E9.1	similarity to collagen chain alpha	-11.04
K02E2.4	ins-35	-11.11
CC8.1		-11.18
ZK39.6	lectin c-type domain short and long forms	-11.19
F16H11.3	similarity to hnp36 protein	-11.21
F11A5.6		-11.6
K02A6.3		-11.94
T24C4.2		-12.01
Y57A10A.T		-12.09
ZK470.2A	hypothetical 19.0 kda protein	-12.14
C29E6.4		-12.14
T05G11.1	zinc finger, c2h2 (2 domains)	-12.34
F49H6.5	molybdenum cofactor synthesis-step 1 protein a splice type 1	-12.68
F17A9.6	homeobox protein	-12.73
AH9.2	conserved hypothetical protein	-12.85
B02H1.2	hypothetical 43.9 kda gtp-binding protein	-12.91
F46E10.H		-12.99
B0299.1	calcium-activated potassium channel nkl3	-13.93
Y39G8C.A	inner nuclear membrane protein	-14.29
F52G3.2		-14.41
ZK512.5	human hypothetical protein	-14.87
F49F1.11		-14.95
T24E12.9		-15.41
Y65B4BL.C		-15.88
W08E12.2	silk moth chorion class high-cysteine hcb protein 13 precursor	-16.37
C55C2.5	amino acid permease	-16.78
T04D3.5		-17.83
R08E3.4	c2h2-type zinc finger	-20.79
B0222.7	similarity to a part of the triple-helical region of collagen alpha chain	-20.97
T26C11.6	ceh-21 homeobox	-21.56
M7.10	similar to keratins in a glycine-rich region	-21.95
Y75B8A.17		-22.39
T07C4.6	t-box protein 9	-23.5
W02D9.5		-26.29
CD4.8	cd4.8 protein	-27.19
F53C3.8		-26.98
Y47D7A.M	dkptp homolog	-29.64
C04B4.2		-29.76
B0202.6	reverse transcriptase	-29.85
F44E5.4	heat shock hsp70 proteins	-30.21
F26G5.1		-34.89
C09G9.3		-38.46
W07A12.7		-43.82
Y46G5A.22B		-45.62
C07F11.1	tol-1	-46.45
T28F12.3	guanine nucleotide exchange factor for ras	-54.53
ZK757.3C		-68.42
C39B5.5	putative 32.8 kda lipase	-74.56
F35E8.5		-85.03
Y38E10A.13		-141.28
W05B2.1	similar to cuticular collagen	-183.35
B0222.6	similarity to the a portion of the triple-helical region of collagen alpha chain	-724.05

CHAPTER 4

IDENTIFICATION OF *LIN-26*, A NOVEL GENE THAT AFFECTS CELL DEATH UPON IONIZING RADIATION IN *C. ELEGANS*

Preface

The microarray experiment and the subsequent analysis of the results provided me with a list of genes potentially to be involved in a DNA damage signaling network, regulating the responses of *C. elegans* to ionizing radiation. In the previous chapter I already gave a short description of some of the candidates – I will now focus on one gene for which there was a mutant available at the beginning of my project.

4.1. The history of LIN-26

4.1.1. The *C. elegans* LIN-26 is required to specify and/or maintain all non-neuronal ectodermal cell fates

The story of this chapter has its onset in the year 1987, when the group of Robert Horvitz became interested in understanding how patterns of cell divisions and cell fates are specified during the development of the nematode *C. elegans*. In a series of genetic screens, a number of mutations were recovered to cause homeotic transformations in the fates of individual cells. The genetic pathway for the specification of the vulval cell fate was the one affected. This finding suggested that these lineages might be specified by a series of decisions distinguishing between alternative cell fates (Ferguson *et al.*, 1987).

One of the twenty-three genes that were assigned to particular steps of the vulval cell fate pathway, was *lin-26*, for which the *n156* mutation caused the normally hypodermal precursor cells to adopt neuronal fates. The first in-depth study occurred seven years later when three new alleles of the same gene were isolated that caused embryonic lethality and defects in all categories of hypodermal cells (Labouesse *et al.*, 1994). The strongest alleles, *mc1* and *mc4*, caused many hypodermal cells to die during embryogenesis. As a consequence, embryos did not elongate and died. Another embryonic lethal mutation, *mc2*, caused hypodermal cells to fail to enclose the embryo properly. The position of these mutations in *lin-26* is shown in Figure 2.

Further insight into the three potential roles of LIN-26, either as a factor to specify, or allow the acquisition or maintain the differentiated state of hypodermal cells came from expression pattern studies. It was proven that during asymmetric cell divisions that generate a neuronal and a non-neuronal cell, the protein is symmetrically segregated and then lost from the former (Labouesse *et al.*, 1996). Its expression in all the hypodermal cells and all glial-like cells (socket and sheath cells) was biologically important, considering the structural and functional defects in the *lin-26(n156)* mutant. The authors concluded that *lin-26* is required to specify and/or maintain the fates of hypodermal cells and of all the other non-neuronal ectodermal in *C. elegans*. A possible mechanism of action would be repressing the expression of neuronal-specific genes in non-neuronal cells.

A new function for LIN-26 emerged as being required for the formation of the somatic gonad epithelium. Tissue-specific knock outs revealed that the protein's similar role in the non-neuronal ectoderm and the somatic gonad is to express epithelial characteristics (den Boer *et al.*, 1998). Loss of LIN-26 activity in the somatic gonad gave rise to five penetrant phenotypes, these being sterility, endomitotic oocytes, a protruding vulva, a germline proliferation defect, or even complete absence of the gonad arms. Although the authors analyzed the expression of the protein in Z1 and Z4 somatic gonad precursors and the gradual disappearance in their daughter cells, no information about its presence in the germ cells during adulthood was enclosed; a fact which will be discussed in paragraph 4.2.3.

Reaching the end of a series of studies to understand the mechanisms that establish epithelial cell identity, it was revealed that LIN-26 is one of the genes

needed for the regulation of epithelial-specific factors. Ectopic LIN-26 expression could reprogram the normal cell fates to trigger epithelial differentiation without, though, conferring tissue/organ specificity (Quintin *et al.*, 2001).

In this chapter I present a novel function for LIN-26, a switch from the pathways that specify ectodermal cell fate to the mechanisms that execute the cell death fate.

4.2. *lin-26*: structure and expression patterns

4.2.1. Genomic organization of *lin-26*

The *lin-26* gene possesses an interesting chromosomal organization, residing in two overlapping operons, with two other genes that all together define a novel class of proteins (Figure 1). The gene exists in three splicing forms, a long isoform referred to as *lin-26A* (F18A1.2b in WormBase); another one that is trans-spliced to SL2 at the third *lin-26A* exon, referred to as *lin-26B*; and a shorter one that lacks the fifth *lin-26A* exon, mentioned as *lin-26C* and considered to be a minor isoform expressed only in a subset of cells (Dufourcq *et al.*, 1999). The neighboring genes that are called *lir-2* and *lir-1* (*lin-26*-related genes) are present in a major and a minor isoform, and in three alternative splice variants, respectively. The proposed model for the chromosomal organization of the *lir-2*/*lir-1*/*lin-26* gene complex is two operons that partially overlap, one that includes *lir-2* and long *lir-1* isoforms (operon 1) and another that includes short *lir-1* isoforms and *lin-26* (operon 2) (Figure 1) (Dufourcq *et al.*, 1999).

4.2.2. *lin-26* belongs to the C2H2-type zinc finger gene family

Based on the longest cDNA sequence, the predicted amino acid sequence of LIN-26 is 472 amino acids long and is shown in Figure 2. Five potentially important functional domains are illustrated: an amino-terminal region with 25% serines or threonines; a middle region with 25% glutamines; a carboxy-terminal region containing several negatively charged amino acids; two copies of cysteine-histidine motif and a potential protein degradation PEST sequence (proline/glutamic acid/serine/threonine) found in proteins with a short half-life.

The Cys/His motifs might form zinc fingers since they are related to but are distinct from the classical zinc fingers of the TFIIIA transcription factor. In particular, the first motif is characterized by the presence of five additional amino acids between the second Cys and the first His (17 instead of 12), and by the absence of the conserved phenylalanine normally located four amino acids after the second Cys. The second motif, though, is more canonical. The residues separating the second Cys and the first His are mainly polar and basic, implicating this region in particular in nucleic acid binding. The zinc finger motif is an unusually small, self-folding domain in which Zn is a crucial component of its tertiary structure, which interacts with nucleotides in the major groove of the nucleic acid (SMART nrdb database). Zinc fingers have the ability to bind to both RNA and DNA, a versatility not demonstrated by the helix-turn-helix motif (Nardelli *et al.*, 1991). It has also been suggested that a Zn-centered domain could be used in a protein interaction, e.g. in protein kinase C.

A search into the human proteome for members that show high similarity with LIN-26 yielded a number of proteins that belong to the Krüppel-type of Zinc Finger

family proteins (ZNF). Figure 3A shows members of the human Krüppel-type superfamily that were randomly selected to align with LIN-26, in the sequence encompassing the C2H2 type zinc finger motif. The various but comparable degrees of similarity or identity fall all in the range that would place LIN-26 in the same set of structurally related proteins. Trying to identify the closest matching protein, two human proteins appeared the most frequently: HKR18 and HKR1 displayed 57% and 60% similarity within the stretch of sequence that contains the zinc finger motif (Figure 3B). The function of the two proteins and their potential relation with LIN-26 are further discussed in paragraph 4.7.

A closer look at the C-terminus of the LIN-26 protein identified an unconventional KRAB motif, a feature encountered in the HKR1 protein (Figure 4A). The Krüppel-associated box (KRAB) domain is a 75-amino acid transcriptional repressor module commonly found in the N-terminal part of about one third eukaryotic zinc finger proteins. It is enriched in charged amino acids and can be divided into subregions A and B, which are predicted to fold into two amphipathic alpha-helices (Figure 4B). The KRAB domain functions as a transcriptional repressor when tethered to the template DNA by a DNA-binding domain. Gene silencing requires binding to the RING-B box-coiled-coil domain of the co-repressor KAP-1. The functions currently known for members of the KRAB-containing protein family include transcriptional repression of RNA polymerase I, II, and III promoters, binding and splicing of RNA, and control of nucleolus function (InterProScan description, EBI database).

Of the mutations that have been isolated and studied in the past (by the Labouesse group), four affect the first potential zinc finger motif and are depicted in Figure 2. Two of them, the *ga91* and the *n156*, I used in this study to investigate the DNA

damage response phenotypes of *lin-26*. Recently the first deletion allele, *ok939*, became available at the CGC. The deletion removes a 156 nucleotide fragment downstream of the ATG, which eliminates 77% of the ORF, rendering it a null (Figure 2).

4.2.3. Germline expression of the *lin-26* gene and protein

The germline is the only tissue where DNA damage responses become apparent in the sense that, phenotypes are easily or solely detectable and amenable to quantification. To manifest a potential role for *lin-26* in the DNA damage signaling network, I first examined whether it is localized in the germline tissue.

Figure 5A shows the immunostaining pattern of LIN-26 in a dissected gonad using a polyclonal antibody against the N-terminus (offered by the Labouesse lab). The protein seems to be associated with the nucleolar compartments of the germline. A closer view at the premeiotic nuclei and the transition zone is shown in 5B. In the first case where DAPI-stained chromatin (in blue) is widely dispersed throughout the volume of the cell, between the nuclear periphery and a centrally located nucleolus, the protein (in red) is localized on both the chromosomes and the nucleolus. In the transition zone where the chromosomes congregate towards one side of the nucleus, the protein achieves a highly polarized spatial organization and adopts an off-center position, opposite to the clustered chromosomes. The sharing of the protein between the two compartments could either imply a different role according to the location or a shuttling from one to another to secure a proper function.

Not only the protein but also the *lin-26* mRNA displays a germline expression pattern (Figure 5C), spreading from the mitotic region until the end of the proximal

arm (pointed by the arrowheads). These are *in situ* hybridization data found in the NEXTDB (Nematode Expression Pattern DataBase).

An additional piece of evidence, telling of the possible role of *lin-26* in processes related to responses to genotoxic stress, emerges from gene expression maps. Those were designed by assembling data from various *C. elegans* microarray experiments and contain genes that are grouped together when co-regulated (Kim *et al.*, 2001). In Figure 5D part of such a map, called a mountain, is illustrated, containing all the genes whose expression topology coordinates are within a certain radius. The genes are visualized in a three-dimensional manner that shows correlations of gene expression profiles as distances in the two dimensions and gene density in the third dimension. This mountain (1465 genes in total) includes genes that are germline-specific (101), genes expressed in oocytes (60), some death-related genes including *ced-4* and is particularly enriched in repair genes. The latter ones are represented by members of the nucleotide excision repair machinery (Met18, XPF, ERCC1 and ERCC1 homologs), the double strand break repair and recombination pathway (Mus81, LIG3, *rad-54*, *rev-1*), the mismatch and oxidative damage repair process (Mlh1, Mms1 homologs, *apn-1*), as well as various other checkpoint genes. The *lin-26* gene clusters among this group. The fact that it is co-regulated with a relevant to the DNA damage response pathway set of known genes, implies possible networking interactions with critical factors that mediate these processes.

4.2.4. Isoform specificity of *lin-26* in the germline and upon ionizing radiation

Initial studies on *lin-26* to determine the organization of the gene revealed, as already mentioned in paragraph 4.2.1, more than one isoforms (Dufourcq *et al.*,

1999). Whole animal studies proved that the *lin-26B* isoform (F18A1.2a in WormBase) is the most abundant one. Rescuing experiments proved that the *lin-26A* isoform is non-functional, since it failed to rescue the lethality and sterility of severe alleles.

I tested the possibility of isoform specificity in the germline tissue and the potential that only some of them might respond to DNA damage. I followed the transcription of isoform specific mRNAs by Q-RT-PCR (Table 1). To distinguish between germline and somatic expression I made use of the *glp-4(bn2)* mutants that lack a germline in the restrictive temperature. The values are presented as relative abundance of isoform B over isoform A. They show that the germline contains more of the short isoform B, reflecting the overall affluence in the animal. The difference in the amount, though, between the soma and the germline suggests that the latter is enriched in the long isoform A.

To investigate a potential isoform preference in the activation of *lin-26* upon ionizing radiation, I used a similar Q-RT-PCR approach to compare the change in mRNA levels in the germline with ones in the soma (Table 2). Isoform A, previously thought to be a non-functional transcript, was found to be induced three hours upon irradiation in the germline. Accompanying this increase, is a reduction in transcription of the short isoform from the rest of the animal. This finding is of particular interest, because it assigns a functionality to a so far seemingly futile *lin-26* isoform.

At the moment it is not known how *lin-26* expression is initiated or established in the germline. The protein, though, has a complex spatial and temporal expression pattern. A molecular dissection of the promoter of the gene could identify almost all the elements necessary to establish such a pattern (Landmann *et al.*, 2004). The

regulation of the gene is achieved to a large extent through tissue-specific *cis*-regulatory elements, which act redundantly or synergistically to drive expression in different cells.

A similar mode of regulation of the gene expression to the one in the epithelial cells of ectoderm and mesoderm could be utilized for the germline. A hypothesis would be that so far unidentified promoter elements, under the right combination, could synergize for its expression in germ cells.

4.3. *lin-26* is required for DNA damage-induced cell death

4.3.1. *lin-26* mutants are defective for ionizing radiation-induced apoptosis

In order to identify an actual involvement of *lin-26* in the DNA damage responses triggered by ionizing radiation in the *C. elegans* germline, I used the already existing mutants at that time to look for relevant phenotypes. Recently a deletion mutant became also available and I integrated this into the analysis.

In the DIC pictures of Figure 6, some of the phenotypic germline characteristics of the *lin-26* mutants are depicted. The *n156* animals show a vulvaless (Vul) and a egg laying defective (Egl) phenotype, and they are slightly small and fat with hypodermal and support cell defects. The germline looks normal, with proliferation rates similar to wild-type: 21.2±2.9 versus 23.2±1.7 for the wt in a 50 μm distance from the DTC. The *ga91* animals display a protruding vulva (Pvl) and a Egl phenotype. They have a wild-type compartmentalization in the germline with slightly decreased numbers of

proliferating nuclei: 18.4±2.6 versus 23.2±1.7 for the wt. The larval arrest (Lva) phenotype of the *ok939* animals makes it impossible to check the germline characteristics of an adult animal. The heterozygote under the mIn1 balancer mutants appear wild-type under the DIC.

I used the *ga91* and *n156* alleles (bearing a point mutation) described above to perform a time course analysis, after exposing them to 60 Gy of X-rays (Figure 7). Apoptotic corpses were scored in the meiotic region of one gonad arm of young adult animals, having the response of wild-type animals as a control. Both in the short- and the long-term response to ionizing radiation, the two *lin-26* mutants display a defect in inducing IR-induced cell death. The defect appears to be of similar severeness for both alleles. I further used the *ok939* allele in a similar time course analysis (Figure 8). Animals that were heterozygote for the deletion (*ok939*/mIn1) were exposed to 120 Gy of X-rays. The apoptotic response to IR is strongly compromised, resulting in only a 1.5 to 2.7-fold increase in the number of corpses above the control levels. To exclude that this would be an effect of the high dose or irradiation used, I repeated the experiment with the application of 60 Gy of X-rays (Figure 9). Both curves totally overlap, suggesting that the apoptotic defect remains after high and medium doses. What remains, though, to be done is score the three alleles for a hypersensitive upon IR phenotype, by using very low doses of X-rays. If the mutants cannot cope with low levels of DNA damage because the protein has a dispensable role under such conditions, then they are expected to show a normal if not increased apoptotic response.

Having obtained a defective apoptotic response with the balanced *lin-26(ok939)* mutant, I had to examine the possibility that the phenotype is not due to some kind of interference from the mIn1 balancer chromosome. For that reason I crossed this strain into wild-type to provide a normal copy of the gene from an intact wild-type chromosome. Apoptotic corpses were scored at two different time-points after treatment with 120 Gy of X-rays (Figure 10). Both *lin-26(ok939)*/mIn1 and *lin-26(ok939)*/+ mutants show a similar lack of IR-induced apoptosis. The observation that animals with a wild-type copy of the gene still present exhibiting a phenotype upon treatment with X-rays, raises the issue of the actual nature of the phenotype. Either a dominant negative phenotype with the mutated gene product (if present) poisoning the functional copy, or a haploinsufficient phenotype, with the normal gene copy not producing enough functional protein, could explain the defective apoptotic behavior of the animals upon ionizing radiation. More insight into that will be gained once a deficiency that covers the *lin-26* locus is studied for induction of apoptosis upon DNA damage. A similar to the above phenotype will strongly point into the second case and needs to be further explored as a gene dosage sensitivity phenomenon. There is considerable evidence in the cancer field suggesting that this haploinsufficiency can facilitate tumor progression by blocking apoptosis (Santarosa & Ashworth, 2004).

4.3.2. *lin-26* mutants fail to respond to endogenous DNA damage

Apart from damage caused by an external source of genotoxic stress, double-strand breaks can occur normally during meiotic prophase as the initiating events in meiotic recombination. In *C. elegans* such breaks can initiate apoptosis (Gartner at al., 2000).

Inhibition of *rad-51*, a member of the RecA family that catalyzes the invasion of DNA single-strand overhangs into a recipient double-strand DNA to initiate the formation of D loops and the later steps of meiotic recombination, results in unresolved DNA breaks. This, in turn, leads to increased germ cell death. Mutants for the IR responsive pathway, such as *hus-1(op244)*, *mrt-2(e2663)* and *clk-2(mn159)* as well as for the p53 homolog *cep-1(gk138)* can suppress *rad-51(lf)*-induced cell death, suggestive of its nature as DNA damage-induced.

To test whether *lin-26* can exert the same function as the above checkpoint and pro-apoptotic genes, I inactivated *rad-51* by using RNAi and scored the germline of *lin-26(ga91)* and *lin-26(n156)* mutants for the presence or not of excessive cell death (Figure 11). Loss of *rad-51* function is suppressed by both mutations in *lin-26*, suggesting that endogenously DNA damage-induced cell death does not occur properly in the absence of LIN-26. The fact that artificially induced DNA double strand breaks have the same effect as breaks caused by irradiation regarding the lack of activation of apoptosis, may place *C. elegans lin-26* in the DNA damage signaling network.

4.4. Physiological cell death is normal in *lin-26*

4.4.1. *lin-26* lies upstream of the apoptotic machinery

The failure of germ cells to undergo apoptosis in response to DNA damage in a *lin-26* mutant background could also raise the question of how efficient the apoptotic machinery itself is in this mutant. Such a possibility can underlie two different

occurrences: Either the death activity of *ced-3* and *ced-4* is compromised, or there is a death-suppressing activity present.

To explore this issue, I scored apoptotic corpses in the germline of animals carrying both the *ga91* mutation and the *n1950*, a strong loss-of-function mutation in the cell death suppressing gene, *ced-9* (Figure 12). The latter results in increased levels of germ cell death, consistent with the protective role of *ced-9* in the germline (Gumienny at al., 1999). The *ga91* mutation in *lin-26* does not suppress loss of *ced-9* function, suggesting that LIN-26 acts upstream of a functional apoptotic machinery. To corroborate the finding about the lack of DNA damage-induced apoptosis in *lin-26* mutants, I additionally irradiated the above double mutant. After 120 Gy of X-rays I observed no further increase in the number of corpses. The *ced-9(n1950)* single mutant similarly does not display a significant increase upon IR, probably due to a saturation effect in the volume of the germline.

In addition, to prove that physiological cell death can occur unperturbed, I scored apoptotic corpses in the germline of animals carrying both the *ga91* mutation and the two loss-of-function mutations in genes that affect germline apoptosis, *gla-1* and *gla-3* (Figure 13). The *op234* and *op216* mutations, respectively, result in increased levels of germ cell death under physiological conditions, although the mechanism of action is still not so clear (Milstein, PhD thesis, 2001). The *ga91* mutation in *lin-26* does not suppress loss of function in the *gla* genes, suggesting that LIN-26 does not affect physiological cell death. Or at least, it does not interfere with something that activates the apoptotic machinery in the absence of external DNA damage in those two mutants.

4.5. Understanding the mode of LIN-26 function

4.5.1. LIN-26 does not have a direct effect on the apoptotic machinery

In an effort to investigate the mode of LIN-26 action following DNA damage, I first examined the possibility of a direct effect on the members of the cell death apparatus. Being or presumably having the characteristics of a transcription factor, LIN-26 could exert its function by regulating the transcriptional levels of either *ced-3*, *ced-4* or *ced-9*. To this point, I applied Q-RT-PCR to measure their mRNA levels before and after treatment with ionizing radiation (Figure 14). In both *lin-26* mutant alleles, *ga91* and *n156*, I did not observe any profound change in the number of transcripts. As is the case with the wild-type, the transcriptional levels of *ced-3*, *ced-4* and *ced-9* remain unchanged. This makes it plausible that the effect of LIN-26 on DNA damage-induced cell death occurs at a step more upstream.

4.5.2. LIN-26 affects the transcriptional activation of *egl-1* and *ced-13*

An important element of the apoptotic DNA damage response in *C. elegans* is the transcriptional activation of *egl-1* and *ced-13*, the only two genes coding for BH3-only domain proteins. This HUS-1 and CEP-1- dependent process triggers the increased germ cell apoptosis following ionizing radiation (Hofmann *et al.*, 2002).

Taken that DNA damage-induced germ cell death is abrogated in *lin-26* mutants, I examined the induction of *egl-1* and *ced-13* by measuring the change in their mRNA levels by Q-RT-PCR, three hours following treatment with 120 Gy of X-rays (Figure 15). As expected, in both *lin-26(ga91)* and *lin-26(n156)* mutants induction is

compromised to a significant degree, showing a 4-10-fold decrease for *egl-1* and an 8-fold decrease for *ced-13*, compared to the wild-type situation.

Thus, LIN-26 is required for the activation of the two BH3 domain-bearing genes in *C. elegans*. This finding, on the other hand, does not unveil any information about the order of action of *lin-26* and other genes that show a similar defect in the transcriptional induction of *egl-1* and *ced-13*. It is still possible that *lin-26* acts in the principal DNA damage pathway comprising *hus-1* and *cep-1*. Alternatively, it can exert its function in a pathway parallel to the previous one and still diverge with it at the level of the two pro-apoptotic molecules. Notably, though, the significant decrease in mRNA induction is still distinguishable from the total abolishment observed in a *cep-1* loss-of-function.

With the experiments described below and in the following paragraph I tried to approach the epistatic relationship between *lin-26* and *cep-1*, based on the hypothesis that they might be connected through a transcriptional relation.

I started asking whether LIN-26 could act via CEP-1, partially by making the presumption that the former could serve the role of a transcription factor. I, therefore, measured the *cep-1* levels in *ga91* and *n156* mutant animals, before and after irradiation, by using real time Q-RT-PCR (Table 3). Although it is known that it is the post-translational modifications to p53 that affect its overall appearance and activity in response to various types of stress (Brooks & Gu, 2003), a regulation at the level of transcription cannot be totally excluded. The initial transcript levels of *cep-1* are expressed in arbitrary units and no significant difference is observed between the *lin-26* mutants and the wild-type. Similarly, following irradiation, the fold-change shows

a comparable picture to what is observed for the wild-type, in the range of 2-3-fold increase.

I conclude that there is no LIN-26-dependent activation of the *cep-1* gene existing. The possibility, though, that the former acts upstream and is genetically connected to CEP-1 in an indirect way, is still open.

4.5.3. *lin-26* transcriptional levels are elevated in the absence of CEP-1

Continuing with the examination of an epistatic relationship between the *lin-26* and *cep-1* genes, the reverse question of what is described in paragraph 4.5.3 arose. To test whether CEP-1 can be responsible for the transcriptional activation of *lin-26* following DNA damage, I measured the *lin-26* mRNA levels with real time Q-RT-PCR in wild-type worms and *cep-1(gk138)* mutants and expressed the results in arbitrary units (Table 4). It seems that there is a relative abundance in the transcript copy numbers of *lin-26* in the absence of CEP-1 protein and under physiological conditions, that reaches the value of 17-fold increase compared to the wild-type. Moreover, when the initial *lin-26* levels are compared with the ones upon treatment with ionizing radiation, comparable to the wild-type values are obtained.

A possible and appealing explanation for this finding would be that CEP-1 keeps the steady-state levels of *lin-26* transcription under control, and thus acts upstream of the latter in the hierarchy of the DNA damage signaling cascade.

Indeed, in a search for putative p53 binding sites in the *lin-26* gene, I was able to identify two of them (Figure 16). I used the consensus p53 binding site consisting of two copies of a stretch of the following nucleotides: 5'-

PuPuPuC(A/T)(A/T)GPyPyPy-3'. These are arranged head to head and are separated by 0 to 13 nucleotides, as has been deduced from a set of genes known to be regulated by the mammalian p53. One of the putative binding sites was identified in the promoter region, 893 nucleotides upstream of the ATG, whereas the other is located in the second exon of the gene. The CG residues depicted in orange in Figure 16 and the A/T residues depicted in blue are well conserved in both cases. The nucleotides flanking this core and shown in bold letters are less perfectly matched. The presence of these sequences does not prove anything about the actual biological process that is occurring. Biochemical experiments are needed to establish the validity of such a hypothesis.

4.5.4. The LIN-26 protein is modified by phosphorylation upon ionizing radiation

Whether LIN-26 is an alternative mode of activating the CEP-1-depedent induction of DNA damage-induced germ cell death, or whether it is a co-factor for the transcriptional regulation of the CEP-1 target genes (*egl-1* and *ced-13*) still remains elusive. Critical DNA damage signaling molecules, on the other hand, are post-translationally regulated mainly by phosphorylation and acetylation, modifications which have a profound effect on their stability and function.

To test such a potent mode of regulation, I performed a western analysis using a polyclonal anti-LIN-26 antibody against the N-terminus (offered by the Labouesse lab). Wild-type animals at the young adult stage were irradiated with 120 Gy or left untreated and protein samples were collected 3 h later (Figure 17). In the irradiated sample a molecular weight shift occurred, a pattern that denotes some kind of

modification. When a fraction of the irradiated sample was subjected to phosphatase treatment, the shift disappeared suggesting that LIN-26 is modified by phosphorylation. Considering that the protein possesses such a property, *lin-26* claims an engaging role in the DNA damage signaling network.

The challenge that follows such a finding is to identify which the upstream kinase responsible for this phosphorylation is. Looking at the amino acid sequence of LIN-26 and subjecting it into bioinformatic analysis, a number of candidate phosphorylation sites were recognized (Figure 18). Underlined in red and black, respectively, are two putative ATM and three putative DNA PK phosphorylation sites shown. The consensus sequences were derived from mammalian data sets and the residues expected to be modified are marked with a box. These sequences match the already established ones with various degrees of statistical significance. The predictions are purely speculative and should be used with caution, though, because they are based on the assumption that the peptide library data is correct. Double underlined are stretches that are known to be recognized by CDK and PKCε kinases.

To decide on the actual kinase(s) for the phosphorylation event, the western analysis has to be repeated in the respective mutant genetic background. Unless there is redundancy, LIN-26 should fail to become phosphorylated. Apart from this candidate based approach which might give information to some extent, a complementary method would be to locate the phosphorylation site(s). For this we have established a contract with the Functional Genomics Center in Zurich (FGCZ) to use the Mass Spectrometry technique in order to precisely map the phosphorylated sequences on LIN-26 (p155 Project Proposal).

4.6. Additional DNA damage phenotypes of *lin-26*

4.6.1. *lin-26* mutants have a abnormal cell cycle arrest upon IR

An important aspect of the DNA damage responses in *C. elegans* is the cell cycle proliferation arrest that occurs in the mitotic zone of the germline tissue. This is a response spatially distinct from the apoptotic response. Cell cycle arrest is initiated when checkpoints become activated. These are regulatory mechanisms that do not allow the initiation of a new phase of the cell cycle before the previous one is completed, or temporarily arrest cell-cycle progression in response to genotoxic stress.

In order to study if the cell cycle arrests properly upon IR in the *lin-26* mutants I made use of a cyclin B1 assay that we have developed in the lab (Deplazes, Diploma thesis, 2002). Transgenic worms carrying the CYB-1::YFP reporter transgene (*opIs76*) have all the germ cells marked with YFP, although some of them are particularly highlighted in the mitotic zone (Figure 19E). We assume that, in a population of cells which undergo different phases of the cell cycle, these represent cells being in the G2 phase, where the expression of cyclin B1 peaks. Upon application of ionizing radiation, the previous patched pattern disappears giving rise to a well-defined zone where all mitotic cells are highlighted (Figure 19F). As early as 3 h following treatment with X-rays, this characteristic pattern appears and stays up even after 12 h, as the figure shows.

In a *lin-26(ga91)* mutant background the *opIs76* marker reveals a variation in mitotic nuclei size under normal conditions (Figure 19A, B). The closed arrows represent big nuclei visualized in the already non-treated cells. These are interspersed

among normal-sized nuclei. Upon irradiation there is no accumulation of the YFP signal in the mitotic zone. Instead of a homogenous staining, some highlighted big nuclei can be detected in a population of cells that varies a lot in size (Figure 19C, D). The small nuclei are represented by open arrows in this case.

For the moment it is not possible to predict the nature of the abnormally sized nuclei. It may well be that the big cells in the non-treated animals are cells that already bear some damage and therefore arrest, or conversely, the small cells in the treated animals could be cells that presumably fail to arrest. In that case, a checkpoint function could be assigned to LIN-26. As known from other systems, DNA damage activates specific checkpoints at the G1/S and G2/M boundaries and in the S phase, with each one based on a different mechanism. In *C. elegans*, although some of the components mediating this response upon IR have already been identified (Hofmann *et al.*, 2002, Ahmed *et al.*, 2001), it is not very clear yet how this process is coordinated. Whether checkpoints are activated in all different phases or there is a preference for the G2/M, as the cyclin B assay reveals, remains to be determined. *lin-26* could be a candidate gene to mediate this checkpoint.

4.6.2. DNA damage is sensed properly in the absence of *lin-26*

The cell cycle usually arrests when excessive damage is present in the cells to cope with while cycling. Repair mechanisms are readily initiated to restore the normal situation in cells, and only when there is need to facilitate them, the cycle ceases. In *C. elegans*, genes that are involved in repair can be identified by the phenotypes the

respective mutants display. Increased accumulation of repair factors to distinct nuclear sites is a good way to exemplify increased damage in a mutant.

To test a potential involvement of LIN-26 in repair, I took advantage of the HUS-1::GFP assay described in Hofmann *et al.* Transgenic animals show a diffuse GFP signal in the proliferating germ cell nuclei under normal conditions. The presence of external damage due to ionizing radiation results in the formation of bright foci that overlap with chromatin, most probably representing actual sites of DNA damage or ongoing repair. Young adult wild-type or *lin-26(ga91)* mutant animals expressing the *opIs34* transgene were irradiated with low doses of X-rays (15 Gy) and mitotic cells in a 50 μm distance from the DTC were scored 8 h later (Figure 20). *lin-26* mutants show the same density of foci after irradiation, suggesting that external damage caused by ionizing radiation is properly sensed by the HUS-1 protein complex. Moreover, the foci are kept low in number before treatment in both backgrounds, indicating that there is no endogenous damage accumulated in the absence of LIN-26 and that the latter is not directly linked to the repair process.

4.6.3. Loss of *lin-26* function results in hypersensitivity upon IR

A sensitive measure for the ability towards DNA damage responses, accounting for the combined effects on apoptosis, cell cycle arrest and repair, is the radiation sensitivity assay. The survival of the embryos generated from mitotic cells that have been exposed to the damaging effects of radiation is assessed that way.

I used this method to determine whether animals with impaired *lin-26* activity are sensitive to the irradiation, as is the case for known checkpoint genes. Animals from different genetic backgrounds were irradiated at the L4 stage with 120 Gy or were left

untreated. Twenty-four hours later they were let lay eggs and finally unhatched embryos were counted and expressed as a fraction of the total number laid. As is shown in Figure 21, *lin-26* exhibits moderate levels of embryonic lethality under normal conditions (12.5%). Based on the results of paragraph 4.6.2, the lack of ability to repair endogenous damage is excluded as a cause of this embryonic lethality. However, the most likely explanation would be an essential function for the protein during embryogenesis that results in decreased progeny survival. Following treatment with X-rays, this percentage increases up to 56% and reaches similar levels with the ones for *hus-1(op244)* and *clk-2(mn159)* checkpoint mutants. This effect could probably be the result of inability to cope with the inflicted damage.

Interestingly, simultaneous loss of the *hus-1* and *clk-2* checkpoint genes in the *lin-26* background under normal conditions gives rise to a synthetic lethal phenotype with 28.4 and 42.2% F1 lethality, respectively. This dramatic effect in survivorship often implies that possible genetic interactions might exist to insure either proper repair in the germline or proper propagation of the embryos. In contrast to that, combined loss of *lin-26* and *atm-1* does not confer any increase in the severeness of the phenotype. Evidence for and discussion on the role of *atm-1* in the DNA damage responses, including a synthetic lethal phenotype in the absence of other checkpoints, is provided in Chapter 5.

4.7. Is there a linkage of *lin-26* to cancer biology?

Structural studies of zinc finger proteins have shed light into their extraordinary diversity of structure and function. However, only a limited number has been structurally and mechanistically characterized, despite the large number of putative zinc finger motifs identified. What is clear so far, though, is that these protein motifs play a vital role in regulating a broad panel of biological functions. Even the classical C2H2 zinc finger motif performs more than the initial nucleic acid binding assignment, more than DNA or RNA recognition and packaging (Laity *et al.*, 2001).

Studies of the past few years have revealed that the eukaryotic genomes contain actually a large number of zinc finger genes (ZNF), widespread and well conserved among various organisms. In the human genome more precisely, there is evidence accumulating that the systematic isolation and mapping of ZNF genes could provide a useful approach for the identification of novel candidate disease genes.

Indeed, the engagement of researchers to isolating human zinc finger-encoding cDNAs with a putative involvement in developmental and malignant disorders, returns promising results: members of the zinc finger Krüppel family (ZNF131-140, 142, 143, 148, 151, 154, and 155), or genes containing a KRAB (Krüppel-associated box) segment (ZNF133, 136, and 140) localize to regions involved in deletions and/or translocations associated with various syndromes (Williams syndrome, split hand and foot disease (SHFD1), and Beckwith-Wiedemann syndrome). Some of these map to regions commonly deleted in solid tumors including thyroid adenoma, neuroblastoma, colon cancer and others. In addition, several of the ZNFs map to regions implicated in

recurrent chromosomal rearrangements in hematological malignancies (Tommerup and Vissing, 1995).

A series of other studies have demonstrated that ZBP-89, a Krüppel-type zinc finger protein, inhibits cell proliferation. Overexpression of the protein in immortalized rat pituitary (GH4) cell lines inhibits DNA synthesis and progression to S phase is blocked (Remington *et al.*, 1998).

Towards a similar mode of action, KS1 (KRAB/zinc finger suppressor protein 1) mRNA is inducible by serum and epidermal growth factor, suggesting a role for this gene in cell growth regulation. KS1 suppresses transformation by the potent oncogenes H-ras, Galpha12, and Galpha13, indicating a potential for the protein to protect against neoplastic transformation (Gebelein *et al.*, 1998).

Zinc finger proteins can confer not only protection against proliferation but also sensitization to apoptotic cell death. The ZK1 gene, for example, is one of early response genes by exposure to ionizing radiation, and may have some functions on radiation-induced apoptotic cell death on hematopoietic cells (Katoh *et al.*, 1998). The transcriptional levels of this KRAB domain bearing gene in human leukemia cells lines, CMK86 and U937, are increased after exposure to ionizing radiation, and stably transfected murine myeloid precursor 32D cells have higher sensitivity to ionizing radiation.

KLF6 (Krüppel-like factor 6) is a ubiquitous zinc finger suggested to be a candidate tumor suppressor gene in prostate cancer and astrocytic glioma (Ito *et al.*, 2004). KLF6 mutations are present in tumors with either microsatellite or chromosomal instability and in most colorectal cancers it is inactivated by loss and/or mutation with rates similar to those of TP53 and K-RAS (Reeves *et al.*, 2004).

Moreover, it is frequently down-regulated and suppresses tumor growth via induction of apoptosis in non-small cell lung cancer cells (NSCLCs), suggesting that it might also be a tumor suppressor for these cells (Ito *et al.*, 2004).

The study of zinc finger proteins has revealed their potential to act as either tumor suppressors or oncogenes. ZK7, a novel zinc finger gene, is induced by vascular endothelial growth factor (VEGF) in hematopoietic cells. ZK7-overexpressing cells have lower sensitivity to ionizing radiation and the chemotherapeutic agent etoposide, the same way as VEGF inhibits radiation-induced apoptosis in the leukemia cell line CMK86. Therefore, ZK7 protein may be involved in the inhibitory effect of VEGF on apoptotic cell death in human hematopoietic cells (Kuramoto *et al.*, 2000). Moreover, the mRNA levels of ZK7 in HNSCC (head and neck squamous cell carcinomas) clinical specimens exposed to platinum drugs and/or ionizing radiation are higher than those in non-exposed specimens, and ZK7 over-expressing cells have low sensitivity to the chemotherapeutic agent cisplatin and to ionizing radiation. These results suggest that ZK7 may inhibit apoptotic cell death in HNSCC (Miyake *et al.*, 2002).

From the closest matching proteins of LIN-26, HKR18 and HKR1 (Figure 3B), the former was found to be a protein of 94kDa with 20 zinc fingers in its C terminus. The gene is ubiquitously expressed in all the human tissues tested, with a slight enrichment in ovary and testis as well as fetal kidney (Mark *et al.*, 2001). In all cases, two mRNA transcripts were found to be present. However, the HKr18 gene does not seem to belong to any known larger subfamily of KRAB zinc finger genes in the human genome. It might therefore define a group on its own. There is no additional

information available, though, about the role of the protein in the tissues where it is expressed.

The HKR1 gene product was identified in a study for factors that mediate the signaling pathway activated by exposure to platinum drugs (Oguri *et al.*, 1998). The authors focused on the C2H2 type of zinc finger transcription factors and screened human lung-cancer cell lines for genes that are induced following exposure to cisplatin. The gene is expressed in low levels in normal lung tissues, compared to tissues derived from lung adenocarcinomas and not previously exposed to any treatment. Furthermore, treatment of clinical samples with cisplatin also results in elevation of the expression levels. It is not yet clear, though, how HKR1 overexpression is associated with increased proliferation in a cancerous situation, on one hand, and with an additional response to a DNA damaging agent under this condition, on the other. More experiments would be needed to clarify whether HKR1 responds to cisplatin or other damaging agents under normal conditions, mediating a general response to genotoxic stress. It could also be that its role is connected with drug metabolism or resistance in cancer cells. One important observation is that the gene is located on a chromosomal region that is implicated in advanced ovarian and cervical cancer (Arnold *et al.*, 1996, Heselmeyer *et al.*, 1997). The possibility that HKR1 is involved in the progression of cancers is still open.

During the years, therefore, it has become evident that the family of zinc finger proteins is expanding rapidly with a challenging connection to cancer biology. The resemblance of LIN-26 to members of the ZNF superfamily provokes the hypothesis that the protein might somehow be involved in the interplay between cell death and cell survival. Although at the moment I cannot exclude the possibility of LIN-26

binding an RNA molecule, the above mentioned similarity strongly points to its role as a transcription factor. The protein could, therefore, act either as a transcriptional activator or a transcriptional repressor. If the gene encodes an activator, making an equivalent hypothesis to that in the studies of Labouesse *et al.*, the targets in the germline would be pro-apoptotic genes. In case of a repressor, LIN-26 would have to negatively regulate an anti-apoptotic factor, or a negative regulator of a pro-apoptotic factor in the germline, both of which would be active in its absence.

As revealed from its structure, LIN-26 most likely belongs to a new group of zinc finger proteins, with no obvious members in *C. elegans*, other than the LIN-26-related proteins from the same operon. Although with only two zinc finger motifs it appears as a protein that doesn't conform to the usual type or expected pattern of the human ZNF proteins discussed, it may still share a similar function. Moreover, the atypical KRAB motif that possibly resides at the C-terminus (paragraph 4.2.2; Figure 4) reinforces this hypothesis.

Differentiation is actually known to be largely regulated by transcription factors controlling gene expression. One interesting possibility for the KRAB zinc fingers proteins is that, by getting expressed in a certain type of cells, they are involved in silencing genes expressed in closely related, yet different, cell lineages. And in that way they participate in differentiation and thereby in cell and organ development. This mode of action is reminiscent of the so far known way of LIN-26 function in *C. elegans* proposed by Labouesse *et al.* The novel function that is proposed in this chapter could also be related to the previous one: if LIN-26 is repressing the expression of certain pro-survival genes, it may be involved in stabilizing the

commitment of the dying cells to the death fate. Inactivation or deregulation of the protein may contribute to the development of a situation where damaged cells survive. No evidence so far, though, excludes a more direct role in initiating germ cell death upon DNA damage in *C. elegans*.

References

Ahmed, S., Alpi, A., Hengartner, M.O. & Gartner, A. *C. elegans* RAD-5/CLK-2 defines a new DNA damage checkpoint protein. *Curr Biol.* **11(24)**, 1934-44 (2001).

Alpi, A., Pasierbeck, P., Gartner, A. & Loidl, J. Genetic and cytological characterization of the recombination protein RAD-51 in *Caenorhabditis elegans*. *Chromosoma* **112(1)**, 6-16 (2003).

Arnold, N., Hagele, L., Walz, L., Schempp, W., Pfisterer, J., Bauknecht, T. & Kiechle, M. overrepresenation of 3q and 8q material and loss of 18q material are recurrent findings in advanced human ovarian cancer. Genes Chromosomes Cancer **16**, 46-54 (1996).

den Boer, B.G.W., Sookhareea, S., Dufourcq, P. & Labouesse, M. A tissue-specific knock-out strategy reveals that *lin-26* is required for the formation of the somatic gonad epithelium in *Caenorhabditis elegans*. *Development* **125**, 3213-3224 (1998).

Brenner, S. The genetics of Caenorhabditis elegans. *Genetics* **77(1)**, 71-94 (1974).

Brooks, C.L. & Gu, W. Ubiquitination, phosphorylation and acetylation: the molecular basis for p53 regulation. *Curr Opin Cell Biol.* **15(2)**, 164-71 (2003).

Deplazes, A. Studies of cell cycle kinetics and regulation in the germ line of C. elegans. Diplomarbeit. University of Zurich, Switzerland (2002).

Dufourcq, P., Chanal, P., Vicaire, S., Camut, E., Quintin, S., den Boer, B.G.W., Bosher J.M. & Labouesse, M. *lir-2*, *lir-1* and *lin-26* encode a new class of zinc-finger proteins and are organized in two overlapping operons both in *Caenorhabditis elegans* and in *Caenorhabditis briggsae*. *Genetics* **152**, 221-235 (1999).

Ferguson, E.L., Sternberg, P.W. & Horvitz, H.R. A genetic pathway for the pecification of the vulval cell lineages of *Caenorhabditis elegans*. *Nature* **326**, 259-267 (1987).

Gartner, A., Milstein, S., Ahmed, S., Hodgkin, J. & Hengartner, M.O. A conserved checkpoint pathway mediates DNA damage--induced apoptosis and cell cycle arrest in *C. elegans*. *Mol. Cell* **5**, 435-443 (2000).

Gebelein, B., Fernandez-Zapico, M., Imoto, M. & Urrutia, R. KRAB-independent suppression of neoplastic cell growth by the novel zinc finger transcription factor KS1. *J Clin Invest*. **102(11)**, 1911-9 (1998).

Gumienny, T., Lamble, E., Hartwieg, E., Horvitz, H.R. & Hengartner, M.O. Genetic control of programmed cell death in the *Caenorhabditis elegans* hermaphrodite germline. *Development* **126**, 1011-1022 (1999).

Heselmeyer, K., Macville, M., Schröck, E., Blegen, H., Hellström, A.C., Shah, K., Auer, G. & Ried, T. Advanced-stage cervical carcinomas are defined by a recurrent pattern of chromosomal aberrations revealing high genetic instability and a consistent

gain of chromosome arm 3q. Genes Chromosomes Cancer **19**, 233-240 (1997).

Hofmann, E.R., Milstein, S., Boulton, S.J., Ye, M., Hofmann, J.J., Stergiou, L., Gartner, A., Vidal, M. & Hengartner, M.O. *Caenorhabditis elegans* HUS-1 is a DNA damage checkpoint protein required for genome stability and EGL-1-mediated apoptosis. *Curr. Biol.* **12**, 1908-1918 (2002).

Ito, G., Uchiyama, M., Kondo, M., Mori, S., Usami, N., Maeda, O., Kawabe, T., Hasegawa, Y., Shimokata, K. & Sekido, Y. Krüppel-like factor 6 is frequently down-regulated and induces apoptosis in non-small cell lung cancer cells. *Cancer Res.* **64(11)**, 3838-43 (2004).

Kamath, R.S., Fraser, A.G., Dong, Y., Poulin, G., Durbin, R., Gotta, M., Kanapin, A., Le Bot, N., Moreno, S., Sohrmann, M., Welchman, D.P., Zipperlen, P., & Ahringer, J. Systematic functional analysis of the Caenorhabditis elegans genome using RNAi. *Nature* **421(6920)**, 231-7 (2003).

Katoh, O., Oguri, T., Takahashi, T., Takai, S., Fujiwara, Y. & Watanabe, H. ZK1, a novel Krüppel-type zinc finger gene, is induced following exposure to ionizing radiation and enhances apoptotic cell death on hematopoietic cells. *Biochem Biophys Res Commun*. **249(3)**, 595-600 (1998).

Kim, S.K., Lund, J., Kiraly, M., Duke, K., Jiang, M., Stuart, J.M., Eizinger, A., Wylie, B.N. & Davidson, G.S. A gene expression map for *Caenorhabditis elegans*. *Science* **293(5537)**, 2087-92 (2001).

Kuramoto, K., Uesaka, T., Kimura, A., Kobayashi, M., Watanabe, H. & Katoh O. ZK7, a novel zinc finger gene, is induced by vascular endothelial growth factor and inhibits apoptotic death in hematopoietic cells. *Cancer Res*. (2000) **60(2)**, 425-30 (2004).

Labouesse, M., Hartwieg, E. & Horvitz, H.R. The *Caenorhabditis elegans* LIN-26 protein is required to specify and/or maintain all non-neoronal ectodermal cell fates. *Development* **122**, 2579-2588 (1996).

Labouesse, M., Sookhareea, S. & Horvitz, H.R. The *Caenorhabditis elegans* gene *lin-26* is required to specify the fates of hypodermal cells and encodes a presumptive zinc-finger transcription factor. *Development* **120**, 2359-2368 (1994).

Laity, J.H., Lee, B.M. & Wright, P.E. Zinc finger proteins: new insights into structural and functional diversity. *Curr Opin Struct Biol*. **11(1)**, 39-46 (2001).

Landmann, F., Quintin, S., Labouesse, M. Multiple regulatory elements with spatially and temporally distinct activities control the expression of the epithelial differentiation gene *lin-26* in *C. elegans*. *Dev Biol*. **265(2)**, 478-90 (2004).

Mark, C., Looman, C., Abrink, M. & Hellman, L. Molecular cloning and preliminary functional analysis of two novel human KRAB zinc finger proteins, HKr18 and HKr19. *DNA Cell Biol*. **20(5)**, 275-86 (2001).

Milstein, S. Genetic analysis of programmed cell death in the *Caenorhabditis elegans* germline. PhD thesis. State University of New York, New York (2001).

Miyake, N., Katoh, O., Hirata, S., Kimura, S., Watanabe, H. & Yajin, K. Expression of the Krüppel-type zinc finger gene, ZK7, in head and neck squamous cell carcinoma and normal mucosa. *Cancer Lett*. **185(1)**, 111-8 (2002).

Nardelli, J., Gibson, T.J., Vesque, C. & Charnay, P. Base sequence discrimination by zinc finger DNA-binding domains. *Nature* **349**, 175-178 (1991).

Oguri, T., Katoh, O., Takahashi, T., Isobe, T., Kuramoto, K., Hirata, S., Yamakido, M. & Watanabe, H. The Krüppel-type zinc finger family gene, HKR1, is induced in lung cancer by exposure to platinum drugs. *Gene* **222**, 61-67 (1998).

Quintin, S., Michaux, G., McMahon L., Gansmuller, A. & Labouesse, M. The *Caenorhabditis elegans* gene *lin-26* can trigger epithelial differentiation without conferring tissue specificity. *Dev. Biol*. **235**, 410-421 (2001).

Reeves, H.L., Narla, G., Ogunbiyi, O., Haq, A.I., Katz, A., Benzeno, S., Hod, E., Harpaz, N., Goldberg, S., Tal-Kremer, S., Eng, F.J,, Arthur, M.J., Martignetti, J.A. & Friedman, S.L. Krüppel-like factor 6 (KLF6) is a tumor-suppressor gene frequently inactivated in colorectal cancer. *Gastroenterology* **126(4)**, 1090-103 (2004).

Remington, M.C., Tarle, S.A., Simon, B. & Merchant, J.L. ZBP-89, a Krüppel-type zinc finger protein, inhibits cell proliferation. *Biochem Biophys Res Commun*. **237(2)**,

230-4 (1997).

Santarosa, M. & Ashworth, A. Haploinsufficiency for tumour suppressor genes: when you don't need to go all the way. *Biochim Biophys Acta*. **1654(2)**:105-22 (2004).

Tommerup, N. & Vissing, H. Isolation and fine mapping of 16 novel human zinc finger-encoding cDNAs identify putative candidate genes for developmental and malignant disorders. *Genomics* **27(2)**, 259-64 (1995).

Methods

Genetics. All strains were grown at 20ºC on NGM agar seeded with *E. coli* OP50 (Brenner, 1974). The Bristol N2 strain was used as the wild-type strain. The following alleles and transgenic strains were used: LGI: *atm-1(gk186)*, *cep-1(gk138)*, *hus-1(op244)*, *gla-1(op216)*, *gla-3(op234)*, *glp-4(bn2)*; LGII: *lin-26(n156)*, *lin-26(ga91)*, *lin-26(ok939)*; LGIII: *clk-2(mn159)*, *ced-9(n1653ts)*; *opIs34* (HUS-1::GFP), *opIs76* (CYB-1::YFP). The *lin-26(ok939)* strain was maintained as *lin-26(ok939)*/mIn1[mIs14 *dpy-10(e128)*] II.

Germline apoptosis. Young adult staged worms from different genetic backgrounds were exposed to 60 or 120 Gy of X-rays and corpses were scored in the meiotic region of one gonad arm during the course of time or at indicated time points, using Nomarski optics. For the RNAi experiments, L1 staged worms were put on plates seeded with the respective RNAi clone (Kamath *et al.*, 2003) and young adults were scored for germline apoptosis at the indicated time points.

Cell cycle arrest studies. The cell cycle arrest phenotype was visualized using a cyclin B1 reporter construct. *opIs76* transgenic animals bearing low copies of CYB-1::YFP in a wild-type or a *lin-26(ga91)* background were treated with 120 Gy of X-rays 12 h post the L4 stage. Images from dissected gonads were captured 10 h later using an ORCA-ER digital CCD camera and were processed with the Openlab software.

Relative quantification of transcripts. Total RNA was extracted from wild-type, *lin-26(n156)*, *lin-26(ga91)*, *cep-1(gk138)* and *glp-4(bn2)* mutants after treatment with 120 Gy of X-rays and/or from untreated worms. cDNA synthesis and quantitative real-time RT-PCR were performed as previously described (Hofmann *et al.*, 2002). Transcripts of the *lin-26* long and short isoforms, the cell death genes *ced-9*, *ced-4*, *ced-3* and the pro-apoptotic genes *egl-1*, *ced-13* and *cep-1* were measured after normalization with 18SrRNA mRNA, which was used as internal control. The average fold-change upon treatment was deduced based on three independent experiments.

Immunostaining of LIN-26. Antibody staining of gonads was performed using standard procedures. Briefly, animals were dissected and fixed with 3% para-formaldehyde/0.1 M K2HPO4 (pH 7.2) for 50 min at room temperature followed by a 10 min incubation with 100% methanol on ice. Gonads were blocked in 5% BSA/PBS-Tween-20 0.1% for 1 h and incubation with a polyclonal anti-LIN-26 antibody against the N-terminal 331 amino acids (offered by the Labouesse lab) was done overnight at 4ºC (Alpi *et al.*, 2003). The tissues were co-stained with DAPI before mounting. Fluorescent images were captured with a Leica microscope equipped with an ORCA-ER digital CCD camera and were processed with the Openlab software.

Immunoblotting of LIN-26. Whole worm protein extracts from wild-type animals were used for SDS-PAGE and subsequently probed with the anti-LIN-26 polyclonal antibody, using standard molecular methods. Proteins were collected before and 3 h

following treatment with 120 Gy of X-rays, with or without having been subjected to λ-phosphatase treatment (New England, Biolabs).

Embryonic lethality assay. Animals from different genetic backgrounds, 48 h post the L1 stage, were subjected to 120 Gy of X-rays and one day later were left lay eggs for 4-6 h. Non-hatched eggs were scored the next day as a positive embryonic lethal phenotype and expressed as a fraction of the total eggs laid. Data shown is the average percent lethality of 50 animals. Error bars indicate SEM.

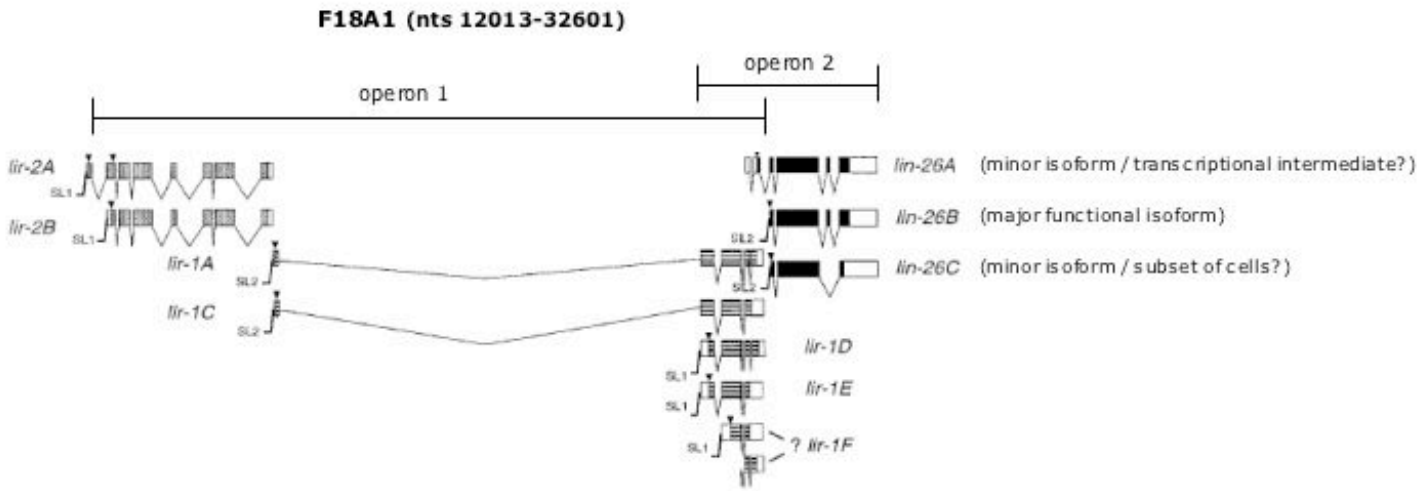

Figure 1. Genomic organization of the *lin-26* and the *lir-*(*lin-26*-related) genes

The genes *lir-1*, *lir-2* and *lin-26* form two overlapping operons, one that includes *lir-2* and long *lir-1* isoforms (operon 1) and another that includes short *lir-1* isoforms and *lin-26* (operon 2). Boxes represent exons and open triangles represent introns. UTRs are shown in white and inverted triangles show the position of the potential methionine initiation codons. *lin-26B* is the major isoform, whereas *lin-26A* is a minor isoform, probably a transcriptional intermediate. *lin-26C*, on the basis of its relative abundance, is required only in a subset of cells (Dufourcq *et al*., Genetics, 1999). The figure is adapted from Dufourcq *et al*.

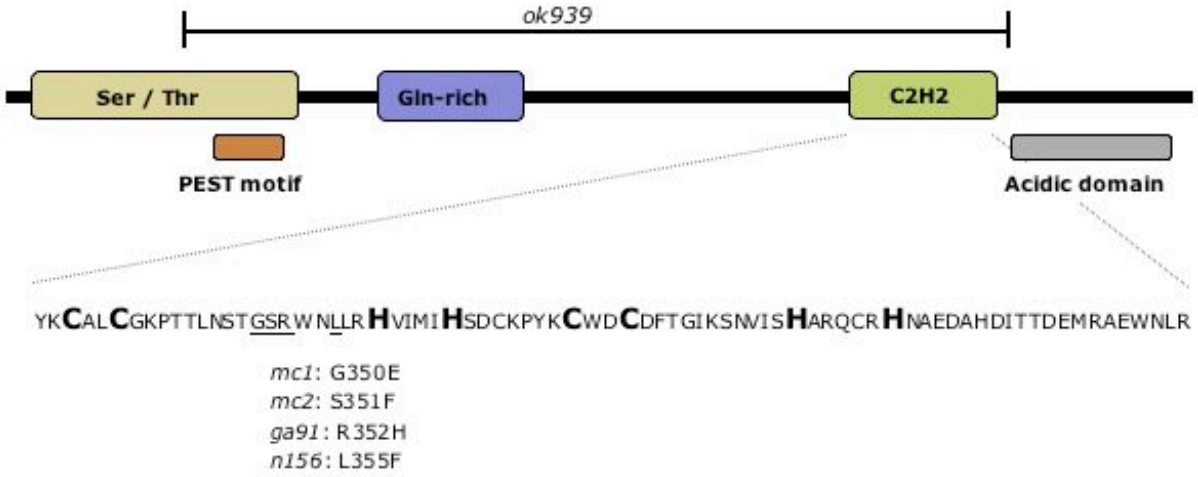

Figure 2. Protein structure of LIN-26

The predicted amino acid sequence of the longest *lin-26* cDNA is shown. The deduced protein is 472 amino acids long. Five potentially important functional domains are illustrated: an amino-terminal region with 25% serines or threonines, a middle region with 25% glutamines, a carboxy-terminal region containing several negatively charged amino acids, two copies of cysteine-histidine motif and a potential protein degradation PEST sequence (proline/glutamic acid/serine/threonine). The Cys/His motifs might form zinc fingers. The four mutations that are depicted affect the first potential zinc finger (isolated by the Labouesse group). A recently isolated deletion, *ok939*, that removes 77% of the ORF was obtained by the CGC.

Figure 3. LIN-26 belongs to the Krüppel-type of Zinc Finger family proteins

(A) Alignment of the zinc finger region from LIN-26 with selected members of the human Krüppel-type Zn finger superfamily. (B) Sequence comparison of the zinc finger motif of LIN-26 with the respective domain from human HKR18 and HKR1 proteins that best match it (57% and 60% similarity within this stretch with each one). The highly conserved residues are marked with asterisks. The first and the second C2H2 motif are shown in orange and green, respectively.

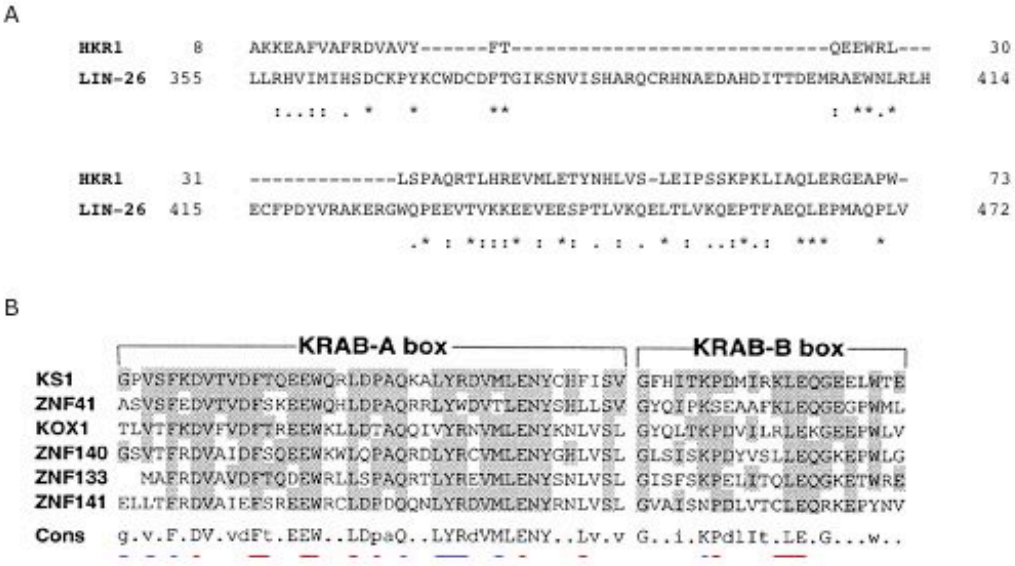

Figure 4. Potential KRAB motif at the C-terminus of LIN-26

(A) Alignment of the residues 355-472 from LIN-26 with the human HKR1 protein, a Krüppel-type Zn finger protein that best matches it. (B) Sequence comparison of the KRAB-A and B structural domains from other zinc finger proteins. identical residues are shaded. A consensus sequence is derived, where uppercase letters represent highly conserved residues. The red underlined residues denote amino acids that are conserved in the LIN-26 sequence, whereas the blue one denote less conserved, similar amino acids.

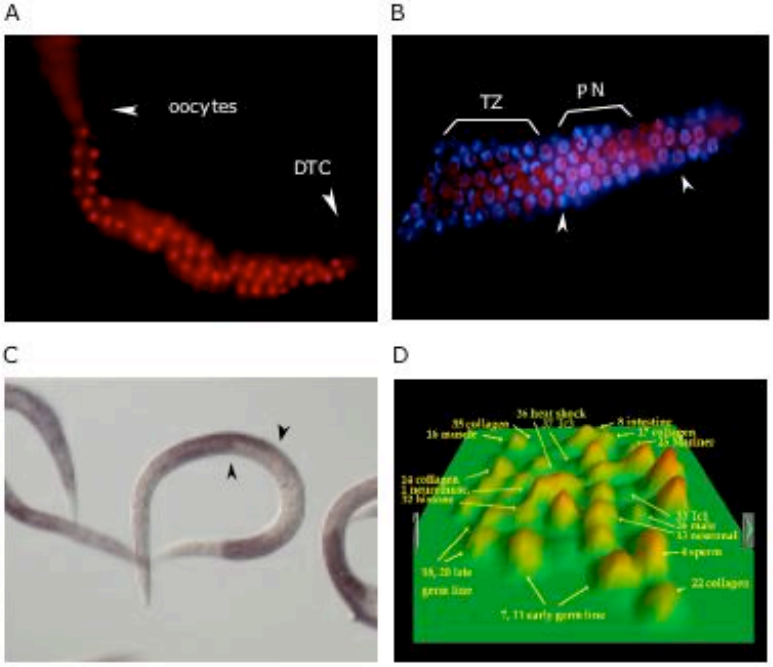

Figure 5. LIN-26 is expressed in the germline tissue of *C. elegans*

(A, B) Immunostaining of a dissected gonad using a polyclonal antibody against LIN-26 (red), reveals localization of the protein in the nucleolar compartments of the germline. DNA staining with DAPI is in blue. TZ and PN denote the transition zone and the premeiotic nuclei, respectively. (C) RNA *in situ* hybridization performed by the Kohara group showing expression of the *lin-26* transcript in both the mitotic and meiotic zone of the germline. (D) Part of the gene expression map of *C. elegans* (Kim *et al.*, Science 2001) showing "mountain 2" enriched in germline and DNA repair genes that are co-regulated. *lin-26* clusters among this group of genes.

Table 1. Isoform B, the short *lin-26* form, is the most abundant transcript in both the germline and the whole animal

Primers were designed to independently measure the mRNA levels of the two *lin-26* isoforms with real time Q-RT-PCR. Wild-type worms as well as *glp-4(bn2)* mutants were used to compare the levels in the germline with the ones in the whole animal. Values are expressed as relative abundance.

	isoform B compared to A (relative abundance)
germline	18
whole animal	1.0E+6

Table 2. Isoform A, the long *lin-26* form, is the transcript up-regulated upon ionizing radiation in the *C. elegans* germline

The change in mRNA levels of the two *lin-26* isoforms were determined upon ionizing radiation (3 h post 120 Gy) with real time Q-RT-PCR. Wild-type worms as well as *glp-4(bn2)* mutants were used to compare the levels in the germline with the ones in the whole animal. Values are expressed as fold-change.

	change upon IR	
	isoform A	isoform B
germline	5.5	-2.9
whole animal	-1.2	-0.4

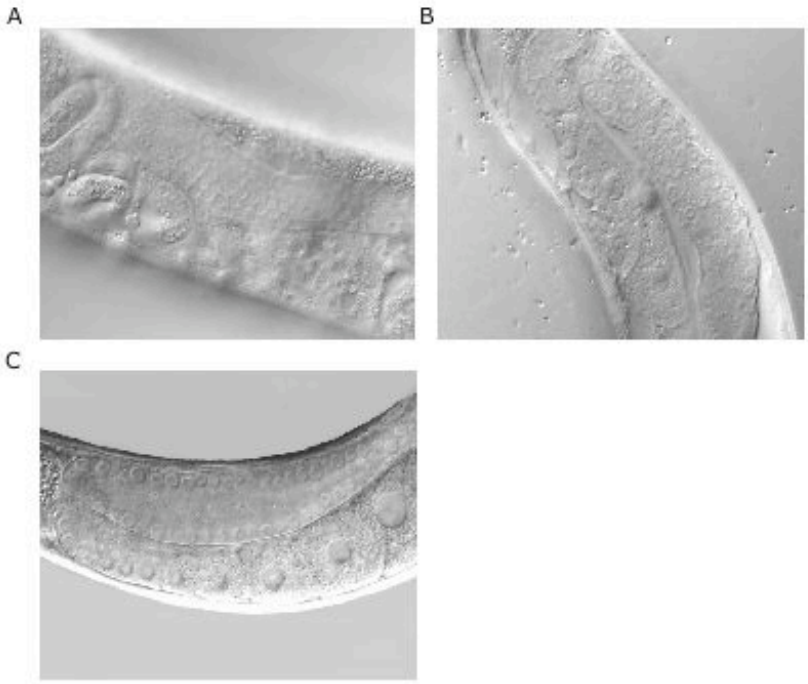

Figure 6. Phenotypic germline characteristics of some of the *lin-26* mutants

DIC pictures of the germlines of the *n156*, *ga91* and *ok939*/mIn1 alleles used in this study are depicted. (A) *n156* animals have a normal-looking germline, with proliferation rates similar to wild-type. Elsewise, they show a Vul (vulvaless) and a Egl (egg laying defective) phenotype and they are slightly small and fat with hypodermal and support cell defects. (B) *ga91* animals have a wild-type compartmentalization in the germline with slightly decreased numbers of nuclei. They also display a Pvl (protruding vulva) and a Egl phenotype. (C) *ok939* animals have a Lva (larval arrest) phenotype making it impossible to determine the germline characteristics in adulthood. The heterozygote over the mIn1 balancer animals appear wild-type.

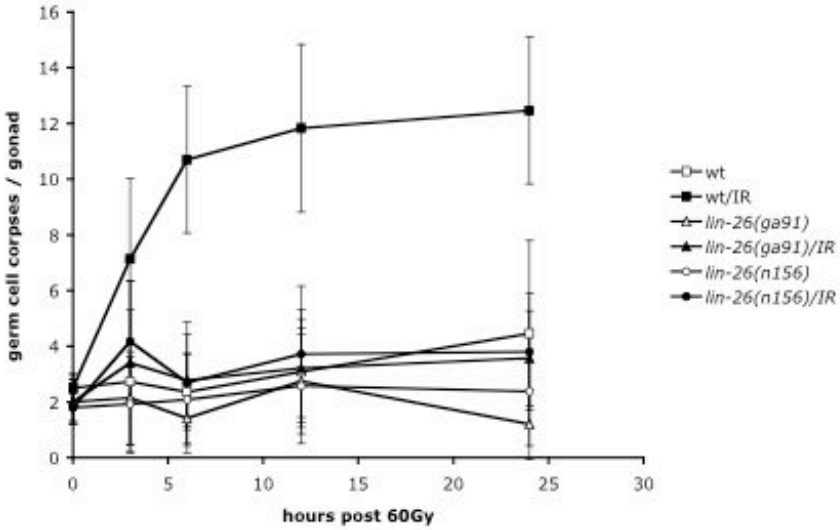

Figure 7. *lin-26* mutants are defective for ionizing radiation-induced apoptosis

Time course analysis was performed with wild-type animals, *lin-26(ga91)* and *lin-26(n156)* mutants. Apoptotic corpses were scored in the meiotic region of one gonad arm of young adult animals, during the course of time and following 60 Gy of X-rays. Data shown represent the average number of three independent experiments ± SD.

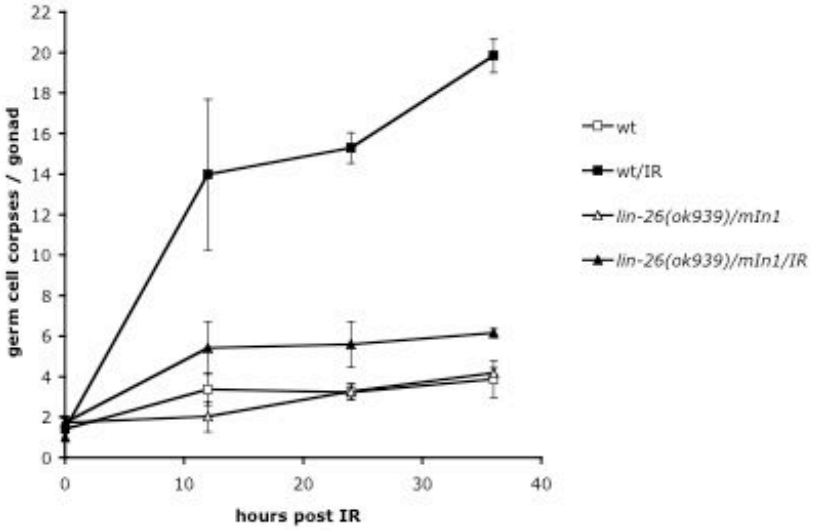

Figure 8. *lin-26* mutants are defective for ionizing radiation-induced apoptosis

Time course analysis was performed with wild-type animals and *lin-26(ok939)* mutants. Apoptotic corpses were scored in the meiotic region of one gonad arm of young adult animals, during the course of time and following 120 Gy of X-rays. Data shown represent the average number of three independent experiments ± SD.

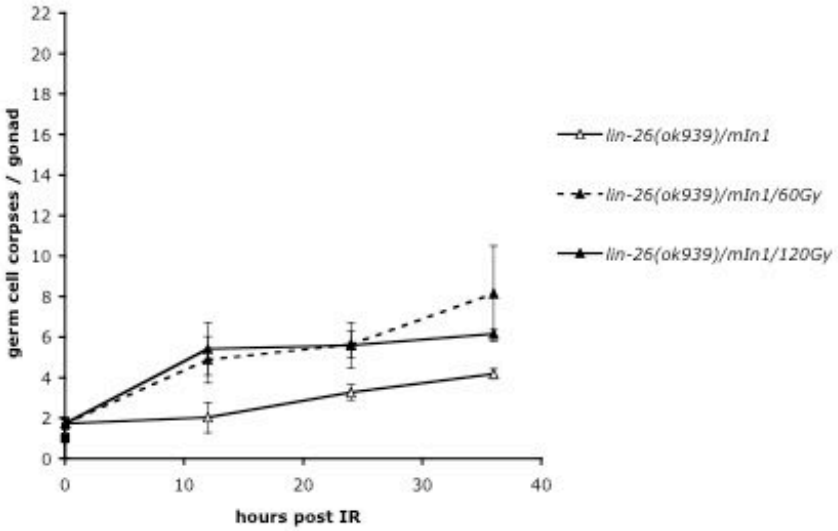

Figure 9. *lin-26* mutants are defective for ionizing radiation-induced apoptosis

Time course analysis was performed with wild-type animals and *lin-26(ok939)* mutants. Apoptotic corpses were scored in the meiotic region of one gonad arm of young adult animals, during the course of time and following either 60 Gy or 120 Gy of X-rays. Data shown represent the average number of two independent experiments ± SD.

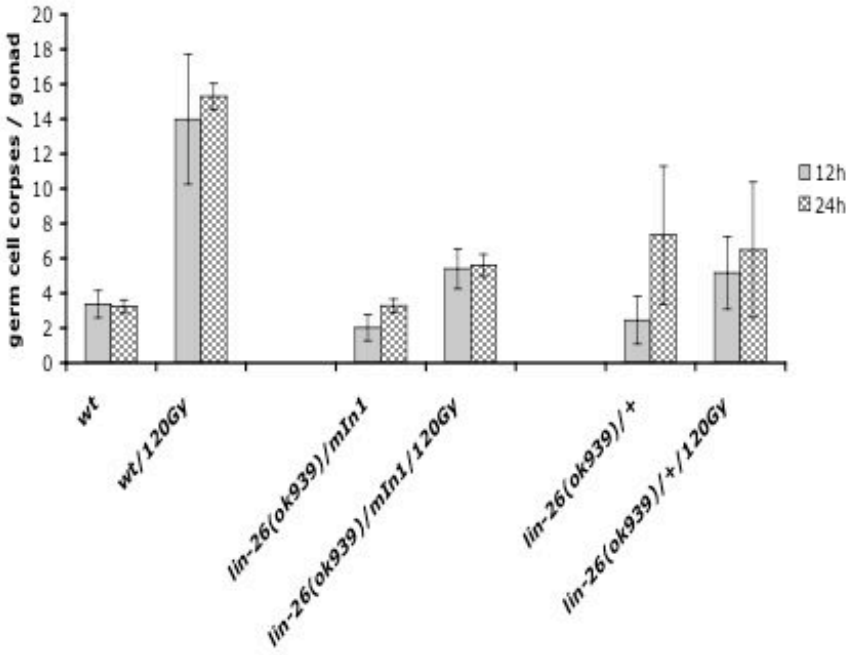

Figure 10. *lin-26* probably acts in a haploinsufficient manner to induce apoptosis upon ionizing radiation

Young adult animals of the following genotypes were used in this apoptotic assay: wild-type, *lin-26(ok939)*/mIn1 and *lin-26(ok939)*/+ mutants. Apoptotic corpses were scored in the meiotic region of one gonad arm, at two different time-points and following 120 Gy of X-rays. Data shown represent the average number of two independent experiments ± SD.

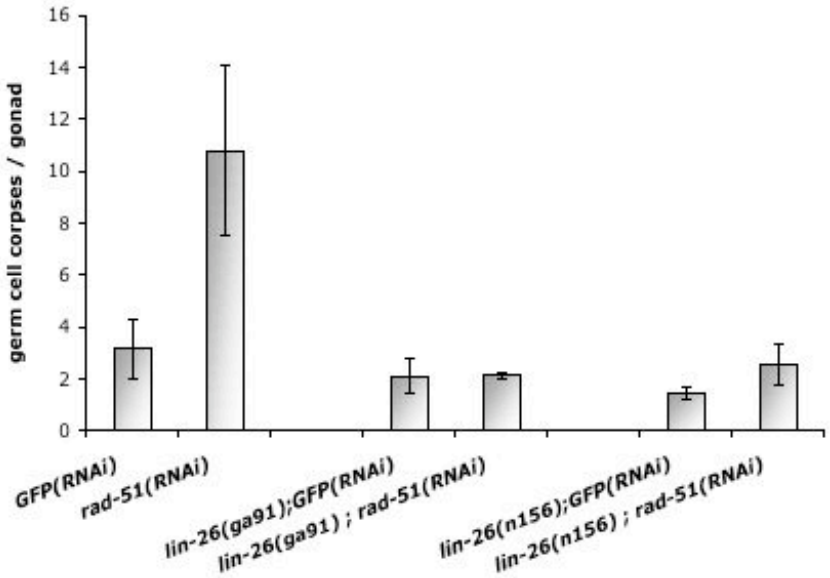

Figure 11. Loss of *rad-51* function is suppressed by the *ga91* and *n156* mutations in *lin-26*, suggesting that endogenously DNA damage-induced cell death does not occur properly in the absence of LIN-26

Apoptotic corpses were scored in the meiotic region of one gonad arm of young adult *lin-(ga91)* and *lin-26(n156)* that were subjected to either GFP or *rad-51*(RNAi) 12 h after the young adult stage. GFP(RNAi) and *rad-51*(RNAi) were used as controls. Data shown represent the average number of two independent experiments ± SD.

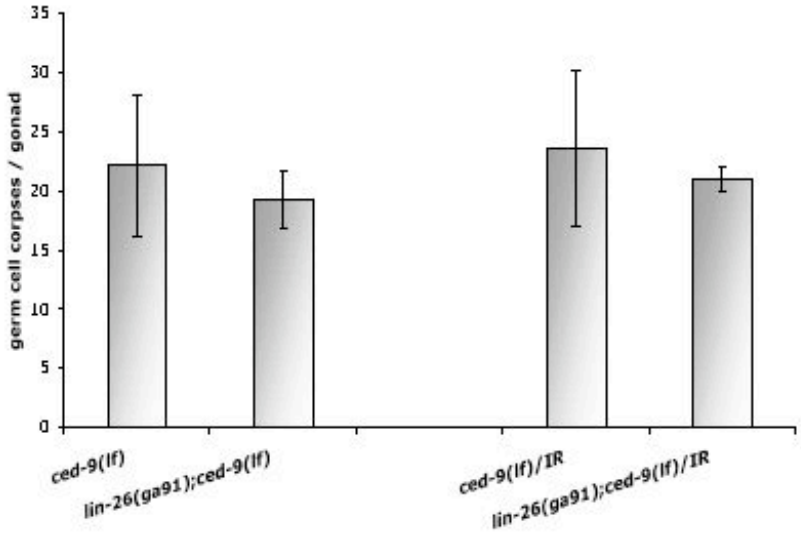

Figure 12. The *ga91* mutation in *lin-26* does not suppress loss of *ced-9* function, suggesting that LIN-26 acts upstream of a functional apoptotic machinery

Apoptotic corpses were scored in the meiotic region of one gonad arm of young adult *ced-9(n1653)* and *lin-26(ga91);ced-9(n1950)* animals before and 12 h after the application of 60 Gy of X-rays. Data shown represent the average number of three independent isolates of double mutants ± SD.

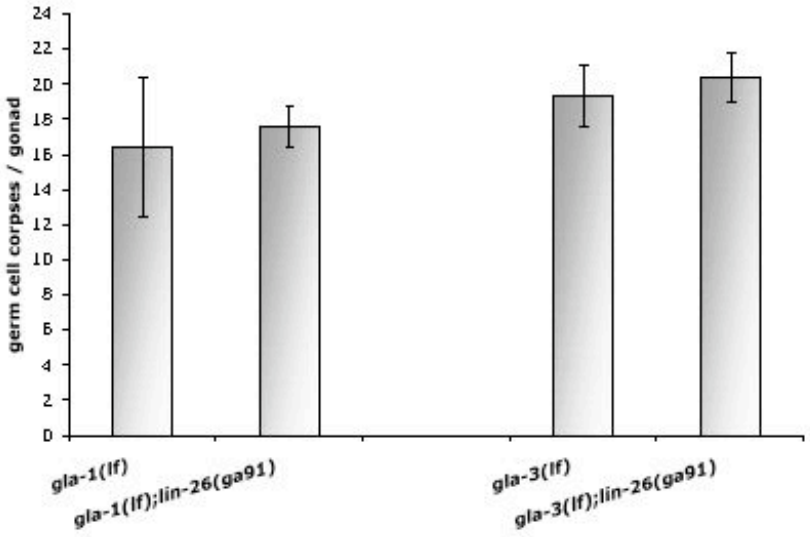

Figure 13. Loss-of-function mutations in *gla-1(op234)* and *gla-3(op216)* are not suppressed by the *ga91* mutation in *lin-26*, suggesting that LIN-26 does not affect physiological cell death

Apoptotic corpses were scored in the meiotic region of one gonad arm of young adult *gla-1(op234)*, *gla-3(op216)* and *gla-1(op234);lin-26(ga91)*, *gla-3(op216);lin-26(ga91)* animals 12 h after the young adult stage. Data shown represent the average number of independent isolates of double mutants ± SD.

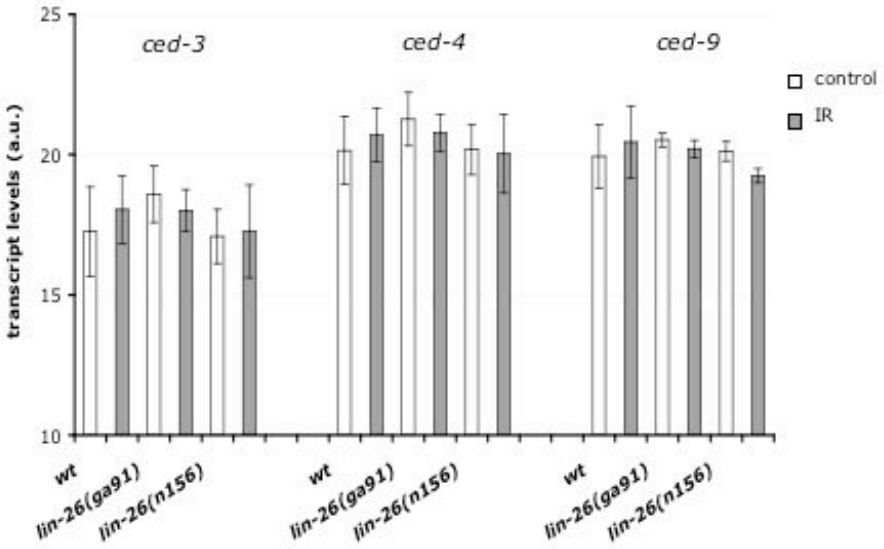

Figure 14. Loss of function in *lin-26* does not affect the transcriptional levels of *ced-3*, *ced-4* and *ced-9*, neither before or after ionizing radiation

The change in the mRNA levels of *ced-3*, *ced-4* and *ced-9* was determined by real-time Q-RT-PCR, 3 h following treatment with 120 Gy of X-rays. Data shown is the average fold-change of three independent experiments ± SD.

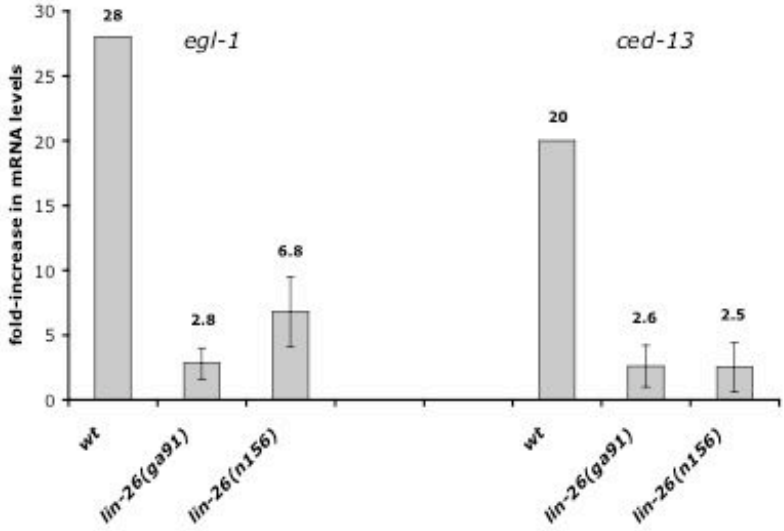

Figure 15. Transcriptional induction of *egl-1* and *ced-13* upon ionizing radiation is compromised in *lin-26* mutants

The change in the mRNA levels of *egl-1* and *ced-13* was determined by real-time Q-RT-PCR, 3 h following treatment with 120 Gy of X-rays. Data shown is the average fold-change of three independent experiments ± SD.

Table 3. Mutations in *lin-26* do not affect the transcriptional levels of *cep-1*, neither under normal conditions, nor upon ionizing radiation

cep-1 levels were measured with real time Q-RT-PCR in wild-type worms, *ga91* and *n156* mutant animals and were expressed in a.u. Fold-change upon IR was determined by comparing the final with the initial *cep-1* levels in the corresponding genetic background.

	***cep-1* initial transcript levels** (au)	**fold-induction 3h upon 120Gy**
wt	2.1 ± 0.4	2.9
lin-26(ga91)	1.0 ± 0.4	2.0
lin-26(n156)	1.5 ± 0.9	2.0

Table 4. *lin-26* transcriptional levels are elevated in a *cep-1(gk138)* mutant background under normal conditions

lin-26 levels were measured with real time Q-RT-PCR in wild-type worms and *cep-1(gk138)* mutants and were expressed in a.u. The initial *lin-26* levels were compared with the ones upon treatment with ionizing radiation.

	lin-26 **transcript levels (au)**		
	initial	**3h upon**	
		40Gy	**120Gy**
wt	1.0 ± 1.9	1.0 ± 1.0	1.0 ± 2.1
cep-1(gk138)	17 ± 2.8	1.9 ± 2.9	1.8 ± 1.4

F18A1 (nts 27251-28300)

gctcatGGACAAGCTGgactttcaACACTAGAAAatgttcgcttgtaatggatctccgaacggtggtgatg
tacttcgcagaaagacgccgtctcggaaagctgaagattcaataaaagctacgtgtaaagtatgtggaca
tgatgtaatgtattctcctcaaaggacttggaacttgatgcgtcacgtatggattatgcaccaatcatca
aaaccgaatcagtgttcaatatgcggatattctcacatcaagccatatgttaggaaacatatcgagtctc
agcataagcatgattcaaatgcaacgataattgacttaaagtgagttttacatttctcagtttgataaaa
ttgtcaatttgattttcagatcaccagaactagaagctgaatggagtcaattgttagatcaatgcttcgg
agtcacatatcgaaagtggaagcatcataaggaggatacgcagcacaccggtgggttactgttcgatgac
gacgagttgagagggtgagcgagagcgtcaccgacatcaactgaagaccgccagtgtagtctttgcagcg
ggtgatgaagattacggtcacgagcatcatttttcaccggaggaagatgtaatgacaactttatgattct
tcatggctttcacttgtcgacgtcttcccattgtcttccattcatctttcgtcatctcttcatatttcac
tcaatcactgccttgtgcgatcatgtaatttcaaactattgtaattcgttgaaattatcaaataataaat
ttaatcaggttattattgaatgtttatgtaacctattccatctcacaatgagttaatacaactcttgaat
acttgaatacctttcatccctcgcttacttttttttaaaatttttaattgattattttcagATGctttctaa
atttgtggtagtcgaagtaagcaactcaaataacacaatgacactggtggaatacttggtatgtttatca
tttaaaaagttcgattaacattggtattttcaggtaACGCATGGATtCGACAAGTTTgcagttgtaacag

p53 consensus binding site: 5'-PuPuPuC(A/T)(A/T)GPyPyPy-3'

Figure 16. Putative p53 binding sites were identified in the promoter region and the second exon of the *lin-26* gene

A stretch of nucleotides from the *lin-26* gene coding region and the upstream sequences is depicted. The sequences in bold and underlined match the consensus p53 binding site, consisting of two copies of 5'-PuPuPuC(A/T)(A/T)GPyPyPy-3', arranged head to head and separated by 0 to 13 nucleotides. The start codon of the gene is also shown.

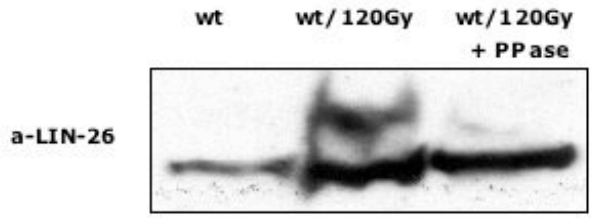

Figure 17. LIN-26 is phosphorylated upon ionizing radiation

Wild-type animals at the young adult stage were irradiated with 120 Gy or left untreated. Protein samples were collected 3 h later and a fraction of the irradiated sample was subjected to phosphatase treatment. Western analysis was performed using a polyclonal anti-LIN-26 antibody against the N-terminal 331 amino acids (offered by the Labouesse lab).

LIN-26

MILHGFHL**STSSHCLPFIFRHLFIFHSITALCDHMLSKFVVVEVSNSNNTMTLVEYLVTHGFD**
KFAVVTDLVDHPSFKYKDGSSSPESPSTTASTAAQHTPPRTAVSTPTSINTPVPPHQNKQRHS
IDKIAANLSTKKVSPSSIEKQLQRTSHNPLHQLSTPHALSQLQKLLEEQHKINQMNIQKKEQE
RQQAEIQRILLQQANAAQINHSFGLERLTPEYDDNHHSETISKASSEDLKTEPDSTDFGLGTS
DDQVRASMLHLLHPVFAPAFGMLDAENIFGAASKPTTPASKRRNTDSNGAPSKKHRWLPVNEL
EESRSSRGKNCGRVHC*KATYKCALCGKPTTLNSTGSRWNLLRHVIMIHSDCKPYKCWDCDFTG*
*IKSNVISHARQCRHNAEDAH*DITTDEMRAEWNLRLHECFPDYVRAKERGWQPEEVTVKKEEVE
ESPTLVKQELTLVKQEPTFAEQLEPMAQPLV

Figure 18. Putative phosphorylation sites by ATM and DNA PK were identified in the amino acid sequence of LIN-26

The amino acid sequence of LIN-26 is depicted. Two putative ATM phosphorylation sites and three putative DNA PK phosphorylation sites, are shown underlined in red and black, respectively. The residue to be modified lies in a box. Double underlined are stretches that are known to be recognized by CDK and PKCε kinases. The Gln-rich domain is illustrated in blue, the Ser/Thr stretch in bold letters, the PEST domain in brown, whereas italicized is the Zn finger domain. Searches were conducted using the http://scansite.mit.edu/ online tool.

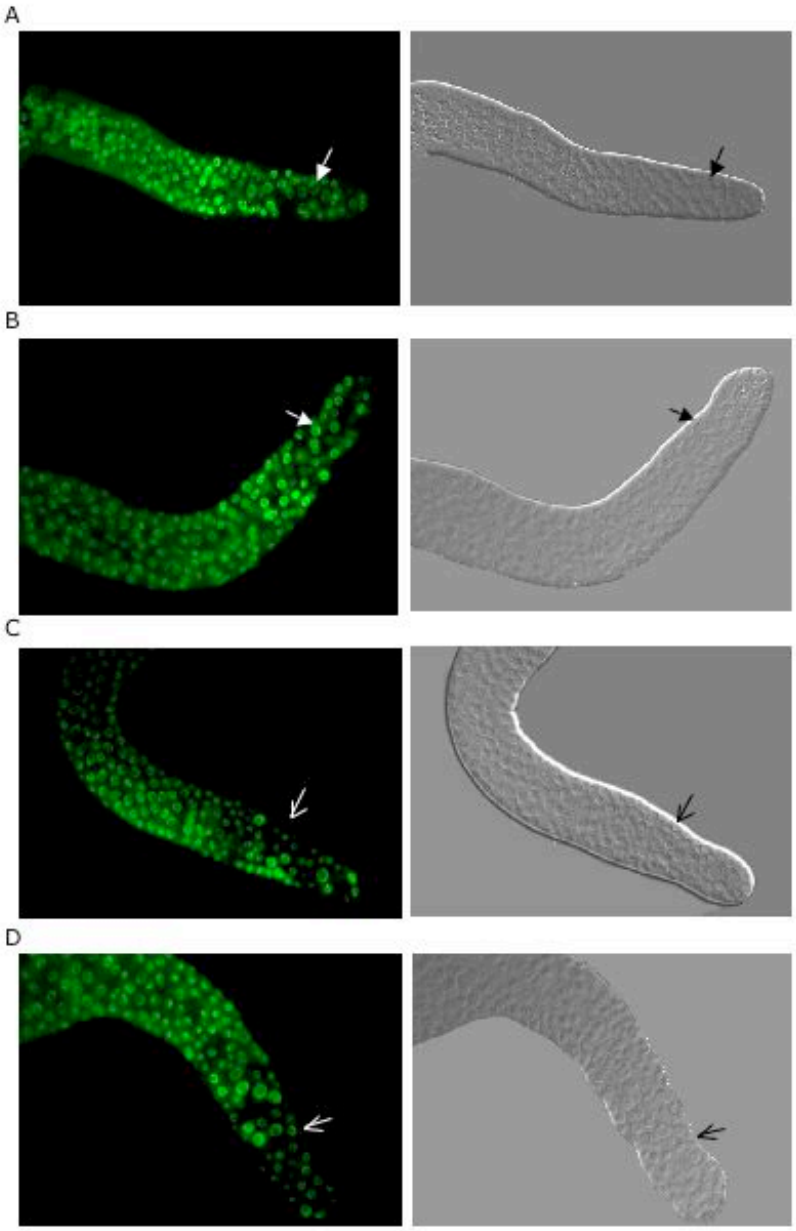
A
B
C
D

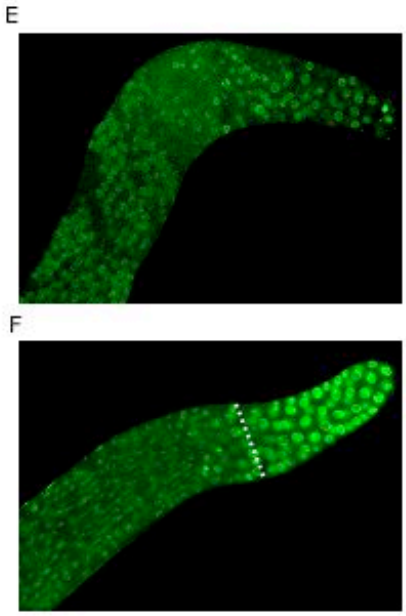

Figure 19. *lin-26* mutants display an abnormal cell cycle arrest phenotype

lin-26 mutant animals carrying a CYB-1::YFP marker (*ga91*;*opIs76*) were either irradiated with 120 Gy of X-rays at the 12 h-post-L4 stage or were left untreated. All nuclei can be visualized by the presence of YFP. Closed arrows represent big nuclei in the non-treated cells (A and B), whereas open arrows represent cells that probably failed to arrest upon treatment (C and D). As a control, animals carrying only the *opIs76* transgene were left untreated (E) or similarly irradiated with 120 Gy (F). Dashed line indicates the border line of the arrested zone.

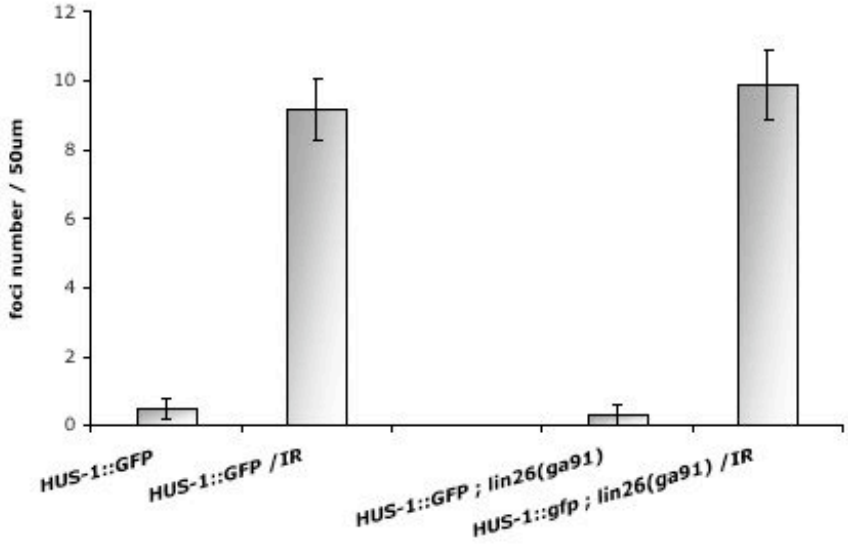

Figure 20. In *lin-26* mutants, DNA damage caused by ionizing radiation is properly sensed by the HUS-1 complex

Young adult wild-type or *lin-26(ga91)* mutant animals expressing HUS-1::GFP (*opIs34*) were irradiated with low doses of X-rays (15 Gy) and proliferating germ cells were scored 8 h later for the appearance of foci formation. Foci were counted in a 50 μm distance from the DTC. Error bars represent SEM.

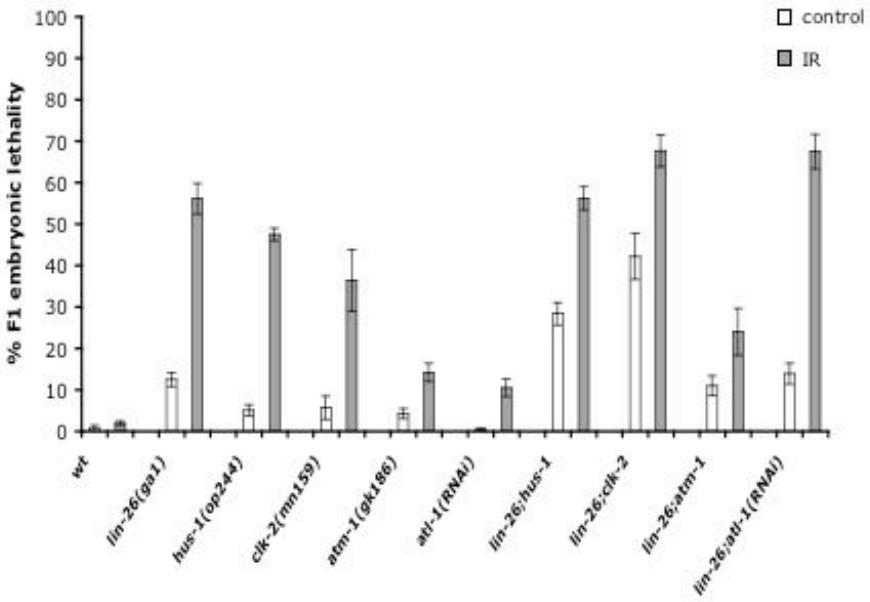

Figure 21. Loss of *lin-26* function results in hypersensitivity upon ionizing radiation and a synthetic lethal phenotype in the absence of HUS-1 and CLK-2, but not ATM-1

Animals at the L4 stage of the indicated genotype were irradiated with 120 Gy or left untreated. After 12 h they were let lay eggs and finally unhatched embryos were counted and expressed as a fraction of the total number laid. Data shown is the average percent lethality of 50 animals for each genotype. Error bars indicate SEM.

CHAPTER 5

GENETIC CONTROL OF UV-INDUCED APOPTOSIS IN THE NEMATODE *C. ELEGANS*

Manuscript under preparation

Preface

To preserve genomic stability it is essential to obstruct the road to cancers. Although cancers are characterized by extreme diversity and heterogeneity, there is a small number of critical steps whose occurrence impels the uncontrolled expansion and invasion: in almost all instances, deregulated cell proliferation and suppressed cell death together provide the underlying platform for cancer progression. Deficiencies in repair mechanisms also contribute to carcinogenesis by creating a permissive environment for genetic instability and accumulation of gene mutations, permitting disobedience of cell cycle checkpoints, which would normally induce apoptosis.

Genetic defects that perturb the mechanisms of checkpoint activation, repair and apoptosis almost invariably cause severe syndromes that are characterized by the degeneration of specific tissues (especially the nervous and immune system), sensitivity to specific DNA-damaging agents and predisposition to cancer.

The ataxia telangiectasia (A-T) disease has long intrigued the research community due to the broad spectrum of defects it encompasses, including neurodegeneration, immune dysfunction, growth and developmental retardation, premature signs of aging, chromosomal instability, radiosensitivity and cancer predisposition. The underlying molecular cause of the disease is mutations in the ATM gene, and the biology beneath dictates defective cellular responses to DNA damage.

This last point is the driving force for researchers to try to understand the fundamental processes of the development of the disease and proceed to exploit them

therapeutically. The conservation of the gene throughout evolution and therefore the immense amount of informational input from different fields is what renders this goal accessible.

I embarked on this project after it became known to the worm community that *C. elegans* possesses an ATM homolog. With so many diverse targets and different partners already known, the network where ATM is involved can only expand. The aim of this study was to unveil the DNA damage signaling cascades, in which the *C. elegans* ATM-1 functions and potentially discover new relationships that might shed light on the full complement of human biology.

Following the manuscript that is under preparation, I present additional data that I generated in order to learn more in the context of ATM-1 signaling and the UV responsive pathway.

Genetic Control of UV-Induced Apoptosis in the Nematode *C. elegans*

Lilli Stergiou, Kimon Doukoumetzidis & Michael Hengartner

Institute of Molecular Biology

University of Zurich

Winterthurerstrasse 190

CH-8057 Zurich, Switzerland

tel.: +41 1 635 3140

fax.: +41 1 635 6861

email: michael.hengartner@molbio.unizh.ch

July, 2005

ABSTRACT

Surveillance mechanisms called checkpoints favor repair processes in case of cellular damage. Failure for the lesions to be restored may trigger apoptosis to eliminate damaged cells. Studies in the model organism *C. elegans* have revealed the presence of DNA damage responses with well-conserved components in mammals. In the current study we report on the existence of a UV apoptotic pathway in the *C. elegans* germline, which is mediated by the p53 homolog and ATL-1 (Ataxia Telangiectasia and Rad3-related). Blockage of the nucleotide excision repair pathway (NER) severely affects the apoptotic response, whereas ATM-1 (Ataxia Telangiectasia mutated) has an assistant role in its proper induction. Interestingly, application of cisplatin and camptothecin, two potent antitumor agents, renders the worms resistant to the apoptotic response when *atm-1* is mutated. Moreover, known checkpoint and repair genes differentially regulate cell cycle arrest and the subsequent death sentence. We conclude that repair components constitute an important determinant for the outcome of DNA damage signaling initiated by the *C. elegans* ATR, based on the induction of UV-induced cell cycle arrest and germ cell death.

INTRODUCTION

Eukaryotic cells preserve their genome integrity by exhibiting a properly regulated response to damaged DNA. Lesions can be naturally occurring as the result of replication errors, oxidative damage by free radicals, endogenous alkylating species, meiotic recombination intermediates or spontaneous alterations in DNA. Otherwise, they might be caused by exogenous factors, such as ionizing radiation, UV light and chemical mutagens.

The cells respond through the action of systems that detect the aberrant DNA structures and trigger the activation of transducers to amplify and diversify the signal by targeting a series of downstream effectors. The output of these responses is the activation of surveillance mechanisms, called cell cycle checkpoints, with which cell cycle is arrested and DNA repair mechanisms are favored.

Nucleotide excision repair (NER) is the major and most flexible repair pathway for the removal of lesions that distort the DNA double helix, including the UV-induced cyclobutane pyrimidine dimers (CPDs) and 6-4 photoproducts (6-4 PPs), as well as adducts produced by the chemotherapeutic agents cisplatin and 4-nitroquinoline oxide (Balajee and Bohr, 2000). The two branches of NER, global genome repair (GGR) and transcription coupled repair (TCR) are initiated somewhat differently but require common enzymatic steps for execution (Prakash and Prakash, 2000, Costa *et al.*, 2003). The NER reaction is carried out by the orchestrated and sequential recruitment of more than 25 factors and key steps include damage recognition, DNA unwinding and damaged strand incision, followed by repair synthesis and ligation. In mammals, XPC initially recognizes DNA distortions and with the help of HR23B recruits the XPB and XPD helicase complex. Damage verification by the XPA-RPA complex

results in continuation of repair (Prakash and Prakash, 2000, Costa *et al.*, 2003, Thoma and Vasquez, 2003) that includes the action of XPF and XPG endonucleases.

Opposed to that and as a sequence of the occurrence of double-strand breaks (DSBs), an alternative repair pathway is activated. Based on the dependence of sequence homology for repair, the main mechanisms involve the error-prone non-homologous-end joining (NHEJ) and the error-free recombinational repair (RR). In the former, recognition of and binding to damaged DNA occurs by the Ku70-Ku80 complex, followed by association with the catalytic subunit, DNA-PKcs. The holoenzyme then activates the ligation process by XRCC4-ligase 4 (Valerie and Povirk, 2003, Dasika *et al.*, 1999). The RR pathway comprises a large number of proteins, including the MRN (Mre11-Rad50-Nbs1) complex for processing of the initial damage and the RAD51 recombinase responsible for homolog pairing and strand exchange after being loaded onto the resected breaks. Several RAD51-associated proteins, the RAD52 DNA single-strand annealing protein and the RAD54 helicase for ATP-dependent DNA unwinding are also involved. The latter one may stimulate the activity of RAD51 by changing the DNA topology (Valerie and Povirk, 2003, Dasika *et al.*, 1999).

Parallel to repair processes, several signaling cascades can be triggered by DNA lesions and members of the PI3 kinase family are major orchestrators in these events (Yang *et al.*, 2003, Shiloh 2001). The ATR and ATM proteins are involved in sensing and processing the presence of certain aberrant DNA structures, formed either naturally during DNA metabolism, or inflicted by exogenous damaging agents. The response to DSBs occurs primarily through ATM, whereas response to both IR- and UV-induced lesions, as well as stalled replication forks occurs via ATR. Having several downstream phosphorylation targets, they can both subsequently activate cell

cycle checkpoints at the G1/S and G2/M boundaries and prevent ongoing DNA synthesis. These events facilitate repair processes, therefore cellular survival. In cases, though, that damage overwhelms the repair capacity of the cell, the death fate is executed to eliminate hazardous or potentially tumorigenic cells.

The physiological importance of the DNA damage response pathways is illustrated in a number of genetic diseases known as "genomic instability syndromes". Ataxia telangiectasia (A-T), that arises when the ATM gene is affected, is a complex genetic disorder inherited in an autosomal recessive manner (Shiloh 2003, Shiloh 1997). Profound defects in neuromotor functions and the immune responses are among the clinical signs of A-T patients. Another hallmark of the disease is the striking predisposition to cancer, lymphomas and lymphoid leukemias in particular, and an increased radiosensitivity to DNA damaging agents. ATR, on the other hand, although absolutely crucial for embryonic development, is not directly linked to a human genetic disorder (Brown and Baltimore, 2000).

Despite our fair understanding about the checkpoint events triggered by ATR and ATM, the mechanism of choice between attempt of survival and programmed cell death is not completely understood. Furthermore, although the already identified ATR and ATM substrates are numerous, the list is not yet saturated, since many ATR/ATM-dependent death processes might involve unknown targets. For these reasons, the establishment of an easily accessible system to dissect these interactions is required. The nematode *C. elegans* is a good model system to study DNA damage responses since it possesses key cell cycle checkpoint genes, like *hus-1* and *clk-2*, as well as the major executioner of apoptosis, p53 (reviewed by Stergiou & Hengartner, 2004). DNA damage responses are restricted in the worm's germline where, so far only ionizing radiation (IR) has been shown to induce both cell cycle arrest and

apoptosis, two responses spatially separated (Gartner *et al.*, 2000). The latter occurs after the exit from pachytene in the meiotic compartment and is dependent on the core apoptotic machinery (CED-3/caspase - CED-4/Apaf1 - CED-9/Bcl-2). For execution it requires the activation of a BH3-only domain-containing protein, EGL-1, which, in turn, is transcriptionally regulated by p53 (Hofmann *et al.*, 2002). Cell proliferation arrest in the mitotic zone is visualized as large nuclei, few in number.

In this work we demonstrate that a UV-induced signaling pathway is also present in *C. elegans* and comprises the already known basic components of the IR pathway, *cep-1*, *hus-1* and *clk-2* and in addition the checkpoint kinase *chk-2*. ATL-1, the *C. elegans* ATR homolog (Ataxia Telangiectasia and Rad3-related), is essential for the execution of UV-induced cell death. We present evidence that components of the NER machinery are required for both cell cycle arrest and apoptosis following UV treatment, presumably by immediate sensing of the damage. ATM-1, the *C. elegans* ATM homolog (Ataxia Telangiectasia mutated), seems also to play an important role in these two processes and further reacts to the UV-mimetic drug cisplatin and the potent antitumor antibiotic camptothecin. Simultaneous loss of ATM-1 and the NER damage recognizing factor, XPA-1, appears to affect the recombinational repair steps initiated upon UV damage processing. Our results establish the action of repair components as a requirement for the initiation of ATR/ATM signaling cascade triggered by UV and *C. elegans* as a valid system to unveil complexities of the DNA damage signaling network.

RESULTS

UV-C radiation induces apoptosis in the *C. elegans* germline, via transcriptional activation of *egl-1* and *ced-13* and dependent on conserved checkpoint genes

The effects of DNA damage in the *C. elegans* germline have been previously described as being part of a cell arrest and an apoptotic response (Gartner *et al.*, 2000). To study the potential role of UV radiation as a source of damage and subsequent inducer of DNA damage signaling, we used different doses of UV-C light (254nm) and measured the apoptotic events in the wild-type animal's germline. We observed a gradual, though not linear, increase in the number of apoptotic corpses after the exit from pachytene zone, an effect similar to that of ionizing radiation (Fig. 1a, b). The apoptotic response was further followed up in a time course after exposure to 100 J/m^2 of UV-C radiation. As is the case with X-rays, the number of apoptotic corpses increases over time (Fig. 1c).

An important element of the apoptotic DNA damage response in *C. elegans* is the transcriptional activation of *egl-1* and *ced-13*, the two genes coding for the BH3-only domain proteins. This HUS-1 and CEP-1-dependent process is what triggers the increased germ cell apoptosis following ionizing radiation (Hofmann *et al.*, 2002). We tested whether UV-induced apoptosis proceeds via the same manner by measuring the change in the mRNA levels of *egl-1* and *ced-13* by real-time Q-RT-PCR (Fig. 1d). Both genes are transcriptionally upregulated following treatment with UV, yet in a less prominent degree compared to IR.

IR-induced cell death in the *C. elegans* germline requires the p53 homolog, *cep-1* (Derry *et al.*, 2001, Schumacher *et al.*, 2001), and the checkpoint genes *hus-1*, *mrt-2* and *clk-2* (Gartner *et al.*, 2000, Hofmann *et al.*, 2002, Ahmed *et al.*, 2001). To investigate whether these well-conserved components in the DNA damage signaling cascade mediate the observed apoptotic response, we scored the respective mutants for germline apoptosis following UV radiation. Whereas loss of *cep-1* and *clk-2* completely abrogated UV-induced cell death (Fig. 1e), absence of *hus*-1 or *mrt-2* severely compromised this response (Fig. 1f).

In our effort to gain insight into the UV responsive pathway in *C. elegans*, we turned our attention to the checkpoint kinase CHK-2. In mammals Chk2 is known to activate p53 to induce apoptosis upon genotoxic stress (Hirao *et al.*, 2002). In worms *chk-2* mutants retain a functional IR-induced checkpoint, yet are defective for the pachytene checkpoint in response to RAD-51 depletion (MacQueen and Villeneuve, 2001). Based on this differential behavior and the different nature of damage elicited by UV, we tested two known alleles of *chk-2* for their apoptotic response. Whereas IR caused an increase in cell death indistinguishable from wild-type confirming previous data, UV failed to cause such an effect (Fig. 1g). Our findings place CHK-2 in the UV responsive pathway most probably conveying the UV generated signal to CEP-1. Whether the latter is a direct target of CHK-2 remains to be elucidated.

ATL-1, the *C. elegans* ATR homolog, is necessary to activate UV-induced germ cell apoptosis

Eukaryotic cells respond to DNA damage with a rapid activation of cell cycle checkpoints that are initiated at the ATR and ATM protein kinase level (Shiloh 2001). We wanted to test whether apoptosis in the *C. elegans* germline can be the output originating from the activation of these kinases. We used a strain that bears an insertion/deletion of 700 nt in the 10.5 kb *atl-1* ORF, resulting in no mRNA transcript and most likely being a null (Supplementary Fig. 2b). The strain is kept balanced due to a maternally rescued embryonic lethal phenotype. We measured the induction of germ cell death upon UV both in homozygous and heterozygous for the mutation animals, and found that they completely lack UV-induced apoptosis (Fig. 2a). Following treatment with ionizing radiation we observed a similar defect (Fig. 2b), suggesting that ATL-1 is necessary for DNA damage-induced germ cell death in worms. We excluded the possibility that the defect is due to the balancing chromosome since *atl-1(tm853)*/+ animals appear to have the same defect (Fig. 2c). We examined the possibility for this phenotype to be either a dominant negative or a haploinsufficient phenotype by scoring worms that carry different deletions in the *atl-1* locus (*sDf29*/+ and *mDf1*/+) and obtained the same with the heterozygotes phenotype. This result suggests that *atl-1* is haploinsufficient for the induction of DNA damage-induced apoptosis in *C. elegans.*

We anticipated that the transcriptional induction of *egl-1* and *ced-13* would be similarly abrogated in the *atl-1(lf)*. Figure 2d shows the fold-change in the mRNA levels in both heterozygotes and homozygotes *atl-1(tm853)* mutants. Indeed, the lack

of activation of the two BH3 domain-bearing genes reflects the death phenotype and the haploinsufficiency of *atl-1*.

UV-induced apoptosis relies on ATM-1, the *C. elegans* ATM homolog

Whereas mammalian ATR responds primarily to UV or stalled replication forks, ATM reacts mainly to double-strand breaks (Shiloh 2001). We used a mutant strain that carries a 550 nt deletion in the 4.9 kb *atm-1* ORF, which gives rise to a truncated transcript, although resulting in a premature stop codon if translated (Supplementary Fig. 2a). Since the kinase domain is downstream of the deleted part, we infer that the mutant is likely a null. Following treatment with X-ray ionizing radiation *atm-1(gk186)* mutants show a normal death response that is dose-dependent (Fig. 3b). After a dose response analysis upon UV, the animals fail to respond with the same wild-type levels of death (Fig. 3a). The observed partial defect is not a time point specific effect but the mutants' response is compromised during the course of time, with the number of corpses being reduced to nearly half (Fig. 3c). Moreover, both the short-term and the long-term apoptotic response is affected in the *atm-1(gk186)* mutants, as indicated by the time course performed in short intervals (Fig. 3c). Our results reveal an involvement of ATM-1 in UV-triggered cell death.

To determine whether UV and IR affect the transcriptional activation of *egl-1* and *ced-13* in the *atm-1(lf)* we measured the fold-change in their mRNA levels (Fig. 3d). As expected, there is no effect in the induction of either genes following X-rays. Upon UV treatment *ced-13* induction is reduced by 7-fold, whereas *egl-1* levels

remain largely unaffected, suggesting that ATM-1 preferentially channels its activity into *ced-13*.

Drug-induced apoptosis requires ATM-1 in *C. elegans*

We further documented the role of ATM-1 in responding to the same type of lesions that UV radiation causes by treating worms with cisplatin, one of the most potent antitumor agents. Cisplatin interacts with DNA and forms adducts mainly intrastrand and to a lesser degree interstrand crosslinks (Monjardet *et al.*, 2002), which are thought to be eliminated by the nucleotide excision repair machinery (NER) (Siddik *et al*). Wild-type worms fed with the drug display an apoptotic response that gradually increases over time, while *atm-1(gk186)* mutants fail to respond (Fig. 3e). If so, the death levels are somewhat lower, implying an impact of the drug on the proliferation rate of germ cells. Therefore, we were able to mimic the UV damage with a chemotherapeutic drug that does not cause double strand breaks *per se*.

Camptothecin, on the other hand, inhibits DNA relaxation by topoisomerase I, by stabilizing the enzyme on DNA in a cleavable complex (Thomas *et al.*, 2004). Both such cleavage complexes and UV lesions lead to replication- and transcription-mediated DNA damage (Pommier 2004). We, therefore, studied the effect of camptothecin on *atm-1(gk186)* mutants. Wild-type worms exposed to the drug show an increase in germ cell apoptosis over time, a response that is abrogated in the mutants (Fig. 3f). This finding implicates the protein in the sensing and/or signaling of a well-defined set of lesions that block the replication process or interfere with chromatin structure.

Conversely, EMS is known to cause base methylation, a single base modification that would require the base excision repair components to be fixed (Christmann *et al*, 2003). Treating wild-type worms with two different concentrations of the agent gives a strong apoptotic response that can be also observed in the case of *atm-1(gk186)* mutants (Fig. 3g). Our results predispose the involvement of a certain damage recognition process by the respective repair components before the actual cell death decision is taken.

ATM-1 is involved in repair of endogenous and exogenous damage

With the assumption that ATM-1 might be required for the recognition of a certain type of lesions, we speculated that it might also be involved in the equivalent repair process. We tested that by looking at the formation of HUS-1::GFP foci, which has been previously shown to represent sites of damage and/or ongoing repair (Hofmann *et al.*, 2002). Although in wild-type worms the number of foci in the mitotic zone of the germline is kept low, in a loss of *atm-1* situation the levels are increased, suggesting that endogenous damage occurs more often in *atm-1(gk186)* mutants (Supplementary Fig. 1a). Upon exogenous damage by UV or IR there is no further increase in the number of foci, presumably either due to a saturation effect or because ATM-1 is required for the activation of such repair processes. Alternatively, ATM-1 could be necessary for the stability of these complexes on chromosomes.

Moreover, we performed progeny survival studies to show that *atm-1(gk186)* mutants have moderate levels of embryonic lethality and an increased sensitivity to UV by displaying around 30% lethality (Supplementary Fig. 1b). The latter effect could again be explained by the inability to deal with additional damage.

Simultaneous loss of the *hus-1* and *clk-2* checkpoint genes under normal conditions gives rise to a synthetic lethal phenotype, reaching the levels of 80% and 50%, respectively. This phenomenon implies that possible genetic interactions might exist between proteins or pathways to ensure proper repair in the germline.

The nucleotide excision repair (NER) machinery is required for triggering UV-induced cell death

The DNA damage response occurs by transduction of the damage signal to the cell cycle checkpoints, as well as the DNA-repair machinery. In fact, the combination of the two can be proven protective for the cell in cases of low levels of damage. Because of the induction of apoptosis in our system as a result of genomic injury, we hypothesized that recruitment of repair components might precede and activate the cell death process.

We started by testing components of the NER machinery and more specifically the *C. elegans* homologs for the mammalian XPC and XPA damage recognition proteins, to assess the induction of death upon UV.

xpc-1(ok734) mutants carry a deletion that removes 1.7 kb of an intron, so a transcript of the right size is detectable in the mutant, though it's less abundant (Supplementary Fig. 2d). In this genetic background, the levels of UV-induced cell death are reduced by half, whereas IR-induced cell death occurs normally (Fig. 4a). We believe that the apoptotic defect in the first case is due to a defect in the UV damage recognition process, probably a requirement to initiate cell death. On the other hand, the eukaryotic XPC is known to be implicated in only one of the two branches of the NER pathway, serving as a recognition factor for the global genome

repair (GGR) (Costa *et al.*, 2003). That could probably explain the reduction we observed.

The *xpc-1* defect is strongly reinforced by the apoptotic behavior of the *xpa-1(ok698)* mutants. *xpa-1* mutants carry a deletion that removes half of the ORF, resulting in no mRNA transcript and most likely being a null (Supplementary Fig. 2e). It was previously shown that *xpa-1* mutants exhibit a hypersensitive phenotype at all developmental stages and a growth arrest upon UV (Park *et al.*, 2002, Astin *et al.*, 2004). UV-induced apoptosis is completely abolished in the absence of XPA-1 (Fig. 4b), consistent with the hypothesis that lack of proper damage recognition can disturb the signal to the apoptotic machinery. Notably, the mutants have elevated death levels before the treatment with UV (Fig. 4b), presumably due to accumulation of endogenous damage. Lack of the ability to repair this damage could result in the spontaneous activation of cell death in *xpa-1* mutants. Simultaneous loss of ATM-1 in this mutant background restores death to normal levels, suggesting that each one of these proteins is sufficient to activate apoptosis in the presence of unrepairable intrinsic damage, but both are necessary for this step. Moreover, upon UV treatment the apoptotic defect still persists in the *atm-1(gk186) xpa-1(ok698)* mutant animals (Fig. 4b).

In contrast to UV, IR-induced apoptosis still occurs in the absence of XPA-1, although with somewhat reduced levels compared to the wild-type (Fig. 4c). This could be the consequence of X-rays not being a clean source of double strand breaks, rather than causing a broad variety of lesions. Our results confirm the connection between the defect upon UV with the nature of lesion inflicted and failed to be detected by the NER factors.

In agreement with the pro-apoptotic role of *xpa-1*, the protein is present in the germline, with a higher intensity in the meiotic nuclei. Figure 4d shows expression of a low-copy integrated transgene carrying GFP fused to the *xpa-1* coding sequence. The expression pattern does not change significantly upon treatment with UV, apart from a slight increase in the mitotic zone (data not shown), probably because the protein is not regulated at the translational level.

Cell cycle arrest upon UV requires a distinct but overlapping with IR set of genes

DNA repair pathways can be facilitated in the removal of lesions when followed by cell cycle arrest. After exposure to IR, proliferation of mitotic nuclei in the *C. elegans* germ line tissue also ceases and the size of the cells becomes larger (Gartner *et al.*, 2000). We assessed the effect of UV on cell cycle progression by measuring the number of nuclei in a certain volume of the mitotic compartment. Similar to the IR case, wild-type animals arrest proliferation, whereas the *hus-1(op244)* and *clk-2(mn159)* checkpoint mutants fail to do so (Fig. 5). In contrast to that, *cep-1(gk138)* mutants known not to mediate the arrest response upon IR (Derry *et al.*, 2001) were found to be required for UV-induced cell cycle arrest (Fig. 5). This behavior is also shared by the checkpoint kinase *chk-2*, consistent with the apoptotic results, placing both proteins in the same pathway mediating the UV response in *C. elegans*. Similarly, *atm-1* falls into the above group, where it is wholly responsible for the cell proliferation arrest. On the other hand, *atl-1(tm853)* mutants seems to follow the wild-type pattern, where arrest can occur upon treatment with both IR and UV radiation (Fig. 5). Moreover, mutants for *atm-1* and *atl-1* kinases have a functional intra-S

checkpoint (data not shown). When tested with hydroxyurea, a drug that depletes the deoxynucleotide pool and DNA synthesis is inhibited, premeiotic nuclei arrest normally like in wild-type animals. Last, *xpa-1* belongs to the already described pathway that mediates cell cycle arrest upon UV, but not following IR.

RAD-51 accumulates in mitotic nuclei upon UV in an ATM-1- and XPA-1-dependent manner

The RAD-51 protein is required for homolog pairing and DNA strand exchange during recombinational repair (Baumann & West, 1998 and Alpi *et al.*, 2003). We postulated that a fraction of the UV lesions would be converted to double-strand breaks during processing by the NER machinery (Bessho *et al.*, 1997, Galli & Schiestl, 1999, Dunkern & Kaina, 2002). In such a case, RAD-51 would be detected on the chromatin of mitotic nuclei following UV radiation. Indeed, multiple foci appear in the germline of wild-type treated animals (Fig. 6a). The foci are still present in an *atm-1* mutant background, making the ATM-1 protein redundant for the loading of RAD-51 onto sites of double strand breaks.

In accordance with this conclusion, *atm-1(gk186)* mutants do not suppress the enhanced apoptosis conferred by loss of *rad-51* function (Fig. 6b). The combination of the two loss-of-function situations rather has an additive effect in the apoptotic induction. We conclude that, the potent role of RAD-51 in initiating repair of double-strand breaks arising from processed UV lesions is uncoupled from its role in resolving meiotic recombination intermediates.

Similarly, elimination of the XPA-1 protein does not influence the appearance of UV-induced foci either (Fig. 6a). When, on the other hand, both proteins are absent in

the *atm-1(gk186) xpa-1(698)* background, we can detect virtually no foci. This presumably assigns a cooperative role to the nucleotide excision repair components and to ATM-1 in transducing the signal downstream to the double strand break repair machinery.

Recombinational repair (RR) can occur following the induction of UV damage

The analysis with components of the NER machinery revealed a link with ATM-1 and a role for both sides to initiate a signaling process that would require the presence of RAD-51 (Fig. 6a). Since the recombinational repair pathway is the main mechanism responsible for the removal of double strand breaks, we assessed a potent connection with the some of its components.

We chose to examine the response of mutants lacking RAD-54, the human counterpart of which is known to functionally interact with Rad51 during recombinational repair. Both human and yeast proteins possess DNA-dependent ATPase activity that stimulates strand exchange by modifying the topology of breaks (Petukhova *et al.*, 1998, Jaskelioff *et al.*, 2003). For this study we used a strain that bears an insertion/deletion of about 1 kb including the start codon, resulting in no mRNA transcript and most likely being a null (Supplementary Fig. 2f). The strain is kept balanced due to a maternally rescued embryonic lethal phenotype. *rad-54(ok615)* mutants exhibit a strong increase in germ line apoptosis (Fig. 7a), which we could also phenocopy with RNAi (Fig. 7b). This death is *cep-1*-dependent, suggesting that it is induced by DNA damage. Moreover, by knocking down the enzyme generating the double strand breaks during recombination, SPO-11 (Roeder, 1997), this death is

alleviated, suggesting that it is due to the accumulation of recombination intermediates (Fig. 7b).

Application of exogenous damage in the form of X-rays failed to further increase the death levels in *rad-54(ok615)*, consistent with our hypothesis that inactivation of repair factors constitute a negative parameter for the initiation of the death process. In agreement with this argument, application of UV radiation had no effect on the initial levels of death (Fig. 7c), strongly implying that recombination takes place after the induction of UV lesions. To exclude the possibility that the lack of further increase is due to a saturation effect from the apoptotic corpses in the germline, we performed the same experiment in the absence of SPO-11. *spo-11(ok79)* mutants respond normally to both stimuli, demonstrating their ability to respond to additional damage caused in their genomes (Fig. 7d). Simultaneous loss of *rad-54* function impairs this response, an effect that is stronger in the case of UV.

Interestingly, both the *atl-1(tm853)* and the *atm-1(gk186)* mutations suppressed the *rad-54* inactivation-dependent apoptosis (Fig. 7e), suggesting that the two kinases are required to trigger apoptosis upon unrepaired DNA damage resulting from the recombinational repair process. This likely places ATM-1 and ATL-1 upstream of a signaling cascade that leads to the resolution of recombination intermediate structures.

CEP-1 protein levels change upon UV radiation in an ATL-1-dependent manner

It is well established that the p53 tumor suppressor is a tightly regulated protein that acts by arresting cell cycle and triggering apoptosis. Upon genotoxic stress it is subject to post-translational modifications, which result in its stabilization,

accumulation and activation in the nucleus (Bode & Dong, 2004). We used a worm specific antibody against the *C. elegans* p53, CEP-1 (Schumacher *et al.*, 2005), to investigate whether the protein is post-translationally altered upon UV treatment (Fig. 8). In the wild-type animals we observed an increase in the amount of protein, which was even more pronounced in the *atm-1(gk186)* mutants, suggesting that either protein translation rates increase or the protein is stabilized. In both *xpa-1(ok698)* and *atm-1(gk186) xpa-1(ok698)* mutant animals the effect of UV radiation on protein amount changed only slightly, despite the *in vivo* data about complete lack of UV-induced apoptosis in these genetic backgrounds. We assume that the change in the protein levels is not sufficient to induce cell death. Minor changes in the CEP-1 levels were also observed in the *chk-2(gk212)* mutants, probably due to input coming from proteins upstream of CHK-2. However, there was no difference in the CEP-1 protein levels between the control and the UV-treated *atl-1(tm853)*/nT1 mutant animals. This is consistent with the requirement of ATL-1 for the UV-mediated cell death and renders it the sole apoptotic regulator for CEP-1 induction. We predict that this might account for the abundance of the CEP-1 protein levels in a loss of ATM-1 function situation (Fig. 8).

DISCUSSION

The power of *C. elegans* as a system to genetically identify proteins that regulate apoptosis has been well established (reviewed by Kinchen & Hengartner, 2004). Recent analyses have also identified a conserved checkpoint pathway that mediates the DNA damage signal to the cell death machinery (Gartner *et al*., 2000). However, these studies have been restricted to ionizing radiation as the sole source of genotoxic stress, therefore hampering further identification of critical factors involved.

In the present study we show that UV is an alternative way to induce DNA damage responses in the germline of *C. elegans*, both in the form of cell cycle arrest and apoptosis. We have managed to mimic the nature of damage with the application of the chemotherapeutic agent, cisplatin, to which worms react in a similar way, making it a promising model for the testing and development of chemical drugs.

We were able to show that a primary initiator of the DNA damage responses in mammals, ATR, is the major player in responses upon both UV and IR in *C. elegans*. ATL-1 is the factor that influences the decision of a cell to undergo apoptosis in case of excessive existing damage. Interestingly, animals that are devoid of one wild-type copy of the *atl-1* gene respond with the same kinetics to UV as the homozygote mutants. This might be implicative of the mode of ATL-1 function. For instance, the mammalian ATM was shown to be activated through an alteration in its oligomerization status by an *in trans* phosphorylation event (Bakkenist & Kastan, 2003). Very recently, though, accumulating evidence indicates that DNA breaks are sensed directly by the MRN complex, which binds DNA, unwinds the ends, recruits

ATM, and dissociates the ATM dimer to activate it (Lee & Paull, 2005). Such a mode of activation for ATR has not been proven yet to occur. It has been reported, though, that ATR is associated with moderate affinity with a smaller protein called ATRIP and certain functions of the former are stimulated by that interaction (Cortez *et al.*, 2001, Kacmaz & Sancar, 2004). Our observations for such a dosage effect could be the consequence of any of the above possibilities.

However, there are intriguing differences in the cellular reactions regarding the activation of checkpoints stemming from ATL-1 kinase. It seems that its role in imposing a cell proliferation arrest, in any of the boundaries of the cell cycle phases, is dispensable. Likewise, we could not specify a function for it in the intra-S phase checkpoint, a role that would fit more with the involvement of a protein in sensing stalled replication fork-induced damage. Our results, though, point to the ATM homolog in worms for a checkpoint activator. In contrast to the IR case, cell cycle arrest is abolished in the *atm-1* mutants upon induction of UV damage. Following the same pattern, animals lacking homologs of both the transcription factor p53 and Chk2 kinase, which are known to phosphorylate cell cycle components and influence the outcome of cell cycle progression in mammals, are also defective. This differential behavior sheds some light on the identity of the UV pathway, which is distinct from the branch that is activated upon ionizing radiation.

Of great interest, though, is the observation that ATM-1 is involved in repair of cellular damage, either endogenous or exogenously inflicted. The engagement of ATM-1 in this task was documented by the finding that numerous damaged sites exist in the genomic background of *atm-1* mutants under normal conditions. In addition,

the synthetic embryonic lethal phenotype observed during the simultaneous loss of other checkpoint genes, like *hus-1* and *clk-2*, reveals potential genetic interactions to maintain genome integrity.

Regarding apoptosis, on the other hand, ATM-1 appears to have an assistant role or be partially involved in the UV signaling that culminates in the elimination of the cell. Notably, its absence leads to a complete defect following treatment with the antitumor agents cisplatin and camptothecin. The cytotoxicity of cisplatin is primarily ascribed to its interaction with nucleophilic sites of purine bases to form DNA–protein and DNA–DNA interstrand and intrastrand crosslinks. Interstrand diadducts is an abundant and the primary cytotoxic form of lesion, capable of terminating DNA synthesis (Siddik 2003, Chaney & Sancar, 1996). The mechanism of camptothecin action involves the inhibition of DNA relaxation by DNA topoisomerase I, and more specifically the stabilization of a covalent binary DNA–topo I complex. Its S-phase cytotoxicity is therefore attributed to cessation of DNA synthesis and double-strand breakage when the replication fork encounters such a site (Thomas *et al*., 2004). Although the two damaging agents obviously belong to different classes of chemotherapeutics, the common response of ATM-1, along with its role in UV signaling, raises the issue of selective substrate specificity in response to different genotoxic stimuli. Whether it is the different adducts themselves or some intermediate or ultimate processed damage structures these cause that triggers cell death, still has to be elucidated.

This study revealed that the repair system largely determines the outcome of DNA damage signaling concerning the induction of germ cell death. A component of the

nucleotide excision repair machinery, the XPA-1 damage recognition factor, was found to be expressed in the death sensitive zone of the pachytene region of meiotic nuclei. Both XPA-1 and XPC-1 damage binding proteins are required for the activation of apoptosis following UV, but not IR. Whether the initial sensing of the lesion or the relay of an already sensed signal is performed by repair factors remains to be determined. In humans, NER protects DNA against the mutagenic effects of carcinogens and UV, and individuals with a hereditary defect in this system suffer from xeroderma pigmentosum (XP) with a marked incidence of skin cancer (Mitchell *et al*., 2003, de Boer & Hoeijmakers, 2000). Generating mouse models for this human disease has been proven helpful as to studying cancer predisposition, but not thorough. Since certain aspects of NER are considerably different between rodents and humans (Hanawalt 2003) and since certain mammalian NER genes give rise to a lethal phenotype when mutated (de Boer 1999), alternative model organisms should emanate. *C. elegans* seems to possess all the factors required for a functional NER system. Regardless the absence of the disease from worms, our results implicate the UV-inflicted or some type of spontaneous damage in such a biological context that requires NER factors to either repair it or lead the damaged cell to death.

Our findings also make it clear that recombinational repair (RR) factors are activated upon UV-induced damage. Indeed, interstrand crosslinks (ICLs) processing is likely to be initiated during replication when the fork progression is stalled, and elimination of the lesions occurs via the combined actions of excision repair and recombination systems (McHugh *et al*., 2001, de Silva *et al*., 2000). The engagement of the RR pathway after the induction of UV damage in *C. elegans* would also explain the partial involvement of HUS-1 and MRT-2 protein complex in the induction of cell death, to deal with this subset of lesions. Here we showed that *rad-54* recombination

mutants exhibit high levels of germline apoptosis under normal conditions. We suspect that the lack of the ability to proceed with damage fixation results in a high susceptibility towards cell death. The lack of further increase upon additional damage caused either by UV or IR treatment strongly implies that recombinational repair activation is a prerequisite for cell death initiation, presumably by presenting strong signals to the death apparatus. Underlying these results, disruption of homologous recombination genes like Rad54 and Rad51 paralogs in yeast and chicken cells, leads to a dramatic decrease in the frequency of spontaneous and psoralen- or mitomycin C-induced recombination events, respectively (Sasaki *et al.*, 2004, Saffran *et al.*, 2004). Moreover, significant levels of lethality were observed in such chicken DT40 mutant cells or in CHO lines mutated for the XRCC2 and XRCC3 recombinational repair components (de Silva *et al.*, 2000, Saffran *et al.*, 2004). The activation of the RR pathway in *C. elegans* as a consequence of a specific type of lesions caused by UV is reinforced by the focal appearance of RAD-51 on damaged chromosomal sites. Neither disruption of the NER activity in the *xpa-1* mutants, nor the absence of ATM-1 alters the foci pattern formation. Contrariwise, elimination of both functions results in the disappearance of RAD-51 from the affected sites. This observation can either be explained by the hypothesis that ssDNA invasion is unable to occur in the first place, or that the protein stabilization on the sites of damage is too low. Alternatively, it might be that an upstream step of complex assembly, for instance, is compromised in the double deficiency. At the moment we can only support that ATM-1 together with XPA-1 have a leading role in transducing the signal downstream, for the RR completion to occur.

A common nominator in the two repair processes described so far is the ability of a cell to die that gets compromised when critical repair factors are missing. The apoptotic potential is translated into CEP-1 activation and subsequent death triggering. Upon DNA damage, mammalian p53 is subject to a number of post-translational modifications that influence its transactivational capacity (Bode & Dong, 2004). Phosphorylation is a common way to increase protein stability and lead to accumulation in the nucleus. Using an anti-CEP-1 antibody we could show a change in the pattern of the worm homolog upon UV treatment, in terms of either increased protein synthesis or protein stability. Even in the absence of critical factors of the pathway, such as in mutants for *xpa-1*, *atm-1*, *chk-2* and the combination of the first two, the CEP-1 protein status is altered to a, however, different extent. This is in part in contrast with the complete or partial lack of death observed in these mutant backgrounds, but could be justified by the redundancies expected to be present: the same p53 site is phosphorylated by several different protein kinases and distinct protein kinases also phosphorylate several sites on p53. Elsewise, multiple and well-orchestrated actions of several factors are necessary for a proper CEP-1 activation. In the *atl-1* mutant animals, however, the protein status remains the same, placing ATL-1 at the upstream end of the UV pathway.

In spite of the complexities encountered in the DNA damage signaling, charged with all the extensive crosstalk among the numerous processes operated by a cell to ensure propagation and continuation, the biological outcome is relatively simple in its layout. The results of this study expand the current knowledge on DNA damage responses in *C. elegans* and set up the ground for succeeding efforts. The identification of an intrinsic interplay between repair factors and death components

might facilitate the understanding of the interplay between molecular factors that either promote death of the cancer cell or survival and resistance acquisition. Many genes responsible for maintaining genome stability have been identified over the last years. Some of these are linked to human cancers and often function in evolutionarily conserved biological pathways (Shiloh 2003, Bernstein *et al.*, 2002). Using *C. elegans* as a model organism to dissect fundamental processes as such would help define the signaling networks underlying defective DNA damage responses. Furthermore, the use of already established agents towards the treatment of cancer diseases in a system like *C. elegans* and the accomplishment of the desirable outcome provides a promising field for drug research. Development and testing of chemical compounds for potent chemotherapeutics might become a fast reality since new branches and interconnecting points are currently emerging.

REFERENCES

1. Balajee, A.S. & Bohr, V.A. Genomic heterogeneity of nucleotide excision repair. *Gene* **250(1-2)**, 15-30 (2000).

2. Prakash, S. & Prakash, L. Nucleotide excision repair in yeast. *Mutat Res.* **451(1-2)**, 13-24 (2000).

3. De Silva, I.U., McHugh, P.J., Clingen, P.H. & Hartley, J.A. Defining the roles of nucleotide excision repair and recombination in the repair of DNA interstrand cross-links in mammalian cells. *Mol. Cell. Biol.* **20**, 7980–7990 (2000).

4. Costa, R.M.A., Chigançcas, V., Galhardo, R., Carvalho, H., Menck, C.F.M. The eukaryotic nucleotide excision repair pathway. *Biochimie* **85**, 1083–1099 (2003).

5. Thoma, B.S. & Vasquez, K.M. Critical DNA damage recognition functions of XPC-hHR23B and XPA-RPA in nucleotide excision repair. *Mol. Carcin.* **38**, 1-13 (2003).

6. Valerie, K. & Povirk, L.F. Regulation and mechanisms of mammalian double-strand break repair. *Oncogene* **22**, 5792–5812 (2003).

7. Dasika, G.K., Lin, S-C.J., Zhao, S., Sung, P., Tomkinson, A. & Lee, E.Y-H.P. DNA damage-induced cell cycle checkpoints and DNA strand break repair in development and tumorigenesis. *Oncogene* **18**, 7883-7899 (1999).

8. Yang, J., Yu, Y., Hamrick, H.E. & Duerksen-Hughes, P.J. ATM, ATR, and DNA-PK: initiators of the cellular genotoxic stress responses. *Carcinogenesis* **24(10)**, 1571-1580 (2003).

9. Shiloh, Y. ATM and ATR: networking cellular responses to DNA damage. *Curr. Opin. Genet. Dev.* **11**, 71-77 (2001).

10. Shiloh, Y. ATM and related protein kinases: safeguarding genome integrity. *Nat. Rev. Cancer* **3(3)**, 155-168 (2003).

11. Shiloh, Y. Ataxia-telangiectasia and the Nijmegen breakage syndrome: related disorders but genes apart. *Annu. Rev. Genet.* **31**, 635-662 (1997).

12. Brown, E.J. & Baltimore, D. ATR disruption leads to chromosomal fragmentation and early embryonic lethality. Genes Dev. **14(4)**, 397-402 (2000).

13. Stergiou, L. & Hengartner, M.O. Death and more: DNA damage response pathways in the nematode *C. elegans*. *Cell Death Differ.* **11**, 21–28 (2004).

14. Gartner, A., Milstein, S., Ahmed, S., Hodgkin, J. & Hengartner, M.O. A conserved checkpoint pathway mediates DNA damage--induced apoptosis and cell cycle arrest in *C. elegans*. *Mol. Cell* **5**, 435-443 (2000).

15. Hofmann, E.R., Milstein, S., Boulton, S.J., Ye, M., Hofmann, J.J., Stergiou, L., Gartner, A., Vidal, M. & Hengartner, M.O. *Caenorhabditis elegans* HUS-1 is a DNA damage checkpoint protein required for genome stability and EGL-1-mediated apoptosis. *Curr. Biol.* **12**, 1908-1918 (2002).

16. Derry, WB., Putzke, AP. & Rothman, JH. *Caenorhabditis elegans* p53: role in apoptosis, meiosis, and stress resistance. *Science* **294**, 591-595 (2001)

17. Schumacher, B., Hofmann, K., Boulton, S. & Gartner, A. The *C. elegans* homolog of the p53 tumor suppressor is required for DNA damage-induced apoptosis. *Curr. Biol.* **11**: 1722-1727 (2001).

18. Ahmed, S., Alpi, A., Hengartner, M.O. & Gartner, A. *C. elegans* RAD-5/CLK-2 defines a new DNA damage checkpoint protein. *Curr. Biol.* **11**, 1934-1944 (2001).

19. Ahmed, S. & Hodgkin, J. MRT-2 checkpoint protein is required for germline immortality and telomere replication in C. elegans. *Nature* **403**, 159-164 (2000).

20. Hirao, A. *et al.* Chk2 is a tumor suppressor that regulates apoptosis in both an ataxia telangiectasia mutated (ATM)-dependent and an ATM-independent manner. *Mol. Cell Biol.* **22(18)**, 6521-32 (2002).

21. MacQueen, AJ. & Villeneuve, AM. Nuclear reorganization and homologous chromosome pairing during meiotic prophase require *C. elegans chk-2*. *Genes Dev.* **15**, 1674-1687 (2001).

22. Monjardet-Bas, V., Chottard, J.C. & Kozelka, J. Fast interstrand cross-linking of cisplatin-DNA monoadducts compared with intrastrand chelation: a kinetic study using hairpin-stabilized duplex oligonucleotides. *Chemistry* **8(5)**, 1144-50 (2002).

23. Siddik, Z.H. Cisplatin: mode of cytotoxic action and molecular basis of resistance. *Oncogene* **22**, 7265-7279 (2003).

24. Thomas, C.J., Rahier, N.J. & Hecht, S.M. Camptothecin: current perspectives. *Bioorg. Med. Chem.* **12**, 1585-1604 (2004).

25. Pommier, Y. Camptothecins and topoisomerase I: a foot in the door. Targeting the genome beyond topoisomerase I with camptothecins and novel anticancer drugs: importance of DNA replication, repair and cell cycle checkpoints. *Curr Med Chem Anti-Canc Agents* **4(5)**, 429-34 (2004).

26. Christmann, M., Tomicic, M.T., Roos, W.P., Kaina, B. Mechanisms of human DNA repair: an update. *Toxicology* **193**, 3–34 (2003).

27. Park, H.K., Yook, J.S., Koo, H.S., Choi, I.S. & Ahn, B. The *Caenorhabditis elegans* XPA homolog of human XPA. Mol Cells. **14(1)**, 50-5 (2002).

28. Astin, J., O'Neil N. & Kuwabara P. Characterization of an *xpa-1* mutant in *C. elegans*. European Worm Meeting 2004

29. Petukhova, G., Stratton, S. & Sung, P. Catalysis of homologous DNA pairing by yeast Rad51 and Rad54 proteins. *Nature* **393(6680)**, 91-4 (1998).

30. Jaskelioff, M., Van Komen, S., Krebs, J.E., Sung, P. & Peterson, C.L. Rad54p is a chromatin remodeling enzyme required for heteroduplex DNA joint formation with chromatin. *J. Biol Chem.* **278(11)**, 9212-9218 (2003).

31. Roeder, G.S. Meiotic chromosomes: it takes two to tango. *Genes Dev.* **11(20)**, 2600-21 (1997).

32. Baumann, P. & West, S.C. Role of the human RAD51 protein in homologous recombination and double-stranded-break repair. *Trends Biochem Sci.* **23(7)**, 247-251 (1998).

33. Bessho, T., Mu, D. & Sancar, A. Initiation of DNA interstrand cross-link repair in humans: the nucleotide excision repair system makes dual incisions 5' to the cross-linked base and removes a 22- to 28-nucleotide-long damage-free strand. *Mol Cell Biol.* **17(12)**, 6822-30 (1997).

34. Galli, A. & Schiestl, R.H. Cell division transforms mutagenic lesions into deletion-recombinagenic lesions in yeast cells. *Mutat Res.* **429(1)**, 13-26 (1999).

35. Bode, A.M. & Dong, Z. Post-translational modification of p53 in tumorigenesis. *Nat. Rev. Cancer* **4**, 793-805 (2004).

36. Schumacher, B., Hanazawa, M., Lee, MH.., Nayak, S., Volkmann, K., Hofmann, R., Hengartner, M., Schedl, T. & Gartner, A. Translational repression of C. elegans p53 by GLD-1 regulates DNA damage-induced apoptosis. *Cell* **120(3)**, 357-68 (2005).

37. Kinchen, J.M. & Hengartner M.O. Tales of cannibalism, suicide, and murder: programmed cell death in *C. elegans*. *Curr. Top. Dev. Biol.* **65**, 1-45 (2004).

38. Bakkenist, C.J. & Kastan, M.B. DNA damage activates ATM through intermolecular autophosphorylation and dimer dissociation. *Nature* **421(6922)**, 499-506 (2003).

39. Lee, J.H. & Paull, T.T. ATM activation by DNA double-strand breaks through the Mre11-Rad50-Nbs1 complex. *Science* **308(5721)**, 551-4 (2005).

40. Cortez, D., Guntuku, S., Qin, J. & Elledge, S.J. ATR and ATRIP: partners in checkpoint signaling. *Science* **294(5547)**, 1713-6 (2001).

41. Unsal-Kacmaz, K. & Sancar, A. Quaternary structure of ATR and effects of ATRIP and replication protein A on its DNA binding and kinase activities. *Mol Cell Biol.* **24(3)**, 1292-300 (2004).

42. Chaney, S.G. & Sancar, A. DNA repair: enzymatic mechanisms and relevance to drug response. *J Natl Cancer Inst.* **88(19)**, 1346-60 (1996).

43. Mitchell, J.R., Hoeijmakers, J.H.J. & Niedernhofer, L.J. Divide and conquer: nucleotide excision repair battles cancer and ageing. *Curr. Opin. Cell Biol.* **15**, 232–240 (2003).

44. De Boer, J. & Hoeijmakers, J.H.J. Nucleotide excision repair and human syndromes. *Carcinogenesis* **21(3)**, 453-460 (2000).

45. Hanawalt, P.C. Revisiting the rodent repairadox. *Environ Mol Mutagen.* **38(2-3)**, 89-96 (2001).

46. de Boer, J. & Hoeijmakers J.H. Cancer from the outside, aging from the inside: mouse models to study the consequences of defective nucleotide excision repair. *Biochimie* **81(1-2)**, 127-37 (1999).

47. McHugh, P.J., Sones, W.R. & Hartley, J.A. Repair of intermediate structures produced at DNA interstrand cross-links in Saccharomyces cerevisiae. *Mol. Cell. Biol.* **20**, 3425–3433 (2000).

48. McHugh, P.J., Spanswick, V.J. & Hartley, J.A. Repair of DNA interstrand crosslinks: molecular mechanisms and clinical relevance. *Lancet Oncol.* **2(8)**, 483–490 (2001).

49. Sasaki, M.S., Takata, M., Sonoda, E., Tachibana, A. & Takeda, S. Recombination repair pathway in the maintenance of chromosomal integrity against DNA interstrand crosslinks. *Cytogenet. Genome Res.* **104(1-4)**, 28-34 (2004).

50. Saffran, W.A., Ahmed, S., Bellevue, S., Pereira, G., Patrick, T., Sanchez, W., Thomas, S., Alberti, M. & Hearst, J.E. DNA repair defects channel interstrand DNA cross-links into alternate recombinational and error-prone repair pathways. *J. Biol. Chem.* **279(35)**, 36462-36469 (2004).

51. Bernstein, C., Bernstein, H., Payne, C.M., Garewal, H. DNA repair/pro-apoptotic dual-role proteins in five major DNA repair pathways: fail-safe protection against carcinogenesis. *Mut. Res.* **511**, 145–178 (2002).

52. Alpi, A., Pasierbeck, P., Gartner, A. & Loidl, J. Genetic and cytological characterization of the recombination protein RAD-51 in *Caenorhabditis elegans*. *Chromosoma* **112(1)**, 6-16 (2003).

53. Praitis, V., Casey, E., Collar, D. & Austin, J. Creation of low-copy integrated transgenic lines in Caenorhabditis elegans. *Genetics* **157(3)**, 1217-26 (2001).

54. Brenner, S. The genetics of Caenorhabditis elegans. *Genetics* **77(1)**, 71-94 (1974).

55. Kamath, R.S., Fraser, A.G., Dong, Y., Poulin, G., Durbin, R., Gotta, M., Kanapin, A., Le Bot, N., Moreno, S., Sohrmann, M., Welchman, D.P., Zipperlen, P., & Ahringer, J. Systematic functional analysis of the Caenorhabditis elegans genome using RNAi. *Nature* **421(6920)**, 231-7 (2003).

METHODS

Genetics. All strains were grown at 20ºC on NGM agar seeded with *E. coli* OP50 (Brenner, 1974). The Bristol N2 strain was used as the wild-type strain. The following alleles and transgenic strains were used: LGI: *atm-1(gk186)*, *hus-1(op244)*, *xpa-1(ok698)*, *cep-1(gk138)*, *rad-54(ok615)*; LGIII: *clk-2(mn159)*, *mrt-2(e2663)*; LGIV: *xpc-1(ok734)*, *spo-11(ok79)*/nT1[*unc-?(n754) let-?*](IV;V); LGV: *atl-1(tm853)*/nT1[qIs51](IV;V), *chk-2(me64)*, *chk-2(gk212)*; *opIs183* (XPA-1::GFP). *chk-2(me64)* and *atl-1(tm853)* strains were maintained as *chk-2(me64) rol-9(sc148)/unc-51(e369) rol-9(sc148)* and *atl-1(tm853)*/nT1[qIs51](IV;V), respectively.

Germline apoptosis. Young adult staged worms from different genetic backgrounds were exposed to 100 Joule/m^2 of UV light (254 nm) or to 120 Gy of X-rays and corpses were scored in the meiotic region of one gonad arm at indicated time points using Nomarski optics. For the treatment with the chemotherapeutic agents cisplatin and camptothecin, worms 12 h-post the L4 stage were transferred to OP50 plates containing 1mM and 0.1mM of the drugs and left grown there during the time course. For the EMS treatment, they were incubated for 30 min in M9 buffer containing 37.5 and 75 mM of the methylating agent and scored for corpses at the indicated time points after removed and washed off. For the RNAi experiments, L1 staged worms were put on plates seeded with the respective RNAi clone (Kamath *et al.*, 2003) and young adults were scored for germline apoptosis in the course of time.

Relative quantification of transcripts. Total RNA was extracted from wild-type, *atm-1(gk186)*, *atl-1(tm853*/nT1*)* and *atl-1(tm853)* mutants after treatment with UV-C

light or X-rays or from untreated worms. cDNA synthesis and quantitative real-time RT-PCR were performed as previously described (Hofmann *et al.*, 2002). Transcripts of *egl-1* and *ced-13* were measured after normalization with 18SrRNA, *tbp-1* and *pgk-1* mRNAs, which were used as internal controls, and average fold-change upon treatment was deduced based on three independent experiments.

Cell cycle arrest studies. Worms at the L4 stage from different genotypes were either treated with UV (100 J/m^2) or X-rays (120 Gy) or were left untreated. The cell cycle arrest phenotype was assessed 7 h later by counting the number of mitotic nuclei in a volume of 75 μm away from the distal tip cell, after images were captured using an ORCA-ER digital CCD camera.

Transgenic animals. An XPA-1::GFP vector was built using 3 kb of upstream sequences and the whole gene coding region fused C-terminally to GFP. The rescuing *unc-119(+)* genomic sequence from pPD135.83 (gift of A. Fire) was subcloned into it and the construct was inserted into *unc-119(ed3)* worms using the microparticle bombardment technique as previously described (Praitis *et al.*, 2001). Integration was determined by loss of visible Unc progeny. Fluorescence was observed in dissected gonads of young adult worms, after images were captured using an ORCA-ER digital CCD camera and processed with the Openlab software.

Immunostaining of RAD-51. Antibody staining of gonads was performed using standard procedures. Briefly, animals were dissected and fixed with 3% para-formaldehyde/0.1 M K2HPO4 (pH 7.2) for 50 min at room temperature followed by a 10 min incubation with 100% methanol on ice. Gonads were blocked in 5%

BSA/PBS-Tween-20 0.1% for 1 h and incubation with anti-RAD-51 (Alpi *et al.*, 2003) was done overnight at 4ºC. The tissues were co-stained with DAPI before mounting. Fluorescent images were captured with a Leica microscope equipped with an ORCA-ER digital CCD camera and were processed with the Openlab software.

Immunoblotting of CEP-1. Whole worm protein extracts from different genetic backgrounds were used for SDS-PAGE and subsequently probed with an anti-CEP-1 polyclonal antibody after pre-absorption (Schumacher *et al.*, 2005), using standard molecular methods. Proteins were collected before and 4 h following treatment with 100 J/m^2 of UV-C. Tubulin was used as an internal loading control.

Embryonic lethality assay. Animals from different genetic backgrounds, 48 h post the L1 stage, were subjected to 100 J/m^2 of UV-C and one day later were left lay eggs for 4-6 h. Non-hatched eggs were scored the next day as a positive embryonic lethal phenotype and expressed as a fraction of the total eggs laid. Data shown is the average percent lethality of 50 animals. Error bars indicate SEM.

FIGURE LEGENDS

Figure 1 UV-C radiation induces apoptosis in the *C. elegans* germline via transcriptional activation of *egl-1* and *ced-13* and dependent on conserved checkpoint genes.

(a) Corpses were scored in the meiotic region of one gonad arm of young adult animals at the 12 h-time point following treatment with different doses of UV-C radiation. **(b)** A similar dose response was repeated with different doses of X-rays. **(c)** The two apoptotic responses were further followed up in a time course after exposure to 100 J/m^2 of UV-C radiation and 120 Gy of X-rays. **(d)** The fold-increase in the mRNA levels of *egl-1* and *ced-13* was determined by real-time Q-RT-PCR, 12 h following treatment with either 120 Gy of X-rays or 100 J/m^2 of UV-C. Data shown is the average fold-change of three independent experiments ± SD. **(e)** Time course analysis with the *cep-1(gk138)*, *clk-2(mn159)*, **(f)** *hus-1(op244)*, *mrt-2(e2663)* and **(g)** *chk-2(me64)*, *chk-2(gk212)* mutants following 100 J/m^2 and/or 120 Gy of X-rays. Apoptotic corpses were scored in the meiotic region of one gonad arm of young adult animals. Data shown in all dose responses and time courses represent the average number of three independent experiments ± SD.

Figure 2 ATL-1, the *C. elegans* ATR homolog, is necessary to activate UV-induced germ cell apoptosis, in an *egl-1* and *ced-13*-dependent manner.

(a) Corpses were scored in the meiotic region of one gonad arm of mutant animals that lack both or one copy of *atl-1* (*atl-1(tm853)* homozygotes and *atl-1(tm853)*/nT1 balanced animals, respectively) at the indicated time points following exposure to 100 J/m^2 of UV-C radiation or **(b)** 120 Gy of X-rays. Data shown represent the average number of three independent experiments ± SD. **(c)** Corpses were scored

in the meiotic region of one gonad arm of young adult animals of the following genotypes: wild-type, *atl-1(tm853)*, *atl-1(tm853/nT1)*, *atl-1(tm853/+)*, *sDf29/+* and *mDf1/+*, the last two being deficiencies in the *atl-1* locus. The 12 h and the 24 h time-points were selected to score for apoptosis upon 100 J/m^2 of UV-C. Data shown represent the average number of two independent experiments ± SD. **(d)** Transcriptional induction of *egl-1* and *ced-13* upon UV-C radiation is dependent on *atl-1*. The fold-increase in the mRNA levels of *egl-1* and *ced-13* was determined by real-time Q-RT-PCR, 12 h following treatment with either 120 Gy of X-rays or 100 J/m^2 of UV-C, in the indicated genetic backgrounds. Data shown is the average fold-change of three independent experiments ± SD.

Figure 3 DNA damage-induced germ cell apoptosis is compromised in *atm-1(gk186)* mutants after UV treatment, whereas it occurs normally upon X-ray irradiation.

(a) Corpses were scored in the meiotic region of one gonad arm of young adult *atm-1(gk186)* animals at the 12 h-time point following treatment with different doses of UV-C and **(b)** X-ray radiation. **(c)** The apoptotic response was also followed up in a time course after exposure to 100 J/m^2 of UV-C radiation and 120 Gy of X-rays. **(d)** Transcriptional induction of *ced-13* upon UV irradiation is dependent on *atm-1*. The fold-increase in the mRNA levels of *egl-1* and *ced-13* was determined by real-time Q-RT-PCR, 12 h following treatment with either 120 Gy of X-rays or 100 J/m^2 of UV-C, in the indicated genetic backgrounds. Data shown is the average fold-change of three independent experiments ± SD. **(e)** ATM-1 responds to certain chemotherapeutic agents. 1 mM cisplatin and **(f)** 0.1 mM camptothecin were applied to 12 h-post the L4 stage wild-type and *atm-1(gk186)* animals and corpses were scored at the indicated time points. **(c)** Similarly, animals were incubated in M9 medium containing EMS at the concentrations of 37.5 and 75 mM and germ cell

corpses were similarly scored. Data shown in all dose responses and time courses represent the average number of three independent experiments ± SD.

Figure 4 The Nucleotide Excision Repair (NER) machinery is required for triggering the UV-induced cell death.

Germ cell corpses were scored in the meiotic region of one gonad arm of young adult **(a)** *xpc-1(ok734)*, **(b)** and **(c)** *xpa-1(ok698)* and *atm-1(gk186) xpa-1(ok698)* animals at the indicated time points following exposure to 100 J/m^2 of UV-C radiation and / or 120 Gy of X-rays. Data shown represent the average number of three independent experiments ± SD. **(d)** Fluorescent microscopy of germ cells expressing a XPA-1::GFP low-copy transgene. Image of dissected gonads were captured using an ORCA-ER digital CCD camera and processed with the Openlab software.

Figure 5 UV irradiation causes cell cycle arrest in the mitotic zone of the germline.

(a) Animals in the L4 stage of the following genotypes were irradiated with X-rays (120 Gy) and UV-C (100 J/m^2) or left untreated: wild-type, *hus-l(op244)*, *clk-2(mn159)*, *cep-1(gk138)*, *chk-2(gk212)*, *atl-1(tm853)*, *atm-1(gk186)* and *xpa-1(ok698)*. Proliferating germ cell nuclei were counted in a 50μm distance from the distal tip cell 7h after the treatment. Data shown represent the average number from 40 gonads ± SEM.

Figure 6a RAD-51 accumulates in the mitotic nuclei in a ATM-1- and XPA-1-dependent manner.

(a) Wild-type nuclei and nuclei from *atm-1(gk186)*, *xpa-1(ok698)* and *atm-1(gk186) xpa-1(ok698)* animals were stained with an anti-RAD-51 antibody (red) and co-stained with DAPI (blue), 4 h after worms were irradiated with 100 J/m^2 of UV-C. Foci

are detected as bright dots that co-localize with chromatin and are denoted with white arrowheads. **(b)** *atm-1* loss-of-function does not suppress *rad-51(RNAi)*-induced apoptosis. *atm-1(gk186)* animals at the L1 stage were treated with RNAi against *rad-51* and germ cell corpses were scored at the indicated time points 12 h after the L4 stage. GFP(RNAi) on wild-type and *atm-1* mutants, and *rad-51(RNAi)* on wild-type were used as controls. Data shown represent the average number of three independent experiments ± SD.

Figure 7a Recombinational repair can occur following the induction of UV damage. **(a)** *rad-54(lf)*-enhanced germline apoptosis is suppressed by *cep-1(lf)*. Germ cell corpses were scored in the meiotic region of one gonad arm of young adult *rad-54(ok615)* animals at the indicated time-points. The same time course was repeated after animals were exposed to *cep-1(RNAi)* starting at the L1 stage. **(b)** *rad-54(lf)*-enhanced germline apoptosis is suppressed by *spo-11(lf)*. Corpses were scored during a time course in a *spo-11(ok79)* background, before and after the animals were exposed to *rad-54(RNAi)* at the L1 stage. GFP(RNAi) on wild-type and *spo-11* mutants, and *rad-54(RNAi)* on wild-type were used as controls. **(c)** *rad-54* mutants fail to induce apoptosis in response to UV and IR. Corpses were scored during a time course in *rad-54(ok615)* animals following exposure to 100 J/m^2 of UV-C radiation and 120 Gy of X-rays. **(d)** The previous time course analysis described in **(b)** was repeated before and after treatment with 100 J/m^2 of UV-C and 120 Gy of X-rays. GFP(RNAi) on *spo-11* mutants was used as control. **(e)** *rad-54(lf)*-enhanced germline apoptosis is suppressed by *atm-1(lf)* and *atl-1(lf)*. Corpses were scored during a time course in *atm-1(gk186)* and *atl-1(tm853)* mutants, before and after the animals were exposed to *rad-54(RNAi)* at the L1 stage. GFP(RNAi) was used as

control. Data shown in all cases represent the average number of three independent experiments ± SD.

Figure 8 CEP-1 protein levels change upon UV in a ATL-1-dependent manner. Western analysis using an anti-CEP-1 antibody in the following genetic backgrounds: wild-type, *atm-1(gk186)*, *xpa-1(ok698)*, *atm-1(gk186) xpa-1(ok698)*, *atl-1(tm853)*, *chk-2(gk212)* and *cep-1(gk138)*. Total protein extracts from untreated or previously exposed to 100 J/m^2 of UV-C radiation animals were probed 4h later with the CEP-1 polyclonal antibody. Probing against tubulin was used as an internal control

Supplementary Fig. 1 Loss of *atm-1* function leads to genomic instability. **(a)** Quantification of the HUS-1::GFP foci in wild-type and *atm-1(gk186)* mutants. Young adult worms expressing HUS-1::GFP (*opIs34*) were either irradiated with low doses of X-rays (15 Gy) or UV-C light (30 J/m^2) and proliferating germ cells were scored 8 h later for the appearance of foci formation. Foci were counted in a 75μm distance from the DTC and are expressed as numbers per germ cell. Error bars represent SEM. **(b)** Embryonic lethality assay upon UV irradiation. *atm-1(gk186)* mutants display increased embryonic lethality after UV treatment and a synthetic lethal phenotype in the *hus-1(op244)* and *clk-2(mn159)* background. The percentage of unhatched embryos was determined in the indicated single and double mutants. The animals had left laid eggs 24 h following treatment with 100 J/m^2 of UV-C at the L4 stage. White bars represent the non-treated and grey bars the UV-treated condition. Data shown is the average percent lethality of 50 animals ± SEM.

Supplementary Fig. 2 RT-PCR analysis to determine the absence or not of transcripts in the mutants used in this study. Primers were designed to flank the

deletions in the genetic loci of the following mutants: **(a)** *atm-1(gk186)*, **(b)** *atl-1(tm853)*, **(c)** *chk-2(gk212)*, **(d)** *xpc-1(ok734)*, **(e)** *xpa-1(ok698)*, and **(f)** *rad-54(ok615)*. Total mRNA from wild-type animals and the corresponding mutants was used in a RT-PCR reaction, with 18SrRNA as an internal control.

Stergiou, *et al.*, 2005 ; Figure 1a

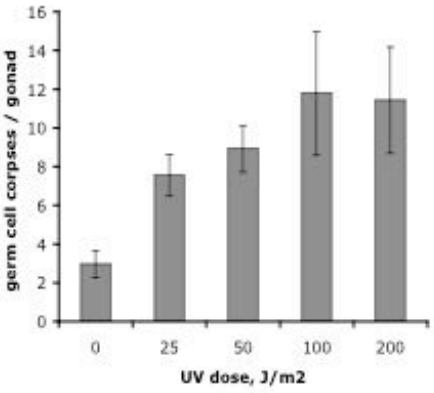

Stergiou, *et al.*, 2005 ; Figure 1b

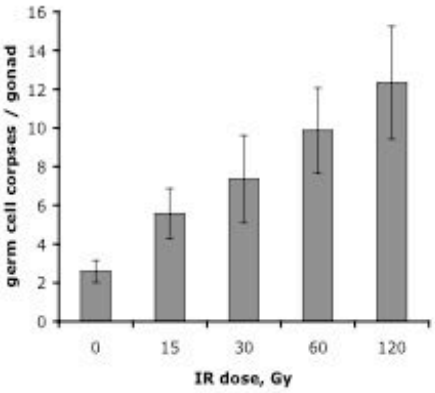

Stergiou, *et al.*, 2005 ; Figure 1c

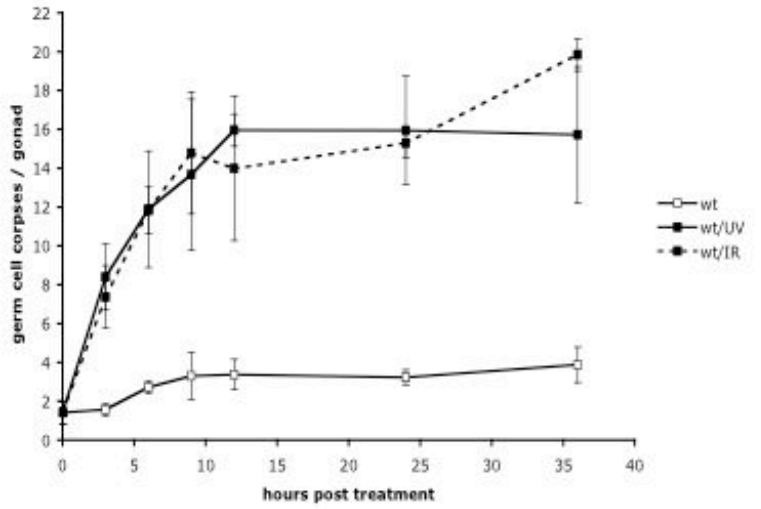

Stergiou, *et al.*, 2005 ; Figure 1d

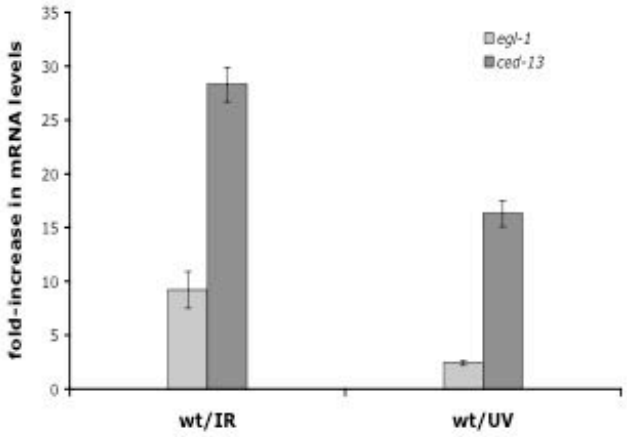

Stergiou, *et al*., 2005 ; Figure 1e

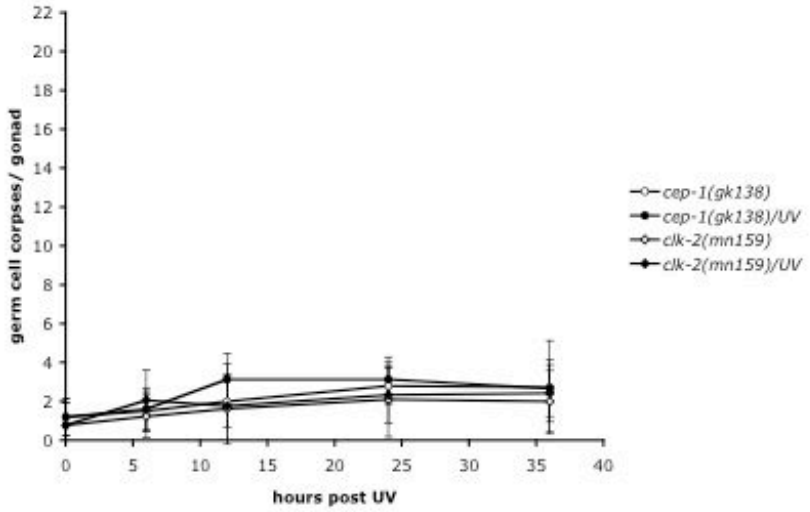

Stergiou, *et al.*, 2005 ; Figure 1f

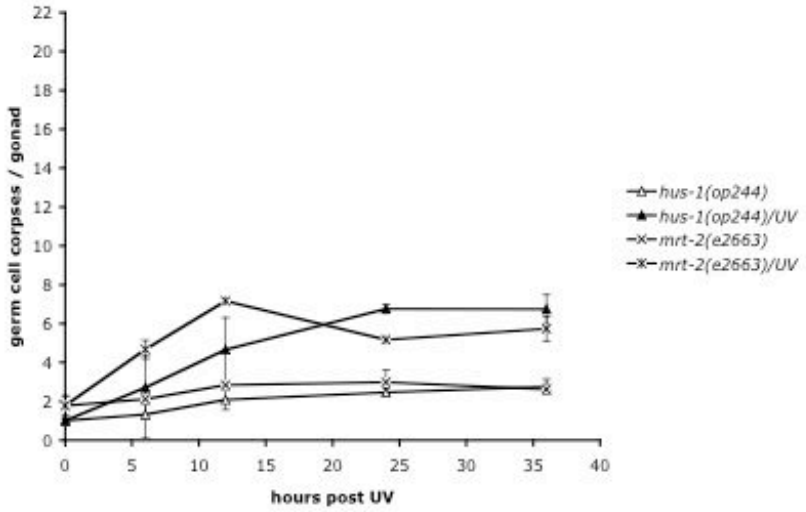

Stergiou, *et al.*, 2005 ; Figure 1g

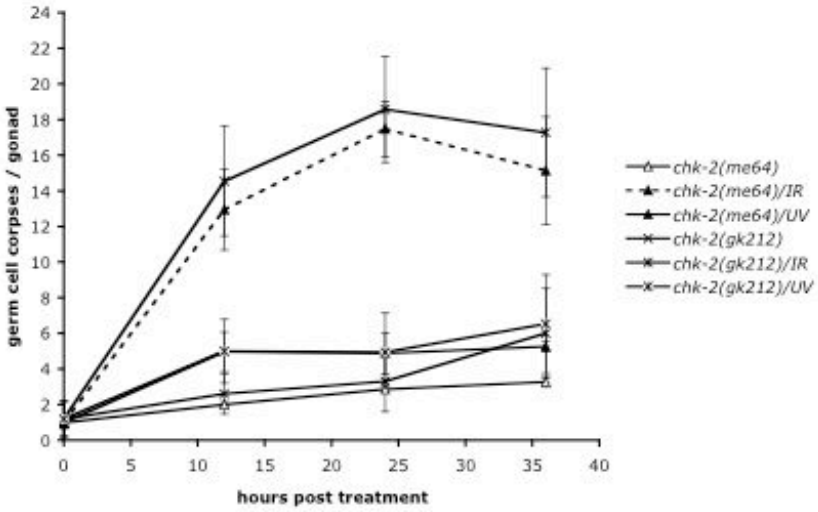

Stergiou, *et al.*, 2005 ; Figure 2a

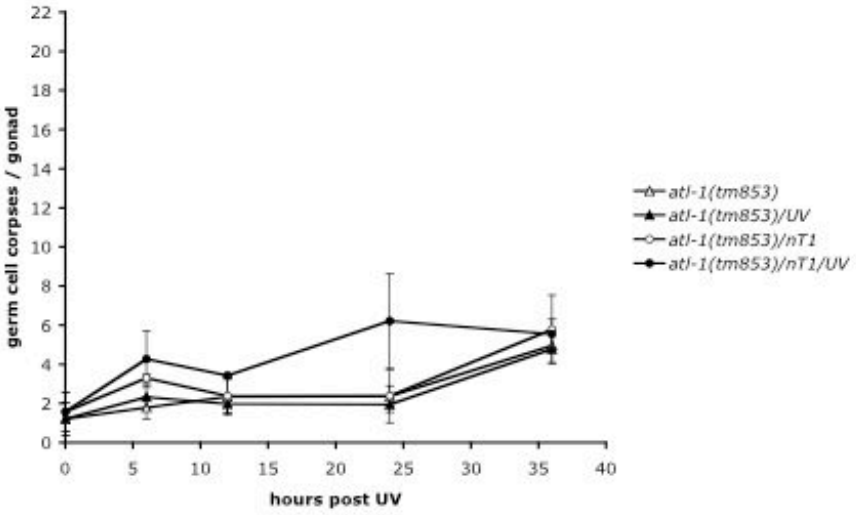

Stergiou, *et al.*, 2005 ; Figure 2b

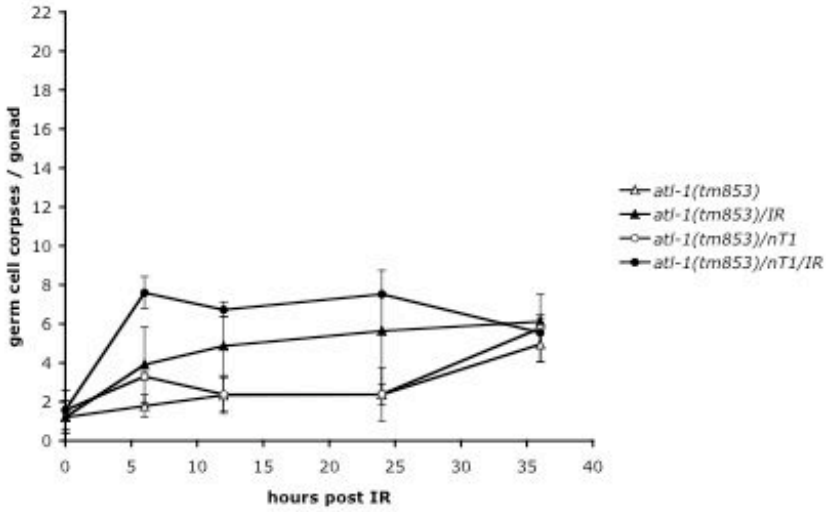

Stergiou, *et al.*, 2005 ; Figure 2b

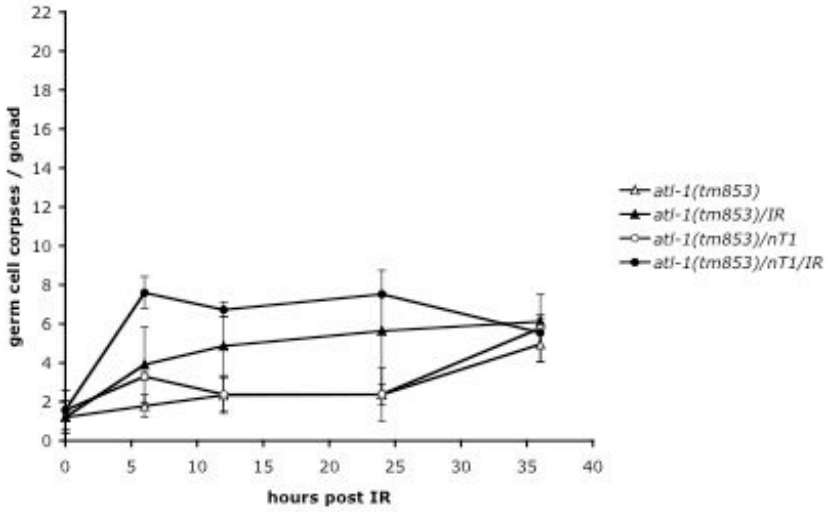

Stergiou, *et al.*, 2005 ; Figure 2c

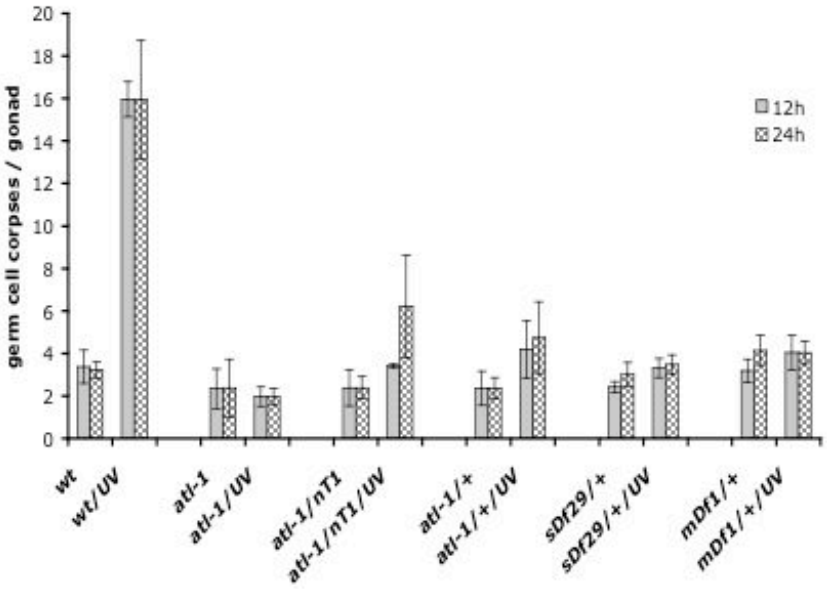

Stergiou, *et al.*, 2005 ; Figure 2d

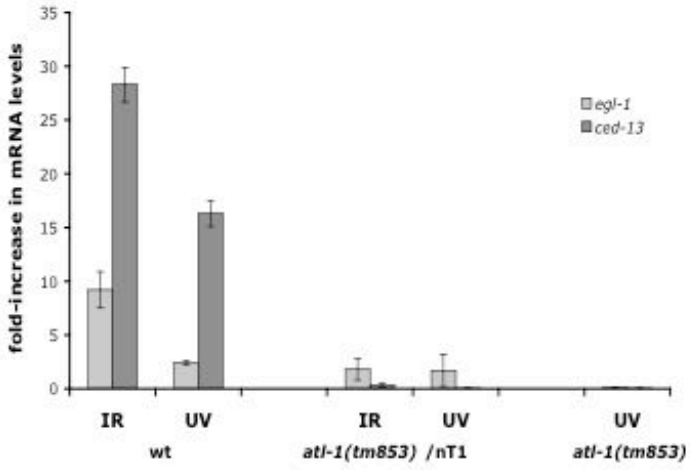

Stergiou, *et al.*, 2005 ; Figure 3a

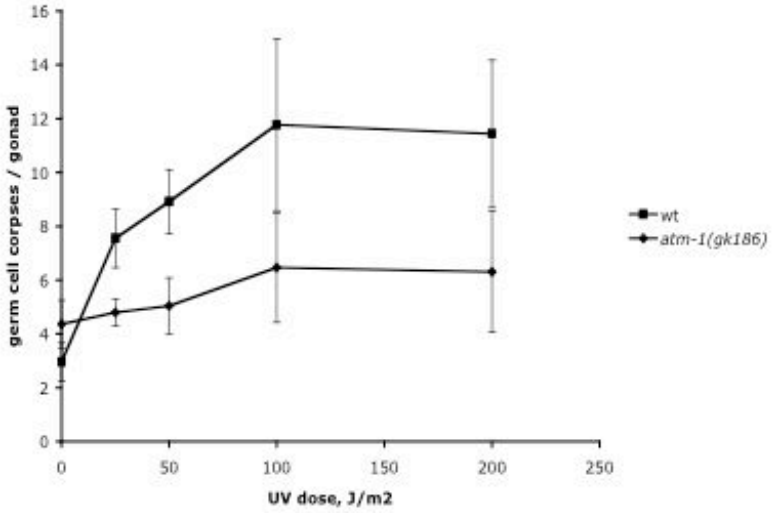

Stergiou, *et al.*, 2005 ; Figure 3b

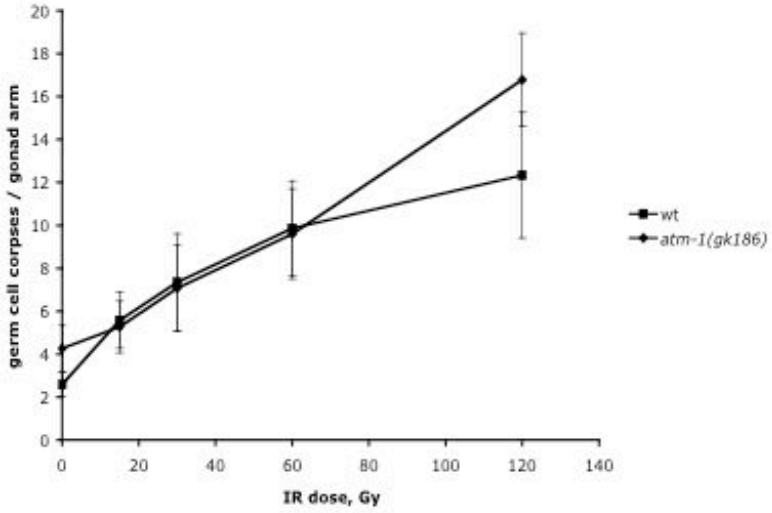

Stergiou, *et al.*, 2005 ; Figure 3c

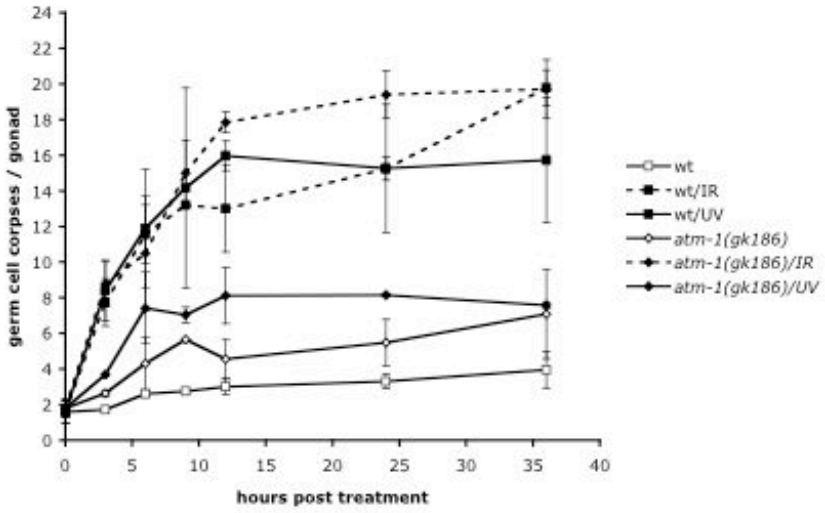

Stergiou, *et al.*, 2005 ; Figure 3d

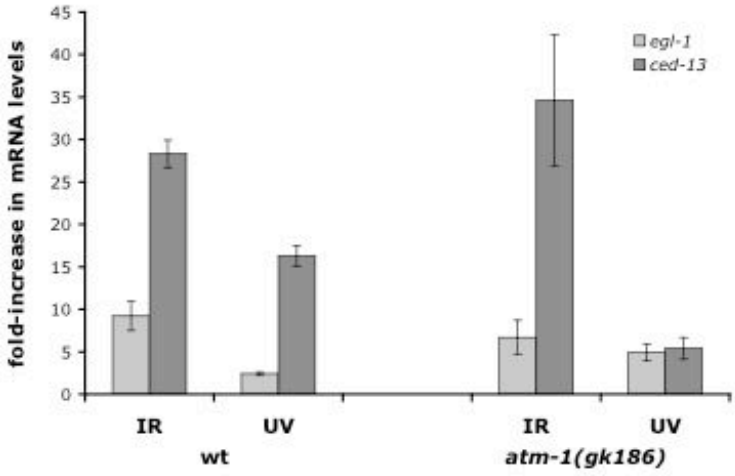

Stergiou, *et al.*, 2005 ; Figure 3e

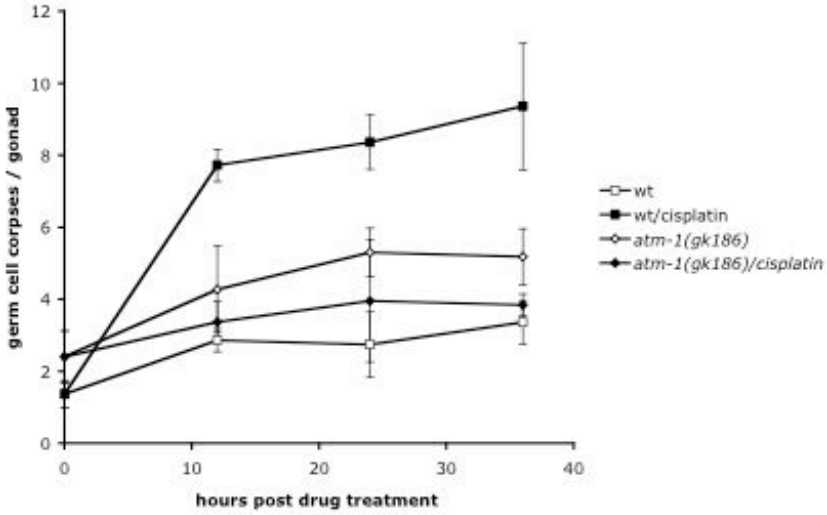

Stergiou, *et al.*, 2005 ; Figure 3f

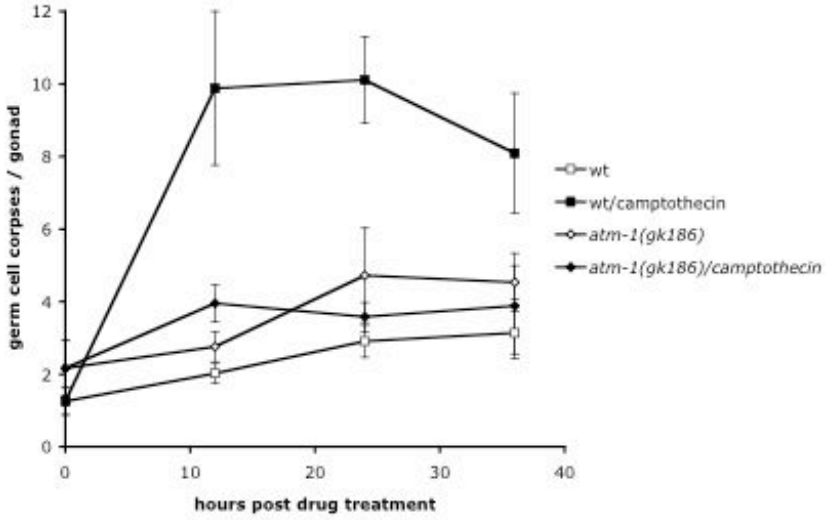

Stergiou, *et al.*, 2005 ; Figure 3g

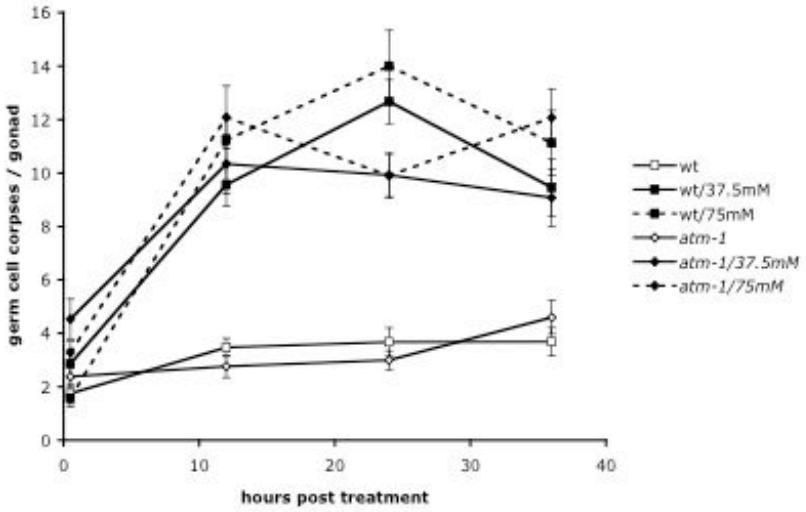

Stergiou, *et al.*, 2005 ; Figure 4a

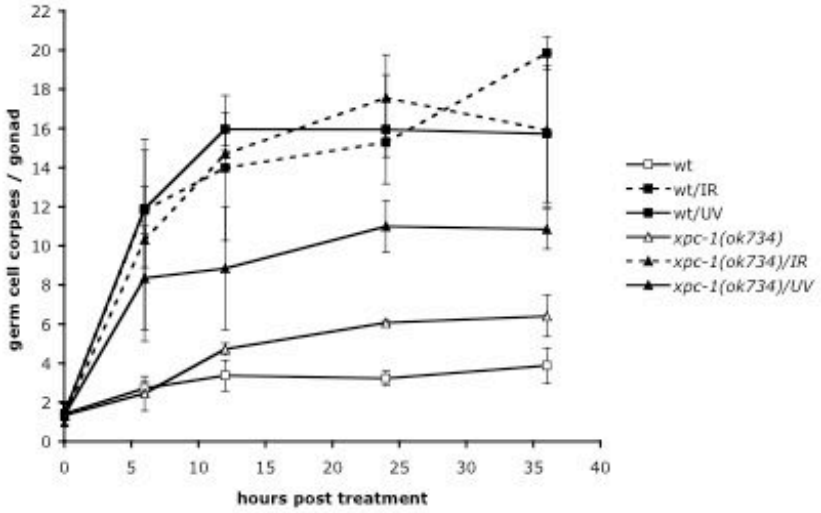

Stergiou, *et al.*, 2005 ; Figure 4b

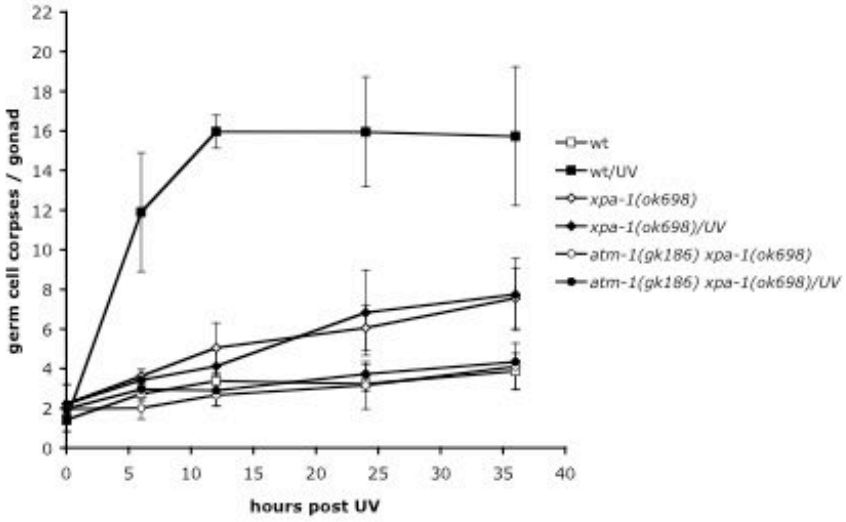

Stergiou, *et al*., 2005 ; Figure 4c

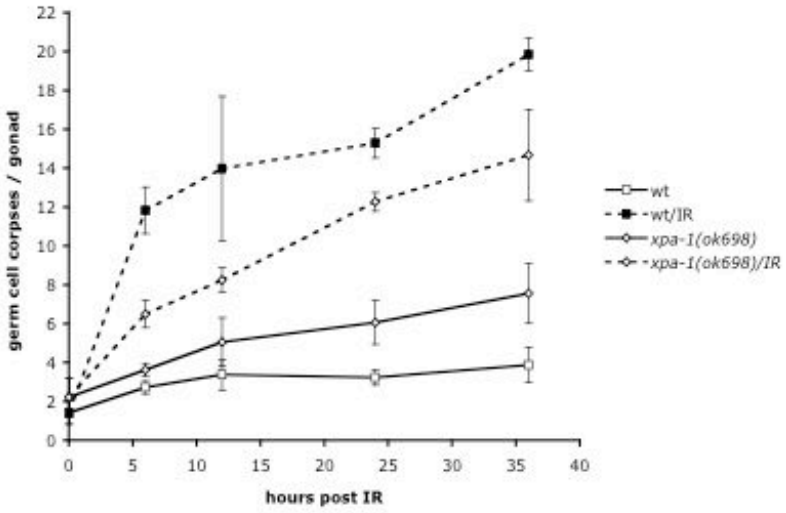

Stergiou, *et al.*, 2005 ; Figure 4d

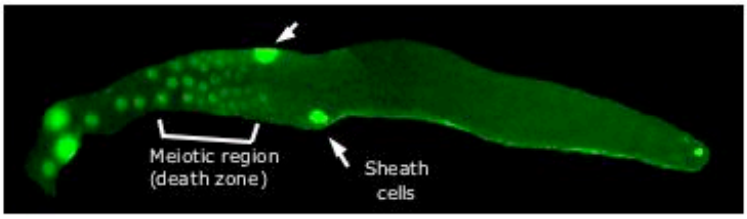

Stergiou, *et al.*, 2005 ; Figure 5

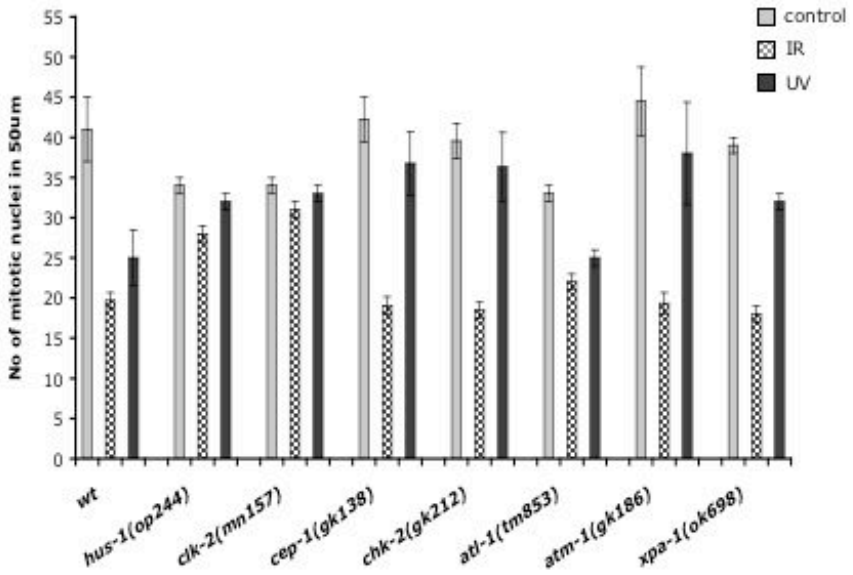

Stergiou, *et al.*, 2005 ; Figure 6a

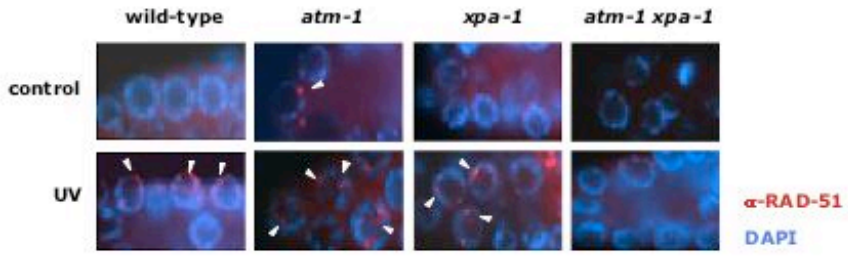

Stergiou, *et al.*, 2005 ; Figure 6b

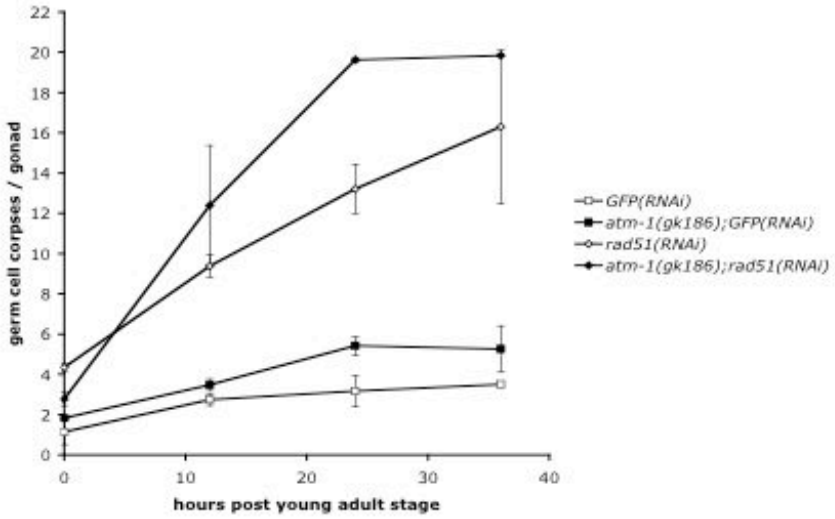

Stergiou, *et al.*, 2005 ; Figure 7a

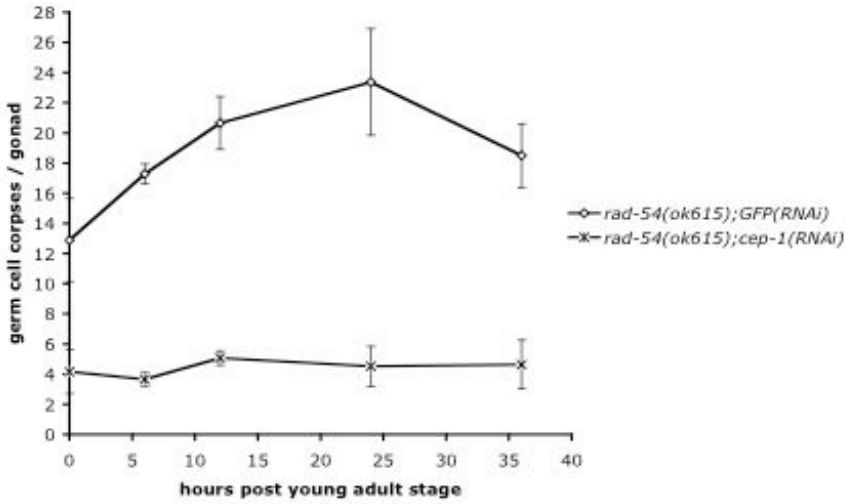

Stergiou, *et al.*, 2005 ; Figure 7b

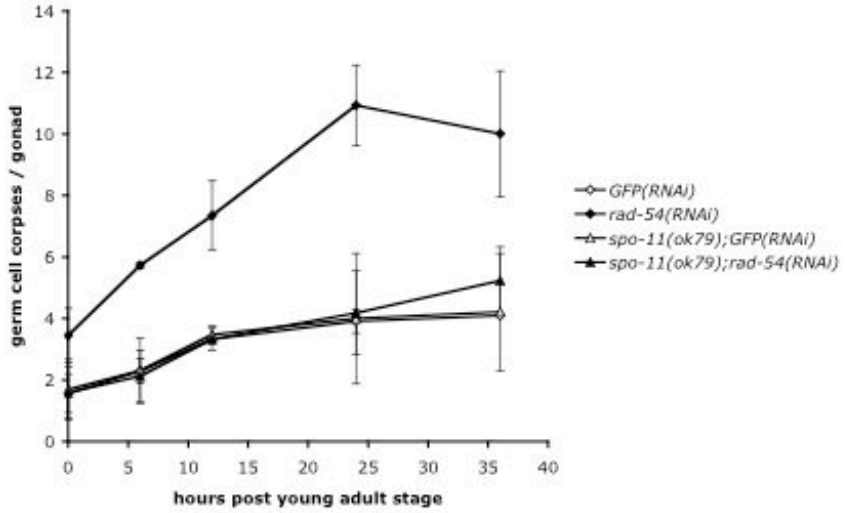

Stergiou, *et al.*, 2005 ; Figure 7c

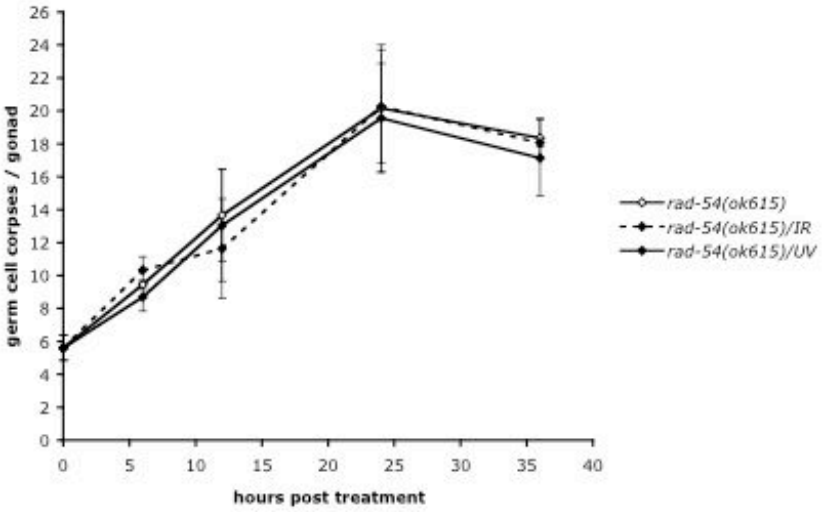

Stergiou, *et al.*, 2005 ; Figure 7d

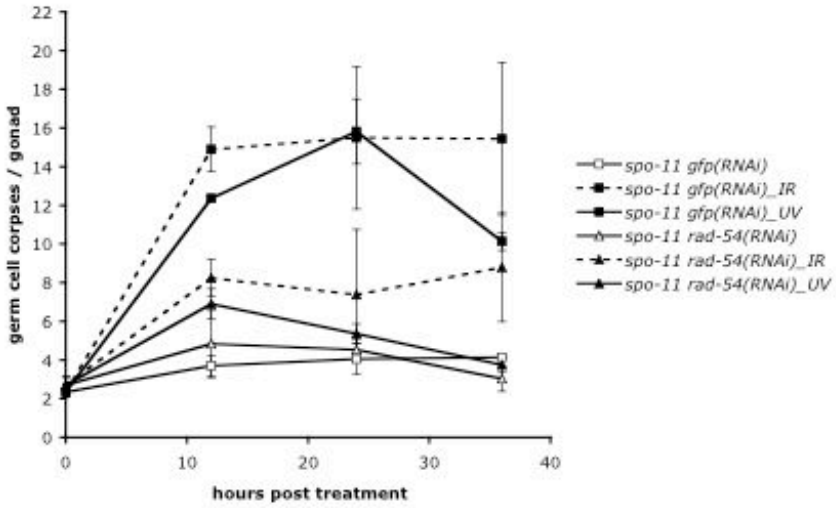

Stergiou, *et al.*, 2005 ; Figure 7e

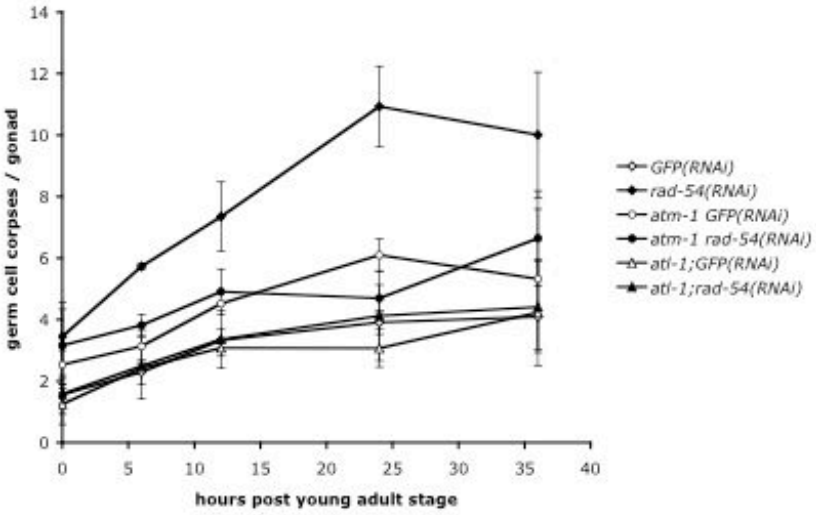

Stergiou, *et al.*, 2005 ; Figure 8

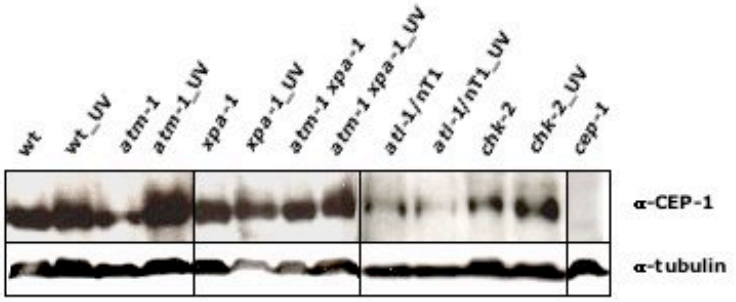

Stergiou, *et al.*, 2005 ; Supplementary Fig. 1a

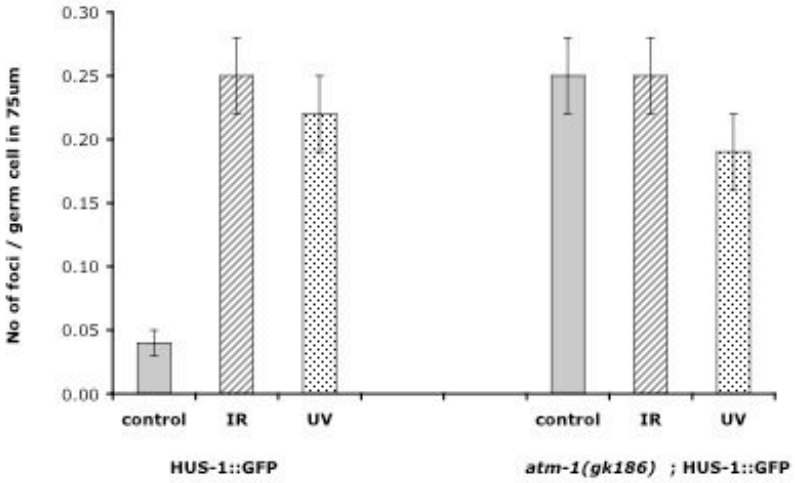

Stergiou, *et al.*, 2005 ; Supplementary Fig. 1b

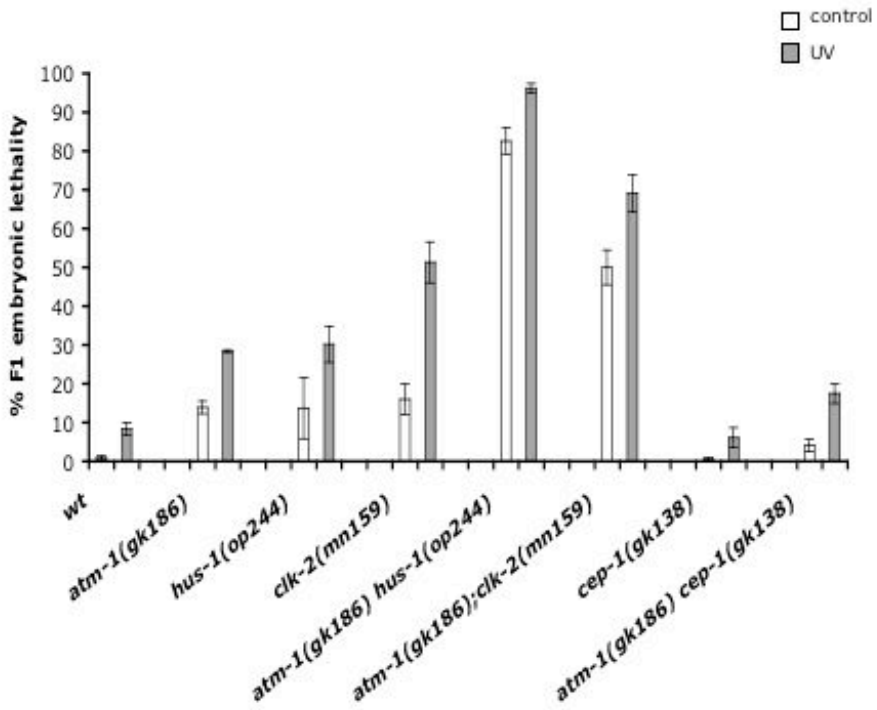

Stergiou, *et al.*, 2005 ; Supplementary Fig. 2

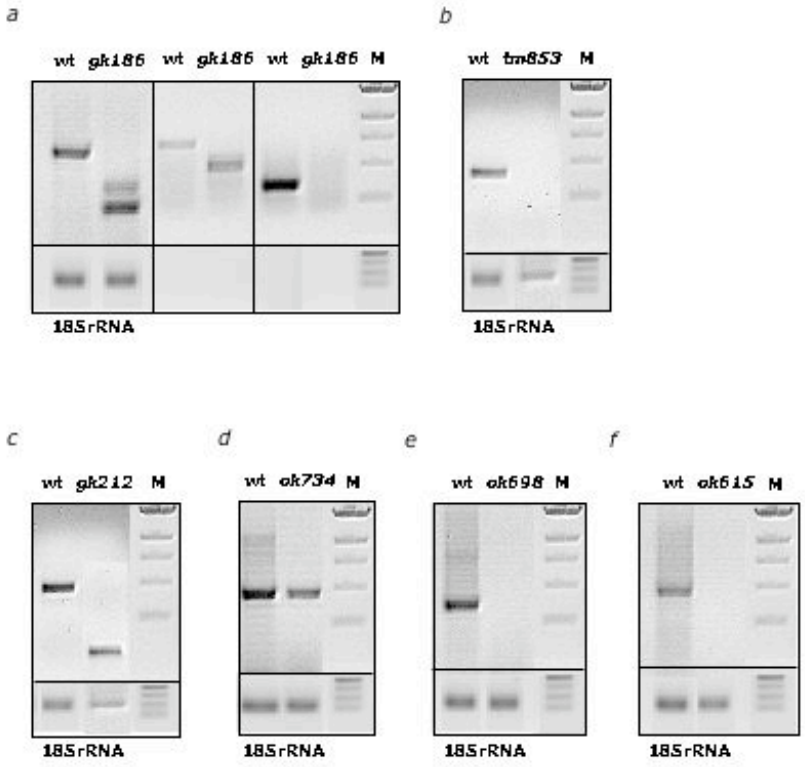

Preface

In addition to the data described and discussed for the purposes of the manuscript, I conducted a few other experiments that either supplement the previous ones or confer more information into this knowledge.

Below I include a list of figures and a short discussion regarding the results obtained. The subjects of the following paragraphs are independent of each other.

5.1. The *C. elegans* ATM-1 and ATL-1

5.1.1. Conservation with members among other eukaryotes

ATM and ATR belong to the superfamily of phosphatidylinositol 3-kinases (PI3-kinase), isoforms of which participate in diverse cellular processes. Despite the significant homology to lipid kinases, no lipid kinase activity has been demonstrated for any of the PIK-related kinases, namely ATM/ATR, TOR (target of rapamycin) and DNA-dependent kinase. This subgroup of proteins has been extensively studied due to its involvement in the critical processes of cell growth, the regulation of cell cycle progression, DNA damage checkpoints, recombination, and maintenance of telomere length.

Both of the *C. elegans* proteins share the same domains, a kinase catalytic domain, a FAT domain and a FATC-terminal domain. To determine how conserved these proteins are with those of other organisms I aligned the full-length sequences from seven different species. The output was used to generate an unrooted phylogenetic tree (Figure 1). Each one of the worm ATM-1 and ATL-1 proteins cluster among members of the same group, well separated from each other. Based on the kinase domains only, there is a 35% and a 31% similarity with the human ATM and ATR, respectively, those being the closest related sequences from all the species tested.

5.2. Cell cycle arrest studies

5.2.1. Cell cycle arrest upon UV requires *atm-1* and *cep-1*

Following exposure to UV-C radiation proliferation of mitotic nuclei in the *C. elegans* germ line tissue ceases and the size of the cells becomes larger. I used this phenotypic assay previously to quantify cell cycle arrest in different mutant backgrounds, and among the genes required to initiate this response I found *atm-1* and *cep-1*.

Alternatively, I used the visible marker CYB-1::YFP that was previously established in the lab to describe this event in wild-type animals and *atm-1(gk186)* and *cep-1(gk138)* mutants. Under normal cycling conditions, only cells that undergo the mitotic phase of the cell cycle express high levels of YFP giving rise to a patched pattern (Figure 2A). Upon Ionizing Radiation or UV-C treatment a distinct zone where all cells are highlighted is formed in the wild-type (Figure 2 B, C). This is indicative of the cells accumulating in the same phase, presumably the G2/M. Ionizing Radiation has the same effect on *atm-1* mutants whereas UV brings no change in the pattern of the control (Figure 2E, F).

An analogous situation occurs in the *cep-1* mutants, where IR causes a normal cell cycle arrest, while UV disrupts this response (Figure 3E, F). The results with the cyclin B1 marker similarly indicate that a checkpoint is abrogated and render both ATM-1 and CEP-1 a requirement for triggering cell cycle arrest in the presence of UV-induced DNA damage.

5.2.2. The intra-S phase checkpoint is functional in *atm-1* and *atl-1* mutants

To probe the role of *C. elegans atm-1* and *atl-1* in the DNA replication checkpoint, I tested the ability of the mutants to respond to hydroxyurea treatment. The drug depletes the deoxynucleotide pool and DNA synthesis is inhibited. Thus, it results in a reduction in the number and an enlargement in size of the premeiotic nuclei of wild-type worms (Figure 4A, B). The same pattern is observed after loss of *atm-1* function, revealing that the intra-S phase checkpoint is normally activated in *atm-1* mutants upon replication block (Figure 4C, D). Likewise, I could not specify a function for *atl-1* mutants in the intra-S phase checkpoint (Figure 4E, F), a role that would fit more with the involvement of a protein in sensing stalled replication fork-induced damage.

5.3. ATM-1 expression studies

5.3.1. A transcriptional *atm-1* reporter shows germline expression

To determine the expression pattern of ATM-1 I first turned my efforts into a transcriptional GFP reporter. Part of the coding region and a 2.5 kb stretch of sequences preceding the start codon were used to fuse to GFP. In the transgenic animals generated all the cells throughout the germline are highlighted (Figure 5). Whether this pattern is an actual perinuclear expression pattern, or represents protein molecules that due to folding or trafficking reasons reside in the ER compartment is elusive.

5.3.2. ATM-1 displays perinuclear expression that partially overlaps with DNA, following UV-C

In order to follow the localization of ATM-1 I obtained a human antibody from the Lavin lab that recognizes the last 16-amino acid stretch at the C-terminus (Watters *et al.*, 1999). Figure 6 shows dissected gonads from wild-type animals, 4 h following treatment with UV-C. A very weak cytoplasmic signal is present, similar to the non-treated situation. Although the majority of cells appear to be devoid of any strong expression, distinct cells in the transition zone are highlighted. The halo-like pattern is reminiscent of the transcriptional GFP signal shown in Figure 5. Moreover, there is a restricted overlap with the DNA as becomes clear from the merged color.
This subset of germ cells presumably represent damaged cells, that are either undergoing repair processes or are fated to undergo apoptosis once they pass through the death sensitive zone.

5.4. XPA-1 expression studies

5.4.1. XPA-1 is expressed in various tissues

Consistent with a role of *xpa-1* in the death decision, the gene product is expressed in the meiotic region and has a nuclear localization. However, several other tissues in the XPA-1::GFP transgenic animals, exhibit an interesting expression pattern.

The respective tissues are shown in Figure 7. Embryos in the one-, two- and 50 cell-stage show GFP signal in both the nucleus and the cytoplasm (A). This strongly

implies a role of *xpa-1* in the developing embryo, which can either be fundamental or related to repair to ensure faithful transmission of the genetic information during the fast cycling of the embryos.

Different head neurons (B), intestinal cells (C) and somatic sheath cells (D) show strong cytoplasmic expression. The existence of protective mechanisms in neurons is gradually being recognized as an important aspect of their function. Nowadays, self-repair processes in the post-embryonic neuron cells are considered of major importance (Proceedings of the 2005 International Workshop on A-T, ATM and the DNA damage responses). The possibility that neurons and other somatic tissues have active repair processes in *C. elegans* as well is very tempting and needs further exploration.

The oocytes have an expression pattern of particular interest (E) and (F). The fourth fully developed oocyte displays an intense GFP signal, whereas the third has a weaker one. The first two oocytes lack GFP expression. The reason for this alternation is currently unknown, although the idea itself of expressing repair factors in cells that will give rise to embryos is quite rational. Apart from the cells in the latest stages of prophase I, occasionally early meiotic cells exhibit a nuclear pattern (G). My hypothesis is that these could represent cells with a heavily on-going repair activity to protect against severe spontaneous damage. Finally, apoptotic corpses are highlighted with GFP (H), underlying the notion that *xpa-1* could be involved in more than the decision steps of DNA damage-induced apoptosis.

5.5. The double strand break repair following UV

5.5.1. Recombinational repair, rather than non homologous end joining predominates in the repair of UV lesions

There are two main pathways for double-strand break repair, homologous recombination (HR) and non-homologous end joining (NHEJ), which are error-free and error-prone, respectively. In simple eukaryotes like yeast, HR is the main pathway, whereas mammals predominantly use NHEJ, although a cell cycle phase specific preference also exists. NHEJ is carried out in part by DNA-PK, a holoenzyme consisting of the catalytic subunit (DNA-PKcs) and a DNA binding and a regulatory subunit, Ku. The reaction is initiated by Ku (Ku70/Ku86 association), which, upon binding with the damaged ends recruits the catalytic subunit. The complex aligns the ends to allow their ligation by DNA ligase IV, which among other factors and activities completes NHEJ DNA repair (Bernstein *et al.*, 2002, Valerie & Povirk, 2003, Christmann *et al.*, 2003).

To support my finding that double strand break repair components are involved in the death decision upon UV-induced damage, with RAD-54 and RAD-51 proteins being implicated, I turned into components of the NHEJ pathway. In *C. elegans* there are homologs of both *cku-80* and *lig-4*. The former has been studied in a context other than repair and no information available exists for the latter (Clejan *et al.*, 2003). *cku-80(ok861)* mutants carry a deletion that removes the whole Ku-core domain, which includes the central DNA-binding beta-barrels and polypeptide rings and the C-terminal arm. Therefore, the mutant is probably a null. *lig-4(ok716)* mutants, on the other hand, bear a deletion that disrupts the second functional domain of the protein.

This is a domain that is not shared by all ATP-dependent DNA ligase enzymes, but its disruption decreases the affinity for nicked DNA in certain species. It is, therefore, thought to be involved in DNA binding and catalysis (InterProScan description, EBI database).

I performed time course analyses with the two mutants following treatment with X-rays and UV-C radiation (Figures 7, 8). Both mutations result in increased levels of germline apoptosis, probably due to accumulation of unrepaired damage, as is the case for mutations in components of the NER pathway. This phenotype, however, is stronger in the *cku-80(ok861)* mutants. In contrast to previous reports, it seems that non-homologous end-joining appears to play some role in the repair of double-strand DNA breaks, at least in the germline of *C. elegans* (Clejan *et al.*, 2003). Upon treatment both mutants respond with an increase in apoptotic levels, although for both the total fold-increase is half of that in wild-type.

Although these phenotypes need further experimental evidence to understand their nature, the ability of the *cku-80* and *lig-4* mutants to respond to genotoxic stress distinguishes them from the mutants of the other major pathway. This is an indirect proof for the involvement of the HR components only, in the processing of UV-type lesions.

5.6. Additional phenotypes of the *atm-1* mutants

5.6.1. *atm-1* mutants exhibit a mild mutator phenotype

Checkpoint genes function to prevent cells with damaged genomes from progressing through the cell cycle without correcting the DNA lesions. Mutations in repair genes or genes that regulate these checkpoints have been shown to display higher spontaneous mutation frequencies ([1]Myung *et al.*, 2001, [2]Myung *et al.*, 2001).

As previously discussed, *atm-1(gk186)* mutants were shown to have moderate levels of embryonic lethality and an increased sensitivity to UV by displaying embryonic lethality (Supplementary Fig. 1b). Moreover, they have increased number of HUS-1 foci in the germline under normal conditions (Supplementary Fig. 1a). These data suggested that endogenous damage occurs more often in *atm-1(gk186)* mutants and point towards their involvement in repairing this damage.

To look at spontaneous mutation frequencies in *atm-1* mutants, I used the well-characterized *unc-93* reversion assay. The *unc-93(e1500)* gain-of-function mutation results in severe paralysis that can be suppressed by loss of function in any one of five different genes; this loss of function includes inactivating second site mutations within the *unc-93* gene itself (Greenwald & Horvitz, 1980). I found the spontaneous suppression frequency of *unc-93(e1500)* worms to be 7.9×10^{-5} (Figure 9). In two independent *atm-1(gk186);unc-93(e1500)* strains (F1.1 and F1.2), the mutation frequency was 12 times higher than in the control strain. What has been previously reported for the *hus-1(op244)* mutant, the fold-increase in the mutation rate is up to 25, compared to a 1×10^{-6} of the control strain. These results are suggestive of the fact

that loss of *atm-1* function leads to genomic instability, probably due to defects of repair.

5.6.2. *atm-1* mutants have a normal lifespan

One of the phenotypic characteristics of Ataxia-Telangiectasia patients is premature aging. This, in part, is associated with the most commonly observed defect that affects telomeres, that being telomeric fusions particularly in T lymphocytes (Metcalfe *et al.*, 1996). A-T cells not only have higher rates of chromosome end associations in metaphase and interphase, but also show chromosomal breaks at metaphase and fewer telomeric signals (Pandita *et al.*, 1995). Similar to the human situation, in Drosophila spontaneous telomere fusions and other chromosomal abnormalities are also common in cells lacking ATM (Silva *et al.*, 2004).

Since it is believed that it is the repair functions of ATM kinase that promote telomere maintenance by inhibition of illegitimate recombination or fusion events, and since the *C. elegans* ATM-1 is involved in repair, I measured the lifespan of *atm-1(gk186)* mutant animals. In two independent experiments, the average lifespan coincides with that of wild-type (Figure 10). Therefore, no 'premature aging' phenotype is observed in the worm mutants. However, to test the role of *C. elegans* ATM-1 in the maintenance of normal telomeres and chromosome stability, I would need to examine the length of telomeres.

References

Clejan, I., Meier, B. & Ahmed, S. *cku-80* and lifespan in *C. elegans*. *International Worm Meeting* 2003.

Greenwald, I.S. & Horvitz, H.R. *unc-93(e1500)*: A behavioral mutant of *Caenorhabditis elegans* that defines a gene with a wild-type null phenotype. *Genetics* **96(1)**, 147-64 (1980).

Libina, N., Berman, J.R. & Kenyon, C. Tissue-specific activities of *C. elegans* DAF-16 in the regulation of lifespan. *Cell* **115(4)**, 489-502 (2003).

[1]Myung, K., Chen, C. & Kolodner, R.D. Multiple pathways cooperate in the suppression of genome instability in *Saccharomyces cerevisiae*. *Nature* **411(6841)**, 1073-6 (2001).

[2]Myung, K., Datta, A. & Kolodner, R.D. Suppression of spontaneous chromosomal rearrangements by S phase checkpoint functions in Saccharomyces cerevisiae. *Cell* **104(3)**, 397-408 (2001).

Proceedings of the 2005 *International Workshop on A-T, ATM and the DNA damage responses*. Italy, 2005.

Watters, D., Kedar, P., Spring, K., Bjorkman, J., Chen, P., Gatei, M., Birrell, G.,

Garrone, B., Srinivasa, P., Crane, D.I. & Lavin, M.F. Localization of a portion of extranuclear ATM to peroxisomes. *Biol Chem*. **274(48)**, 34277-82 (1999).

Methods

Cell cycle arrest studies. The cell cycle arrest phenotype was alternatively visualized using a cyclin B1 reporter construct. *opIs76* transgenic animals bearing low copies of CYB-1::YFP, in a wild-type and an *atm-1(gk186)* or a *cep-1(gk138)* mutant background, were treated with 100 J/m^2 of UV-C or 120 Gy of X-rays 12 h post the L4 stage. Images from dissected gonads were captured 10 h later using an ORCA-ER digital CCD camera and were processed with the Openlab software.

Hydroxyurea studies. Standard NGM agar plates were prepared containing HU at a final concentration of 25 mM. Wild-type worms or *atl-1(tm853)* and *atm-1(gk186)* mutants at the L4 stage were grown for 7 h there until gonads were dissected and stained with Hoechst 33342 (0.5 g/mL). The functionality of the intra-S checkpoint was assessed by the morphological view of the distal end of the gonads.

Transgenic animals. An P*atm-1*::GFP vector was built using 2.5 kb of sequences upstream of the predicted start codon and 2 kb of the ORF, and was fused C-terminally to GFP. The rescuing *unc-119(+)* genomic sequence from pPD135.83 (gift of A. Fire) was subcloned into it and the construct was inserted into *unc-119(ed3)* worms using the microparticle bombardment technique as previously described (Praitis *et al.*, 2001). Integration was determined by loss of visible Unc progeny. Fluorescence was observed in dissected gonads of young adult worms, after images were captured using an ORCA-ER digital CCD camera and processed with the Openlab software.

***unc-93(e1500)* reversion assay.** Mutants of each genotype were singled out (*unc-93*, n=100 ; *atm-1;unc-93*, n=100) and monitored for three generations until plates were starved. Animals were then newly transferred and plates with revertants were scored as independent events. Reversion frequency was determined by dividing these with the number of haploid genomes screened for each genotype.

Lifespan analysis. Lifespan assays were performed at 20°C and were initiated at the L4 larvae stage with 80-100 worms. Animals were transferred away from their progeny to new plates every other day until the end of the reproductive period (in case of sterility, they were kept on the same plates). I used the Excel software to carry out statistical analysis and to determine mean lifespans. Animals that crawled off the plate, "exploded" (e.g., had a gonad extruding through their vulva), or "bagged" (e.g., died from internal hatching) were censored at the time of the event and were not included into the final data set.

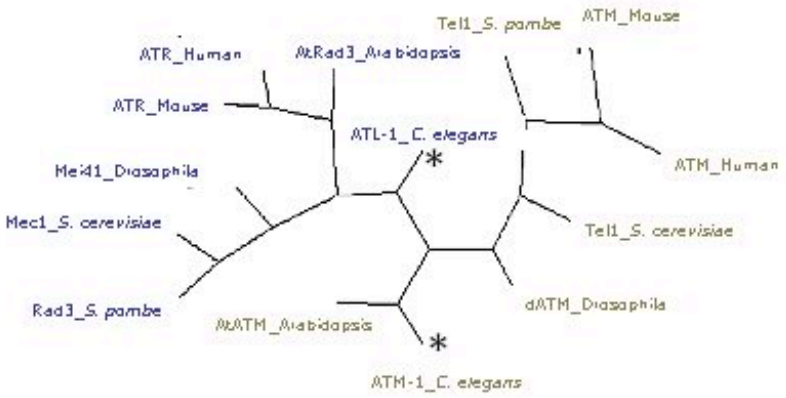

Figure 1. Phylogenetic tree of members of the ATM/ATR superfamily

The *C. elegans* ATM-1 and ATL-1 cluster among members of other eukaryotes. Whole protein sequences of ATM and ATR from different species were aligned using the ClustalW tool and the output was used to generate a phylogenetic tree using the TreeTop prediction program. The unrooted tree was the product of the topological algorithm.

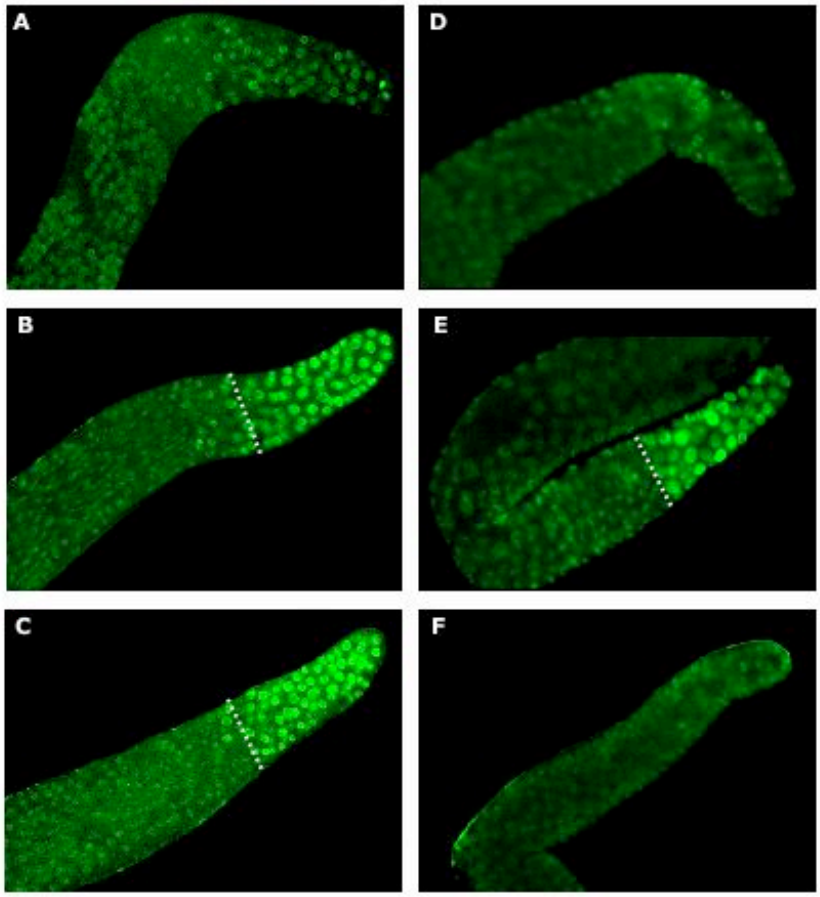

Figure 2. *atm-1* mutants display a cell cycle arrest defect upon UV

Wild-type or *atm-1* mutant animals carrying a CYB-1::YFP marker (*gk186*;*opIs76*) were either irradiated with 120 Gy of X-rays (B, E) or 100 J/m^2 of UV-C (C, F) at the 12 h-post-L4 stage, or were left untreated (A, D). All nuclei can be visualized by the presence of YFP. Dashed line indicates the border line of the arrested zone.

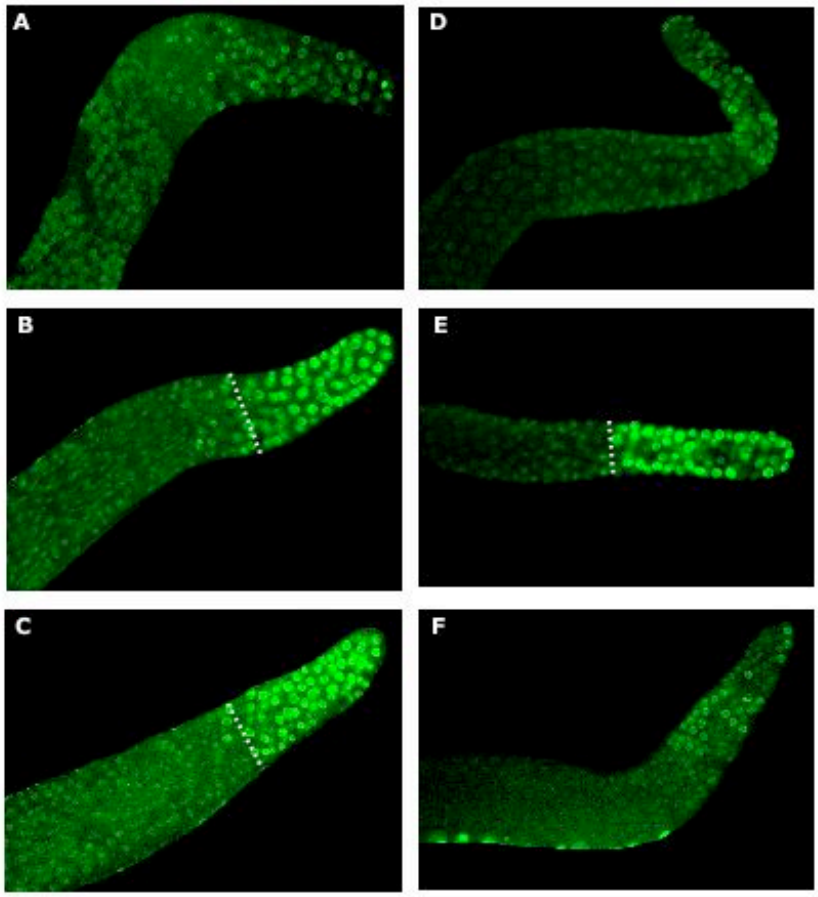

Figure 3. *cep-1* mutants display a cell cycle arrest defect upon UV

Wild-type or *cep-1* mutant animals carrying a CYB-1::YFP marker (*gk138*;*opIs76*) were either irradiated with 120 Gy of X-rays (B, E) or 100 J/m^2 of UV-C (C, F) at the 12 h-post-L4 stage, or were left untreated (A, D). All nuclei can be visualized by the presence of YFP. Dashed line indicates the border line of the arrested zone.

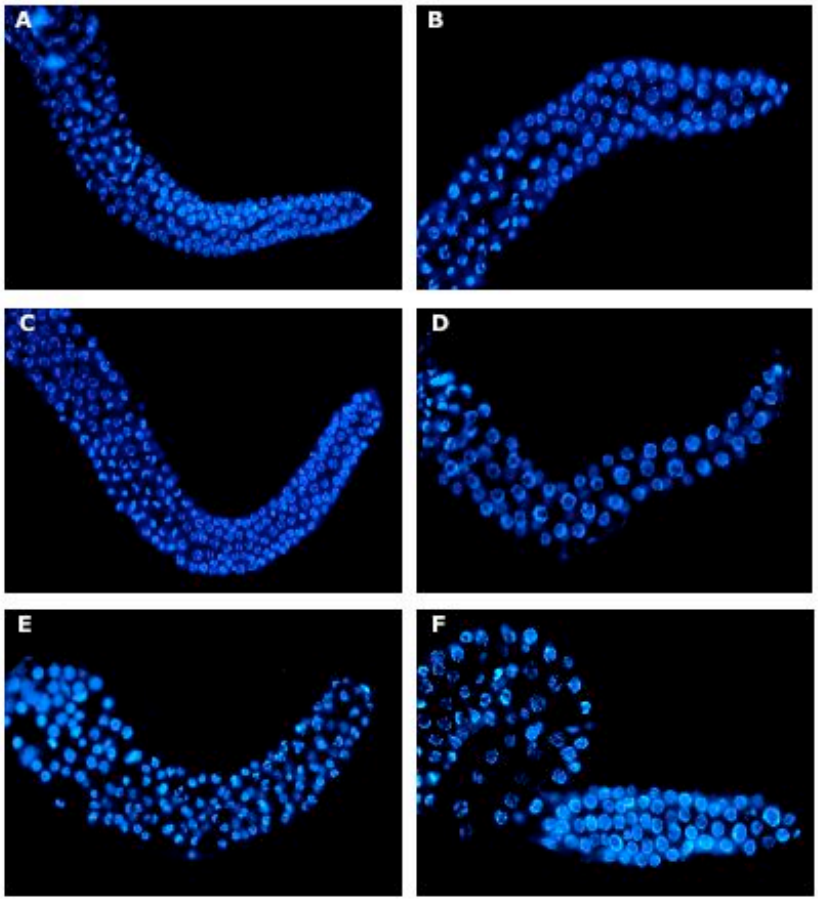

Figure 4. The intra-S checkpoint is functional in *atm-1* and *atl-1* mutants

Wild-type, *atm-1(gk186)* and *atl-1(tm853)* mutant animals were either fed on 25mM hydroxyurea for 7 h after the L4 stage (B, D, F) or were left untreated (A, C, E). Dissected gonads were stained with Hoechst 33342 and visualized under a fluorescence microscope. Arrested nuclei manifest an enlarged size, compared to the control situation.

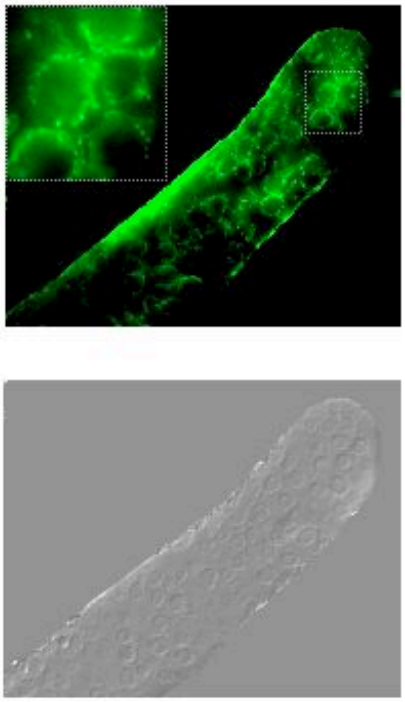

Figure 5. A transcriptional *atm-1* reporter reveals germline expression

Fluorescence and DIC microscopy of a transgenic animal expressing a low-copy P*atm-1*::GFP construct. All the cells in the germline are highlighted with GFP.

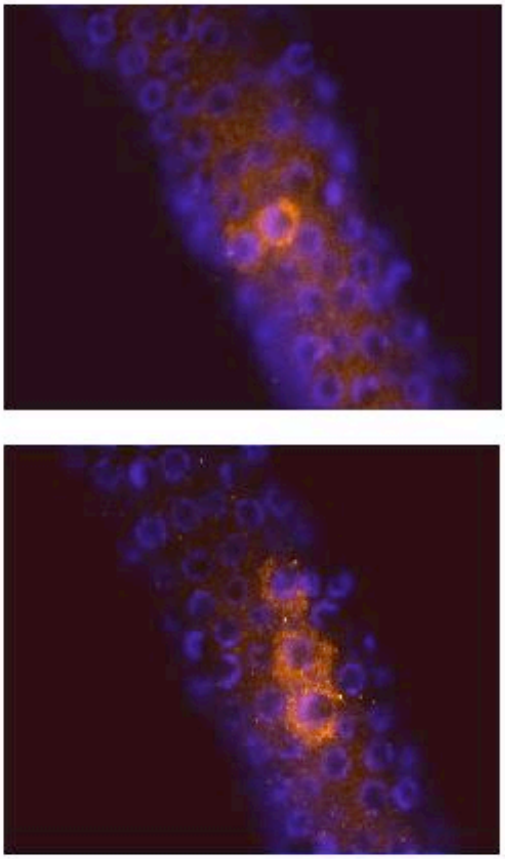

Figure 6. ATM-1 has a localized perinuclear expression that partially overlaps with DNA, following UV-C

Immunostaining using a monoclonal antibody against the C-terminal part of the human protein. Dissected gonads from wild-type and 5 h UV-treated animals were stained with the CT1 and co-stained with DAPI. Images were processed with the Openlab software.

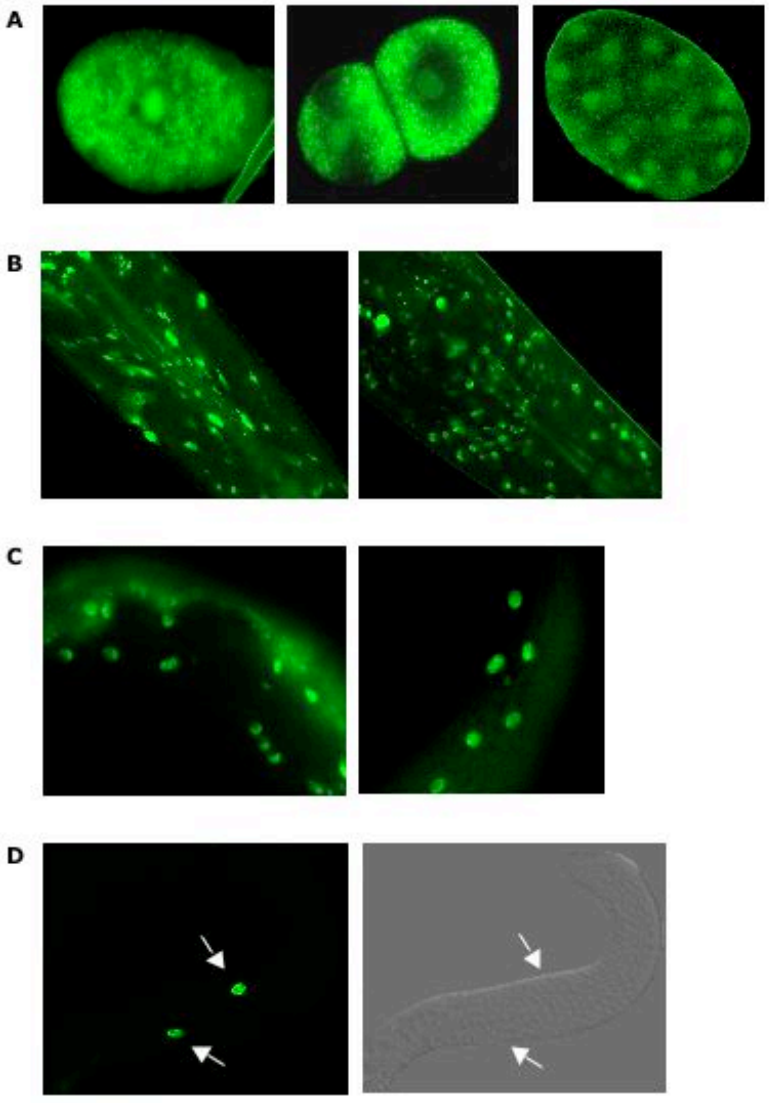
A
B
C
D

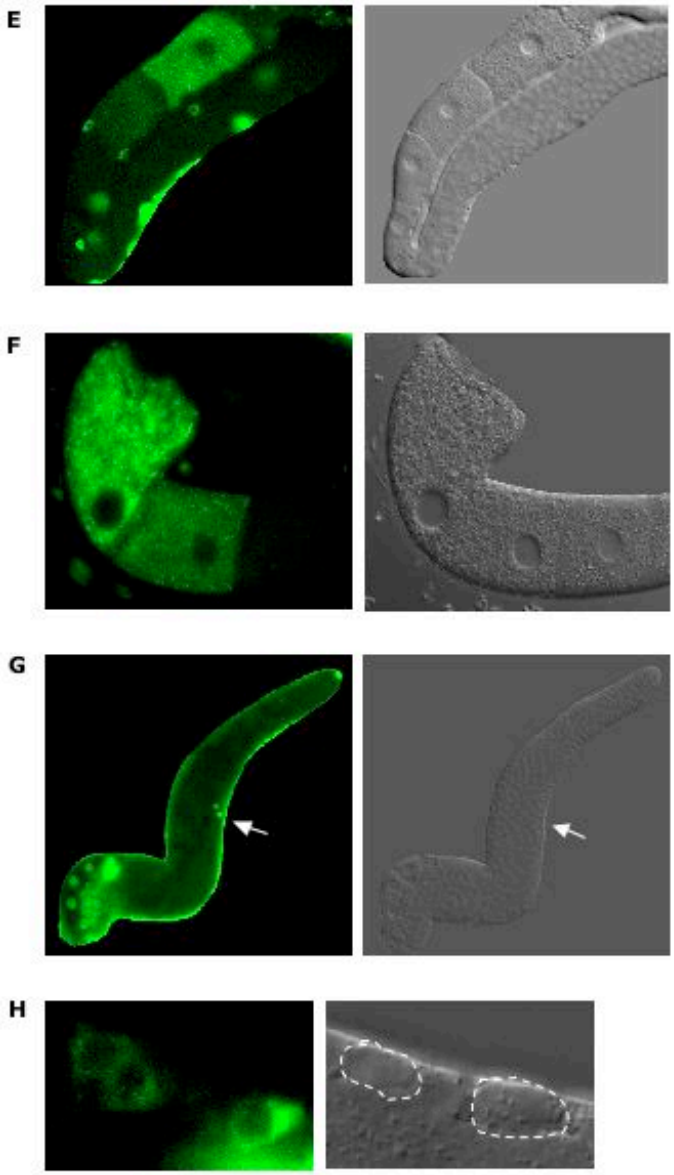
E
F
G
H

Figure 7. Expression pattern of XPA-1::GFP in *C. elegans*

Fluorescence microscopy of different tissues expressing a low-copy XPA-1::GFP transgene. (A) One-, two- and 50 cell-embryos, (B) different head neurons, (C) intestinal cells, (D) somatic sheath cells, (E) and (F) the fourth and third fully developed oocytes and (G) cells in the latest stages of prophase I and occasional early meiotic cells exhibit a GFP signal. (H) Moreover, apoptotic corpses are highlighted with GFP.

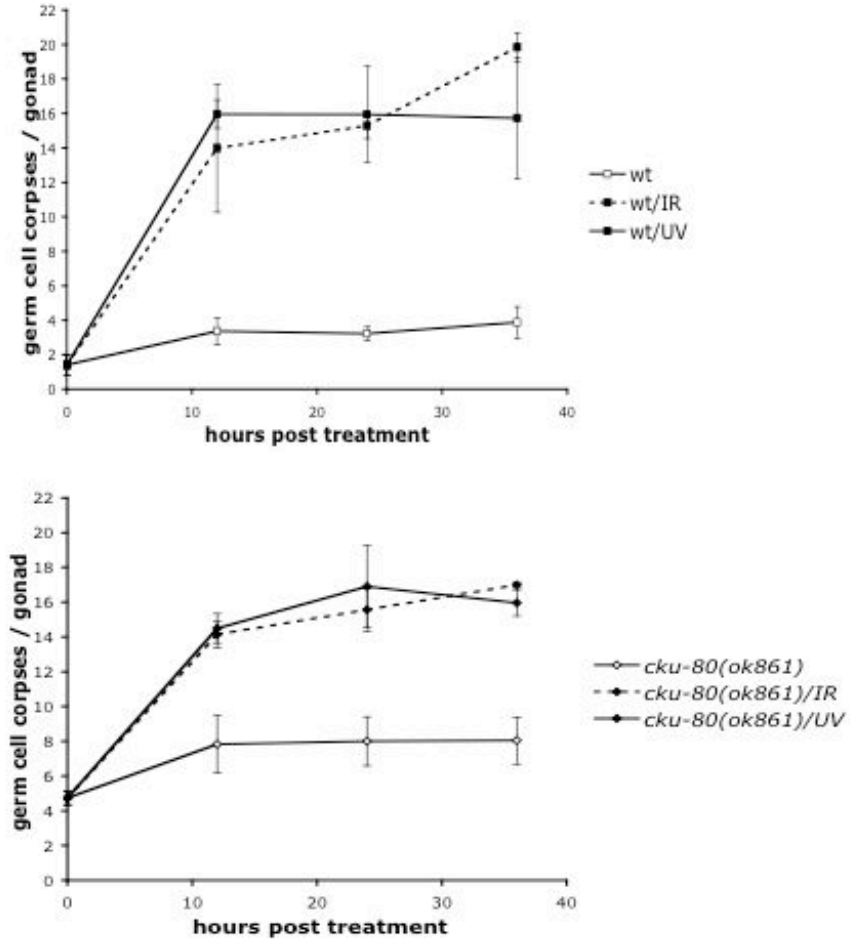

Figure 8. *cku-80* mutants respond to Ionizing Radiation and UV-C

Time course analysis was performed with wild-type animals and *cku-80(ok861)* mutants. Apoptotic corpses were scored in the meiotic region of one gonad arm of young adult animals, during the course of time and following 120 Gy of X-rays and 100 J/m^2 of UV-C. Data shown represent the average number of two independent experiments ± SD.

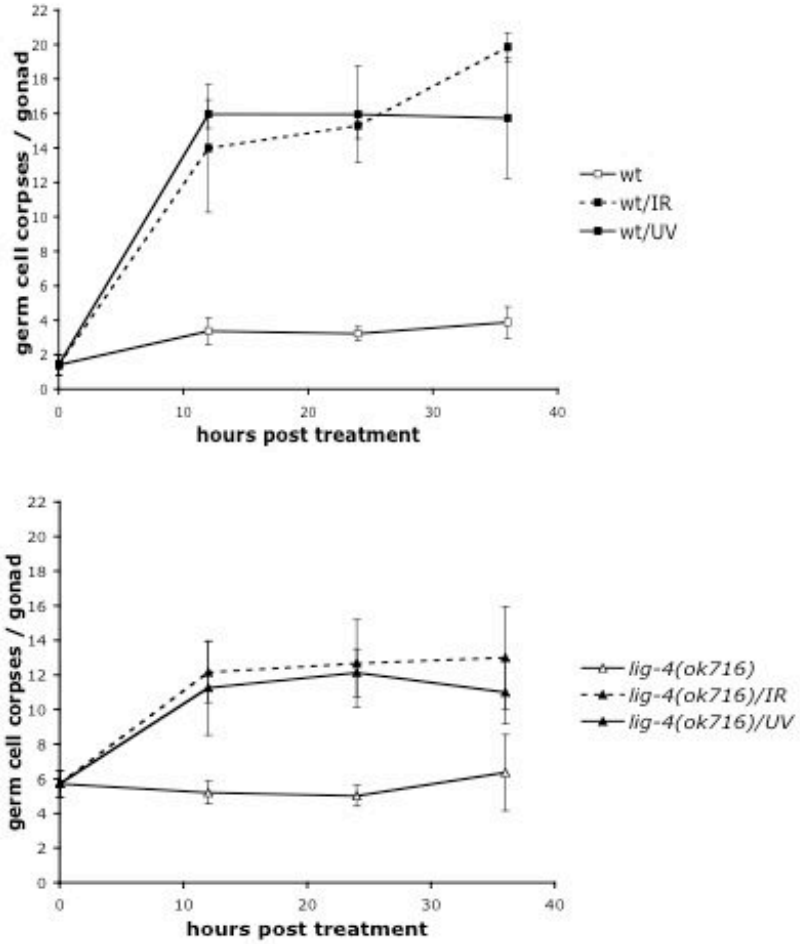

Figure 9. *lig-4* mutants respond to Ionizing Radiation and UV-C

Time course analysis was performed with wild-type animals and *lig-4(ok716)* mutants. Apoptotic corpses were scored in the meiotic region of one gonad arm of young adult animals, during the course of time and following 120 Gy of X-rays and 100 J/m^2 of UV-C. Data shown represent the average number of two independent experiments ± SD.

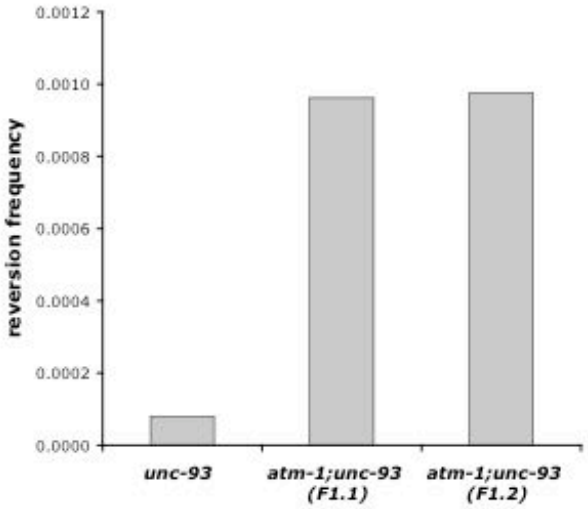

Figure 10. *atm-1* mutants exhibit genomic instability, based on the reversion of an Unc phenotype

Spontaneous *unc-93(e1500)* reversion frequencies in *atm-1*(+) and two independently generated *atm-1(gk186);unc-93(e1500)* strains, F1.1 and F1.2.1. The assay was performed according to Hofmann *et al.*

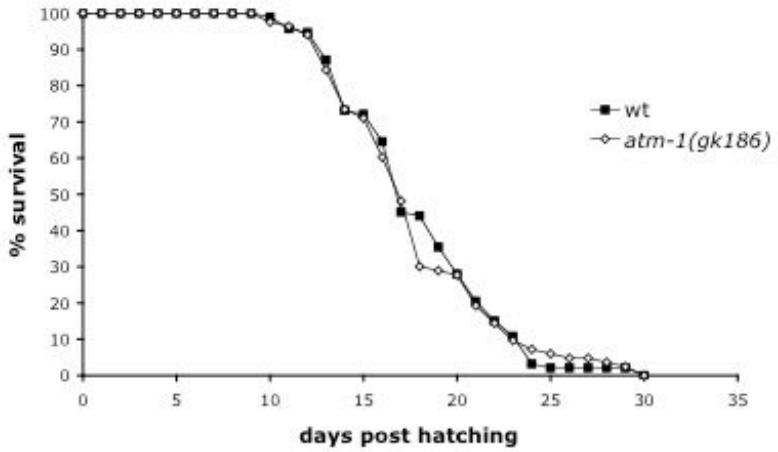

Figure 11. *atm-1* mutants show a lifespan similar to the wild-type

Adult lifespan assay of wild-type and *atm-1(gk186)* mutants grown on OP50 plates. Between 80 and 100 animals were used in this assay and the data-points represent the average of two independent experiments.

CHAPTER 6

A ROLE FOR A PROTEIN SIMILAR TO A SPLICE VARIANT OF THE HUMAN RNA POL I BETA SUBUNIT IN DNA DAMAGE RESPONSES IN THE *C. ELEGANS* GERM LINE

Preface

The work in our lab aims to decipher the mechanisms by which eukaryotic cells detect various forms of DNA damage and then signal the presence of these structures to the DNA repair machinery, the cell cycle engine and the apoptotic device. As many aspects of the DNA damage response have been highly conserved throughout eukaryotic evolution, we are analyzing proteins involved in these pathways in the model organism of *C. elegans*.

Having defined the basal components that constitute the DNA damage signaling pathway initiated following exposure of the *C. elegans* germ cells to ionizing radiation, we turned our efforts to identify new players. In this chapter I describe the work initiated by Randy Hofmann, a former post doc in the Hengartner lab and continued by myself during the third year of my PhD thesis.

6.1. Identification of *rpo-1*

6.1.1. A forward genetic screen for mutants defective in cell cycle arrest upon ionizing radiation

Forward genetic screens in *C. elegans* is an important component of studies to unveil genes that, when mutated, disrupt a certain biological process. In the cell death field, labor-intensive screens under a compound microscope have been proven very useful for the identification of new genes (Ellis *et al.*, 1991, Hengartner *et al.*, 1992).

To identify novel genes that participate in the initiation of cell arrest upon treatment of the *C. elegans* germ cells with ionizing radiation, such a forward screen was conducted. It was performed as a F1 clonal screen using DIC microscopy to observe the desired phenotype. The parental generation of wild-type worms was mutagenized using the chemical alkylating agent EMS (1.25mM) and two generations afterwards the animals were exposed to 120 Gy of γ-rays. The rationale of this screen was based on the fact that germ cells that normally undergo cell cycle arrest in the mitotic zone exhibit the phenotype of few in number but large in size nuclei. A mutation disrupting the function of a gene involved in this response would suppress this phenotype. After screening 2000 haploid genomes, the *op259* mutation was recovered. Figure 1a shows the germline from a wild-type worm and an *op259* mutant under the DIC microscope, before and after treatment with IR. The difference in size of the mitotic nuclei upon treatment between the two genotypes is visible and easily detectable. The arrowheads in these two panels mark subcellular structures that become visible upon IR and they will be discussed further in paragraph 6.5.5 (Figure 14).

To quantify the phenotype that the *op259* mutants exhibit, Randy measured the population of cells that reside in a 50μm distance from the distal tip cell, 12 h after treatment with increasing doses of X-rays (Figure 1b). The initial number of germ cells that the untreated *op259* mutants possess is lower by 30% compared to the wild-type, probably due to a proliferation defect that the animals exhibit. Indeed the mutation causes a slow growth phenotype, estimated to be around 12 h later than the normal rate. Following treatment the wild-type animals show a sudden decrease in the number of cells, already with 30 Gy of X-rays. Upon the maximum dose used, the decrease is 68% from the initial levels. *op259* mutants, on the other hand, display only a 34% reduction in the number of proliferating germ cells at this dose. Although the cell cycle arrest response seems to be half as strong compared to the wild-type, the mutants do exhibit a decrease upon ionizing radiation, with kinetics similar to wild-type as the doses increases. An alternative method to quantify the response to IR and decide on whether the mutants are actually defective, is presented in paragraph 6.5.2. Nevertheless, the cell cycle arrest defect seems to be not the most prominent phenotype of *op259* mutants.

6.1.2. Mapping the *op259* mutation at the F14B4.3 locus

With a combination of three-factor and two-factor mapping techniques, Randy mapped the *op259* mutation on the right arm of chromosome I, near the center. A series of fine mapping and finally sequencing determined its position and the gene affected turned out to be F14B4.3. The expected amino acid sequence of the gene that was subsequently named *rpo-1* is 1127 long (Figure 2A). The gene is predicted to

code for the beta subunit of the DNA-directed RNA polymerase I, comprising seven domains.

Domain 1, which is also known as the protrusion domain, forms one of the two distinctive lobes of the Rbp2 structure in mammals. DNA has been demonstrated to bind to the concave surface of the lobe domain, and plays a role in maintaining the transcription bubble (Cramer *et al*., 2001). The other lobe is nested within this domain (domain 2). Domain 3 is also known as the fork domain and is proximal to catalytic site, whereas domain 5 is known as the external 2 domain. Between domain 3 and 5 lies domain 4, but shows no homology to the equivalent domain of the mammalian Rpb2. The external domains in multisubunit RNA polymerase (those most distant from the active site) are actually known to demonstrate more sequence variability. Domain 6 represents the hybrid-binding and the wall domain. In the Pol II transcription elongation complex, the hybrid-binding domain binds the nascent RNA strand/template DNA strand. It contains the important structural motifs, switch 3 and the flap loop and binds an active site metal ion. The structural domains anchor and clamp are part of domain 7. The clamp region (C-terminal) contains a zinc-binding motif and a region termed switch 4. The switches within the polymerase are thought to signal different stages of transcription (Cramer *et al*., 2001) (InterProScan description, EBI database).

The *op259* mutation resides in the first domain of the RNA Pol beta subunit and results in the alteration of amino acid 70 from a proline to a serine. To find whether the mutation affects a specially conserved residue, I selected a stretch around that region (residues 50-203) to identify similarities with proteins from other organisms. I subsequently aligned RPO-1 with the proteins that best matched it: the human RNA

polymerase I polypeptide beta (hPolIbeta), the human RNA polymerase I 135kDa polypeptide (hRpa135) and the equivalent from *S. cerevisiae* named yRPA135 (Figure 2B). Although the first two human proteins share 99% similarity, a stretch of 56 amino acids is missing from hRpa135. With a similarity between 40 and 45%, RPO-1 is most likely the homolog of the human RNA polymerase I polypeptide beta and the yeast Rpa135 (discussed further in paragraph 6.6.1). This result changes the initial notion that *rpo-1* is the actual second largest subunit of RNA PolI.

6.2. *rpo-1* is required for DNA damage-induced cell death

6.2.1. *rpo-1* mutants are defective for ionizing radiation- and UV-induced apoptosis

The cell cycle arrest is only one aspect of the DNA damage responses in the germline of *C. elegans*. To look for an involvement of *rpo-1* in the DNA damage-induced germ cell death, the mutants were followed in the course of time, after exposure to different doses of X-rays. Apoptotic corpses were scored in the meiotic region of one gonad arm of young adult animals, having the response of wild-type animals as a control (Figure 3a). Under all doses tested, the *rpo-1(op259)* mutants exhibit a defect in mounting an apoptotic response to ionizing radiation. Moreover, to test whether *rpo-1* is also involved in the UV apoptotic pathway which, as discussed in Chapter 5, has some different genetic requirements from the IR pathway, the mutants were exposed to Ultraviolet Light (254nm). A similar time course analysis was performed using 120 Gy of X-rays and 40 J/m^2 of UV-C light, as shown in Figure

3b. *rpo-1(op259)* mutants are defective for both ionizing radiation and Ultraviolet Light-induced apoptosis.

6.2.2. *rpo-1* mutants fail to respond to endogenous DNA damage

Apart from damage caused by an external source of genotoxic stress, double-strand breaks can occur normally during meiotic prophase as the initiating events in meiotic recombination. In *C. elegans* such breaks can initiate apoptosis (Gartner *et al.*, 2000). Inhibition of *rad-51*, a member of the RecA family that catalyzes the invasion of DNA single-strand overhangs into a recipient double-strand DNA to initiate the formation of D loops and the later steps of meiotic recombination, results in unresolved DNA breaks. This, in turn, leads to increased germ cell death. Mutants for the IR responsive pathway, such as *hus-1(op244)*, *mrt-2(e2663)* and *clk-2(mn159)* as well as for the p53 homolog *cep-1(gk138)* can suppress *rad-51(lf)*-induced cell death, suggestive of its nature as DNA damage-induced.

To test whether *rpo-1* can exert the same function as the above checkpoint and pro-apoptotic genes, the germline of *rad-51(lg8701)* and *rpo-1(op259);rad-51(lg8701)* mutants was scored for the presence or not of excessive cell death. The *rad-51* homozygote mutants have a maternally rescued embryonic lethal phenotype and are therefore kept balanced with the nT1 balancer chromosome. Both homozygotes and heterozygotes animals, though, have increased germline apoptosis and they are both equally hypersensitive to the effects of ionizing radiation (Figure 4A). Increased cell death due to loss of *rad-51* function is suppressed by the *op259* mutation, suggesting that endogenously DNA damage-induced cell death does not occur properly in the mutants. Moreover, the hypersensitivity upon radiation treatment is also suppressed

by the *op259* mutation in *rpo-1*, supporting the previous finding that ionizing radiation-induced cell death fails to take place in the absence of RPO-1 (Figure 4B).

To corroborate this result, Randy examined the genetic relationship between *rpo-1* and *abl-1*. The latter is the homolog of human c-Abl, a conserved nonreceptor tyrosine kinase that integrates genotoxic stress responses, acting as a transducer of both pro- and antiapoptotic effector pathways. In *C. elegans* the gene serves an anti-apoptotic purpose in the germ line acting as a negative regulator of the pathway initiated by the checkpoint genes *hus-1*, *mrt-2* and *clk-2* and leading to the activation of the p53 homolog, *cep-1*. Worms carrying a deletion in the *abl-1* gene are specifically hypersensitive to radiation-induced apoptosis in the germline (Deng *et al.*, 2004).

Apoptotic corpses were, therefore, scored in the meiotic region of one gonad arm of *abl-1(ok171)* and *rpo-1(op259);abl-1(ok171)* mutant animals, that were either treated with 120 Gy of X-rays or were left untreated. The increased baseline in germ cell apoptosis observed in *abl-1(ok171)* mutants is inhibited by loss of *rpo-1* function (Figure 5). This suggests that, death arising from endogenous damage probably due to environmental stress or meiotic recombination intermediates requires an intact *rpo-1* gene to occur. Additionally, the hypersensitivity of *abl-1(ok171)* mutants upon ionizing radiation is suppressed by the *op259* mutation in *rpo-1*, suggesting once more that radiation-induced cell death does not occur properly in the absence of RPO-1.

The fact that artificially induced DNA double strand breaks have the same effect as breaks caused by irradiation regarding the lack of activation of apoptosis, gives *C. elegans rpo-1* a place in the DNA damage signaling network.

6.2.3. RNAi against *rpo-1* phenocopies the *op259* mutation

To support the finding that *rpo-1(op259)* mutants are defective for any type of DNA damage-induced cell death, I undertook the commonly used approach of the RNAi application. A similar to the mutant phenotype would indicate that the defect we observe is due to a lowering in the activity of the protein under study.

Suppression of the *rpo-1* transcripts using standard conditions applied in the lab (feeding L1 worms with 1mM IPTG) resulted in sterility of the parental worms and severe germline defects. This suggests, in parallel, that the *op259* mutation is hypomorphic and that further interference with the physiological function of the gene affects their normal development. After optimization the conditions required application of RNAi at the L3 larval stage using 2.5mM of IPTG. Apoptotic corpses were subsequently scored in the meiotic region of young adult animals before and 12 h following treatment with 120 Gy of X-rays (Figure 6). In independent experiments using different controls the cells failed to undergo apoptosis in response to DNA damage, proving the validity of our results with the mutant.

In a parallel effort to rescue the apoptotic defect by inserting the wild-type copy of the *rpo-1* gene, the outcome was less successful. Cloning the full length of the gene including promoter sequences was not possible. I therefore used the cosmid that contains the *rpo-1* locus and tried to inject it in the germline of *rpo-1(op259)* mutants, with the help of Jason Kinchen. It is known, however, that insertion of high copies of external DNA is silenced in the germline. For that reason, I looked at the first generation of animals that had obtained the cosmid. Following treatment with X-rays there was a partially penetrant increase in the number of corpses similar to the wild-

type response, showing rescue of the mutant phenotype (data not shown). The cosmid, as expected, was not active in the following generations.

6.3. Physiological cell death is normal in *rpo-1*

6.3.1. *rpo-1* lies upstream of the apoptotic and engulfment machinery

The failure of germ cells to undergo apoptosis in response to DNA damage in a *rpo-1* mutant background could also raise the question of how efficient the apoptotic machinery itself is in this mutant. Such a possibility can underlie two different occurrences: Either the death activity of the apoptotic machinery is compromised, or there is a death-suppressing activity present.

To explore this issue, apoptotic corpses were scored during the course of time in the germline of animals carrying both the *op259* mutation and the *n1950*, a strong loss-of-function mutation in the cell death suppressing gene, *ced-9* (Figure 7a). The latter results in increased levels of germ cell death, consistent with the protective role of *ced-9* in the germline (Gumienny at al., 1999). The *op259* mutation in *rpo-1* does not suppress loss of *ced-9* function, suggesting that RPO-1 acts upstream of a functional apoptotic machinery.

Loss-of-function mutations in genes that function in engulfment result in the accumulation of persistent apoptotic cell corpses and genetically define two partially redundant pathways. It has been proposed that these genes essential for engulfment of apoptotic corpses also play a role in cell killing (Reddien *et al.*, 2001). To exclude

that the defect in DNA damage-induced cell death in the *rpo-1(op259)* mutants is due to an improper function of the engulfment machinery, the *ced-6* mutants were chosen for study. CED-6, an adaptor molecule acting within engulfing cells promotes the engulfment of cells at both early and late stages of apoptosis (Liu and Hengartner, 1998). Apoptotic corpses were then scored in the meiotic region of *rpo-1(op259)* and *rpo-1(op259) ced-6(n1813)* animals in the course of time (Figure 7b). Loss of *ced-6* function is not suppressed by the *op259* mutation in *rpo-1*, suggesting that RPO-1 does not affect the clearance of apoptotic corpses and therefore the lapse of physiological cell death. Furthermore, death in *rpo-1(op259)* is, as expected, suppressed by *ced-3(lf)*, suggesting that it is indeed apoptotic in nature.

In addition, to prove that physiological cell death can occur unperturbed, Randy also scored apoptotic corpses during the course of time in the germline of animals carrying both the *op259* mutation and a loss-of-function mutation in a gene that affects germline apoptosis, *gla-1* (Figure 7c). The *op234* mutation results in increased levels of germ cell death under physiological conditions, although the mechanism of action is still not so clear (Milstein, PhD thesis, 2001). The *op259* mutation in *rpo-1* does not suppress loss of *gla-1* function, suggesting that RPO-1 does not affect physiological cell death. Or at least, it does not interfere with something that activates the apoptotic machinery in the absence of external DNA damage in this mutant.

All the above double mutant analysis with components of both the apoptotic and the engulfment machinery points to the fact that, germ cells in *rpo-1* mutants not only have the intrinsic ability to die, but also to be phagocytosed properly using a fully functional at all stages apoptotic device.

6.4. Understanding the mode of RPO-1 function

6.4.1. RPO-1 affects the transcriptional activation of *egl-1* and *ced-13*

An important element of the apoptotic DNA damage response in *C. elegans* is the transcriptional activation of *egl-1* and *ced-13*, the two genes coding for the BH3-only domain proteins. This HUS-1 and CEP-1- dependent process is what triggers the increased germ cell apoptosis following ionizing radiation (Hofmann *et al.*, 2002).

The observation that DNA damage-induced germ cell death is abrogated in *rpo-1* mutants, made it reasonable to examine the induction of the two genes. I measured the change in the mRNA levels of *egl-1* and *ced-13* by real-time Q-RT-PCR, during a time course and following treatment with 120 Gy of X-rays (Figure 8a). As expected, in *rpo-1(op259)* mutants induction of *egl-1* is compromised to a significant degree, showing an average of 50% reduction compared to the wild-type, for all the time-points tested. The *op259* mutation, on the other hand, has a more severe impact on the induction of *ced-13*, with barely any induction compared to the wild-type situation, especially for the 6 to 24-hour time-window.

Thus, RPO-1 is required for the activation of the two BH3 domain-bearing genes in *C. elegans*. This finding, on the other hand, does not unveil any information about the order of action of *rpo-1* and other genes that show a similar defect in the transcriptional induction of *egl-1* and *ced-13*. It is still possible that *rpo-1* acts in the principal DNA damage pathway comprising *hus-1* and *cep-1*. Alternatively, it can exert its function in a pathway parallel to the previous one and still diverge with it at the level of the two pro-apoptotic molecules. Notably, though, the significant decrease

in mRNA induction is still distinguishable from the total abolishment observed in a *cep-1* loss-of-function.

6.4.2. RPO-1 affects the transcriptional activation of *pme-5* and *dod-22*

To investigate the possibility that RPO-1 is implicated in a pathway that controls general responses to genotoxic stress, other than or additional to those that directly affect the apoptotic machinery, I studied the regulation of *pme-5*. The gene encodes one of the members of the poly (ADP-ribose) polymerase (PARP) conserved family of enzymes. By catalyzing the synthesis of poly (ADP-ribose) and the covalent attachment of this polymer to glutamic acid residues of acceptor proteins such as histones and topoisomerases, it regulates cellular processes such as maintenance of chromatin structure, programmed cell death, and DNA replication and repair. In response to ionizing radiation expression of the *C. elegans pme-5* transcript increases, an activation that requires the DNA damage checkpoint gene *hus-1* (Chapter 7).

I therefore measured the change in the mRNA levels of *pme-5* by real-time Q-RT-PCR, during a time course and following treatment with 120 Gy of X-rays (Figure 8b). Transcriptional induction of the gene remains low in *rpo-1(op259)* mutants relative to the wild-type response, and is at comparable levels for all the different time-points. Interestingly enough, there seem to be two peaks in the expression of *pme-5* in the wild-type animals.

To assess the role of RPO-1 in a signaling network that involves not only responses to genotoxic stress, but is broader to include signals from the environment, I studied the regulation of *dod-22*. In a microarray experiment performed previously

in the Hengartner lab to identify genes that are upregulated in response to ionizing radiation in wild-type worms, the gene *dod-22* was found to be among the ones highly activated (Milstein, PhD thesis, 2001). It turned out that *dod-22* also belongs to a group of genes that act downstream of *daf-16* to influence lifespan in *C. elegans* (Murphy *et al.*, 2003). It is postulated that the insulin/IGF-I pathway exerts its effect on lifespan by upregulating a wide variety of genes, including cellular stress-response genes. How the finding with *dod-22* and presumably other DNA damage responsive genes is integrated to this notion is currently unknown.

I measured the change in the mRNA levels of *dod-22* by real-time Q-RT-PCR, during a time course and following treatment with 120 Gy of X-rays (Figure 8b). As was previously the case, transcriptional induction of the gene is compromised in *rpo-1(op259)* mutants relative to the wild-type response. In addition, the mRNA levels remain constant in all the different time-points tested, compared to the gradual decline observed in the wild-type animals after the 6-hour time-point.

Thus, RPO-1 is required not only for the transcriptional activation of the two pro-apoptotic genes, *egl-1* and *ced-13*, but seems to regulate at least a small set of other DNA damage responsive genes. This fact is not to be generalized until more genes are tested or the exact function of RPO-1 in DNA damage responses is elucidated. Moreover, the link that bridges environmental perturbation with the cellular metabolism and the genomic status is still unidentified.

6.4.3. RPO-1 does not affect the expression pattern of CEP-1 upon ionizing radiation

Given the lack of apoptosis in *rpo-1* mutants following infliction of DNA damage, a phenotype that is also shared by the p53 homolog in *C. elegans*, we thought of examining any possible genetic interaction between the two factors.

For this purpose, Randy followed the localization of CEP-1 in the germline in a *rpo-1* mutant background. Animals carrying integrated copies of a CEP-1::GFP transgene are expressing the fusion protein throughout the germline. The construct is lacking the 3'-UTR of the *cep-1* gene, therefore missing important regulatory elements that would restrict expression in the mitotic and pachytene zone, as recently described (Schumacher *et al.*, 2005). Despite that, it proves itself suitable for this type of analysis to be performed.

Under normal conditions, the expression pattern is largely uniform throughout the tissue in a wild-type background. Following treatment with 120 Gy of X-rays, the signal is redistributed (Figure 9A). Certain cells in the mitotic compartment are highlighted and these usually overlap with the morphologically big cells. However, since *cep-1* is dispensable for cell cycle arrest, these might simply represent damaged cells. Similarly, a number of meiotic germ cells are enriched in GFP signal. In these cells we postulate that CEP-1 has been stabilized, presumably at the posttranslational level, and is competent to exert its pro-apoptotic function. In a *rpo-1* mutant background, the pattern is not at all different from the wild-type situation described above (Figure 9B). Certain cells accumulate increased GFP signal and the protein is preferentially localized in some others.

We therefore conclude that there is no dependency of the CEP-1 localization or expressivity on the presence of a functional RPO-1. This further implies that *rpo-1* might act either downstream or in a pathway parallel to *cep-1* and they both converge at the level of cell death initiation upon DNA damage.

6.4.4. Loss of *rpo-1* function results in hypersensitivity upon IR

A sensitive measure for the ability towards DNA damage responses, accounting for the combined effects on apoptosis, cell cycle arrest and repair, is the radiation sensitivity assay. The survival of the embryos generated from mitotic cells that have been exposed to the damaging effects of radiation is assessed that way.

I used this method to determine whether animals with impaired *rpo-1* activity are sensitive to the irradiation, as is the case for known checkpoint genes. Animals from different genetic backgrounds were irradiated at the L4 stage with 120 Gy or were left untreated. A day later they were let lay eggs and finally unhatched embryos were counted and expressed as a fraction of the total number laid. As is shown in Figure 10, *rpo-1* exhibits considerable levels of embryonic lethality under normal conditions and at 20ºC (21%). The most likely explanation would be an essential function for the protein during embryogenesis that results in decreased progeny survival. However, an involvement of the protein in the process of repairing endogenous damage cannot be excluded. Following treatment with X-rays, this percentage increases up to 42%, a value that lies between the one for *hus-1(op244)* and *clk-2(qm37)* checkpoint mutants. This effect could probably be the result of inability to cope with the inflicted damage.

Interestingly, simultaneous loss of the *hus-1* checkpoint gene under normal conditions gives rise to a synthetic lethal phenotype for *rpo-1* with 54% progeny that

don't survive. This dramatic effect in survivorship often implies that possible genetic interactions might exist to insure either proper repair in the germline or proper propagation of the embryos. In contrast to that, combined loss of *rpo-1* and *clk-2* does not confer any increase in the severeness of the phenotype, resulting in the phenotype of the former. This piece of evidence gives probably a hint as to the pathway where *rpo-1* might be involved. It is very likely that both genes form a genetically distinct pathway in response to DNA damage. Indeed, *clk-2* defines a novel pathway parallel to that of *hus-1*, based on several parameters including embryonic lethality data (Ahmed *et al.*, 2001, Hofmann *et al.*, 2002).

6.5. Additional phenotypic characteristics of *rpo-1*

6.5.1. *rpo-1* mutants have an abnormal nucleus and nucleolus morphology

The overall size of a metazoan is under tight control at the cellular level. Growth occurs by increases in both the size of individual cells and in the actual number of cells. Although these processes are coordinated most of the times, with cells increasing in size and subsequently dividing, they can also become uncoupled. Rapid cleavage divisions, for instance, occur during early embryogenesis without any increase in size. Conversely, growth of cells in a certain tissue can happen in the absence of cell division. It is very well established that cancer arises from uncontrolled cell division, but there is accumulating evidence that inappropriate cell size increase can play a big role in its development and/or progression (Prober and Edgar, 2001, White, 2005, Goberdhan and Wilson 2003).

Studies in bacteria and yeast have previously demonstrated that cell growth is closely linked to translational control and ribosome biogenesis (Nomura *et al.*, 1984). This correlation becomes apparent for example in the diminished transcription of ribosomal RNAs (rRNA and 5S RNA) during quiescence and subsequent increase after stimulation with growth factors.

The nucleolus represents a highly dynamic nuclear compartment of the interphase nucleus. Its major established function is the synthesis of rRNA and the assembly of preribosomal subunits. Among the genes that negatively regulate ribosome synthesis through their ability to inhibit both RNA polymerase I and III transcription, are the drosophila RB retinoblastoma protein (Cavanaugh *et al.*, 1998, White, 1997) and the *C. elegans ncl-1* (Frank and Roth, 1998).

One of the obvious phenotypic characteristics that also led to the isolation of the *rpo-1(op259)* mutants is the small size of the germ cell nuclei. To investigate the underlying events that give rise to such a morphology and attempt to probably connect this feature with the inherent inability of the mutants to respond to DNA damage, I systematically quantified the size of both nuclei and nucleoli.

Animals from different genetic backgrounds at the L4 stage were used to count the diameter of the first mitotic germ cells under the DIC microscope (Figure 11a). In this analysis, DNA damage defective mutants, of the checkpoint gene *hus-1* and the pro-apoptotic factor *cep-1* were included. As a control for lack of cell death, the *ced-3* mutants were also measured. Moreover, mutants for the *ncl-1* gene and animals mutated for both *ncl-1* and *rpo-1* were analyzed. In *C. elegans*, the *ncl-1* gene codes for a B-box zinc finger protein that may be a suppressor of rRNA synthesis and an inhibitor of cell growth. *ncl-1* mutants are larger than wild-type worms and have

larger cells with elevated protein content. In almost all their cells the nucleoli are also enlarged due to higher rates of rRNA synthesis and consequently higher steady state levels of rRNA.

As expected, animals defective in *rpo-1* have significantly smaller nucleoli and animals with compromised *ncl-1* activity are much larger in nucleoli size. Double mutants exhibit the phenotype of the *rpo-1* single mutants, suggesting that *rpo-1* is epistatic to *ncl-1*. The same holds true for the nucleoli size of meiotic germ cells that reside just before the bend of the gonad, leading to the same conclusion for the probable order of action of the two gene products (Figure 11b). The same difference in the size of the nucleoli is also reflected in the nuclei size of the meiotic cells. Moreover, it seems that *hus-1* mutants follow a similar pattern, with their nuclei being smaller than the normal and *cep-1*, although to a lesser degree, falls into the same group. A daring but attractive explanation for this result would be a general tendency for DNA damage signaling mutants to display such phenotypic characteristics that are somehow related to the lack of mounting the proper responses, cell death in particular, upon genotoxic stress. In contrast to that, the observed effect that the *ced-3(n717)* mutation has on nuclei size of the animals could be attributed to the absolute lack of physiological apoptosis. Such a defect results in the accumulation of extra germ cells that lack the appropriate nutrients and this manifests the effect on cell size.

To further support the epistatic relationship between *rpo-1* and *ncl-1* and in parallel to test it in a tissue other than the germline, I measured the diameter of the nuclei in 4-cell stage embryos of all the previous genetic backgrounds (Figure 11c). Also in a somatic tissue the *op259* mutation suppresses the phenotype of the increased nucleus size of *ncl-1*. To speculate on the mode of action of these proteins, both are expected to be necessary for a cell to achieve the balance in transcribing ribosomal DNA at

adequate amounts. In *C. elegans rpo-1* is most probably required to relieve the negative strain posed by *ncl-1* on the ribosomal genes.

6.5.2. The nucleus and nucleolus size of *rpo-1* mutants changes upon ionizing radiation

Using the approach described in the previous paragraph to demonstrate the deviation of *rpo-1* from the normal sized nuclei, it turned out that it could be proven a useful tool to quantify cell cycle arrest in the corresponding mutant. Already in paragraph 6.1.1 it was shown that the mutants exhibit a decrease in the mitotic germ cell number upon ionizing radiation, although not as strong as the wild-type animals.

In this case, wild-type and *rpo-1* mutant animals were picked as L4 and irradiated with 120 Gy of X-rays. Seven hours later the diameter of the nucleus and the nucleolus of the first mitotic cells was measured (Figure 11d). In both cases, there is an increase observed in size that falls into the range of 30-33%. What differs, though, is the initial size of cells in wild-type and *rpo-1* mutants, that counts for 12% and 26% reduction in the latter for the nuclei and the nucleoli, respectively. In conclusion, the increase in size following IR reflects a concomitant decrease in the number of germ cells and points to a largely functional cell cycle checkpoint for *rpo-1*.

6.5.3. Ribosomal RNA synthesis is altered in *rpo-1* mutants

A decrease in the germ cell size is likely to indicate a diminish in protein synthesis and this, in turn, apparently demonstrates the decreased capability for protein synthesis or ribosome production. Because the nuclear and nucleolar size in *rpo-1*

mutants is smaller compared to the wild-type, we hypothesized that the levels of ribosomal RNA might also vary.

The ribosomal RNA genes are arranged in large clusters of usually many hundreds of genes. Each gene unit contains an 18S, 5.8S and 28S gene. These genes are transcribed by the RNA polymerase I as a single precursor rRNA (pre-rRNA) transcript containing external transcribed spacers at the 5'- and 3'-ends, and internal transcribed spacers separating the genes. The pre-rRNAs are processed to mature rRNAs, with a procedure that requires a number of nucleolar proteins, nucleases and small nucleolar ribonucleoprotein particles (snoRNPs).

For the purpose of this experiment I assayed the steady state levels of processed and unprocessed 5.8S rRNA transcripts with real time Q-RT-PCR (Figure 12). I compared the amount of transcripts in the *rpo-1(op259)* mutant with that in wild-type and *ncl-1(e1865)* mutant. Moreover, I used a strain that bears a deficiency in the rDNA locus, *eDf3*/*eDf24*, and one that carries a duplication of that region, *sDp1*. Both the processed and the unprocessed form of the 5.8S rRNA is reduced in the absence of *rpo-1*, in consistency with the small cell size of the mutants. In *ncl-1* only the unprocessed form of transcripts is slightly higher, whereas the processed one is rather lower than the normal levels. A possible explanation for that would be that, having a not properly functional protein only affects the production of the primary transcript, but does not have an effect on the processing itself. In the deficiency strain both primary and mature transcript levels are somewhat above background levels. In contrast to that, in the strain that has a duplicated rDNA locus, these levels are both significantly lowered. This result, although strikingly unconventional considering the capacity of the cells in the two respective genetic backgrounds, could still be explicable. An excess of rRNA transcripts might be toxic for the cells, thereby

repressing mechanisms might occur to control the rate of synthesis. On the other hand, insufficient amounts could lead to an increase in the production of the transcripts, to compensate for the loss.

These results suggest that both the levels of processed and unprocessed 5.8S rRNA transcripts are negatively affected in the *rpo-1(op259)* mutants and that this is reflected to the nuclear and nucleolar size. However, there is no hint about the underlying mechanism. Whether *rpo-1* acts directly or indirectly to control these levels needs to be determined.

6.5.4. *rpo-1* is epistatic to *ncl-1* and mimics the reduction in rRNA levels upon IR

The pro-apoptotic role of *rpo-1* in combination with the unconventional phenotype of the nucleolus in the mutants that were described so far, is challenging the concept of these two facts being linked at the molecular level. Indeed, differences in the morphology and the biosynthetic activity of the nucleoli between normal proliferating and neoplastic cells have been well documented (Busch, 1990, Horky *et al*., 2002). Increased nucleolar activity is coordinated with cell proliferation in tumor cells.

To address the issue of the existence of a relationship between ribosomal RNA production and commitment to cell death upon DNA damage, I quantified the apoptotic response in mutants with deregulated rRNA levels. Apoptotic corpses were scored in the meiotic region of young adult worms of the following genotypes: *rpo-1(op259)*, *ncl-1(e1865)*, *rpo-1(op259);ncl-1(e1865)*, *sDp1*, the already mentioned duplication of the 5.8S rDNA locus, *eDf3*/*eDf24*, the deficiency in that region and +/*rpo-1*Δ, a deletion around the *rpo-1* locus on one chromosome (Figure 13). The

response was measured at the 12- and the 24-hour time-point after application of 120 Gy of X-rays.

As expected, *rpo-1* mutants display a defect in the IR-induced apoptosis, whereas apoptosis in *ncl-1* mutants is comparable to the wild-type levels. In the double mutants apoptosis upon IR is suppressed, consistent with previous data regarding the germ cell size where *rpo-1* was shown to be epistatic to *ncl-1*. The cell death levels following irradiation in the strain carrying a duplication of the ribosomal locus (*sDp1*) are falling within the wild-type range. In contrast to that, when animals are devoid of a whole rDNA locus (*eDf24*), the apoptotic response is strongly compromised. Therefore, the deficiency in the *rpo-1* locus mirrors the *op259* mutation with respect to the inability to mount a proper apoptotic response following genotoxic stress. A similar behavior is observed when a deletion in the genomic region where *rpo-1* lies (+/*rpo-1*Δ) is present. The mutants have increased levels of endogenous apoptosis, for reasons that are not clear at the moment but are probably related to the nature of this allele. Upon treatment with ionizing radiation there is an increase observed, yet the fold-induction is 2-3 times less compared to the wild-type response.

These results point to an involvement of the ribosomal locus in triggering the appropriate DNA damage-induced apoptotic response. Whether it is the compromised production of ribosomal transcripts or the excessive production of these molecules more of an issue to consider is not clear yet. However, the results strongly suggest that the role of *rpo-1* in the DNA damage responses must be more specific, than simply a factor prerequisite for ribosomal synthesis. Titrating out the locus where it belongs already has an effect on cell death. The *op259* point mutation in a homozygous state, however, is likely to disrupt a crucial interaction that results, upon DNA damage induction, in lack of apoptosis activation.

6.5.5. Appearance of intranuclear structures upon IR in wild-type and *rpo-1* mutants

One of the observations that we made while treating wild-type animals with ionizing radiation is the appearance of "nuclear dots" in the mitotic germ cells (Figure 14A). These can have either a uniform round shape or an irregular shape, foci-like, and are scarcely found in the non-irradiated cells. Damage infliction results in a dramatic increase of their number in a 50μm distance from the DTC, both in the wild-type and the *cep-1(gk138)* background and to a lesser degree in the *hus-1(op244)* background (Figure 14B). In *rpo-1(op259)* mutants, however, their frequency under normal conditions is already high and only reaches half the levels achieved by the wild-type when cells are expose to IR. Interestingly, *clk-2(mn159)* mutants appear to show a similar defect in the generation of these "dots", suggesting that the presence and abundance of these intranuclear structures depend predominantly on a functional *rpo-1* and *clk-2* rather than any other pro-apoptotic gene. This is also consistent with the probability of the two forming a genetically distinct pathway (paragraph 6.4.4). Nevertheless, their frequent existence under normal conditions in the absence of *rpo-1*, imply a more sophisticated way of action and a complex type of regulation.

The nature and the possible role of these "dots" are currently unknown. It is reminiscent, however, of different other nuclear compartments and subnuclear domains, whose role in the regulation of gene expression, signaling, and cellular functions is constantly emerging.

Indeed, the nucleus contains a heterogeneous group of intranuclear (nucleoplasmic) structures, situated within the nuclear matrix and distinguished

mainly by morphologic criteria. The so-called nuclear bodies (NBs) include several domains containing granular and fibrillar materials. NBs are implicated in diverse major activities, such as pre-mRNA synthesis and processing, splicing, packaging, and traffic-transport within the nucleus and towards the cytoplasm. Prominent structures of the nucleus comprise the well-characterized Cajal bodies (CBs), the nucleolus, perinucleolar and perichromatin regions, PML bodies and similar intranuclear foci containing multi-molecular complexes with major role in DNA replication, surveillance, and repair, as well as messenger RNA and ribosomal RNA synthesis and assembly (Zimber *et al.*, 2004).

Research over the years has implicated the nuclear bodies in extreme physiological and environmental conditions. A number of diseases are believed to be related to those, ranging from neurodegenerative diseases to predisposition to cancer. The list with these diseases demonstrate that a lack of function due to a loss, structural change, and/or inappropriate localization of such proteins may result in cellular degeneration and death, or in a deregulation of processes such as cell proliferation, differentiation, apoptosis, and DNA surveillance, thus contributing to malignant transformation and degenerative diseases.

A closer focus on the ultrastructure of the observed upon irradiation nuclear structures, for example using electron microscopy, will probably shed light into their origin in the *C. elegans* germ line. Additionally, a search for the proteins that may reside or stored inside these formations could help elucidate their function in DNA damage responses. The lack of abundance in the *rpo-1* mutants may contribute to the rapid recognition of their function, based on the nature of the gene affected in these animals.

6.6. How is RPO-1 connected to the DNA damage signaling network?

6.6.1. RPO-1 is homologous to a splice variant of the second largest subunit of human RNA polymerase I

Despite the generation of all the data to expound the phenotype of *rpo-1(op259)* mutants and the involvement of the protein in the response to both endogenously caused and exogenously inflicted DNA damage, a clear association at the molecular levels is still missing. Further insight into the biological process where the *C. elegans rpo-1* might be implicated, are hampered by the lack of a set of interacting partners.

In an effort to identify proteins that are physically associated with RPO-1, a yeast-two-hybrid approach was undertaken by Randy Hofmann and Stuart Milstein. This attempt yielded no information, probably because the bait was the full-length protein.

Very often a segment of the protein of interest is used to generate the bait, especially since not all the parts of the protein confer to its function. I used the GlobPlot bioinformatics service to identify regions meant to be structured and therefore without any functional domain or, on the other hand, unstructured (disordered) and therefore with small motifs that are important for protein function. According to the Russell-Linding prediction model for the mutated residue in the *rpo-1(op259)* mutants lies within the 61-332 amino-acid segment, a sequence part with perfect order / globularity (Figure 15). This result is also confirmed by applying the "hot loops" parameters, where again the affected amino acid 70 (P) lies in a structured region (Figure 16).

Considering the fact that avoidance of potentially disordered segments in protein expression constructs can increase expression, ability to fold and stability of the

expressed protein, we are undertaking new efforts to exclude regions flanking the mutation that most likely contribute to instability.

The *rpo-1* gene product, though, was identified as part of the map of the interactome network of *C. elegans*, a study initiated to discover most of the existing protein-protein interactions in the nematode (Li *et al.*, 2004). In this data set, RPO-1, used either as a bait or being a prey, was found to interact with some of the subunits of the RNA polymerase I. More specifically, the homologs of the yeast RPA12 subunit, the RPC19 and RPC40 common to RNA polymerases I and III subunits, the common to all RNA polymerases RPB5 subunit, and the large subunit of RNA polymerase I, were the interactors obtained. These all have homologs in the human genome as well.

A closer look at the human proteins that claim to be potential functional homologs of RPO-1 resulted in a single gene named POLR1B. It turned out that the gene has two splicing variant forms, one of them being the second subunit of the RNA polymerase I, alternatively known as hRpa135. For the other isoform (named hPolIbeta in Figure 2B), which lacks exon 2 from the mRNA transcript, no function has been assigned yet. The 56-amino acid stretch that is absent contains the region with the conserved proline residue that is mutated in the worm *rpo-1* product.

This raises the challenging hypothesis that the two proteins in the two different organisms constitute a new group of polypeptides, whose role is distinct from being one of the subunits of the RNA polymerase I complex. Novel functions might arise that are relevant to the cellular response to genotoxic stress, by the utilization of key gene units to control processes of DNA surveillance and cell demise.

6.6.2. RPO-1 is probably a functional homolog of the yeast Rpa135 protein

Interestingly, the yeast genome contains a gene homologous to *rpo-1* and the human RNA polymerase I polypeptide beta. The yRPA135 exerts the same function with the hRpa135, namely is part of the transcription complex, retaining at the same time the stretch that is missing from the human equivalent (see Figure 2B for details). A number of studies using affinity precipitation and two-hybrid experiments to discover interacting partners of the yeast protein, led to 32 proteins with diverse functions (http://db.yeastgenome.org/cgibin/phenotype/phenotype.pl?dbid=S000006214&type=allinteraction). Among members of the RNA polymerase complex, proteins that control chromatin assembly and chromosome function, proteins involved in proper folding or degradation of gene products, proteins required for nuclear transport were identified (Gavin *et al.*, 2002, Ho *et al.*, 2002, Krogan *et al.*, 2004, Flores *et al.*, 1999).

The Rad51 strand exchange protein, involved in the recombinational repair of double-strand breaks in DNA during vegetative growth and meiosis, was one of the interactors of yRPA135. Similar to the situation in worms the protein in yeast accumulates meiosis-specific double strand breaks (DSBs) at a recombination hotspot. Rad51 mutants are also defective for X-ray damage repair and gene conversions. The protein interacts with itself and other members of the *RAD52* epistasis group, all of which are involved in the repair of DSBs in DNA caused by ionizing radiation and MMS. Furthermore they are involved in the maintenance of telomere length and in mitotic and meiotic recombination. This result is of particular

interest since it gives the first link to a process initiated upon DNA damage, such as repair.

One of the four major serine/threonine phosphatases, PP2A, found to be implicated in the negative control of cell growth and division in yeast (Stark, 1996), was identified as another protein interacting with yRPA135. It was recently shown that PP2A interacts with ATM in undamaged cells, regulating its autophosphorylation and activity (Goodarzi *et al.*, 2004). Ionizing radiation induces phosphorylation-dependent dissociation of PP2A from ATM and loss of the associated protein phosphatase activity. Association of different targeting subunits with the core enzyme is known to be an important mechanism of regulating PP2A activity, substrate specificity, and localization to specific cellular microenvironments and/or signaling pathways. Moreover, a well-known cellular event where the phosphatase participates is the regulation of the cell cycle (Mumby and Walter, 1993). All this current knowledge might be proven very useful for the elucidation of the *rpo-1* role in the cellular responses and in DNA damage signaling activation in *C. elegans* and might give insights for new regulatory relationships in mammals.

Among the interactors of yRPA135, two proteins involved in ubiquitin-mediated protein degradation were recognized. Doa1, a WD repeat is known to play a role in controlling the cellular ubiquitin concentration. Additionally, it promotes efficient NHEJ (non-homologous end joining) in the postdiauxic/stationary phase of *S. cerevisiae*, since mutants show a decrease in the NHEJ/SSA (single-strand annealing) ratio (Wilson, 2002). San1, a ubiquitin-protein ligase is known to control the turnover of a specific class of unstable nuclear proteins including Sir4p but not Sir2p or Sir3p,

suggestive of a role of the protein in chromatin-mediated transcriptional silencing (Dasgupta *et al.*, 2004).

The possibility that RPO-1 might be implicated in a post-translational checkpoint to control its stability or activity during DNA damage responses is not to be overlooked. This would be in the same conceptual frame with findings in the mammalian field that there are multiple links between the ubiquitin/proteasome system and the apoptotic machinery. The function of p53, for instance, is substantially controlled through ubiquitylation by the RING-finger-dependent ubiquitin protein ligase Mdm2 and subsequent proteasomal proteolysis (Haupt *et al.*, 1997). Modulation of many cell-cycle regulatory proteins, such as cyclins and CDK inhibitors, also affects apoptosis (Nakayama *et al.*, 2000). In addition to that, various Bcl-2 family members have been identified as substrates of the proteasome, whose inhibition of degradation has been found to influence the outcome of apoptosis (Dimmeler *et al.*, 1999). Finally, the ubiquitin-ligase activity of IAPs (inhibitors of apoptosis) leads to their auto-ubiquitylation and degradation, when a cell needs to commit to apoptosis (Yang *et al.*, 2000).

6.7. Nucleolus: can site and size regulate function?

6.7.1. The "nucleolus and RPO-1 connection" hypothesis

The emergence of the *rpo-1* gene product from a gene that is normally involved in the production of ribosomal RNA, made us turn to the nucleolus as a potentially reference point for the protein function.

The nucleolus has a well-established role in ribosomal subunit assembly. Additional nucleolar functions, not related to ribosome biogenesis, have been discovered, though, within the last decade. One of the more intriguing novel roles is the participation of the nucleolus in sensing cellular stress and transmitting signals to the system that regulates the activity of p53. The latest model dictates that nucleolar disruption is a prerequisite for stabilization of p53 under various stress conditions (UV radiation, anti-cancer drugs, heat shock, hypoxia) (Rubbi and Milner, 2003), and that this stabilization is most likely dependent on the interaction of ARF with MDM2 (Zhang and Xiong, 2001) However, this sensor model may not hold for all cell types, or other nucleolar molecules can mediate the p53 response. A growing body of literature actually points to multiple levels of nucleolar involvement in p53 regulation, including the association of p53 with abundant nucleolar proteins (nucleolin and nucleophosmin) involved in ribosome biogenesis (Daniely *et al*., 2002, Colombo *et al*., 2002). Furthermore, the ribosomal protein L11 negatively regulates MDM2 and mediates a p53-dependent ribosomal-stress checkpoint pathway (Zhang *et al*., 2003).

It is very tempting to hypothesize that the *C. elegans* RPO-1, in analogy, might constitute a link between the nucleolus and DNA damage initiated responses. It is also very critical, though, to determine its precise localization. An association with the

nucleolus could reinforce this hypothesis. Moreover, identification of interacting partners for RPO-1 might help identify additional mechanisms by which a stress signal is perceived and transferred to the apoptotic machinery.

6.7.2. The "cell size and RPO-1 connection" hypothesis

The phenotypic feature of the *rpo-1* mutants with a smaller germ cell nuclei and nucleoli size, in combination with the apoptotic defect that they display upon DNA damage, made us consider the relationship between germ cell growth and proper activation of DNA damage responses.

Ribosome biogenesis is an essential cellular process that is highly coordinated to lead to accurate initiation and regulation of protein synthesis. Increase in rRNA synthesis by inactivating mutations, or alterations in the modification of rRNAs, or mutations and overexpression of ribosomal proteins might have deleterious effects on the cell. This can be manifested either by an increase in ribosome production, thereby leading to an upregulation in total translation, or by alterations in translation of specific mRNAs, which are involved in the regulation of cell proliferation. Furthermore, when key checkpoints important in coordinating ribosome production with accurate cell-cycle progression are lost, 'nucleolar stress' occurs with a subsequent unrestrained cellular proliferation (Ruggero and Pandolfi, 2003). In cancer cells which harbor inactivating mutations in p53 and Rb, for example, deregulation of Pol I and Pol III activity might contribute to tumorigenesis (Cairns and White, 1998, White *et al.*, 1996).

The growth defect of the germ cell nuclei, together with the restricted proliferation in the germline tissue of *rpo-1(op259)* mutants are associated with changes in the rate

of rRNA synthesis (discussed in paragraph 6.5.3). Whether and how *rpo-1* is implicated in the process of ribosome biogenesis needs to be clarified. If so, it is possible that either the global translation or the translation of certain mRNA transcripts is affected. In the second case, the protein synthesis of pro-apoptotic genes under conditions of stress is most likely to be disturbed.

Since one of the most striking visual features of cancer cells is their highly enlarged nucleoli and having the knowledge that several oncogenes and tumor suppressors might regulate malignant progression growth (White, 2005), it is important to consider how RPO-1 interacts with the mechanisms that regulate proper DNA damage responses.

References

Ahmed, S., Alpi, A., Hengartner, M.O. & Gartner, A. *C. elegans* RAD-5/CLK-2 defines a new DNA damage checkpoint protein. *Curr Biol.* **11(24)**, 1934-44 (2001).

Brenner, S. The genetics of *Caenorhabditis elegans*. *Genetics* **77(1)**, 71-94 (1974).

Busch, H. The final common pathway of cancer. *Cancer Res.* **50(16)**, 4830-8 (1990).

Cairns, C.A. & White, R.J. p53 is a general repressor of RNA polymerase III transcription. *EMBO J.* **17(11)**, 3112-23 (1998).

Cavanaugh, A.H., Hempel, W.M., Taylor, L.J., Rogalsky, V., Todorov, G. & Rothblum, L.I. Activity of RNA polymerase I transcription factor UBF blocked by Rb gene product. *Nature* **374(6518)**, 177-80 (1995).

Colombo, E., Marine, J.C., Danovi, D., Falini, B. & Pelicci, P.G. Nucleophosmin regulates the stability and transcriptional activity of p53. *Nat Cell Biol.* **4(7)**, 529-33 (2002).

Cramer, P., Bushnell, D.A. & Kornberg, R.D. Structural basis of transcription: RNA polymerase II at 2.8 angstrom resolution. *Science* **292** 1863-1876 (2001).

Daniely, Y., Dimitrova, D.D. & Borowiec, J.A. Stress-dependent nucleolin

mobilization mediated by p53-nucleolin complex formation. *Mol Cell Biol*. **22(16)**, 6014-22 (2002).

Dasgupta, A., Ramsey, K.L., Smith, J.S. & Auble, D.T. Sir Antagonist 1 (San1) is a ubiquitin ligase. *J Biol Chem*. **279(26)**, 26830-8 (2004).

Deng, X., Hofmann, E.R., Villanueve, A., Hobert, O., Capodieci, P., Veach, D.R., Yin, X., Campodonico, L., Glekas, A., Cordon-Cardo, C., Clarkson, B., Bornmann, W.G., Fuks, Z., Hengartner, M.O. & Kolesnick, R. *Caenorhabditis elegans* ABL-1 antagonizes p53-mediated germline apoptosis after ionizing irradiation. *Nat Genet*. **36(8)**, 906-12 (2004).

Dimmeler, S., Breitschopf, K., Haendeler, J. & Zeiher, A.M. Dephosphorylation targets Bcl-2 for ubiquitin-dependent degradation: a link between the apoptosome and the proteasome pathway. *J Exp Med*. **189(11)**, 1815-22 (1999).

Ellis, R.E., Jacobson, D.M. & Horvitz, H.R. Genes required for the engulfment of cell corpses during programmed cell death in *Caenorhabditis elegans*. *Genetics* **129(1)**, 79-94 (1991).

Flores, A., Briand, J.F., Gadal, O., Andrau, J.C., Rubbi, L., Van Mullem, V., Boschiero, C., Goussot, M., Marck, C., Carles, C., Thuriaux, P., Sentenac, A. & Werner, M. A protein-protein interaction map of yeast RNA polymerase III. *Proc Natl Acad Sci U S A* **96(14)**, 7815-20 (1999).

Frank, D.J. & Roth, M.B. *ncl-1* is required for the regulation of cell size and ribosomal RNA synthesis in *Caenorhabditis elegans*. *J Cell Biol.* **140(6)**, 1321-9 (1998).

Gartner, A., Milstein, S., Ahmed, S., Hodgkin, J. & Hengartner, M.O. A conserved checkpoint pathway mediates DNA damage--induced apoptosis and cell cycle arrest in *C. elegans*. *Mol. Cell* **5**, 435-443 (2000).

Gavin, A.C. *et al.* Functional organization of the yeast proteome by systematic analysis of protein complexes. *Nature* **415(6868)**, 141-7 (2002).

Goberdhan, D.C. & Wilson, C. PTEN: tumour suppressor, multifunctional growth regulator and more. *Hum Mol Genet.* **12 Spec No 2**, R239-48 (2003).

Goodarzi, A.A., Jonnalagadda, J.C., Douglas, P., Young, D., Ye, R., Moorhead, G.B., Lees-Miller, S.P. & Khanna, K.K. Autophosphorylation of ataxia-telangiectasia mutated is regulated by protein phosphatase 2A. *EMBO J.* **23(22)**, 4451-61 (2004).

Gumienny, T., Lamble, E., Hartwieg, E., Horvitz, H.R. & Hengartner, M.O. Genetic control of programmed cell death in the Caenorhabditis elegant hermaphrodite germline. *Development* **126**, 1011-1022 (1999).

Haupt, Y., Maya, R., Kazaz, A. & Oren, M. Mdm2 promotes the rapid degradation of p53. *Nature* **387(6630)**, 296-9 (1997).

Hengartner, M.O., Ellis, R.E. & Horvitz, H.R. *Caenorhabditis elegans* gene *ced-9* protects cells from programmed cell death. *Nature* **356(6369)**, 494-9 (1992).

Ho, Y. *et al.* Systematic identification of protein complexes in *Saccharomyces cerevisiae* by mass spectrometry. *Nature* **415(6868)**, 180-3 (2002).

Hofmann, E.R., Milstein, S., Boulton, S.J., Ye, M., Hofmann, J.J., Stergiou, L., Gartner, A., Vidal, M. & Hengartner, M.O. *Caenorhabditis elegans* HUS-1 is a DNA damage checkpoint protein required for genome stability and EGL-1-mediated apoptosis. *Curr. Biol.* **12**, 1908-1918 (2002).

Horky, M., Kotala, V., Anton, M. & Wesierska-Gadek, J. Nucleolus and apoptosis. *Ann N Y Acad Sci.* **973**, 258-64 (2002).

Kamath, R.S., Fraser, A.G., Dong, Y., Poulin, G., Durbin, R., Gotta, M., Kanapin, A., Le Bot, N., Moreno, S., Sohrmann, M., Welchman, D.P., Zipperlen, P., & Ahringer, J. Systematic functional analysis of the *Caenorhabditis elegans* genome using RNAi. *Nature* **421(6920)**, 231-7 (2003).

Krogan, N.J. *et al.* High-definition macromolecular composition of yeast RNA-processing complexes. *Mol Cell* **13(2)**, 225-39 (2004).

Li, S. *et al.* A map of the interactome network of the metazoan *C. elegans*. *Science* **303(5657)**, 540-3 (2004).

Liu, Q.A. & Hengartner, M.O. Candidate adaptor protein CED-6 promotes the engulfment of apoptotic cells in *C. elegans*. *Cell* **93(6)**, 961-72 (1998).

Milstein, S. Genetic analysis of programmed cell death in the *Caenorhabditis elegans* germline. PhD thesis. State University of New York, New York (2001).

Mumby, M.C. & Walter, G. Protein serine/threonine phosphatases: structure, regulation, and functions in cell growth. *Physiol Rev*. **73(4)**, 673-99 (1993).

Murphy, C.T., McCarroll, S.A., Bargmann, C.I., Fraser, A., Kamath, R.S., Ahringer, J., Li, H. & Kenyon, C. Genes that act downstream of DAF-16 to influence the lifespan of *Caenorhabditis elegans*. *Nature* **424(6946)**, 277-83 (2003).

Nakayama, K., Nagahama, H., Minamishima, Y.A., Matsumoto, M., Nakamichi, I., Kitagawa, K., Shirane, M., Tsunematsu, R., Tsukiyama, T., Ishida, N., Kitagawa, M., Nakayama, K. & Hatakeyama, S. Targeted disruption of Skp2 results in accumulation of cyclin E and p27(Kip1), polyploidy and centrosome overduplication. *EMBO J*. **19(9)**, 2069-81 (2000).

Nomura, M., Gourse, R. & Baughman, G. Regulation of the synthesis of ribosomes and ribosomal components. *Annu Rev Biochem*. **53**, 75-117 (1984).

Prober, D.A. & Edgar, B.A. Growth regulation by oncogenes--new insights from model organisms. *Curr Opin Genet Dev*. **11(1)**, 19-26 (2001).

Reddien, P.W., Cameron, S. & Horvitz, H.R. Phagocytosis promotes programmed cell death in *C. elegans*. *Nature* **412(6843)**, 198-202 (2001).

Rubbi, C.P. & Milner, J. Disruption of the nucleolus mediates stabilization of p53 in response to DNA damage and other stresses. *EMBO J.* **22(22)**, 6068-77 (2003).

Ruggero, D. & Pandolfi, P.P. Does the ribosome translate cancer? *Nat Rev Cancer*. **3(3)**, 179-92 (2003).

Schumacher, B., Hanazawa, M., Lee, MH., Nayak, S., Volkmann, K., Hofmann, R., Hengartner, M., Schedl, T. & Gartner, A. Translational repression of *C. elegans* p53 by GLD-1 regulates DNA damage-induced apoptosis. *Cell* **120(3)**, 357-68 (2005).

Stark, M.J. Yeast protein serine/threonine phosphatases: multiple roles and diverse regulation. Yeast **12(16)**, 1647-75 (1996).

White, R.J. Regulation of RNA polymerases I and III by the retinoblastoma protein: a mechanism for growth control? *Trends Biochem Sci*. **22(3)**, 77-80 (1997).

White, R.J. RNA polymerases I and III, growth control and cancer. *Nat Rev Mol Cell Biol*. **6(1)**, 69-78 (2005).

White, R.J., Trouche, D., Martin, K., Jackson, S.P. & Kouzarides T. Repression of RNA polymerase III transcription by the retinoblastoma protein. *Nature* **382(6586)**, 88-90 (1996).

Wilson, T.E. A genomics-based screen for yeast mutants with an altered recombination/end-joining repair ratio. *Genetics* **162(2)**, 677-88 (2002).

Yang, Y., Fang, S., Jensen, J.P., Weissman, A.M. & Ashwell, J.D. Ubiquitin protein ligase activity of IAPs and their degradation in proteasomes in response to apoptotic stimuli. *Science* **288(5467)**, 874-7 (2000).

Zhang, Y. & Xiong, Y. Control of p53 ubiquitination and nuclear export by MDM2 and ARF. *Cell Growth Differ.* **12(4)**, 175-86 (2001).

Zhang, Y., Wolf, G.W., Bhat, K., Jin, A., Allio, T., Burkhart, W.A. & Xiong, Y. Ribosomal protein L11 negatively regulates oncoprotein MDM2 and mediates a p53-dependent ribosomal-stress checkpoint pathway. *Mol Cell Biol.* **23(23)**, 8902-12 (2003).

Zimber, A., Nguyen, Q.D. & Gespach, C. Nuclear bodies and compartments: functional roles and cellular signalling in health and disease. *Cell Signal.* **16(10)**, 1085-104 (2004).

Methods

Genetics. All strains were grown at 20ºC on NGM agar seeded with *E. coli* OP50 (Brenner, 1974). The Bristol N2 strain was used as the wild-type strain. The following alleles and transgenic strains were used: LGI: *hus-1(op244)*, *cep-1(gk138)*, *rpo-1(op259) eDf3*/*eDf24*, *sDp1*; LGIII: *ced-6(n1813)*, *clk-2(mn159)*, *ncl-1(e1865)*, *ced-9(n1653)*; LGIV: *rad-51(lg8701)*, *ced-3(n717)*; LGX: *abl-1(ok171)*. The *rad-51(lg8701)* and *rpo-1(op259)*;*ncl-1(e1865)* strains were maintained as *rad-51(lg8701)*/nT1[qIs51](IV;V) and *rpo-1(op259)*;*ncl-1(e1865)*/hT2[qIs48](I;III), respectively.

Germline apoptosis. Young adult staged worms from different genetic backgrounds were exposed to selected doses of X-rays (30, 60, 120 Gy) or to 40 Joule/m^2 of UV light (254 nm) and corpses were scored in the meiotic region of one gonad arm at the indicated time points using Nomarski optics. For the RNAi experiments, L1 staged worms were put on plates seeded with the respective RNAi clone (Kamath *et al.*, 2000) and young adults were scored for germline apoptosis in the course of time or at the indicated time points.

Cell cycle arrest studies. Wild-type or *rpo-1(op259)* mutant animals at the L4 stage were either treated with X-rays (30, 60 and 120 Gy) or were left untreated. The cell cycle arrest phenotype was assessed 12 h later by counting the number of proliferating germ cell nuclei in a volume of 50 μm away from the distal tip cell, after images were captured using an ORCA-ER digital CCD camera.

Relative quantification of transcripts. Total RNA was extracted from either wild-type and *rpo-1(op259)* mutants before and after treatment with X-rays, or from wild-type, *rpo-1(op259)*, *ncl-1(e1865)*, *eDf3/eDf24* and *sDp1* strains. cDNA synthesis and quantitative real-time RT-PCR were performed as previously described (Hofmann *et al.*, 2002). Transcripts of *egl-1*, *ced-13*, *dod-22*, *pme-5* and 5.8SrRNA were measured after normalization with 18SrRNA and/or *tba-1* mRNAs, which were used as internal controls. Average fold-change upon treatment was deduced based on three independent experiments.

Embryonic lethality assay. Animals from different genetic backgrounds, 48 h post the L1 stage, were subjected to 120 Gy of X-rays and one day later were left lay eggs for 5-8 h. Non-hatched eggs were scored the next day as a positive embryonic lethal phenotype and expressed as a fraction of the total eggs laid. Data shown is the average percent lethality of 50 animals. Error bars indicate SEM.

Cell size measurements. Gonads or 4-cell stage embryos from wild-type, *hus-1(op244)*, *cep-1(gk138)*, *ced-3(n717)*, *rpo-1(op259)*, *ncl-1(e1865)* and *rpo-1(op259);ncl-1(e1865)* mutant animals at the L4 stage were captured using an ORCA-ER digital CCD camera. The nuclei and/or nucleoli diameter was measured in the first mitotic cells and the meiotic cells before the bend of the gonad. Alternatively, photos were taken from wild-type worms and *rpo-1* mutants 7 h following treatment with 120 Gy of X-ray, and the above measurements were repeated.

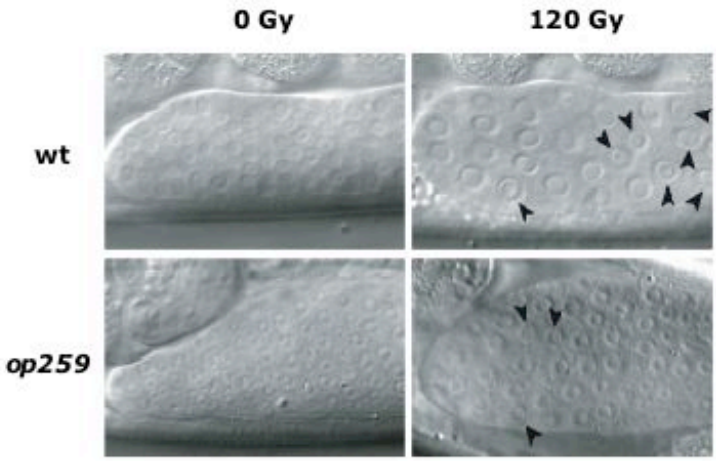

Figure 1a. The *op259* mutation was identified in a screen looking for mutants with defect in cell cycle arrest upon ionizing radiation

DIC microscopy of germlines from wild-type worms and *op259* mutants, before and after 120 Gy of X-rays. Wild-type irradiated nuclei appear fewer in number and bigger in size compared to the untreated ones. Subcellular structures that become visible upon IR in the two genotypes are marked by arrowheads (discussed in Figure 14) (Randy and Jen Hofmann, unpublished data).

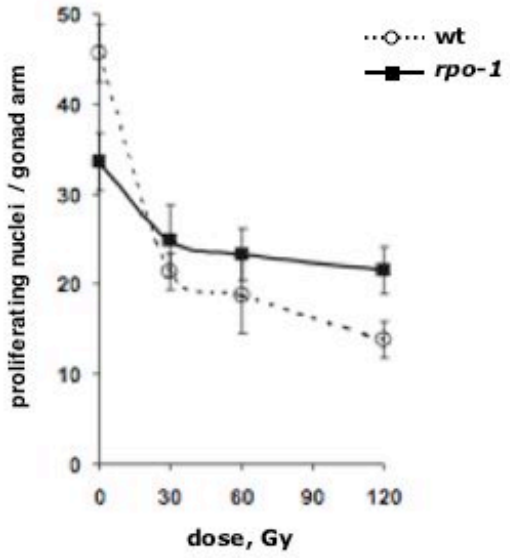

Figure 1b. *op259* mutants exhibit a decrease in the number of proliferating germ cells upon ionizing radiation, with kinetics similar to wild-type

Animals in the L4 stage were irradiated with the indicated doses of X-rays or were left untreated. Proliferating germ cell nuclei were counted in a 50μm distance from the distal tip cell 12 h after the treatment. Data shown represent the average number from 20 gonads ± SEM (Randy and Jen Hofmann, unpublished data).

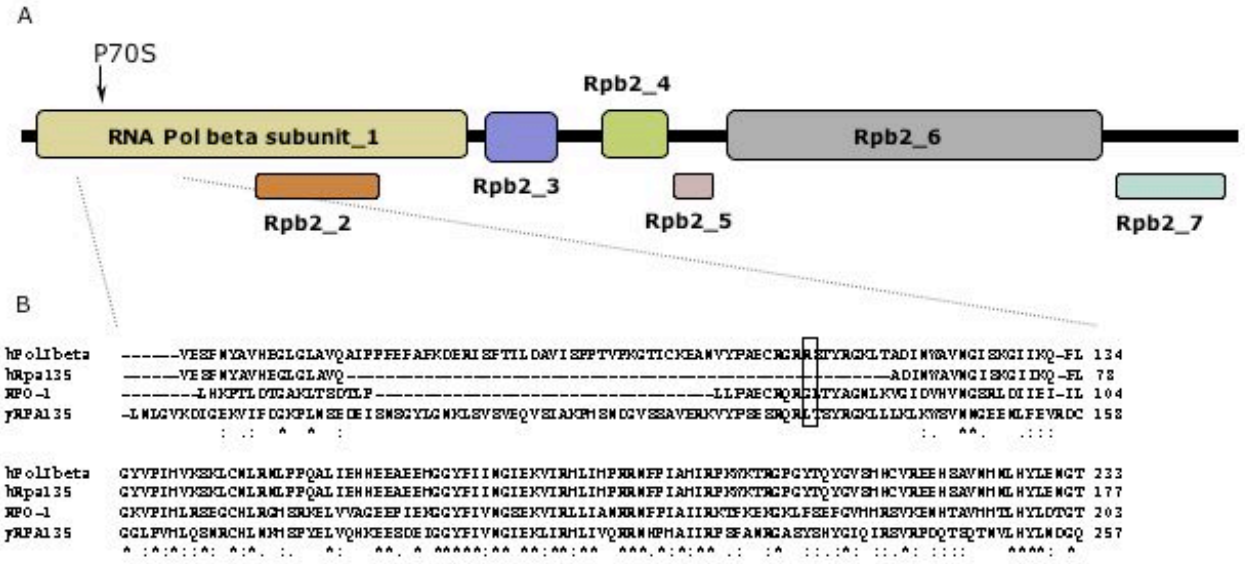

Figure 2. Protein structure of RPO-1

(A) The predicted 1127 amino acid long sequence of the *rpo-1* gene is shown. This is the beta subunit of the DNA-directed RNA polymerase I, comprising seven domains. Domain 1 (also known as protrusion domain) forms one of the two distinctive lobes of the Rbp2 structure. The other lobe is nested within this domain (domain 2). (B) Alignment of the residues 50-203 from RPO-1 with proteins that best match it: the human RNA polymerase I polypeptide beta, the human RNA polymerase I 135kDa polypeptide and the equivalent from *S. cerevisiae*. The *op259* mutation, P70S, affects the beginning of a conserved region shared by these proteins.

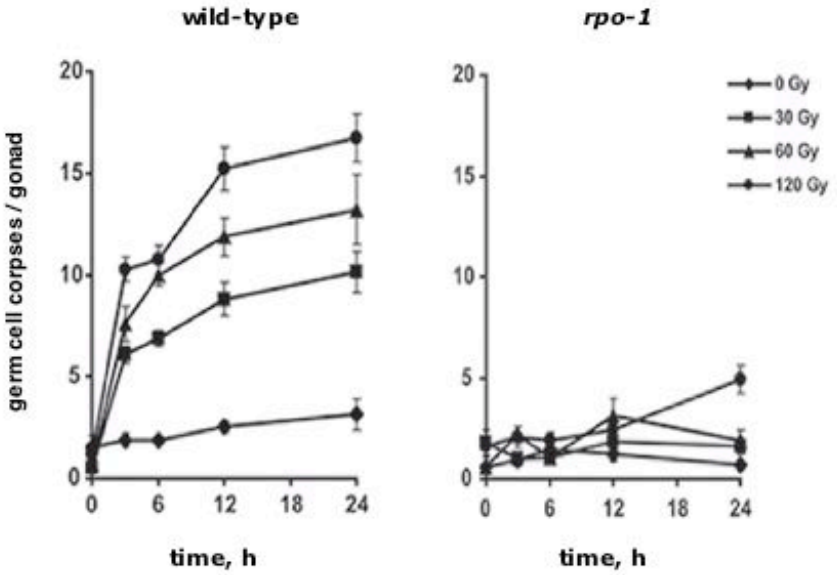

Figure 3a. *rpo-1* mutants are defective for ionizing radiation-induced apoptosis

Time course analysis was performed with wild-type animals and *rpo-1(op259)* mutants. Apoptotic corpses were scored in the meiotic region of one gonad arm of young adult animals, during the course of time and following 30, 60 and 120 Gy of X-rays. Data shown represent the average number of three independent experiments ± SD (Randy and Jen Hofmann, unpublished data).

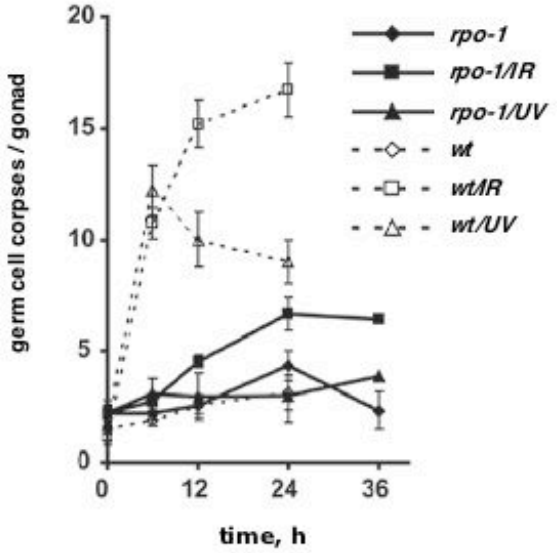

Figure 3b. *rpo-1* mutants are defective for both ionizing radiation and Ultraviolet Light-induced apoptosis, in the course of time

Time course analysis was performed with wild-type animals and *rpo-1(op259)* mutants. Apoptotic corpses were scored in the meiotic region of one gonad arm of young adult animals, during the course of time and following 120 Gy of X-rays and 40 J/m^2 of UV-C light. Data shown represent the average number of three independent experiments ± SD (Randy and Jen Hofmann, unpublished data).

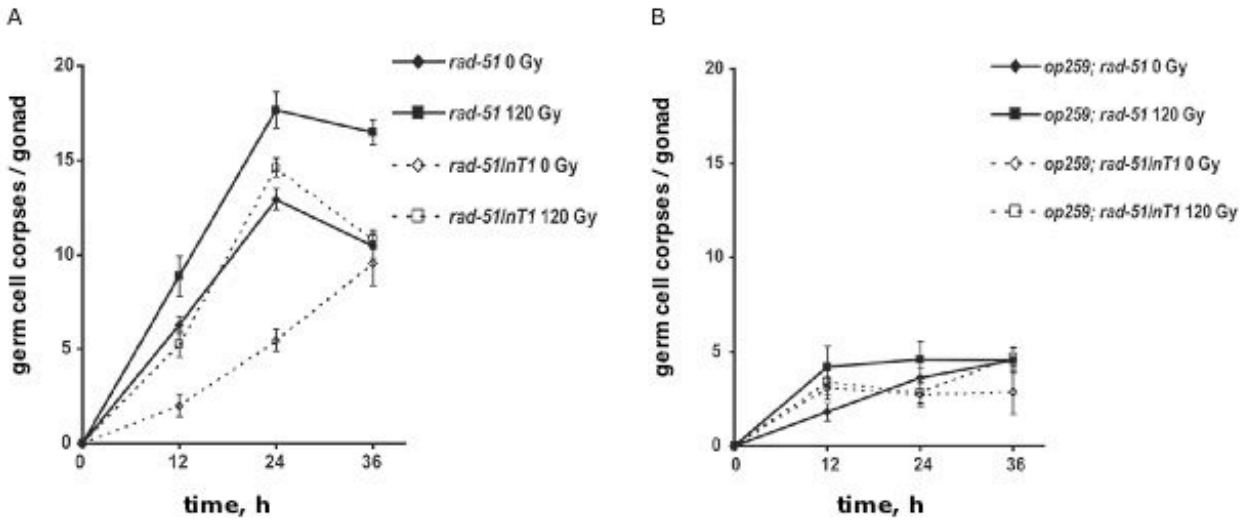

Figure 4. Loss of *rad-51* function, as well as the hypersensitivity upon ionizing radiation is suppressed by the *op259* mutation in *rpo-1*, suggesting that endogenously DNA damage-induced cell death does not occur in the absence of RPO-1

Apoptotic corpses were scored in the meiotic region of one gonad arm of *rpo-1(op259)*, *rad-51(lg8701)/nT1* and *rpo-1(op259);rad-51(lg8701)/nT1* mutant animals, that were either treated with 120 Gy of X-rays or left untreated. Data shown represent the average number of two independent experiments ± SD (Randy and Jen Hofmann, unpublished data).

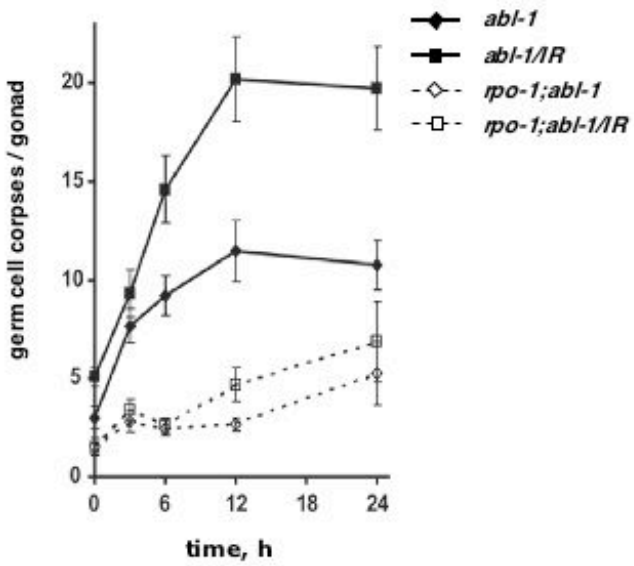

Figure 5. Loss of *abl-1* function, as well as the hypersensitivity upon ionizing radiation is suppressed by the *op259* mutation in *rpo-1*, suggesting that DNA damage-induced cell death does not occur properly in the absence of RPO-1

Apoptotic corpses were scored in the meiotic region of one gonad arm of *abl-1(ok171)* and *rpo-1(op259);abl-1(ok171)* mutant animals, that were either treated with 120 Gy of X-rays or left untreated. Data shown represent the average number of two independent experiments ± SD (Randy and Jen Hofmann, unpublished data).

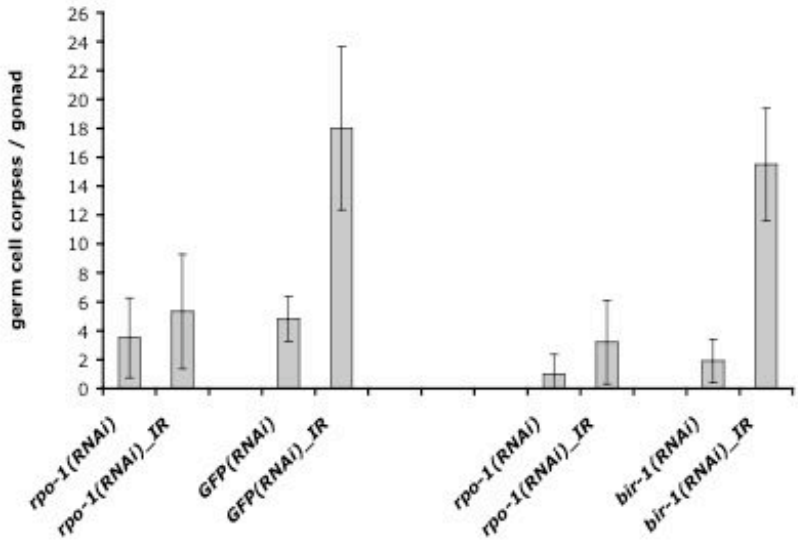

Figure 6. RNAi against *rpo-1* phenocopies the *op259* mutation in terms of apoptosis

Apoptotic corpses were scored in the meiotic region of one gonad arm of young adult animals before and 12 h following treatment with 120 Gy of X-rays. The animals were exposed to *rpo-1*(RNAi) and GFP or *bir-1*(RNAi) at the L3 stage. IPTG was used in a final concentration of 2.5mM. Data shown represent the average number of two independent experiments ± SD.

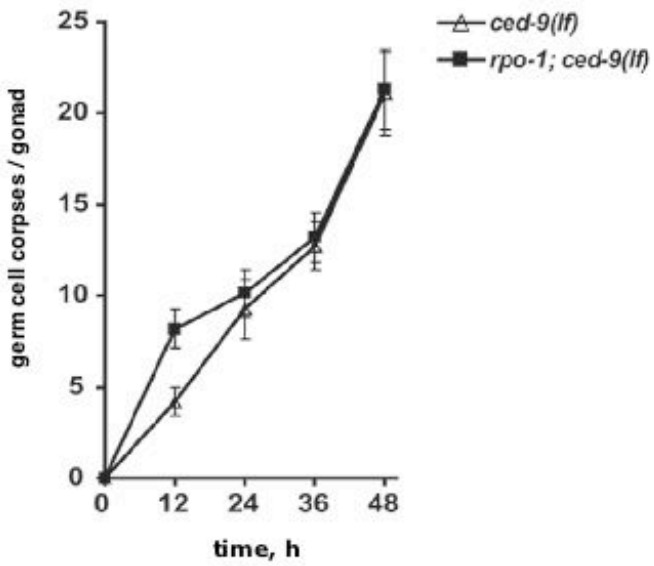

Figure 7a. The *op259* mutation in *rpo-1* does not suppress loss of *ced-9* function, suggesting that RPO-1 acts upstream of a functional apoptotic machinery

Apoptotic corpses were scored in the meiotic region of one gonad arm of *ced-9(n1653)* and *rpo-1(op259);ced-9(n1950)* animals, in the course of time starting from the L4 stage. Data shown represent the average number of two independent experiments ± SD (Randy and Jen Hofmann, unpublished data).

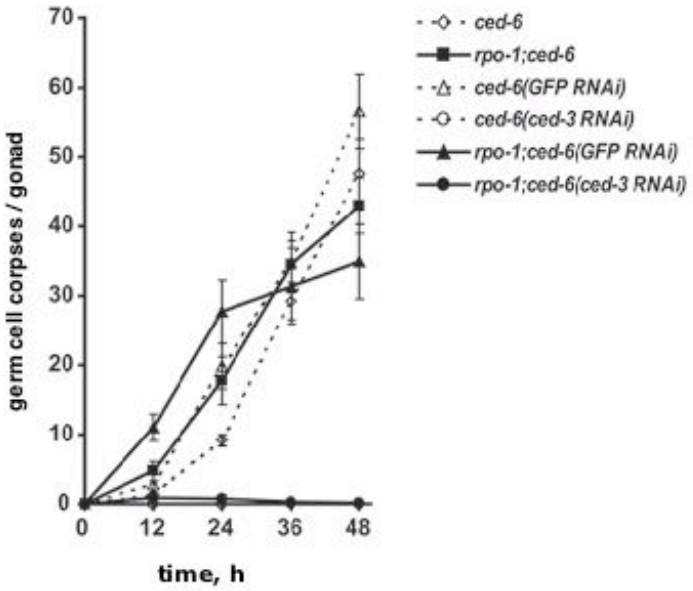

Figure 7b. Loss of *ced-6* function is not suppressed by the *op259* mutation in *rpo-1*, suggesting that RPO-1 does not affect physiological cell death. Death in *rpo-1(op259)*, though, is suppressed by *ced-3(lf)*, suggesting that it is apoptotic in nature.

Apoptotic corpses were scored in the meiotic region of one gonad arm of *rpo-1(op259)* and *rpo-1(op259) ced-6(n1813)* animals before or after applying *ced-3*(RNAi), in the course of time starting from the L4 stage. Data shown represent the average number of two independent experiments ± SD (Randy and Jen Hofmann, unpublished data).

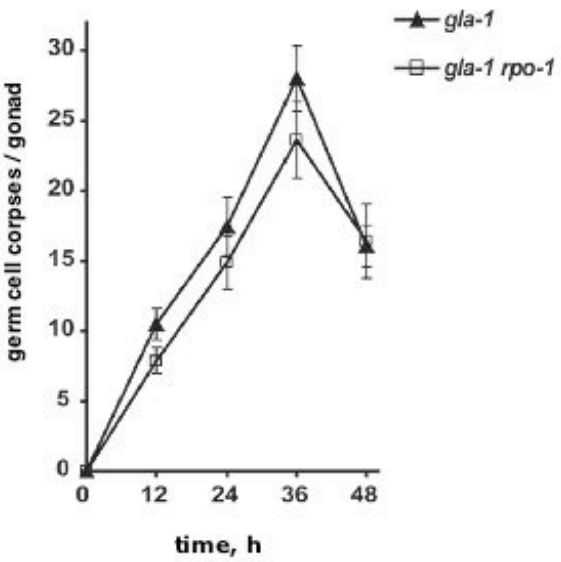

Figure 7c. Loss-of-function mutations in *gla-1(op234)* are not suppressed by the *op259* mutation in *rpo-1*, suggesting that RPO-1 does not affect physiological cell death

Apoptotic corpses were scored in the meiotic region of one gonad arm of *gla-1(op234)* and *gla-1(op234) rpo-1(op259)* animals, in the course of time starting from the L4 stage. Data shown represent the average number of two independent experiments ± SD (Randy and Jen Hofmann, unpublished data).

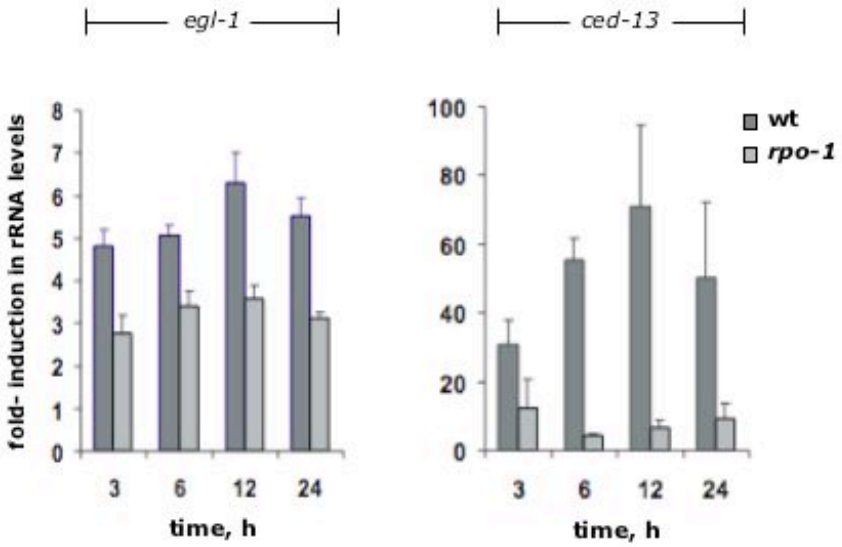

Figure 8a. Transcriptional induction of *egl-1* and *ced-13* upon ionizing radiation is compromised in *rpo-1* mutants

The change in the mRNA levels of *egl-1* and *ced-13* was determined by real-time Q-RT-PCR at the indicated time-points, following treatment with 120 Gy of X-rays. Data shown is the average fold-change of three independent experiments ± SD.

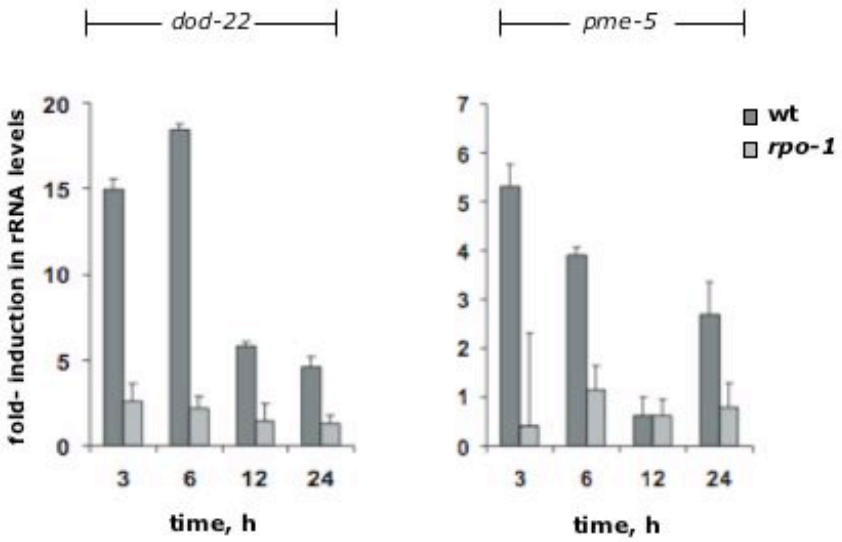

Figure 8b. Transcriptional induction of *dod-22* and *pme-5* upon ionizing radiation is compromised in *rpo-1* mutants

The change in the mRNA levels of *dod-22* and *pme-5* was determined by real-time Q-RT-PCR at the indicated time-points, following treatment with 120 Gy of X-rays. Data shown is the average fold-change of three independent experiments ± SD.

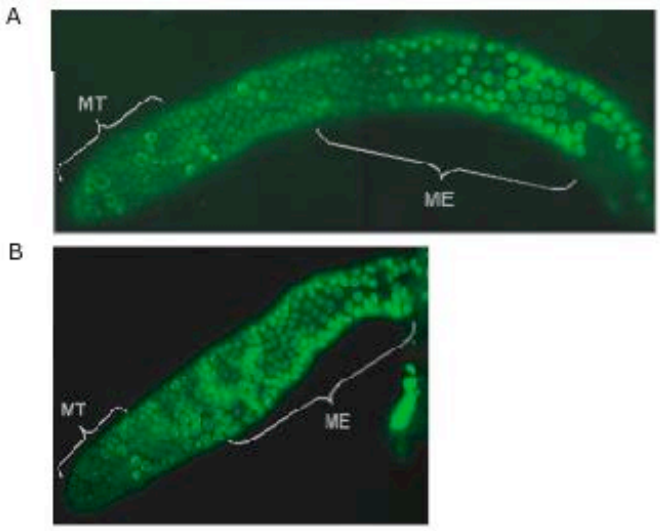

Figure 9. Expression levels of CEP-1 in the *rpo-1* mutants are similar to the ones in wild-type

Fluorescent microscopy of integrated transgenic strains expressing CEP-1::GFP, either in the wild-type background (A) or in the *rpo-1(op259)* mutants (B). Dissected gonads were visualized 12 h after they had been exposed to 120 Gy of X-rays. The mitotic zone (MT) and the meiotic zone (ME) are indicated (Randy and Jen Hofmann, unpublished data).

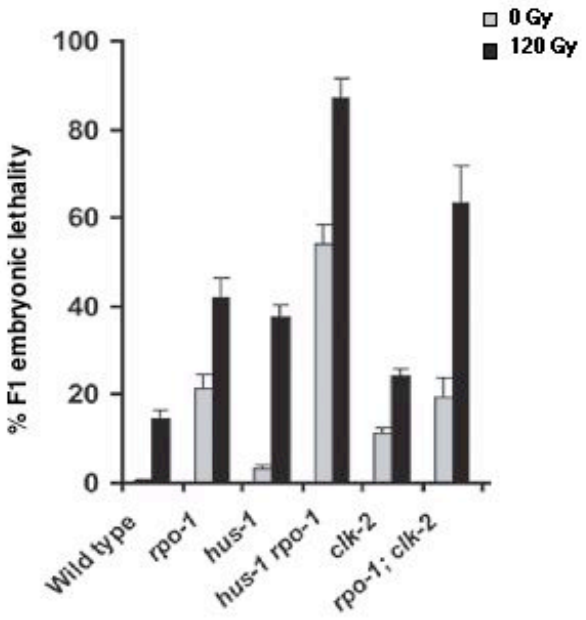

Figure 10. ***rpo-1*** **mutants display embryonic lethality and a synthetic lethal phenotype in the absence of** ***hus-1*****, but not** ***clk-2***

Embryonic lethality assay upon ionizing radiation treatment. Animals from different genetic backgrounds, 48h post the L1 stage, were subjected to 120 Gy of X-rays and one day later were left lay eggs for 5-8h. Non-hatched eggs were scored the day after. Data shown is the average percent lethality of 50 animals ± SD.

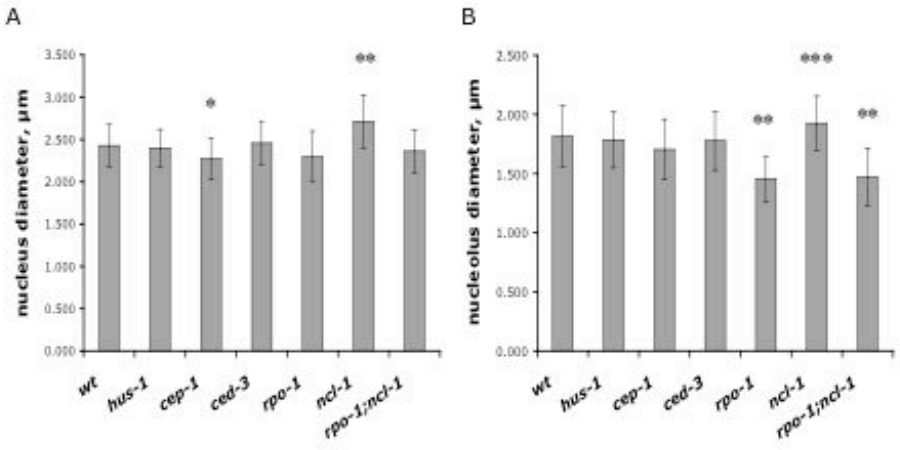

Figure 11a. Phenotypic characteristics of the *rpo-1(op259)* mutants: nucleus and nucleolus size of the mitotic germ cells

The diameter of the nucleus and the nucleolus of the first mitotic germ cells was measured in the following genetic backgrounds: wild-type, *hus-1(op244)*, *cep-1(gk138)*, *ced-3(n717)*, *rpo-1(op259)*, *ncl-1(e1865)* and *rpo-1(op259);ncl-1(e1865)*. Animals were picked as L4 and 4-5 cells from a total number of 10-15 animals were measured after images were captured under a DIC microscope, using the OpenLab software.

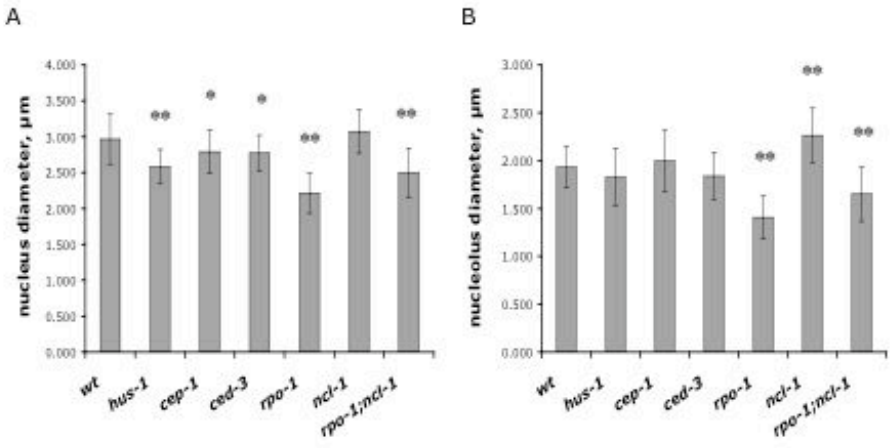

Figure 11b. Phenotypic characteristics of the *rpo-1(op259)* mutants: nucleus and nucleolus size of the meiotic germ cells

The diameter of the nucleus and the nucleolus of meiotic germ cells just before the bend of the gonad was measured in the following genetic backgrounds: wild-type, *hus-1(op244)*, *cep-1(gk138)*, *ced-3(n717)*, *rpo-1(op259)*, *ncl-1(e1865)* and *rpo-1(op259);ncl-1(e1865)*. Animals were picked as L4 and 4-5 cells from a total number of 10-15 animals were measured after images were captured under a DIC microscope, using the OpenLab software.

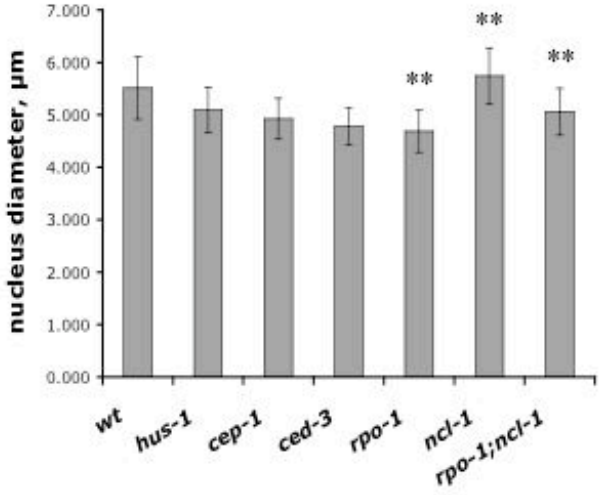

Figure 11c. Phenotypic characteristics of the *rpo-1(op259)* mutants: nucleus size of the embryos

The diameter of the nucleus of 4-cell stage embryos was measured in the following genetic backgrounds: wild-type, *hus-1(op244)*, *cep-1(gk138)*, *ced-3(n717)*, *rpo-1(op259)*, *ncl-1(e1865)* and *rpo-1(op259);ncl-1(e1865)*. Embryos inside a total number of 15-20 animals were measured after images were captured under a DIC microscope, using the OpenLab software.

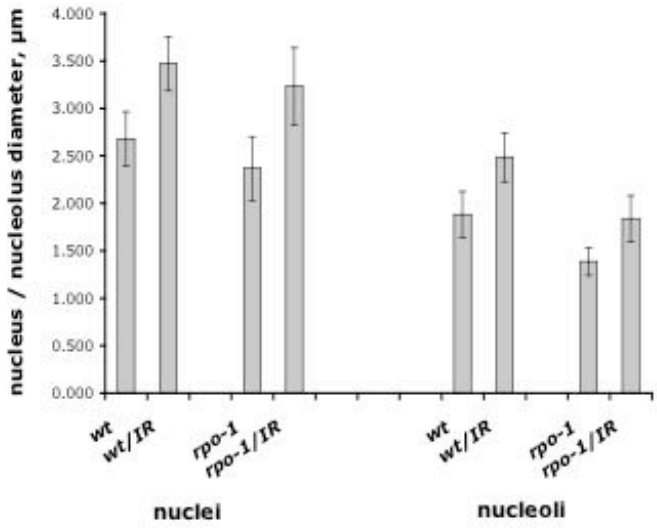

Figure 11d. *rpo-1* mutants exhibit an increase in the size of the nucleus and nucleolus of proliferating germ cells upon ionizing radiation, similar to wild-type

The diameter of the nucleus and the nucleolus of the first mitotic germ cells was measured in wild-type animals and *rpo-1(op259)* mutants. Animals were picked as L4 and irradiated with 120 Gy of X-rays. Seven hours later, 5 cells from a total number of 10-15 animals were measured, after images were captured under a DIC microscope, using the OpenLab software.

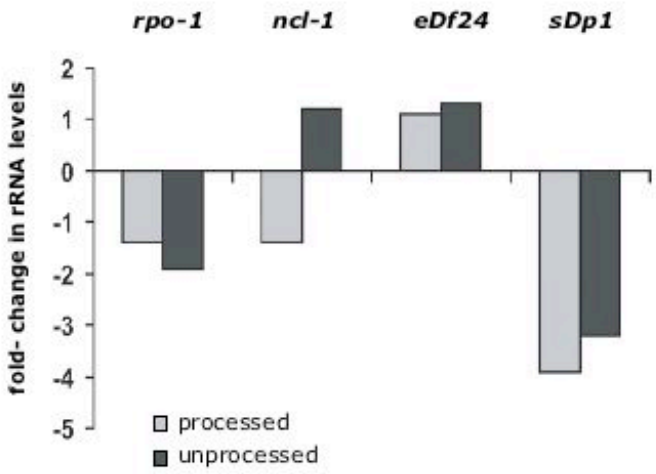

Figure 12. The levels of processed and unprocessed 5.8S rRNA transcripts are reduced in the *rpo-1(op259)* mutants

The levels of 5.8S rRNA transcripts, both in their processed and unprocessed form, were determined by real-time Q-RT-PCR in the following genetic backgrounds: *rpo-1(op259)*, *ncl-1(e1865)*, *eDf3/eDf24*, a deficiency in the 5.8S rDNA locus, and *sDp1*, a duplication of that region. Data shown is the average fold-change of three independent experiments.

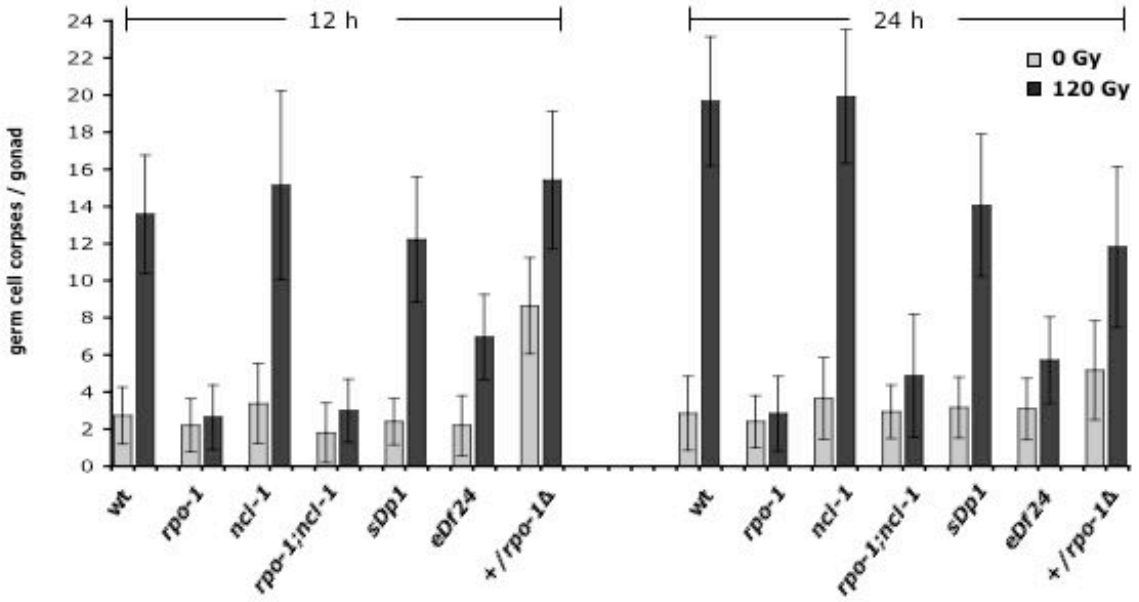

Figure 13. The *rpo-1* mutation is epistatic to *ncl-1(e1865)* and mimics the reduction in the rRNA levels in terms of cell death induction upon ionizing radiation

Apoptotic corpses were scored in the meiotic region of one gonad arm of young adult worms of the following genotypes: *rpo-1(op259)*, *ncl-1(e1865)*, *rpo-1(op259);ncl-1(e1865)*, *sDp1*, a duplication of the 5.8S rDNA locus, *eDf3/eDf24*, a deficiency in that region and +/*rpo-1*Δ. The 12 h and the 24 h time-points were selected to score for apoptosis upon 120 Gy of X-rays. Data shown represent the average number of two independent experiments ± SD.

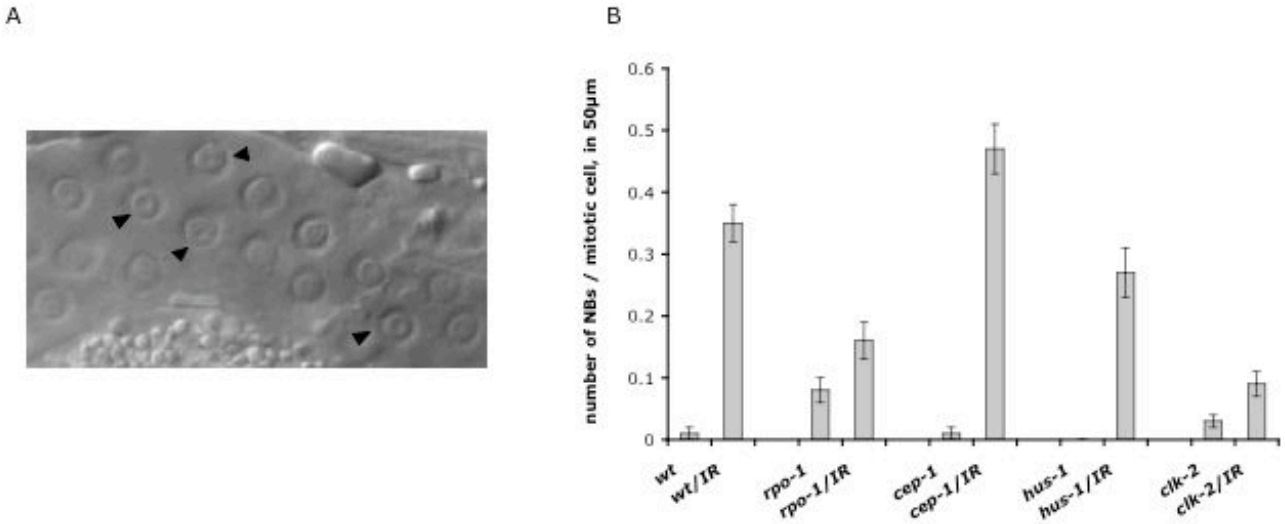

Figure 14. Intranuclear structures that appear after ionizing radiation in the nucleoli of mitotic germ cells are less abundant in the *rpo-1(op259)* mutants

(A) Arrowheads represent intranuclear structures in the nuclei of wild-type mitotic germ cells (called Nucleolar Bodies in the text). (B) The number of the above structures was measured in wild-type animals, *rpo-1(op259)*, *cep-1(gk138)*, *hus-1(op244)* and *clk-2(mn159)* mutants. Animals were picked as L4 and irradiated with 120 Gy of X-rays. Seven hours later, a total number of 15-20 animals were scored in a region of 50 μm from the DTC, after images were captured under a DIC microscope, using the OpenLab software.

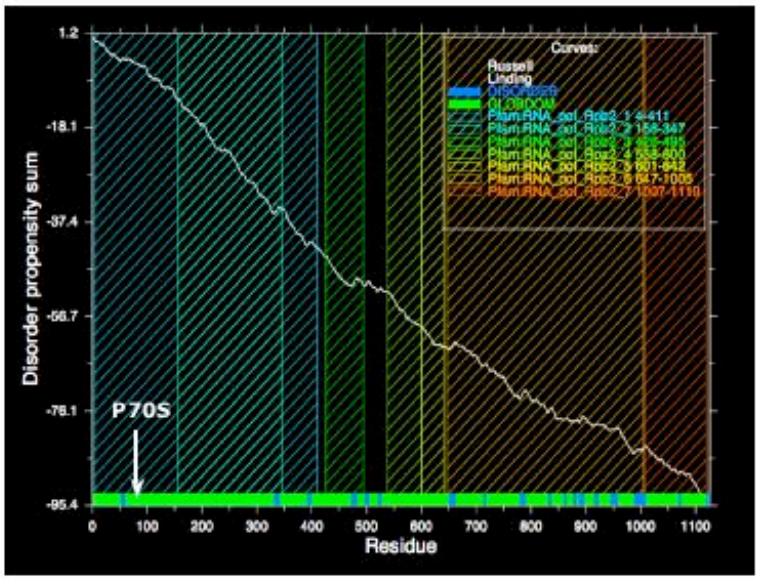

Figure 15. The affected by the *op259* mutation amino acid lies in a domain segment without any obvious motif or recognized domain

Russell-Linding prediction model for ordered (globular) and disordered (potentially functional) regions in the RPO-1 protein. The *op259* mutation, which results into a P70S substitution, lies within the 61-332 amino-acid segment, predicted to be ordered.

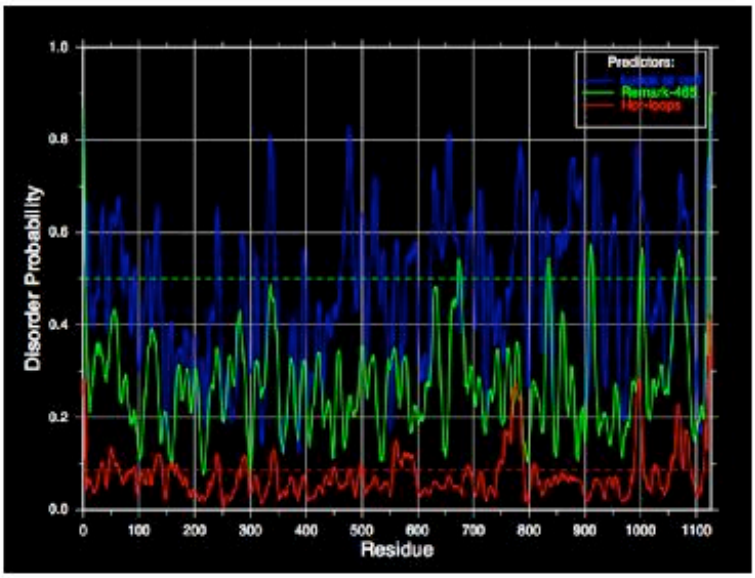

Figure 16. The affected by the *op259* mutation amino acid lies in an ordered domain segment

Prediction model for ordered (globular) and disordered (potentially functional) regions in the RPO-1 protein, according to the "Hot Loops" parameters (coils with high temperature factors). The *op259* mutation lies within a predicted ordered amino-acid segment.

CHAPTER 7

THE *C. ELEGANS* GENE *PME-5*: MOLECULAR CLONING AND ROLE IN THE DNA-DAMAGE RESPONSE OF A TANKYRASE ORTHOLOGUE

DNA Repair

Volume 3, p. 171-182

Preface

In the presence of DNA strand breaks eukaryotic cells activate signal transduction pathways that trigger cell cycle arrest and repair mechanisms leading ultimately to cell survival or programmed cell death. Central to pathways that maintain genomic integrity is the immediate modification of histones and nuclear proteins by ADP-ribose polymers catalyzed by poly(ADP-ribose) polymerases (PARPs). Although PARP1 has been mostly studied, the research in the field is expanding due to the presence of less characterized subgroups, including tankyrase-1 and -2, PARP-2 and -3, sPARP-1 and VPARP (Tong *et al.*, 2001, Ame *et al.*, 2004, Oei *et al.*, 2005).

My participation in the project presented in this chapter started when the group of Dr. S. Desnoyers, from the Department of Pediatrics at the CHUL Research Centre and Laval University, decided to further explore the precise role of tankyrases in *C. elegans*. The paper deals mainly with the molecular cloning of *pme-5* (*poly(ADP-ribose) metabolism enzyme-5*), a potential tankyrase homolog, and my task was to investigate a connection, if any, with DNA damage responses. Following the paper presented below is my contribution to this.

Available online at www.sciencedirect.com
SCIENCE DIRECT®
DNA Repair 3 (2004) 171–182
DNA REPAIR
www.elsevier.com/locate/dnarepair

The *C. elegans* gene *pme-5*: molecular cloning and role in the DNA-damage response of a tankyrase orthologue

Catherine Gravel [a,1], Lilli Stergiou [b,1], Steve N. Gagnon [a], Serge Desnoyers [a,*]

[a] *Department of Pediatrics, CHUL Research Centre and Laval University, 2705 Boulevard Laurier, Sainte-Foy, Qué., Canada G1V 4G2*
[b] *Institute of Molecular Biology, University of Zürich, Winterthurerstrasse 190, 8057 Zürich, Switzerland*

Accepted 24 October 2003

Abstract

Tankyrases are recently identified proteins characterized by ankyrin repeats and a poly(ADP-ribose) polymerase (PARP) signature motif. In vertebrates, tankyrases mediate protein–protein interactions via the ankyrin domain. Many partners have been identified that could function in telomere maintenance, signal transduction in vesicular transport, and cell death. To further our knowledge of tankyrases and to study their function in development, we sought and found a tankyrase-related gene in *Caenorhabditis elegans* that we named *pme-5* (*poly(ADP-ribose) metabolism enzyme-5*). The protein encoded includes a large ankyrin domain and a catalytic PARP domain containing the well-conserved PARP signature sequence and the regulatory region. Unlike other tankyrases, PME-5 lacks a sterile-α module (SAM), but has a coiled coil domain which may mediate oligomerization. We also found that *pme-5* mRNA is alternatively spliced at the fifth exon, producing a long (PME-5L) and a short (PME-5S) transcript. Both isoforms are constitutively expressed during the life cycle of *C. elegans*. We also show DNA damage increases expression of *pme-5*, a response that requires the DNA damage checkpoint gene *hus-1*. Moreover, DNA damage-induced germ cell apoptosis was slightly increased in *pme-5(RNAi)* hermaphrodites. Altogether, these data indicate that *pme-5* is part of a DNA damage response pathway which leads to apoptosis in *C. elegans*.

Keywords: Poly(ADP-ribose)polymerase; *trans*-Splicing; Gene structure and expression; Ionizing radiation; Apoptosis

1. Introduction

Tankyrases are conserved proteins, having orthologues reported in mouse, rat, chicken and the fruit fly. Tankyrases are enzymes that could function in telomere maintenance and vesicular transport signaling pathways [1–3]. They are related to both ankyrins (ANK) and poly(ADP-ribose) polymerases (PARP), possessing both ANK and PARP domains. ANKs are well known structural proteins which link membrane receptors and channels to the cytoskeleton [4]. PARPs are a family of enzymes that play a major role in stabilizing eukaryote genome. PARPs catalyze the posttranslational modification of certain acceptor proteins through synthesis of negatively charged poly(ADP-ribose) polymers [5,6], using nicotinamide adenine dinucleotide (NAD^+) as substrate [7]. The addition of poly(ADP-ribose) polymers on acceptor proteins usually results in the inhibition of those protein's functions. Moreover, tankyrases constitute a cytoplasmic site for poly(ADP-ribosyl)ation, which was considered to be exclusively nuclear until recently.

Human tankyrase-1 was first discovered through its interaction with telomeric repeat binding-factor 1 (TRF1) [1], a negative regulator of telomere length [8,9]. Human tankyrase-1 is a 142 kDa modular protein that contains a large ANK central domain, located between a N-terminal histidine, proline, serine rich region (HPS), and a C-terminal sterile-α module (SAM). The PARP catalytic domain is located at the C-terminus [1]. The ANK domain of tankyrase-1 possesses 20 ANK repeats, organized into five subdomains

Abbreviations: ANK, ankyrin; PARP, poly(ADP-ribose) polymerase; SAM, sterile-α module; NAD^+, nicotinamide adenine dinucleotide; PME, poly(ADP-ribose) metabolism enzyme; MAPK, mitogen-activated protein kinase; ORF, open reading frame; UTR, untranslated region; EST, expressed sequence tag; SL, splice leader; $(PR)_2AMP$, diphosphoribose-adenosine-monophosphate; BER, base excision repair; GSP, gene-specific primer; GFP, green fluorescent protein; RNAi, RNA interference; dsRNA, double stranded RNA

* Corresponding author. Tel.: +1-418-654-2296; fax: +1-418-654-2761.
E-mail address: serge.desnoyers@crchul.ulaval.ca (S. Desnoyers).
[1] These authors contributed equally to this work.

1568-7864/$ – see front matter © 2003 Elsevier B.V. All rights reserved.
doi:10.1016/j.dnarep.2003.10.012

providing redundant protein–protein binding sites for its interacting partners [10,11]. Tankyrase-1 binds TRF1 through its ANK domains [2,11,12]. TRF1 poly(ADP-ribosyl)ation mediated by nuclear-localized tankyrase-1 is thought to release TRF1 from telomeric DNA, thus relaxing telomeric structure. This would provide access to telomerase [2,12], an enzyme that duplicates and maintains telomeres through multiple cell cycles [13,14]. Tankyrase-1 was therefore proposed to be a positive regulator of telomere length [2].

However, in addition to its effect on telomere length, tankyrase-1 involvement has also been implicated in vesicular targeting because it binds and modifies the cytosolic tail of the insulin-responsive aminopeptidase (IRAP). This enzyme resides within specialized endosomes called GLUT4 vesicles [3]. These can be scattered throughout the cytoplasm or can be associated with the *trans*-Golgi network. Under the action of insulin, these vesicles translocate to the cytoplasmic membrane, mediating both the uptake of glucose by the GLUT4 transporter, and the degradation of vasoactive peptides by IRAP [15]. Moreover, tankyrase-1 is a substrate of mitogen-activated protein kinase (MAPK) and is stochiometrically phosphorylated by insulin, PDGF, or EGF stimulation. Phosphorylation of tankyrase-1 enhances its PARP activity, suggesting a possible role for tankyrase-1 as a signaling molecule in vesicular transport [3].

Tankyrase-1 shares more than 80% overall sequence similarity with tankyrase-2; they both share the same structural organization except the latter does not have a N-terminal HPS rich region. Tankyrase-2 is 130 kDa protein, 1,166 amino acids in length [16]. It was previously described as a novel antigen associated with immune response in patients with meningioma [17] and breast cancer [18]. Tankyrase-2 was also isolated from a yeast two-hybrid screen as a Grb14 binding partner [16], a small SH2-containing adaptor protein thought to be a signaling component of the insulin-mediated pathway [19,20]. Tankyrase-2, like tankyrase-1, binds and modifies IRAP as well as TRF1 [10], and overexpression of nuclear-targeted tankyrase-2 releases endogenous TRF1 from telomeres [12]. Both tankyrases have similar subcellular localizations and they can form homo- and heterodimers through their SAM domain [10,21]. This, along with their high structural similarity, suggests overlapping functions for tankyrases, although tankyrase-1 expression is higher in testis and adipocytes [1,10], and tankyrase-2 expression is higher in the placenta and skeletal muscle [10,16]. In addition, overexpression of tankyrase-2, but not tankyrase-1, induces necrotic cell death [22]. Therefore, despite similar activities, tankyrase-1 and -2 probably possess certain separate and unique functions. Yeast two-hybrid screens have revealed many other tankyrase-interactions such as with the spindle pole marker nuclear/mitotic apparatus protein (NuMA) [23], the Bcl-2 family member myeloid cell leukemia-1 (Mcl-1) [24], and the newly discovered tankyrase associated 182 kDa binding proteins (TAB182) [11]. Thus, it is clear that tankyrases are multivalent proteins, interacting with many different factors.

Molecular characterization of tankyrases from vertebrates as well as identification of many interactors have provided many clues for their physiological roles. To further explore the more precise function of tankyrase, we sought and identified a gene in *Caenorhabditis elegans* that encodes a protein related to human tankyrase. Here we describe the molecular characterization of poly(ADP-ribose) metabolism enzyme 5 (*pme*-5), the unique *C. elegans* tankyrase-related gene. Amino acid sequence analysis of PME-5 revealed a protein sharing structural similarities with human tankyrases, but having some unique structure of its own. We also demonstrate that *pme-5* expression is significantly up-regulated following γ-irradiation, suggesting a role for PME-5 in DNA-damage response. The DNA damage checkpoint gene *hus-1* is also needed for the up-regulation of *pme-5*. Moreover, when *pme-5* is knocked-down by RNAi a slight increase in germ cell apoptosis is observed suggesting that some damage may persist in the absence of PME-5.

2. Materials and methods

2.1. C. elegans strains and culture

C. elegans N2 (Bristol strain) and *hus-1(op244)* were handled, cultured, and staged as described previously and according to standard techniques [25].

2.2. Nematode irradiation and RNA preparation

For the time-course experiment regarding *pme-5* up-regulation (Fig. 6A), L4 nematodes were distributed in five polypropylene 50-ml clear tubes (1 ml of nematode pellet/tube). Four nematode pellets were γ-irradiated at 120 Gy (^{60}Co), and one was kept as the non-irradiated control. Nematode pellets were then flash-frozen in liquid nitrogen after 0, 5, 30 and 60 min following irradiation and stored at −80 °C. Total RNA was isolated from frozen nematode pellets using TRIzol reagent (Gibco BRL/Invitrogen) [26].

For the experiment regarding the *hus-1* dependent *pme-5* expression (Fig. 6B), synchronized wild-type and *hus-1(op244)* adult hermaphrodites were irradiated with 120 Gy of X-rays and left for 3 h to recover. Total RNA was isolated using RNAzolB (ams Biotechnology), treated with DNaseI and further purified with the RNeasy kit (Qiagen).

2.3. Cloning of cDNA encoding C. elegans tankyrase

An expressed sequence tag (yk470c3) encoding the 3′-end of *pme-5* cDNA was obtained from Dr. Yuji Kohara (Japan). The yk470c3 phagemid was excised and circularized using a standard method [27]. The resulting plasmid was named pBS-yk470c3 and its sequence was obtained by automated DNA sequencing. To obtain the full-length *pme-5* cDNA, the 5′-end of *pme-5* was obtained by a reverse transcriptase (RT)-PCR reaction performed with the pre-amplification

system for first-strand cDNA synthesis (SuperScript II Kit™; Gibco BRL/Invitrogen). First-strand was obtained using oligo(dT) 12-18 oligonucleotides and total RNA prepared from mixed-stage culture as described before. To amplify the 5′-end of *pme-5* cDNA from first-strand synthesis, specific oligonucleotides based on the putative ZK1005.1 gene (WormBase, version WS86, http://wormbase.org) and yk470c3 sequence were used. The forward primer, TCCCCGCGGCCGCATGGCTCGTCGTGTTAATAA (predicted initiation codon underlined) contained *Sac*I and *Not*I restriction sites, whereas the reverse primer, CGTTTCCGAACGCGTAGTGA, was a gene specific primer containing the unique *Mlu*I restriction site found in yk470c3 (*Mlu*I site underlined). After amplification (94 °C, 45 s; 55 °C, 45 s; 72 °C, 6 min; 35 cycles with *Pfu* DNA polymerase), the PCR product (3,400 pb) was gel-purified (Qiaquick gel extraction kit; Qiagen), digested by *Not*I-*Mlu*I restriction enzymes, and ligated into the pBS-yk470c3 plasmid also digested by *Not*I-*Mlu*I restriction enzymes. The resulting plasmid, pBS-pme5, was sequenced by automated DNA sequencing and the full-length cDNA thus reconstructed.

2.4. Determination of alternatively spliced pme-5 isoforms

RT-PCR was used to amplify the sequence containing the presumed exon 5 in *pme-5* mRNA. The forward primer, selected at the end of exon 4, was TTCCAATGAAAGTTTACGG and the reverse primer, selected at the beginning of exon 6, was GATTCTGTTGATGCCTTCCA. PCR amplification was done on first-strand cDNA and the PCR reaction was a "two-step"-type amplification: a denaturing step at 94 °C for 1 min; a two-step sequence of 94 °C for 30 s followed immediately by a step at 55 °C for 15 s repeated 35 times, and a final step at 72 °C for 5 min. The predicted sizes of PCR products were 501 and/or 387 pb, corresponding to the presence and absence of exon 5 (114 pb), respectively.

2.5. PCR amplification of the 5′-terminal regions

First-strand cDNA was synthesized with polyadenylated [poly(A)$^+$] RNA from mixed-stage (MS) nematode cultures using the SuperScript II RT Kit™ according to the manufacturer's recommendations (Gibco BRL/Invitrogen). PCR amplification was done using a gene-specific forward primer: ATGGCTCGTCGTGTTAATAA (start codon underlined), and a reverse gene-specific primer: AACGGCTCTGGTGATCCATCT, generating a 423 pb amplicon. Amplification of the splice leader was done with SL1 (GTTTAATTACCCAAGTTTGAG) or SL-2 (GGTTTTAACCCAGTTACTCAAG) sequences as forward primer and the same gene-specific reverse primer. The PCR reaction was a "two-step"-type amplification and was previously described [28].

2.6. RT-PCR relative quantification of pme-5 expression

Postirradiation (Fig. 6A) or developmental (Fig. 4B) expression of *pme-5* was measured by real-time quantitative RT-PCR using fluorogenic probe (Taqman) and the ABI Prism® 7000 Sequence Detection System (Applied Biosystems). The *ama-1* gene, a known reference for quantitative PCR, was used as an endogenous control [29,30]. Primers and fluorogenic probes (see Table 1) were designed using PrimerExpress software and selected to span exon junctions to minimize contamination by genomic DNA amplification. PCR amplification of the target (*pme-5*) and the endogenous control (*ama-1*) mRNA were done in separate tubes, using the Brilliant® Single-Step QRT-PCR Master Mix (Stratagene). Reactions were performed in a volume of 25 μl including 100 ng of total RNA for each unknown samples, 200 nM of fluorogenic probe (Integrated DNA Technology), 300 nM of each primer and 1:50 dilution of reference dye. MS total RNA was used to produce a 5-point linear standard curve, ranging from 0.1 to 1000 ng. All points and samples were tested four times. The RT-PCR reaction was done in three steps: (1) 30 min at 50 °C (RT reaction); (2) 10 min at 95 °C (RT enzyme inhibition); (3) 15 s at 95 °C followed by 1 min at 60 °C for 40 cycles (PCR amplification). According to previous optimization test results, setup templates were done to read the reference dye ROX (carboxy-x-rhodamine) and the probe reporter 6-FAM (6-carboxyfluorescein), but no quencher reporter was selected for the Black Hole Quencher (BHQ), which produce little or no secondary emission.

For the experiment regarding the *hus-1*-dependent *pme-5* expression (Fig. 6B), cDNA synthesis was performed using 250 U MultiScribe Reverse Transcriptase and random primers (Applied Biosystems). Relative amounts of *pme-5* transcripts were determined by quantitative real-time RT-PCR in a 7900HT Sequence Detection System, by using primers that span the 7th intron. 18S rRNA was used as an internal control to normalize the results. Fold-induction

Table 1
Primers and fluorogenic probe sets used in real-time RT-PCR

Gene		Primers (5′-3′)	Probe (5′-3′)	Product size (pb)
pme-5	Forward	CAGGAAAATTGATGGGCAAATC	FAM-CACGGACTCCGTCCACAACTCGTCT-BHQ[a]	70
	Reverse	GCGTTGACGGGACGACTT		
ama-1	Forward	ATCCGATGAATGATGGAAAGAAG	FAM-TGATAGCGACCGCATCCACCT-BHQ[a]	70
	Reverse	CCGACACGGCGGTATGAT		

[a] BHQ: Black Hole Quencher.

represents the relative expression of *pme-5* following irradiation compared to the untreated samples.

2.7. pme-5 inactivation using RNAi

A 1,155 bp PCR product of *pme-5* was obtained using genomic DNA and was ligated into linearized T-tailed L4440 vector that contains T7 promoter sites flanking each side of the multiple cloning site. The plasmid was transformed into the HT115(DE3) bacterial strain, in which expression of T7 polymerase is induced by the addition of 1 mM IPTG. RNAi of *pme-5* was performed by feeding synchronized L1 larvae with the bacterial culture grown for 8 h [31]. GFP dsRNA-synthesizing bacteria were used as a reference.

2.8. Analysis of DNA damage-induced apoptosis in the germline

Synchronized RNAi-fed nematodes at the young adult stage were exposed to 60 Gy of X-rays and analyzed at 6 h intervals after mounting onto glass slides. Apoptotic cell corpses in one gonad arm were scored by using Nomarski optics as described by Gartner et al. [32].

2.9. Computer analysis

Database searches were conducted using the TBLASTN of the BLAST program [33]. Analysis of sequence data, sequence comparisons, and predicted phylogenic relationship were performed using the CLUSTAL method with PAM250 residue weight table within the MegAlign Lasergene package (DNASTAR, Madison, WI, USA). Protein and amino acid sequence analyses were performed using the program *PSORT II* from Dr Kenta Nakai (Human Genome Center, IMS, U. Tokyo, Japan), the protein family database *Pfam* (Sanger Institute and Washington University in St-Louis), NetPhos 2.0 server (http://www.cbs.dtu.dk/services/NetPhos/), and the database of protein families and domain *ScanProsite* (Swiss Institute of Bioinformatics).

3. Results

3.1. PME-5 is a protein related to vertebrate tankyrase

We searched the *C. elegans* data base WormBase (http://www.wormbase.org) using the BLASTp program for protein containing a motif known as PARP signature (amino acids 859–908) derived from huPARP-1 (accession no. P09874). Four loci were identified: Y71F9AL.18 or *pme-1*, E02H1.4 or *pme-2*, ZK1005.1 or *pme-5*, and AC8.1 or *pme-6*. The genes *pme-1*, *pme-2* and *pme-6* have been characterized already [28]. This study is centered on the characterization of *pme-5* which is localized on chromosome V. It encodes a predicted protein that shares many similarities with tankyrases from other species.

3.2. Structural analysis of PME-5 and tankyrase related proteins

Computer analysis of the predicted PME-5 amino acid sequence revealed a primary structure related to higher-eukaryote tankyrases (Fig. 1). Human tankyrases are modular enzymes containing a large ankyrin domain (ANK) formed by 18–19 full-ANK repetitions, a sterile-α module (SAM) and a poly(ADP-ribose) polymerase-like catalytic domain (PARP). Human tankyrases-1 and -2 can be distinguished by a histidine, proline and serine rich domain (HPS) found only in tankyrase-1 N-terminal region. *Drosophila* tankyrase-like protein (drTANK) has the same structural organization and shares 50% sequence similarity with both tankyrase-1 and 2 (Fig. 1A). PME-5 does not have a SAM motif but possesses a large ANK domain (at least 19 full-ankyrin repeats) and a PARP domain containing both the catalytic and the regulatory region as found in the well-known PARP-1 enzyme. In addition, PME-5 contains an aspartate rich region (D), a coiled coil domain, and nuclear localization signals (NLS); three domains not found in human and *Drosophila* tankyrases. Sequence analysis [34] of the 38 amino acids encoded by the exon 5 revealed a possible tyrosine phosphorylation site (data not shown). Although the putative kinase that may phosphorylate this site is not known, it is interesting to note that mammalian tankyrase-1 is phosphorylated by a MAP kinase.

Standard protein-protein BLAST on GenBank® protein database with PME-5 sequence identified a closely-related protein named ADPRT-3 (*ADP-ribose transferase-3*, accession no. CAD59239) in *Dictyostelium discoideum*. The *D. discoideum* tankyrase orthologue (ddTANK) shares 26% identity and 44% similarity with amino acids from PME-5. Like PME-5, ddTANK lacks a SAM domain but possesses an aspartate rich sequence (D), a coiled coil region, nuclear localization signals, and a PARP domain containing the regulatory module. ddTANK also has two glutamate (E) and one threonine (T) rich sequences, and the larger ANK domain found in tankyrase-like protein to this date, with 26 ankyrin repeats (Fig. 1B).

3.3. PARP-1 and tankyrases catalytic domain analysis

Human PARP-1 (huPARP-1) is perhaps the most studied PARP to date. Its catalytic domain, representing the last C-terminal 40 kDa, has been well characterized and contains a 50 amino acids motif (amino acids 859–908) well conserved among the vertebrate (100%) and highly conserved among all species (92%) [35]. This motif, the PARP signature, is found in all functional PARP-like enzymes including tankyrases. To investigate the PARP domain of tankyrase orthologues and the one of PMEs in *C. elegans*, we compared their PARP signature with huPARP-1 (Fig. 2).

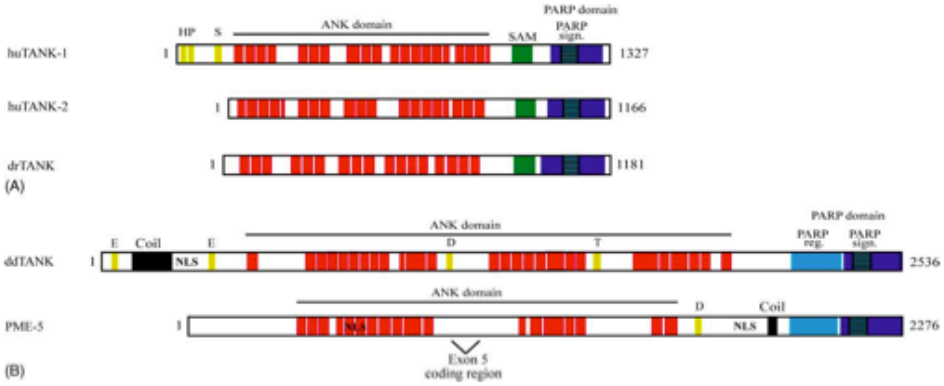

Fig. 1. PME-5 is structurally related to higher-eukaryotes tankyrases but is a close relative to the *D. discoideum* tankyrase orthologue. Schematic primary structure of various tankyrases orthologues (human tankyrase-1 (huTANK1, accession no. AAC79841); human tankyrase-2 (huTANK2, accession no. AAK13463); *Drosophila* tankyrase like protein (drTANK, accession no. AAD34784); *D. discoideum* tankyrase like protein (ddTANK, accession no. CAD59239); and *C. elegans* tankyrase like protein (PME-5L, accession no. AAN40683)). Tankyrases are modular enzymes containing at least two common domains: a large ANK repeat domain and a catalytic PARP domain. A highly conserved motif in the catalytic domain called the PARP signature (PARP sign.) is also present. (A) Human tankyrases are close relatives, which can be differentiated by the histidine, proline and serine rich region (HPS) present in tankyrase-1 only. A sterile-α module (SAM) is also present in human and *Drosophila* tankyrases orthologues. (B) ddTANK and PME-5L do not have a SAM domain but they both have a PARP regulatory domain (PARP reg.), a coiled coil region, a glutamate rich sequence and many nuclear localization signals (only regions containing bipartite NLS are shown). ddTANK also has a glutamate (E) and a large threonine (T) rich sequence. PME-5 exon 5 encoded sequence is shown.

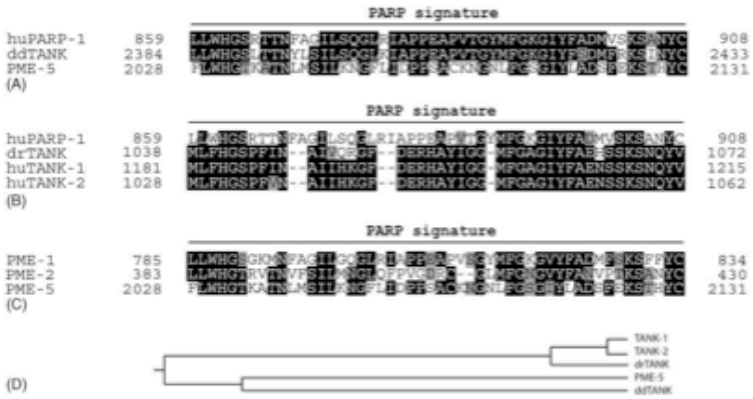

Fig. 2. PME-5 PARP signature is more related to huPARP-1 than to huTankyrase-1 and -2 signature. Alignment of the deduced amino acid sequences of PME-5 PARP signature with various orthologues. (A) Alignment of huPARP-1 signature domain (accession no. PO9874, amino acids 859-908) with *D. discoideum* tankyrase like protein (ddTANK) and PME-5 PARP signature. (B) Alignment of huPARP-1 signature with *Drosophila* like tankyrase (drTANK), human tankyrase-1 (huTANK1) and human tankyrase-2 (huTANK2) PARP signature. (C) Alignment of huPARP-1 and -2 *C. elegans* orthologues (PME-1 and PME-2) with PME-5 PARP signature. (D) Predicted phylogenetic relationship between the PARP signature motifs of tankyrases orthologues. PME-5 and ddTANK are members of a major branch while drTANK and the human tankyrases compose the other branch. Identical amino acids are boxed in black, conserved substitutions are in grey.

Sequence alignment of PARPs signature from tankyrases orthologues and huPARP-1 revealed that ddTANK and PME-5 both have a catalytic domain highly related to huPARP-1 (Fig. 2A). PME-5 PARP signature shares 50% sequence similarity with huPARP-1 signature, only 24.4% similarity with human tankyrase-1 and tankyrase-2, and 52% with ddTANK. We also found that huPARP-1 and ddTANK PARP signatures seem to be very close to one another as they share 82% sequence similarity. Human tankyrase-1 and -2 and their *Drosophila* orthologue are very close relatives, sharing 89–98% sequence similarity over their entire amino acid sequence (Fig. 2B). However, the common PARP signature of huTANK-1 and huTANK-2 only shares 24, 31 and 38% sequence similarity with the ones from PME-5, ddTANK and huPARP-1 PARP signatures respectively. Consequently, PME-5 and ddTANK PARP signatures share more similarities with huPARP-1 than any other tankyrases PARP signature. We also compared PME-1, PME-2, and PME-5 PARP signatures. Sequence alignment shows a relatively well-conserved amino acid pattern, with 42–48% sequence similarity (Fig. 2C). This result can be compared to the 38% sequence similarity between huPARP-1 and tankyrases PARP signatures.

3.4. Heterogeneity of *pme-5* mRNAs

The gene *pme-5* is composed of 11 exons distributed over 9,241 nucleotides (WormBase WS89 and Fig. 3). The full-length *pme-5* cDNA sequence contains 6,885 nucleotides, including a 5′-untranslated region (5′UTR) consisting of 38 nucleotides, and a 3′UTR region of 130 nucleotides including the poly(A)$^+$ tail. The four nucleotides (CAGC) upstream of the initiation codon ATG are different from the vertebrate [(A/G)CC] or the *C. elegans* (AAAA) consensus sequence for translational initiation [36]. The usual *C. elegans* poly(A)$^+$ signal, namely AAUAAA, is located 11-16 nucleotides upstream of the poly(A)$^+$ tail. Another polyadenylation signal (AAUAAU) is located 42 nucleotides upstream of the poly(A)$^+$ tail [36]. The *pme-5* coding sequence contains 6,831 nucleotides and encodes a predicted protein of 2,276 amino acids, having a calculated molecular weight of 254.604 kDa and a p*I* of 8.63.

However, we cloned a 6,717 bp ORF cDNA from our cDNA library [28] where nucleotidic sequence from exon 5 was missing. Examination of the sequence of the EST yk470c3 revealed the presence of the last 96 nucleotides of exon 5. This suggests at least two mRNA isoforms are transcribed from *pme-5*: a long form (PME-5L) composed of all 11 exons, and a short form (PME-5S) where exon 5 is missing.

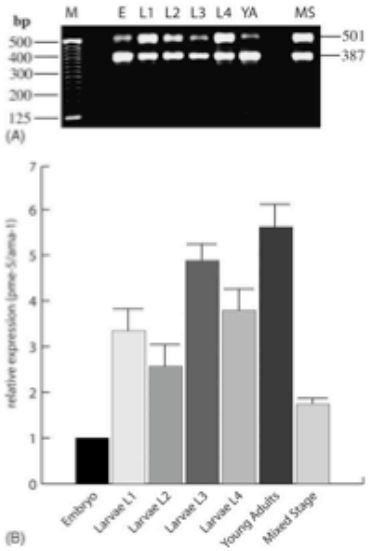

Fig. 4. PME-5 transcript is alternatively spliced on the fifth exon and expressed throughout the life cycle of *C. elegans*. (A) RT-PCR amplification of the region containing the exon 5 of PME-5 transcript. A pair of primer overlapping the region containing the exon 5 was selected to yield 387 and 501 bp products that correspond to the absence and presence of exon 5 respectively. Reaction was performed on embryos (E), L1, L2, L3 and L4 larvae, on young adult (YA) and mixed-stage (MS) cDNA. M: 25-bp DNA marker. (B) Total RNA from each nematode pellet was extracted as described in Section 2.2 and submitted to relative quantification (see Section 2.6). Data are normalized in relation to *ama-1* gene expression, and compared to the embryo values defined as the calibrator. Values are means ± S.E. of two determinations.

Therefore, we verified that PME-5S and PME-5L were both expressed during the life cycle of *C. elegans* under normal conditions of culture. This was done using a RT-PCR reaction performed with cDNA from each developmental stage using primers selected at the end of the exon 4 (forward primer) and at the beginning of the exon 6 (reverse primer). We were able to detect two PCR

Fig. 3. Schematic representation of the genomic organization of *pme-5* gene. Start codon (ATG) and stop codon (TAA) are indicated. Open numbered boxes indicates exons. Exon 5 is alternatively spliced, producing a long and a short transcript.

products having an estimated difference of 114 pb in all developmental stages (Fig. 4A). The sequence of PME-5 has been deposited in GenBank® database with accession no. AAN40683. Analysis of *pme-5* genomic sequence revealed that the *C. elegans* intronic 3′ splice consensus sequence (UUUUCAG) [36] is present and relatively well conserved in every *pme-5* introns. The three last nucleotides, CAG, are always present, except in the intron preceding the fifth exon, which end with UAG. This may explain the existence of the alternatively spliced isoform PME-5S.

PME-5S contains 6,717 nucleotides and encodes a predicted protein of 2,238 amino acids with a calculated molecular weight of 250.381 kDa and an estimated p*I* of 8.59. The predicted protein isoforms encoded by *pme-5* have a global primary structure related to higher-eukaryote tankyrases (Fig. 1).The relative distribution of *pme-5* mRNAs in the life cycle of *C. elegans* was also determined (Fig. 4B). Expression is low in embryos compared to larvae expression where it is between 2.5–4.8 times more abundant. It seems to peak at the young adult stage where it is 5.6 times higher than embryo. The low level expression in the mixed-stage culture may represent a uneven representation of the different stages.

3.5. Structure analysis of mRNA 5′-end

trans-Splicing of mRNAs in *C. elegans* is a common phenomenon. A study revealed that approximately 70% of *C. elegans* mRNA are *trans*-spliced with splice leader 1 or 2 at their 5′-end [37]. To characterize the 5′-end of *pme-5* mRNAs, RT-PCR was done on mixed-stage *C. elegans* cultures using either SL-1 or SL-2 sequence primer. Amplification was obtained only with SL-1, suggesting that *pme-5* mRNAs are *trans*-spliced by SL-1 (Fig. 5A). Automated DNA sequencing of the PCR product revealed a unique 38 nucleotides 5′UTR containing SL-1 sequence and 16 genomic nucleotides (Fig. 5B).

3.6. Postirradiation regulation of pme-5 mRNA expression

PME-5 is part of the PARP family and their members are well-known for their role in DNA repair [38]. Poly(ADP-ribosyl)ation is also one of the first cellular responses to DNA damage [7]. In order to test the hypothesis that PME-5 may play a role in DNA damage signaling, we monitored its response at the transcriptional level. Young L4 nematodes were γ-irradiated at 120 Gy, a dose known to induce DNA damage and germ cell apoptosis in *C. elegans* [32]. We followed *pme-5* expression by real-time quantitative RT-PCR using fluorogenic probe. Results show that *pme-5* mRNA level gradually increases after irradiation, reaching a plateau at 30 min postirradiation, and four times more mRNA compared with the non-irradiated control (Fig. 6). These results suggest a role for *pme-5* in DNA damage response.

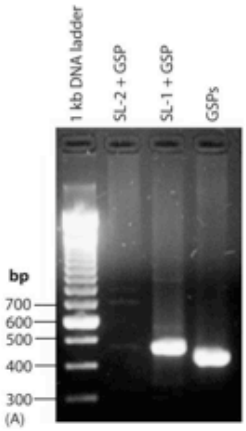

GGTTTAATTACCCAAGTTTGAGccgtaatccgaacagcATGGCTCGTC....
(B)

Fig. 5. PME-5 transcript is *trans*-spliced by SL-1 splicing factor. RT-PCR amplification of the 5′-end of PME-5 transcript. (A) Two PCR amplifications were performed using SL-1 and SL-2 as forward primer, and a gene-specific primer (GSP) ending at the base 423 from the start codon as reverse primer. A third amplification using a gene-specific primer beginning at the start codon as forward primer, and the same gene-specific reverse primer were also performed. (B) Sequence determination of the 5′-end of PME-5 transcipt from PCR product using SL-1 and GSP. Plain capital letters indicate the splice leader sequence, small letters indicate genomic untranslated region, and bold capital letters indicate translated sequence with the start codon underlined.

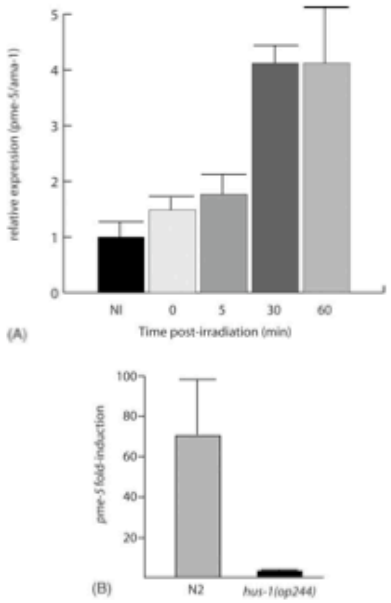

Fig. 6. DNA damages induce *pme-5* expression which is under the control of *hus-1*. (A) Nematodes were γ-irradiated with 120 Gy and flash-frozen in liquid nitrogen at 0, 5, 30 and 60 min following irradiation. Total RNA from each nematode pellet was extracted as described in Section 2.2 and submitted to relative quantification (see Section 2.6). Data are normalized relatively to *ama-1* gene expression, and compared to the non-irradiated control (NI) value defined as the calibrator. Values are means ± S.E. of four determinations. (B) Nematodes were treated with X-rays (120 Gy) and left 3 h to recover. RNA was extracted as described in Section 2.2. Relative amounts of *pme-5* transcripts were determined by quantitative real-time RT-PCR. Fold-induction represents the relative expression of *pme-5* following irradiation compared to the untreated samples.

3.7. Increased DNA damage-induced apoptosis in the germ line of pme-5(RNAi) nematode

Apoptosis can be induced in the germ line of hermaphrodites by DNA damaging agents such as gamma and X-rays [32]. Some of the genes required for programmed cell death in *C. elegans* as well as checkpoint proteins are also needed for DNA damage-induced apoptosis [32].

We observed DNA damage-induced apoptosis by using microscopy and the apoptotic cell corpses were counted in the gonad arms of RNAi fed animals in presence or absence of X-rays. In unirradiated GFP(RNAi) control animals, the number of corpses was low for all time points whereas *pme-5(RNAi)* animals have a slightly higher number (Fig. 7). The number of corpses were significantly higher when animals, both control GFP and *pme-5(RNAi)*, were irradiated. Moreover, *pme-5(RNAi)* animals have more corpses than

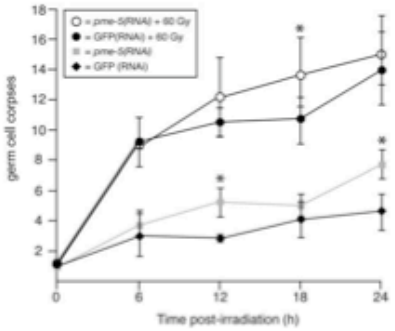

Fig. 7. *pme-5* weakly modulates the response to DNA damage-induced apoptosis in the germ line. Synchronized RNAi-fed animals at the young adult stage were exposed to 60 Gy of X-ray and analyzed at 6 h intervals after mounting onto glass slides. Apoptotic cell corpses in one gonad arm were scored by using Nomarski optics. Between 10 and 24 animals from each group for each time point were used in these experiments. Averages ± S.E. of two independent experiment are shown. The symbol (*) indicates a significant difference in the number of corpses ($P \leq 0.038$ by ANOVA).

control at time points 12, 18 and 24 h (Fig. 7). Therefore, DNA damage-induced apoptosis is increased in the absence of *pme-5*, and may suggest a persistence of some damage after irradiation. Otherwise, the *pme-5(RNAi)* animals displayed a wild-type phenotype in their morphology and behavior.

3.8. pme-5 transcript up-regulation is dependent on the checkpoint gene hus-1

The protein HUS-1 (hydroxyurea sensitive 1) in *C. elegans* is a recently identified DNA damage checkpoint required for genome stability [39]. It also controls the induced up-regulation of *egl-1* after radiation treatment. EGL-1 is a BH3 domain protein that activates the apoptotic machinery in *C. elegans*. It is transcriptionally regulated for the activation of programmed cell death during normal somatic development [40]. In order to further characterize the *pme-5* up-regulation following ionizing radiation, we used quantitative RT-PCR to measure its induction in wild-type and *hus-1(op244)* animals background. We found that *pme-5* transcription is dramatically up-regulated 3 h after irradiation in wild-type nematodes (Fig. 6B). Induction is significantly lower in animals with a defective *hus-1* gene. Therefore, *pme-5* is likely to be in the same pathway than *hus-1* for the DNA damage-induced apoptosis.

4. Discussion

To date, knowledge of tankyrases relies mostly on biochemical and cellular studies. To elucidate the function

of tankyrase in the context of a whole animal, we have identified and characterized the *pme-5* gene of *C. elegans*, which encodes a protein related to tankyrases. The predicted protein product(s) are structurally similar to vertebrate tankyrases in their overall structural arrangement. Moreover, comparison between the vertebrate and invertebrate protein sequences showed several highly conserved motifs, which in vertebrate tankyrase are known to mediate protein–protein interactions. PME-5 protein also contains a PARP catalytic motif, present and active in vertebrate tankyrases. The presence of similar motifs in the *C. elegans* protein may indicate functional conservation. Interestingly, two genes coding for two tankyrases are found in higher-eukaryote like human, mouse, rat, chicken, and many others [21]. Whereas in *Drosophila* and *C. elegans* only one has been discovered. This may suggest that higher eukaryotic types of tankyrases arose from a single ancestor already present in organisms not far in the evolutionary scale such as *C. elegans* and the fruit fly. It may also suggest that functions performed by the single gene present in nematode and *Drosophila* may be divided among tankyrases in higher eukaryotes (Fig. 2D).

4.1. Molecular conservation of the ANK and PARP motifs

PME-5 amino acid analysis revealed a central ANK domain with 18 ankyrin repeats, and a catalytic PARP domain containing the conserved PARP signature motif. PARP signature sequence alignment of tankyrases orthologues and huPARP-1 revealed that ddTANK and PME-5 have a PARP signature very similar to huPARP-1 (Fig. 2). Indeed, the huPARP-1 signature motif shares 50% sequence similarity with PME-5 signature, and 82% with ddTANK. Surprisingly, the percentage similarity is much lower (38%) with both human tankyrases. Moreover, PME-5 and ddTANK both contain the PARP regulatory domain also found in huPARP-1, but not in human tankyrases. This suggests that the overall PARP catalytic domain of *C. elegans* and mycet tankyrases may be structurally closer to huPARP-1 as compared with their human orthologues.

PARP-1 catalyzes initiation, elongation, and branching of ADP-ribose polymers [7]. However, analysis of polymers synthesized by tankyrase-1 failed to show the presence of $(PR)_2AMP$, suggesting absence of branching activity [41]. It is not known if this feature is common to all tankyrases across species. However, considering the high similarity of its PARP signature with huPARP-1, and the presence of the PARP regulatory region, it would not be surprising that PME-5, and especially ddTANK, catalyzes the branching of poly(ADP-riboses). Moreover, we verified the presence of specific amino acids that participate in the branching of poly(ADP-ribose) in PME-5 and ddTANK sequence [42]. Some of them seem to be conserved, and some are also found in human tankyrase-1. However, the simple presence of those specific amino acids is not sufficient to estimate the branching capacity of PARPs. Subsequent experiments and analysis of PME-5 poly(ADP-riboses) will be needed to verify the structure of the polymer. Although not demonstrated in the present study, it is likely that PME-5 is a functional PARP and contributes to the overall endogenous poly(ADP-ribosyl)ation activity found in the nematode [28].

4.2. Identification of other motifs in PME-5

Unlike the classic tankyrase PARP domain, PME-5 isoforms contain the regulatory region also found in PARP-1 [43,44]. The role of the PARP regulatory domain is thought to relay the signal from PARP-1 binding to nicked DNA to the catalytic domain by a relative rearrangement, thereby giving rise to the NAD^+ binding mode more favorable for catalysis [43]. Similarly, the PARP regulatory region in PME-5 might mediate conformational rearrangement in response to protein interaction with the ANK domain. Notably, PME-5 does not contain the SAM module, which is thought to mediate homo- and heterodimerization between other SAM containing proteins [45]. However, PME-5 possesses a possible coiled coil domain in its C-terminal portion, just before the PARP domain where the SAM module is usually found. Coiled coil structure is known as a highly versatile protein folding oligomerization motif [46]. It is composed of 2–5 α-helices showing a 3.5-residue periodicity, which twist around each other in a supercoil. Coiled coil structures are found in structural and skeletal proteins, like the motor protein myosines [47], kinesines and dyneins, the intermediate filament proteins α-keratine and vimentin, and in some DNA-binding proteins (review in [46]). Therefore, despite the lack of SAM motif, PME-5 isoforms may be able to form homo- and heterodimers *via* their coiled coil regions, as reported for chicken and human tankyrases [10,48]. Another special feature found in PME-5 is the nuclear localisation signals (NLS). Indeed, eight motifs for NLS, including two-bipartite type, were found during amino acid analysis, predicting a nuclear localization for PME-5.

4.3. trans- and cis-splicing of PME-5

Like *pme-1* (PARP-1 *C. elegans* orthologue), *pme-5* mRNA was shown to be *trans*-spliced by SL-1. This particularity is characteristic of genes that are not localized in operon-like structures [28,36]. PME-5 mRNAs are thus members of a very large group of transcripts having their 5′-end equipped with the special feature SL1.

The fifth exon of *pme-5* was also shown to be alternatively spliced, producing two isoforms of the protein (Fig. 4). Exon 5 encodes a sequence of 38 amino acids located in the middle of the PME-5 ankyrin domain, where no ANK motif is found. Alternative splicing is frequent in ankyrin genes [49]. There are indeed three ankyrin genes in human and they all encode different isoforms as a result of alternative splicing events [4,49]. It may be the case for PME-5 as well because it is part of the ankyrin family.

According to amino acids analysis, the long and the short PME-5 isoform seem to have the same structural organization. However, the exon 5 encodes a peptide containing a possible tyrosine phosphorylation site (result not shown), suggesting that PME-5S may be resistant to some phosphorylation events compared with PME-5L. Moreover, exon 5 skipping may bring secondary and/or tertiary structure differences in PME-5 isoforms, thereby creating divergent binding sites for PME-5 ANK motif interacting partners.

4.4. Molecular phylogeny of pme-5 and its relationship to ddTANK

Much similarity was found between PME-5 and *D. discoideum* tankyrase-like protein (ddTANK). This protein contains 2,536 amino acids with 26 ANK motifs, and a catalytic PARP domain containing both the regulatory and the signature region. It also possesses a coiled coil domain but alignment with the one from PME-5 revealed no similarity. Finally, ddTANK seems to contain many NLS with 10 motifs, including five bipartite-type all in the same region. The finding of bipartite NLS in both *C. elegans* and *D. discoideum* tankyrases supports the predicted role of tankyrase in telomere maintenance, and also suggests a loss of those NLS in the evolution of higher *Coelomata* organisms.

4.5. Developmental and DNA damage-induced expression of pme-5

Expression patterns of PME-5S and PME-5L mRNAs were studied by conventional RT-PCR and quantitative RT-PCR, and both mRNA were detected at all developmental stages (Fig. 4A and B), suggesting that there is at least two different tankyrases expressed in the nematode throughout its life cycle. The physiological significance of this splicing remains to be determined. It is likely that the two isoforms have different functions or at least altered activities because the shorter isoform lacks a potential phosphorylation site (see Section 4.3).

The nuclear huPARP-1 protein is known for its functions in genomic integrity. That enzyme possesses two DNA-binding zinc fingers that allow recognition of DNA-strand breaks. Following DNA damage, PARP-1 activity increases up to 500-fold, and poly(ADP-ribosyl)ation of DNA-associated proteins is believed to modulate chromatin structure [7]. Relaxation of chromatin is essential for DNA transcription, replication, and repair. Indeed, PARP-1 seems to be a component of the base excision repair (BER) system and its presence is needed for effective DNA repair [50]. Tankyrases do not possess known DNA-binding domain and seem to lack NLS. However, some tankyrase molecules reach the nucleus probably by interacting with other nuclear proteins like TRF-1 [12]. Interestingly, PME-5 possesses its own bipartite NLS suggesting that it may be present largely in the nucleus. To investigate potential functions of PME-5, expression profile of *pme-5* mRNA following γ-irradiation was studied by quantitative RT-PCR using a fluorogenic probe that was designed to recognize a common segment in PME-5 isoforms. Results showed an increase in PME-5 mRNA level with time. This is the first time that tankyrase expression is associated with DNA damage. The fact that this induction is dependent on *hus-1* provides a molecular link between DNA damage and tankyrase. The way PME-5 may participate to DNA-damage response still remains unclear. However, as *pme-5* knock-down showed, it may be possible that PME-5 is involved in the DNA repair process. In its absence some damage may persist and direct cells toward apoptosis. This would suggest that long term absence of PME-5 may be deleterious for *C. elegans* as accumulation of damage over time can kill the animals. PME-5 may be required to keep the telomeric chromatin open via its PARP activity, and thereby, facilitating the repair of telomeric DNA. Through its ANK domain, PME-5 may also interact with many transcriptional factors or DNA-binding proteins and regulate their functions in response to damaging conditions.

It would be interesting to test if other checkpoint proteins in *C. elegans* have the same influence over *pme-5* expression. These include CEP-1, the recently found orthologue of p53 in *C. elegans* [51], MRT-2 and HRP-9. Further characterization of *pme-5* in *C. elegans* may prove important in discerning the function of this gene in vivo. The work presented here provides the foundation necessary for pursuing study of tankyrase function in *C. elegans*.

Acknowledgements

We are grateful to Dr. Yuji Kohara for providing the clone yk470c3 and Susanne Richardson for editorial review. This work is supported by the Grant 218712-99 from the Natural Sciences and Engineering Research Council of Canada and The Foundation for Research into Children's Diseases. S.D is a Junior I Research Fellow from the Fonds de la Recherche en Santé du Québec.

References

[1] S. Smith, I. Giriat, A. Schmitt, T. de Lange, Tankyrase, a poly(ADP-ribose) polymerase at human telomeres, Science 282 (1998) 1484–1487.
[2] S. Smith, T. de Lange, Tankyrase promotes telomere elongation in human cells, Curr. Biol. 10 (2000) 1299–1302.
[3] N.W. Chi, H.F. Lodish, Tankyrase is a golgi-associated mitogen-activated protein kinase substrate that interacts with IRAP in GLUT4 vesicles, J. Biol. Chem. 275 (2000) 38437–38444.
[4] M.A. Batrukova, V.L. Betin, A.M. Rubtsov, O.D. Lopina, Ankyrin: structure properties and functions, Biochemistry (Mosc) 65 (2000) 395–408.
[5] S. Shall, Poly (ADP-ribosylation): a common control process? Bioessays 24 (2002) 197–201.
[6] S. Smith, The world according to PARP, Trends Biochem. Sci. 26 (2001) 174–179.

[7] D. D'Amours, S. Desnoyers, I. D'Silva, G.G. Poirier, Poly(ADP-ribosyl)ation reactions in the regulation of nuclear functions, Biochem. J. 342 (1999) 249–268.
[8] A. Bianchi, S. Smith, L. Chong, P. Elias, T. de Lange, TRF1 is a dimer and bends telomeric DNA, EMBO J. 16 (1997) 1785–1794.
[9] B. van Steensel, T. de Lange, Control of telomere length by the human telomeric protein TRF1, Nature 385 (1997) 740–743.
[10] J.I. Sbodio, H.F. Lodish, N.W. Chi, Tankyrase-2 oligomerizes with tankyrase-1 and binds to both TRF1 (telomere-repeat-binding factor 1) and IRAP (insulin-responsive aminopeptidase), Biochem. J. 361 (2002) 451–459.
[11] H. Seimiya, S. Smith, The telomeric poly(ADP-ribose) polymerase, tankyrase 1 contains multiple binding sites for telomeric repeat binding factor 1 (TRF1) and a novel acceptor, 182-kDa tankyrase-binding protein (TAB182), J. Biol. Chem. 277 (2002) 14116–14126.
[12] B.D. Cook, J.N. Dynek, W. Chang, G. Shostak, S. Smith, Role for the related poly(ADP-Ribose) polymerases tankyrase 1 and 2 at human telomeres, Mol. Cell. Biol. 22 (2002) 332–342.
[13] E.H. Blackburn, C.W. Greider, E. Henderson, M.S. Lee, J. Shampay, D. Shippen-Lentz, Recognition and elongation of telomeres by telomerase, Genome 31 (1989) 553–560.
[14] C.I. Nugent, V. Lundblad, The telomerase reverse transcriptase: components and regulation, Genes Dev. 12 (1998) 1073–1085.
[15] J.W. Slot, H.J. Geuze, S. Gigengack, D.E. James, G.E. Lienhard, Translocation of the glucose transporter GLUT4 in cardiac myocytes of the rat, Proc. Natl. Acad. Sci. U.S.A. 88 (1991) 7815–7819.
[16] R.J. Lyons, R. Deane, D.K. Lynch, Z.S. Ye, G.M. Sanderson, H.J. Eyre, G.R. Sutherland, R.J. Daly, Identification of a novel human tankyrase through its interaction with the adaptor protein Grb14, J. Biol. Chem. 276 (2001) 17172–17180.
[17] D. Monz, A. Munnia, N. Comtesse, U. Fischer, W.I. Steudel, W. Feiden, B. Glass, E.U. Meese, Novel tankyrase-related gene detected with meningioma-specific sera, Clin. Cancer Res. 7 (2001) 113–119.
[18] A.N. Kuimov, D.V. Kuprash, V.N. Petrov, K.K. Vdovichenko, M.J. Scanlan, C.V. Jongeneel, M.A. Lagarkova, S.A. Nedospasov, Cloning and characterization of TNKL, a member of tankyrase gene family, Genes Immun. 2 (2001) 52–55.
[19] R.J. Daly, G.M. Sanderson, P.W. Janes, R.L. Sutherland, Cloning and characterization of GRB14, a novel member of the GRB7 gene family, J. Biol. Chem. 271 (1996) 12502–12510.
[20] A. Kasus-Jacobi, D. Perdereau, C. Auzan, E. Clauser, E. Van Obberghen, F. Mauvais-Jarvis, J. Girard, A.F. Burnol, Identification of the rat adapter Grb14 as an inhibitor of insulin actions, J. Biol. Chem. 273 (1998) 26026–26035.
[21] M. De Rycker, R.N. Venkatesan, C. Wei, C.M. Price, Vertebrate tankyrase domain structure and sterile alpha motif (SAM)-mediated multimerization, Biochem. J. 372 (2003) 87–96.
[22] P.G. Kaminker, S.H. Kim, R.D. Taylor, Y. Zebarjadian, W.D. Funk, G.B. Morin, P. Yaswen, J. Campisi, TANK2, a new TRF1-associated poly(ADP-ribose) polymerase, causes rapid induction of cell death upon overexpression, J. Biol. Chem. 276 (2001) 35891–35899.
[23] J.I. Sbodio, N.W. Chi, Identification of a tankyrase-binding motif shared by IRAP, TAB182, and human TRF1 but not mouse TRF1. NuMA contains this RXXPDG motif and is a novel tankyrase partner, J. Biol. Chem. 277 (2002) 31887–31892.
[24] J. Bae, J.R. Donigian, A.J. Hsueh, Tankyrase 1 interacts with Mcl-1 proteins and inhibits their regulation of apoptosis, J. Biol. Chem. 278 (2003) 5195–5204.
[25] I. Hope (Ed.), *C. elegans*: A Practical Approach, Oxford University Press, Oxford, 1999.
[26] I.L. Johnston, Molecular Biology, in: I.A. Hope (Ed.), *C. elegans*: A Practical Approach, Oxford University Press, Oxford, 1999, pp. 201–225.
[27] J. Sambrook, E.F. Fritsch, T. Maniatis, Molecular Cloning: A Laboratory Manual, Cold Spring Harbor, 1989.
[28] S.N. Gagnon, M.O. Hengartner, S. Desnoyers, The genes *pme-1* and *pme-2* encode two poly(ADP-ribose) polymerases in *Caenorhabditis elegans*, Biochem. J. 368 (2002) 263–271.
[29] I.L. Johnstone, J.D. Barry, Temporal reiteration of a precise gene expression pattern during nematode development, EMBO J. 15 (1996) 3633–3639.
[30] C.G. Larminie, I.L. Johnstone, Isolation and characterization of four developmentally regulated cathepsin B-like cysteine protease genes from the nematode *Caenorhabditis elegans*, DNA Cell. Biol. 15 (1996) 75–82.
[31] R.S. Kamath, A.G. Fraser, Y. Dong, G. Poulin, R. Durbin, M. Gotta, A. Kanapin, N. Le Bot, S. Moreno, M. Sohrmann, D.P. Welchman, P. Zipperlen, J. Ahringer, Systematic functional analysis of the *Caenorhabditis elegans* genome using RNAi, Nature 421 (2003) 231–237.
[32] A. Gartner, S. Milstein, S. Ahmed, J. Hodgkin, M.O. Hengartner, A conserved checkpoint pathway mediates DNA damage-induced apoptosis and cell cycle arrest in *C. elegans*, Mol. Cell 5 (2000) 435–443.
[33] S.F. Altschul, T.L. Madden, A.A. Schaffer, J. Zhang, Z. Zhang, W. Miller, D.J. Lipman, Gapped BLAST and PSI-BLAST: a new generation of protein database search programs, Nucleic Acids Res. 25 (1997) 3389–3402.
[34] N. Blom, S. Gammeltoft, S. Brunak, Sequence and structure-based prediction of eukaryotic protein phosphorylation sites, J. Mol. Biol. 294 (1999) 1351–1362.
[35] G. de Murcia, J. Ménissier-de Murcia, Poly(ADP-ribose) polymerase: a molecular nick-sensor, Trends Biochem. Sci. 19 (1994) 172–176.
[36] L.D. Riddle, T. Blumenthal, B.J. Meyer, J.R. Priess (Eds.), *C. elegans* II, Cold Spring Harbor Laboratory Press, Cold Spring Harbor, 1997.
[37] D.A.R. Zorio, N.N. Cheng, T. Blumenthal, J. Spieth, Operons as a common form of chromosomal organization in *C. elegans*, Nature 372 (1994) 270–272.
[38] A. Bürkle, V. Schreiber, F. Dantzer, F.J. Oliver, C. Niedergang, G. de Murcia, J. Ménissier-de Murcia, Biological significance of poly(ADP-ribosyl)ation reactions: molecular and genetic approaches, in: G. de Murcia, S. Shall (Eds.), From DNA Damage and Stress Signaling to Cell Death: Poly ADP-Ribosylation Reactions, Oxford University Press, New York, 2000, pp. 91–111.
[39] E.R. Hofmann, S. Milstein, S.J. Boulton, M. Ye, J.J. Hofmann, L. Stergiou, A. Gartner, M. Vidal, M.O. Hengartner, *Caenorhabditis elegans* HUS-1 is a DNA damage checkpoint protein required for genome stability and EGL-1-mediated apoptosis, Curr. Biol. 12 (2002) 1908–1918.
[40] B. Conradt, H.R. Horvitz, The TRA-1A sex determination protein of *C. elegans* regulates sexually dimorphic cell deaths by repressing the *egl-1* cell death activator gene, Cell 98 (1999) 317–327.
[41] J.F. Rippmann, K. Damm, A. Schnapp, Functional characterization of the poly(ADP-ribose) polymerase activity of tankyrase 1, a potential regulator of telomere length, J. Mol. Biol. 323 (2002) 217–224.
[42] V. Rolli, M. O'Farrell, J. Ménissier-de Murcia, G. de Murcia, Random mutagenesis of the poly(ADP-ribose) polymerase catalytic domain reveals amino acids involved in polymer branching, Biochemistry 36 (1997) 12147–12154.
[43] A. Ruf, J. Ménissier-de Murcia, G. de Murcia, G.E. Schulz, Structure of the catalytic fragment of poly(ADP-ribose) polymerase from chicken, Proc. Natl. Acad. Sci. U.S.A. 93 (1996) 7481–7485.
[44] A. Ruf, G. de Murcia, G.E. Schulz, Inhibitor and NAD+ binding to poly(ADP-ribose) polymerase as derived from crystal structures and homology modeling, Biochemistry 37 (1998) 3893–3900.
[45] J. Schultz, C.P. Ponting, K. Hofmann, P. Bork, SAM as a protein interaction domain involved in developmental regulation, Protein Sci. 6 (1997) 249–253.
[46] P. Burkhard, J. Stetefeld, S.V. Strelkov, Coiled coils: a highly versatile protein folding motif, Trends Cell Biol. 11 (2001) 82–88.

[47] C. Cohen, D.A. Parry, A conserved C-terminal assembly region in paramyosin and myosin rods, J. Struct. Biol. 122 (1998) 180–187.
[48] M. De Rycker, R.N. Venkatesan, C. Wei, C.M. Price, Vertebrate tankyrase domain structure and sterile-alpha motif (SAM) mediated multimerization, Biochem. J. 372 (2003) 87–96.
[49] V. Bennett, A.J. Baines, Spectrin and ankyrin-based pathways: metazoan inventions for integrating cells into tissues, Physiol. Rev. 81 (2001) 1353–1392.
[50] F. Le Page, V. Schreiber, C. Dherin, G. de Murcia, S. Boiteux, Poly(ADP-ribose) polymerase-1 (PARP-1) is required in murine cell lines for base excision repair of oxidative DNA damage in the absence of DNA polymerase beta, J. Biol. Chem. 278 (2003) 18471–18477.
[51] B. Schumacher, K. Hofmann, S. Boulton, A. Gartner, The *C. elegans* homolog of the p53 tumor suppressor is required for DNA damage-induced apoptosis, Curr. Biol. 11 (2001) 1722–1727.

7.1. Hints for involvement of *pme-5* in the DNA damage responses

7.1.1. Induction of *pme-5* transcripts after ionizing radiation (Figure 6B)

Since poly(ADP-ribosyl)ation is known to be part of an immediate response to DNA damage, we hypothesized that there might be a change at the transcriptional levels of *pme-5* upon ionizing radiation. Three hours after the application of 120 Gy of X-rays the mRNA levels were significantly higher, as measured by real-time quantitative RT-PCR (Figure 6B). Actually the transcript amounts increased four times, soon after 30 min (Figure 6A). To find the genetic requirements for this induction, I turned to *hus-1* that was already known to be required for the transcriptional up-regulation of *egl-1* upon ionizing radiation (Hofmann *et al.*, 2002). In the *hus-1(op244)* mutants *pme-5* induction was totally suppressed (Figure 6B), suggesting that *pme-5* most likely acts downstream of the *hus-1* checkpoint gene in the generation of a DNA damage response signal.

7.1.2. RNAi against *pme-5* results in elevated levels of apoptosis in the germ line (Figure 7)

To gain some insight into the role of the gene in the DNA damage responses, I inactivated it by RNAi and measured the apoptotic response before and after the application of ionizing radiation (Figure 7). A small increase in the levels of endogenous apoptosis was observed, implying an involvement of *pme-5* in the repair of endogenous DNA damage. Following treatment with X-rays the induction of apoptosis was comparable to wild-type, unlike what is stated in the paper.

Considering the efficiency of RNAi as a technique, though, these experiments should be repeated using the mutant that became available in the meantime (*pme-5(ok446)*).

Poly(ADP-ribosyl)ation is an immediate cellular response to DNA damage generated either endogenously or from exogenous factors. The proteins that catalyze this post-translational modification belong to the poly(ADP-ribose) polymerase superfamily (PARPs). By synthesizing poly (ADP-ribose), and by covalently attaching this polymer to glutamic acid residues of acceptor proteins such as histones and topoisomerases, it regulates diverse cellular processes. It has been proposed that maintenance of chromatin structure, DNA replication and repair, recombination, cell proliferation and programmed cell death, are among the functional tasks of PARPs.

What has led to this plethora of functions is the modular architecture of PARPs. A conserved core responsible for the catalytic activity to which a number of specific targeting and regulatory modules have been added, characterizes all the members in the superfamily. PARP-1 and PARP-2 are so far the only members whose catalytic activity is stimulated *in vitro* and *in vivo* by DNA strand-breaks and which catalyze the transfer of the ADP-ribose moiety from NAD^+ to a limited number of acceptor proteins involved in chromatin architecture and in DNA metabolism (Ame *et al.*, 2004, Oei *et al.*, 2005).

Among the other members of the PARP family, tankyrase 1 (TRF1-interacting, ankyrin-related ADP-ribose polymerase, TANK1) was identified as a partner of the human telomeric protein TRF1 in a two-hybrid screening (Smith *et al.*, 1998). Overexpression of TANK1 promotes release of TRF1 from telomeres and telomere

elongation (Smith & Lange, 2000), whereas shutting down its expression blocks the cells during early anaphase, suggesting a role in the resolution of specific cohesion complexes (Dynek & Smith, 2004).

TANK2 interacts with the same set of proteins as TANK1 (e.g. TRF1) and probably mediates overlapping functions in telomere homeostasis and vesicle trafficking. When overexpressed, it induces caspase-independent cell death through the loss of mitochondrial potential (Kaminker *et al*., 2004).

However, the question of how these PARP-like molecules with which *pme-5* shares similarity contribute to genome stability, is still open. To address this issue in *C. elegans*, a number of answers concerning its function either as an ADP(ribose)-polymerase or a tankyrase or both, have to be obtained. First the function of the PARP domain, both the catalytic and the regulatory, has to be deciphered in terms of ability to initiate and polymerize ADP monomers. Similarly, whether *pme-5* possesses a branching activity has to be molecularly proven, despite the presence of conserved amino acids involved in the branching process. In addition, evidence is necessary to prove that the coiled coil domains act as a substitute for the lack of SAM domain, a characteristic feature of tankyrases, and if so, to determine the nature of the potential dimers formed. Finally, important for the documentation of a role for *pme-5* in DNA damage responses is the identification of interacting partners. The clustered ANK repeats could be candidate docking sites for different protein-protein interactions.

References

Ame, J.C., Spenlehauer, C. & de Murcia, G. The PARP superfamily. Bioessays. **26(8)**, 882-93 (2004).

Dynek, J.N. & Smith, S. Resolution of sister telomere association is required for progression through mitosis. *Science* **304(5667)**, 97-100 (2004).

Hofmann, E.R., Milstein, S., Boulton, S.J., Ye, M., Hofmann, J.J., Stergiou, L., Gartner, A., Vidal, M. & Hengartner MO. *Caenorhabditis elegans* HUS-1 is a DNA damage checkpoint protein required for genome stability and EGL-1-mediated apoptosis. *Curr Biol*. **12(22)**, 1908-18 (2002).

Kaminker, P.G., Kim, S.H., Taylor, R.D., Zebarjadian, Y., Funk, W.D., Morin, G.B., Yaswen, P. & Campisi, J.TANK2, a new TRF1-associated poly(ADP-ribose) polymerase, causes rapid induction of cell death upon overexpression. *J Biol Chem*. **276(38)**, 35891-9 (2001).

Oei, S.L., Keil, C. & Ziegler, M. Poly(ADP-ribosylation) and genomic stability. *Biochem Cell Biol*. **83(3)**, 263-9 (2005).

Smith, S. & de Lange, T. Tankyrase promotes telomere elongation in human cells. *Curr Biol*. **10(20)**, 1299-302 (2000).

Smith, S., Giriat, I., Schmitt, A. & de Lange, T. Tankyrase, a poly(ADP-ribose) polymerase at human telomeres. *Science* **282(5393)**, 1484-7 (1998).

Tong, W.M., Cortes, U. & Wang, Z.Q. Poly(ADP-ribose) polymerase: a guardian angel protecting the genome and suppressing tumorigenesis. Biochim Biophys Acta. **1552(1)**, 27-37 (2001).

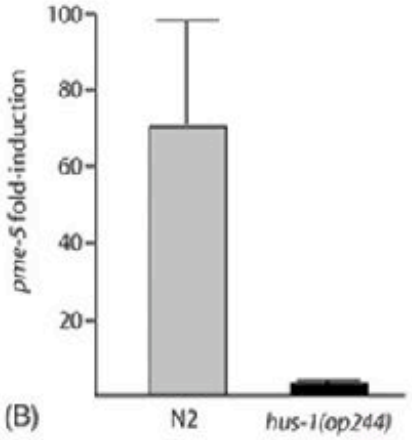

Figure 6B. *pme-5* is transcriptionally induced by irradiation in a *hus-1*-dependent manner

Average fold induction of *pme-5* gene expression in wild-type and *hus-1(op244)* mutants. The transcript levels were determined by real-time quantitative RT-PCR, 3 h following 120 Gy of X-ray irradiation.

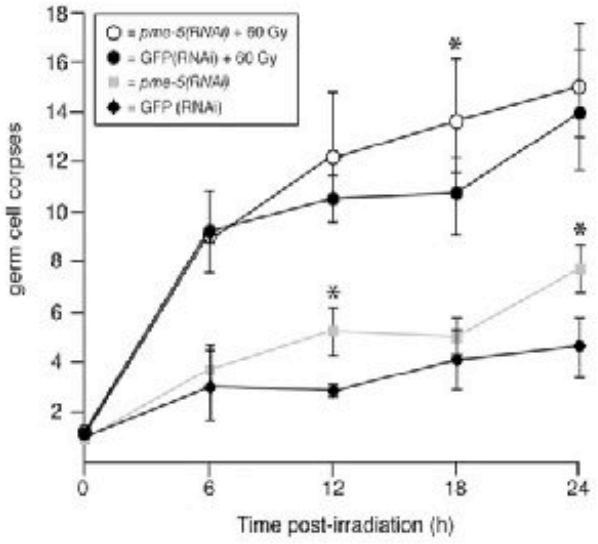

Figure 7. Inactivation of *pme-5* results in slightly increased levels of germline apoptosis

Time course analysis was performed with wild-type animals subjected to RNAi against *pme-5* or GFP as control. Apoptotic corpses were scored in the meiotic region of one gonad arm of young adult animals, before and after treatment with 60 Gy of X-rays. Data shown represent the average number of two independent experiments ± SD.

CHAPTER 8

FUTURE DIRECTIONS

Preface

The work in our lab aims to decipher the mechanisms by which eukaryotic cells detect various forms of DNA damage and then signal the presence of these structures to the DNA repair machinery, the cell cycle engine and the apoptotic device. As many aspects of the DNA damage response are highly conserved throughout eukaryotic evolution, we are analyzing proteins involved in these pathways in the model organism of *C. elegans*.

The current study identified some novel players in the DNA damage responses upon ionizing radiation and helped to explore a novel UV-inducible pathway. Considering the dense networking in these responses, we only have a fragmentary knowledge of some of the events that lead to the different biological outputs, namely the activation of checkpoints, DNA repair and apoptosis.

Below I submit some of the open questions in the field as well as some of the ways to approach them.

How is CEP-1 regulated upon genotoxic stress? If protein modification, e.g. phosphorylation, is a positive mode of regulation, what are the negative regulators of the protein activity?

It is almost very well-defined by now that the mammalian p53 is regulated in a number of ways that lead to its activation as a gene regulator. Modifications of the protein by chemical alterations or controlling its levels by degradation have been extensively studied in the past (reviewed by Wahl & Carr, 2001, Oren, 2003, Fingerman & Briggs, 2004, Yang *et al*., 2004).

So far knowledge on the *C. elegans* p53 mode of regulation is lacking. Mapping of potent sites of modification by mass spectrometry analysis and subsequent identification of the responsible enzyme, might be a good marker for testing activity of the principle pro-apoptotic molecule in worms.

Moreover, a negative regulator of CEP-1 with a function equivalent to that of Mdm2 ubiquitin protein E3 ligase, is up to now missing from the worm proteome (reviewed by Moll & Petrenko, 2003, Chène, 2004). Whether such an unidentified ligase exists or another one plays that role remains to be determined. In a screen for modifiers of the *cep-1(lf)* situation, the *ned-8* gene coding for an E3 ligase was obtained (Derry *et al*., 2003). Data from my experiments revealed an increased apoptosis phenotype in the germline when knocking down the gene function by RNAi (data not shown). Such observations should be followed up more and a closer look at all genes predicted to function as such has to be undertaken.

How does CEP-1 initiate cell cycle arrest upon exposure to Ultraviolet Radiation? How is cell cycle arrest initiated upon exposure to ionizing radiation?

Having identified a role for CEP-1 in the activation of germ cell proliferation arrest upon UV and in contrast to IR, the question of how this is succeeded arises. Previous studies have excluded the involvement of two cyclin kinase inhibitors, *cki-1* and *cki-2*, homologs of the mammalian p21, as inducible by ionizing radiation genes (Hofmann *et al.*, 2002). With the knowledge that p21 transcription mediates cell cycle arrest in a p53-dependent manner (Bunz *et al.*, 1998), the mRNA levels of the already mentioned worm genes should be examined more carefully during the course of time.

Additionally, a fraction of genes that were found to be regulated upon ionizing radiation in the microarray experiments were linked to the cell cycle progression control. For instance, the yeast APC homolog (Anaphase-Promoting Complex) or the human p27kip1 equivalent gene lies in that group (*mat-1*). A member of the CDC25 family of cell cycle regulators (*cdc-25.3*) is an ENU-regulated gene. The nature of these genes points to a starting point for the elucidation of how the cell cycle arrest is initiated upon genotoxic stress in *C. elegans*.

The knowledge of the exact cell cycle phase that is blocked (through the use of cyclin-specific reporters) will assist the search for such regulators, following exposure to both IR and UV.

Is there an involvement of the C. elegans chk-1 in the DNA damage responses?

The experimental analysis of Chapter 5 identified a role for the *C. elegans chk-2* in mediating both the cell cycle arrest and the apoptotic response upon treatment with Ultraviolet light, but assigned no function to it in the ionizing radiation-induced pathway. The involvement of the yeast and the mammalian *chk-1* homolog in checkpoint activation upon genotoxic stress makes it a reasonable candidate to act downstream of the ATL-1 kinase following IR. Although knocking down the gene function by RNAi did not result in any detectable defect, repeating all the appropriate assays with the mutant animals will be more informative.

Furthermore, initiating a biochemical characterization of the two major damage responsive pathways will complete the current view of how the DNA damage signaling is triggered in *C. elegans* and might constitute an inspirational platform for the design of approaches to identify new players in the field.

What is the precise function of LIN-26 in the execution of cell death upon IR?
Is the molecular function of LIN-26 linked to that of a transcription factor or is it more likely associated with a RNA binding activity?

The deduced amino acid sequence of *lin-26* points to its role either as a transcription factor, with both the transcriptional induction or repression activity equally possible, or as an RNA binding protein. Biochemical experiments in the form of chromatin immunoprecipitation analyses or RNA binding assays are necessary in order to determine the gene or transcript targets, respectively.

Although it is obvious from the preceded analysis that LIN-26 is implicated in the DNA damage responses, it is not known yet where in the signaling pathway the protein acts. It might exert its function in the principal DNA damage pathway comprising *hus-1* and *cep-1*, or in a parallel one and still diverge with the former at the level of the two BH3-only domain molecules. The abundance in the messages of *lin-26* in the absence of the CEP-1 protein under physiological conditions, in combination with the putative p53 binding sites in the gene implies a regulatory relationship between the two molecules. To establish the validity of such a hypothesis, an *in vitro* DNA binding assay using an a-CEP-1 antibody should be performed.

The modification of the LIN-26 protein upon genotoxic stress implicates a protein kinase in the hierarchy of the DNA damage signaling cascade where it acts. Mapping the potent phosphorylation sites on LIN-26 by 2D-gel electrophoresis and subsequent mass spectrometry analysis would reveal a lot of the underlying biology.

The gene dosage effect unveiled by the deletion *lin-26* allele is worth to be further explored since it might be of relevance to cancer biology. Blockage of apoptosis by loss of one functional gene copy is an interesting and common feature of haploinsufficient tumor suppressor genes. The scoring of a deficiency that covers the gene locus will enable to identify the nature of the phenotype and speculate more on the gene function.

How does RPO-1 regulate the cell death decision upon exposure to IR?
Is there any role for the nucleolus in sensing and transducing signals that regulate the activity of proapoptotic genes, e.g. cep-1?

RPO-1 is homologous to a splicing variant of the human second largest subunit of RNA polymerase I, for which no role up to now has been assigned. This raises the challenging hypothesis that the two proteins constitute a new group of polypeptides, and that novel functions might arise by the utilization of key gene units to control processes of DNA surveillance and cell demise.

The embryonic survival studies placed *rpo-1* in the *clk-2* pathway, parallel to the *hus-1* one, to influence the transcriptional activation of the two pro-apoptotic genes, *egl-1* and *ced-13*. Since the *clk-2* pathway has not been described yet, the approach from two different sides might help elucidate its nature.

The mutation in the *rpo-1* gene negatively affects both the levels of processed and unprocessed 5.8S rRNA transcripts and this is reflected to the nuclear and nucleolar size. Titrating out the locus (by genetic deficiencies) has an effect on the activation of cell death, mirroring the *op259* mutation. Whether ribosomal biosynthesis is associated with triggering of the appropriate DNA damage-induced apoptotic response cannot be yet deduced.

A growing body of literature, though, points to multiple levels of nucleolar involvement in the regulation of p53, including its association with abundant nucleolar proteins involved in ribosome biogenesis (Daniely *et al*., 2002, Colombo *et al*., 2002). It is very tempting to hypothesize that RPO-1, in analogy, might constitute

a link between the nucleolus and DNA damage initiated responses. Studies to identify interacting partners upon infliction of damage by the yeast-two-hybrid technique, for example, might shed some light on the issue. Moreover, determining the subcellular localization of the protein before and following DNA damage, by raising specific antibodies against it, would be crucial to prove this hypothesis.

Is there a role for the proteasome machinery in the death decision upon genotoxic stress?

What is the nature of the defect in rpn-9(gk401) mutants?

The microarray analysis revealed a radiation-induced transcriptional activation of the *rpn-9* gene and the mutant analysis identified a defect in the induction of apoptosis. Although the characterization presented in this dissertation is very preliminary, a systematic approach to conclusively establish a mode of function for the gene is necessary. This would involve all the regular assays to identify a potential checkpoint or repair role for the protein and double mutant analyses to determine genetic interactions with known pro- and anti-apoptotic checkpoint proteins.

All of the characterized proteins containing PINT (Proteasome, Int-6, Nip-1 and TRIP-15) domains, like the *rpn-9* gene product, are parts of larger multi-protein complexes. Identification of the components of such a complex upon DNA damage might unveil interesting information on the general role of the proteasome in regulating responses upon conditions of genotoxic stress. Ideally, the protein's interaction with (a) specific substrate(s) might be telling of its specific role in the DNA damage responses.

How is the phospholipid-independent AKT/PKB kinase implicated in the initiation of cell death upon IR?

The microarray analysis also revealed a radiation-induced transcriptional activation of the W04B5.5 gene, coding for a phospholipid-independent AKT/PKB kinase. The human counterpart is also significantly induced in a p53-dependent manner after DNA damage, whereas the budding yeast homolog, known as ksg1, is involved in the control of cell cycle arrest via a phosphoinositide signaling pathway.

The apoptotic defect of animals lacking the respective kinase in *C. elegans* engages the protein in the DNA damage signaling network, at least in the short term apoptotic responses. An extensive genetic study that involves double mutant and epistasis analyses is required to establish a gene function. The starting point would be known components of the stress responsive pathway in *C. elegans*, where the AKT kinases that mediate the DAF-2 signaling are implicated.

Although the AKT/PKB signaling pathway is now recognized as one of the most critical pathways in regulating cell survival, by providing the cells with a signal that allows them to withstand apoptotic stimuli, a new branch might be emerging with the W04B5.5 protein participating in signaling the genotoxic stress stimuli to the apoptotic machinery. It was recently reported, though, that the gene product, named PIAK by the researchers, phosphorylates the mammalian AKT/PKB and activates the survival pathway that may be utilized during periods of cellular quiescence (Li, *et al.*, 2001). Despite that, a pro-apoptotic function during conditions of genotoxic stress cannot be readily excluded.

References

Bunz, F., Dutriaux, A., Lengauer, C., Waldman, T., Zhou, S,, Brown, J.P., Sedivy, J.M., Kinzler, K.W. & Vogelstein, B. Requirement for p53 and p21 to sustain G2 arrest after DNA damage. *Science* **282(5393)**, 1497-501 (1998).

Chene, P. Inhibiting the p53-MDM2 interaction: an important target for cancer therapy. *Nat Rev Cancer* **3(2)**, 102-9 (2003).

Colombo, E., Marine, J.C., Danovi, D., Falini, B. & Pelicci, P.G. Nucleophosmin regulates the stability and transcriptional activity of p53. *Nat Cell Biol*. **4(7)**, 529-33 (2002).

Daniely, Y., Dimitrova, D.D. & Borowiec, J.A. Stress-dependent nucleolin mobilization mediated by p53-nucleolin complex formation. *Mol Cell Biol*. **22(16)**, 6014-22 (2002).

Derry, W.D., Wood, C., Cheam, L., Vang, J., Bierings, R., Fraser, A.G., Kamath, R.S., Ahringer, J. & Rothman, J.H. Unraveling the p53 network using functional genomics *International Worm Meeting* 2003.

Fingerman, I.M. & Briggs, S.D. p53-mediated transcriptional activation: from test tube to cell. *Cell* **117(6)**, 690-1 (2004).

Li, Y., Dowbenko, D. & Lasky, L.A. *Caenorhabditis elegans* PIAK, a phospholipid-independent kinase that activates the AKT/PKB survival kinase. *J Biol Chem*. **276(23)**, 20323-9 (2001).

Moll, U.M. & Petrenko, O. The MDM2-p53 interaction. *Mol Cancer Res*. **1(14)**, 1001-8 (2003).

Oren, M. Decision making by p53: life, death and cancer. *Cell Death Differ*. **10(4)**, 431-42 (2003).

Song, G., Ouyang, G., Bao, S. The activation of Akt/PKB signaling pathway and cell survival. *J Cell Mol Med*. **9(1)**, 59-71 (2005).

Wahl, G.M. & Carr, A.M. The evolution of diverse biological responses to DNA damage: insights from yeast and p53. *Nat Cell Biol*. **3(12)**, E277-86 (2001).

Yang, Y., Li, C.C. & Weissman, A.M. Regulating the p53 system through ubiquitination. *Oncogene* **23(11)**, 2096-106 (2004).